Lawrence Berkeley National Laboratory

Lawrence Berkeley National Laboratory

Title

MAGNETOTELLURIC STUDIES IN GRASS VALLEY, NEVADA

Permalink

https://escholarship.org/uc/item/4x803369

Author

Morrison, H.F.

Publication Date

1979

eScholarship.org Powered by the California Digital Library
University of California

LBL-8646
UC-66b

MAGNETOTELLURIC STUDIES IN GRASS VALLEY, NEVADA

H. Frank Morrison, Ki Ha Lee, Gary Oppliger and Abhijit Dey*

Lawrence Berkeley Laboratory
University of California, Berkeley 94720
Engineering Geoscience
Department of Materials Science and Mineral Engineering

NOTICE

This report was prepared as an account of work sponsored by the United States Government. Neither the United States nor the United States Department of Energy, nor any of their employees, nor any of their contractors, subcontractors, or their employees, makes any warranty, express or implied, or assumes any legal liability or responsibility for the accuracy, completeness or usefulness of any information, apparatus, product or process disclosed, or represents that its use would not infringe privately owned rights.

January 1979

This work was supported by the Division of Geothermal Energy of the U.S. Department of Energy under contract No. W-7405-ENG-48.

*Presently with Chevron Resources, Inc., San Francisco, CA

DISTRIBUTION OF THIS DOCUMENT IS UNLIMITED

DISCLAIMER

This report was prepared as an account of work sponsored by an agency of the United States Government. Neither the United States Government nor any agency Thereof, nor any of their employees, makes any warranty, express or implied, or assumes any legal liability or responsibility for the accuracy, completeness, or usefulness of any information, apparatus, product, or process disclosed, or represents that its use would not infringe privately owned rights. Reference herein to any specific commercial product, process, or service by trade name, trademark, manufacturer, or otherwise does not necessarily constitute or imply its endorsement, recommendation, or favoring by the United States Government or any agency thereof. The views and opinions of authors expressed herein do not necessarily state or reflect those of the United States Government or any agency thereof.

DISCLAIMER

Portions of this document may be illegible in electronic image products. Images are produced from the best available original document.

Contents

Introduction

A program of detailed magnetotelluric soundings was initiated in 1974 in Green Valley, Nevada, as part of the Lawrence Berkeley Laboratory's major study of techniques for geothermal exploration in north central Nevada. The magnetotelluric program had three main goals; the determination of resistivity distribution at depths greater than that conveniently measured with other techniques; a comparison of the interpreted resistivity at shallow depth with the results of the other techniques; and the evaluation of the SQUID or Josephson effect magnetometer in practical field surveys. In addition, new numerical models were developed so that interpretation could be carried out in terms of fairly complex two-dimensional models.

Geological Setting

Beyer et al., (1976) have presented the following summary of the geologic setting of the Leach Hot Springs area.

> Active hot springs areas in the Great Basin are in almost all cases associated with steeply dipping basin and range faults (Hose and Taylor, 1974) often at the intersection of two major orientations of faulting. A possible model for the numerous hot springs in the area is simply that surface waters descend along permeable zones associated with these faults, become heated at depths of only a few kilometers by the higher than normal gradients in this region, and ascend to the surface. Renner, et al. (1975), in their summary of hydrothermal convection systems in the U.S., are however, "skeptical that geothermal gradient alone can sustain high temperatures for the long durations of time indicated for these systems."
>
> Certainly, if the only conduit for geothermal waters is along such permeable fault zones, or at the intersection of two such zones, the volume of the zone would have to be large to constitute a reservoir. The successful model of an economic reservoir must consist of a source of heat, a suitable transport mechanism, and a volume of sufficient porosity and permeability to be exploitable as a reservoir of hot water. Because of lack of definitive geologic information on most hot spring areas, the basis on which the estimates by Renner et al., (1975) of heat content are made involve rather arbitrary assignments of value. For example, for Leach Hot Springs, a subsurface reservoir of an areal extent of 4 square kilometers and a thickness of 2.5 km has been assumed. However, in the absence of direct, or for that matter indirect, information, a simple fault zone model could explain the surface hot spring activity and would entail no appreciable reservoir volume at all.
>
> The Leach Hot Springs area is located in Grass Valley, Nevada approximately 50 km south of Winnemucca. The Sonoma and Tobin Ranges bound the valley on the east, while the valley is constricted

south of the hot springs by the Goldbanks Hills, locus of earlier mercury mining. Grass Valley is bounded on the west by the basalt-capped East Range. The distribution of major lithologic units in the region is illustrated on the geologic map, Fig. 1. The intricate fault and lineament pattern, based strongly on photo interpretation, (Noble 1975) is shown on a separate map, Fig. 2. Paleozoic siliceous clastic rocks and greenstones are the oldest bedrock types in the region. In places in the Sonoma and Tobin Ranges, the Paleozoics are in thrust-fault contact with Triassic siliceous clastic and carbonate rocks. The Paleozoic and Triassic rocks have been intruded by granitic rocks of probable Triassic age in the Goldbanks Hills; elsewhere the granitics are probably of Cretaceous age. Though not exposed in the Leach Hot Springs area, Oligocene-Miocene rhyolitic tuffaceous rocks are probably present in the subsurface. They are overlain by a sequence of interbedded sandstone, fresh water limestone and altered tuffs, which are in turn overlain by coarser conglomeratic sediments (fanglomerates derived from mountain range fronts steepened by the onset of basin and range faulting. The fanglomerates are opalized in places by siliceous hydrothermal activity associated with fault zones; occasionally the locus of mercury mineralization. Opalization of mercury deposits in the Goldbanks Hills and East Range closely resembles the opalized sinter at Leach Hot Springs. The Tertiary sedimentary sequence is overcapped by predominantly basaltic volcanic rocks whose ages, dated by the potassium argon method, range from 14.5 to 11.5 million years.

Characteristic of the hot springs systems observed in northern Nevada, Leach Hot Springs is located on a fault, strongly expressed by a 10 to 15 m high scarp trending NE. Normal faulting since mid-Tertiary has offset rock units vertically several tens to several hundred meters. As shown on the fault and lineament map (Fig. 2) the present-day hot springs occur at the zone of intersection of the NE trending fault and the NNW-SSE trending lineaments.

Total surface flow from the Leach Hot Springs system has been measured at 130 ℓ min^{-1} (Olmsted et al., 1975). Subsurface temperatures of the springs reach 94°C, boiling at their altitude, and water temperatures at depth are estimated to be 155°C to 170°C, based on silica and alkali-element geothermometers (Mariner et al., 1974). Application of mixing-model equations (Fournier, et al., 1974), based on silica contents and temperatures of warm and cold spring waters, indicates that the temperature of hot water at depth within the Leach Hot Springs system may exceed 200°C. Material deposited by Leach Hot Springs, presently and in the past is predominantly SiO_2.

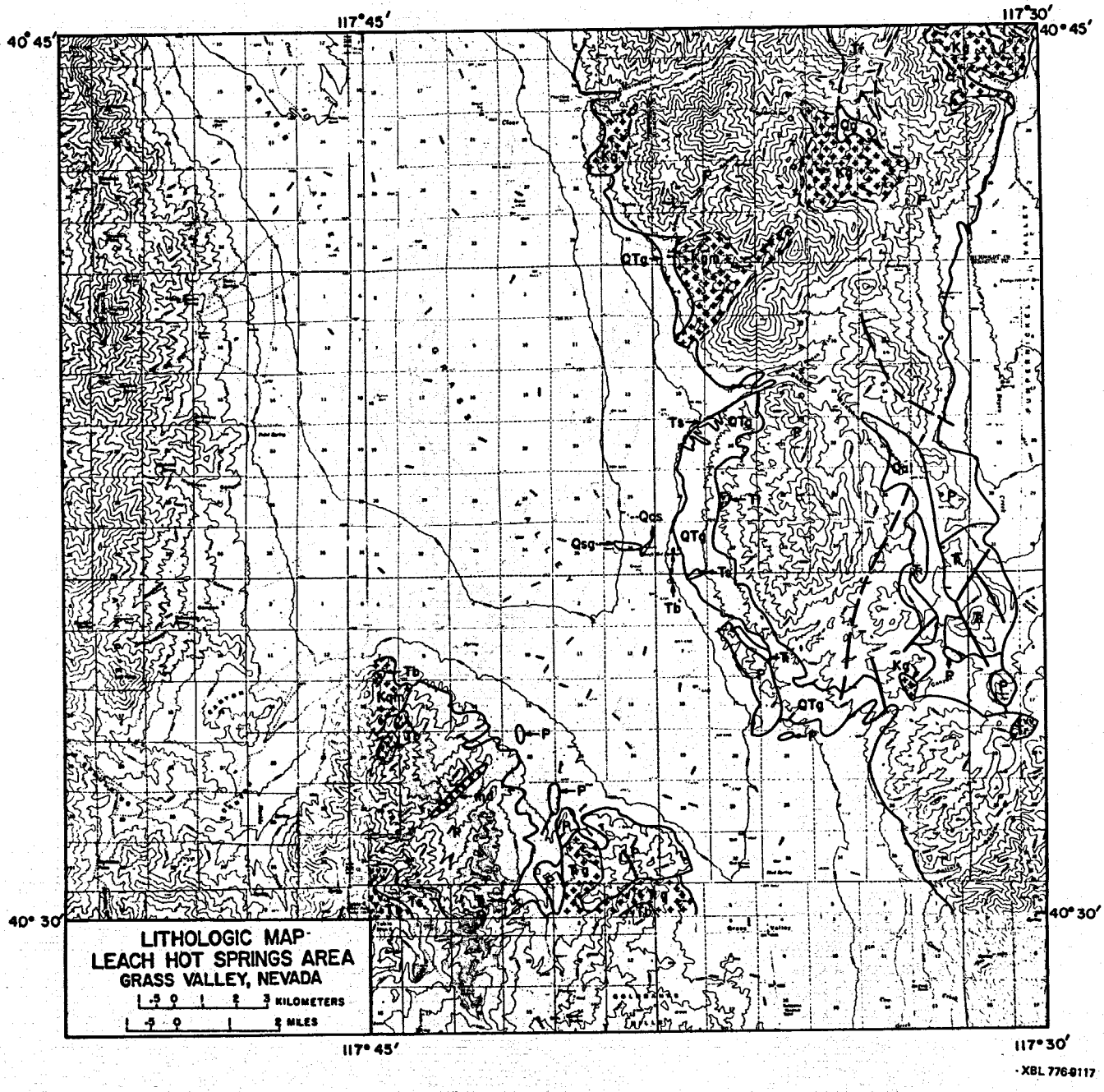

Fig. 1. Lithologic Map, Leach Hot Springs Area. Qal: alluvium, Qos: older sinter deposits, Qsg: sinter gravels, QTg: Quaternary-Tertiary gravels and fanglomerates, Tb: Tertiary basalt, Tr: Tertiary rhyolite, Tt: Tuff, Ts: Tertiarary sedimentary rocks, Kqm: quartz monzonite, Kg: granitic rock, md: mafic dike, TRg: Triassic granitic rocks, TR: undifferentiated Triassic sedimentary rocks, P: undifferentiated Paleozoic sedimentary rocks.

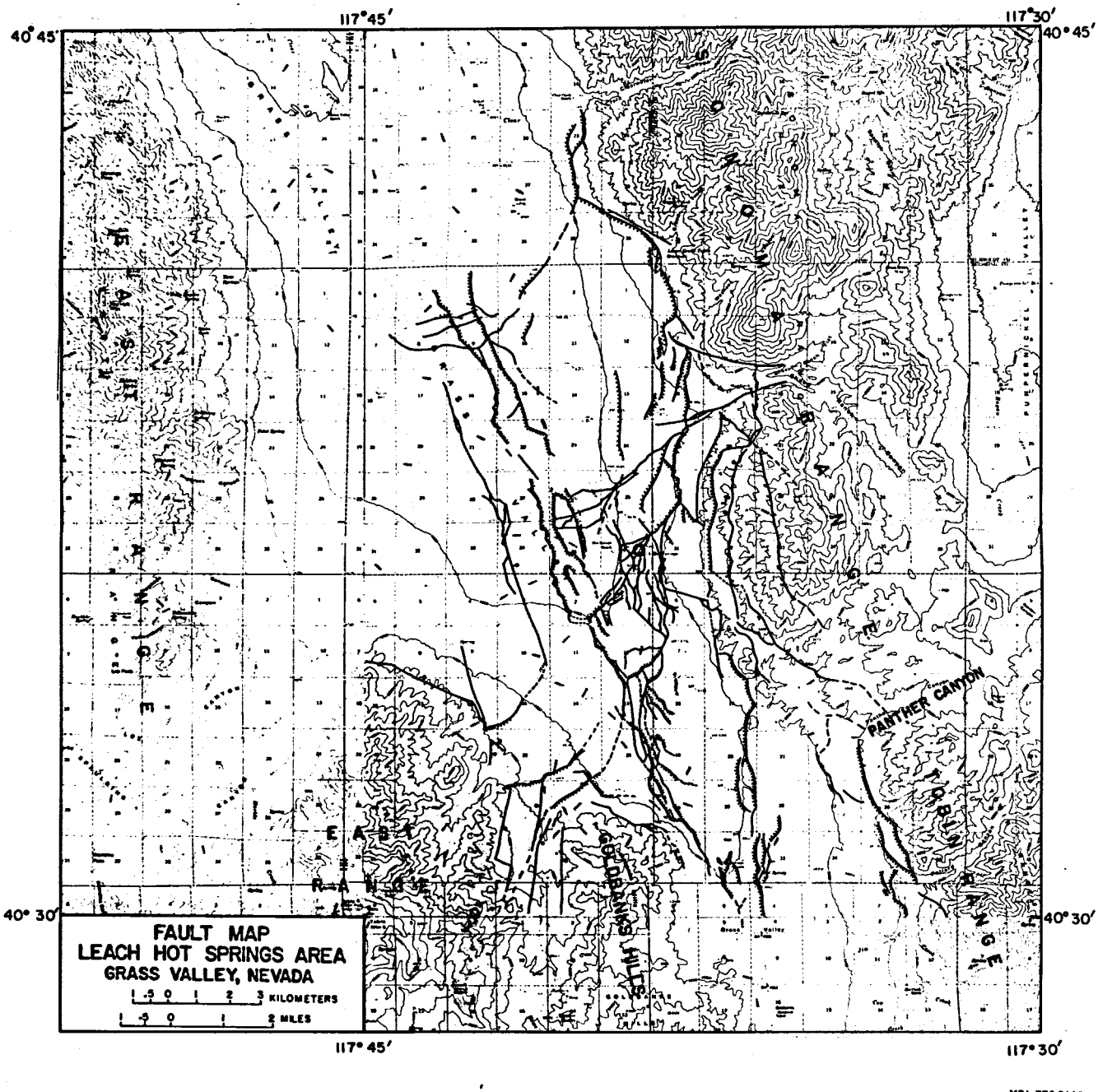

Fig. 2. Fault map of the Leach Hot Springs area. Hachured lines indicate down-faulted sides of scarplets; ball symbol indicates downthrown side of other faults. Leach Hot Springs is denoted by a small circle near the center of the map, and Hot Springs passes through it to the northeast and southwest.

Magnetotellurics

Geothermal exploration has provided increased incentive to develop magnetotelluric field and data processing techniques for practical, or commerical applications. Vozoff (1972) has described the application of magnetotellurics in petroleum exploration but most other studies have been concerned with deep crustal or upper mantle structure. More recently magnetotelluric surveys have been used in geothermal exploration by Stanley et al., (1977), Hermance and Pedersen (1976), Jiracek et al., (1977) and considerable contract work has been carried out by several geophysical survey companies (Geotronics, Geonomics, Terraphysics, and Senturion, to mention a few) but this latter work has not been published. In the case of deep crustal studies only a few stations are occupied, and the measurement interval has to be many days or weeks long to obtain the long periods required for deep penetration. Vozoff (1972) has shown that for the depths of exploration required in petroleum exploration a station may only need to be occupied for one or two days if easily movable equipment is available. The traditional sensors for low frequency magnetic fields are multiturn induction coils. These have a sensitivity of approximately 10^{-3} gamma (γ) at 1 Hz and are large and heavy (~90 kg per coil) This sensitivity is achieved only with considerable attention to detail in the coil construction and in the low-noise preamplifiers. The resistivity distribution that is sought in petroleum exploration may be expected to be less complicated than that in geothermal exploration. The resistivity variations may also be expected to be more subtle in the former; gentle anticlinal structures, layer displacements across faults at great depth, or gradual facies changes laterally within a layer. Thus, in petroleum exploration, one-dimensional layered interpretation is often satisfactory, but the data quality has to be very good to permit the resolution of many layers. Further, in sedimentary sections the resistivities are generally low (<100Ωm) so that frequences as low as 10^{-3} Hz may be required to achieve adequate depths of exploration. This requires long recording periods and taxes the sensitivity and signal to instrument-noise characteristics of the magnetic field sensors.

In geothermal exploration the local resistivity distribution is generally complex. In north central Nevada, for example, hot spring activity is often associated with range front faults separating resistive ranges and conductive alluvium filled valleys. Multiple range-bounding faults and transverse structures which segment the valleys into 3-dimensional blocks all pose serious interpretational difficulties for magnetotellurics. One immediate consequence of this added geologic complexity is that closer station sampling may be needed, and unless the data can be taken and processed quickly the cost of the survey may become unreasonable. On the other hand, since a depth of exploration of only 3-5 km is required to probe the valleys, which rarely exceed 2 to 3 km in sediment thickness, the longer period variations may not be required and adequate data can be obtained in only a few hours at a site.

The development of SQUID magnetometers (e.g., Clark, 1974; Zimmerman and Campbell, 1975) has solved one of the most important field problems for magnetotellurics. Useful sensitivities at least an order of magnitude greater than for induction coils from dc to 1 Hz are readily achievable. Three components of magnetic field are measured by means of a single small, lightweight package, and the electronics are simple and require a minimum of adjustment in the field. The frequency response is flat. While ideally suited for the lowest frequencies ($\leq 10^{-2}$ Hz) the increased sensitivity allows field measurement during periods of relative quiet when the signals are of the same order as the instrument noise in the induction coil systems. Most importantly, the sensor package weighs only 15-20 kg, and is easily deployed on the ground surface. Wind noise is eliminated by placing a light tent or frame around the sensor (Fig. 3). The instrument noise in SQUID systems is easily measured; a superconducting shield, or can, is placed around the sensors so that no external magnetic field can be detected. The output is then a true measure of sensor plus electronics noise. A comparable measurement is very difficult to make with induction coils as they cannot be shielded from external fields. Consequently internal noise sources (such as thermal noise in the mu-metal cores) cannot be evaluated.

In the summer of 1974 preliminary tests of a magnetotelluric system using a SQUID magnetometer were conducted in Grass Valley, Nevada. The instrument was calibrated on-site using a small loop current source. Several operational problems (overheating of electronics, sensor overloading by high amplitude transients (sferics), and inadequate wind motion protection) were encountered that prevented the completion of a full survey of the area. By August 1975 these problems had been corrected and 17 stations were occupied in a two week period in the general vicinity of Leach Hot Springs. The stations were located along two of the main geophysical traverse lines, A-A' and E-E' (Fig. 4). These lines were also used for other survey techniques, such as resistivity and tellurics (Beyer, 1977). Five of these stations were reoccupied in the summer of 1976. The stations were reoccupied for an empirical test of repeatibility and a modified shield was used at one of the stations to obtain data to 10^{-3} Hz.

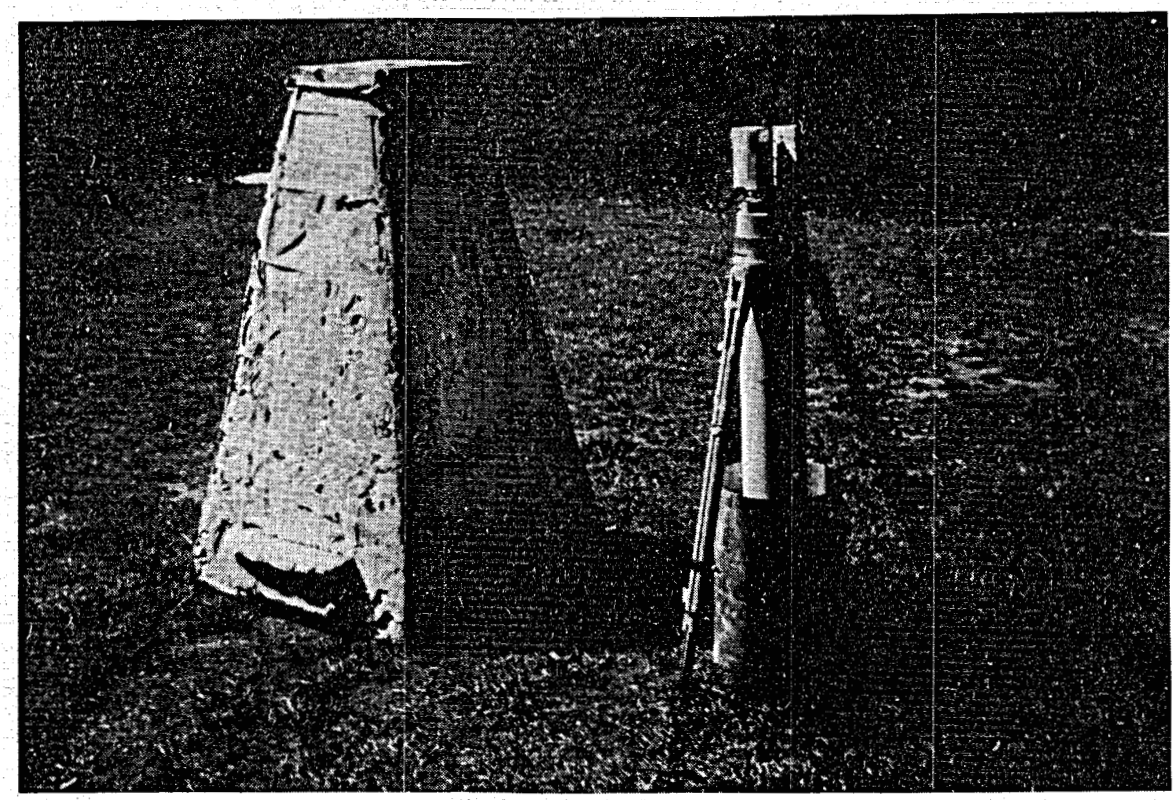

CBB 770-10369

Fig. 3. SQUID magnetometer (in tripod) and plastic foam insulator/windscreen.

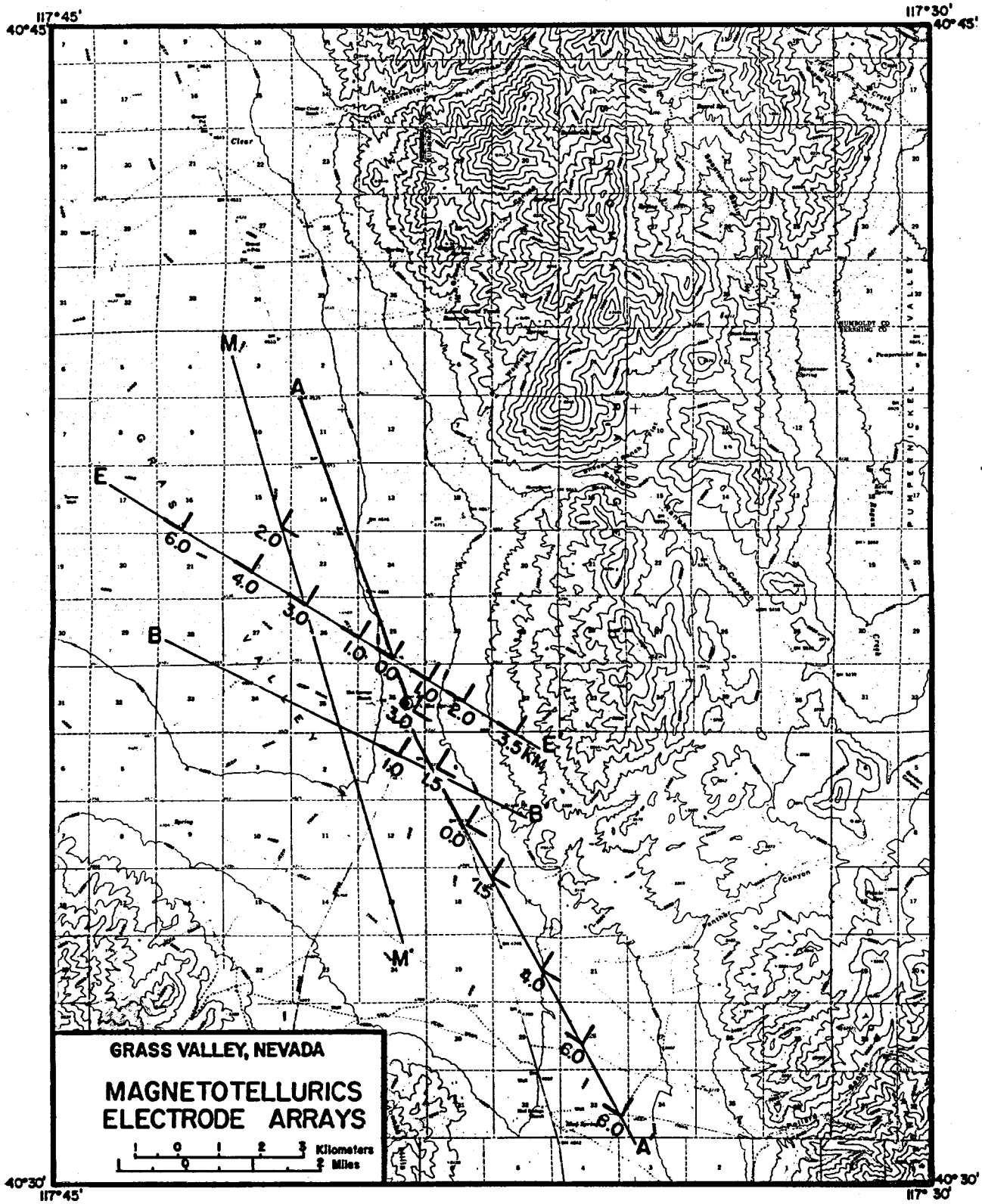

XBL 778-2677

Fig. 4. Magnetotelluric recording sites in Grass Valley, Nevada.

Instrumentation and Data Processing

The sensors, sensor electronics and recorders used for the Grass Valley experiment are shown schematically in Fig. 5. Two SQUID magnetometers were used at different times. A commerically available ac SQUID manufactured by DEVELCO Inc. (Model 8230) was used for most of the data and a new dc SQUID magnetometer developed by Professor John Clarke, University of California, was used at several sites. It was also used simultaneously with the Develco unit for comparative performance studies. The results with the new magnetometer are reported separately (Clarke et al., 1976).

A fundamental aspect of the SQUID magnetometer is that whereas the sensor can respond to very large magnetic field changes, in practical applications the sensor is used as a null detector in a feed-back loop. Therefore the frequency response, dynamic range and slew rate are determined by the feedback electronics. A sensitivity of 10^{-5} γ is available and desirable, but a dynamic range of 100's of gammas and a bandwidth of 100 Hz is needed in a practical magnetometer. Not all these characteristics can be met with existing electronics, and so, for example, most commercial SQUID magnetometers cannot track a 100 γ change at 100 Hz. Another way of stating the problem is that SQUID magnetometers are slew rate limited, the limit defined as the number of γ's per second in a transient signal that the device can follow.

This slew rate limitation poses a problem whenever strong sferic signals are present. These transients are generated by lightning, and may easily produce fields whose rate of change is in excess of the slew rate of the magnetometer. Electronic filtering cannot help, as it does with the induction coils, because the sensor itself is driven by the incident field. If the feedback electronics cannot keep up, magnetic flux enters the sensor loop and when the electronics again "locks in" a dc offset will be observed. These steps, which occur each time the feedback system loses lock, produce long transients in the filters which cannot be removed from the data.

The solution to this problem is to prefilter the field itself by means of electromagnetic shield around the sensor. In the Develco magnetometer the shield is a small 5 cm by 10 cm cylinder of thin copper. This acts like a single pole low pass filter. It was found that even this was not sufficient for summer operation in Nevada and so a second shield in the form of an aluminum can (30 cm diameter, 45 cm long, 1 mm thick) was added around the outside of the cryostat. Since the mutual impedance of the two shields is appreciable the net result remains approximately that of a single pole filter, but with a lower corner frequency. The response of the three-axis SQUID system with the two shield filter is shown in Figs. 6a - 6f.

Despite the double shield severe sferic transients would cause the electronics to lose lock. This is particularly annoying when very long period data are desired, and on these occasions a thick-

walled external aluminum can was used which provided a corner frequency of approximately 1.0 Hz. The external shields are easily removed or exchanged so this prefiltering technique poses no operational difficulties in the field.

Electric fields were measured with orthogonal electric dipoles, 500 m in length, and arrayed in an "L", with one common electrode. Copper-copper sulfate porous pot electrodes were used.

The voltages detected on the receiving electrode pairs were amplified with a Princeton Applied Research (PAR) model 113 preamplifier. The three components of magnetic field and two of electric field were then bandpassed with Ithaco model 4211 electronic filters. These filters were chosen because of the high uniformity of phase and amplitude response for a particular filter setting. Thus, each filter would be within 1.0^{o} and 2%, absolute, within the selected pass band. This is a very desirable characteristic for it eliminates the need to compensate for filter responses in impedance calculations; all channels are affected in exactly the same way. Two pass bands were used so that the signals could be recorded on an FM recorder despite its restricted dynamic range. The low frequency band covered .01 Hz to 5 Hz and the high frequency band covered 1 Hz to 40 Hz. At one of the sites a specially constructed long-period filter was used to cover the band from 0.001 Hz to 0.1 Hz.

The filtered signals were then recorded at 1 7/8 ips on a 0.5 inch, 7-channel FM tape recorder (Honeywell 5600). A read-after-write head on the tape deck permitted the recorded signals to be monitored via paper chart recorders in the field.

A right-hand-coordinate convention was used, the z-axis positive down. All the electrode arrays were oriented in the same direction: E_x at $N59^{o}$ W and E_y at $N31^{o}$ E. The magnetometer axes were aligned to correspond to electric dipole directions.

The tape recorded data and chart records were returned to Berkeley for processing and analysis. Segments containing good data (free from steps, gain changes or periods of very low activity) were selected from the monitor chart records, and the corresponding tape segments were then played back through a Varian 620/L - 100 minicomputer with a multichannel digitizer to produce a five channel multiplexed digital tape compatible with a CDC 7600 computer. To decrease the time spent in laboratory tape processing, the field tapes were played back into the digitizer at 300 ips. Simultaneously, a five-channel paper record was produced directly from the tape with event marks on the margin supplied from the computer or digitizers. These marks indicate the beginning of each record of 300 digitized data points (60 from each of the five channels) on the digital tape. This allows precise correlation between the analog traces and the digitized version. A further selection is then made to find usable contiguous records

to form data segments containing 512, 1024, or 2048 points per channel. As many of these data blocks as possible are made for each site. Table 1 presents the numbers of data blocks obtained in the two pass bands for each site.

Table 1. GRASS VALLEY MT DATA 1975-1976

STATION	No. of Data Sets 100-1 Sec.	No. of Data Sets 1-40 Hz	No. of Points Per Data Sets 100-1 Sec.	No. of Points Per Data Sets 1-40 Hz
		1975 DATA		
3.5 KM E EE'	10	45	2048	1024
2.0 KM E EE'	6	46	2048	1024
1.0 KM E EE'	12	37	2048	1024
0.0 KM E EE'	7	29	2048	1024
1.0 KM E EE'	12	33	2048	1024
2.5 KM W EE'	14	27	2048	1024
4.0 KM W EE'	7	33	2048	1024
6.0 KM W EE'	14	30	2048	1024
3.0 KM N AA'	16	46	2048	1024
1.5 KM N AA'	15	34	2048	1024
0.0 KM AA'	12	35	2048	1024
1.5 KM S AA'	10	29	2048	1024
4.0 KM S AA'	14	28	2048	1024
6.0 KM S AA'	16	30	2048	1024
8.0 KM S AA'	14	43	2048	1024
1.0 KM E BB'	12	43	2048	1024
2.0 KM N MM'	17	37	2048	1024
		1976 DATA		
3.5 KM E EE'	16	40	2048	1024
2.0 KM E EE'	50	41 day/45 night	2048	1024
1.0 KM E EE'	18	40	2048	1024
0.0 KM EE'	14	40	2048	1024
3.0 KM N AA'	24	30		1024
		(1000 sec.-20 sec.) DATA		
1.0 KM W EE'	5		2048	(Data length 8100 sec each)

Note: Nyquist frequency for 100 - 1 sec. band is 2 Hz.
Nyquist frequency for 1-40 Hz band is 78 Hz.

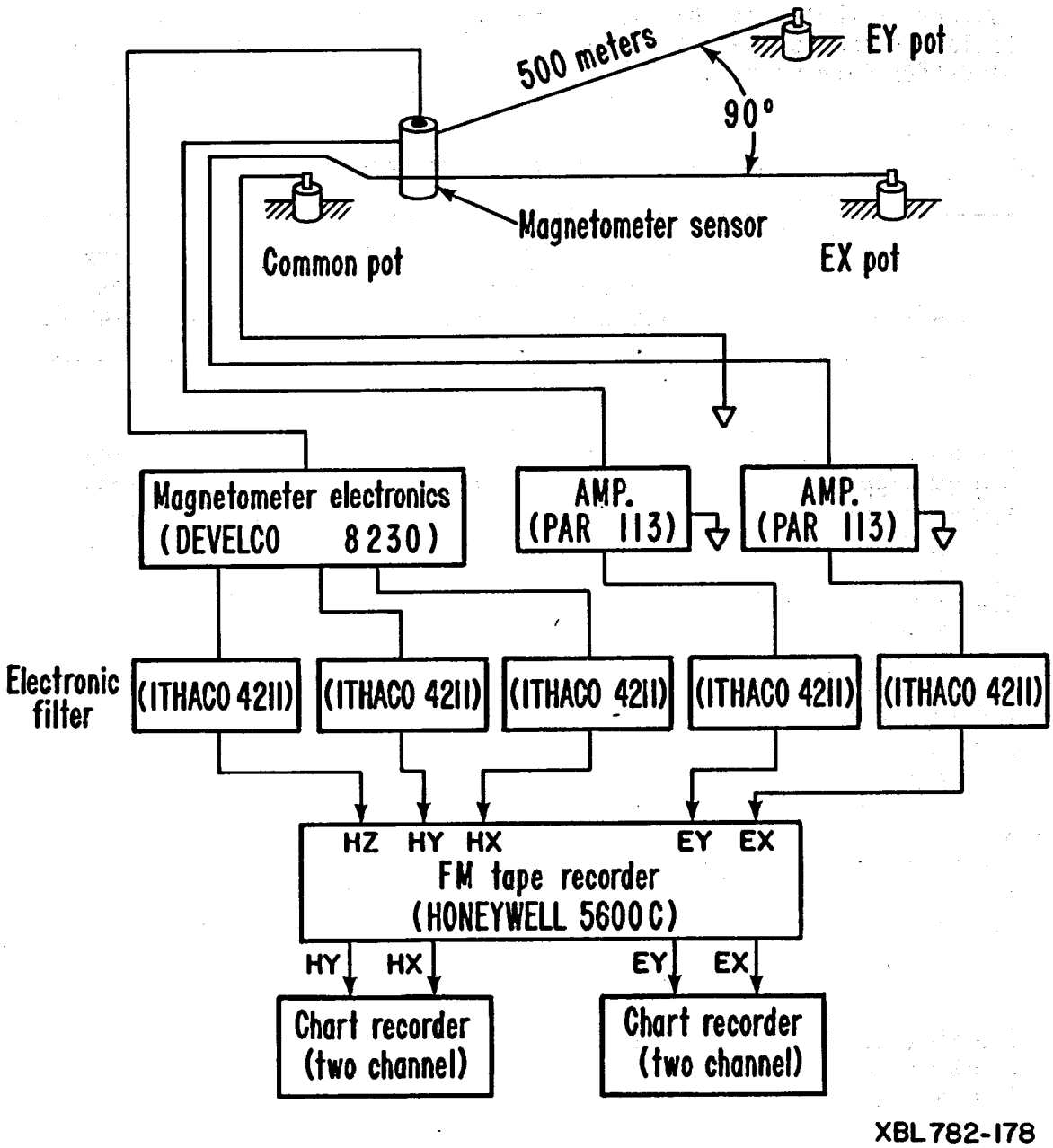

Fig. 5. Schematic of magnetotelluric measurement system.

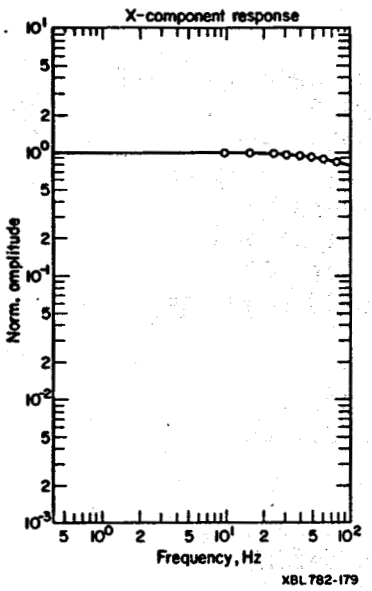

a.

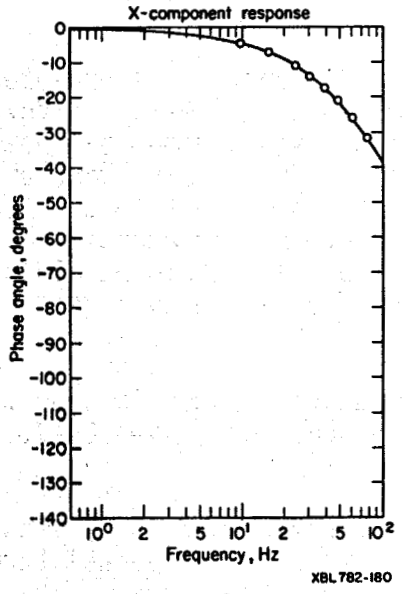

b.

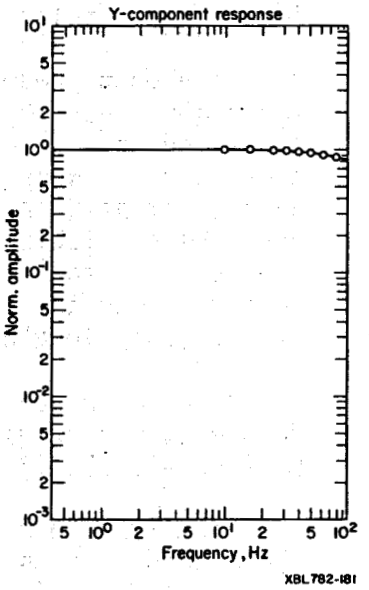

c.

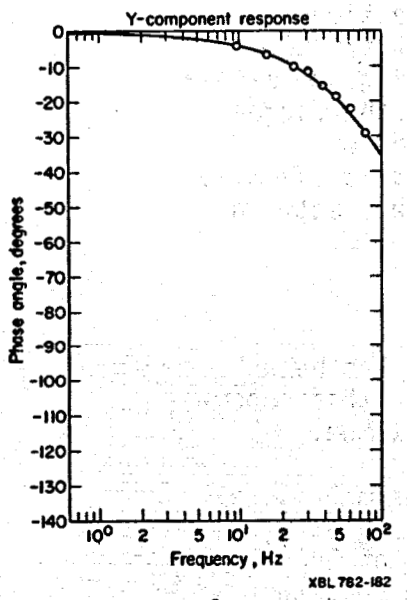

d.

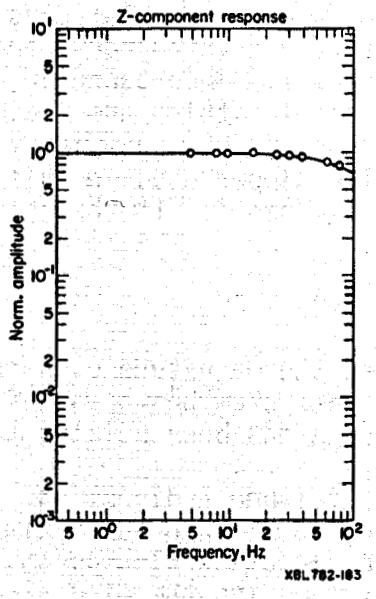

e.

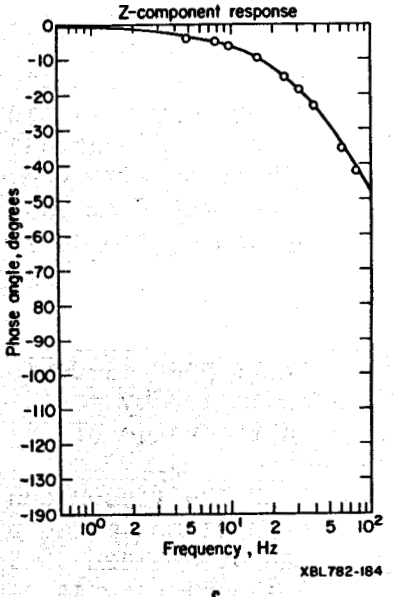

f.

Figs. 6a-6f. Amplitude and Phase response of SQUID Magnetometer. Amplitude response of Hx component. Phase Response of Hx component. Amplitude response of Hy component. Phase response of Hy component. Amplitude response of Hz component. Phase response of Hz component.

Impedance Calculations

The data presented in this report were analyzed using power spectral techniques described by Sims et al., (1971) and Vozoff, (1972). The digitized data were Fourier transformed and all possible auto- and cross-spectra were calculated. The spectra were obtained by averaging over constant Q frequency intervals and then by ensemble averaging over the available data blocks. For frequencies between .01 Hz and 1 Hz the ensemble averages typically contained 10 segments of 500 seconds. For the 1-40 Hz band ensemble averages contained 30 segments of 8 seconds length (Table 1).

The two dimensional impedance tensor is then calculated for each frequency window using the expressions given by Vozoff (1972), and Sims et al. (1971).

The impedance estimates are rotated in 5^0 steps (clockwise) until the diagonal terms are maximized. The diagonal terms then define E_x'/H_y' and E_y'/H_x' in the principal directions. These values are then used to calculate the apparent resistivities ρ_x' and ρ_y' respectively. The magnitude of the skew, a measure of the three dimensionality of the ground, is also calculated as is the tipper, following Vozoff (1972). We have devoted considerable effort to analyzing the tipper because of its importance in resolving the strike direction, assisting in 2-D model fitting and indicating the degree of three dimensionality through its skew and its variation of direction with frequency. The tipper used in this report is slightly different from that defined by Vozoff. If the relationship between H_z and H_x and H_y is written

$$H_z = AH_x + BH_y,$$

the tipper is defined here as the magnitude of A after A has been maximized by rotation. A tipper skew has been defined in this report as the ratio of $|B|/|A|$ after A has been rotated to a maximum.

The tipper can also be assigned a direction. If the magnitude of A is maximized by rotation to A' then the maximizing angle, θ_1, can be defined as the tipper direction with an ambiguity of 180^0. The ambiguity is resolved by choosing the direction such that the phase of A' is in the range of $\pm 90^0$. Thus, a maximized tipper is found by mathematical rotation to angle θ_1. If the phase is found to be within $\pm 90^0$ this is the direction of the tipper. If the phase is outside $\pm 90^0$ then the direction is reversed.

There are two kinds of errors which can affect the impedance estimates. Noise in either electric or magnetic fields alone can produce a bias error in the impedance estimate depending on which combination of auto- and cross-spectra are used in the calculation. This uncorrelated noise are signals in E or H which are not correlated with counterparts in H and E respectively. Thus, local sources of magnetic noise (a vehicle rocking in the wind) would not have an

associated electric field determined by the plane wave impedance relation. The magnetic field would, thus, be uncorrelated with the electric field. Bias errors are difficult to correct although there is theoretically enough data to compute the impedance over a two-dimensional earth without bias. For this report we have used an impedance formula which is not biased by uncorrelated electric field noise.

More specifically, the formulae are based on least-squares fits of complex coefficients for two-input one-output linear systems, where the horizontal magnetic fields are assumed to be noise-free inputs and each of the two electric components is, in turn, considered the system output. If uncorrelated magnetic noise is present the impedance estimates will be biased downwards. This choice is not entirely arbitrary and has been influenced by analysis recently performed by Gamble, Goubau and Clarke (1977) which has shown that, in fact, there is uncorrelated noise in the electric field at the Grass Valley site.

Random errors in the impedance estimates may be estimated following Bendat and Piersol (1971) and this approach has been used by Reddy et al., (1976) to obtain 95% confidence limits for these apparent resistivity values. The same procedure has been used in this analysis.

Finally, the coherence between the measured electric field and the calculated electric field, determined from the impedance estimate and the measured magnetic field, is also calculated. An impedance estimate is not selected for further analysis unless this coherence is greater than 0.5.

The final plots of the data for all 17 stations are presented in Figs. 7–28. Apparent resistivities and other tensor properties are plotted against square root of period T, on standard log-log scale (cm per cycle) which is compatible with all other magnetotelluric analysis carried out in this laboratory. Repeat data taken in 1976 are included for stations 0.0, 1.0 East, 2.0 East, 3.5 East on Line EE' and for station 3.0 North on Line AA'.

A summary of tipper data is presented in Fig. 29. Representative tippers are shown for the band 25-80 seconds (solid line) and 1-20 Hz (dashed line). The arrow indicates the tipper direction as found by maximizing A as discussed above. The arrow length (the length is assigned a scale in Fig. 29) gives the magnitude of A' and the tipper skew is indicated by including the magnitude of B' on a line at 90° to the direction of A'.

The principle resistivity direction, determined from impedance tensor rotation, is also shown in Fig. 29 as a line terminated by a circle.

Some general features of the data can be summarized before a detailed analysis is given. The data quality, indicated by the 95% confidence limits on the apparent resistivities, is poor in the band from .16 seconds to 10 seconds. This is simply a result of little

natural field energy in this band, and despite the long recording intervals not enough signal activity was recorded to provide good estimates. The formula for calculating apparent resistivities is subject to bias from uncorrelated magnetic field noise. It is, therefore, possible that the low apparent resistivities observed in this low signal level band are the result of bias errors rather than a resistivity low in the geologic section. However, it was later determined that the resistivity low is real. Data for several stations were processed using estimators subject to bias from uncorrelated electric field noise and the results were substantially the same. Finally, Gamble, Goubau and Clarke (1977) succeeded in developing several impedance estimators which are unbiased, and they verify the low apparent resistivity.

At all sites the quality of the tipper estimates proved to be significantly worse than the associated impedance estimates. This resulted in a larger degree of scatter in tipper directions than is present in the impedance tensor orientations.

One of the most striking results is that the principal values of apparent resistivity, obtained from the rotated impedances, lie within 0^{o} to 20^{o} of the measurement axes at the majority of stations on the east side of the valley. The maximum resistivity is in the x-direction (sub-parallel to line EE') and the minimum in the y-direction. Except for station 2.5 West on EE' and 1.5 North on AA', all eastern stations have approximately the same principal resistivity axes for the entire frequency range analyzed. No error bars have been calculated for these impedance rotations but in general, reliable rotation angles are obtained when the error bars on the corresponding resistivity estimates are small. If a mean rotation of $+15^{o}$ is selected, the strike would be interpreted as N45^{o}W. The geological strike taken from the fault map (Fig. 2) or from the surface geology (Fig. 1) is complex. The set of faults passing through station 4.0W on Line EE' strike at about N 22^{o}W. The main range front faults and also the topographic demarcation of the edge of the valleys are closer to N 10^{o}W. The axis of the valley defined by gravity is close to N 40^{o}W south of Leach Hot Springs and approximately N 20^{o}W north of the springs. The maximum apparent resistivity axis, thus, appears to be rotated about 20^{o} to the west of the other measures of regional strike.

For almost all stations the ρ_x apparent resistivities reveal a four-layer structure. Since ρ_x is subparallel to the regional strike of the contact separating the valley sediments from the Paleozoic rocks of the ranges, we can associate it with the TE mode of incident field. In a later section it will be shown that for a layered earth interrupted by horizontal discontinuities the TE mode apparent resistivities are the least affected, and an approximate interpretation can be obtained from a one-dimensional (multilayer) analysis. Thus, we use the ρ_x values of most of the stations to obtain a first estimate of the layered structure.

The first layer has a resistivity of between 10 and 20 ohm meters. The curves then drop, indicating a more conductive second layer in the valley sediments. The curves rise again, presumably for the more resistive basement and upper crust. Finally, at depth, there is a conductive roll-over, indicating the presence of a conductive layer or half space, possibly at the base of the crust.

The tipper data, summarized in Fig. 29, indicate the same general structure except that, unlike the impedance data, there are different tipper directions for the high frequency (1-20 Hz) band and for the low frequency (25 to 80 second period) band. At several stations these directions differ by more than 40°, suggesting a pronounced change in the strike direction with depth; i.e., or a three-dimensional effect. The absence of impedance orientation changes of a similar magnitude points to the significant conclusion that tippers may be substantially more sensitive to local structure than are impedances. This has recently been confirmed in 3-D model studies by Jones and Vozoff (Vozoff, 1977, personal communication).

Inasmuch as two-dimensional models cannot explain the discrepancies between principal axes of the impedance tensor and tipper direction (especially as a function of frequency) the effects must be due to the fact that the valley is not well represented by two-dimensional models. Some indications of the three-dimensional nature of the valley can be seen directly in the tipper data. At stations 6.0 km and 8.0 km south, Line AA', the tippers point northwest - suggesting a more resistive terrain to the northwest. Station 4.0 km south, Line AA', has unusually high values of near surface resistivity, 30-35 ohm meters and shows only a suggestion of a more conductive layer between surface and resistive basement. It could, therefore, be presumed that the valley sediments have thinned appreciably at 4.0 km south and then thicken again to the south. This is confirmed very well by the gravity data (Goldstein and Paulsson, 1977) which show that Grass Valley does, in fact, close off in the vicinity of 4.0 km south.

In the center of the valley, stations 4.0 km and 6.0 km west on Line EE', the tippers vary a great deal. In general, the long period vectors point in a southerly direction which may be the result of the proximity of the range on the west side of the valley which trends NW-SE.

It is somewhat disturbing to note how sensitive the tippers and impedance tensors are to features which must be relatively small compared to the gross structure of the valley which is clearly two-dimensional. The gravity interpretation (Goldstein and Paulsson, 1977) does show small transverse features but the structure is clearly dominated by a broad elongated valley filled with low density sediments. The magneto-telluric data, even at long periods, appears to be very sensitive to minor resistivity contrasts and does not give a very good value for the obvious strike of the valley fill.

Figs. 7-28. Data for each station includes: rotated apparent resistivities, impedance rotation angle, impedance skew, tipper magnitude, tipper rotation and tipper skew. Line designations refer to Fig. 4.

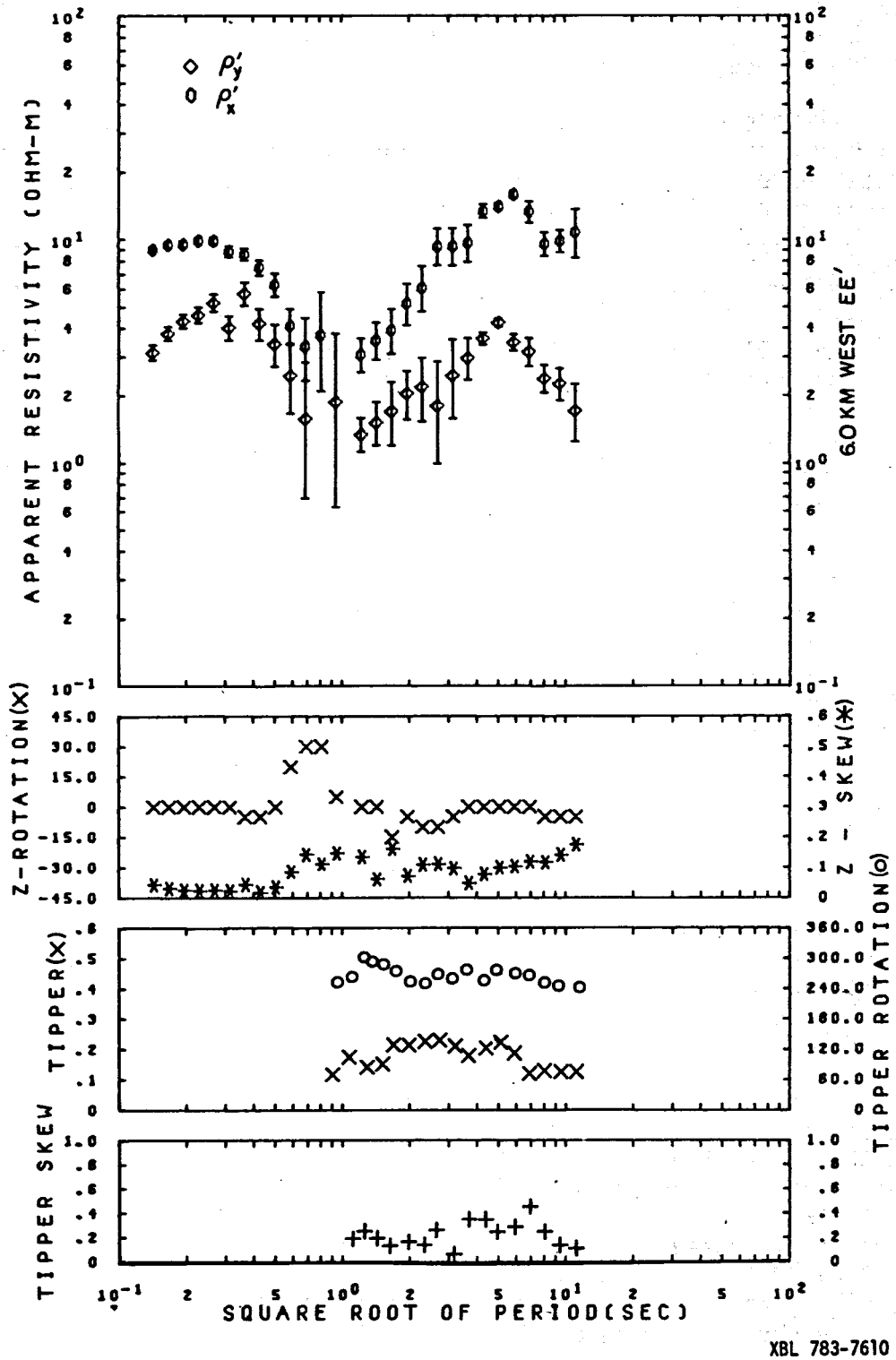

Fig. 7. Station 6.0 kw West, Line EE'.

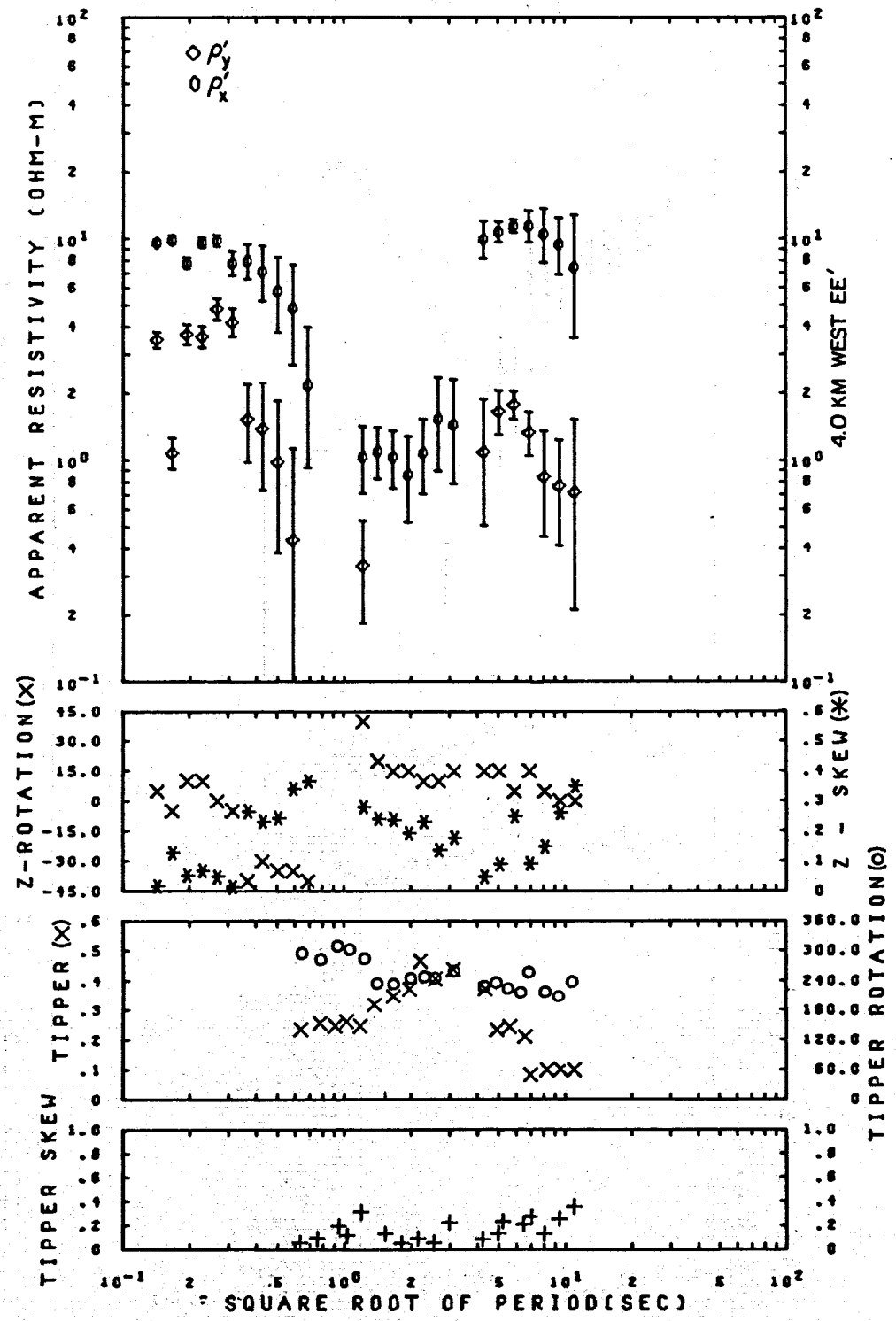

Fig. 8. Station 4.0 kw West, Line EE'.

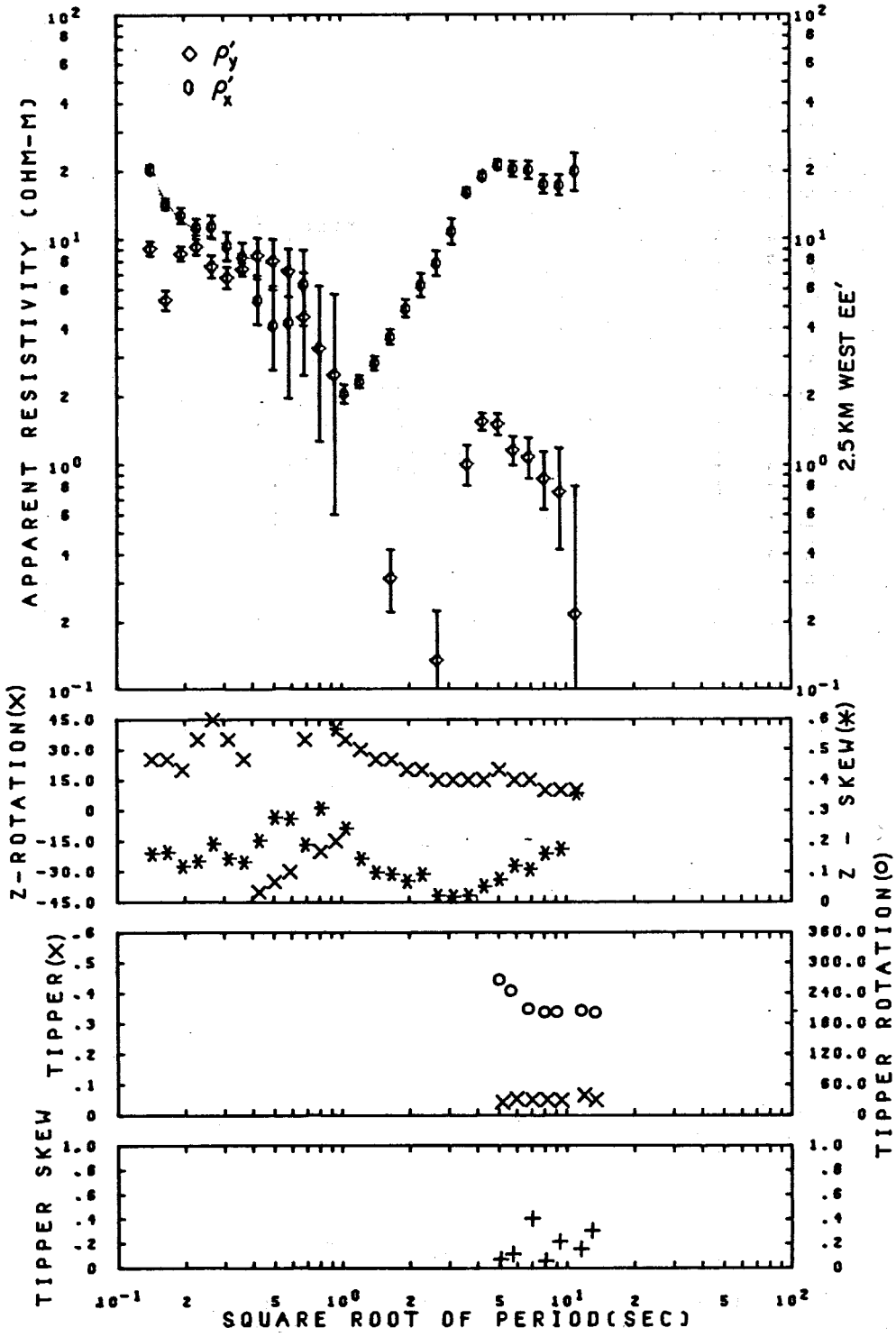

Fig. 9. Station 2.5 kw West, Line EE'.

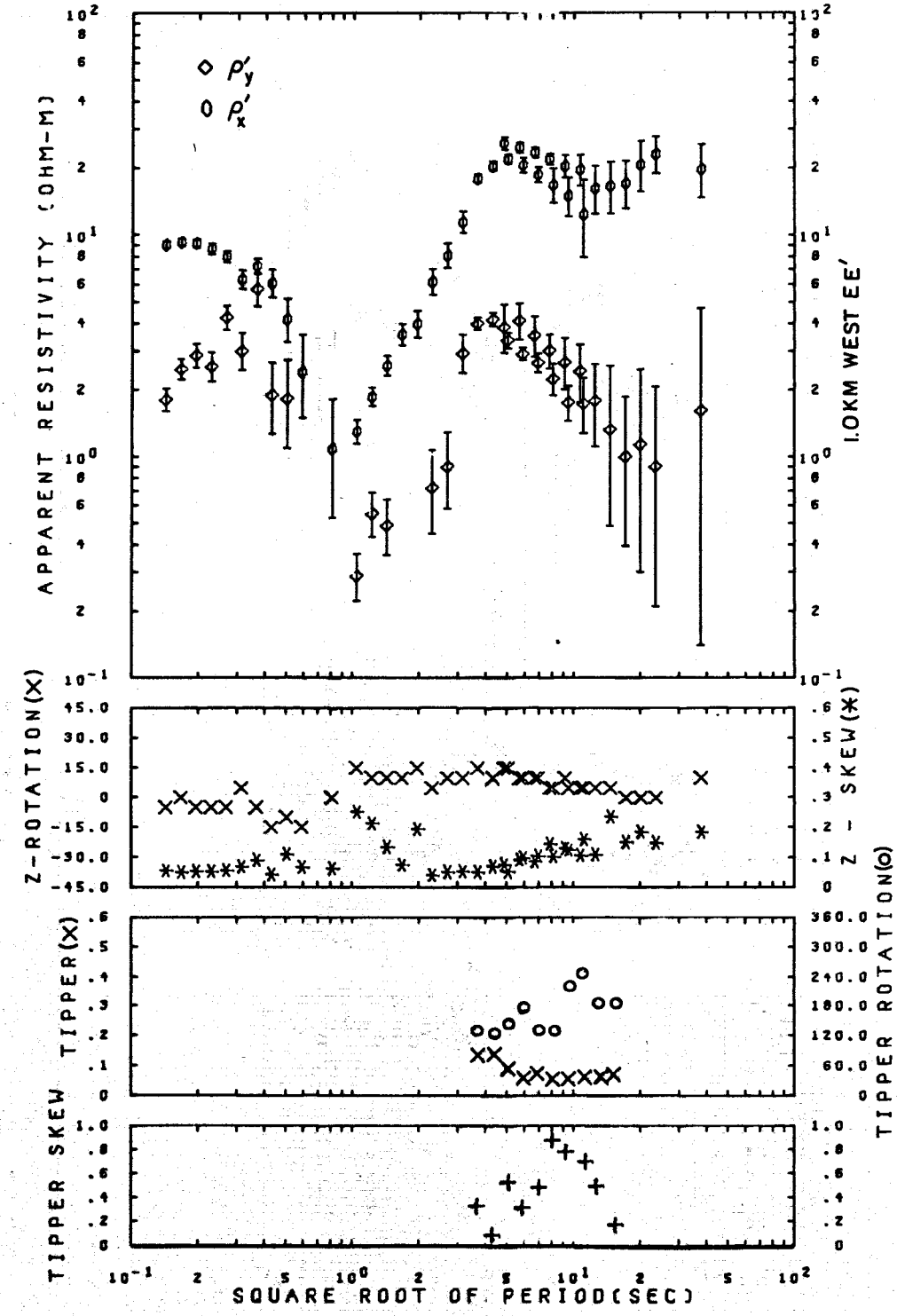

Fig. 10. Station 1.0 kw West, Line EE'.

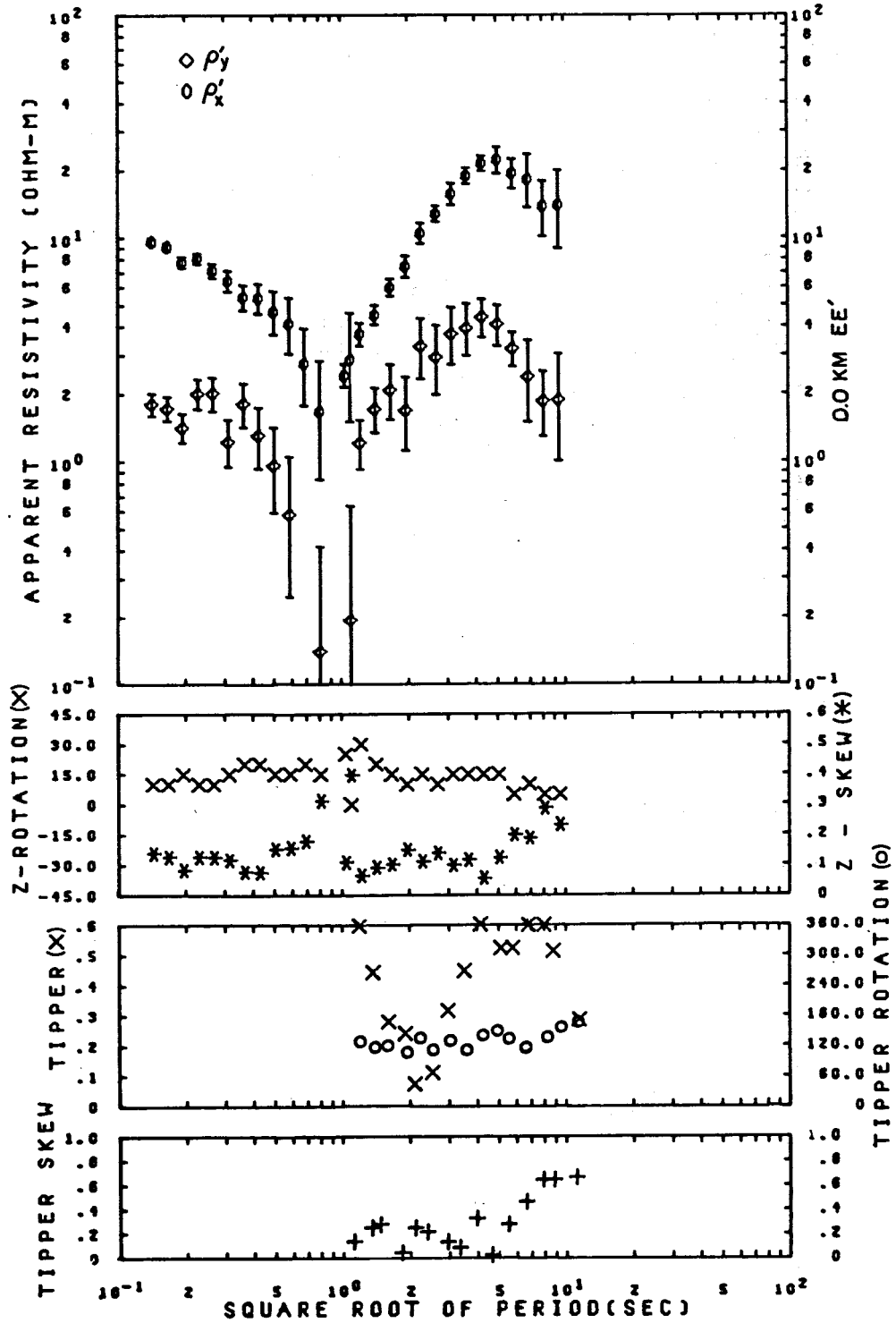

Fig. 11. Station 0.0 km, Line EE'.

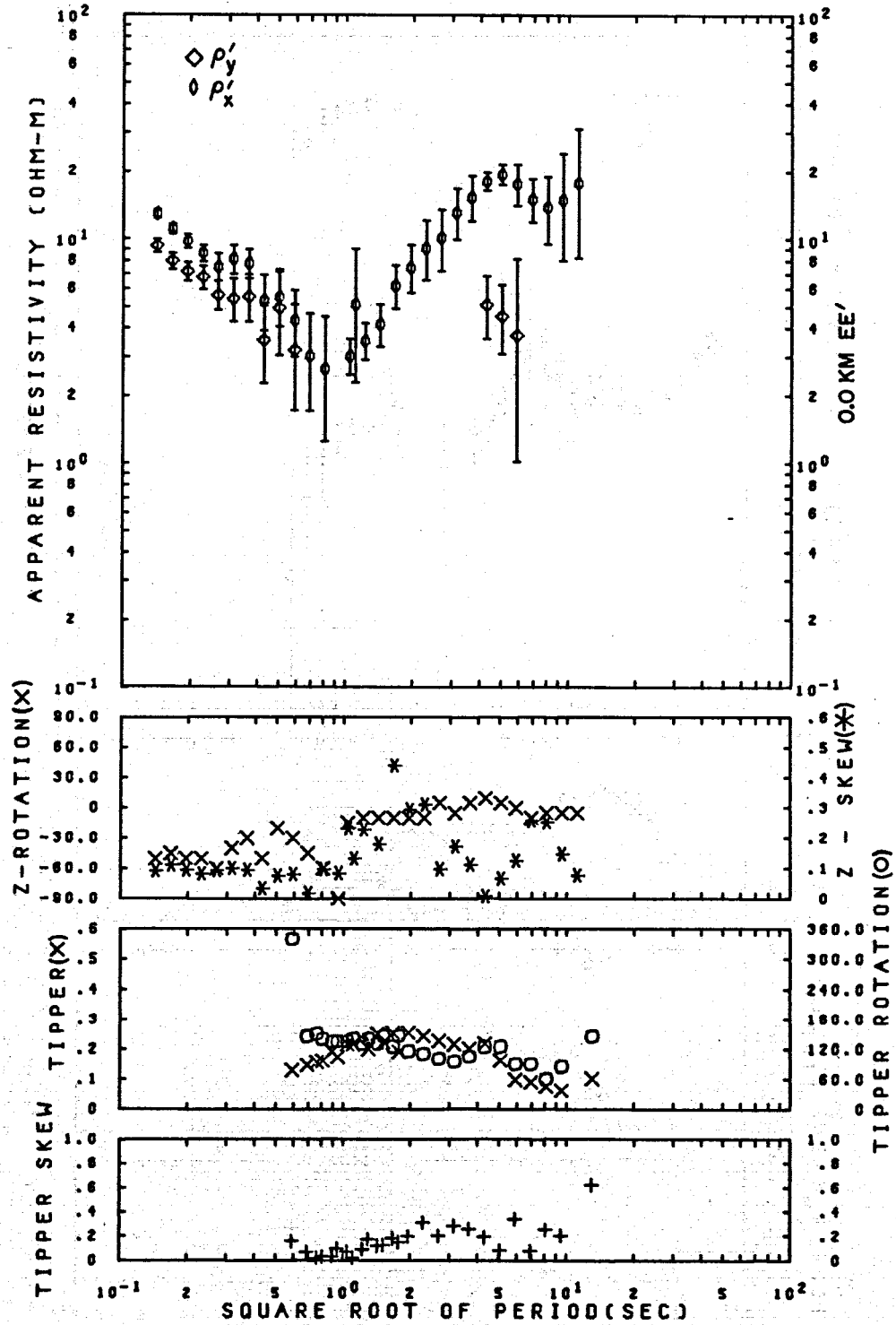

Fig. 12. Station 0.0 km, Line EE'. Repeat Data, 1976.

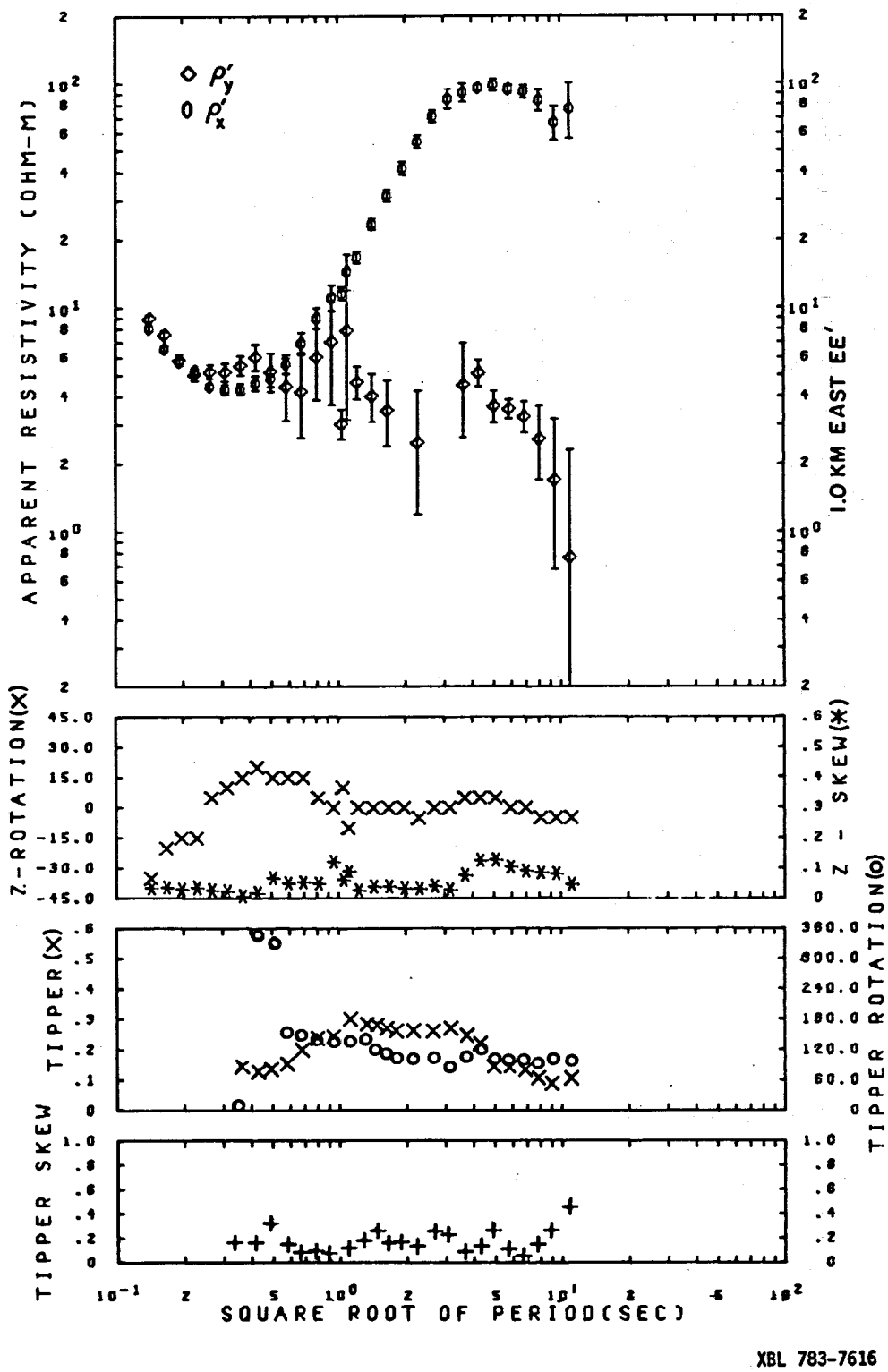

Fig. 13. Station 1.0 km East, Line EE'.

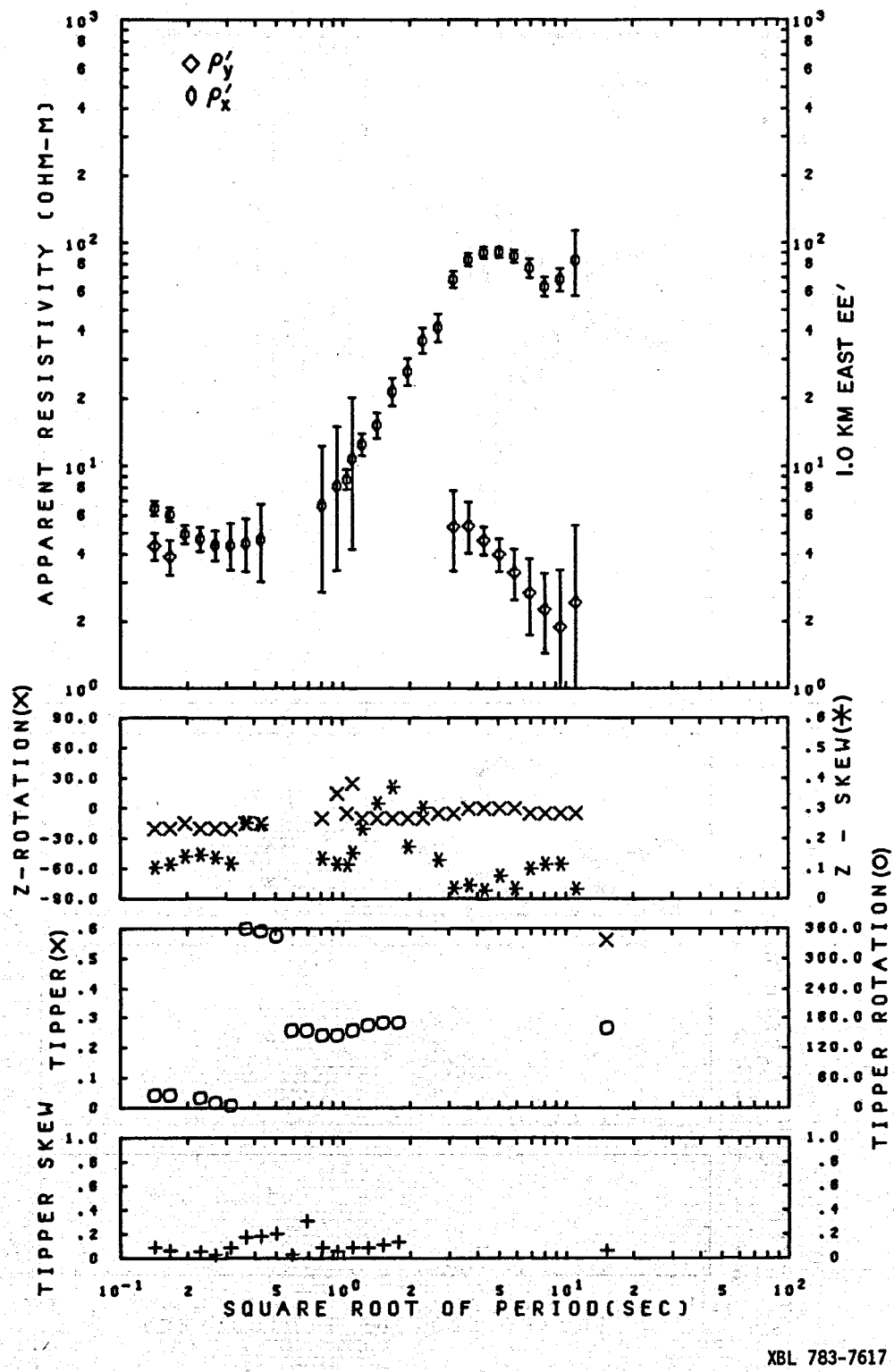

Fig. 14. Station 1.0 km East, Line EE'. Repeat Data, 1976.

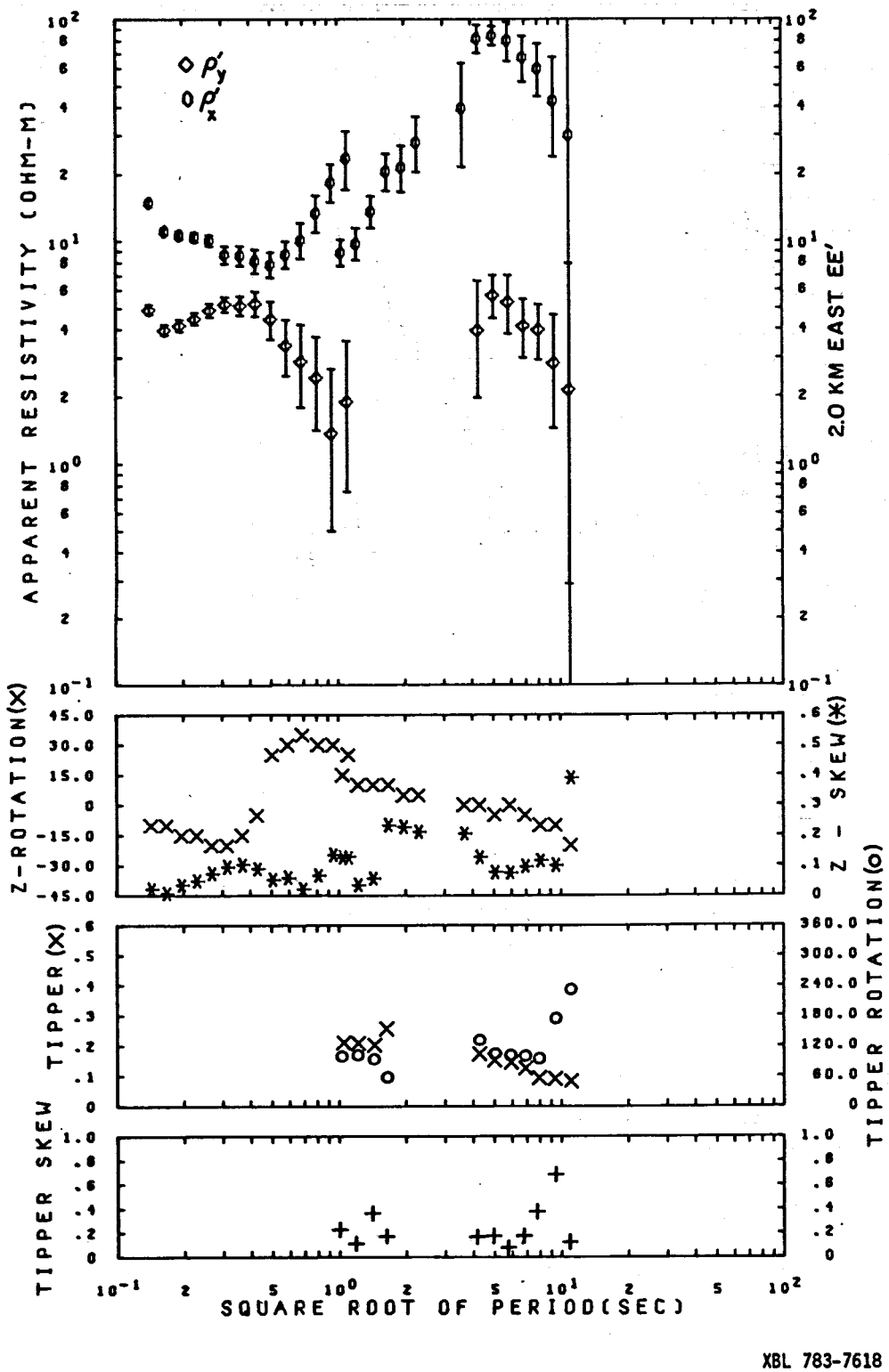

Fig. 15. Station 2.0 km East, Line EE'.

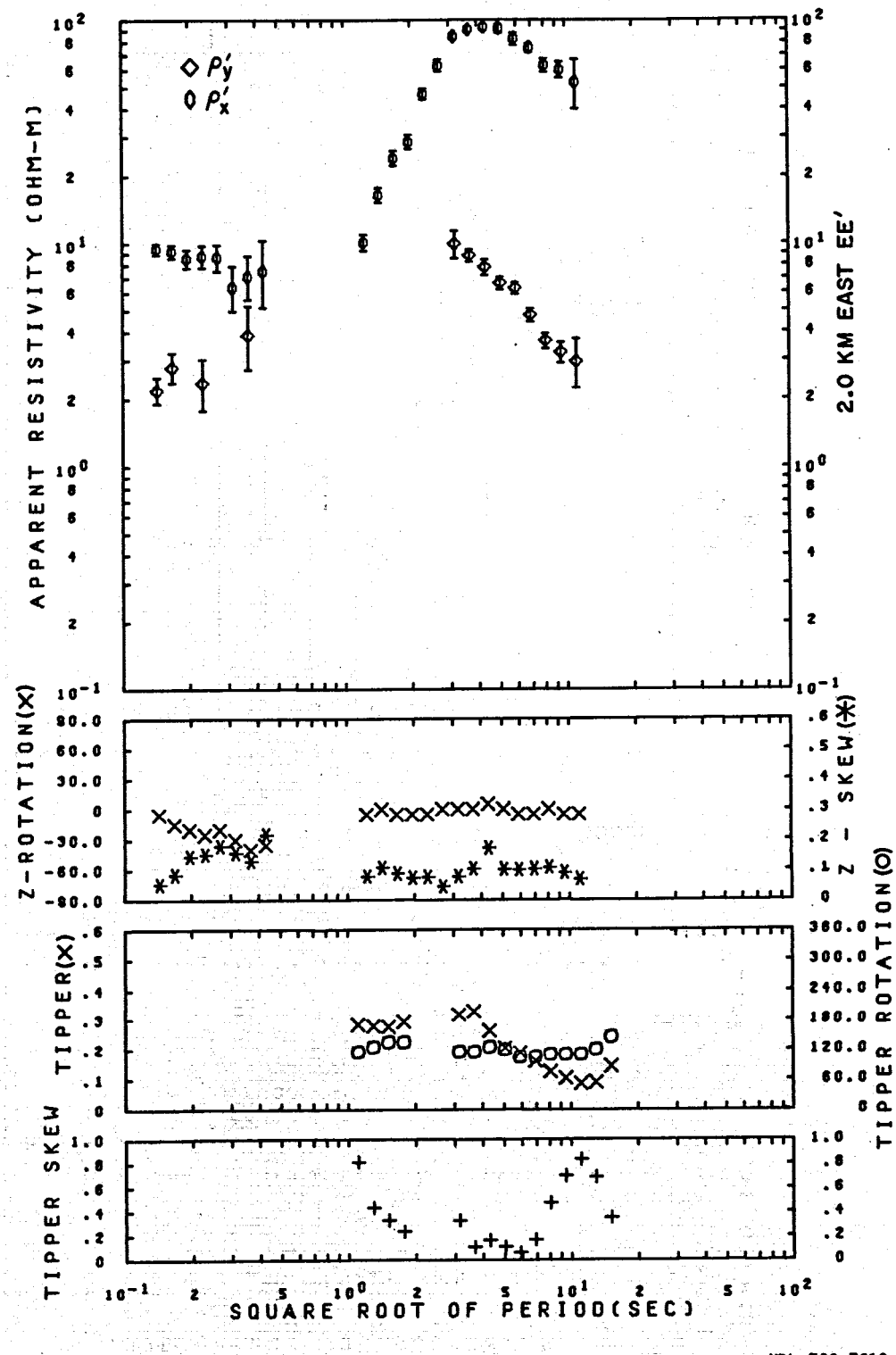

Fig. 16. Station 2.0 km East, Line EE'. Repeat Data, 1976.

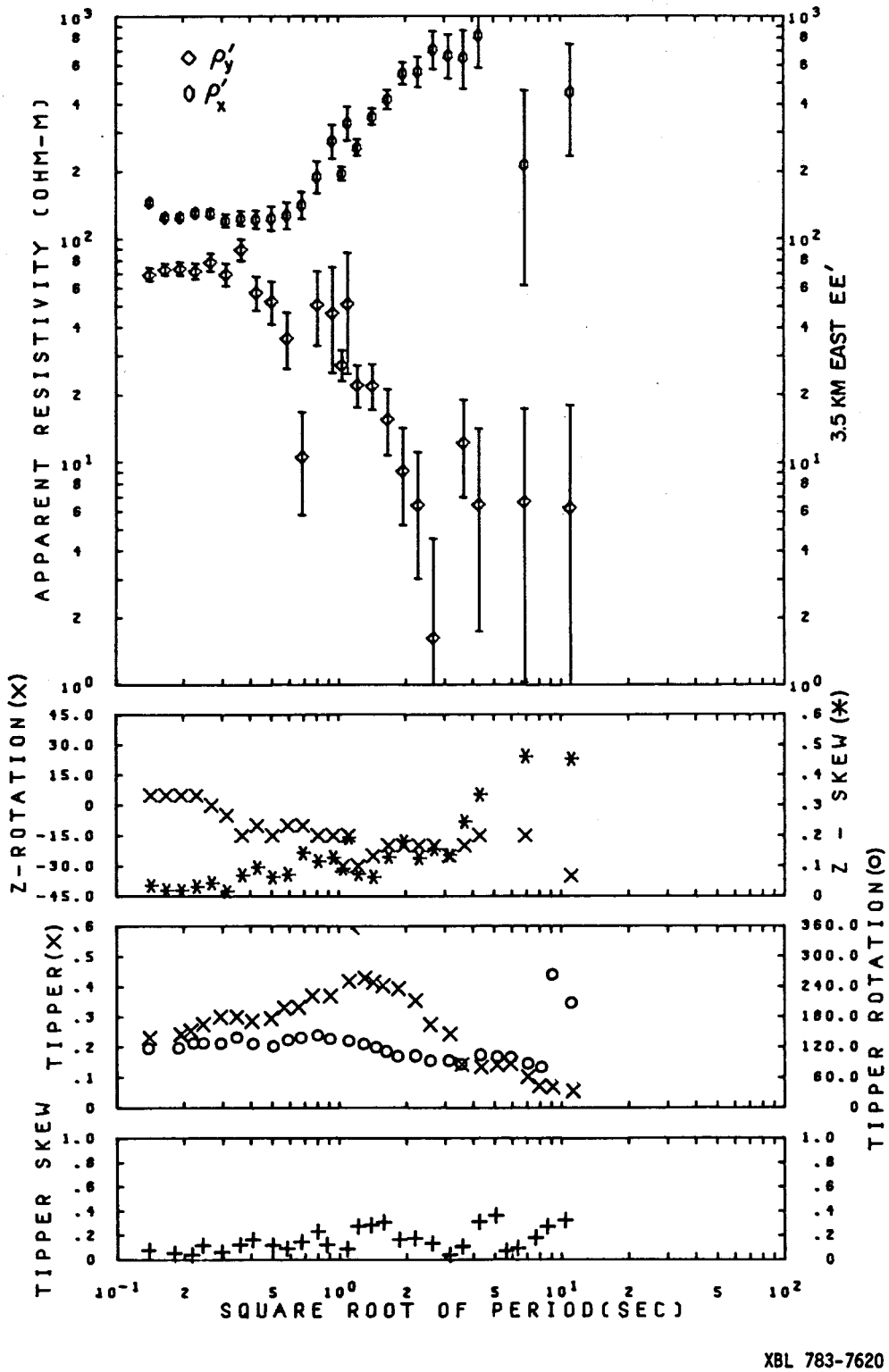

Fig. 17. Station 3.5 km East, Line EE'

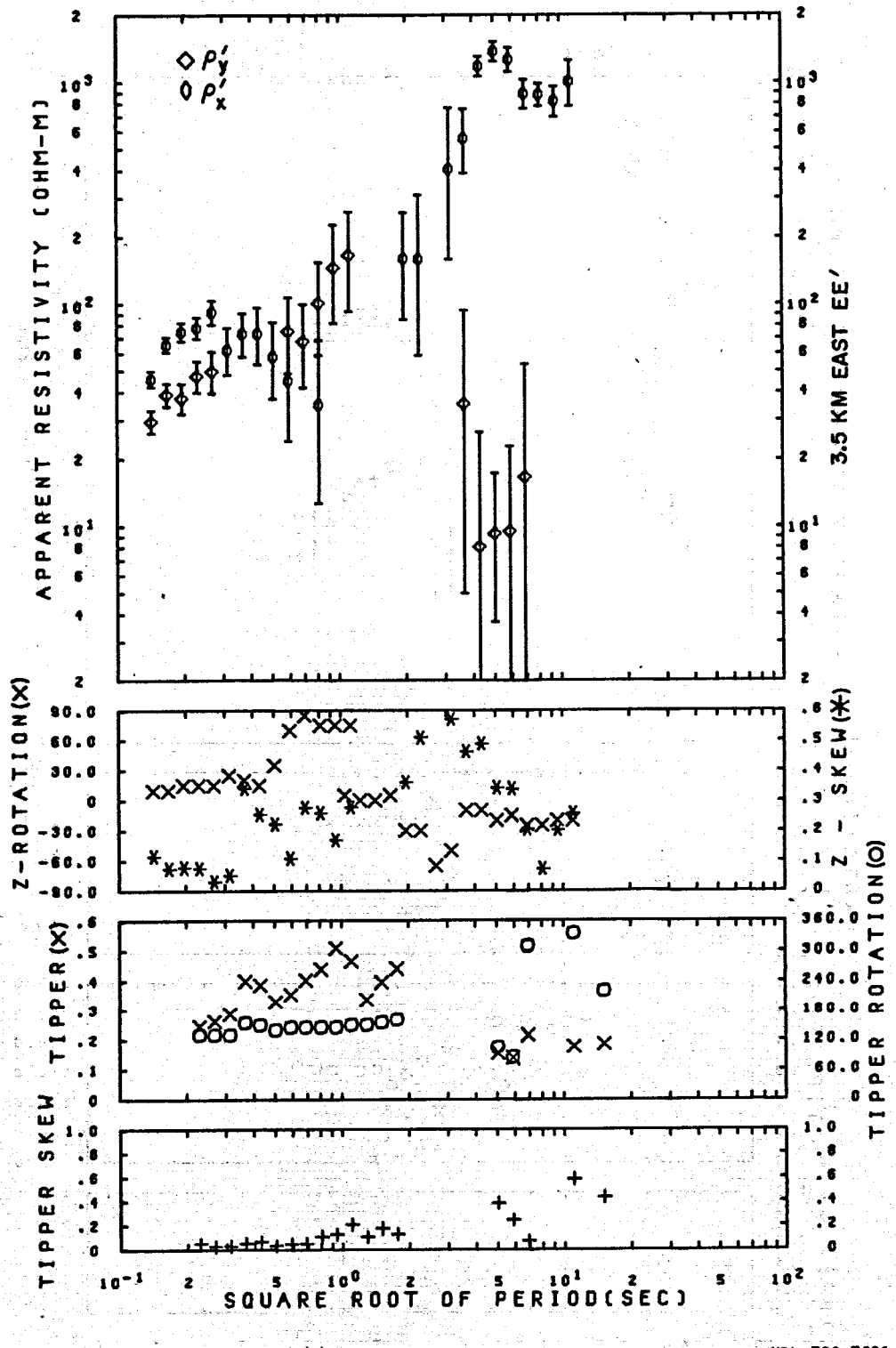

Fig. 18. Station 3.5 km East, Line EE'. Repeat Data, 1976.

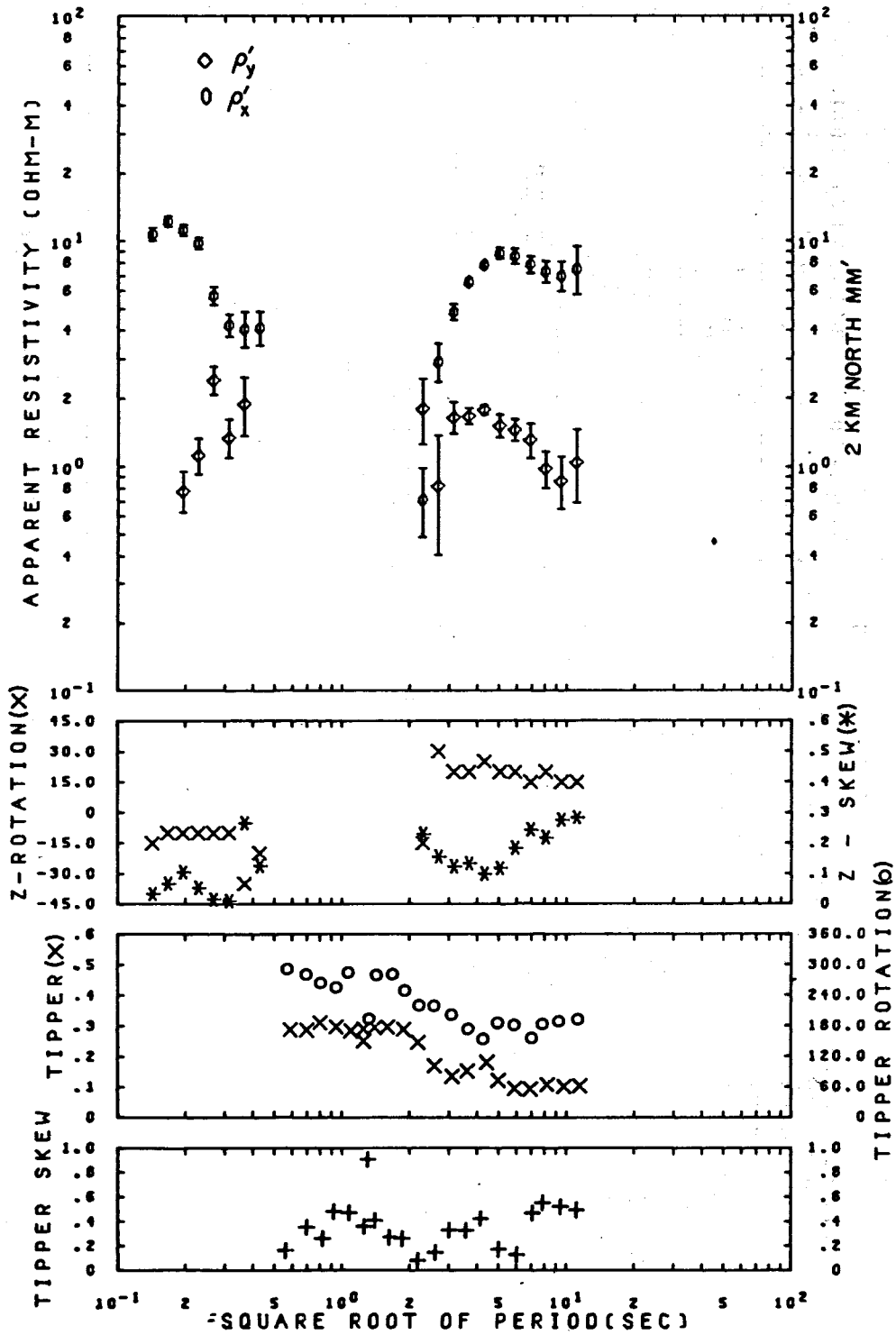

Fig. 19. Station 2.0 km North, Line MM'.

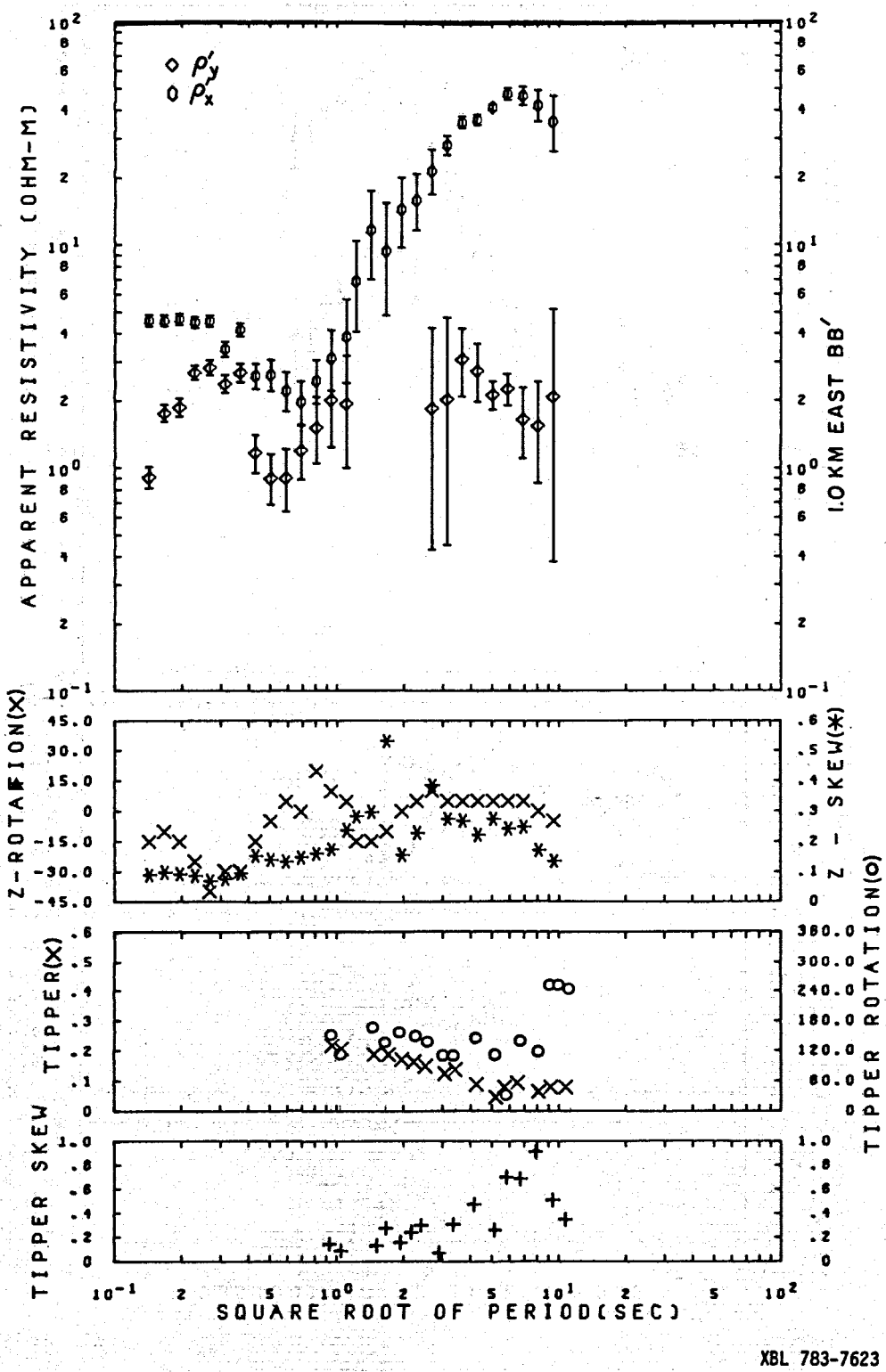

Fig. 20. Station 1.0 km East Line BB'.

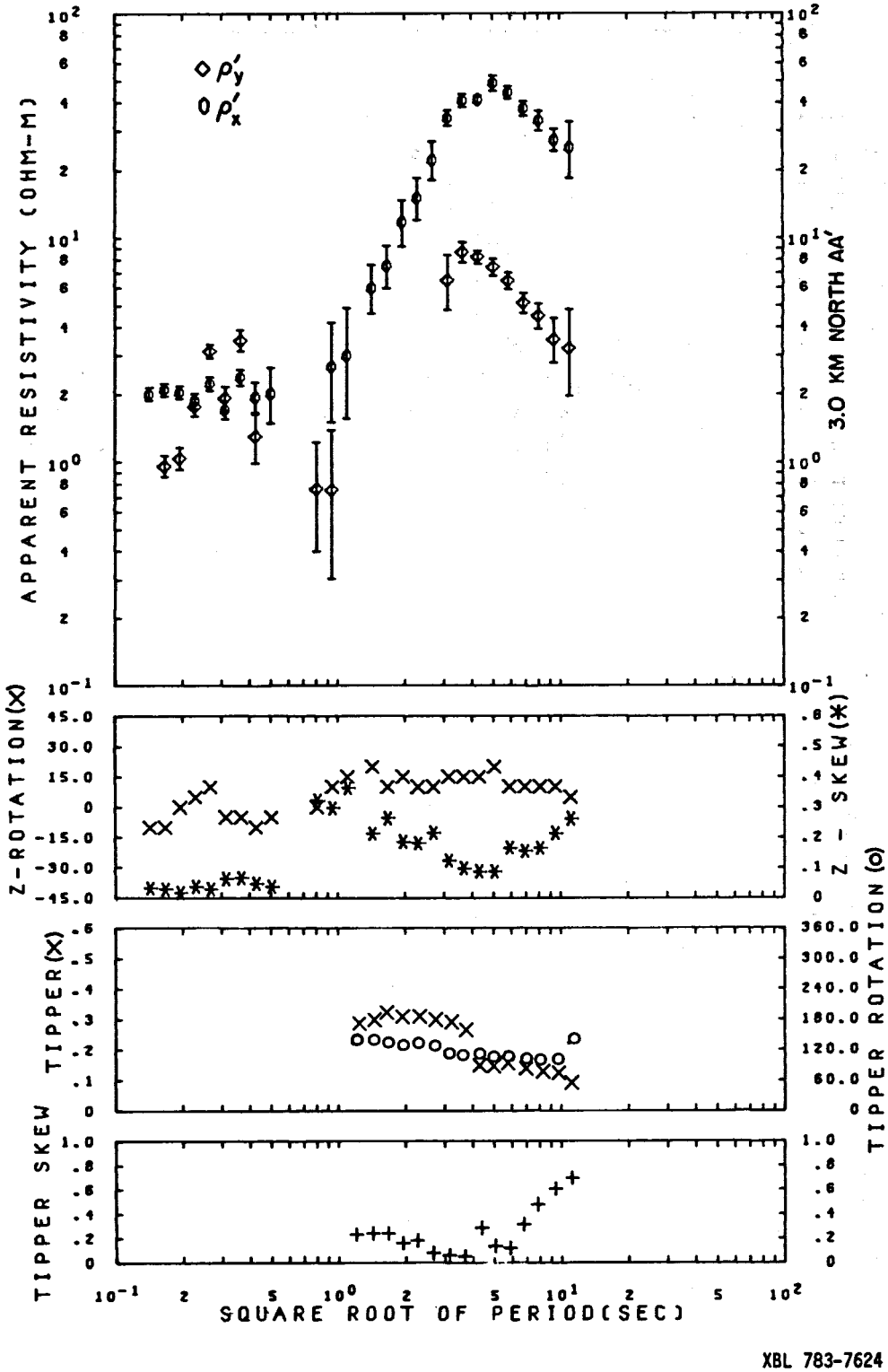

Fig. 21. Station 3.0 km North, Line AA'.

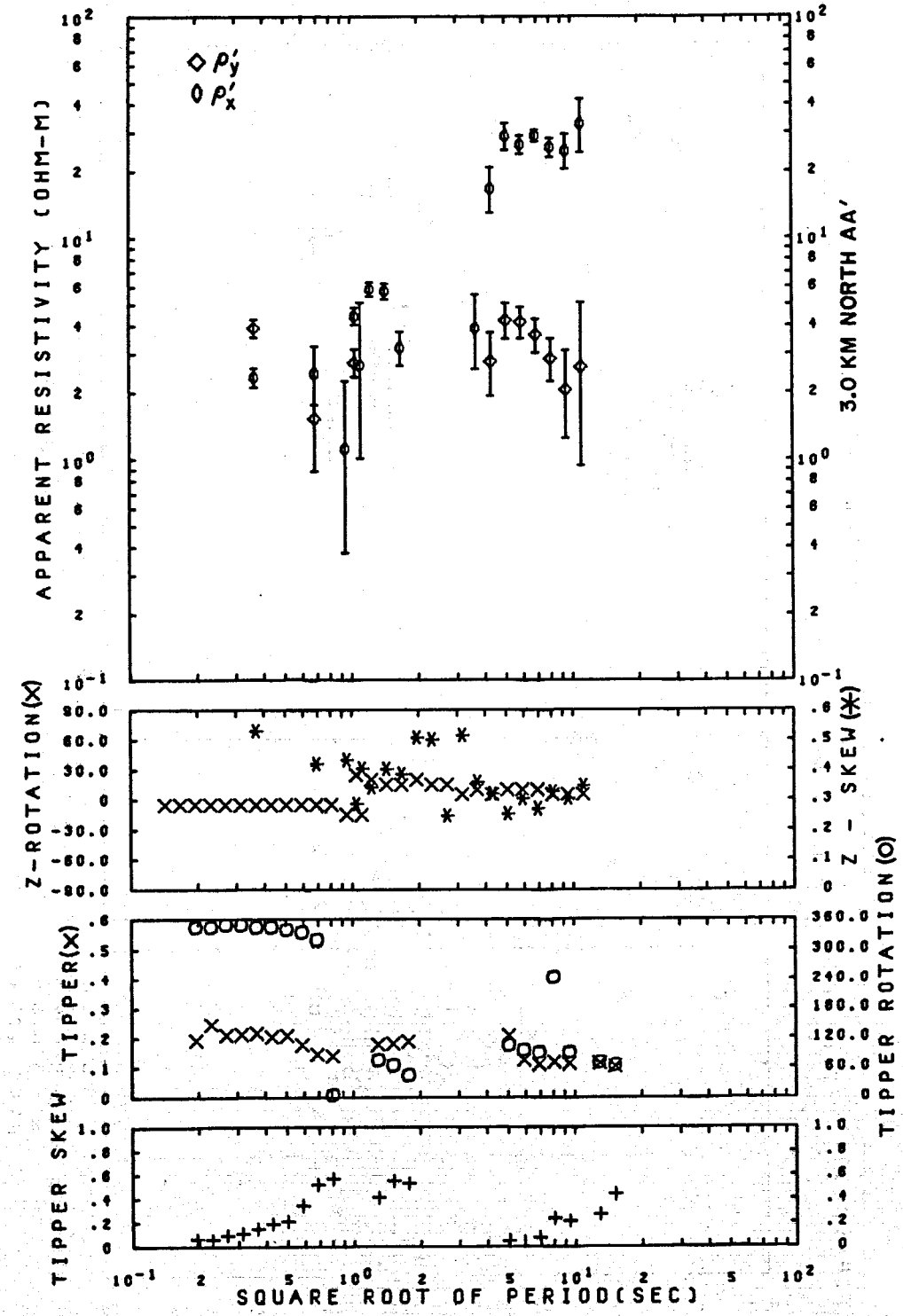

Fig. 22. Station 3.0 km North, Line AA'. Repeat Data, 1976.

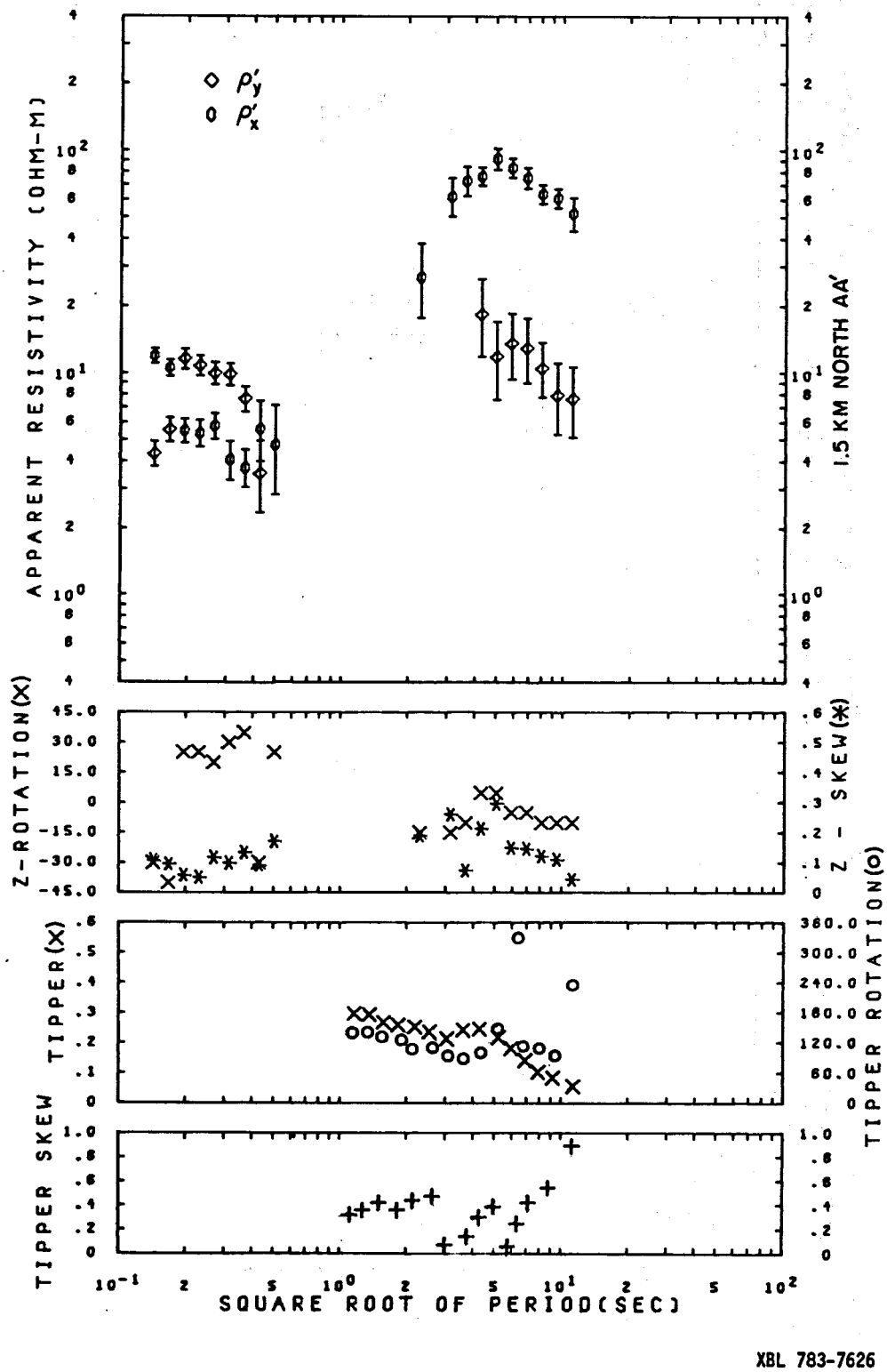

Fig. 23. Station 1.5 km North, Line AA'.

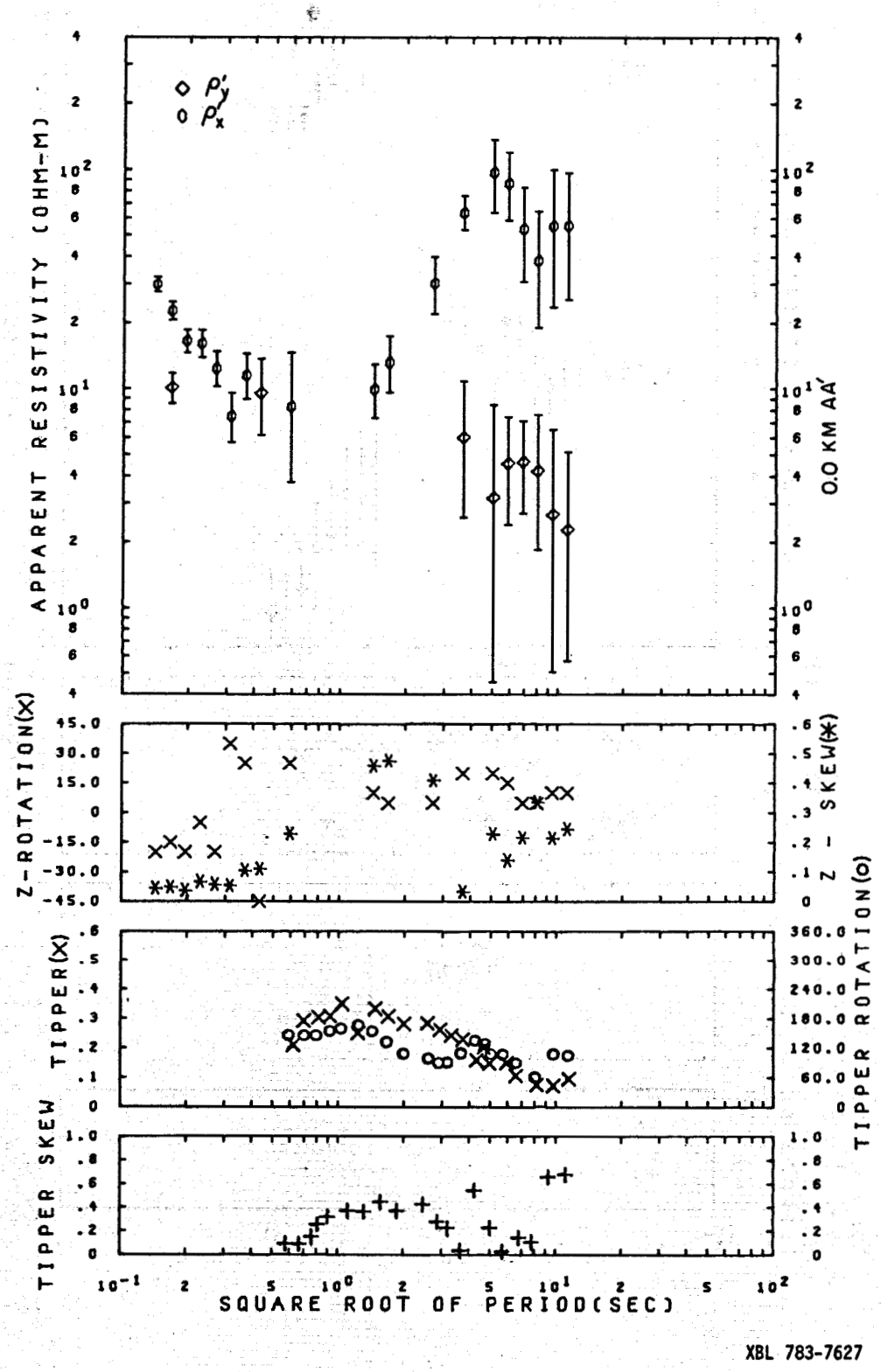

Fig. 24. Station 0.0 km Line AA'.

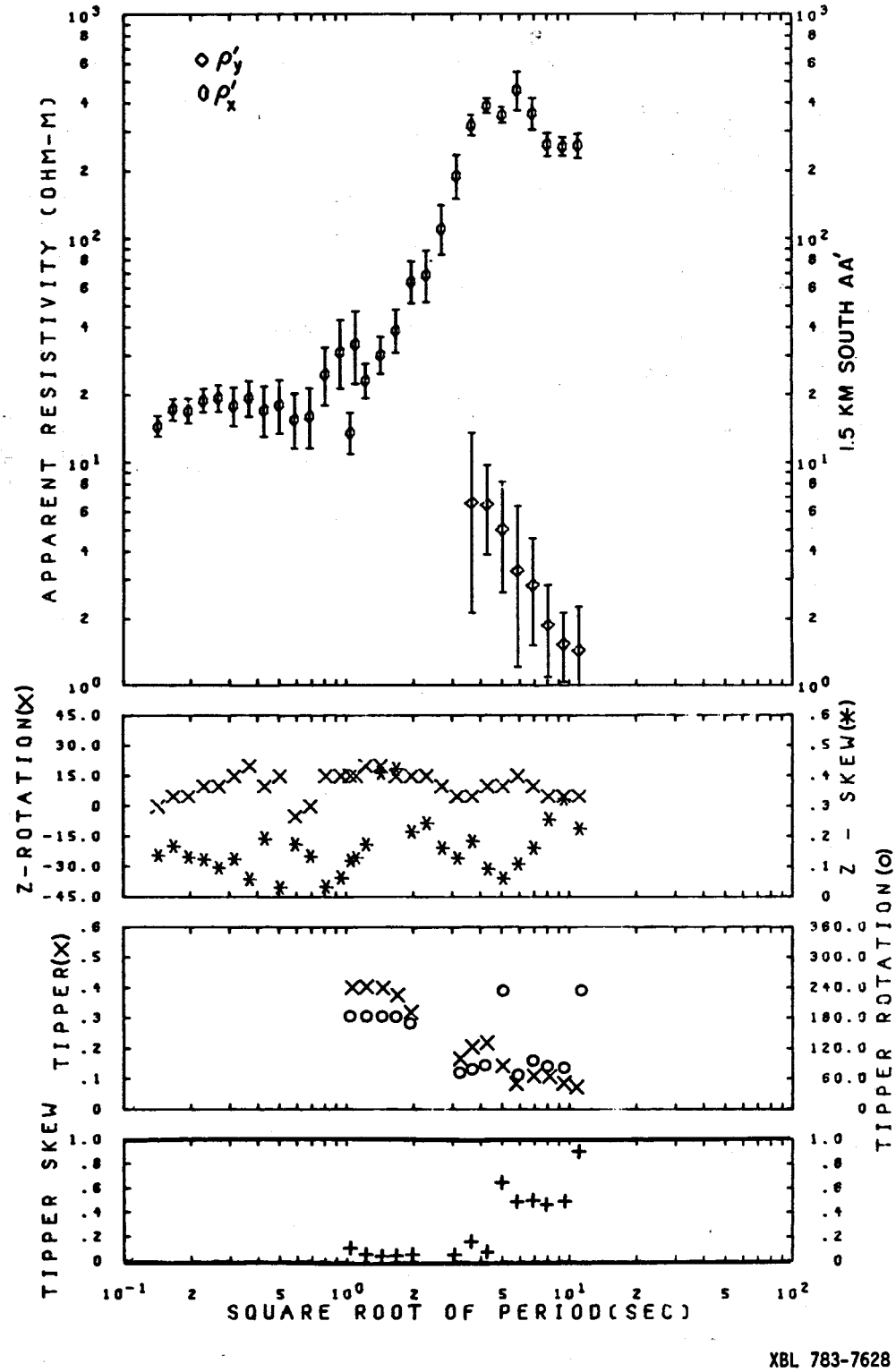

Fig. 25. Station 1.5 km South, Line AA'.

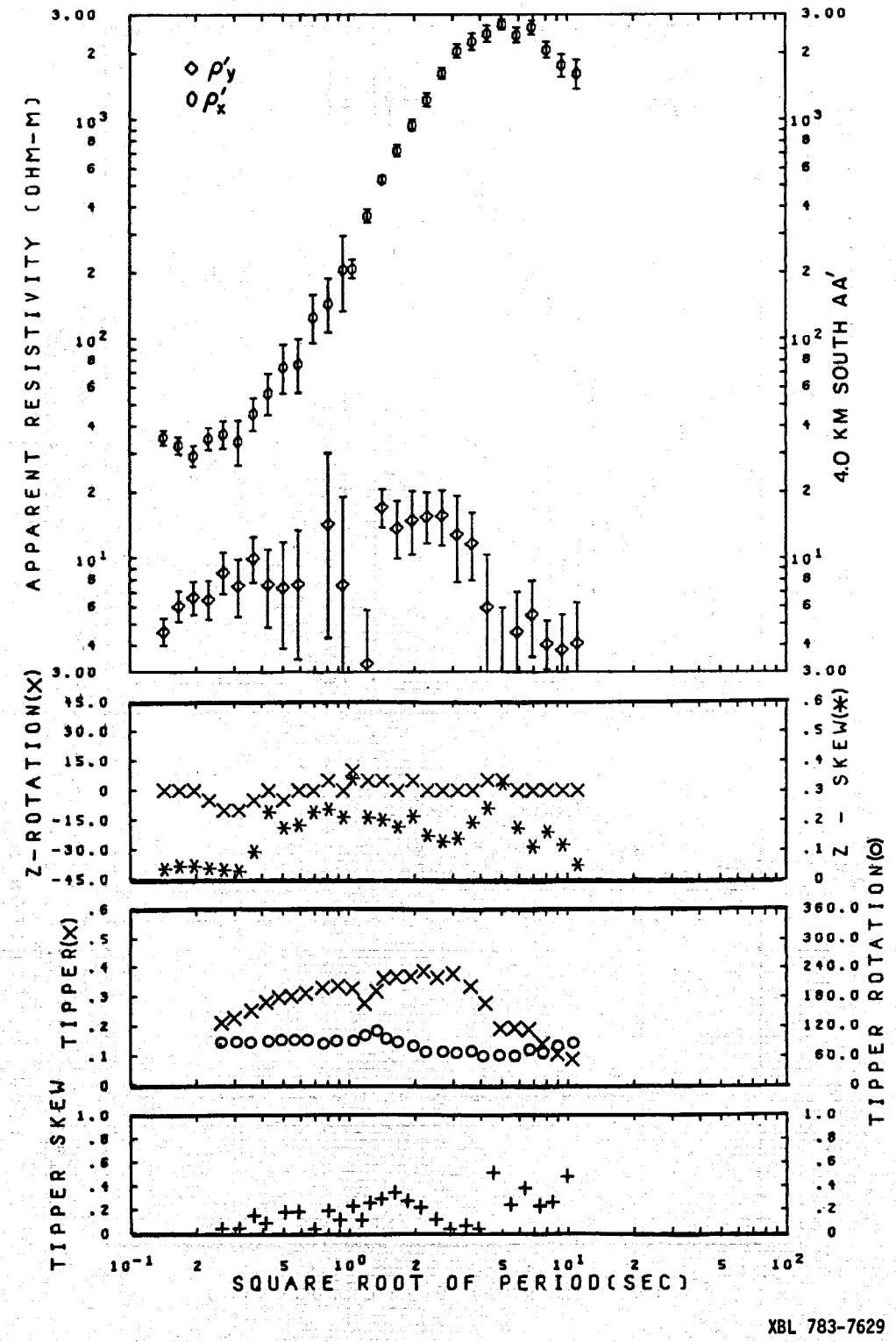

Fig. 26. Station 4.0 km South, Line AA'.

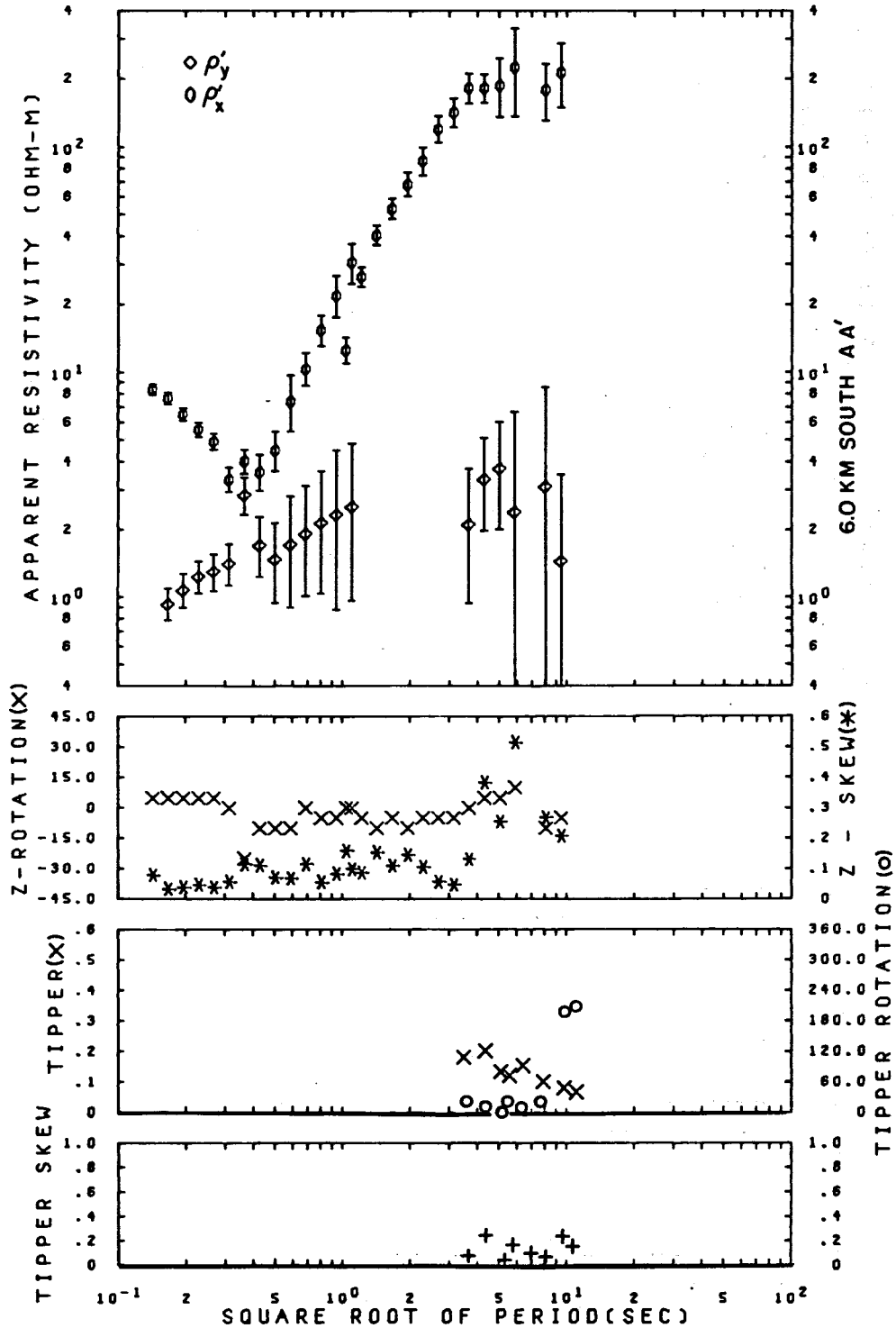

Fig. 27. Station 6.0 km South, Line AA'.

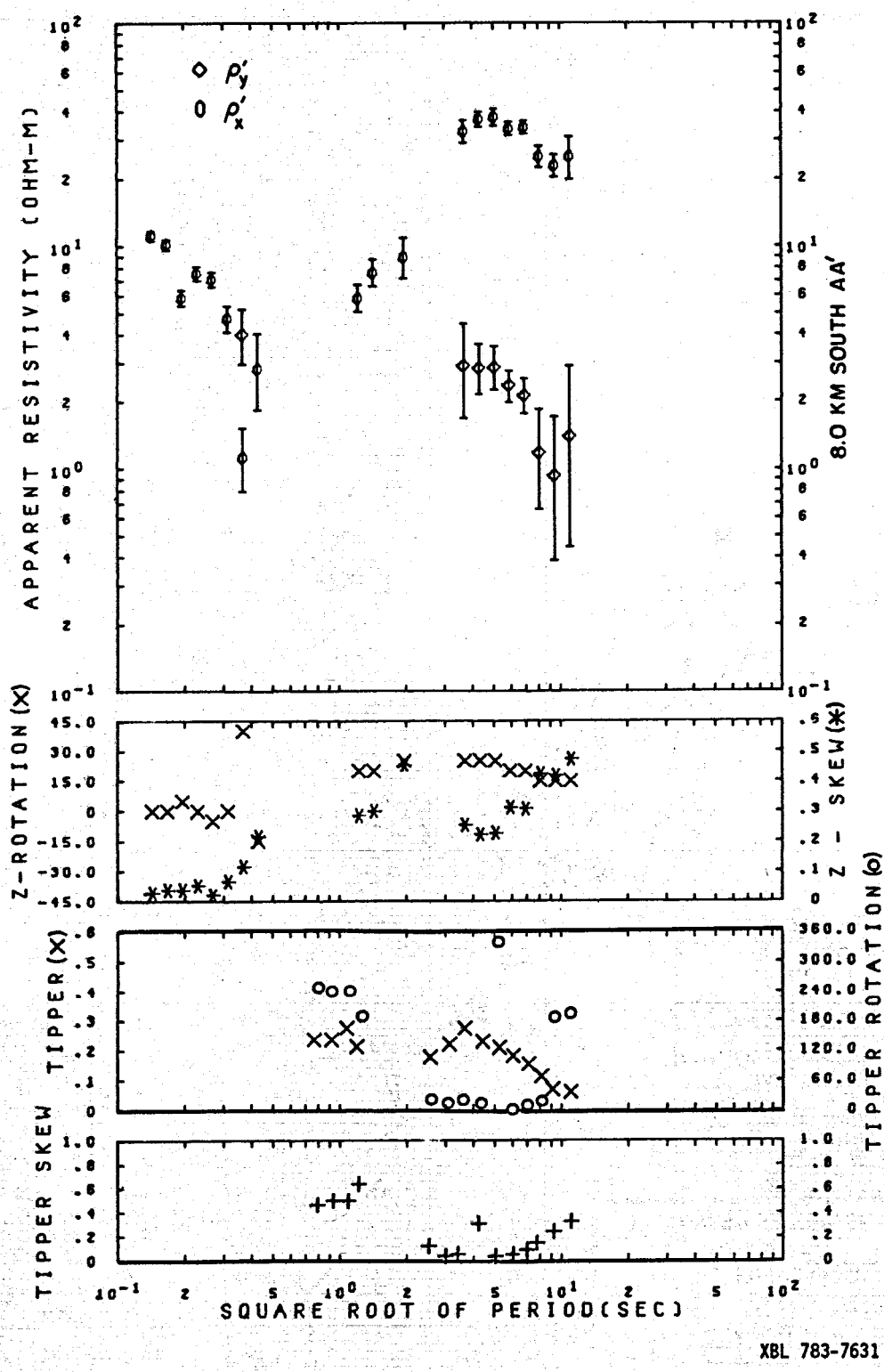

Fig. 28. Station 8.0 km South, Line AA'.

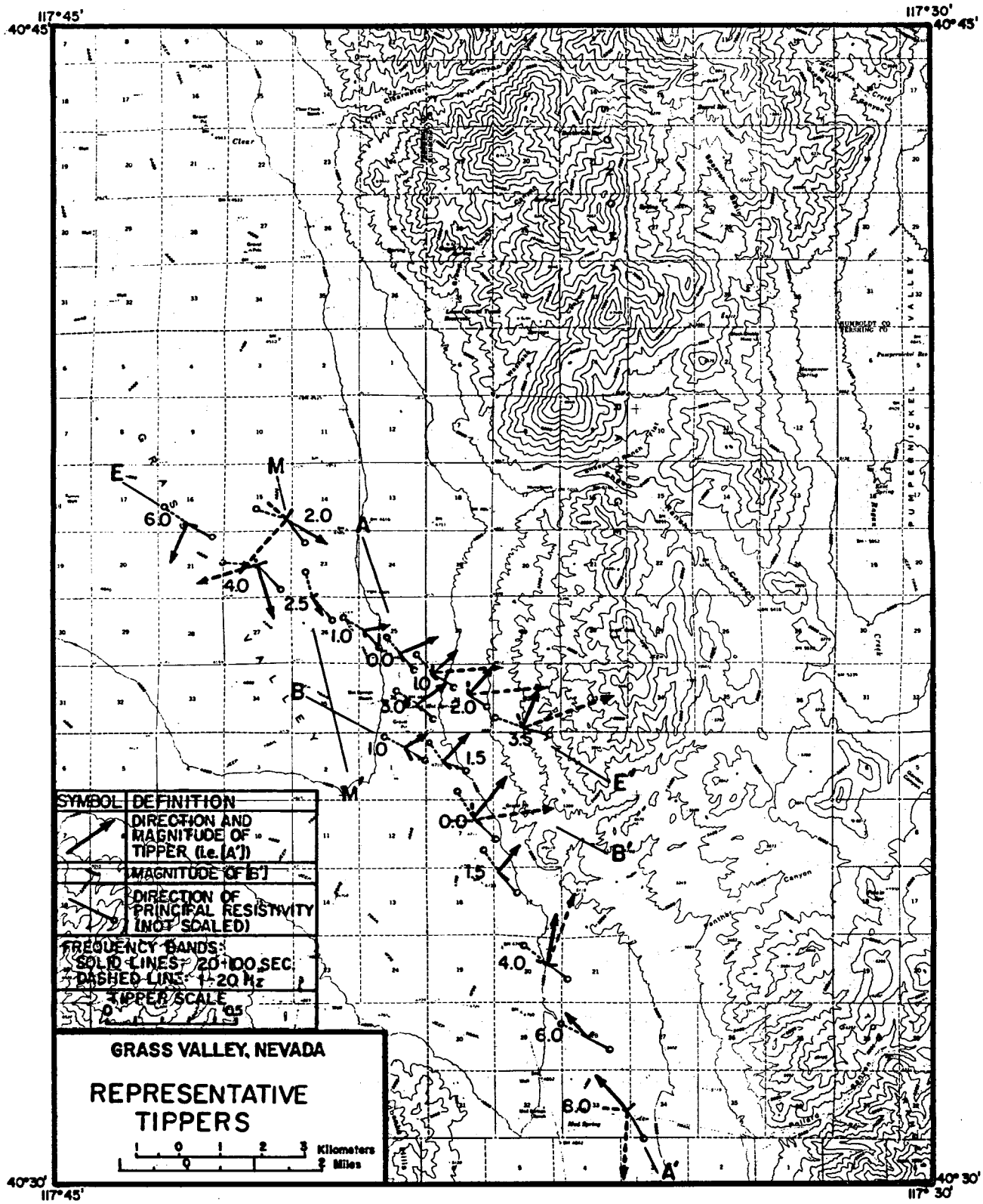

XBL 778-2676

Fig. 29. Summary representation of tipper and impedance data for magnetotelluric stations in Green Valley, Nevada

Detailed Interpretation

The interpretation of magnetotelluric data in other than horizontally layered media involves curve matching the observed results to computer generated data for collections of simple models. We have developed a fast finite-element program for obtaining the principle impedances for TE and TM excitation over two-dimensional models. The program is based on one developed in our group by Ryu (1971) and later modified by K. Lee. A catalogue of apparent resistivity psuedo section for simple two-dimensional models has been issued in an LBL report (Lee, et al., 1978).

The interpretation process is iterative. The interpreter begins with a collection of simple models, the vertical contact, simple valley, etc., to get a rough idea of the relevant model. Successive versions of the model are tried, usually with increasing complexity, until a reasonable fit to the observed apparent resistivities is obtained.

The basic models used in this study are shown in the index of Fig. 1-1 of Appendix 1 and the TE and TM apparent resistivities for various positions on the models are given on the pages following this index. Important features of this model are discussed in the Appendix.

Only very general conclusions about the resistivity distribution in Grass Valley can be drawn from the models in the Appendix. A valley contact with the resistive rocks of the ranges of the east is clearly revealed by the characteristic split of the TE and TM curves at long period (e.g. station 1.0 km east on EE', Fig. 13) and is similar to results of Model 4.3 or 4.4 In fact, the progression of the curve shapes for TE and TM as the distance away from the inferred edge of the valley is increased is very similar to the model results for a wide valley. Stations 4.0 south, 1.5 south and 0.0 on Line AA', and Stations 3.5 east, 2.0 east, 1.0 east on Line EE', have TM values which are depressed below the TE values over the whole range of $\sqrt{T}$ values. For stations to the west of these stations the TM values tend to follow the TE values until separation occurs at the longer period. The fact that the curves remain separated even at 6.0 km west on Line EE' is a good indication of the finite extent of the valley to the west. The extreme separation for 3.5 east on EE', 1.5 and 4.0 south on AA' suggests that they are within .5 km of the contact. The tipper data are unfortunately so erratic that a more precise location of the contact using the data is not possible.

Since all the data allow a good definition of the strike direction the TE and TM directions are also well defined. As a first attempt to define the layer structure in the valley, least-squares parameter fitting was carried out for the TE data of stations 1.0 east, 0.0, 1.0 west on Line EE' and at 1.5 south and 3.0 north on AA'. The curve fitting using a five-layer model is shown in Figs. 30-35. The TE data are repeated in these figures, the theoretical apparent resistivity curve for the best fit model is superimposed on the data, and the

layer parameters are listed below the plot. A composite cross section for Line EE' is given in Fig. 36.

The gross features of the section are evident from Fig. 36. A thin resistive surface layer, a thicker conductive section lying on resistive basement and finally deep in the crust a conductive layer. Because TE apparent resistivity interpretations on the conductive side of such a contact underestimate the thicknesses involved, a series of models were then tried incorporating the resistivities indicated but with greater layer thicknesses.

The models used for this interpretation are Models 6-1, 6-2, 6-3, of the Appendix. Only the general features of the data on Line E are well interpreted with these models. The details of the curves for periods less than 1 sec. are not accounted for at all; this is, presumably, because surficial layers thinner than 250 meters are strongly perturbing the data at these periods. It has been shown that discontinuities in such thin layers unfortunately also perturb the response at long periods. The strong separation of the TE and TM mode apparent resistivities at short periods suggests that caution must be exercised in the interpretation at greater periods.

In an average sense Model 6-2 has the best fit to the data, at least to the TE data to the left of the inferred contact. The results are actually quite sensitive to the resistive surface layer thickness and to the thickness of the conductive layer beneath it. The 1 km layer of 1 ohm meter material in Model 6-3 depresses the apparent resistivities too much and displaces the observed minimum value to longer periods than can be reconciled with the observed data. The bounds on the model are quite good but the true thickness of the conductive layer may lie between .3 and .7 km and may of course vary between these limits all along the line.

A serious problem for interpretation is that the data from stations only 1 km apart display such large variations that there is no possibility of matching the subtle changes in the model results to the field data. Another serious problem is that the TM data are not well fitted by the model. The error bars on the TM data are large, however, that it is not reasonable to carry out more exhaustive modelling to accommodate the data.

A final and rather perplexing observation is that the data for Station 3.5 E seem to indicate that the boundary contact between the conductive valley and resistive range has been crossed. The apparent resistivity values at short periods have jumped by a factor of 10 but the relative values for TE and TM mode have not reversed. The curve shapes are excellent; for example the data for station +0.5 and +1.0 of Model 6-2 would fit the data very well if TE and TM were interchanged. The entire data processing scheme was carefully reviewed to determine if this result was an artifact of the processing. Unless some field error resulted in an exchange of E and H recording channels for this station there is no evidence of a processing error.

Figs. 30-35. Least-squares five-layer model results fitted to the TE apparent resistivity data of that station.

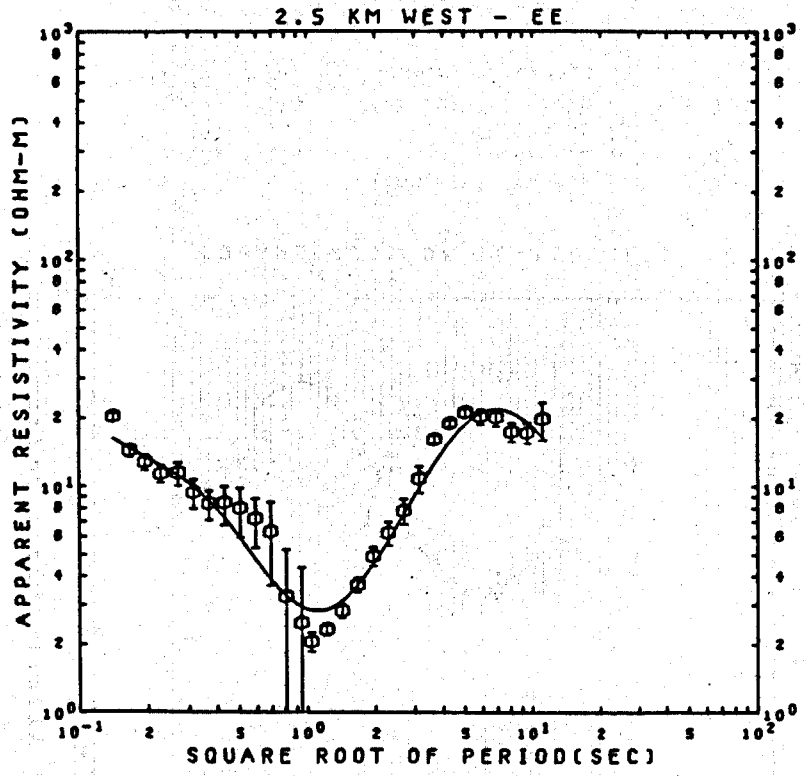

Resis (1) = 30.0 (ohm.m) Thickness (1) = 136.75 m
Resis (2) = 5.13 (ohm.m) Thickness (2) = 266.41 m
Resis (3) = 1.13 (ohm.m) Thickness (3) = 302.8 m
Resis (4) = 142.82 (ohm.m) Thickness (4) = 14.603 km
Resis (5) = 1.05 (ohm.m) Thickness (5) =

Fig. 30. Station 2.5 km West, Line EE'.

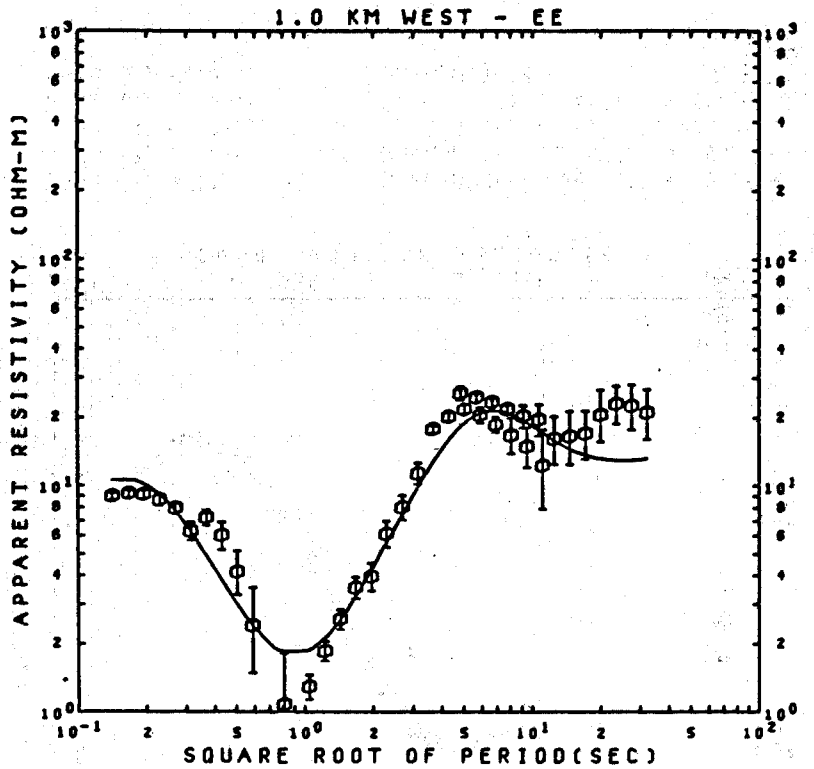

Resis (1) = 9.0 (ohm.m) Thickness (1) =274.4 m
Resis (2) = 0.414 (ohm.m) Thickness (2) = 123.7 m
Resis (3) = 232.66 (ohm.m) Thickness (3) = 16.268 km
Resis (4) = .431 (ohm.m) Thickness (4) = 614.88 m
Resis (5) = 18.76 (ohm.m) Thickness (5)

Fig. 31. Station 1.0 km West, Line EE'.

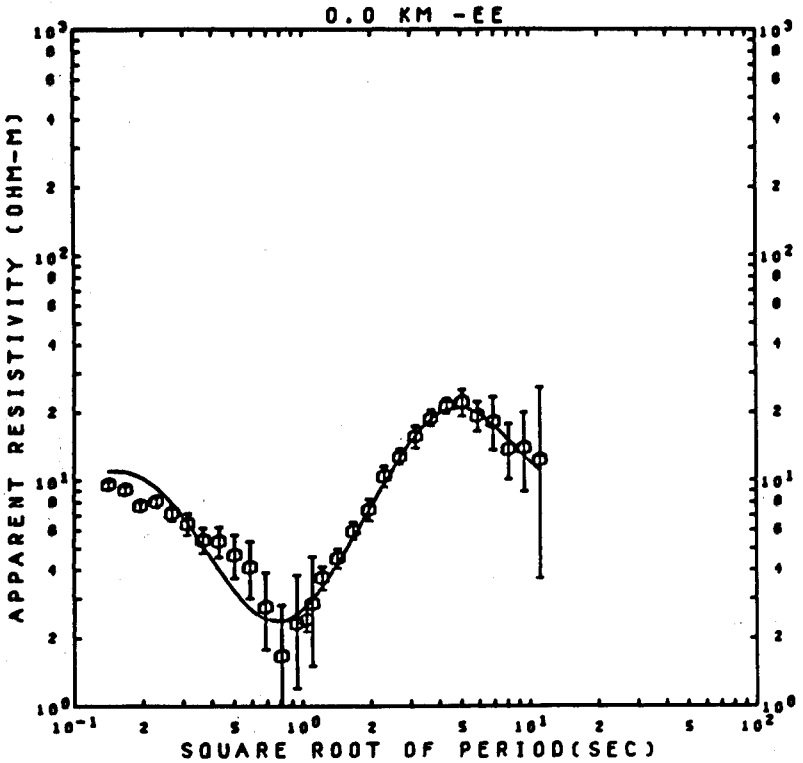

Resis (1) = 9.5 (ohm.m) Thickness (1) = 268 m
Resis (2) = .74 (ohm.m) Thickness (2) = 172 m
Resis (3) = 1373 (ohm.m) Thickness (3) = 10.6 km
Resis (4) = .99 (ohm.m) Thickness (4) = 1.9 km
Resis (5) = 9.3 (ohm.m) Thickness (5)

Fig. 32. Station 0.0 km, Line EE'.

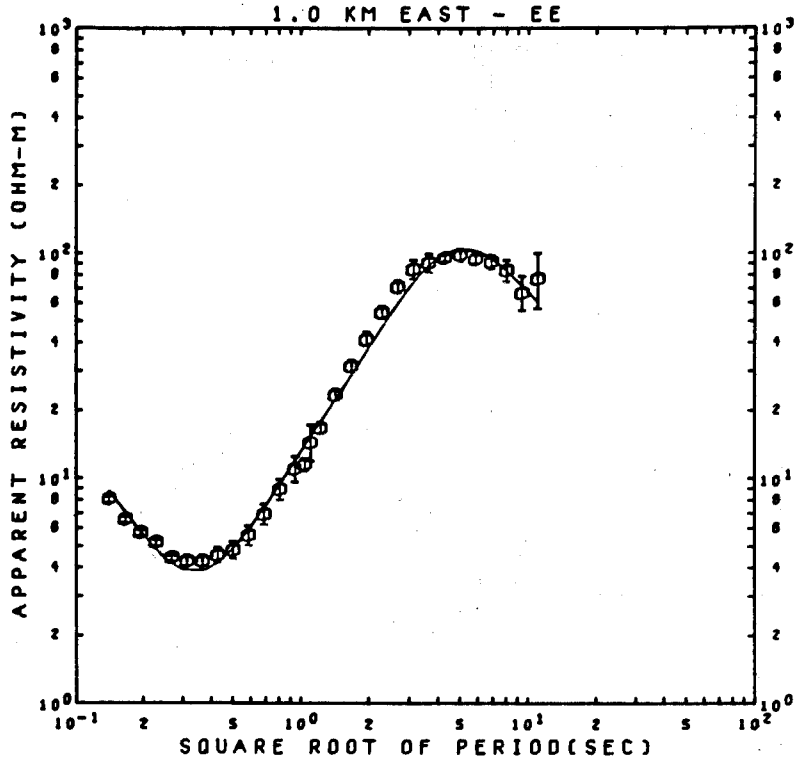

Resis (1) = 21.6 (ohm.m) Thickness (1) = 101.8 m
Resis (2) = 2.29 (ohm.m) Thickness (2) = 185.6 m
Resis (3) = 273.7 (ohm.m) Thickness (3) = 26.29 km
Resis (4) = 2.0 (ohm.m) Thickness (4) = 634.9 m
Resis (5) = 10.38 (ohm.m) Thickness (5)

Fig. 33. Station 1.0 km East, Line EE'.

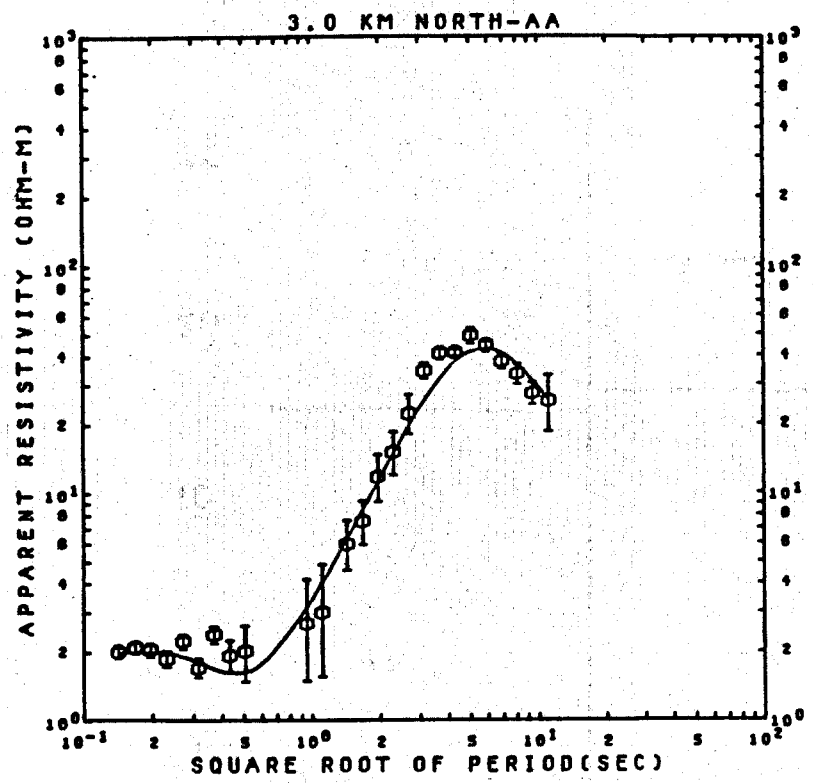

Resis (1) = 2.0 (ohm.m) Thickness (1) = 293.3 m
Resis (2) = 3.43 (ohm.m) Thickness (2) = 150.4 m
Resis (3) = 305.8 (ohm.m) Thickness (3) = 14.2 km
Resis (4) = 34.8 (ohm.m) Thickness (4) = 3.64 km
Resis (5) = 1.38 (ohm.m) Thickness (5)

Fig. 34. Station 3.0 km North, Line AA'.

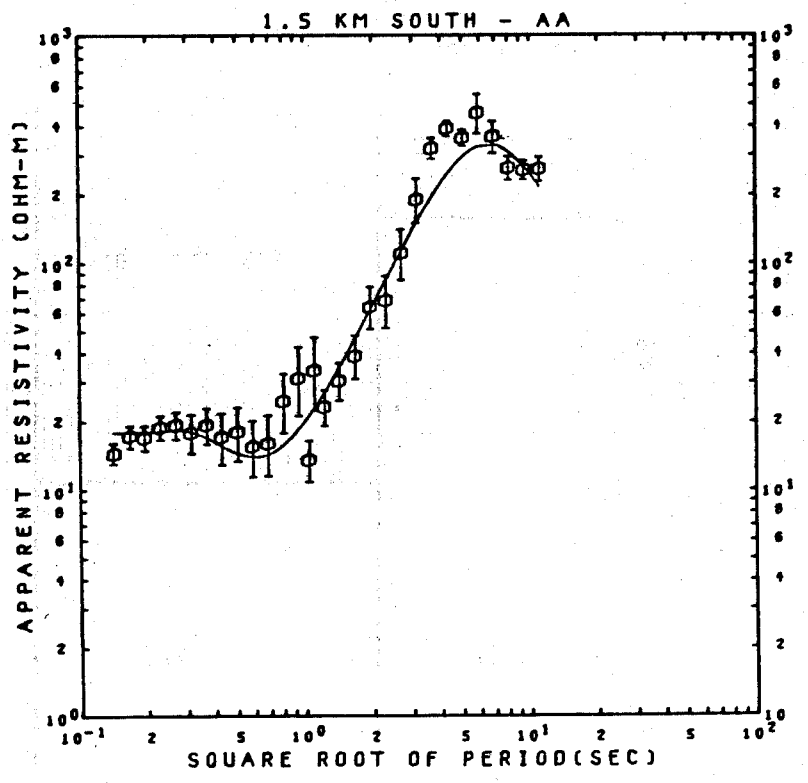

Resis (1) = 18.0 (ohm.m) Thickness (1) = 929.5 m
Resis (2) = 11.8 (ohm.m) Thickness (2) = 381 m
Resis (3) = 3170 (ohm.m) Thickness (3) = 57.6 km
Resis (4) = 2.0 (ohm.m) Thickness (4) = 13.7 km
Resis (5) = 7.05 (ohm.m) Thickness (5)

Fig. 35. Station 1.5 km South, Line AA'.

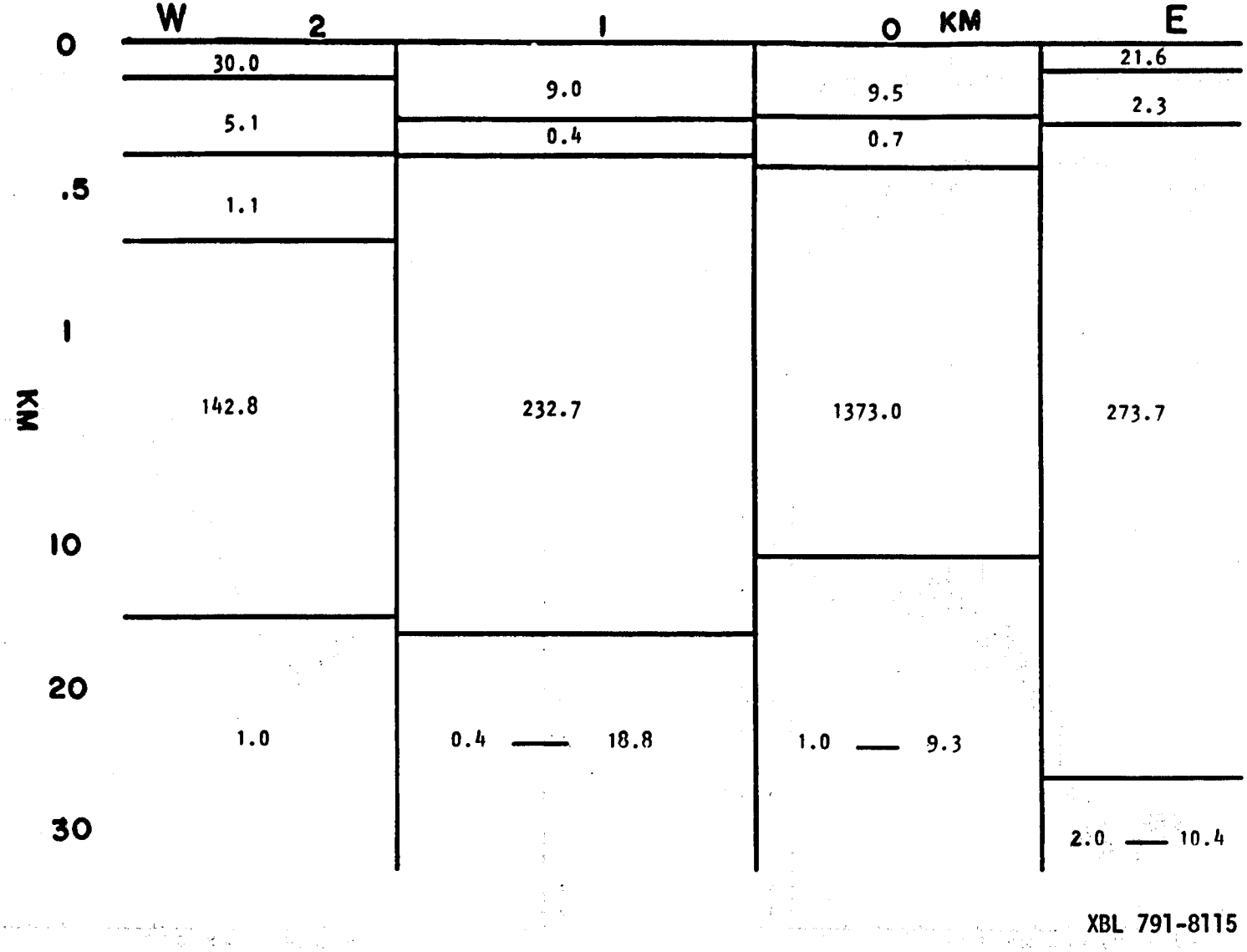

Fig. 36. Resistivity section on Line EE' from five-layer inversion of TE apparent resistivities.

Conclusions

The attempt to carry out a detailed interpretation of a magnetotelluric survey has demonstrated some fundamental problems that must be addressed in future surveys and in future research.

The general features of Grass Valley could have been obtained from data from three or four magnetotelluric stations. Greater station density revealed variations over distances of one or two kilometers that could not be modeled with existing two-dimensional techniques (at least not within reasonable time and computer costs).

The dramatic effect of discontinuities in thin surface layers has been aptly demonstrated both in the models and in the data. TE interpretations of layered models yielded valley thicknesses that were 50% too low. Perhaps more importantly, it can be deduced that if a contact some 10 kilometers away can strongly distort a sounding curve in a two-dimensional model, a three-dimensional feature (a strike closure for the assumed 2-D valley, for example) a similar distance away could similarly distort the impedance. Strike directions inferred from impedance rotation would thus be affected and this may be the cause of the discrepancy between interpreted strike and observed geological strike in Grass Valley.

Near-surface discontinuities probably have a more serious effect on sounding curves than previous investigators had acknowledged. Two major effects are noted. First, the fields are strongly dependent on the length of the electric dipole. This is seen in the model results from stations close to contacts, a good example being the data for Model 1-1 at 0 km where the fields are shown for 500 m electrodes which straddle the contact. Second, the field is distorted over a wide period range and over large spatial extents for shallow bodies. The results for the shallow valley, represented by Model 4-1 and Model 4-2, demonstrate this effect. The TM data are strongly affected over the whole frequency range. The same type of results would be obtained if the station were in a much shallower conductive zone, 10 to 100 meters thick, lying within the larger valley structure. However, there is no guarantee that the shallower features, if two dimensional at all, will be parallel to the layer structure. Thus the strong distortion produced in electric fields perpendicular to a shallow conductor will persist to distort the fields which are parallel to a larger structure underneath.

Even if the above problems did not exist, it is evident that the large errors associated with the field data preclude detailed modelling. The gross features are easily seen through the error bars, but subtle features such as tipper magnitude as a function of lateral position, or details of the TE - TM apparent resistivity curves are masked in this data set. The phase data for the principal impedances have not been presented in this analysis because of the very large scatter observed. This is a serious omission since it represents essential additional information that has been simply discarded.

There may be several reasons for the poor data quality and these probably apply to most magnetotelluric soundings taken in geothermal exploration.

Exploration surveys are typically constrained by economics, which imposes a limit on the length of recording time. Brief recording times plus the low field activity in certain bands, particularly .1 Hz to 1.0 Hz, result in inadequate data to obtain well-determined impedance estimates. A hitherto unsuspected fact that has emerged in a parallel MT study by Clarke et al., (1977) is that there is a significant amount of electromagnetic noise uncorrelated with the desired incident magnetotelluric field. This introduces bias errors in the estimates during periods of low amplitude magnetotelluric fields. The bias errors can be as great as the spatial changes observed at stations only a kilometer apart. It is obviously futile to attempt model refinements at this level until the data can be obtained without bias errors. The method developed by Clarke et al., using a remote reference magnetometer promises to provide data of the required quality.

References

Bendat, J. S., and Piersol, A. G. 1971. Random data: Analysis and measurement procedures, New York: John Wiley and Sons.

Beyer, H., Dey, A., Liaw, A., Majer, E., McEvilly, T. V., Morrison, H. F., and Wollenberg, H. 1976. Geological and geophysical studies in Grass Valley, Nevada. A preliminary report to the Lawrence Berkeley Laboratory, LBL-5262.

Beyer, J. H. 1977. Telluric and D. C. resistivity techniques applied to the geophysical investigation of basin and range geothermal systems, part III: The analysis of data from Grass Valley, Nevada. Ph.D. thesis, Lawrence Berkeley Laboratory report LBL-6325.

Clarke, John 1974. Josephson junction detectors. Science, v. 184, p. 1235.

Clarke, J., Goubau, W. M., and Ketchen, M. B., 1976. Tunnel junction dc SQUID: fabrication, operation, performance. J. Low Temp. Phys., 25, p. 99.

Fournier, R. O., et al. 1974. "Geochemical indicators of subsurface temperature," U. S. Geol. Survey J. of Res. 2 (3).

Gamble, Thomas D., Goubau, W. M., and Clarke, J. 1977. Magnetotelluric data analysis: Tests of methods using data obtained at Grass Valley, Nevada. Lawrence Berkeley Laboratory Report, LBL-6648, submitted to Geophysics.

Goldstein, N. E., and Paulsson, B. 1977. Interpretation of gravity surveys in Grass and Buena Vista Valleys, Nevada. Lawrence Berkeley Laboratory report, LBL-7013, submitted to Geothermics.

Hermance, J. F., and Pedersen, J. 1976. Assessing the geothermal resource base of the southwestern United States: Status report of a regional geoelectromagnetic traverse. Abstract of paper given at the 46th Annual International Meeting, Society of Exploration Geophysicists, Houston, Texas.

Hose, R. K., and Taylor, B. E., 1974. Geothermal systems of northern Nevada. U.S. Geol. Survey open file report 74-271.

Jiracek, G. R., Reddy, I. K., Philips, R. J., and Whitcomb, J. H. 1977. Magnetotelluric soundings of the Rio Grande Rift COORP seismic profile in New Mexico. Abstracts, 47th Annual International Meeting and Exposition, of the Society of Exploration Geophysicists, Calgary, Alberta, Canada, Sept. 18-22, 1977.

Lee, K. H., et al., 1978. Catalogue of magnetotelluric apparent resistivity psuedo-sections over two-dimensional models. Lawrence Berkeley Laboratory Report, LBL-7057.

Mariner, R. H., et al. 1974. The chemical composition and estimated minimum thermal reservoir temperatures of the principal hot springs of northern and central Nevada, U.S. Geol. Survey open file report.

Noble, D. C., 1975. Geologic history and geothermal potential of the Leach Hot Springs Area, Pershing County, Nevada. A preliminary report to the Lawrence Berkeley Laboratory.

Olmsted, F. H., et al. 1975. Preliminary hydrogeologic appraisal of selected hydrothermal systems in northern and central Nevada. U.S. Geol. Survey open file report 75-56.

Reddy, I. K., et al. 1976. Monitoring of time dependent electrical resistivity by magnetotellurics, J. Geomag. and Geoelectr., v. 28, pp. 165-198.

Renner, J. L., White, D. E., and Williams, D. L., 1975. Hydrothermal convection systems. in Assessment of geothermal resources of the United States, 1975. D. E. White and D. L. Williams, eds. Geol. Survey Circular 726.

Ryu, J. 1971. Low frequency electromagnetic scattering. Ph.D. thesis, University of California, Berkeley.

Sims, W. E., Bostick, F. X., and Smith, H. W., 1971. The estimation of magnetotelluric impedance tensor elements from measured data. Geophysics, v. 36, n. 5, pp. 938-942.

Stanley, W. D., et al., 1977. Geothermal significance of magnetotelluric sounding in the eastern Snake River Plain, Yellowstone Region, J. of Geophys. Res. v. 82, n. 17, p. 2501.

Vozoff, K. 1972. The magnetotelluric method in the exploration of sedimentary basins. Geophysics, v 37, n. 1, pp. 98-141.

Zimmerman, J. E., and Campbell, W. H., 1975. Tests of cryogenic SQUID for geomagnetic field measurement." Geophysics, v. 40, n. 2, pp. 269-284.

APPENDIX

Two-Dimensional Model for Interpretation of Magnetotelluric Data

Because a model study was undertaken to analyze the magnetotelluric data from Grass Valley, Nevada, a suite of models was chosen to represent the general features of the known geology and morphology of the valley. Representative dimensions were also chosen on this basis although scaling laws would permit these data to be used in other geologic settings of different dimensions.

The data are presented in both the familiar, apparent resistivity vs square root of period plots, and as pseudo sections. In the latter case the horizontal axis is station spacing on the ground surface, the vertical axis is square root of period, and contours of equal apparent resistivity form the resulting plot. The TE (electric field parallel to strike) and TM (magnetic field parallel to strike) apparent resistivities are plotted on the same graph in the standard ρ_a vs $\sqrt{T}$ figures, but separate plots are given for each mode in the pseudo sections. The tipper values and tipper phases are included with these plots. Each model is presented with a figure showing the model number, a scale drawing of the model and a legend identifying the plotting symobls used for the TE, TM, and tipper values. Following this are the ρ_a vs $\sqrt{T}$ plots and the tipper values for a succession of station locations across the model. For each station, where the section immediately below is layered, the apparent resistivities for an infinite one-dimensional model of the same resistivity and layer thicknesses are shown by means of a dotted curve. Finally, the pseudo sections summarizing the individual ρ_a vs $\sqrt{T}$ plots are presented. We have found the pseudo sections very difficult to use for interpretation. They require considerable practice on the part of the user, and in most cases it is difficult to obtain the field data along continuous profiles; it is, therefore, rare that a good field data pseudo section can be obtained to match with the model pseudo section. Furthermore, important relationships between TE and TM apparent resistivities vs frequency are difficult to recognize in the separated pseudo sections.

It should be noted that there are numerical errors at the highest frequencies that are introduced by the modeling program and which are not always eliminated by the plotting programs. These errors occur when the mesh spacing becomes too small to represent the fields in the surface layer. In all cases run the apparent resistivities have, in fact, become asymptotic to the near-surface value of resistivity. Also, the tipper phase at low values of the tipper are meaningless and should be ignored in the analysis.

For completeness the model set begins with the well known case of a single vertical discontinuity, separating regions of different resistivity, Models 1-1, 1-2, and 1-3. This model has already been discussed previously by d'Erceville and Kunetz (1962) and by Vozoff (1972); the latter presented the tipper results for such a model. It should be noted that the fields recover to their half space values

at roughly 1.5 skin depths away from the contact and that the tipper direction is always towards the resistive side, or in the plus x-direction. The tipper reaches a maximum on the resistive side of the contact. On the resistive side of the contact the TM apparent resistivities are relatively much closer to the true resistivity than the TE apparent resistivities for all frequencies. On the conductive side both modes are about equally influenced by the contact.

In Model 2 a vertical contact exists between two surface layers of 1 and 10 ohm meter resistivity overlying a resistive basement of 300 ohm meters. This model of a thin, discontinuous, surface layer illustrates one of the major difficulties in interpreting magnetotelluric results. For a station located at -3 km from the single vertical contact of Model 1-2 both TE and TM apparent resistivities are within 10% of their half space asymptotic value for values of $\sqrt{T}$ less than 5.0. For the corresponding site in Model 2 TE apparent resistivity is almost 2 times the uniform two layer value and the TM apparent resistivity is about 30% less than the two-layer value. Even at 10 km from the contact the values continue to be strongly affected by the discontinuity. For example, it is only at periods less than 10 seconds (a skin depth of approximately 1.5 km in the surface layer) that the apparent resistivities for TE and TM lie within 10% of the layered half space results. The fields are thus distorted by the contact at distances up to 6 skin depths, compared to only 1.5 to 2 skin depths in the case of the infinite contact.

This effect can be explained using the case of the long period response for an infinite conductive layer over a resistive half space. The electric field will be essentially uniform across the surface layer and will be the value obtained from the surface impedance of the underlying half space. The current flowing in the surface layer will thus be higher than that which would flow in the same thickness of a uniform half space with the resistivity of the surface layer. If a contact or barrier is now placed in the surface layer this current cannot flow, and as we have seen the effect may persist to very large distances from the barrier. In fact, since the current must adjust to this barrier by flowing into the lower half space it might be expected that normal two-layer apparent resistivities would not be reached until distances from the contact of one or two skin depths in the lower medium were achieved.

It can easily be imagined that magnetotelluric soundings in sedimentary sections will be strongly influenced by the edges of the valley or basin. Lateral variations in surface resistivity thus pose as serious a problem in magnetotellurics as they do in dc electrical resistivity surveys. Sufficient stations must be occupied to identify the lateral contacts and this may require profiles whose lengths are up to 20 times the thickness of the conductive section being investigated.

Some features of the apparent resistivity results over the thin discontinuous layer are worth summarizing. First, as in the case of the vertical contact, the TE values are higher than those for the

one-dimensional model on the conductive side of the contact and lower on the resistive side. The TM values behave in the opposite sense; lower on the conductive side and higher on the resistive side. The tipper magnitude increases gradually from each side and peaks close to, but on the resistive side of the contact.

It is often assumed that the observed TE apparent resistivities are a good approximation to the equivalent one-dimensional layered models at some distance from the fault. This is not always the case, as discussed above, and in fact the distortion of the TE apparent resistivity curve is such that an interpretation using a one-dimensional inversion routine would underestimate the thickness of the surface layer. The estimate of the basement resistivity would, however, be better with the TE mode than with the TM mode. For example, at -1.0 km in Model 2 the TE inversion would yield a basement resistivity of 150-300 ohm meters, while the TM estimate would be only 30 to 50 ohm meters. The TM interpretation would, for all sites on the conductive side, overestimate the surface layer thickness.

A final point about Model 2 is that the TM values on the resistive side of the contact can be as much as four times higher, at long periods, than the equivalent layered values. The TE values can be 1/5 the equivalent layered values. These departures from the one-dimensional case are much greater than those observed in the case of a simple vertical contact (Model 1).

While it has been shown that one-dimensional model interpretation will lead to erroneous conclusions about the resistivities and thicknesses for this discontinuous, thin-layer model, an excellent interpretation can be made once the general features of the results are obtained. The tipper always points from the conductive to the resistive side of the contact. Thus, it is always known where the contact is from data at an arbitrary station. The layering structure is guessed approximately from the TE data on the conductive side or from the TM data on the resistive side. A rough estimate of the distance to the contact can be obtained most easily from the change in tipper value at two sites. With this information initial guess estimates for a two dimensional model can be made for the iterative procedure of more detailed interpretation.

The next case considered is that of a buried contact of the type represented by the suite of models 3-1 to 3-3. Here a vertical contact separates two quarter spaces of 10 and 100 ohm meters. An overlying layer of 1, 10, and 100 ohm meters and with thickness 1.0 km completes the simulation of various buried contact sections.

In Model 3-1, TE and TM apparent resistivites to the left of the contact are roughly equal and fall above the equivalent one-dimensional model until a point about 2 km from the contact is reached. At this point both modes indicate a basement resistivity of about twice that of true basement resistivity, and since the tipper values are low, it would be very difficult to tell that there was a buried contact.

Closer to the contact the curves split just as they do approaching a simple vertical contact. In this case, however, the values do not reverse over the contact as they do in the simple contact case; instead the reversal is very subtle and takes place at a point some 3 km to the left of the contact. The TM values remain higher than the TE and, in fact, the TM curve is very close to the equivalent two-layer case even within 0.5 km of the fault. The tipper varies very slowly across the section, never exceeds 0.30, and points to the right (i.e. still in the direction from low to high resistivity in the basement).

In Model 3-2, the overburden layer is assigned a value of 10 ohm meters so the model becomes that of a buried 100 ohm meter quarter space. Approaching the contact from the left, or conductive side, the TE and TM apparent resistivities behave as they do approaching the simple vertical contact of Model 1-3. However, closer than about 3.0 km the separation between the curves does not increase as it does on the simple contact, but begins to decrease until at about -1.5 km the curves merge. Beyond this point, to the right, the TM values again closely approximate the two layer model. Far to the right the curves are close together at short periods but diverge at long periods just as they do in vertical contact model. The tipper behavior is similar to that of Model 3-1. A similar development of apparent resistivity curves occurs for Model 3-3, a buried conductive quarter space.

For all of these cases the general distribution of resistivity can be deduced from several stations spaced across the section. Care must be exercised in interpreting a single station value. It would, for example, be difficult to tell Model 3-3 from Model 1-2 at a station 4 km to the right of the contact in each case. However, there is no ambiguity in differentiating the results of Models 1 or 3 from the thin layer contact case represented by Model 2.

In a step towards models more representative of the conductive valleys of Nevada a collection of simple rectangular troughs is presented in Model 4-1, 4-2, and 4-3. The valley is in all cases 1.0 km thick, has a resistivity of 10 ohm meters and has widths of 5, 10, and 16 km. The surrounding half space resistivity is 150 ohm meters.

The results are quite distinctive in that they possess features which allow a clear differentiation from any of the previous models studied. In Model 4-1 the TE apparent resistivities within the valley show a characteristic two-layer shape, the high and low frequency asymptotes of which are correct, i.e. 10 and 150 ohm meters respectively. The curve is distorted in such a way, however, that a one dimensional interpretation would seriously underestimate the valley thickness. In this respect, the results are similar to that of the thin discontinuous layer in Model 2. The TM apparent resistivities, however, are almost constant as a function of period within the valley, and in the center are below the resistivity of the valley. At the edges, e.g., $\pm$2.0 km, the constant value is depressed to 4 to 6 ohm meters.

The tipper is zero in the center of the valley, positive values to the right and negative to the left. This is again consistent with the conclusion that the tipper points to the higher resistivity. The tipper reaches a maximum of about 0.5 just outside the valley. The tipper peaks at a frequency of about 1 Hz, whereas in Model 1 it increased monotonically with increasing period at all sites. Outside the valley the apparent resistivities appear to approximate the values for an infinite vertical contact (see Model 1-2 at +1.0 km) for periods less than 1 second but with increasing period the TE values begin rising to the appropriate 150 ohm meter asymptote. The TM values just outside are high (400 ohm meters for all frequencies below 1 Hz. As the distance away from the contact increases the TE and TM curves come together and by about 8 km all evidence of the valley is gone. This latter result is very reassuring since it implies that near surface conductive valleys at some distance from a magnetotelluric site do not exert any influence, even at long periods.

These general features are repeated in Models 4-2 and 4-3 as the valley is widened to 10 and 16 km, respectively.

The TE values yield the correct two layer asymptotes but even in the center of the 16 km valley the thickness is underestimated. The TM values in the center are constant but only at periods greater than 1 sec in Model 4-2 and greater than 4 seconds in Model 4-3. The reason for the behavior of the TM apparent resistivities now becomes evident. At a $\sqrt{T}$ of 10, the skin depth in the valley is approximately 15 km. Thus, in both dimensions the size of the valley is comparable to or less than a skin depth. The TM response in this case is very close to the uniform field or dc response at all the low frequencies. To verify this hypothesis a uniform field dc computer program (Dey and Morrison, 1977) was used to calculate the electric field at the center of the two-dimension inhomogeneity of the Model 4-1. This field, normalized to the field outside the inhomogeneity, is plotted on the graph for 0.0 km of Model 4-1.

The section represented by Model 4-4 is that of a valley whose left hand margin is extended to infinity. This model obviously has some of the characteristics of the discontinuous surface layer studied in Model 2 and must represent some sort of asymptote for the progression of ever widening valleys in Models 4-1 through 4-3.

Another model considered here, which was also discussed by Vozoff (1972), is a wide conductive dike below a conductive surface layer of equal thickness, Model 5-1. The conductive dike has virtually no effect on the TM apparent resistivities. The TE values are predictably lower over the dike, and even at 10 km distance the long period TE apparent resistivities are lowered by it. The effect on TE at long periods is caused by the infinite vertical extent of the dike. A surface feature, such as the valley of Model 4-1, does not exert this influence. There is little possibility of confusing this dike model with any of the other models that have been discussed.

A final case which addresses the problem of the effect of surface discontinuities on the response of a deep crustal conductor is analyzed with Model 2-2. This is Model 2 but with the addition of a conductive basement 16 km beneath the surface. In general the TE response is similar to that of Model 2. Its shape and asymptotes are approximately those for the equivalent uniformly layered model. Like the discontinuous single layer model (Model 2), however, an inverse layer fitting for Model 2-2 for all the stations to the left of the contact would greatly underestimate the thickness of the surface layer, but the depth estimate to the basal conductor would be quite accurate.

The effect of the basal conductor on the TM data is very dramatic. The TM fields appear to "sense" the deep conductor at almost an order of magnitude higher frequency than do the TE fields. This lowers TM values considerably even at 10 kilometers away from the contact. On the resistive side of the contact neither TE or TM is close to the equivalent layered model except at large distances from the fault where the TE data is approximately correct.

Some care must be exercised in distinguishing the response of Model 2-2 from the response of the buried resistive quarter space of Model 3-2. At stations over the resistive quarter space the apparent resistivity curves have the same general shape as those over the left hand side of Model 2-2. However the relative values of the TE and TM apparent resistivities are reversed so that in a practical situation there would be no confusion if the TE and TM modes could be correctly identified.

This small collection of simple models can not begin to resolve the question of uniqueness for a two dimensional resistivity distribution. It does indicate, however, that if multiple stations are available, there is no difficulty in distinguishing between the models of this set, especially if the tipper and its direction are available.

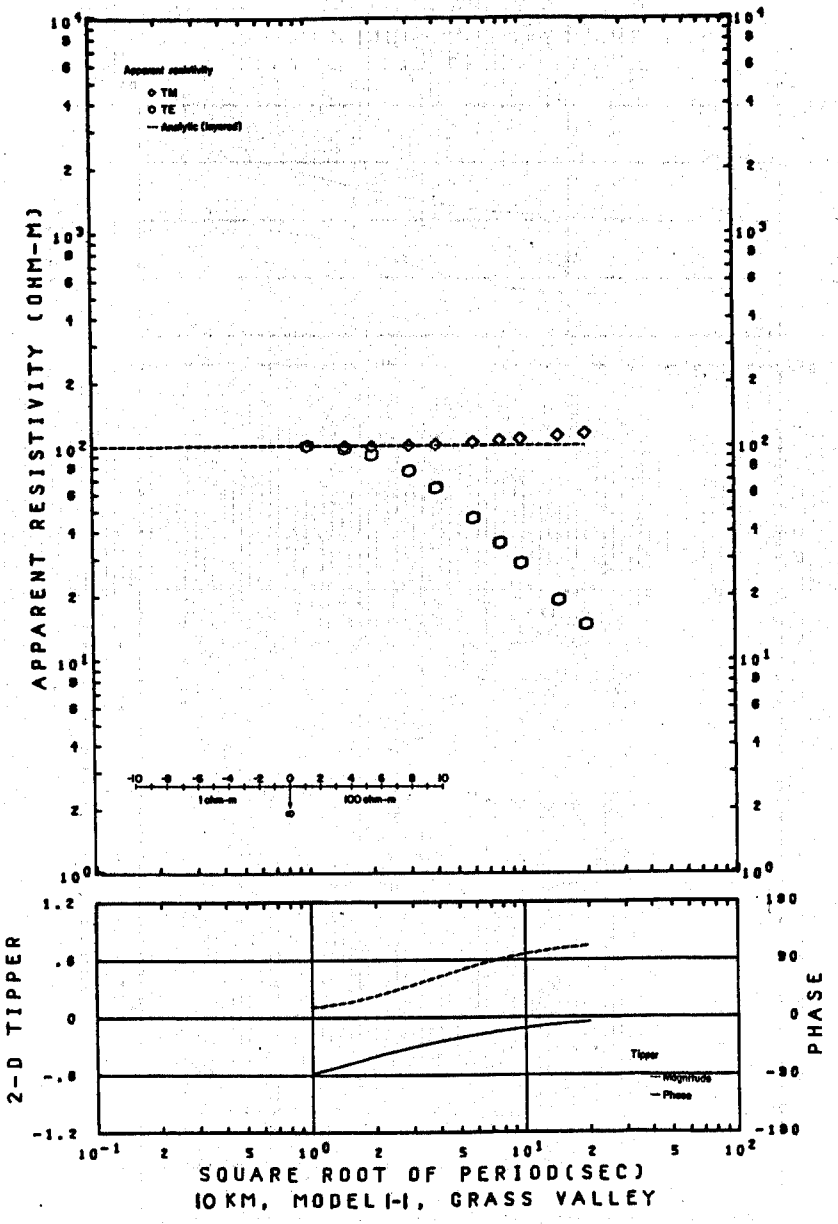

10 KM, MODEL I-I, GRASS VALLEY

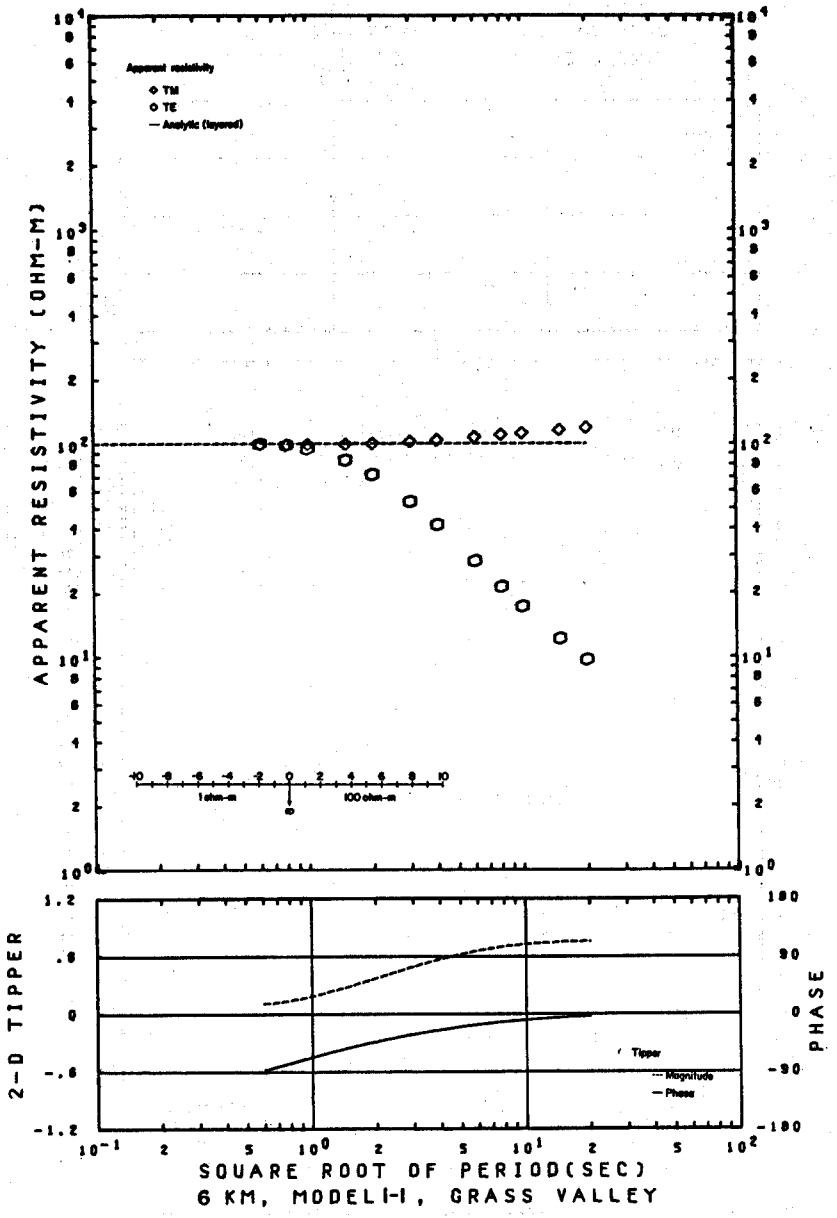

6 KM, MODEL I-I, GRASS VALLEY

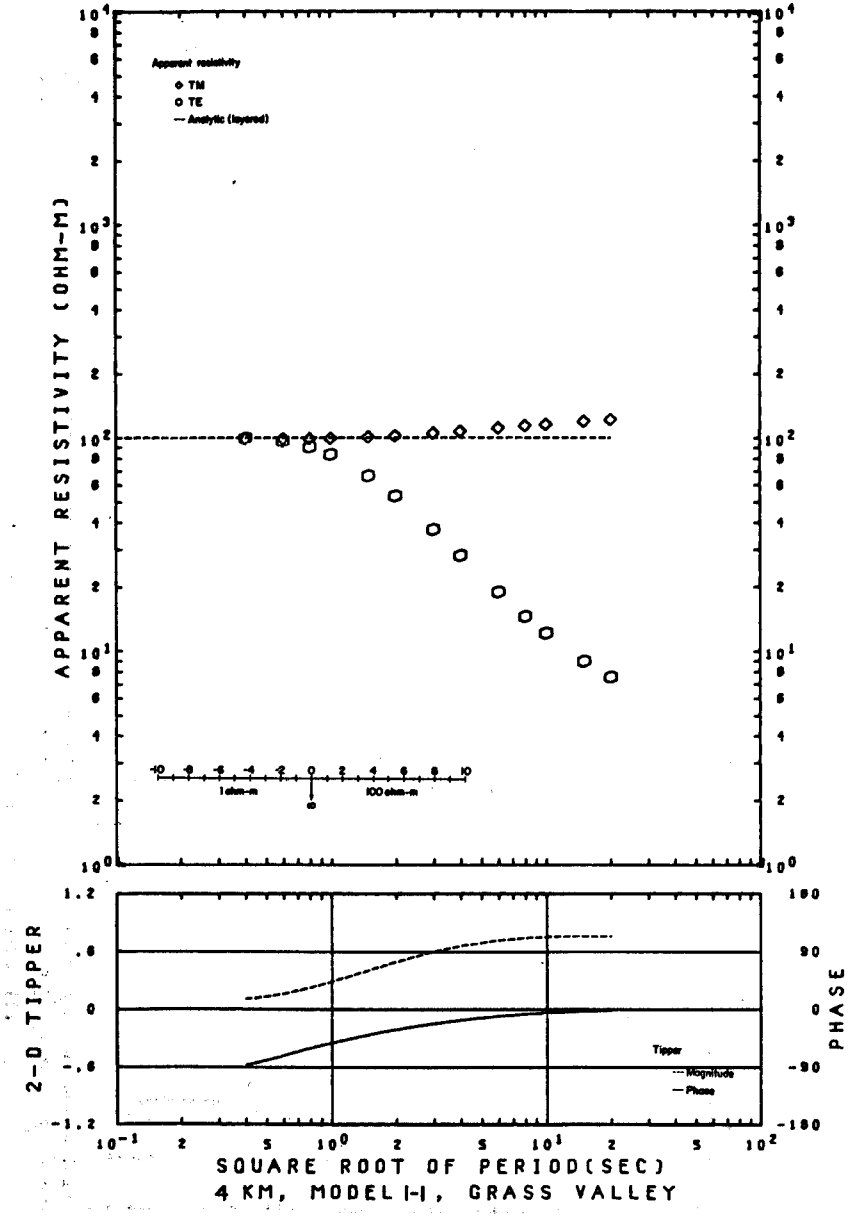
Apparent resistivity
TM
TE
Analytic (layered)
APPARENT RESISTIVITY (OHM-M)
1 ohm-m
100 ohm-m
2-D TIPPER
PHASE
Tipper
Magnitude
Phase
SQUARE ROOT OF PERIOD(SEC)
4 KM, MODEL I-I, GRASS VALLEY

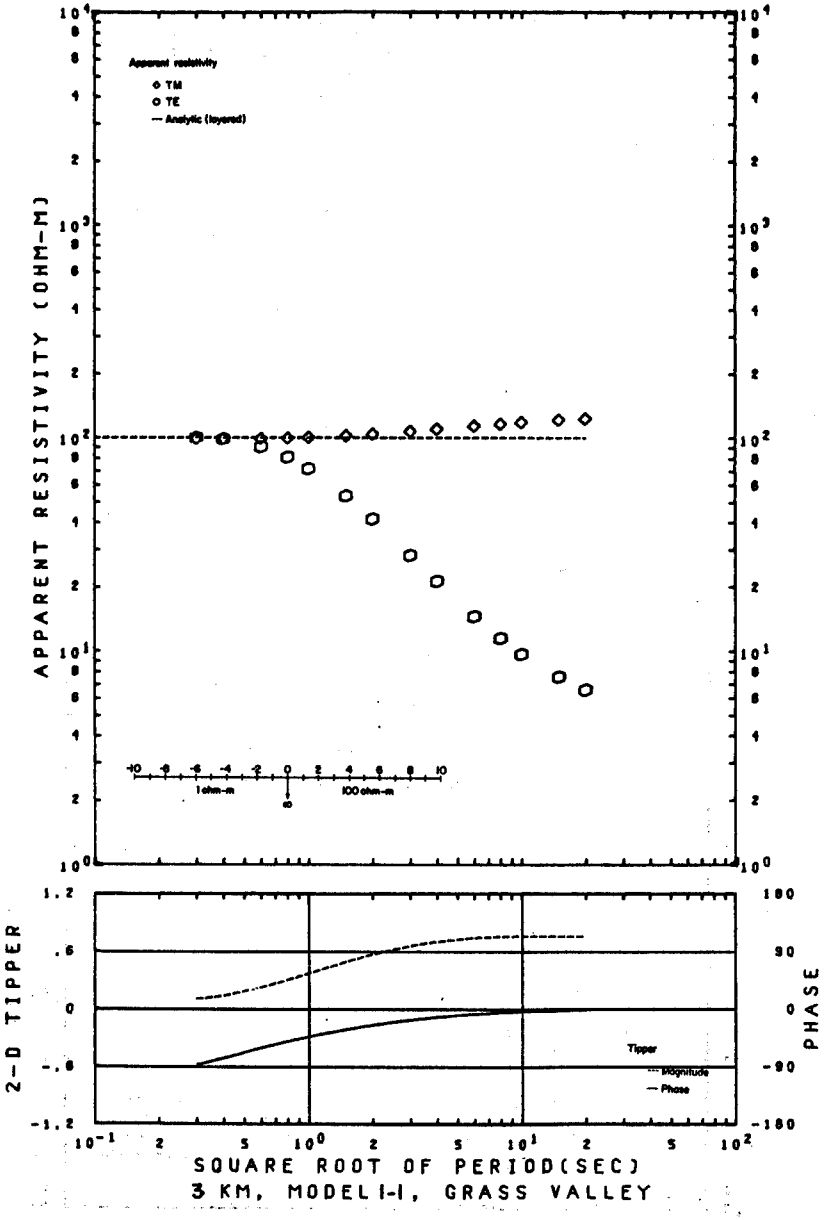
Apparent resistivity
TM
TE
Analytic (layered)
APPARENT RESISTIVITY (OHM-M)
1 ohm-m
100 ohm-m
2-D TIPPER
PHASE
Tipper
Magnitude
Phase
SQUARE ROOT OF PERIOD(SEC)
3 KM, MODEL I-I, GRASS VALLEY

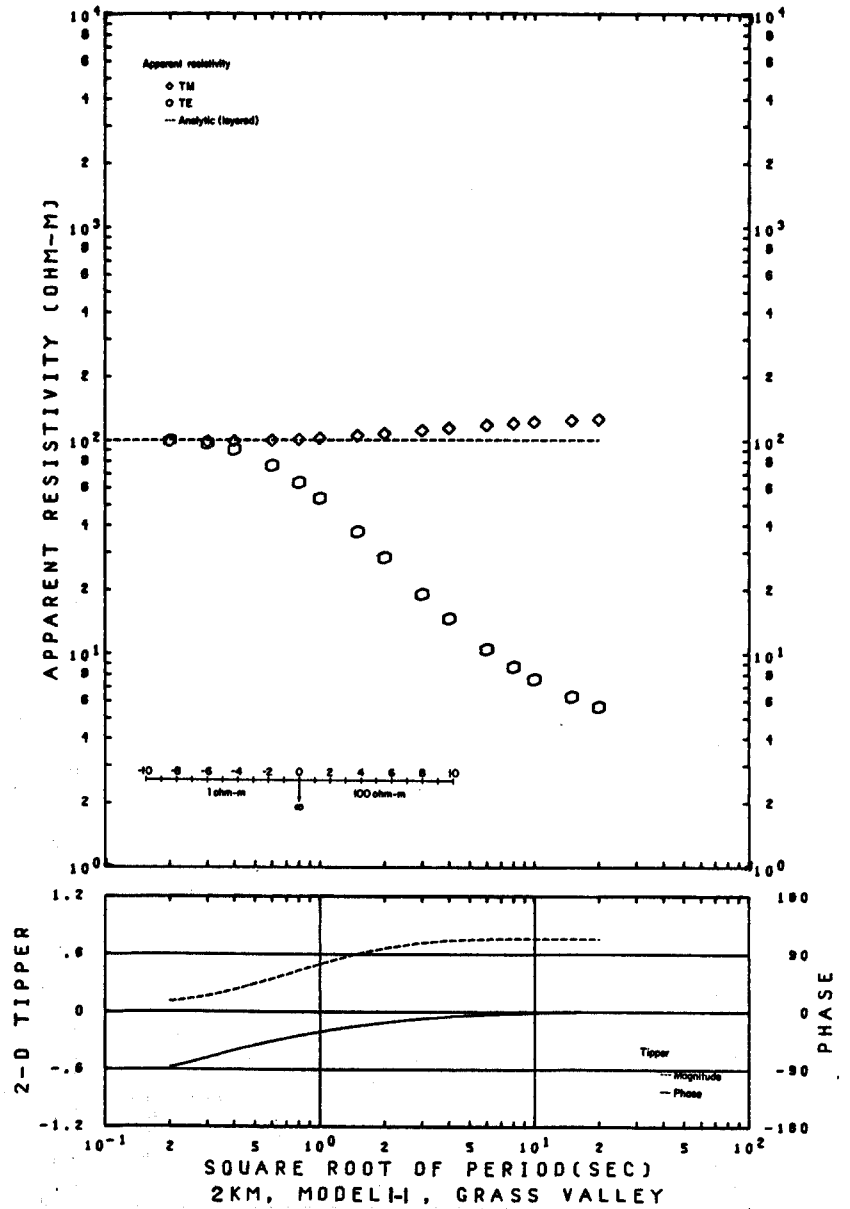
Apparent resistivity
TM
TE
Analytic (layered)
APPARENT RESISTIVITY (OHM-M)
1 ohm-m
100 ohm-m
2-D TIPPER
PHASE
Tipper
Magnitude
Phase
SQUARE ROOT OF PERIOD(SEC)
2KM, MODELI-I, GRASS VALLEY

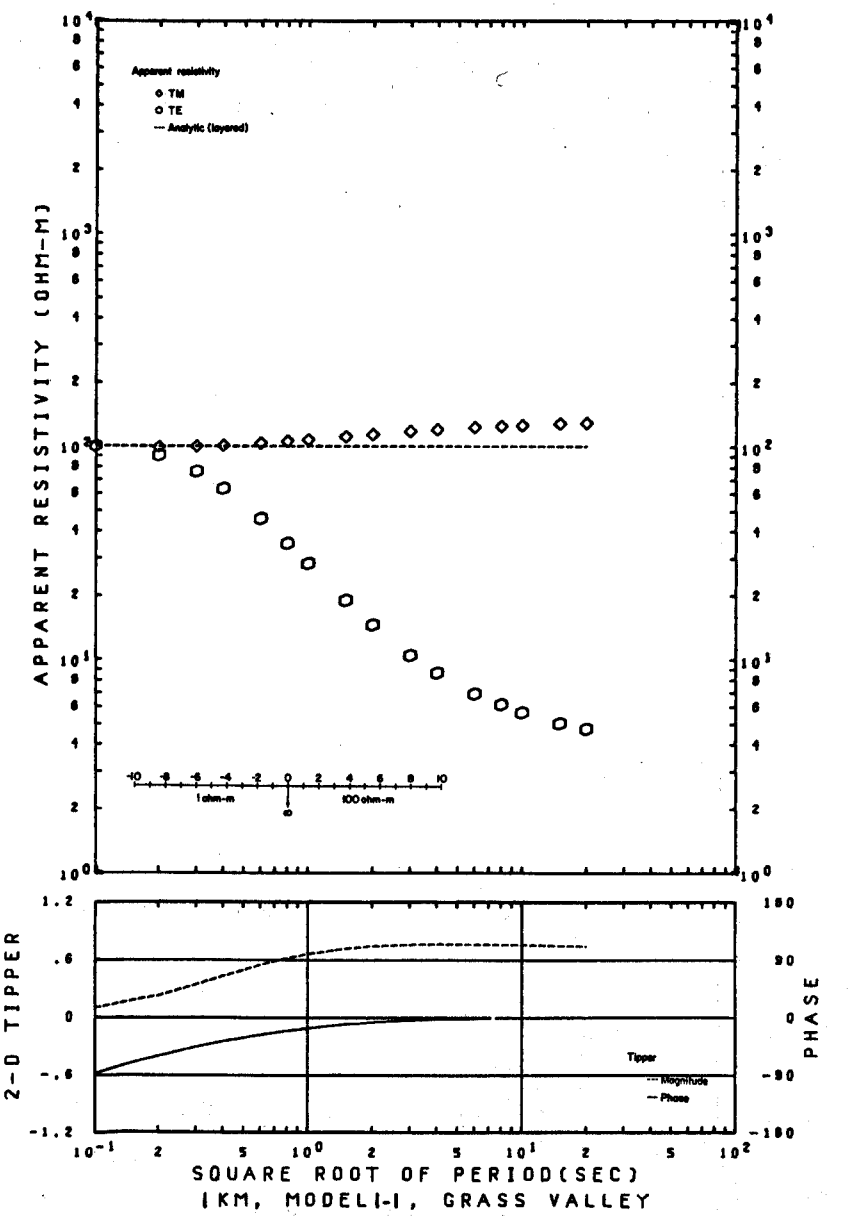
Apparent resistivity
TM
TE
Analytic (layered)
APPARENT RESISTIVITY (OHM-M)
1 ohm-m
100 ohm-m
2-D TIPPER
PHASE
Tipper
Magnitude
Phase
SQUARE ROOT OF PERIOD(SEC)
1KM, MODELI-I, GRASS VALLEY

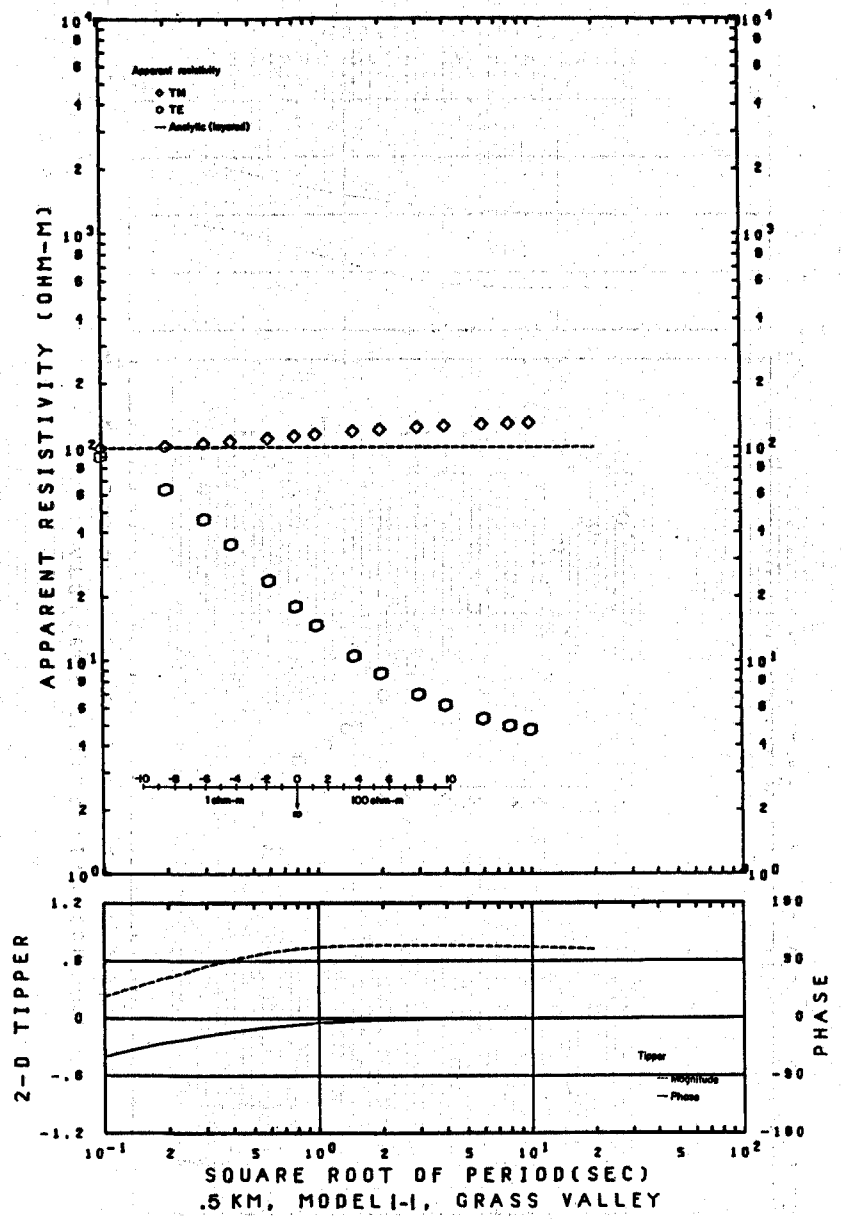
Apparent resistivity
TM
TE
Analytic (layered)
APPARENT RESISTIVITY (OHM-M)
1 ohm-m
100 ohm-m
2-D TIPPER
PHASE
Tipper
Magnitude
Phase
SQUARE ROOT OF PERIOD(SEC)
.5 KM, MODEL I-I, GRASS VALLEY

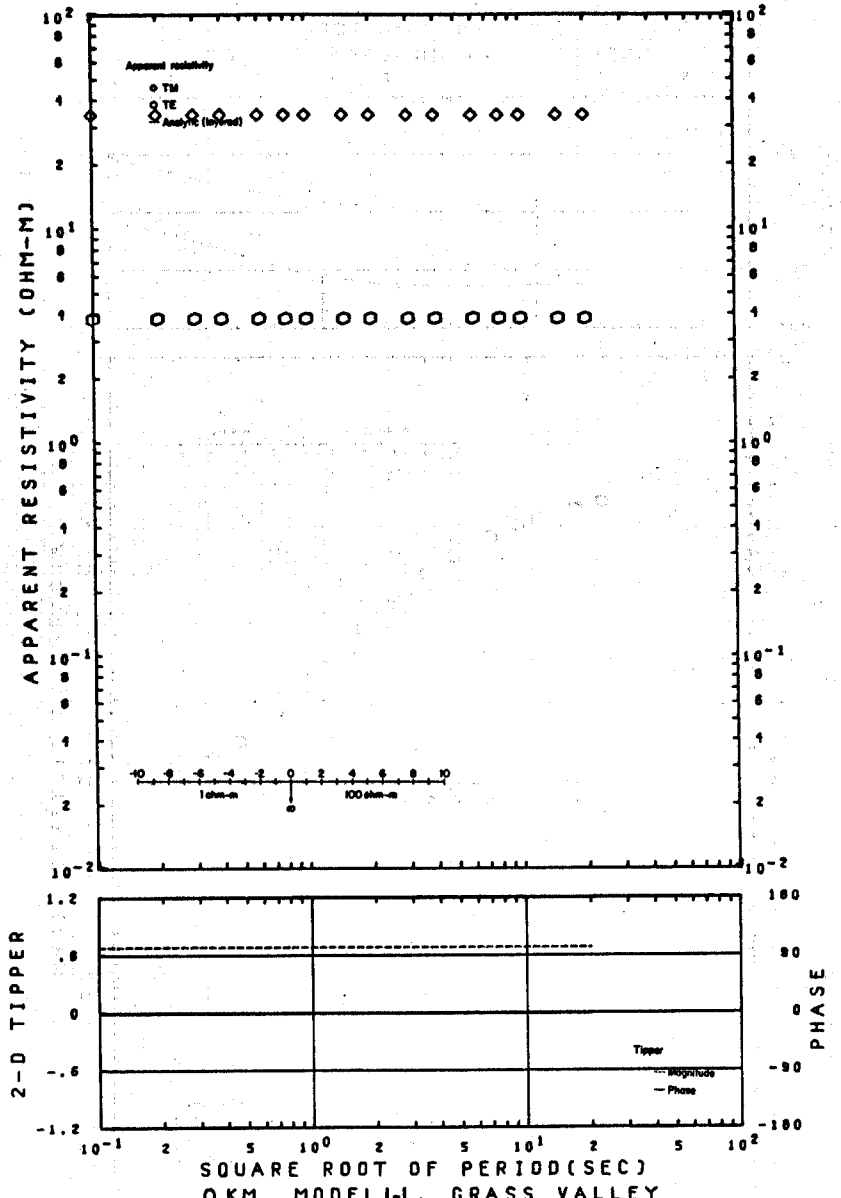
Apparent resistivity
TM
TE
Analytic (layered)
APPARENT RESISTIVITY (OHM-M)
1 ohm-m
100 ohm-m
2-D TIPPER
PHASE
Tipper
Magnitude
Phase
SQUARE ROOT OF PERIOD(SEC)
0 KM, MODEL I-I, GRASS VALLEY

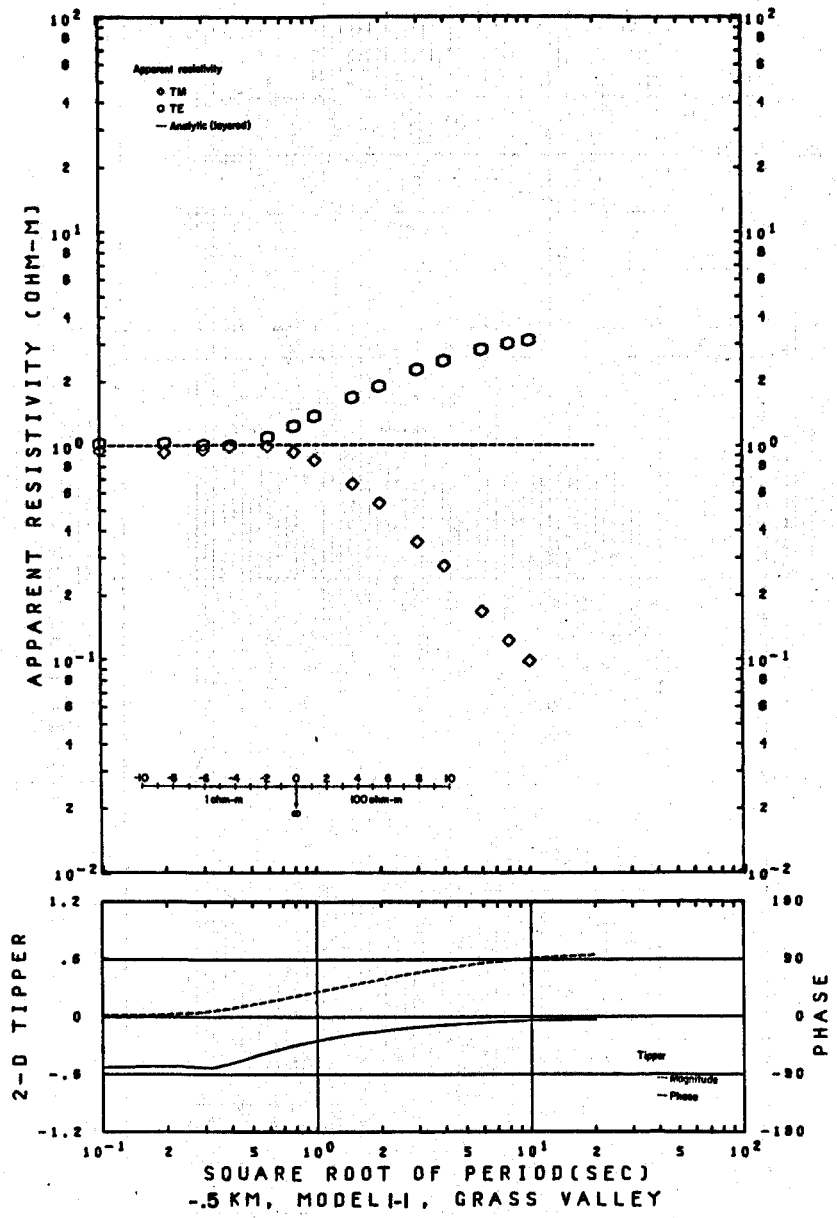
Apparent resistivity
TM
TE
Analytic (layered)
APPARENT RESISTIVITY (OHM-M)
1 ohm-m
100 ohm-m
2-D TIPPER
PHASE
Tipper
Magnitude
Phase
SQUARE ROOT OF PERIOD(SEC)
-.5 KM, MODEL I-I, GRASS VALLEY

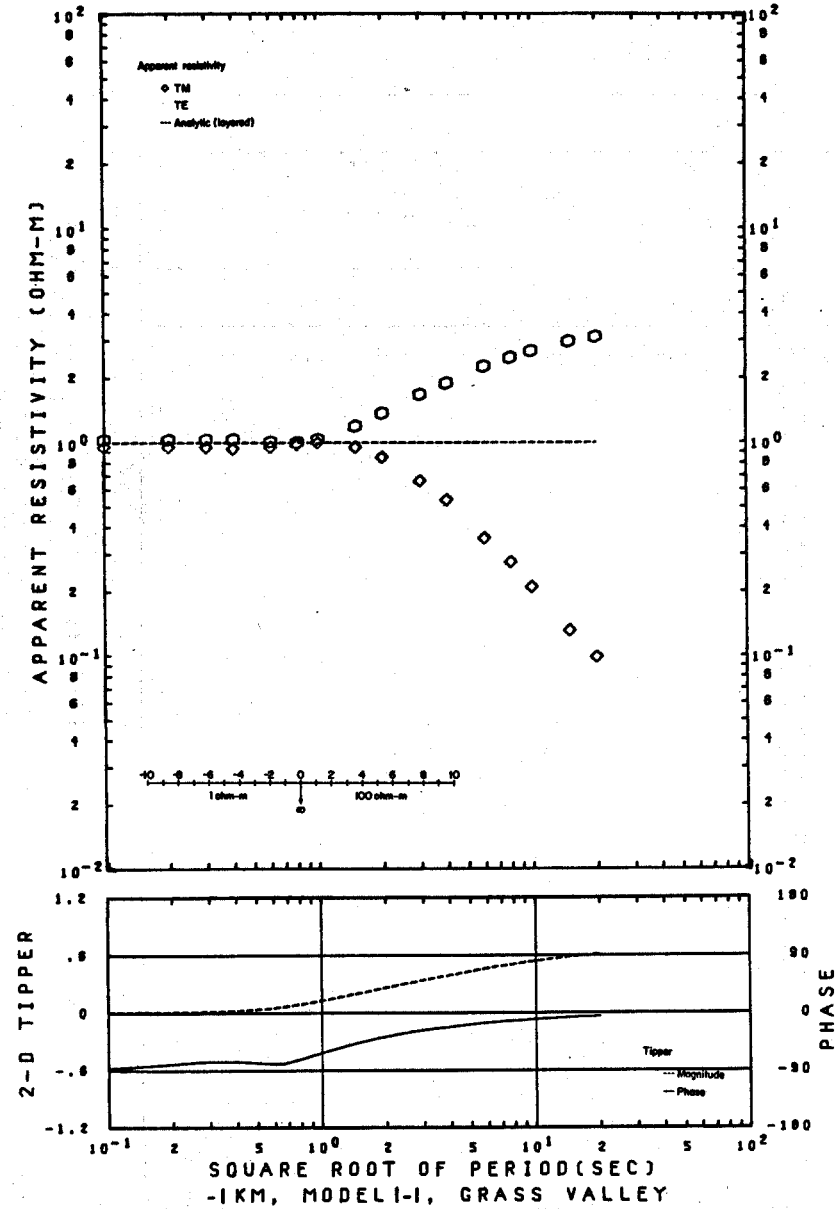
Apparent resistivity
TM
TE
Analytic (layered)
APPARENT RESISTIVITY (OHM-M)
1 ohm-m
100 ohm-m
2-D TIPPER
PHASE
Tipper
Magnitude
Phase
SQUARE ROOT OF PERIOD(SEC)
-1 KM, MODEL I-I, GRASS VALLEY

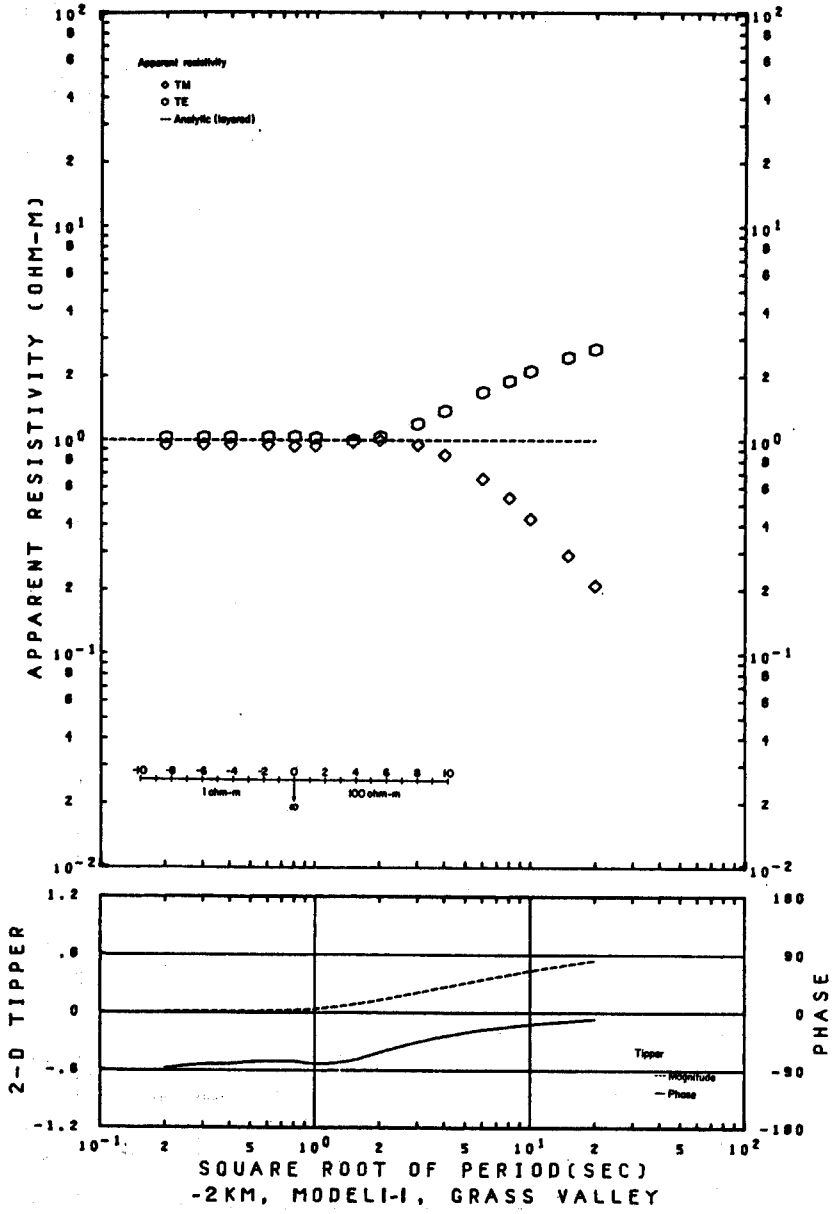

-2KM, MODELI-1, GRASS VALLEY

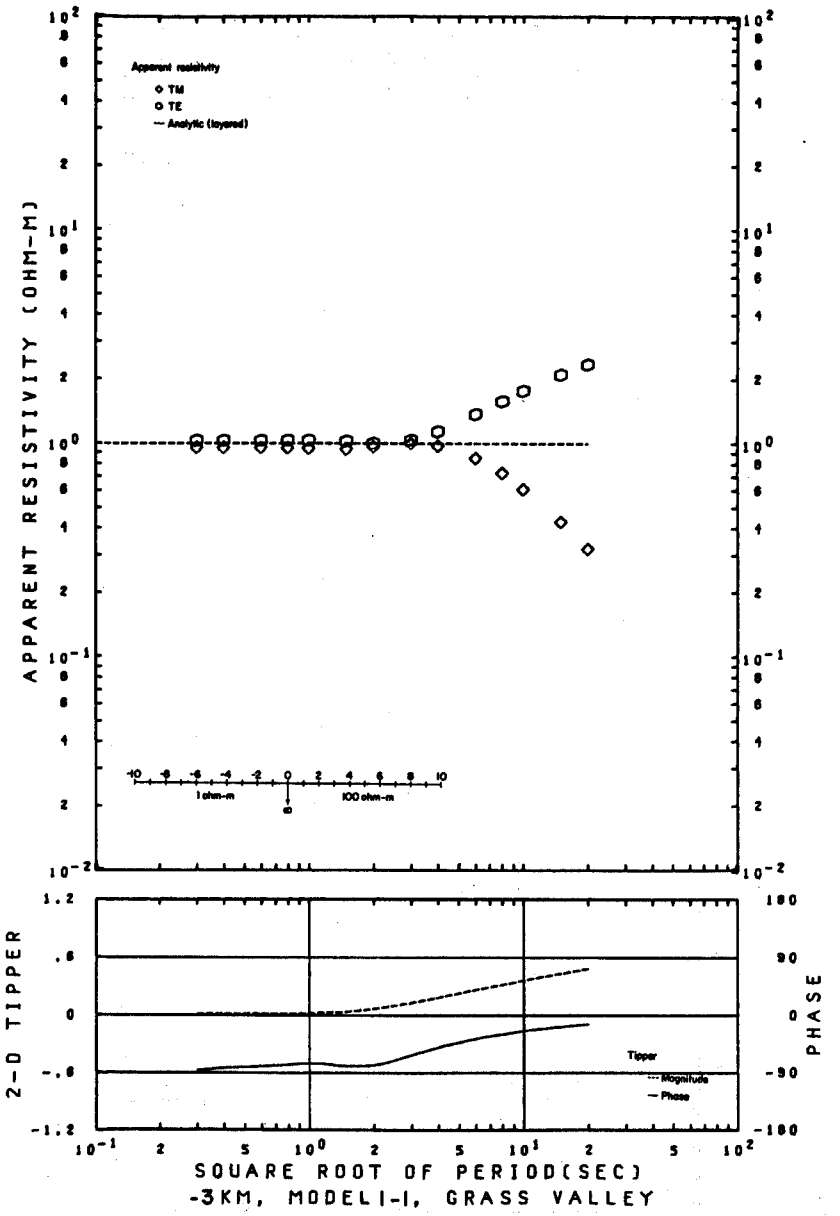

-3KM, MODELI-1, GRASS VALLEY

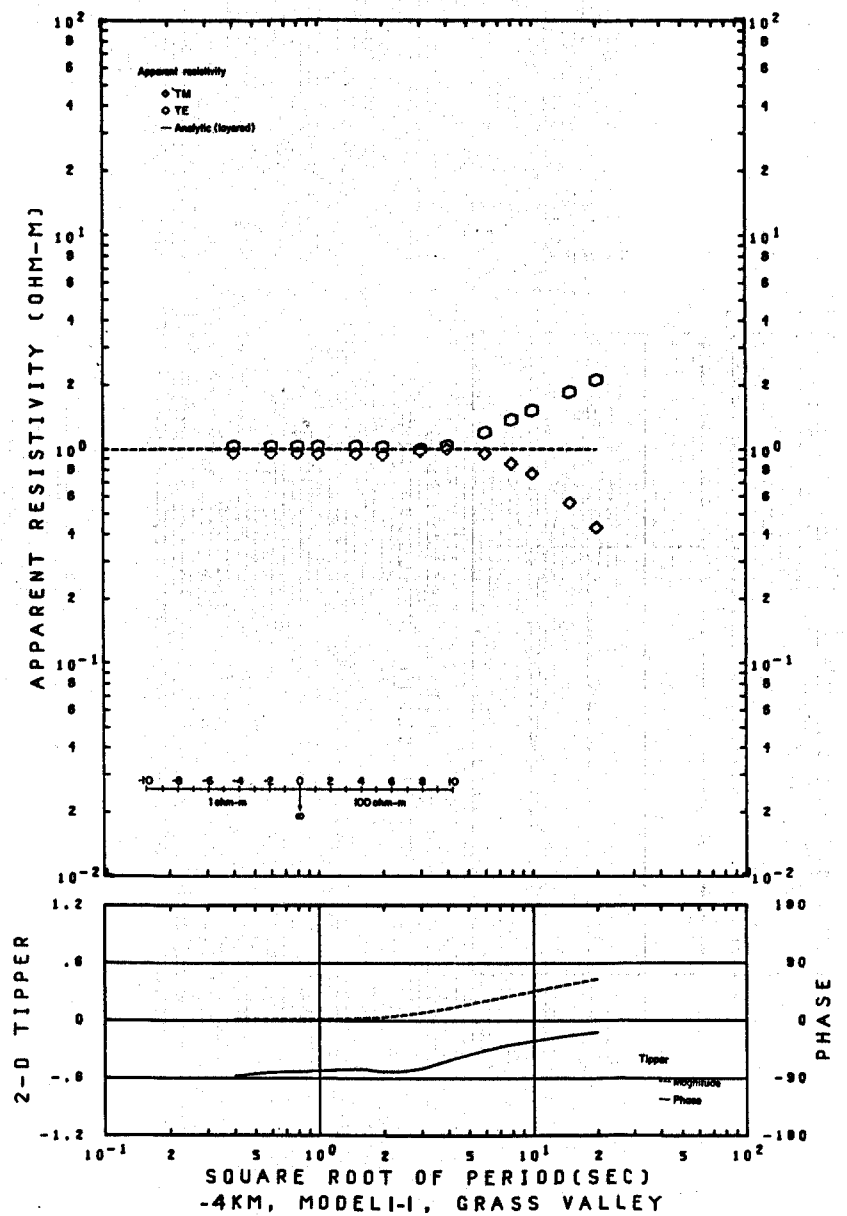

-4KM, MODELI-I, GRASS VALLEY

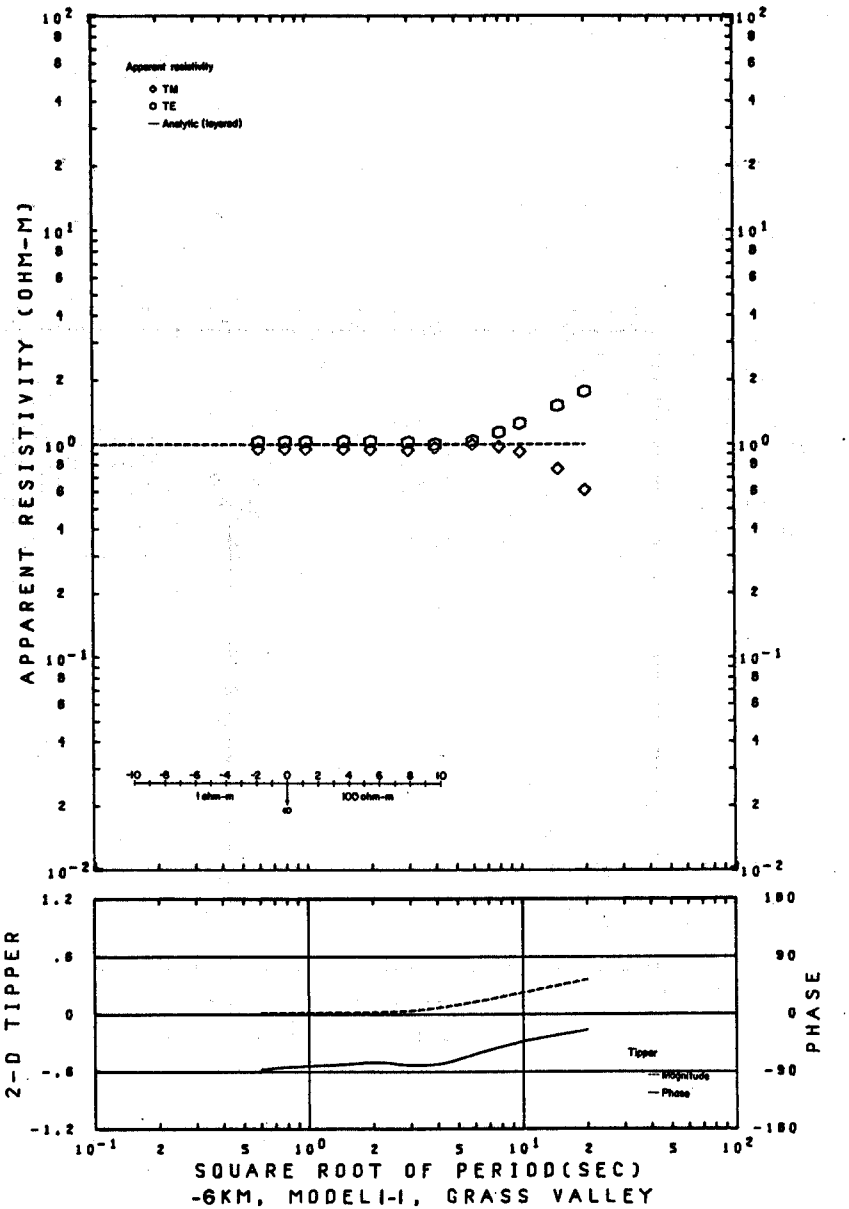

-6KM, MODELI-I, GRASS VALLEY

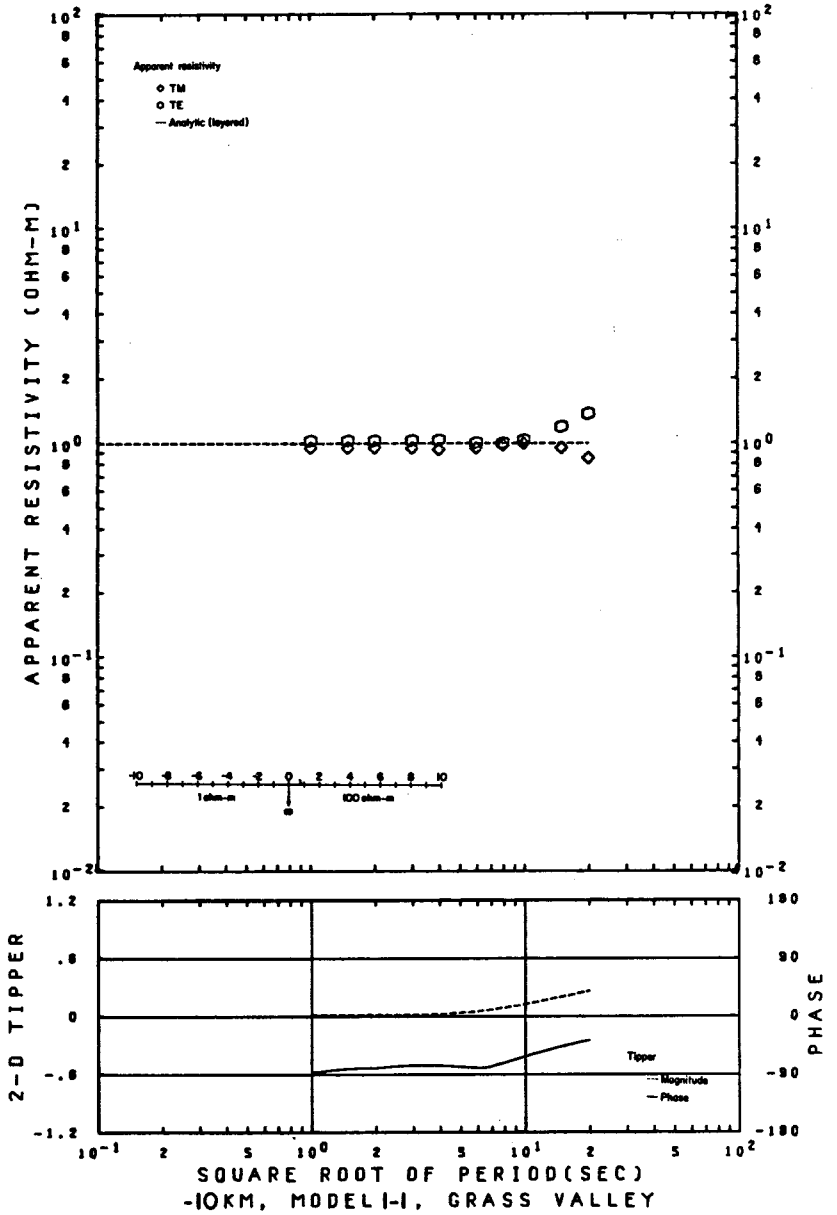
Apparent resistivity
TM
TE
Analytic (layered)
APPARENT RESISTIVITY (OHM-M)
1 ohm-m
100 ohm-m
2-D TIPPER
PHASE
Tipper
Magnitude
Phase
SQUARE ROOT OF PERIOD(SEC)
-10KM, MODEL I-I, GRASS VALLEY

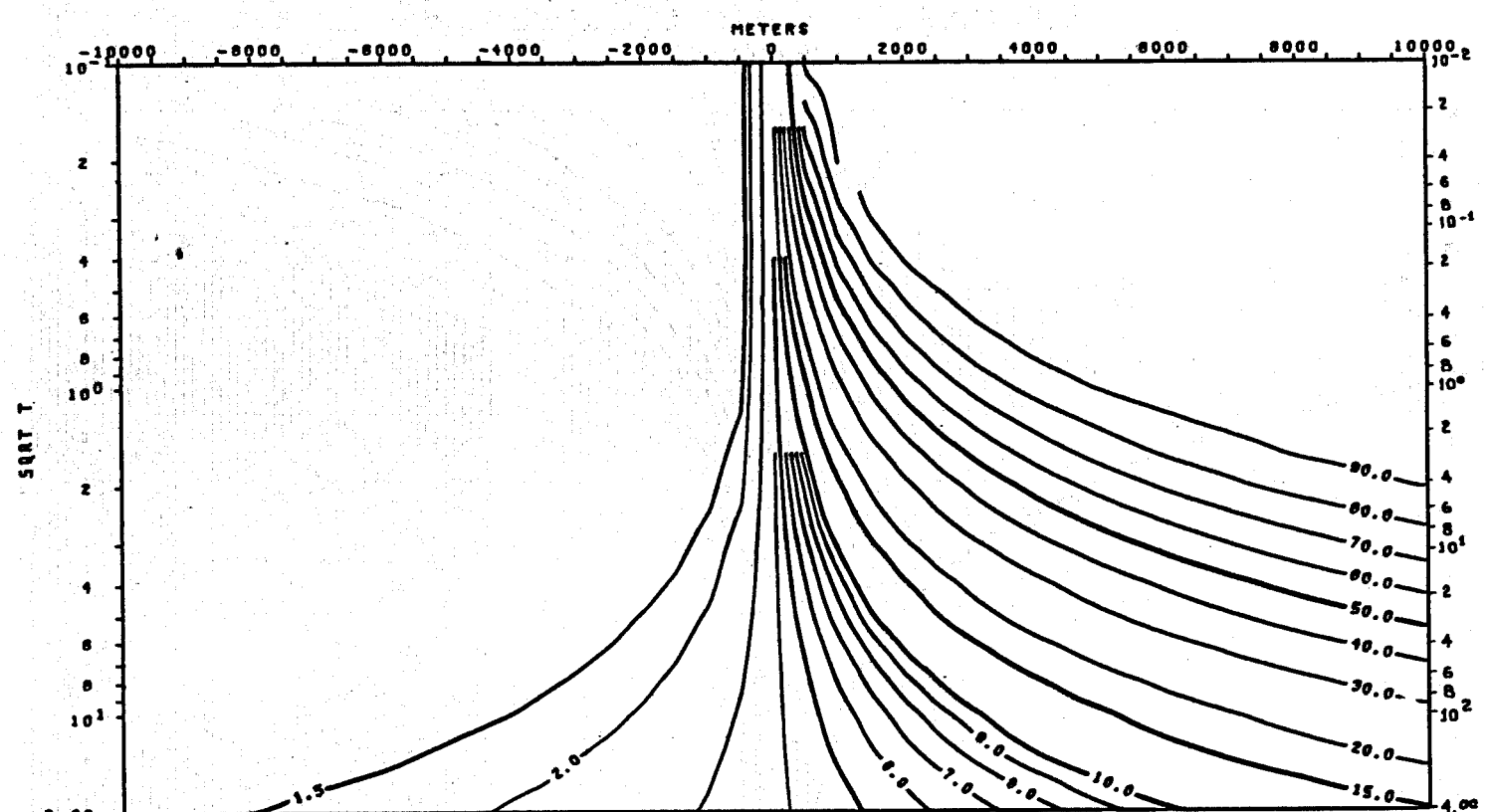

TE MODE
APPARENT RESISTIVITY VS. PERIOD (T)
MODEL 1-1

XBL 786-1903

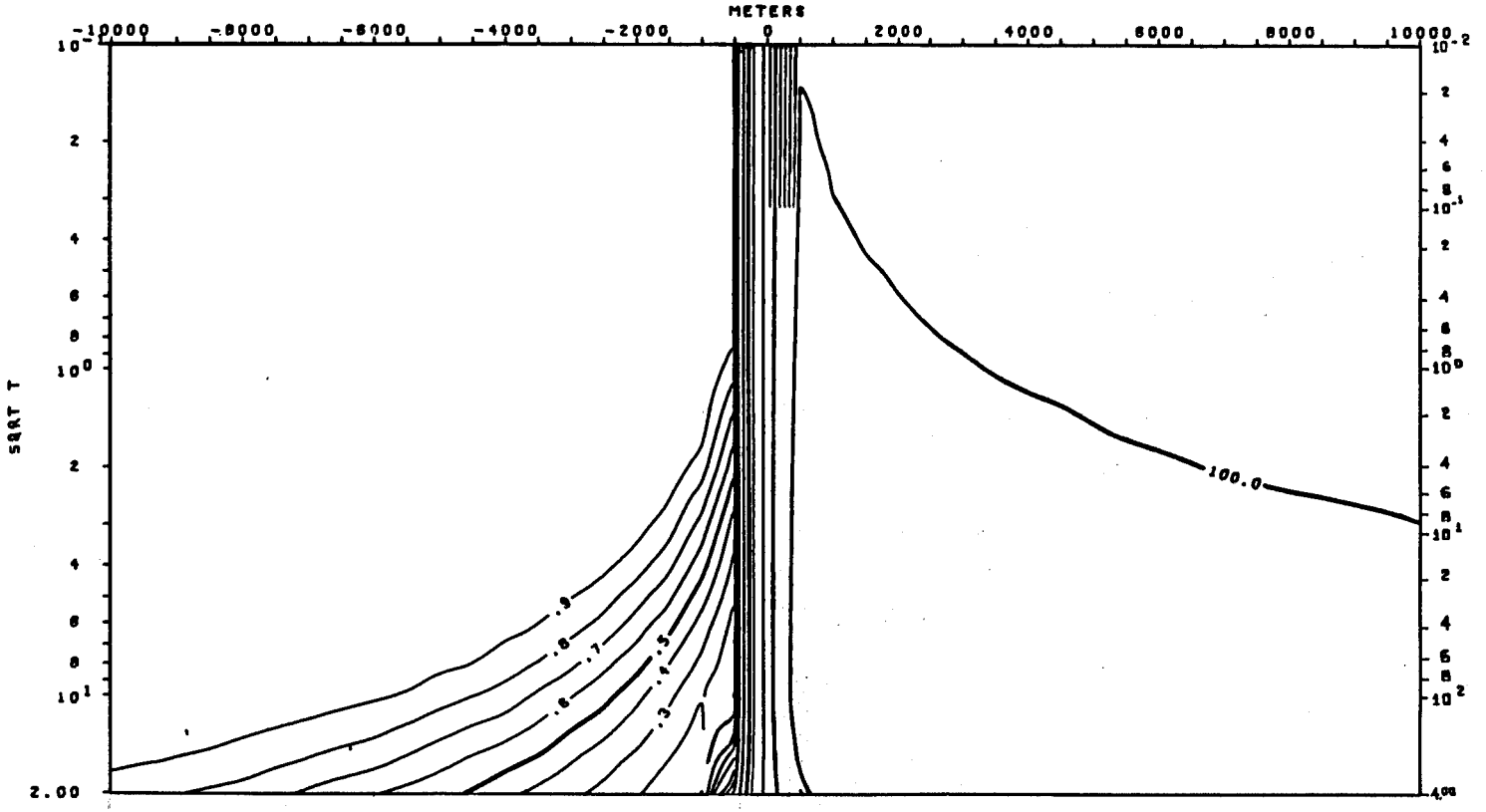

TM MODE
APPARENT RESISTIVITY VS. PERIOD (T)
MODEL 1-1

XBL 786-1929

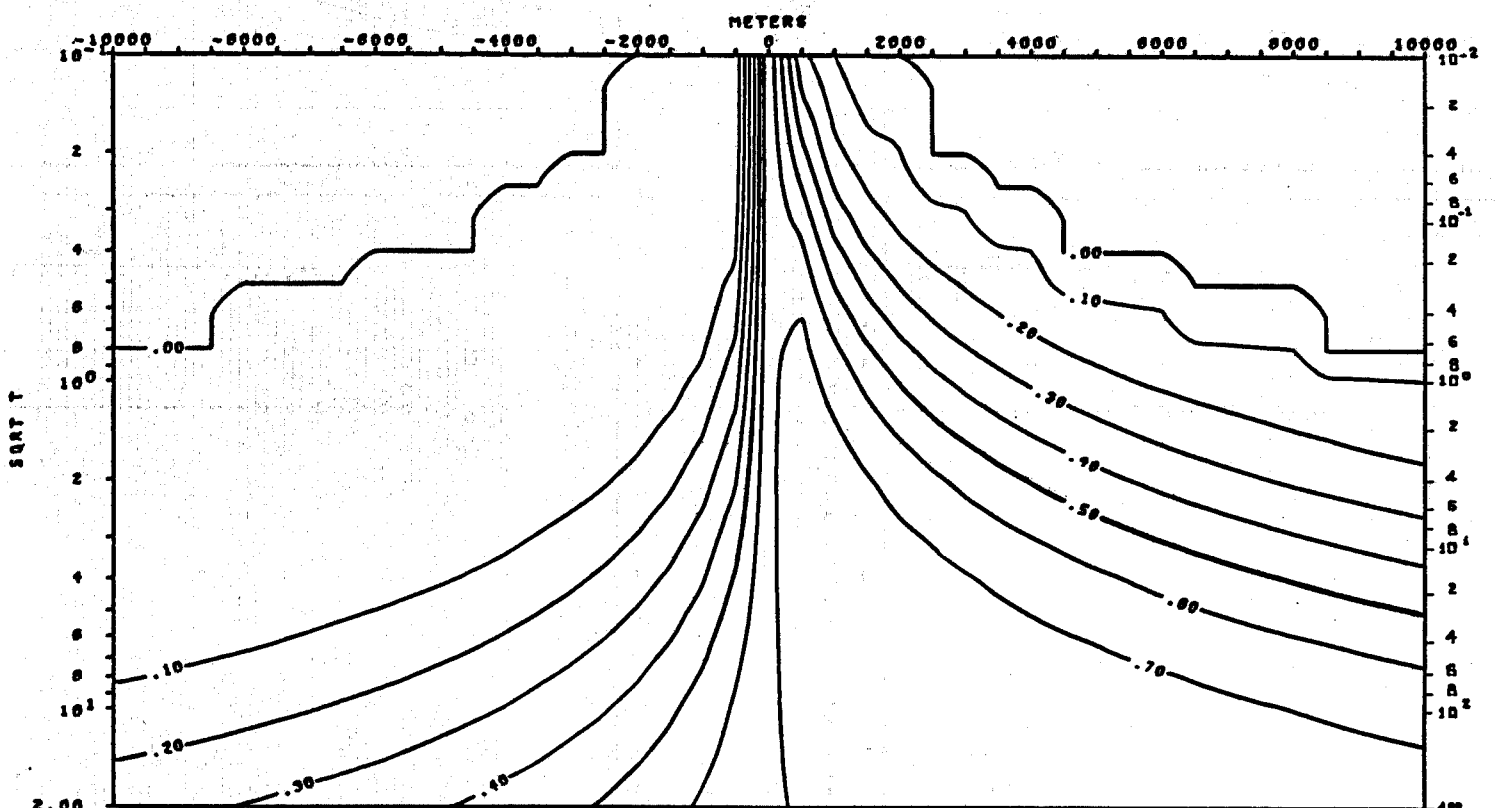

TIPPER VS. PERIOD (T)
MODEL 1-1

XBL 786-1904

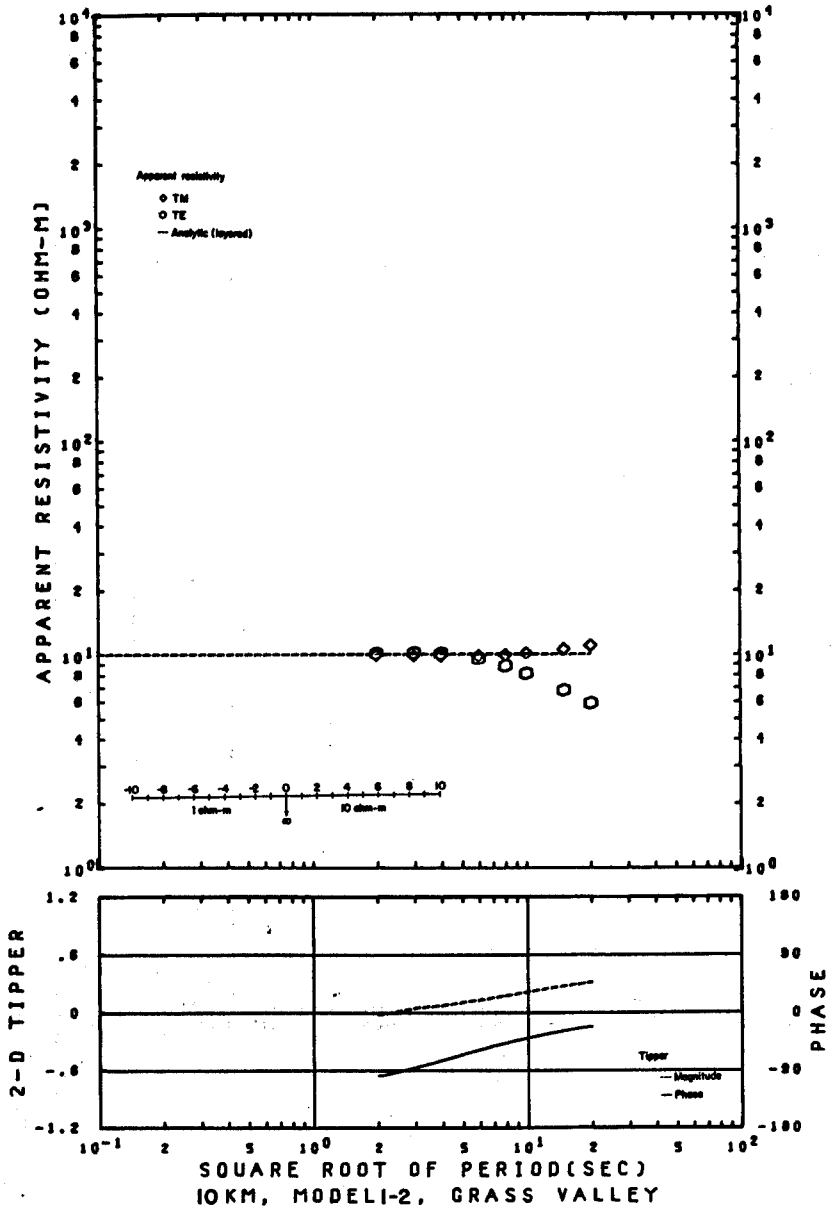
APPARENT RESISTIVITY (OHM-M)
Apparent resistivity
TM
TE
Analytic (layered)
1 ohm-m
10 ohm-m
2-D TIPPER
PHASE
Tipper
Magnitude
Phase
SQUARE ROOT OF PERIOD(SEC)
10KM, MODELI-2, GRASS VALLEY

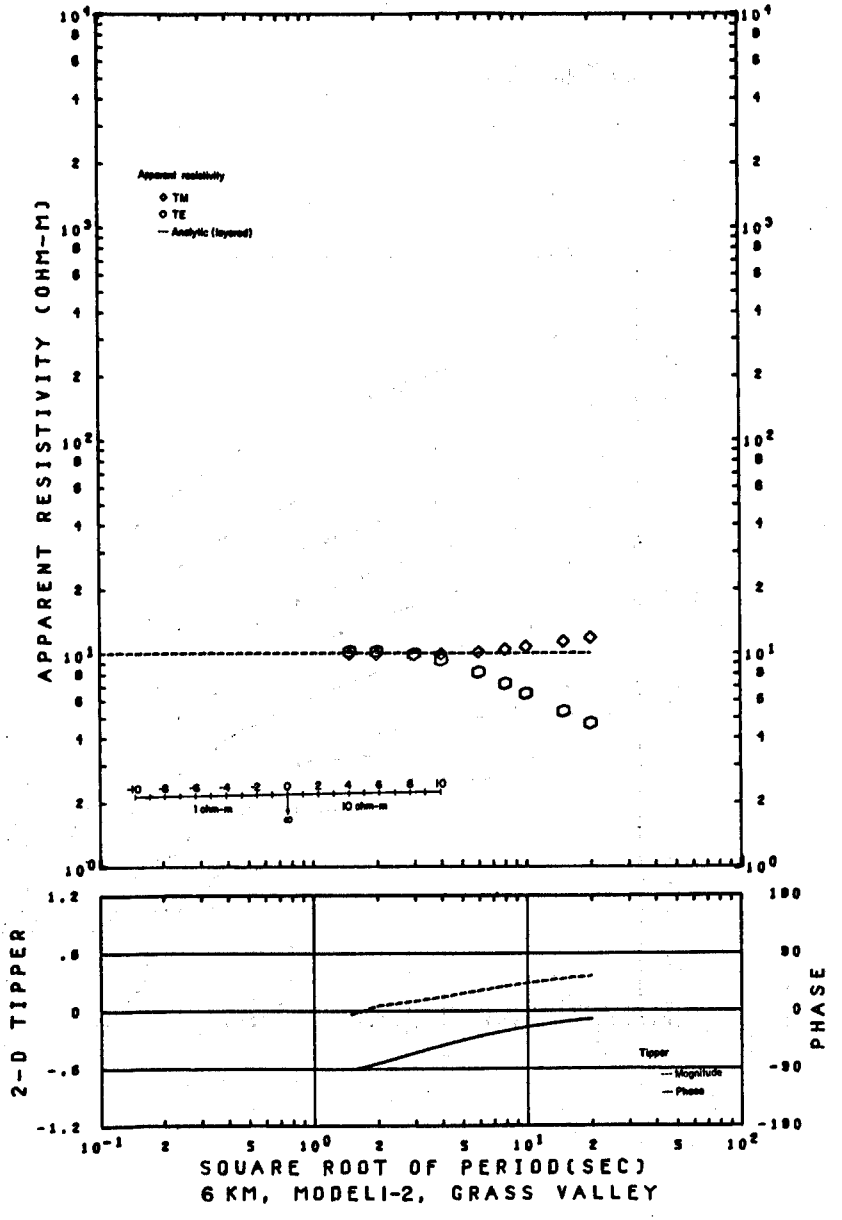
APPARENT RESISTIVITY (OHM-M)
Apparent resistivity
TM
TE
Analytic (layered)
1 ohm-m
10 ohm-m
2-D TIPPER
PHASE
Tipper
Magnitude
Phase
SQUARE ROOT OF PERIOD(SEC)
6 KM, MODELI-2, GRASS VALLEY

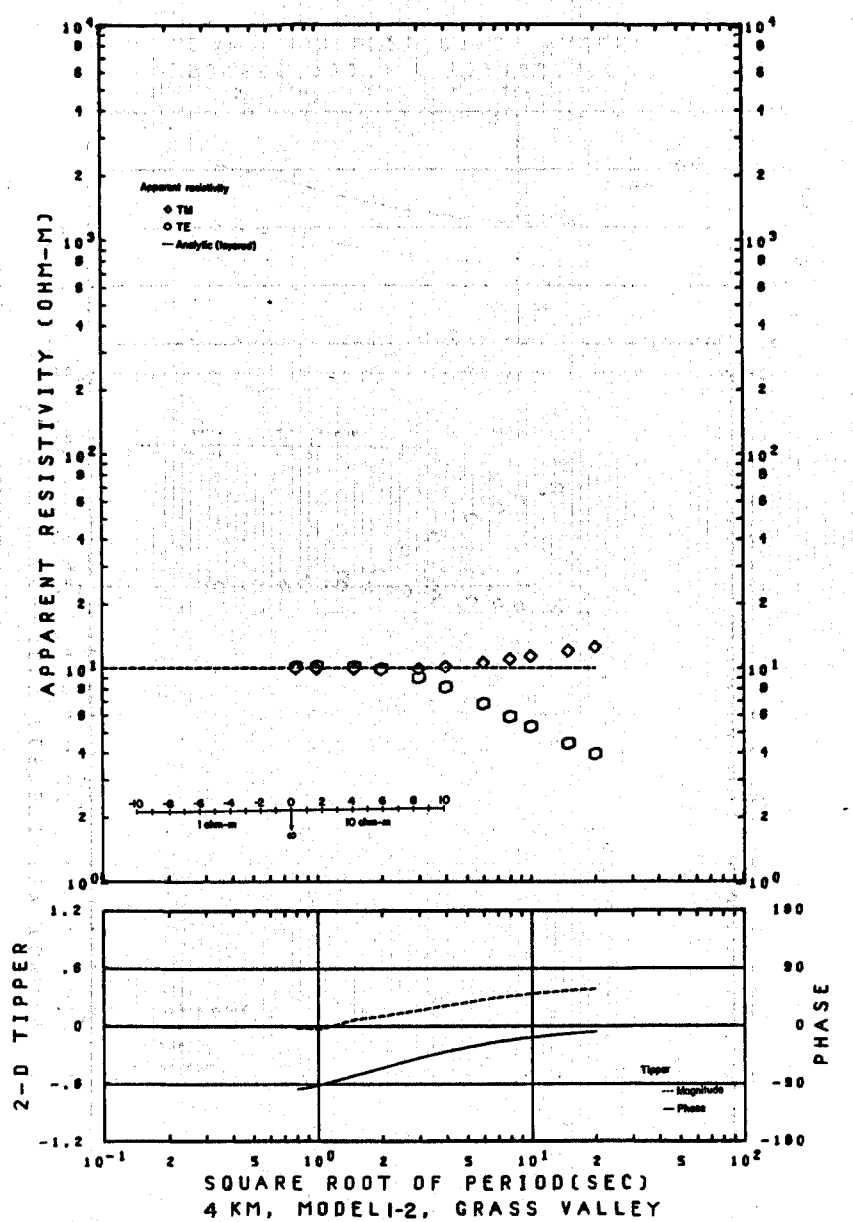
APPARENT RESISTIVITY (OHM-M)
Apparent resistivity
TM
TE
Analytic (layered)
1 ohm-m
10 ohm-m
2-D TIPPER
PHASE
Tipper
Magnitude
Phase
SQUARE ROOT OF PERIOD(SEC)
4 KM, MODEL1-2, GRASS VALLEY

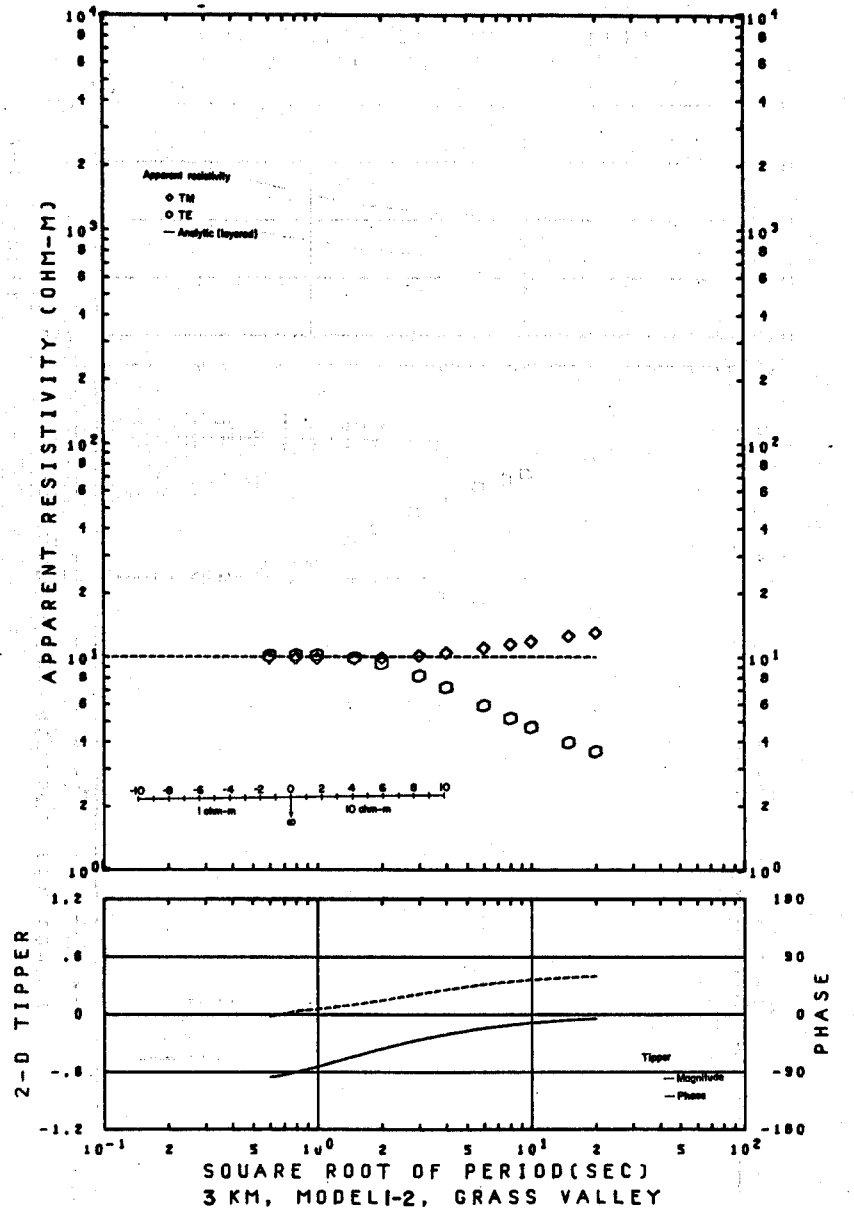
APPARENT RESISTIVITY (OHM-M)
Apparent resistivity
TM
TE
Analytic (layered)
1 ohm-m
10 ohm-m
2-D TIPPER
PHASE
Tipper
Magnitude
Phase
SQUARE ROOT OF PERIOD(SEC)
3 KM, MODEL1-2, GRASS VALLEY

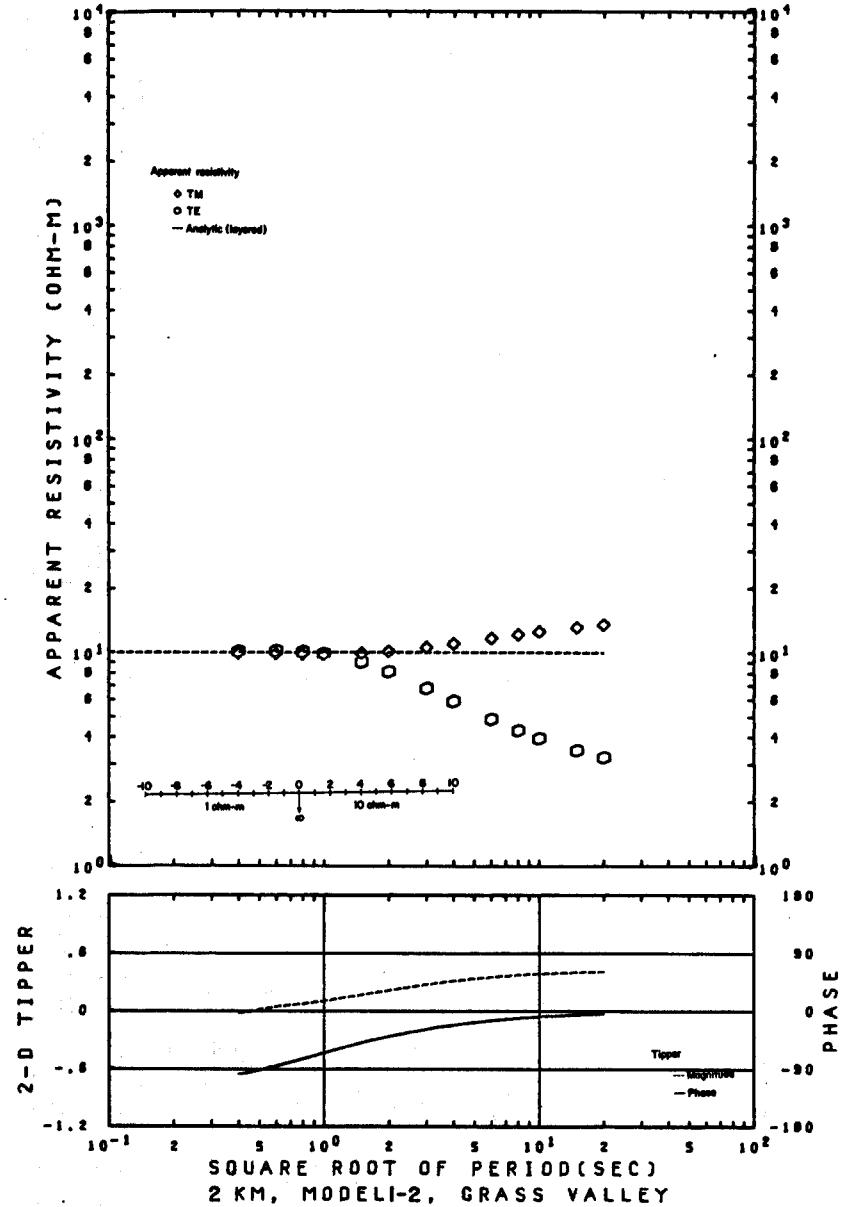
APPARENT RESISTIVITY (OHM-M)
Apparent resistivity
TM
TE
Analytic (layered)
1 ohm-m
10 ohm-m
2-D TIPPER
PHASE
Tipper
Magnitude
Phase
SQUARE ROOT OF PERIOD(SEC)
2 KM, MODELI-2, GRASS VALLEY

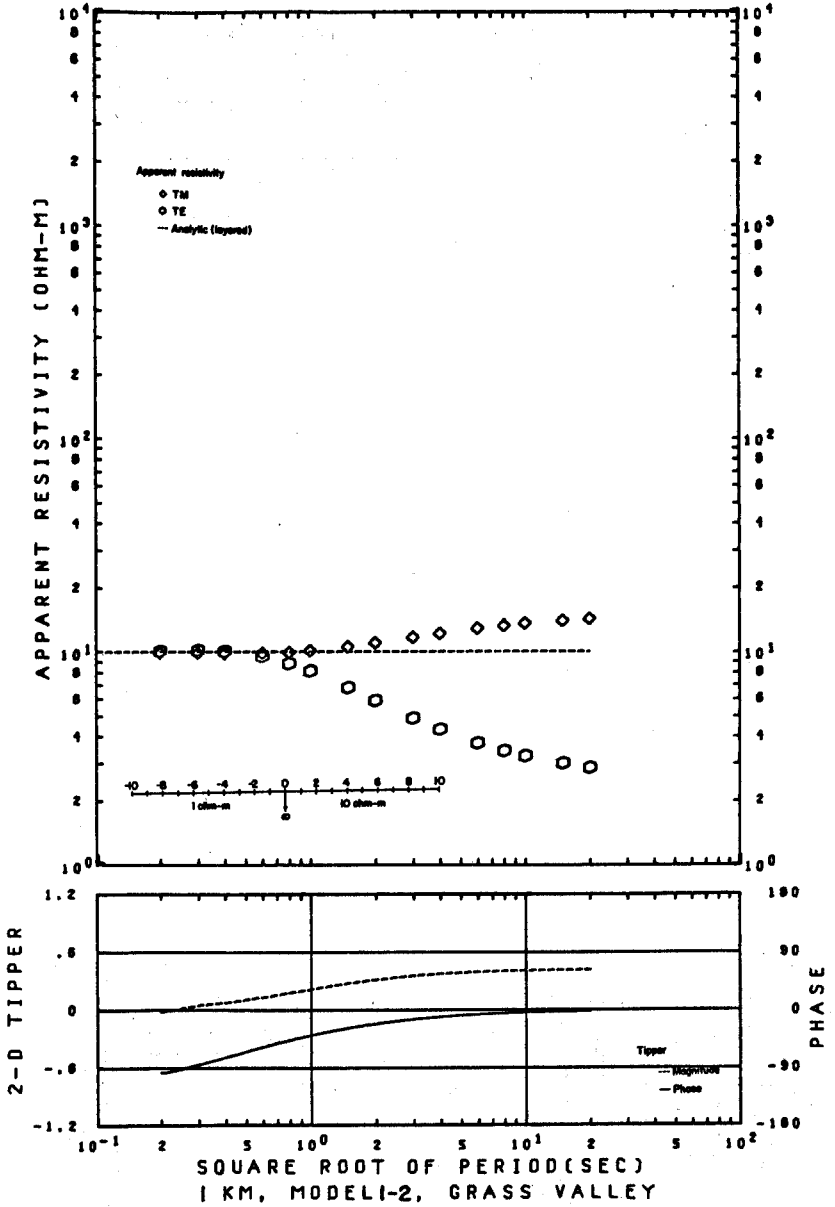
APPARENT RESISTIVITY (OHM-M)
Apparent resistivity
TM
TE
Analytic (layered)
1 ohm-m
10 ohm-m
2-D TIPPER
PHASE
Tipper
Magnitude
Phase
SQUARE ROOT OF PERIOD(SEC)
1 KM, MODELI-2, GRASS VALLEY

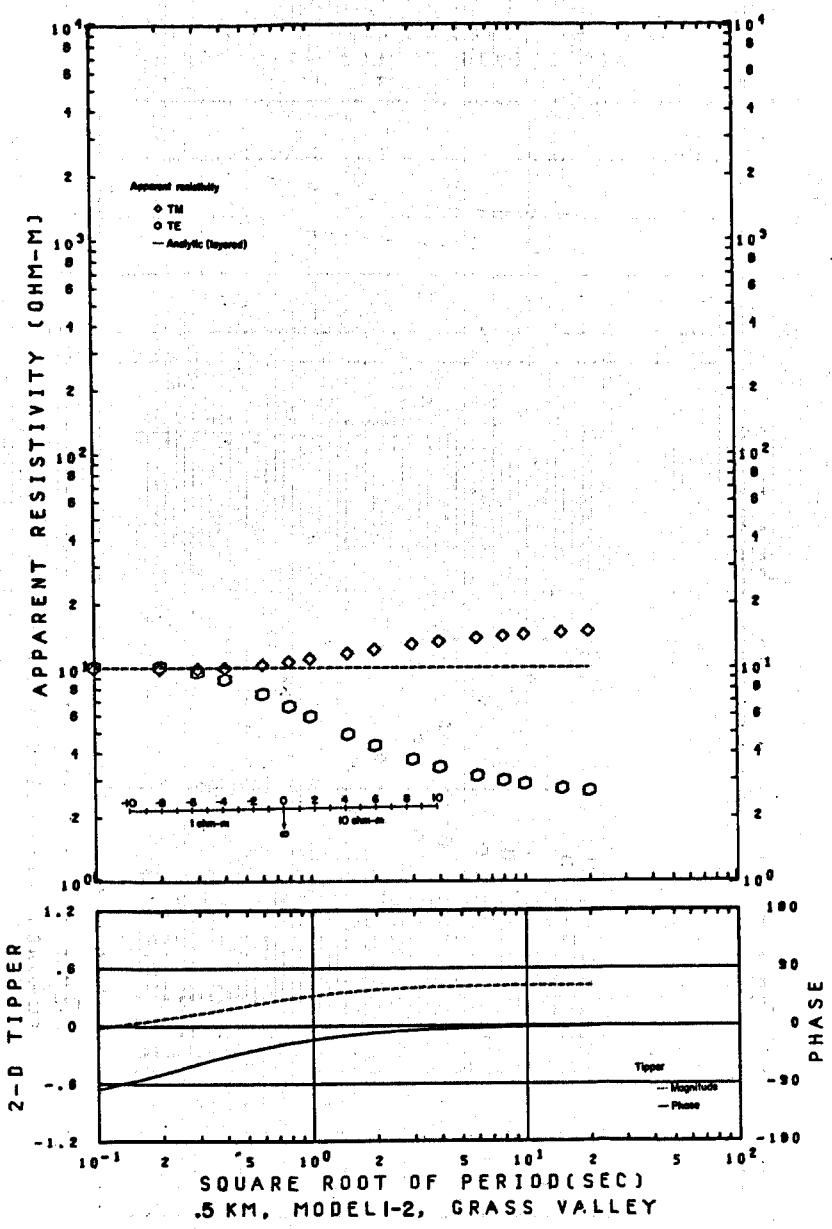
Apparent resistivity
TM
TE
Analytic (layered)
APPARENT RESISTIVITY (OHM-M)
1 ohm-m
10 ohm-m
2-D TIPPER
PHASE
Tipper
Magnitude
Phase
SQUARE ROOT OF PERIOD(SEC)
.5 KM, MODELI-2, GRASS VALLEY

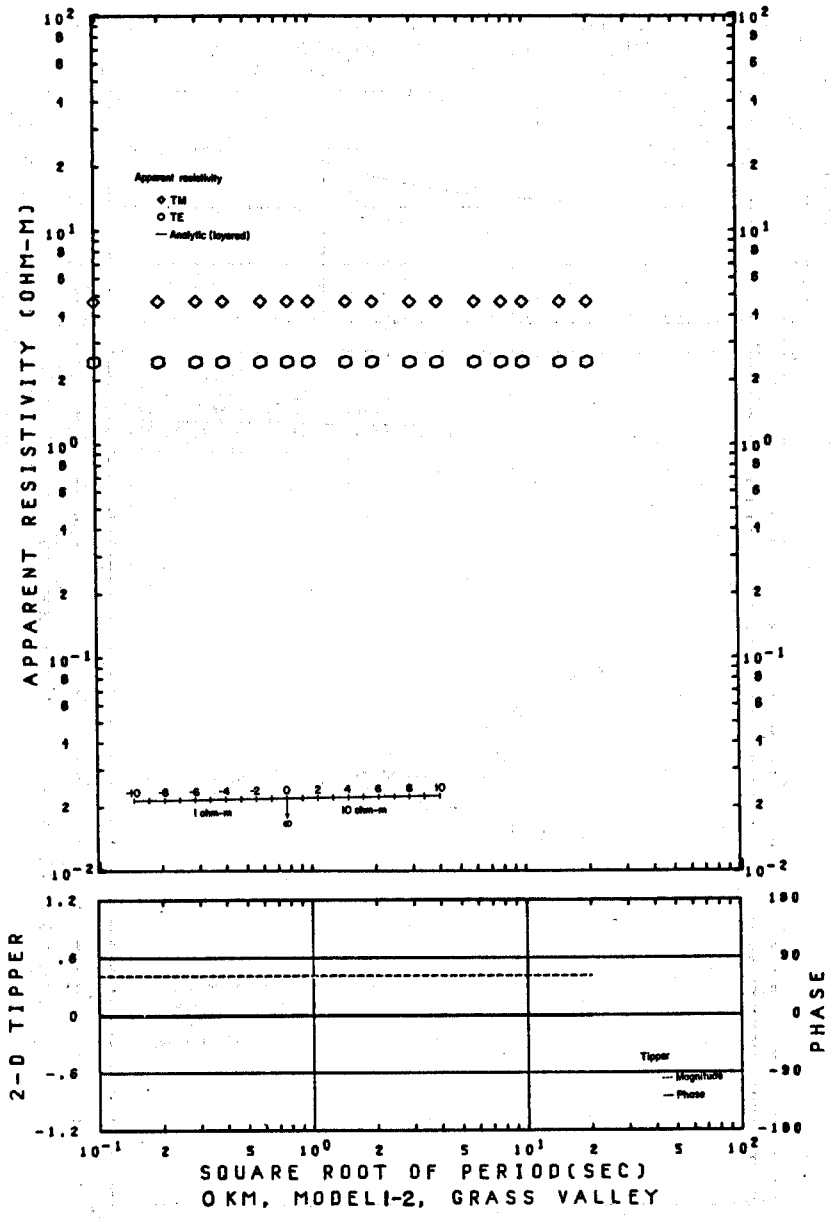
Apparent resistivity
TM
TE
Analytic (layered)
APPARENT RESISTIVITY (OHM-M)
1 ohm-m
10 ohm-m
2-D TIPPER
PHASE
Tipper
Magnitude
Phase
SQUARE ROOT OF PERIOD(SEC)
0 KM, MODELI-2, GRASS VALLEY

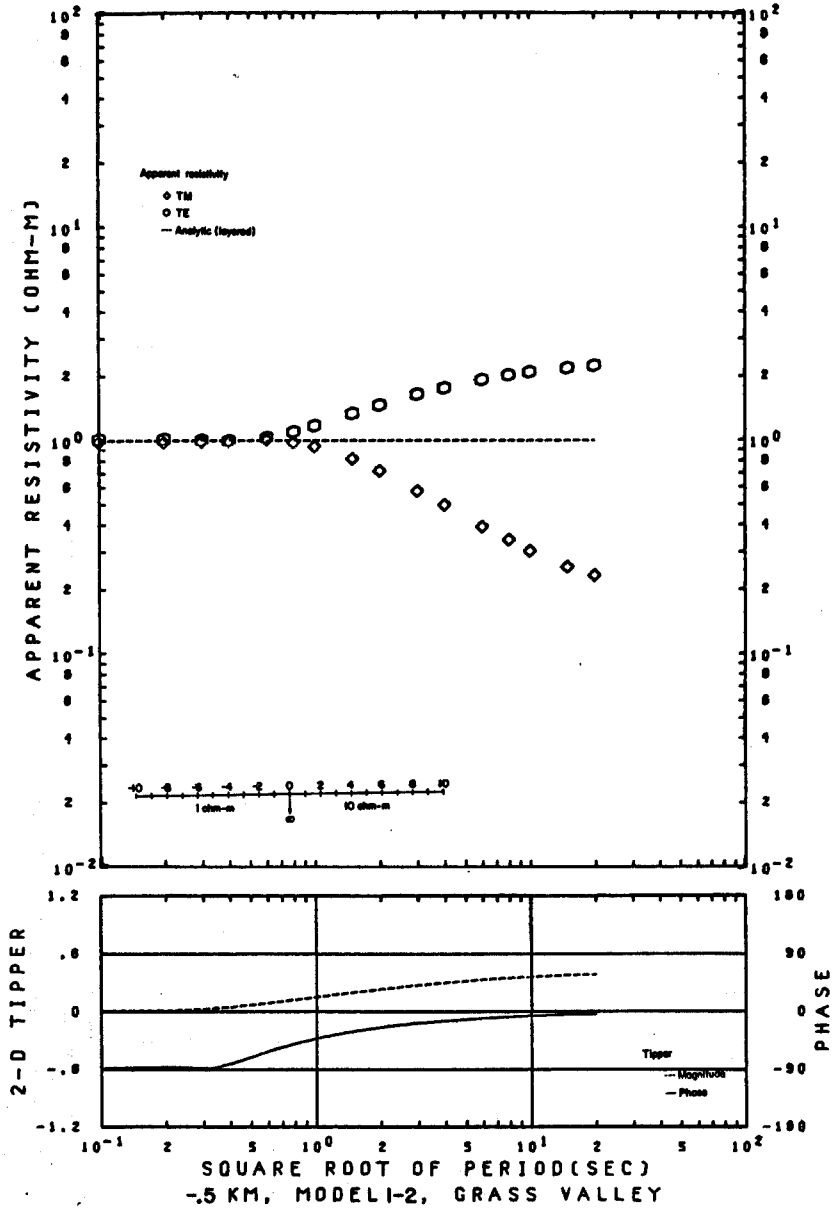
APPARENT RESISTIVITY (OHM-M)
Apparent resistivity
TM
TE
Analytic (layered)
1 ohm-m
10 ohm-m
2-D TIPPER
PHASE
Tipper
Magnitude
Phase
SQUARE ROOT OF PERIOD(SEC)
-.5 KM, MODELI-2, GRASS VALLEY

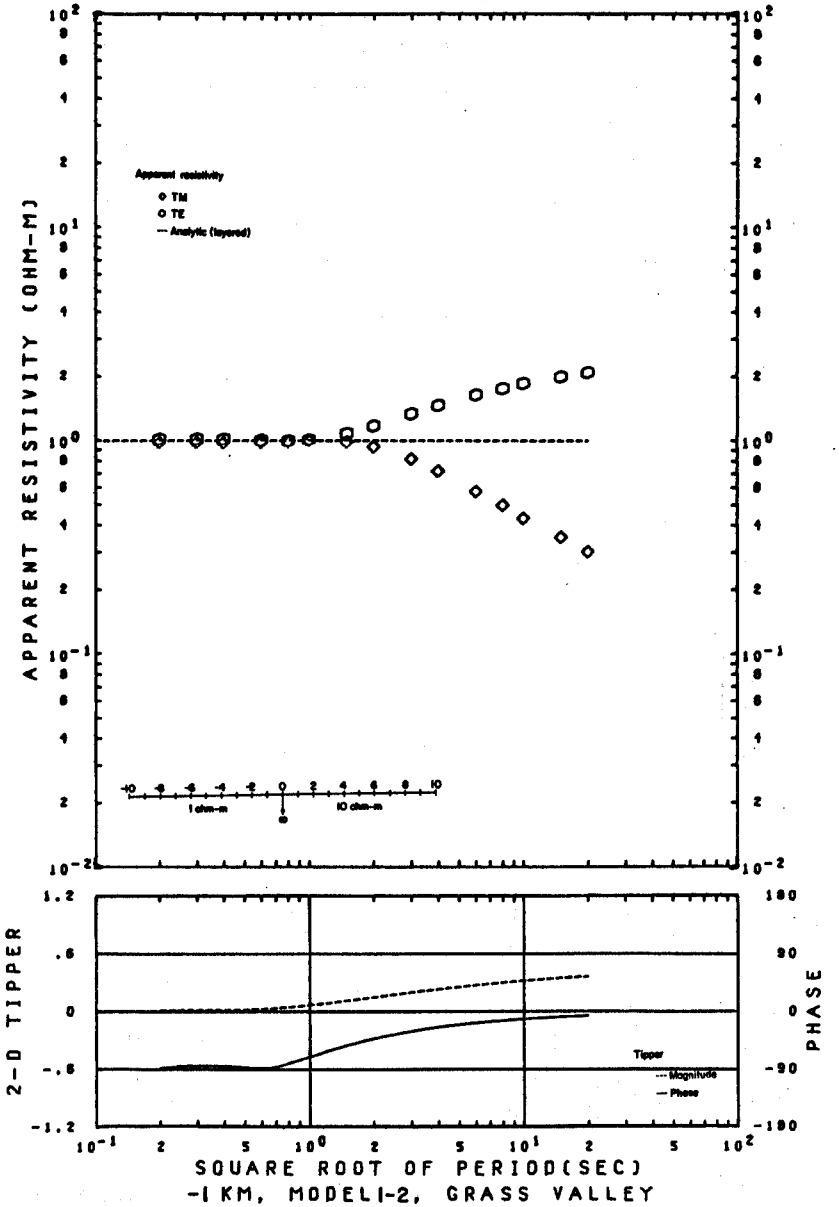
APPARENT RESISTIVITY (OHM-M)
Apparent resistivity
TM
TE
Analytic (layered)
1 ohm-m
10 ohm-m
2-D TIPPER
PHASE
Tipper
Magnitude
Phase
SQUARE ROOT OF PERIOD(SEC)
-1 KM, MODELI-2, GRASS VALLEY

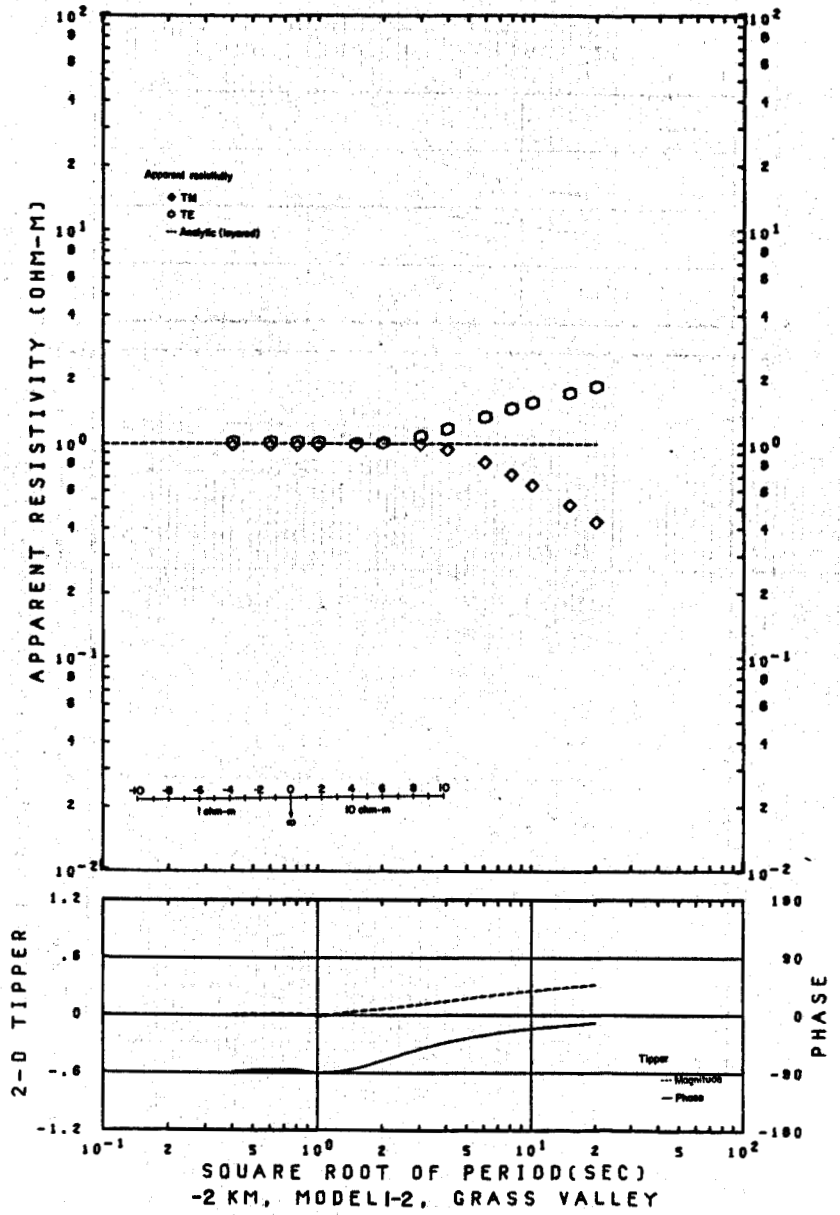

-2 KM, MODELI-2, GRASS VALLEY

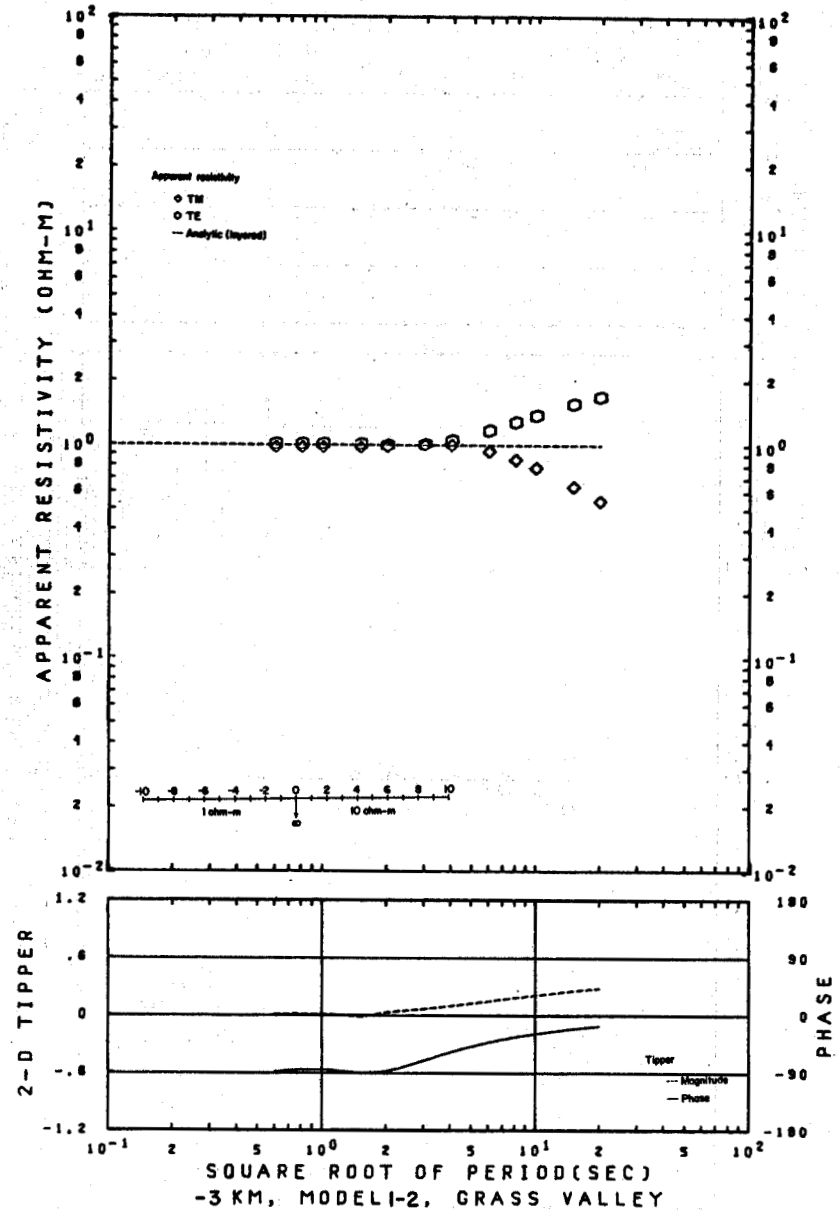

-3 KM, MODELI-2, GRASS VALLEY

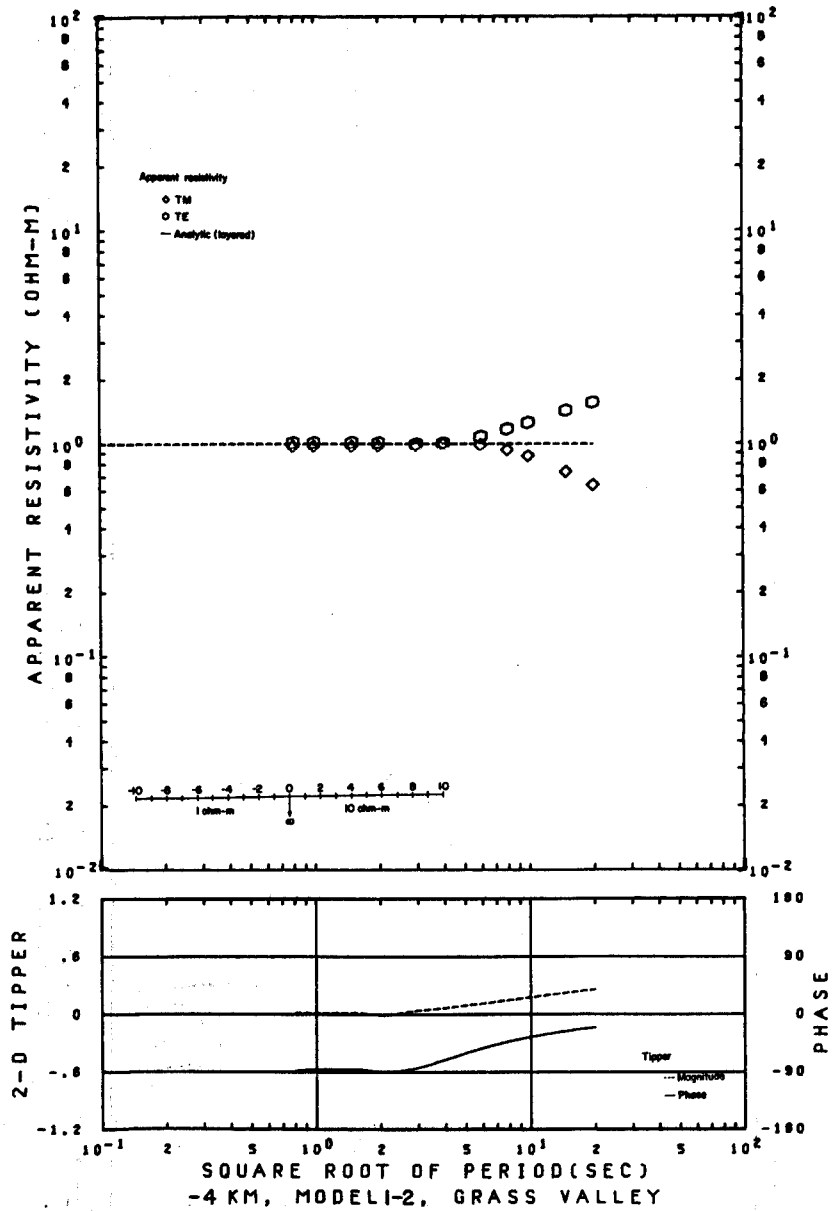
APPARENT RESISTIVITY (OHM-M)
Apparent resistivity
TM
TE
Analytic (layered)
1 ohm-m
10 ohm-m
2-D TIPPER
PHASE
Tipper
Magnitude
Phase
SQUARE ROOT OF PERIOD(SEC)
-4 KM, MODELI-2, GRASS VALLEY

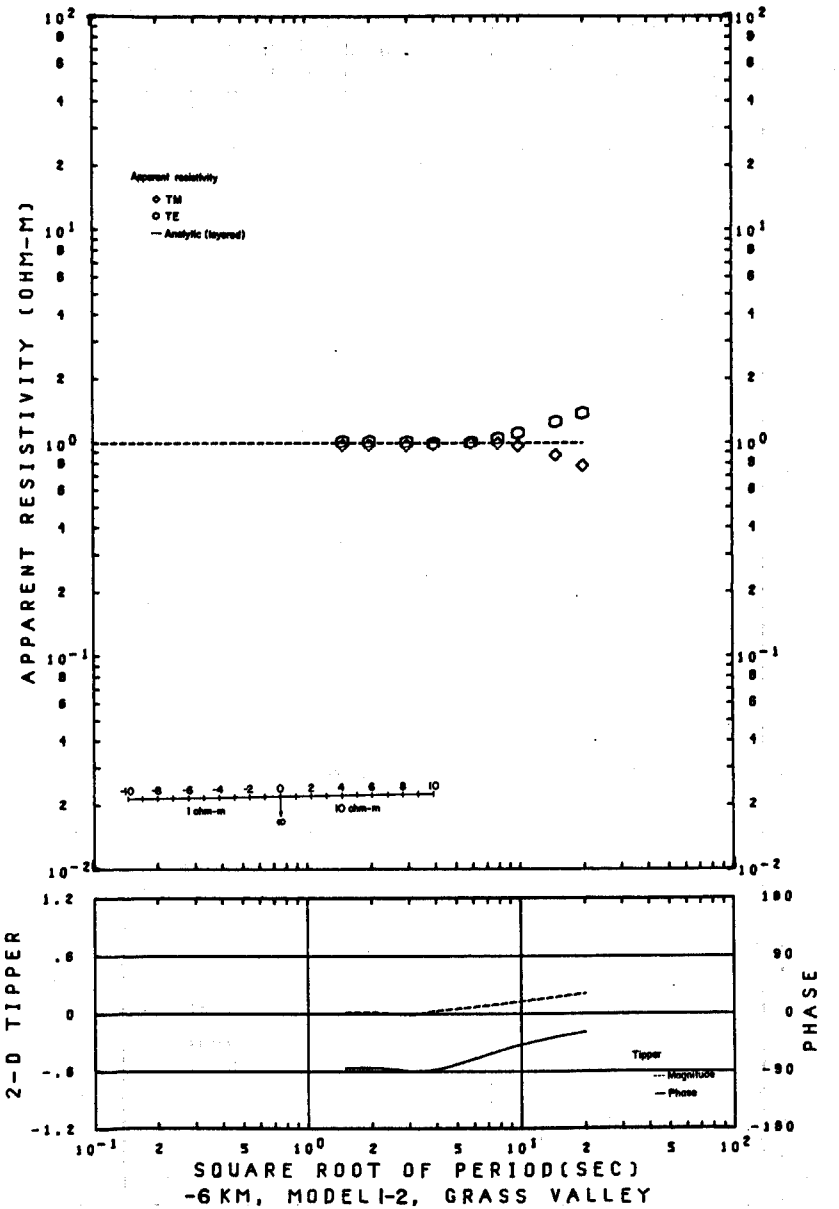
APPARENT RESISTIVITY (OHM-M)
Apparent resistivity
TM
TE
Analytic (layered)
1 ohm-m
10 ohm-m
2-D TIPPER
PHASE
Tipper
Magnitude
Phase
SQUARE ROOT OF PERIOD(SEC)
-6 KM, MODELI-2, GRASS VALLEY

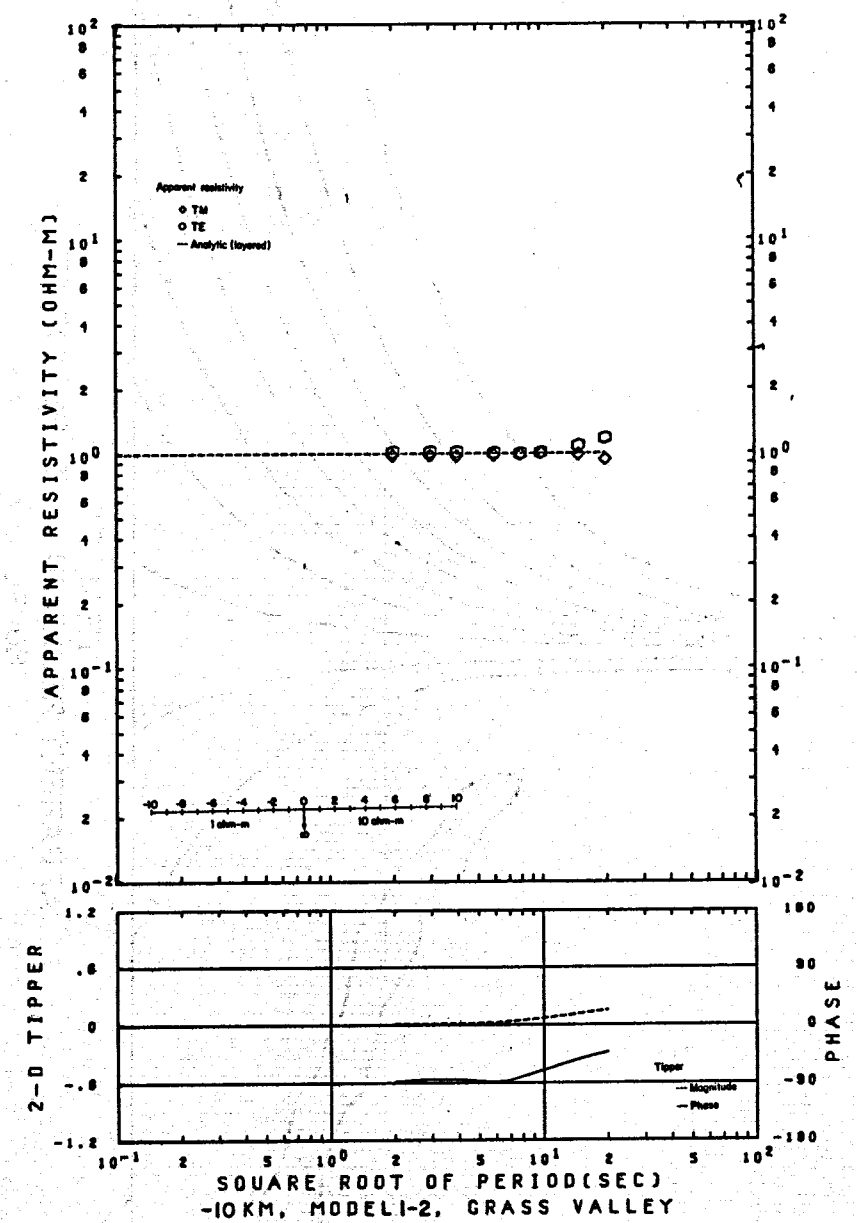
Apparent resistivity
TM
TE
Analytic (layered)
APPARENT RESISTIVITY (OHM-M)
1 ohm-m
10 ohm-m
2-D TIPPER
PHASE
Tipper
Magnitude
Phase
SQUARE ROOT OF PERIOD(SEC)
-10KM, MODEL1-2, GRASS VALLEY

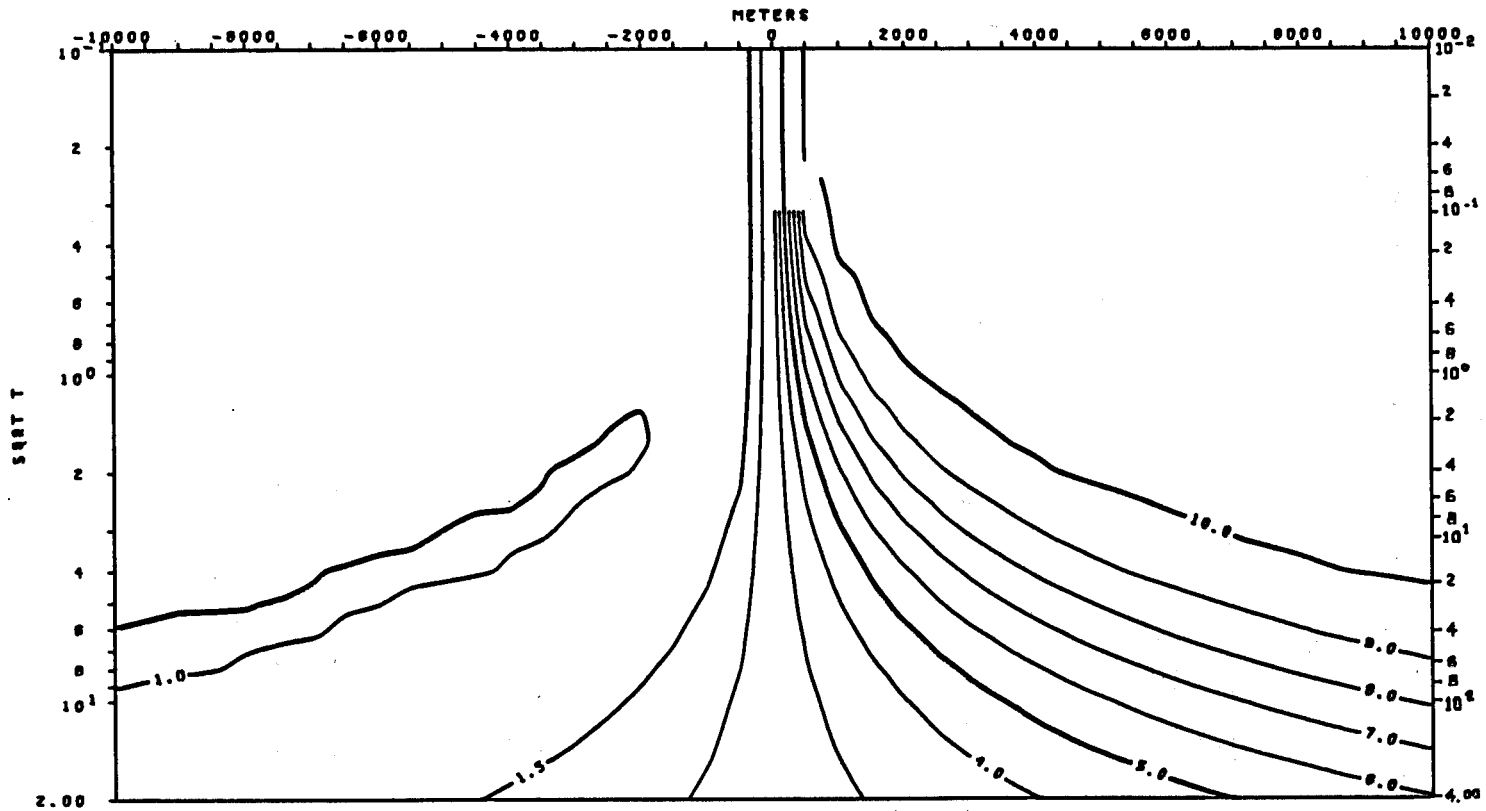

TE MODE
APPARENT RESISTIVITY VS. PERIOD (T)
MODEL 1-2

XBL 786-1916

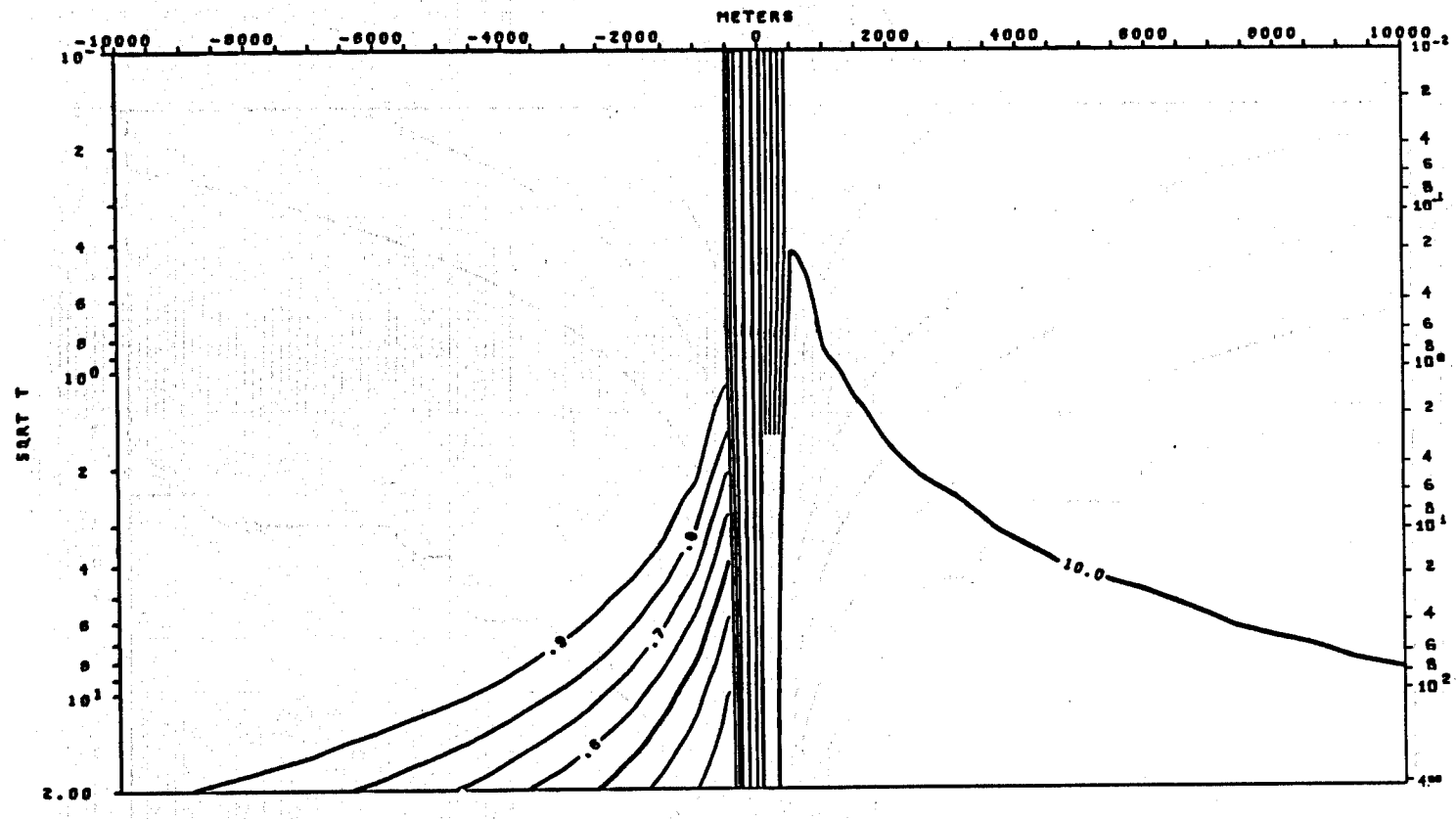

TM MODE
APPARENT RESISTIVITY VS. PERIOD (T)
MODEL 1-2

XBL 786-1915

T

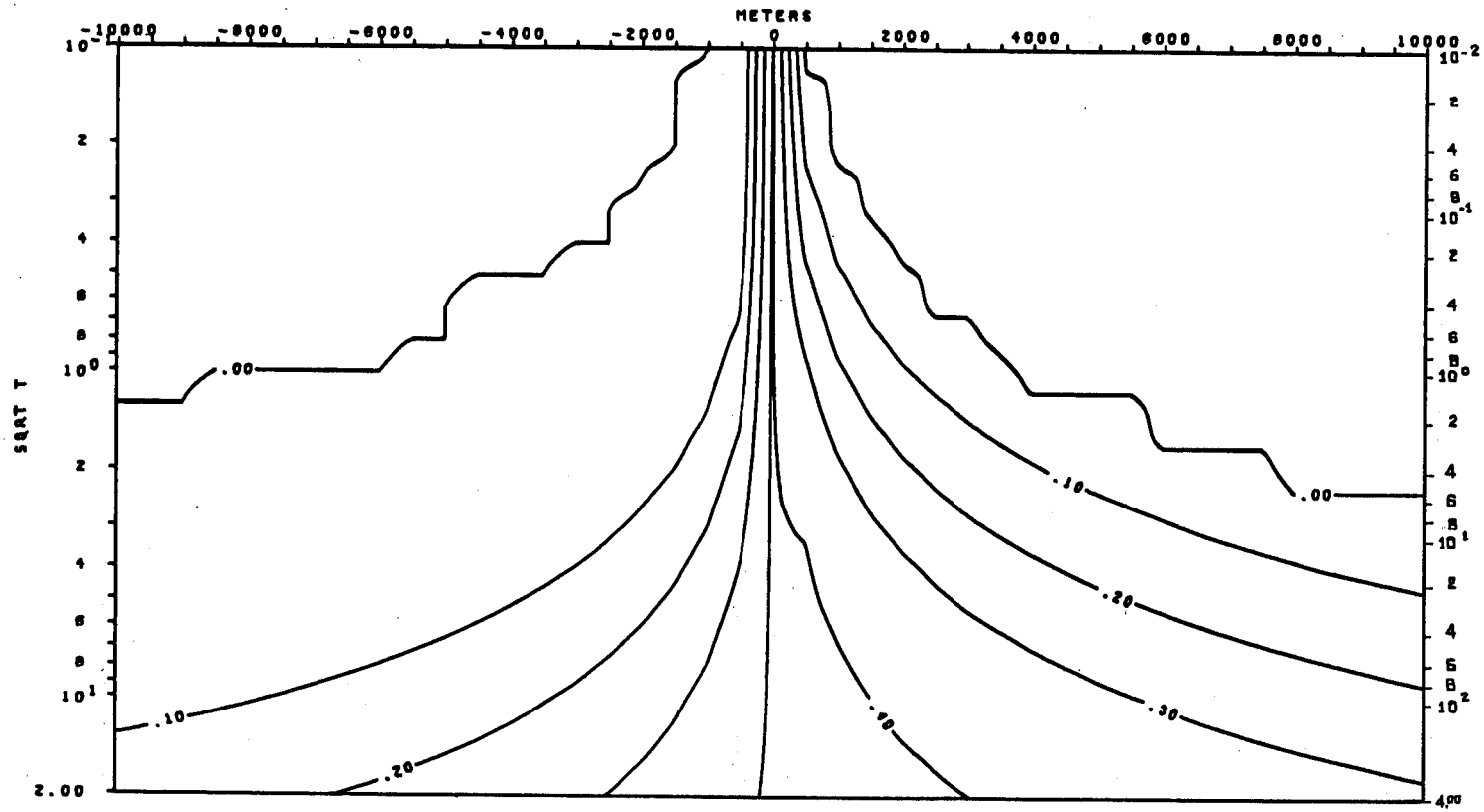

TIPPER VS. PERIOD (T)
MODEL 1-2

XBL 786-1930

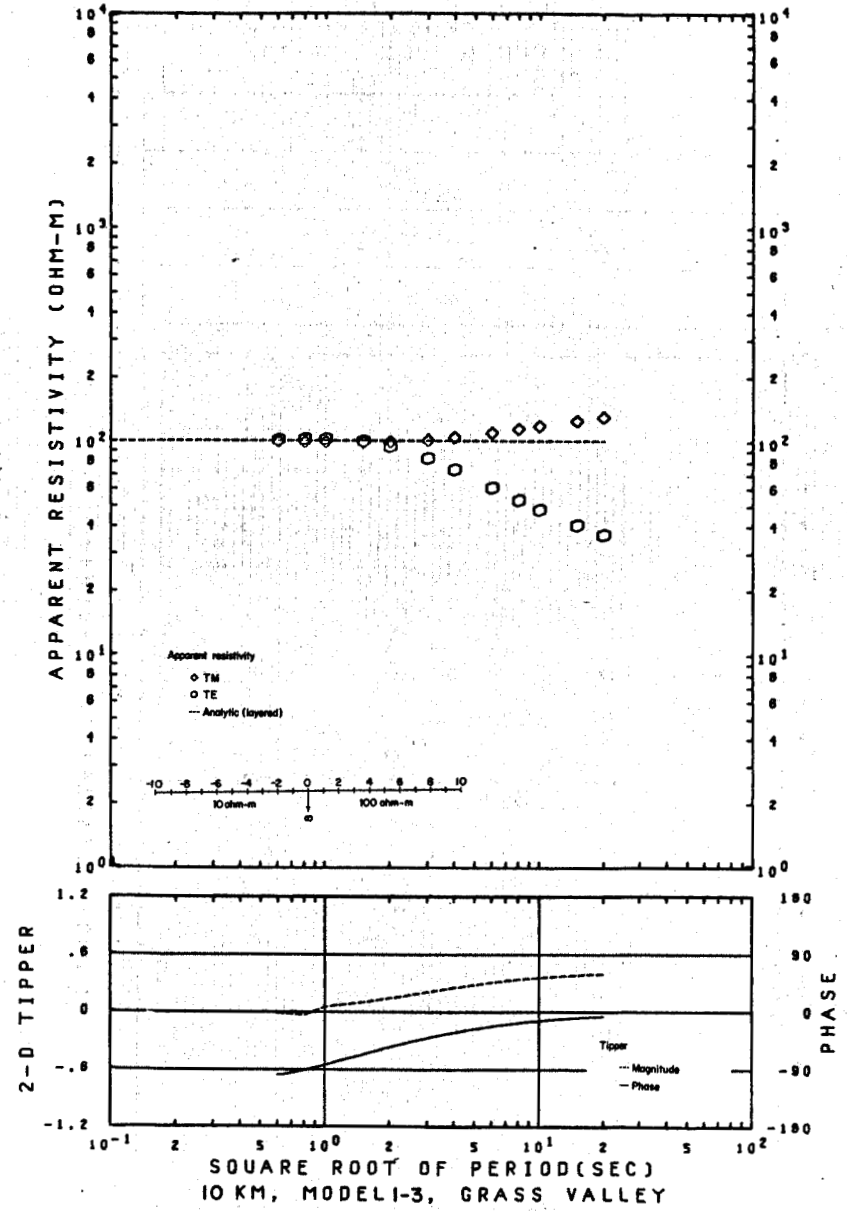

10 KM, MODEL1-3, GRASS VALLEY

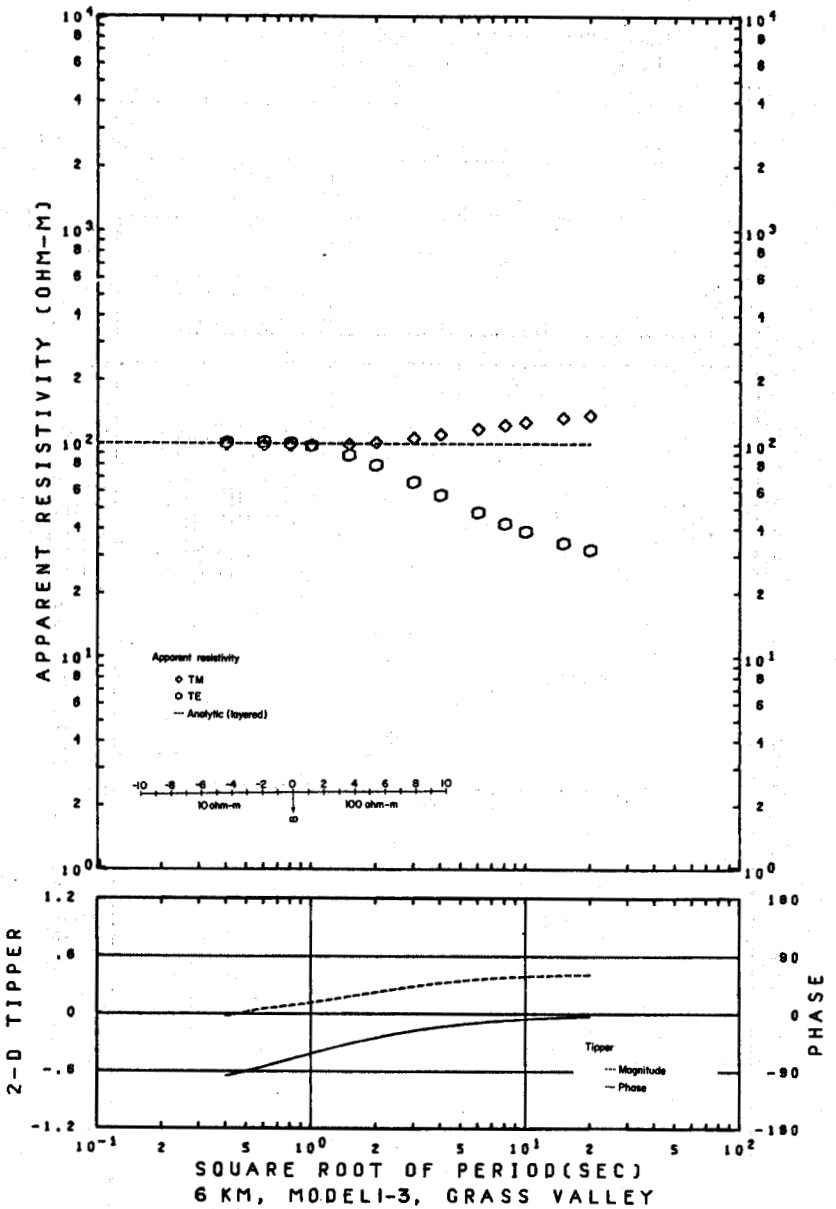

6 KM, MODEL1-3, GRASS VALLEY

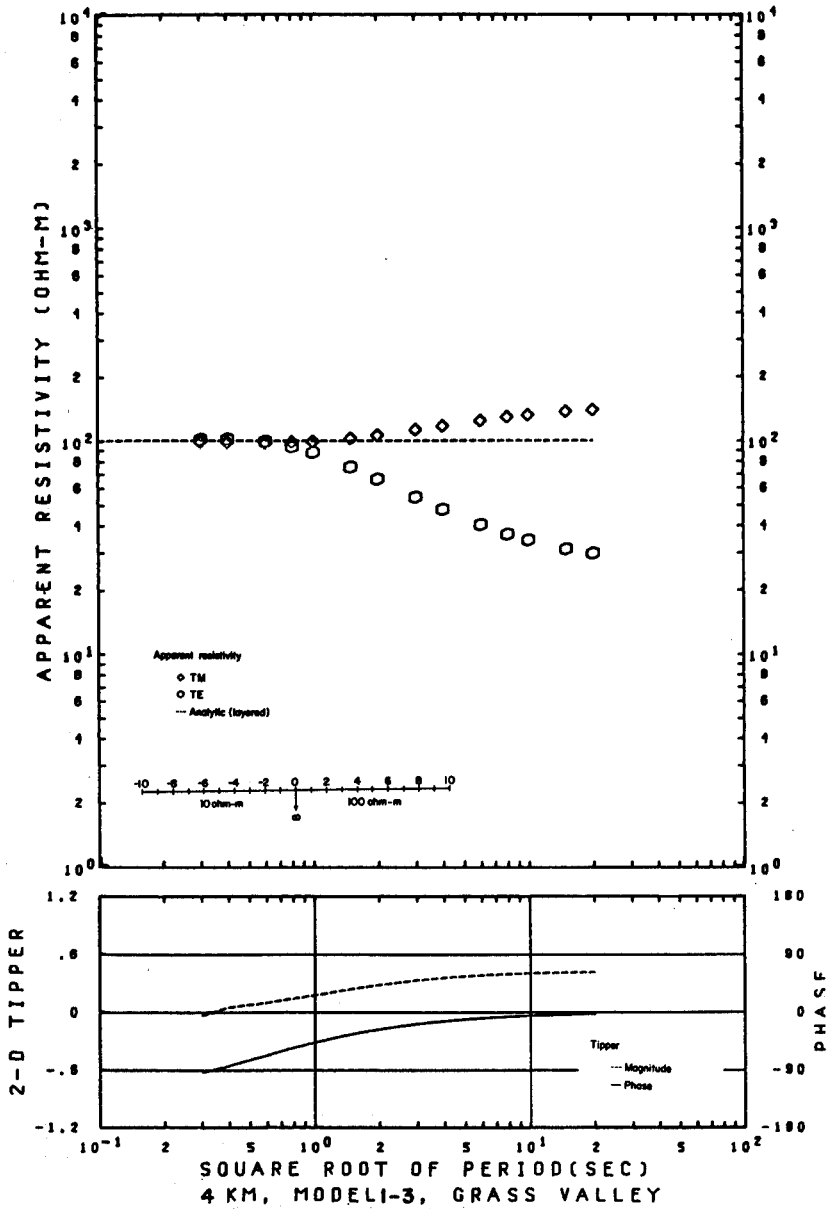
APPARENT RESISTIVITY (OHM-M)
Apparent resistivity
TM
TE
Analytic (layered)
10 ohm-m
100 ohm-m
2-D TIPPER
PHASE
Tipper
Magnitude
Phase
SQUARE ROOT OF PERIOD(SEC)
4 KM, MODELI-3, GRASS VALLEY

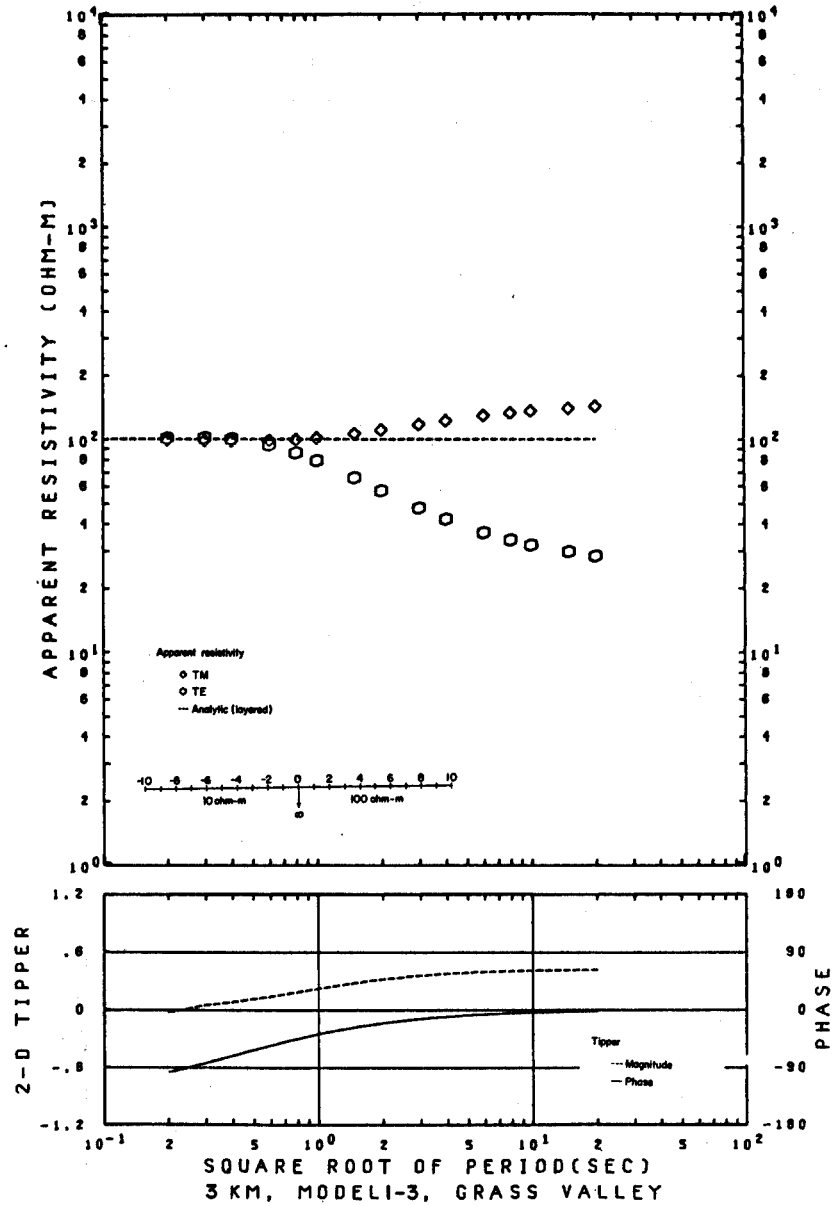
APPARENT RESISTIVITY (OHM-M)
Apparent resistivity
TM
TE
Analytic (layered)
10 ohm-m
100 ohm-m
2-D TIPPER
PHASE
Tipper
Magnitude
Phase
SQUARE ROOT OF PERIOD(SEC)
3 KM, MODELI-3, GRASS VALLEY

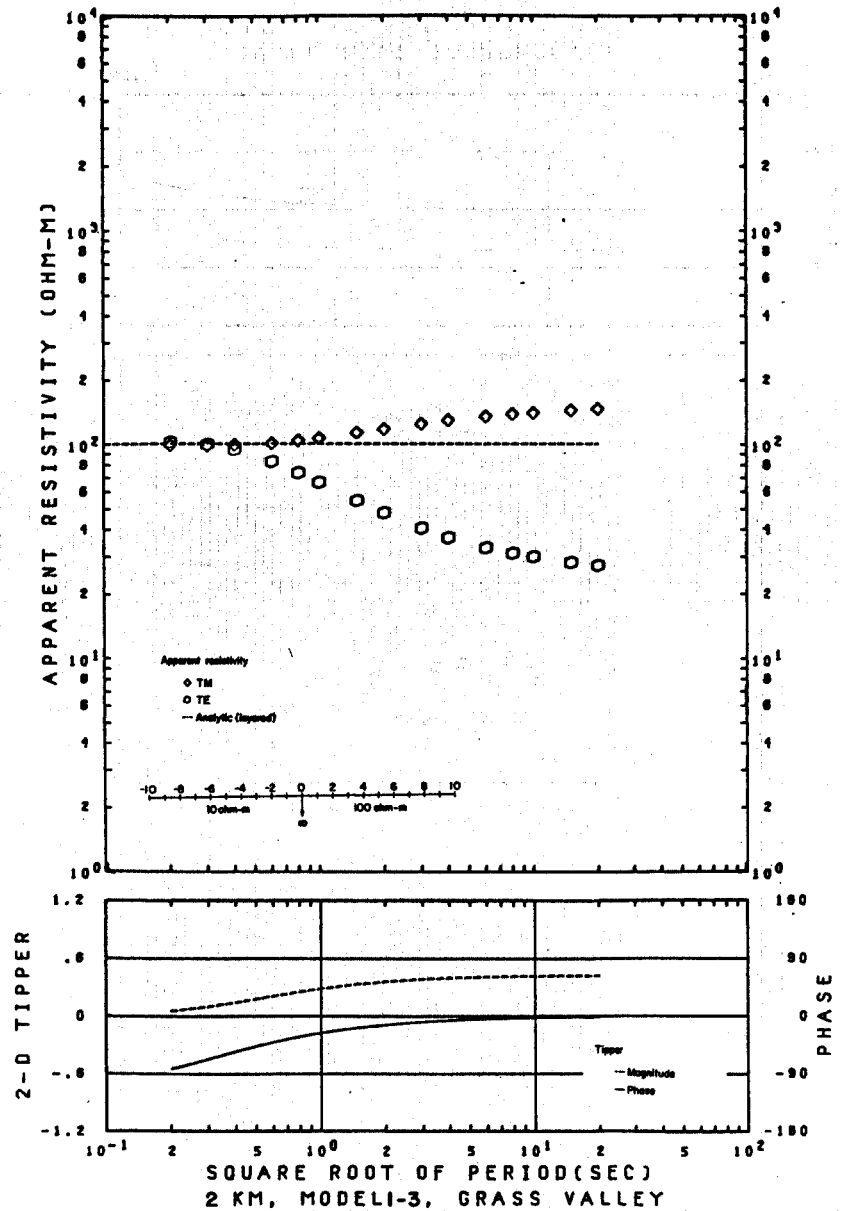
APPARENT RESISTIVITY (OHM-M)
Apparent resistivity
TM
TE
Analytic (layered)
10 ohm-m
100 ohm-m
2-D TIPPER
PHASE
Tipper
Magnitude
Phase
SQUARE ROOT OF PERIOD(SEC)
2 KM, MODELI-3, GRASS VALLEY

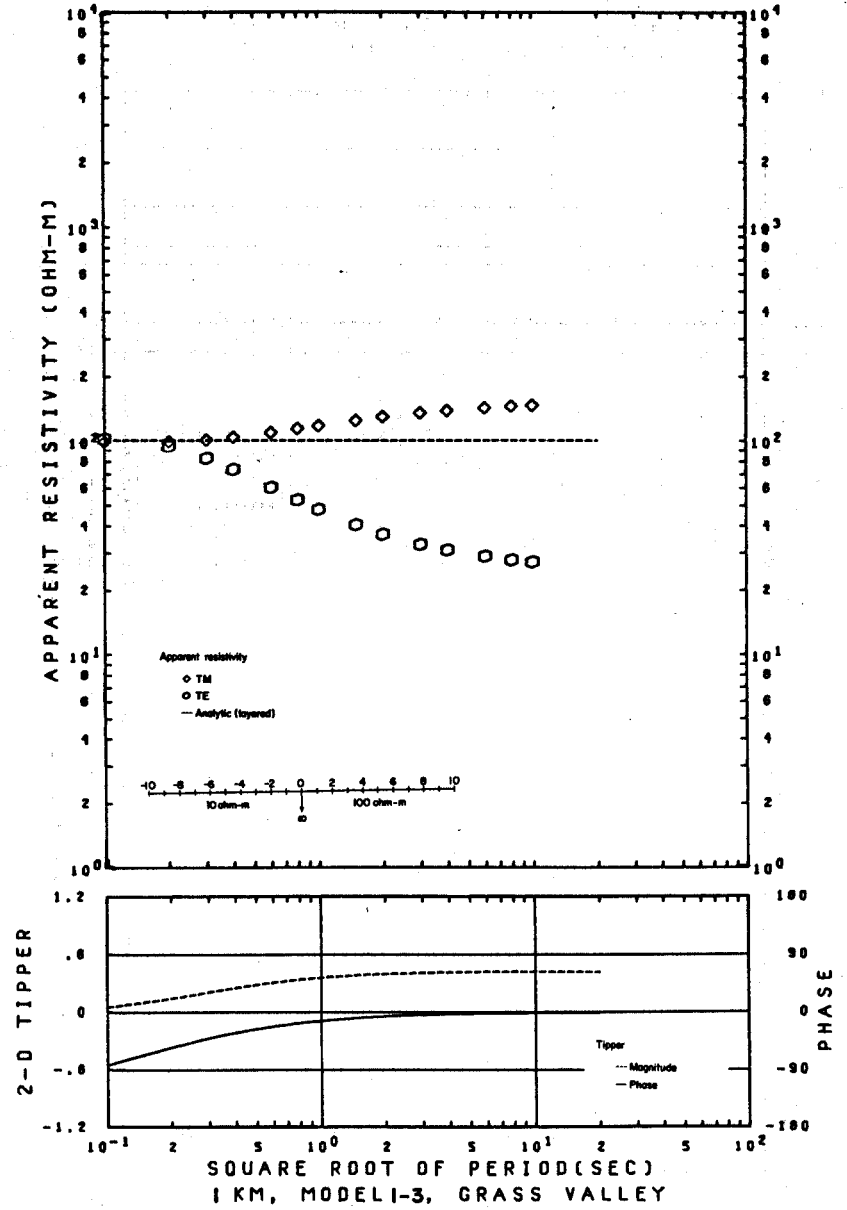
APPARENT RESISTIVITY (OHM-M)
Apparent resistivity
TM
TE
Analytic (layered)
10 ohm-m
100 ohm-m
2-D TIPPER
PHASE
Tipper
Magnitude
Phase
SQUARE ROOT OF PERIOD(SEC)
1 KM, MODELI-3, GRASS VALLEY

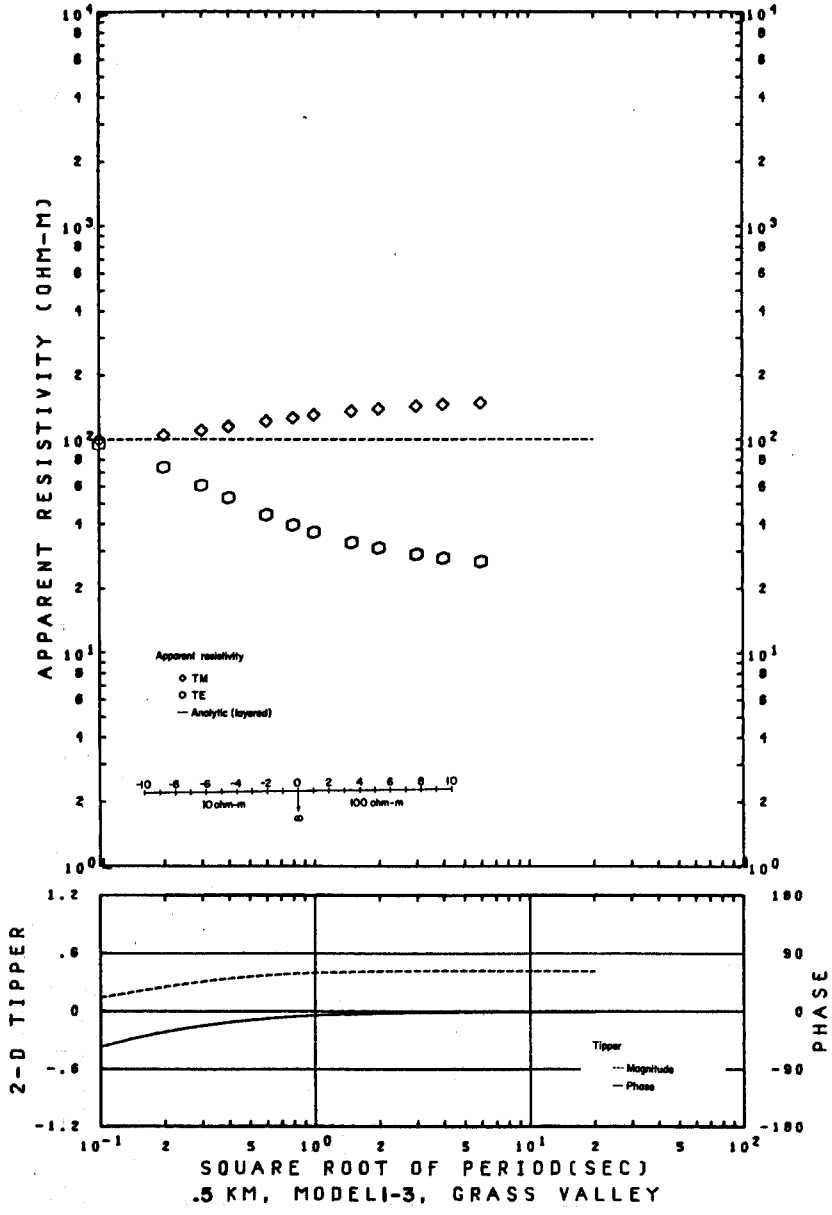
APPARENT RESISTIVITY (OHM-M)
Apparent resistivity
TM
TE
Analytic (layered)
10 ohm-m
100 ohm-m
2-D TIPPER
PHASE
Tipper
Magnitude
Phase
SQUARE ROOT OF PERIOD(SEC)
.5 KM, MODELI-3, GRASS VALLEY

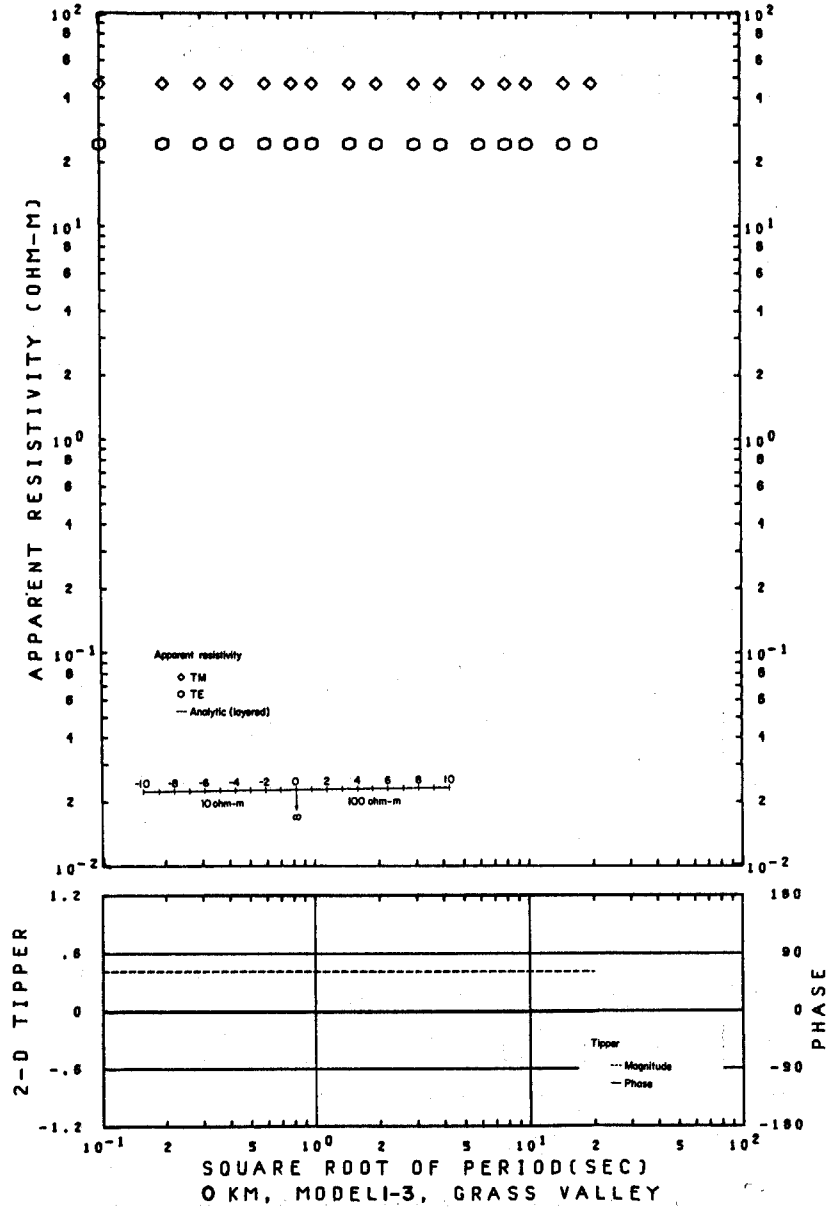
APPARENT RESISTIVITY (OHM-M)
Apparent resistivity
TM
TE
Analytic (layered)
10 ohm-m
100 ohm-m
2-D TIPPER
PHASE
Tipper
Magnitude
Phase
SQUARE ROOT OF PERIOD(SEC)
0 KM, MODELI-3, GRASS VALLEY

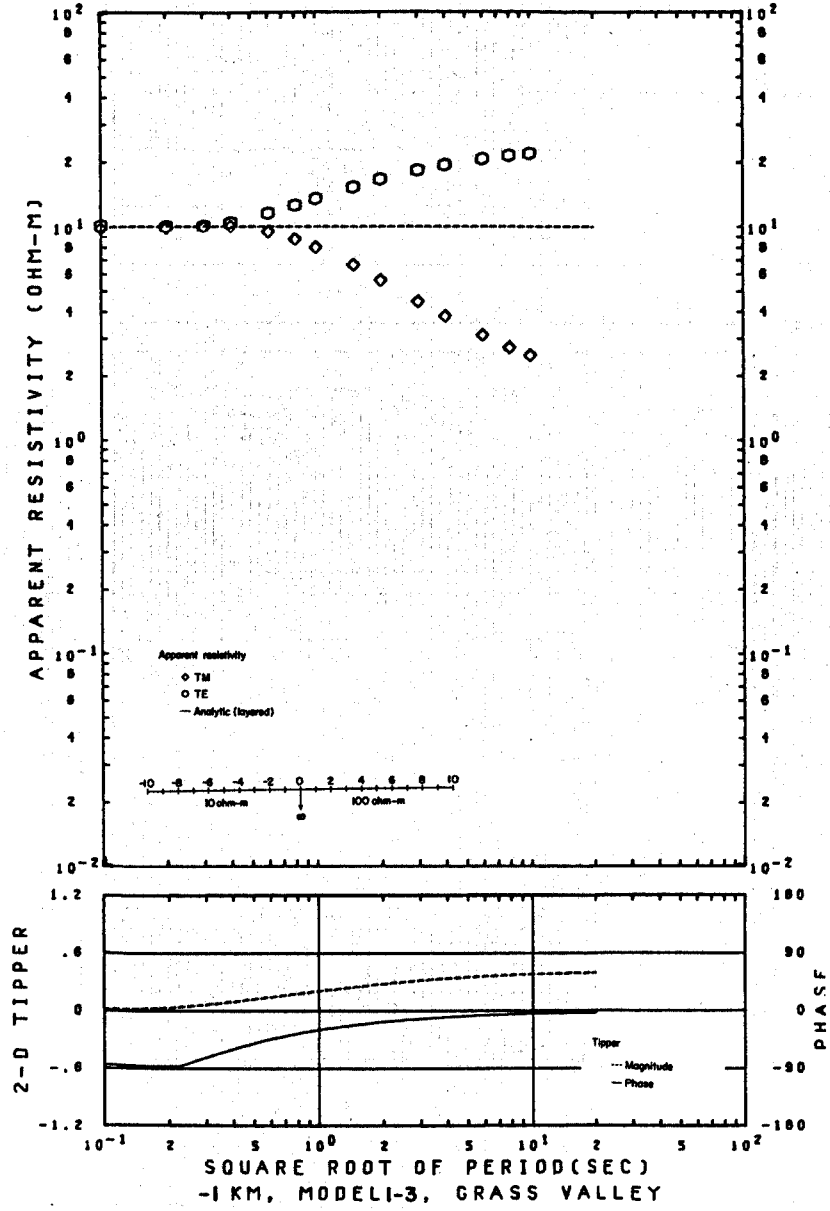
APPARENT RESISTIVITY (OHM-M)
Apparent resistivity
TM
TE
Analytic (layered)
10 ohm-m
100 ohm-m
2-D TIPPER
PHASE
Tipper
Magnitude
Phase
SQUARE ROOT OF PERIOD(SEC)
-1 KM, MODEL1-3, GRASS VALLEY

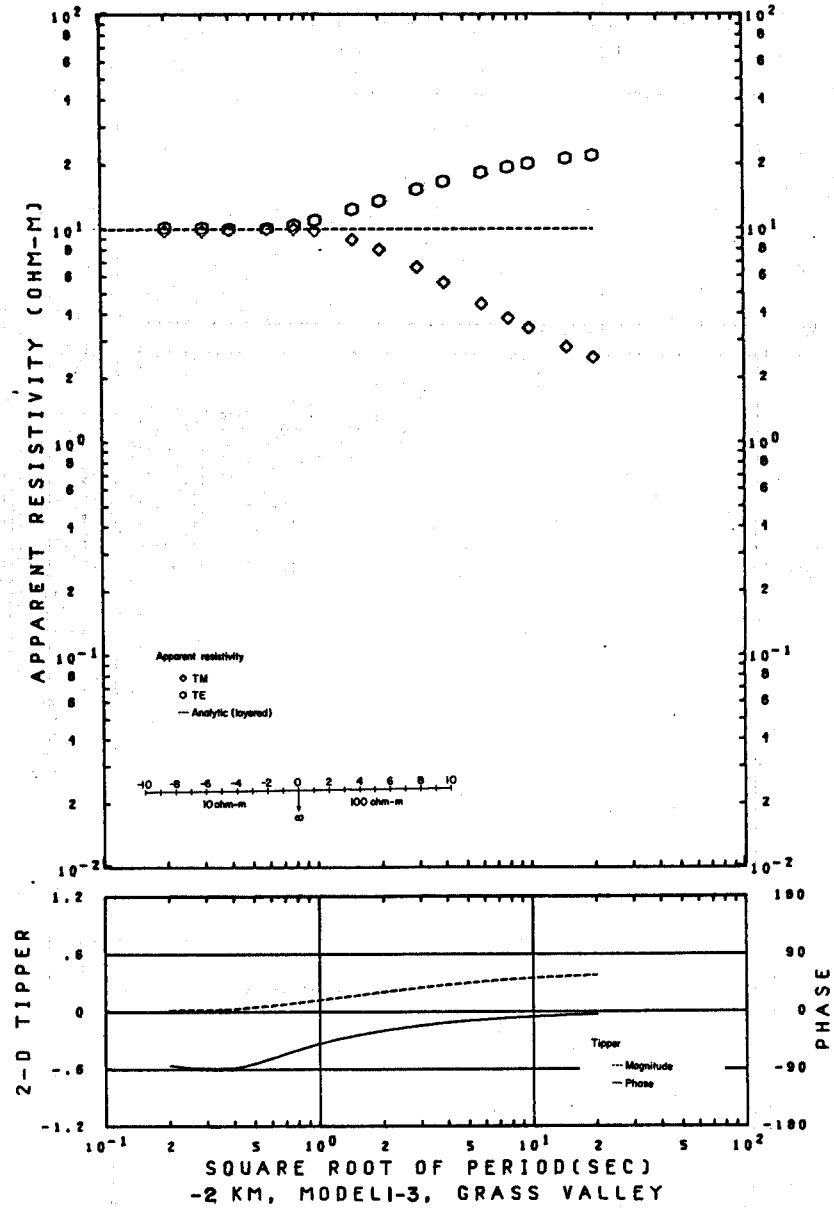
APPARENT RESISTIVITY (OHM-M)
Apparent resistivity
TM
TE
Analytic (layered)
10 ohm-m
100 ohm-m
2-D TIPPER
PHASE
Tipper
Magnitude
Phase
SQUARE ROOT OF PERIOD(SEC)
-2 KM, MODEL1-3, GRASS VALLEY

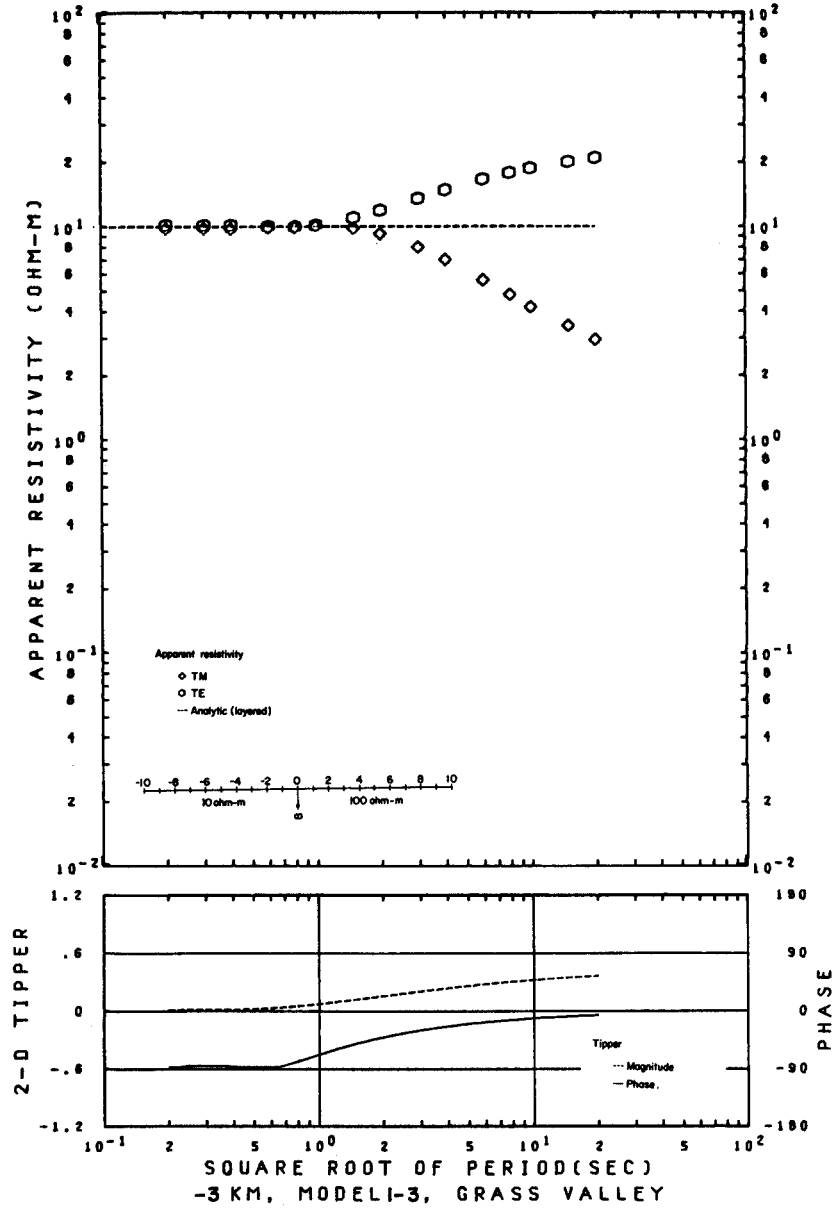
APPARENT RESISTIVITY (OHM-M)
Apparent resistivity
TM
TE
Analytic (layered)
10 ohm-m
100 ohm-m
2-D TIPPER
PHASE
Tipper
Magnitude
Phase
SQUARE ROOT OF PERIOD(SEC)
-3 KM, MODEL1-3, GRASS VALLEY

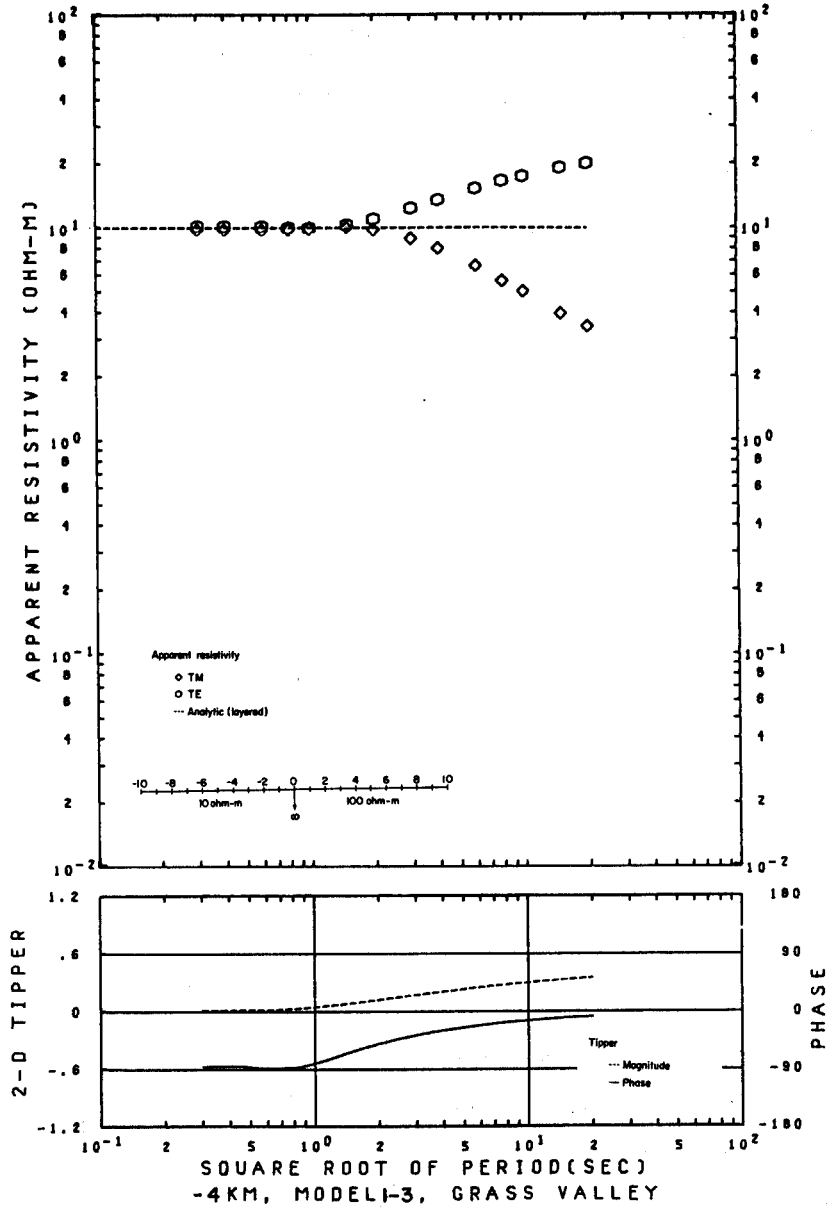
APPARENT RESISTIVITY (OHM-M)
Apparent resistivity
TM
TE
Analytic (layered)
10 ohm-m
100 ohm-m
2-D TIPPER
PHASE
Tipper
Magnitude
Phase
SQUARE ROOT OF PERIOD(SEC)
-4 KM, MODEL1-3, GRASS VALLEY

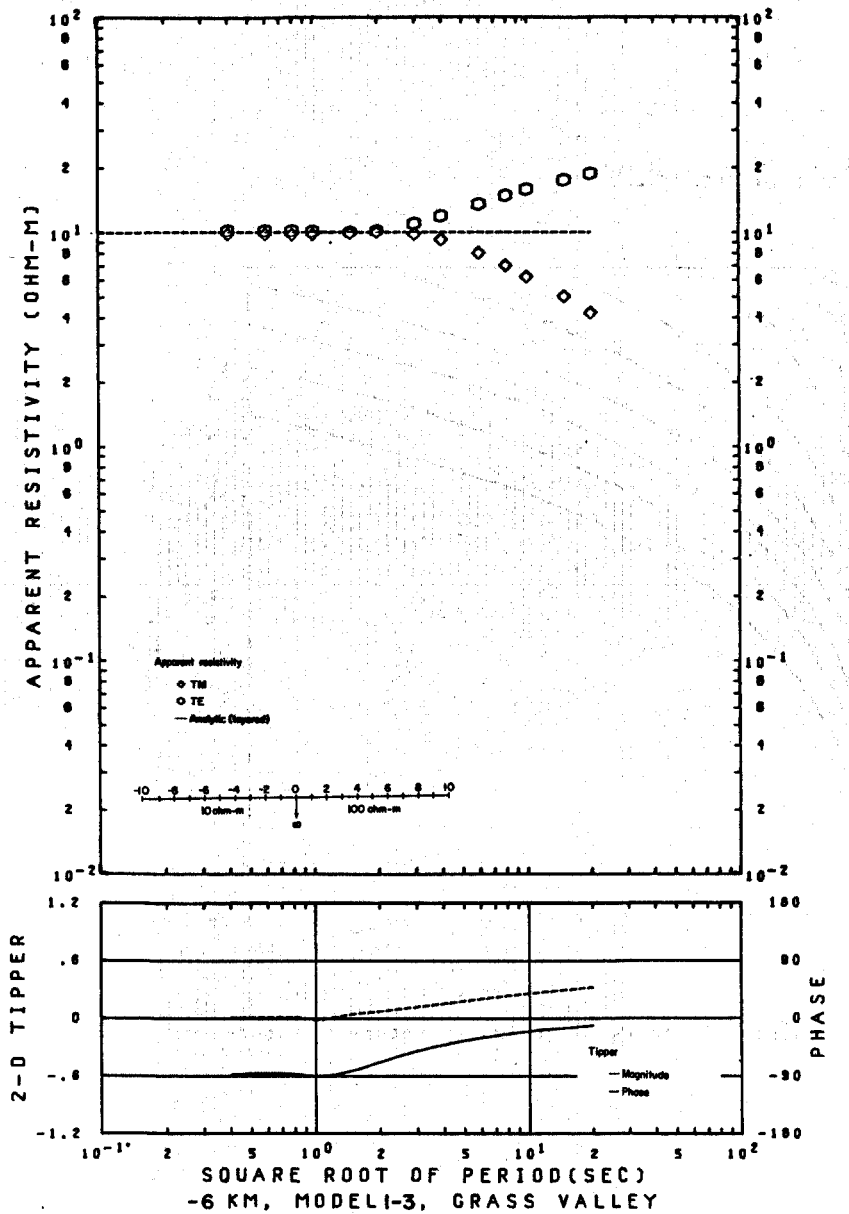

-6 KM, MODEL1-3, GRASS VALLEY

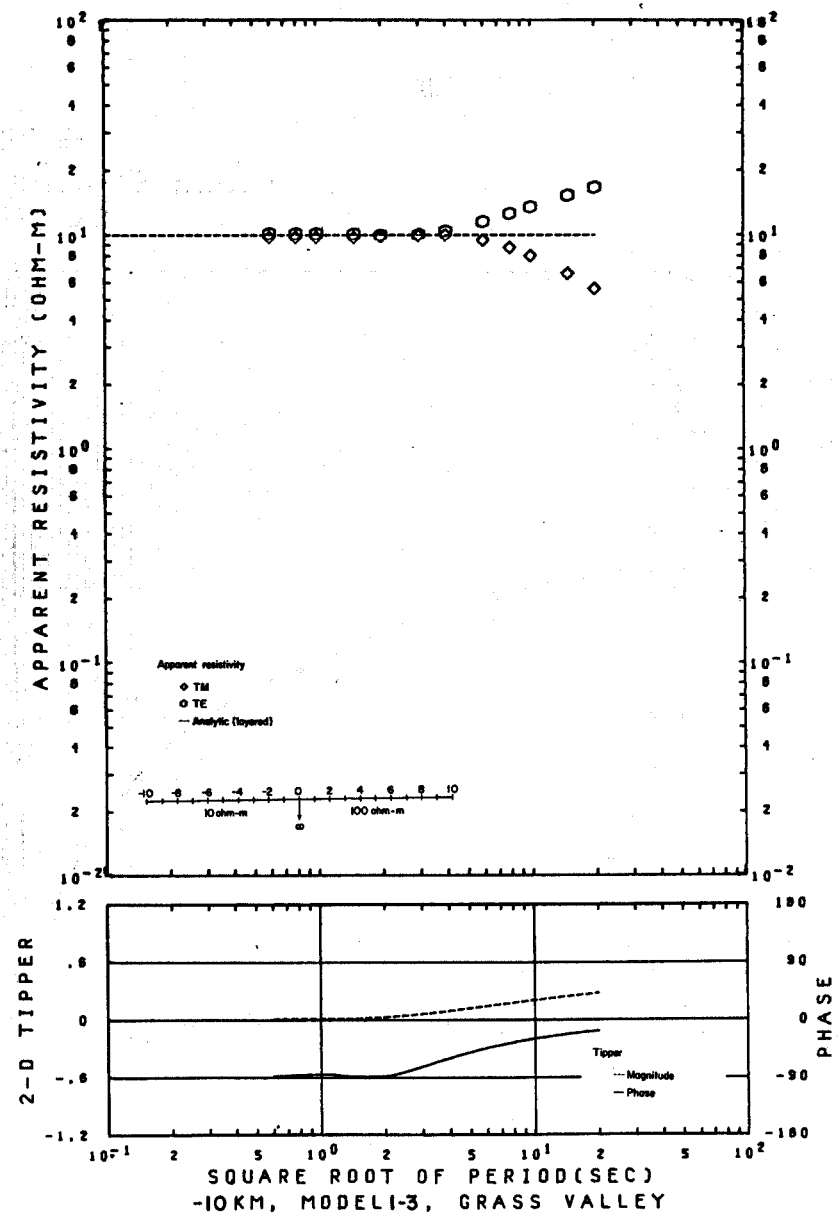

-10KM, MODEL1-3, GRASS VALLEY

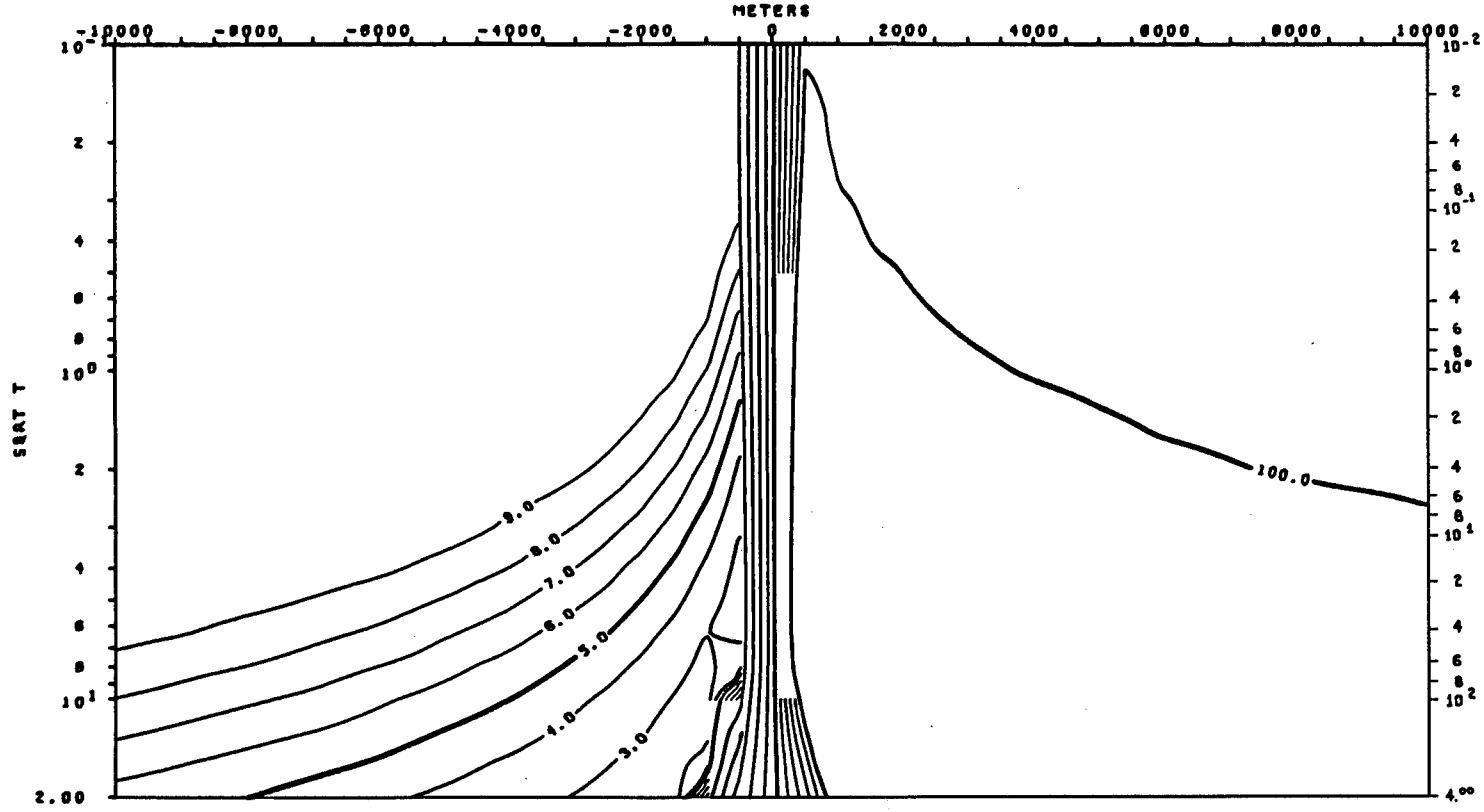

TE MODE
APPARENT RESISTIVITY VS. PERIOD (T)
MODEL 1-3

XBL 786-1906

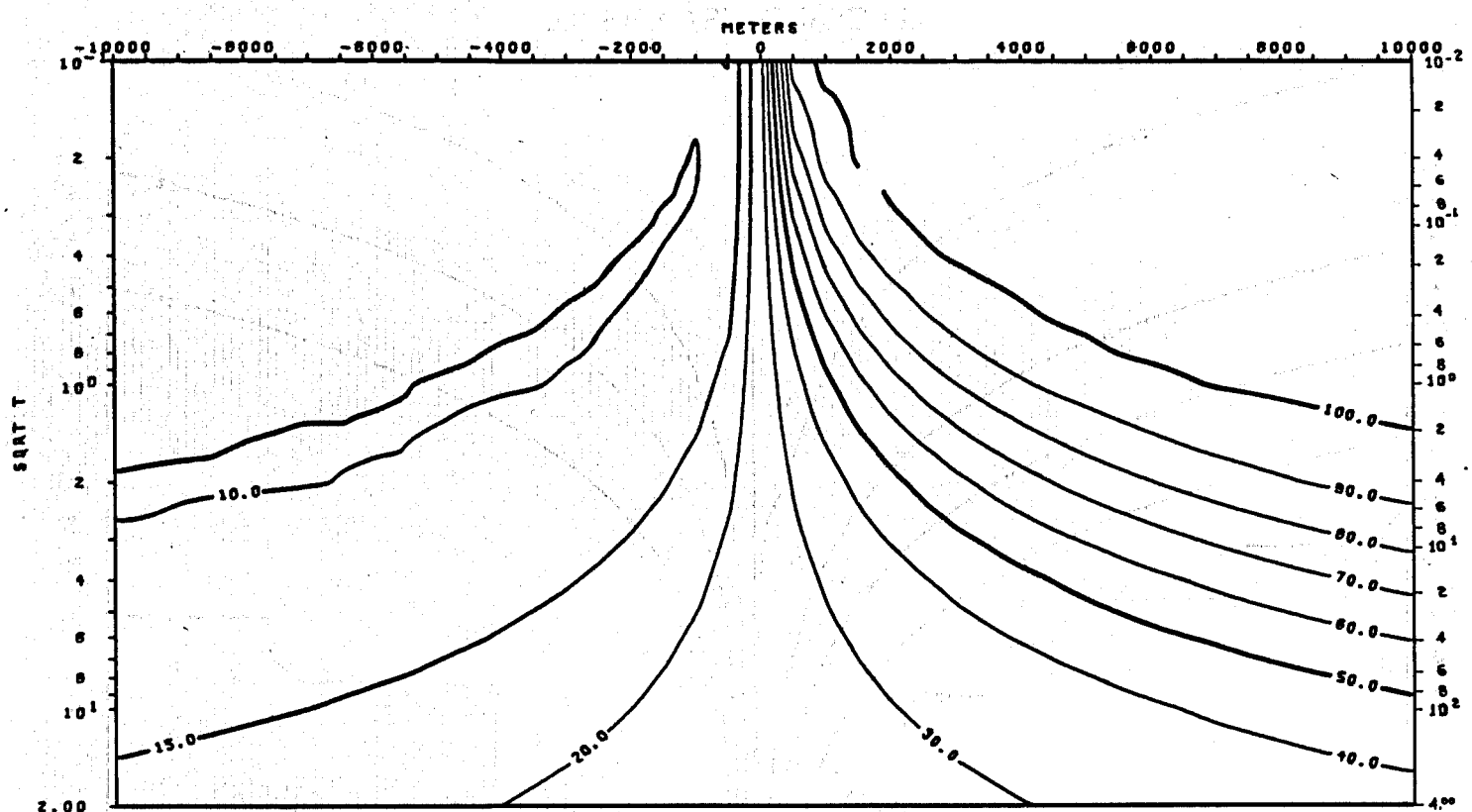

TM MODE
APPARENT RESISTIVITY VS. PERIOD (T)
MODEL 1-3

XBL 786-1902

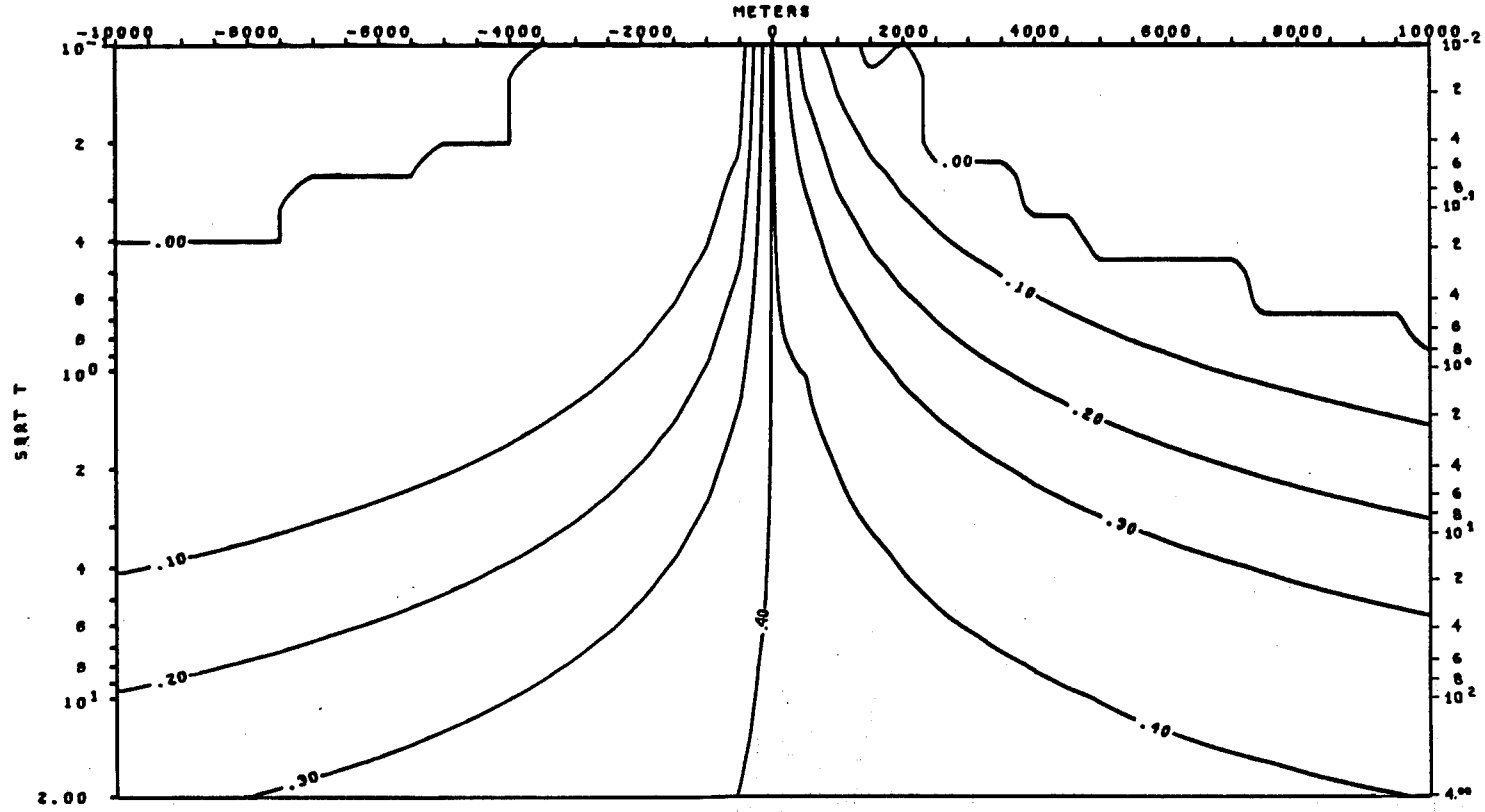

TIPPER VS. PERIOD (T)
MODEL 1-3

XBL 786-1932

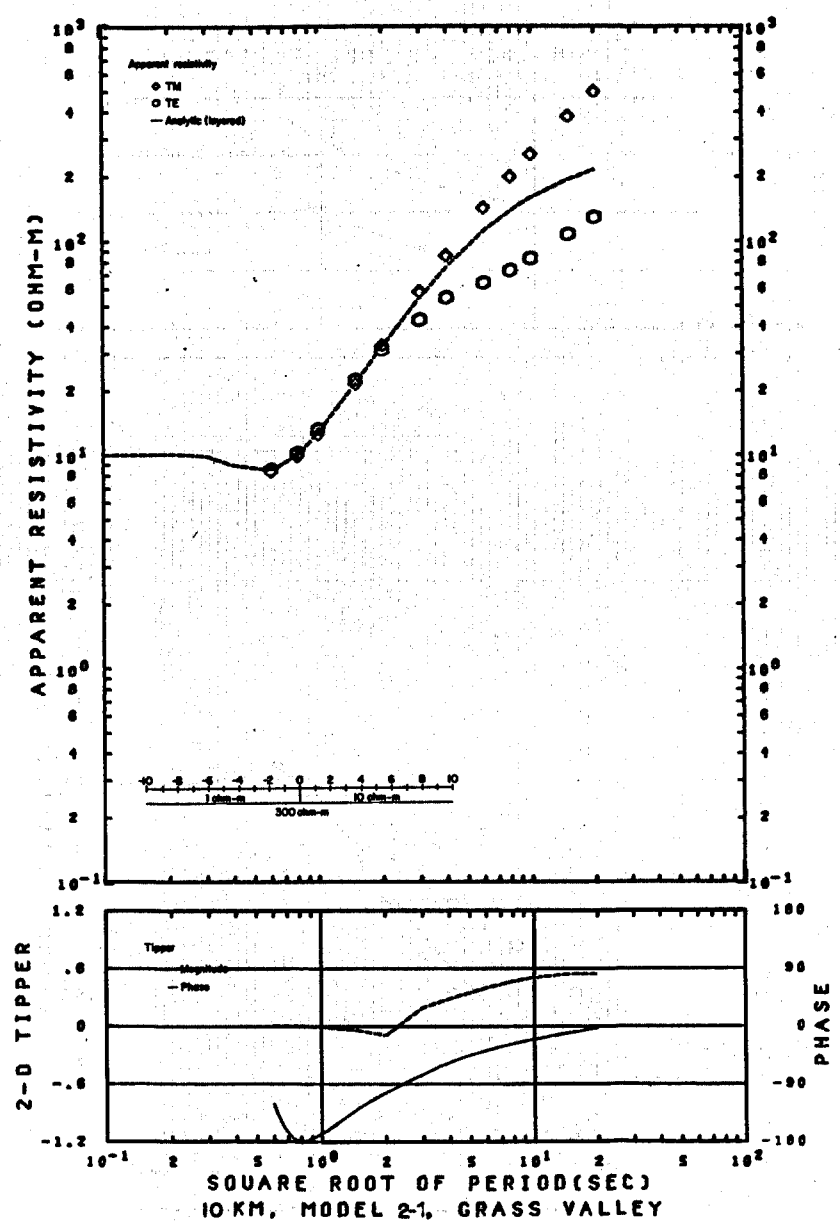

10 KM, MODEL 2-1, GRASS VALLEY

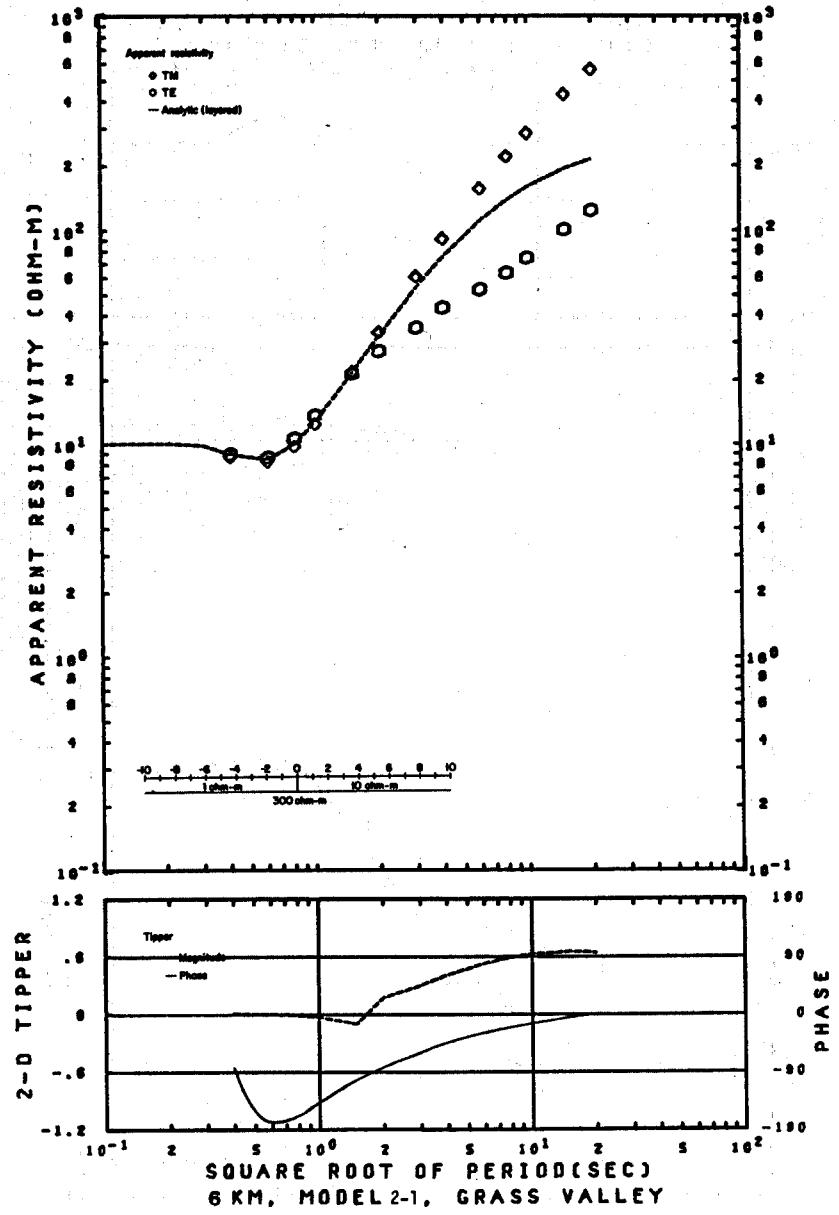

6 KM, MODEL 2-1, GRASS VALLEY

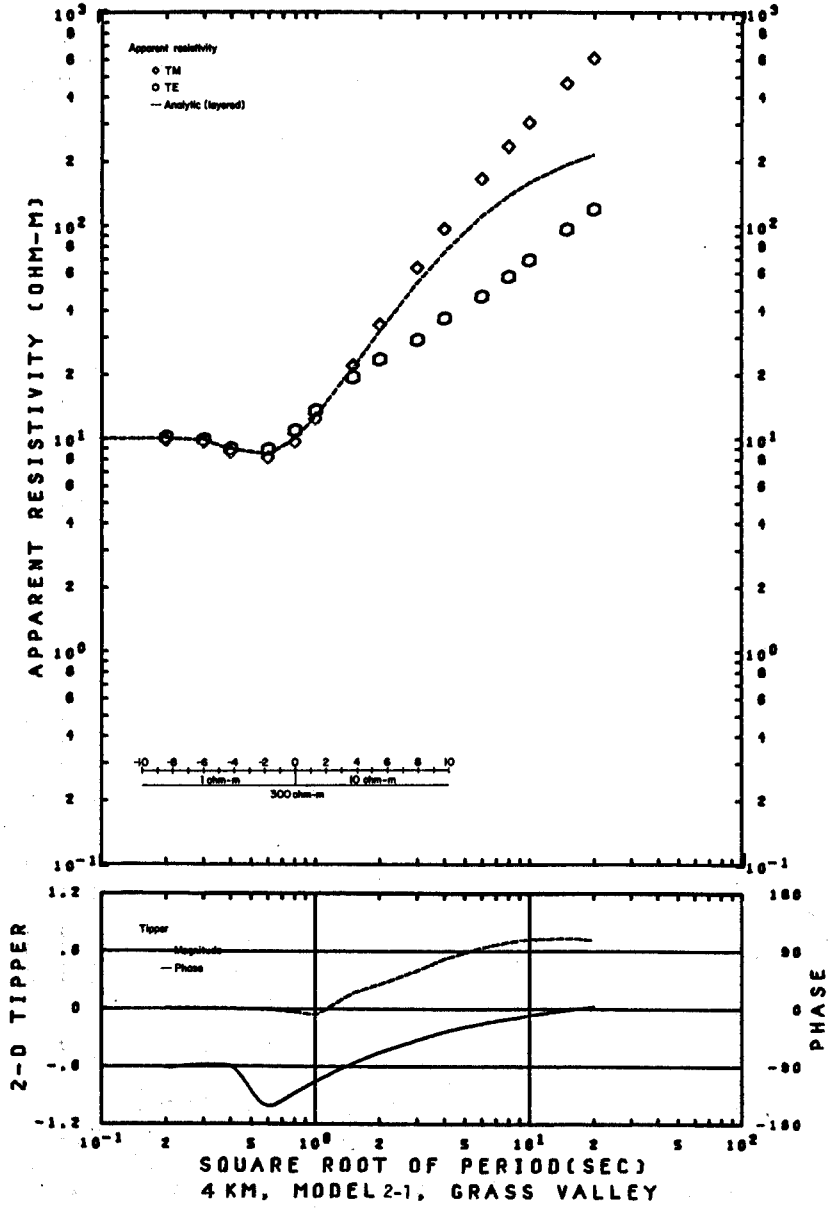
Apparent resistivity
TM
TE
Analytic (layered)
APPARENT RESISTIVITY (OHM-M)
1 ohm-m
10 ohm-m
300 ohm-m
Tipper
Magnitude
Phase
2-D TIPPER
PHASE
SQUARE ROOT OF PERIOD(SEC)
4 KM, MODEL 2-1, GRASS VALLEY

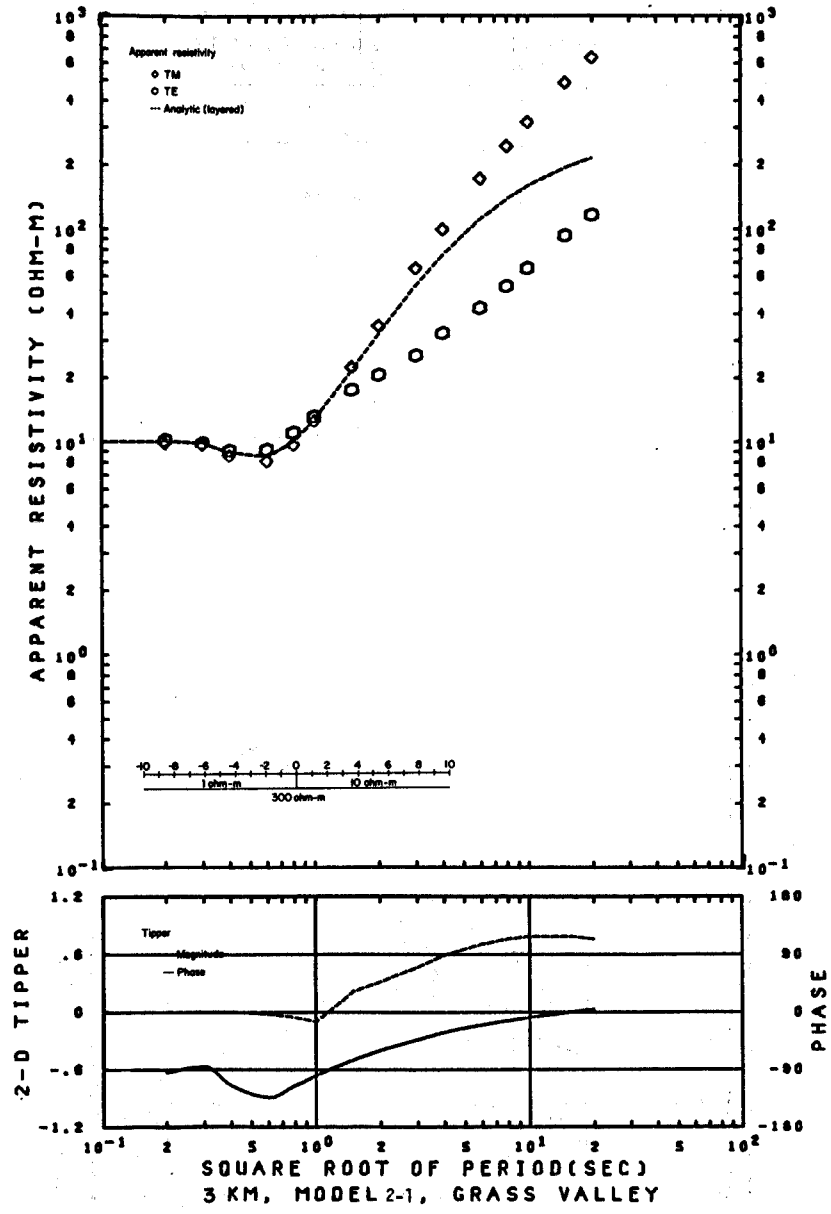
Apparent resistivity
TM
TE
Analytic (layered)
APPARENT RESISTIVITY (OHM-M)
1 ohm-m
10 ohm-m
300 ohm-m
Tipper
Magnitude
Phase
2-D TIPPER
PHASE
SQUARE ROOT OF PERIOD(SEC)
3 KM, MODEL 2-1, GRASS VALLEY

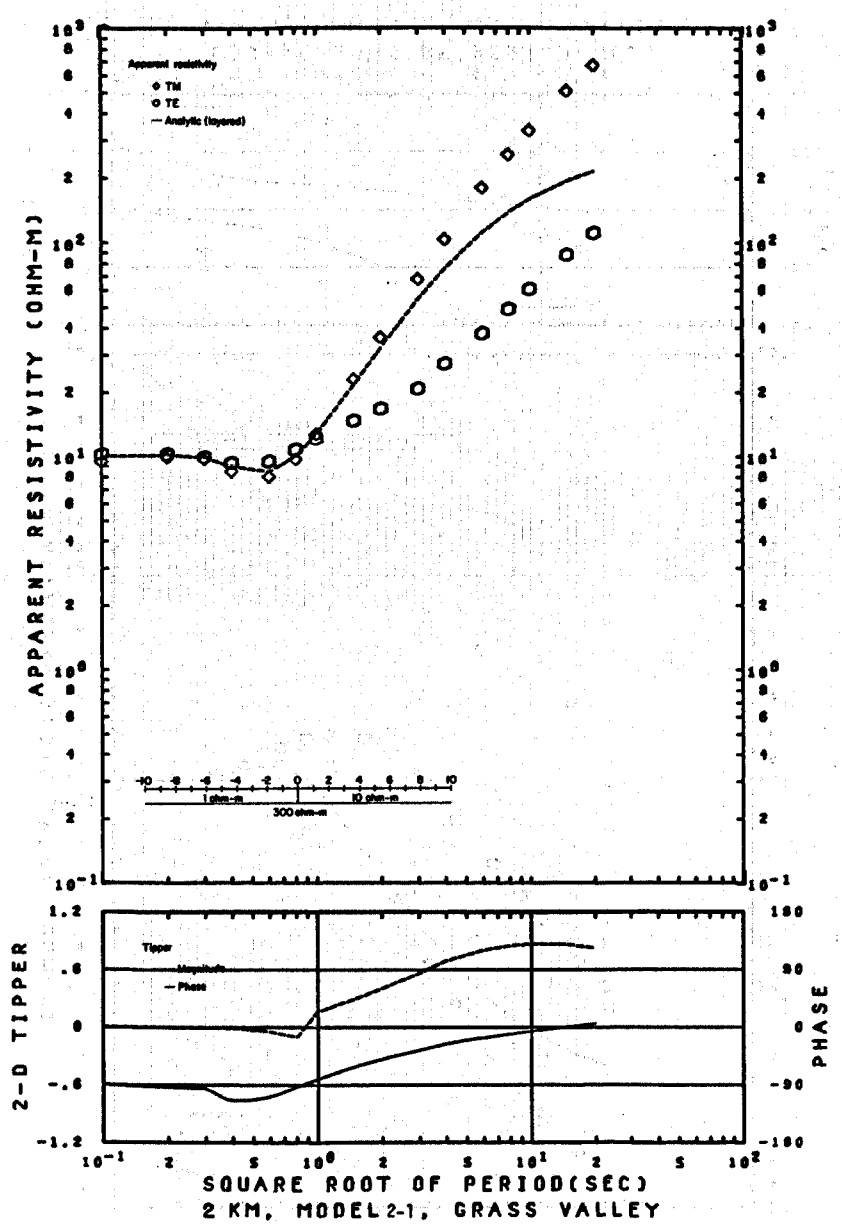

2 KM, MODEL 2-1, GRASS VALLEY

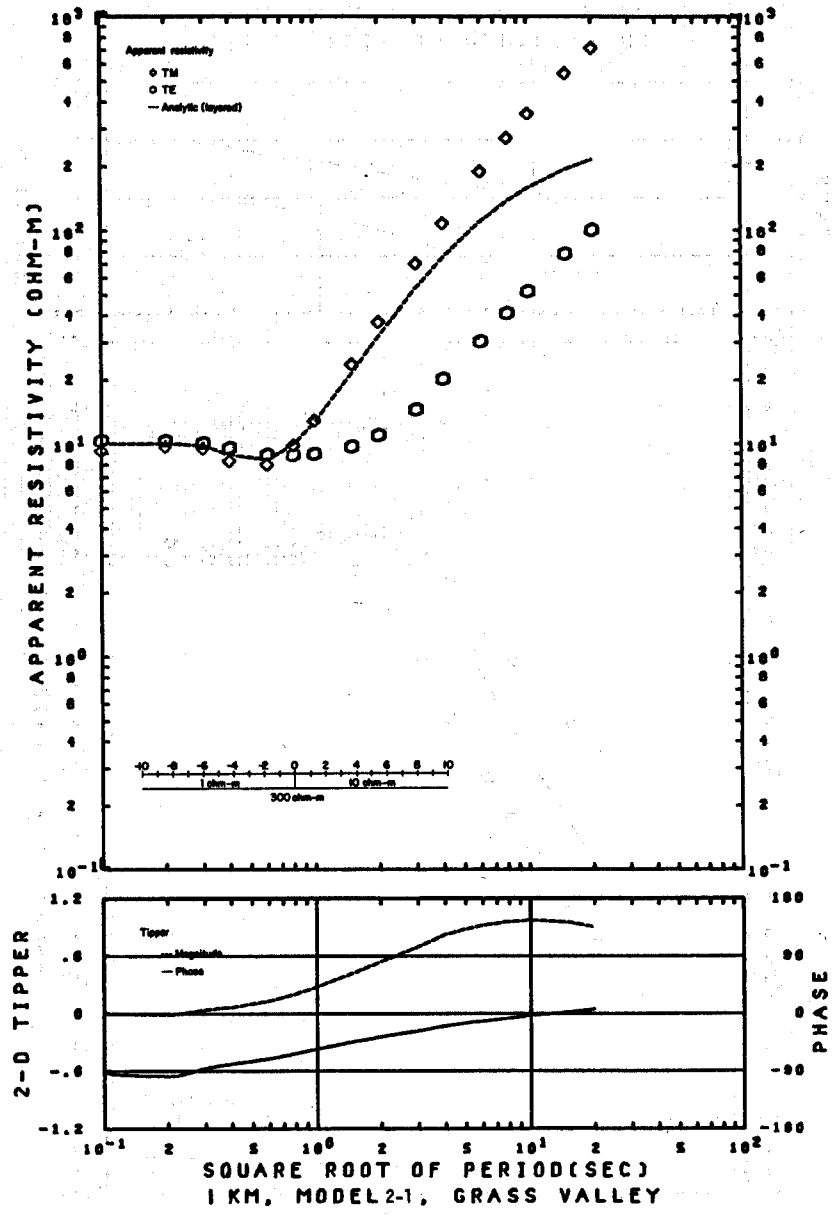

1 KM, MODEL 2-1, GRASS VALLEY

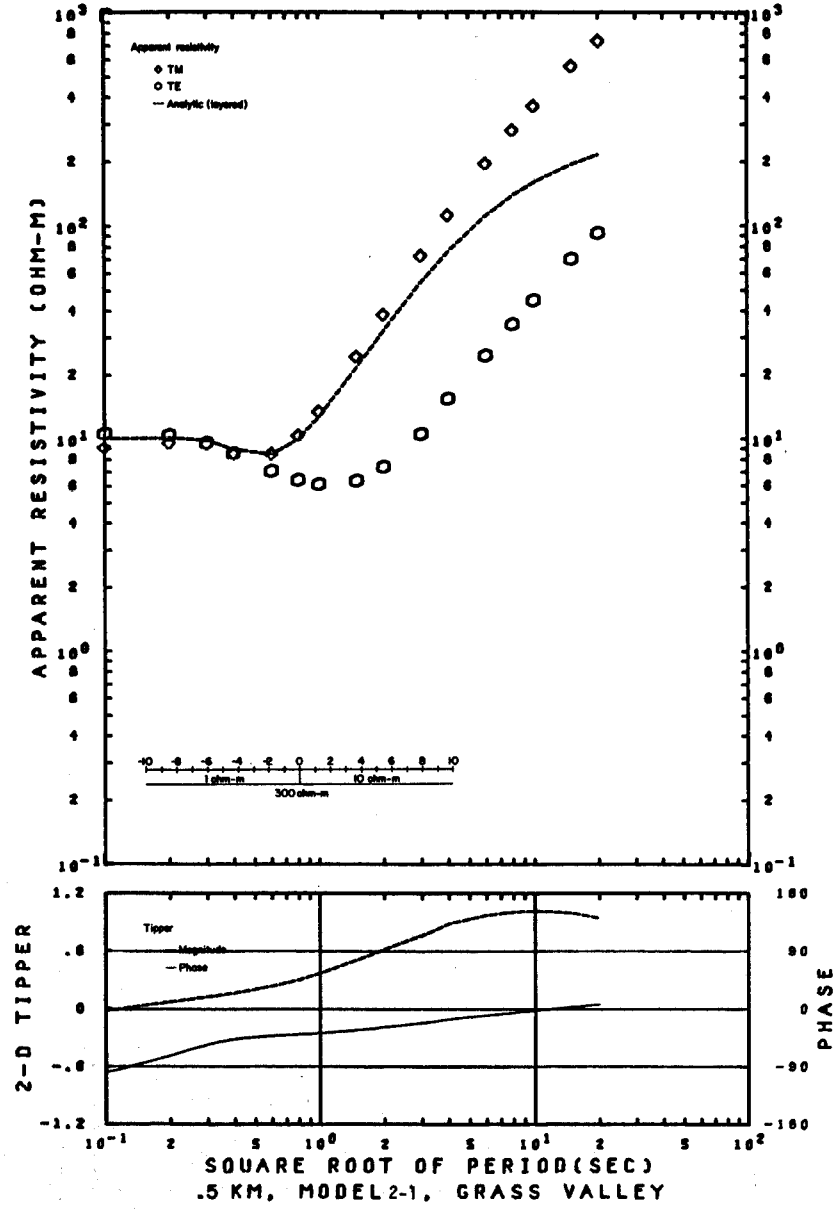
Apparent resistivity
TM
TE
Analytic (layered)
APPARENT RESISTIVITY (OHM-M)
1 ohm-m
10 ohm-m
300 ohm-m
Tipper
Magnitude
Phase
2-D TIPPER
PHASE
SQUARE ROOT OF PERIOD(SEC)
.5 KM, MODEL 2-1, GRASS VALLEY

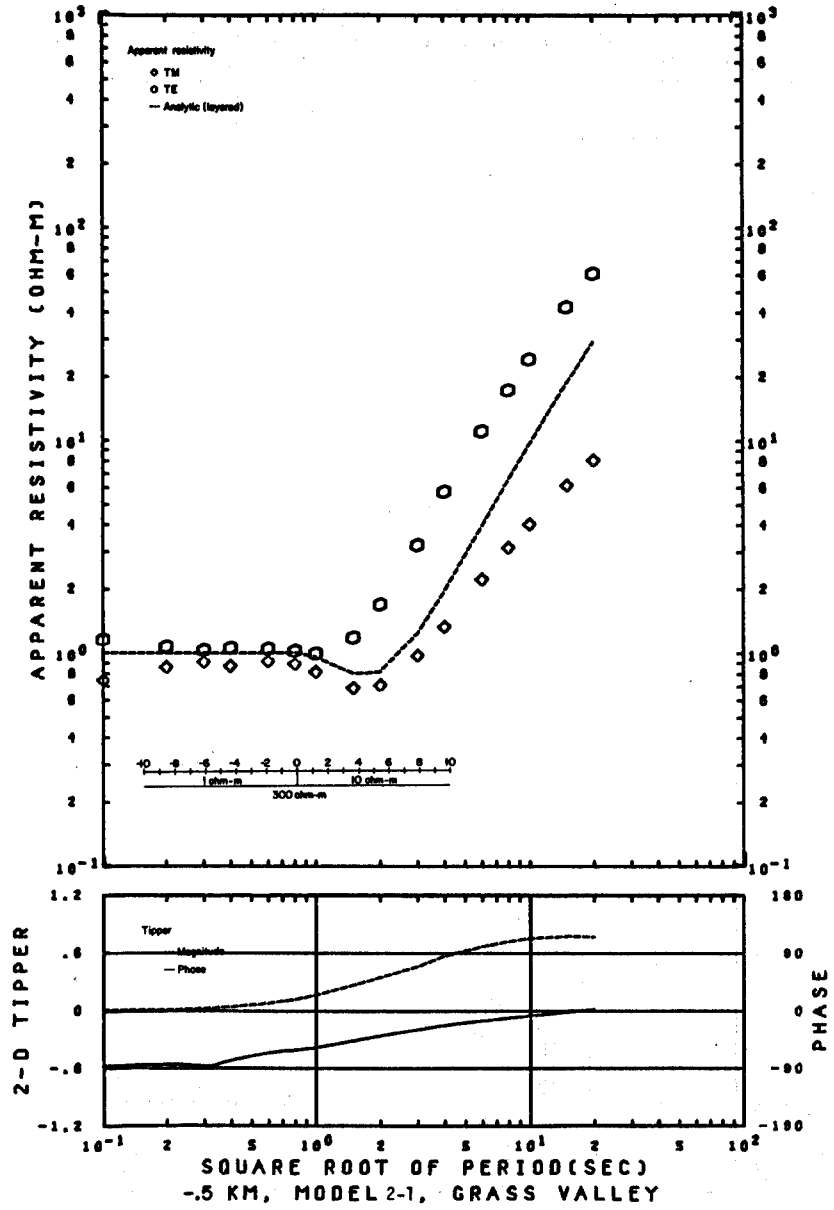
Apparent resistivity
TM
TE
Analytic (layered)
APPARENT RESISTIVITY (OHM-M)
1 ohm-m
10 ohm-m
300 ohm-m
Tipper
Magnitude
Phase
2-D TIPPER
PHASE
SQUARE ROOT OF PERIOD(SEC)
-.5 KM, MODEL 2-1, GRASS VALLEY

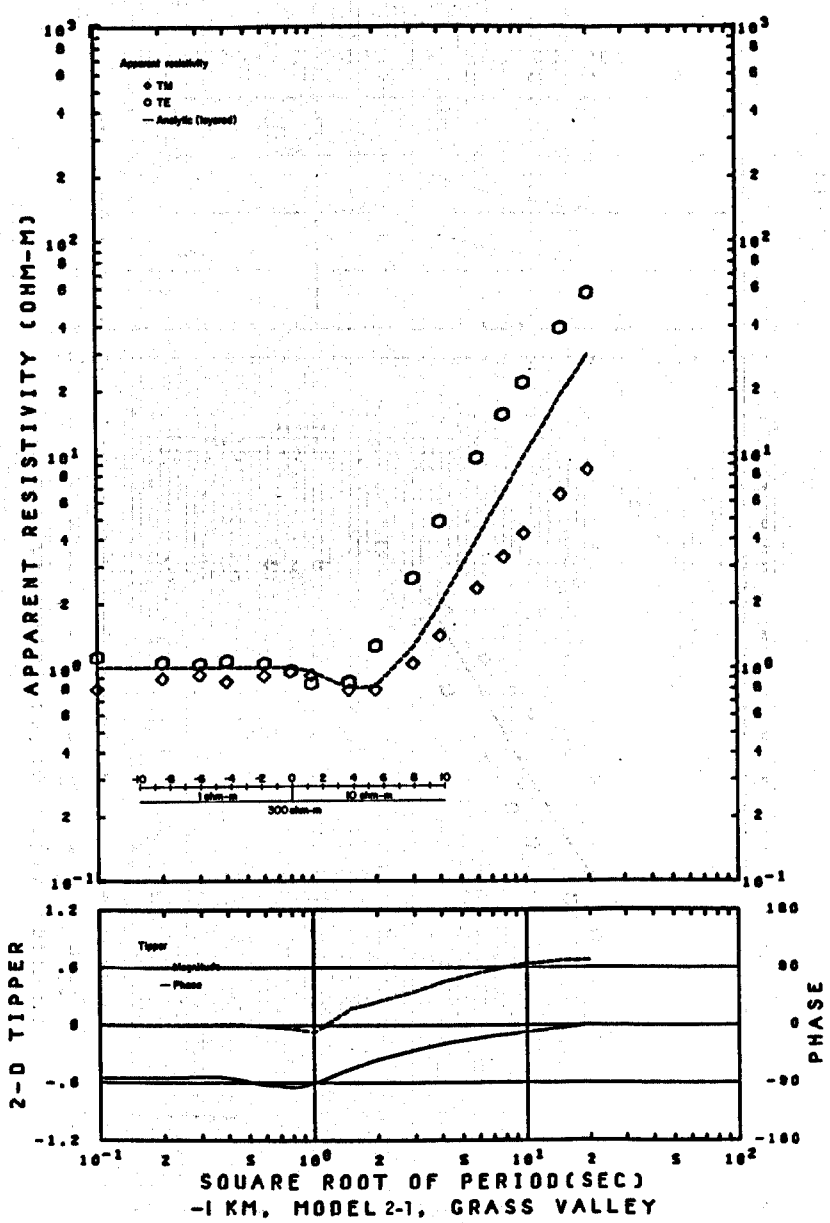

-1 KM, MODEL 2-1, GRASS VALLEY

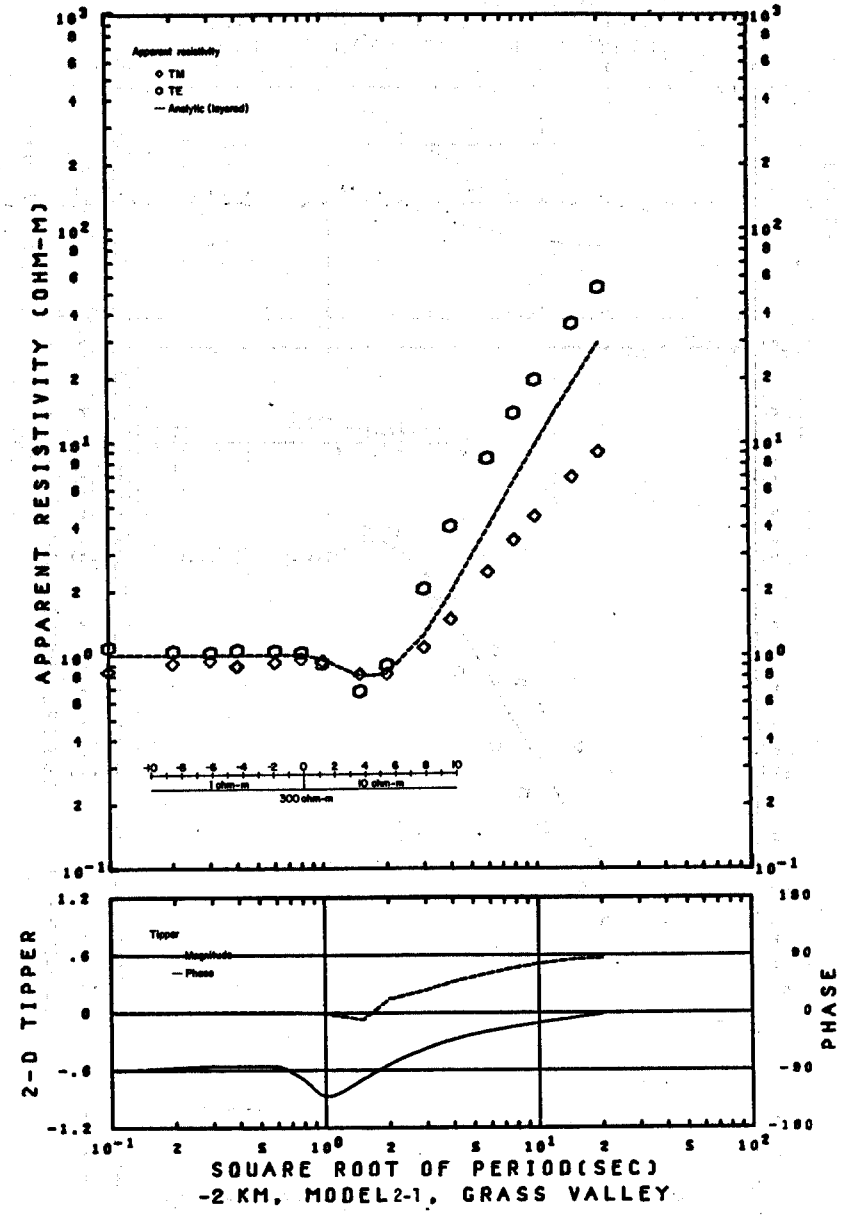

-2 KM, MODEL 2-1, GRASS VALLEY

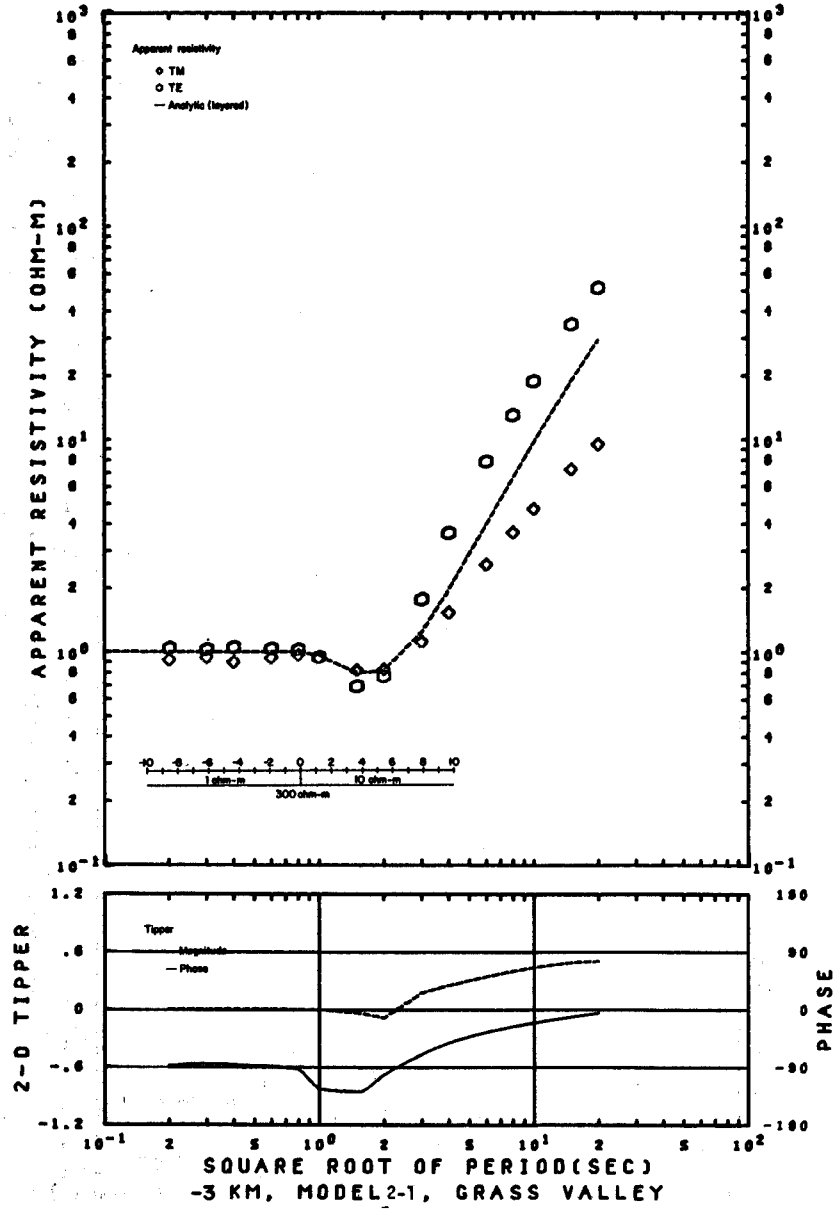

-3 KM, MODEL 2-1, GRASS VALLEY

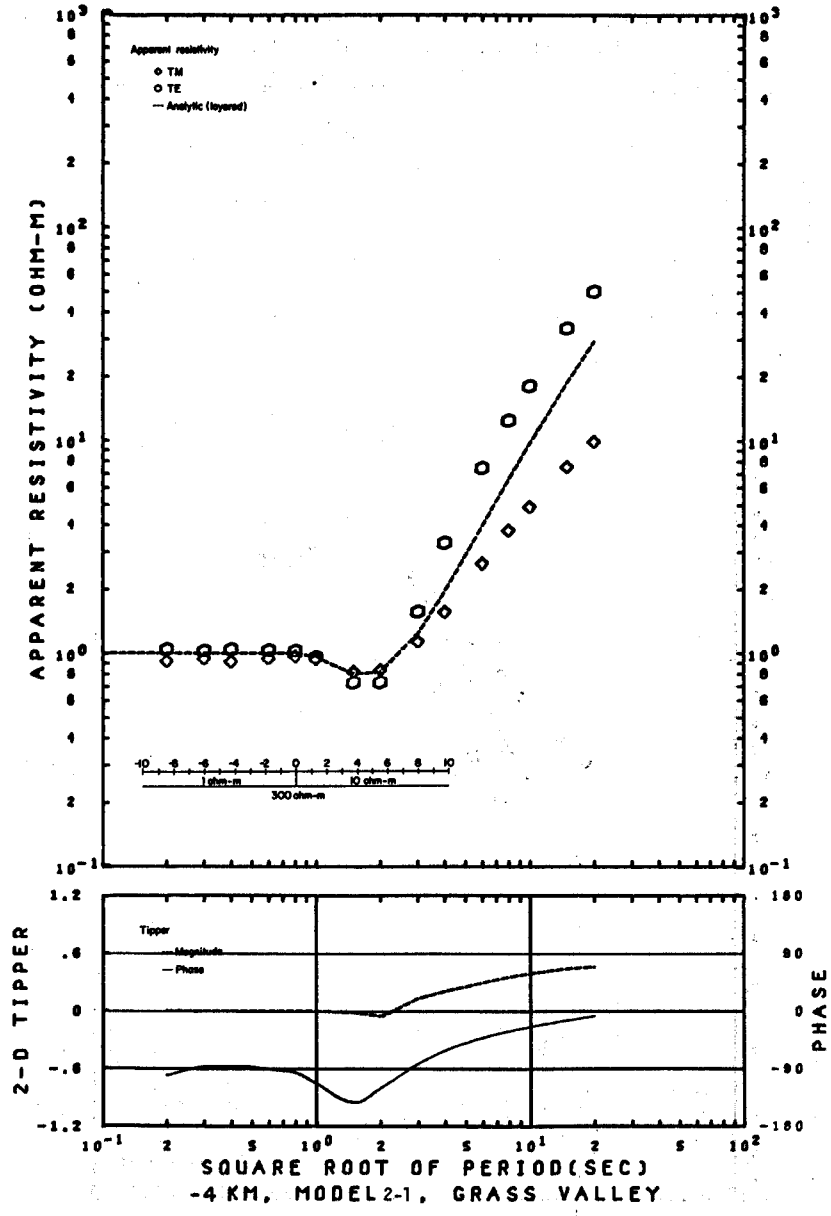

-4 KM, MODEL 2-1, GRASS VALLEY

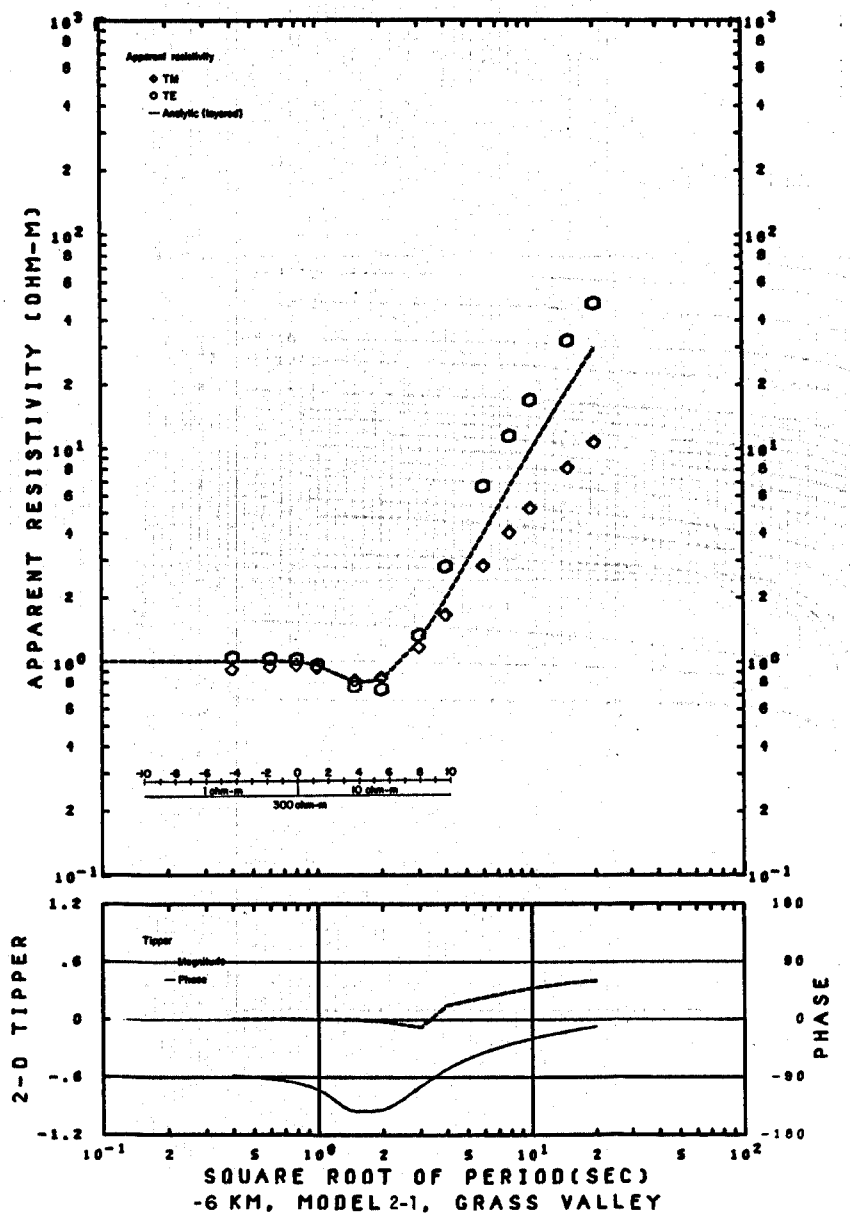

-6 KM, MODEL 2-1, GRASS VALLEY

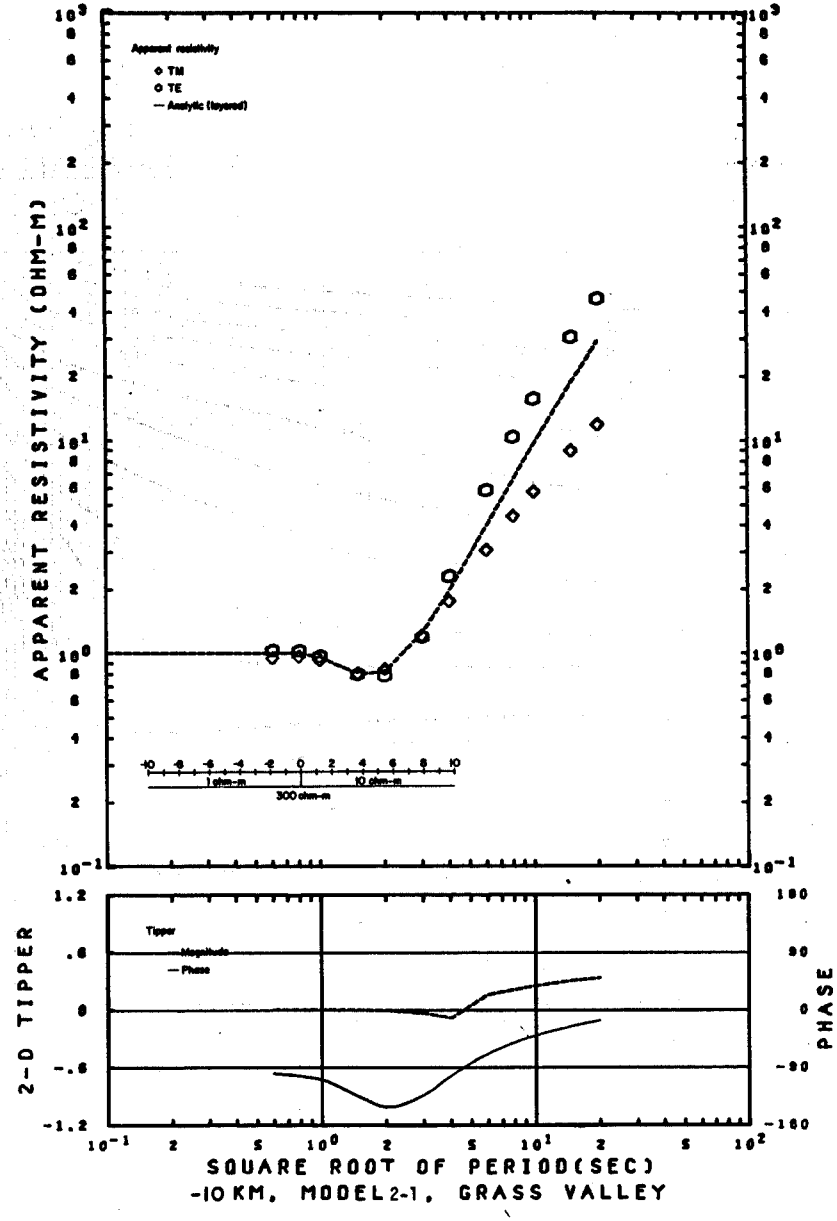

-10 KM, MODEL 2-1, GRASS VALLEY

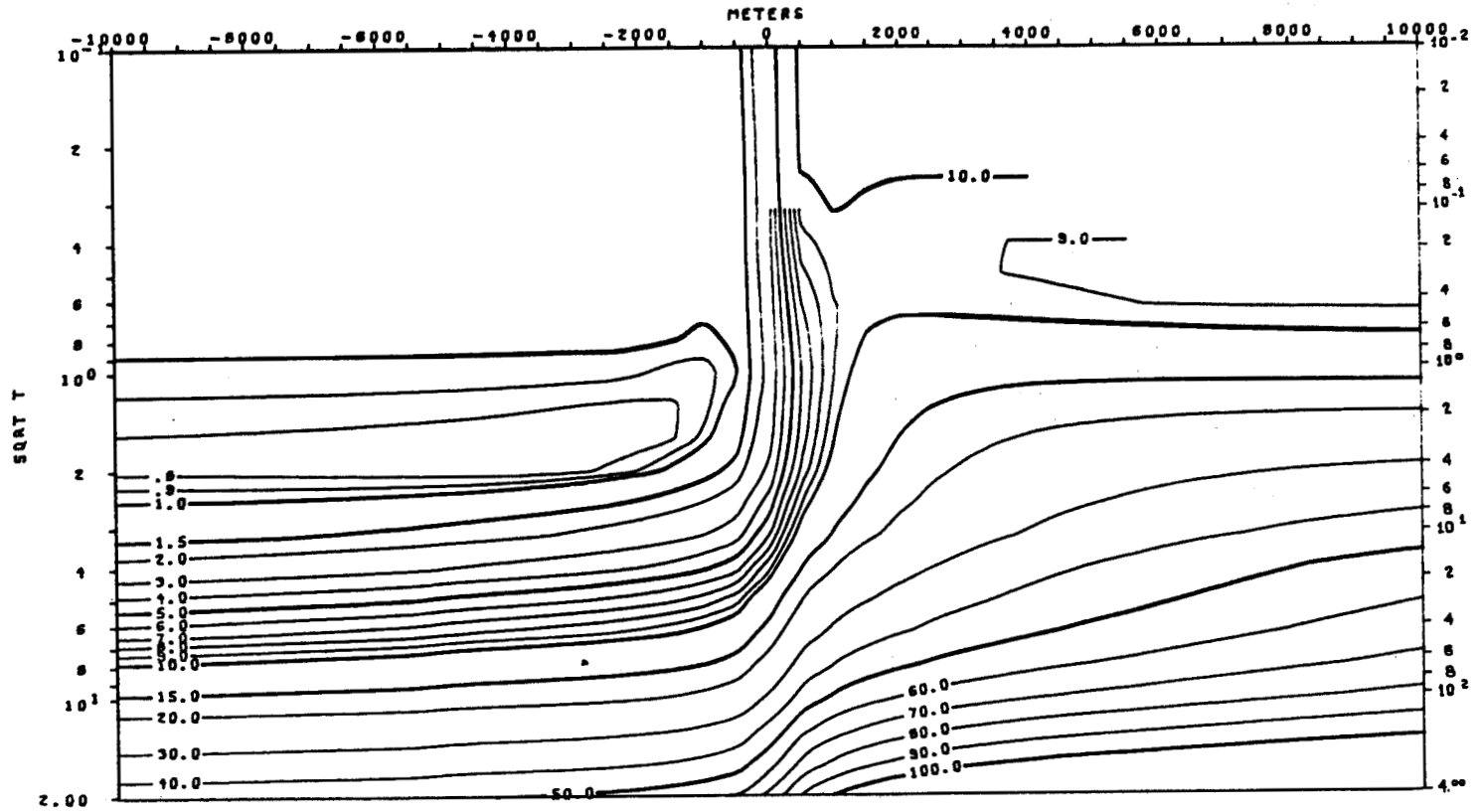

TE MODE
APPARENT RESISTIVITY VS. PERIOD (T)
MODEL 2-1

XBL 786-1943

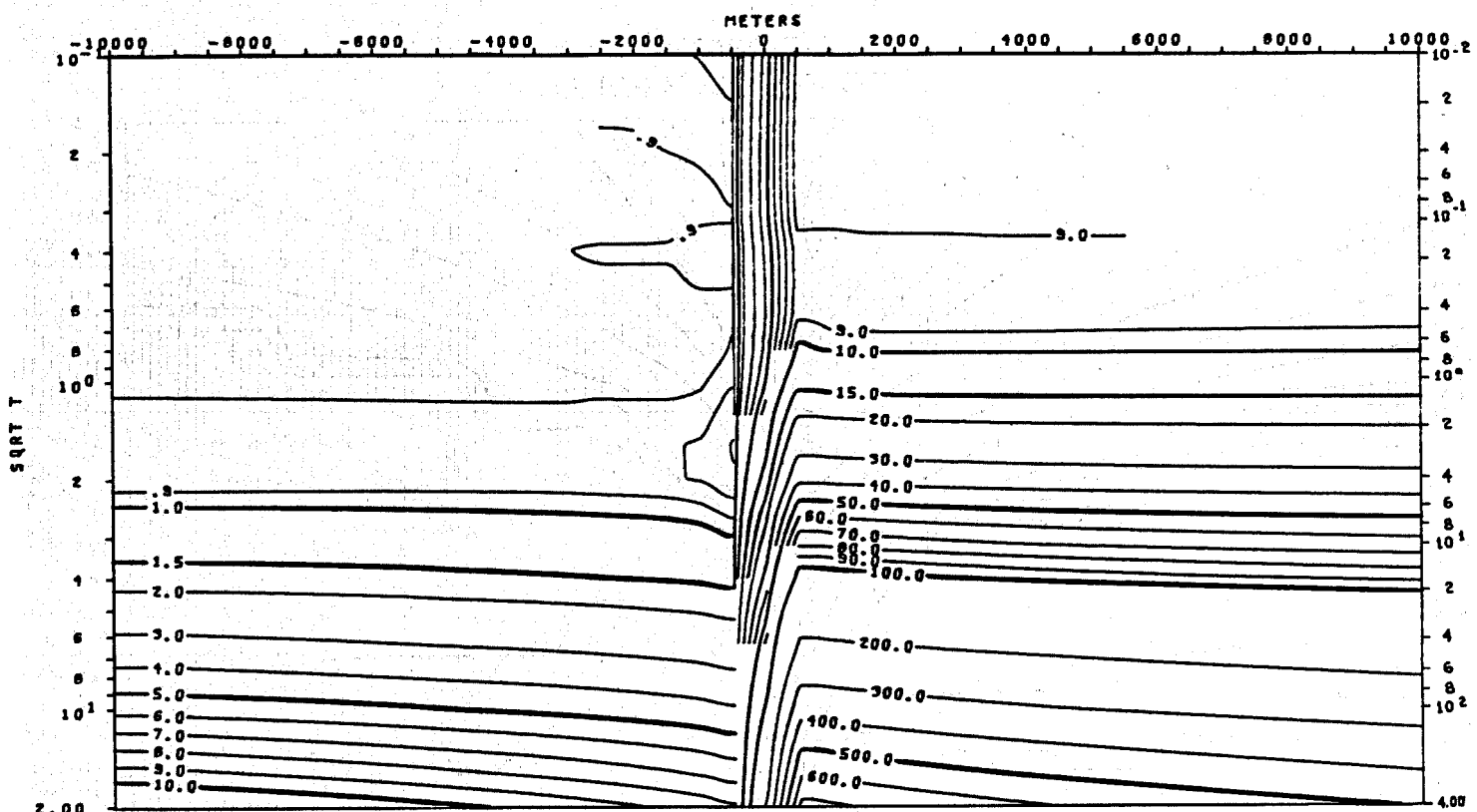

TM MODE
APPARENT RESISTIVITY VS. PERIOD (T)
MODEL 2-1

XBL 786-1925

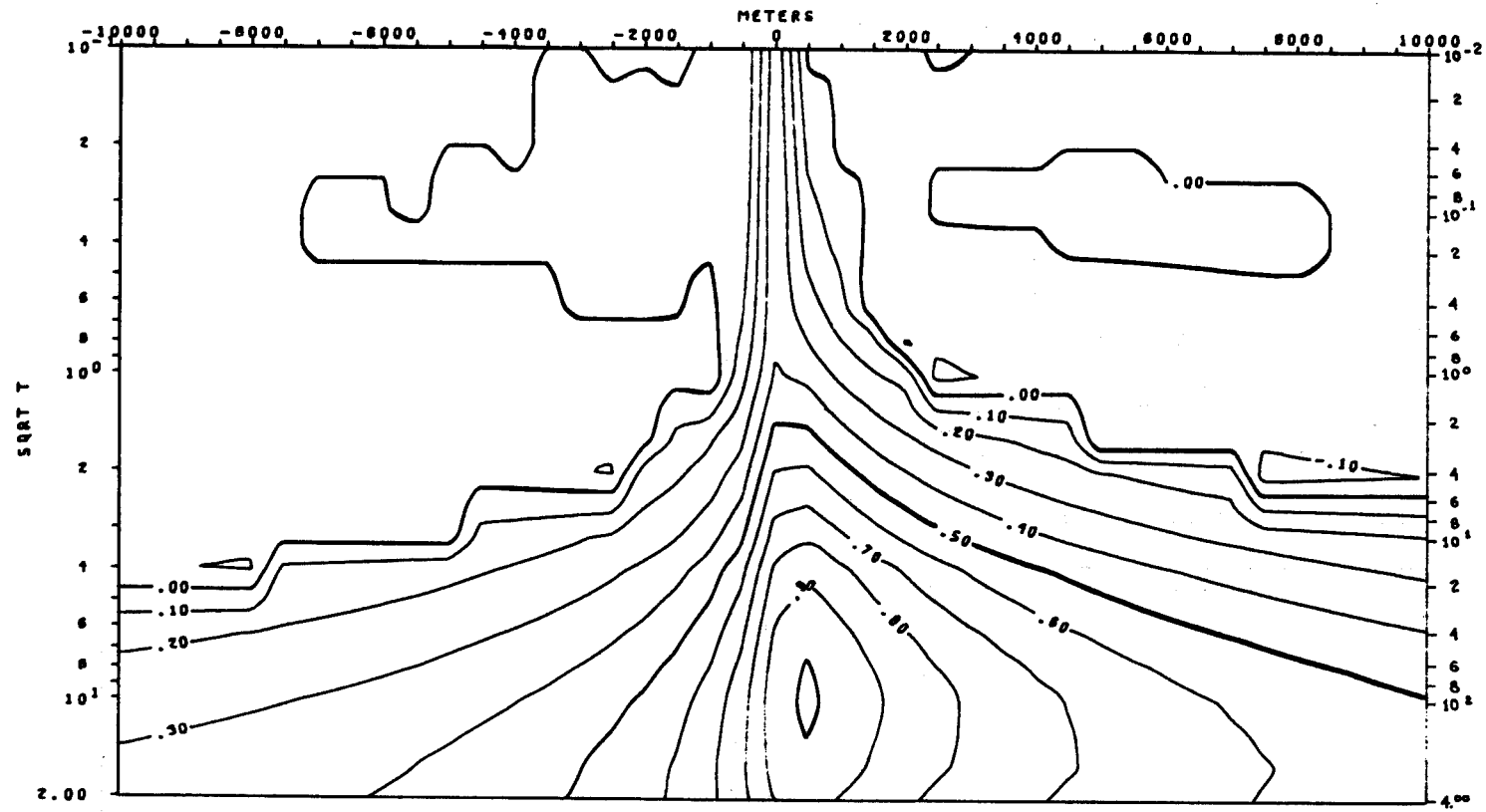

TIPPER VS. PERIOD (T)
MODEL 2-1

XBL 786-1900

T

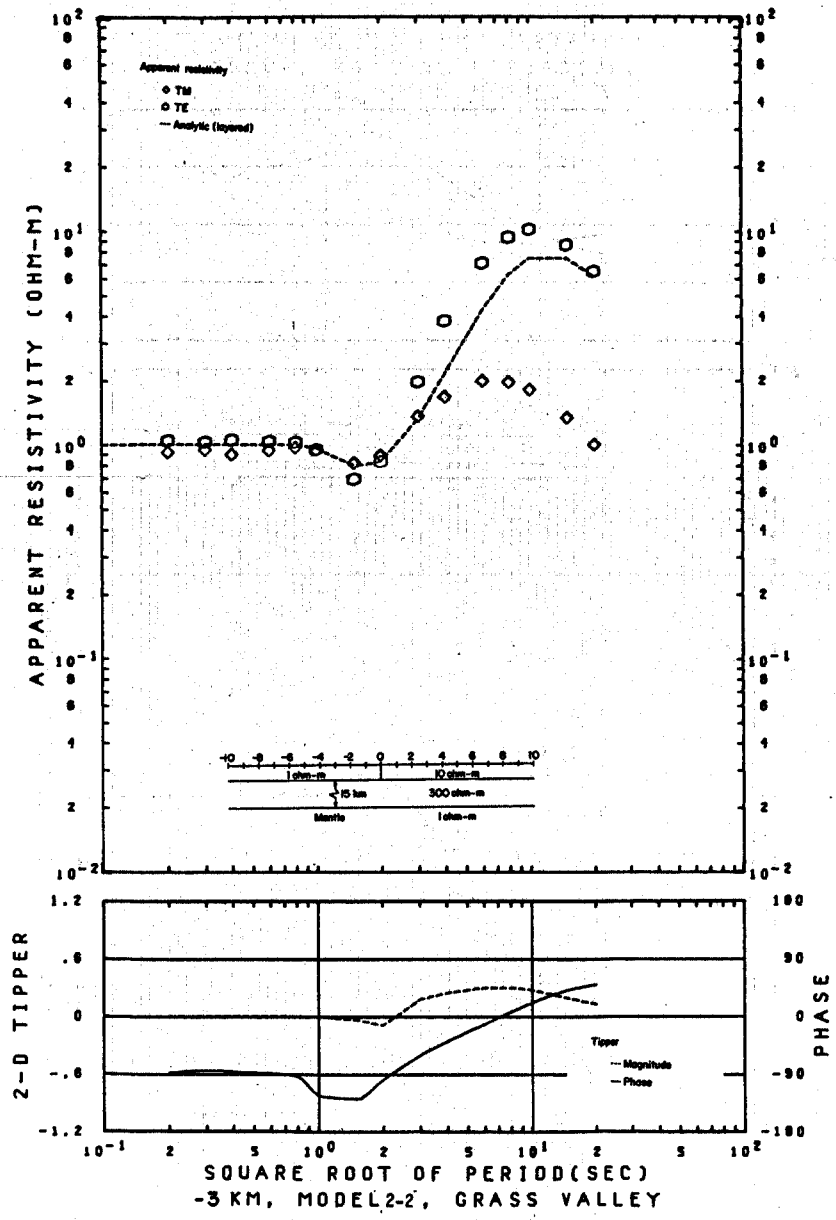
Apparent resistivity
TM
TE
Analytic (layered)
APPARENT RESISTIVITY (OHM-M)
1 ohm-m
10 ohm-m
15 km
300 ohm-m
Mantle
1 ohm-m
2-D TIPPER
PHASE
Tipper
Magnitude
Phase
SQUARE ROOT OF PERIOD(SEC)
-3 KM, MODEL 2-2, GRASS VALLEY

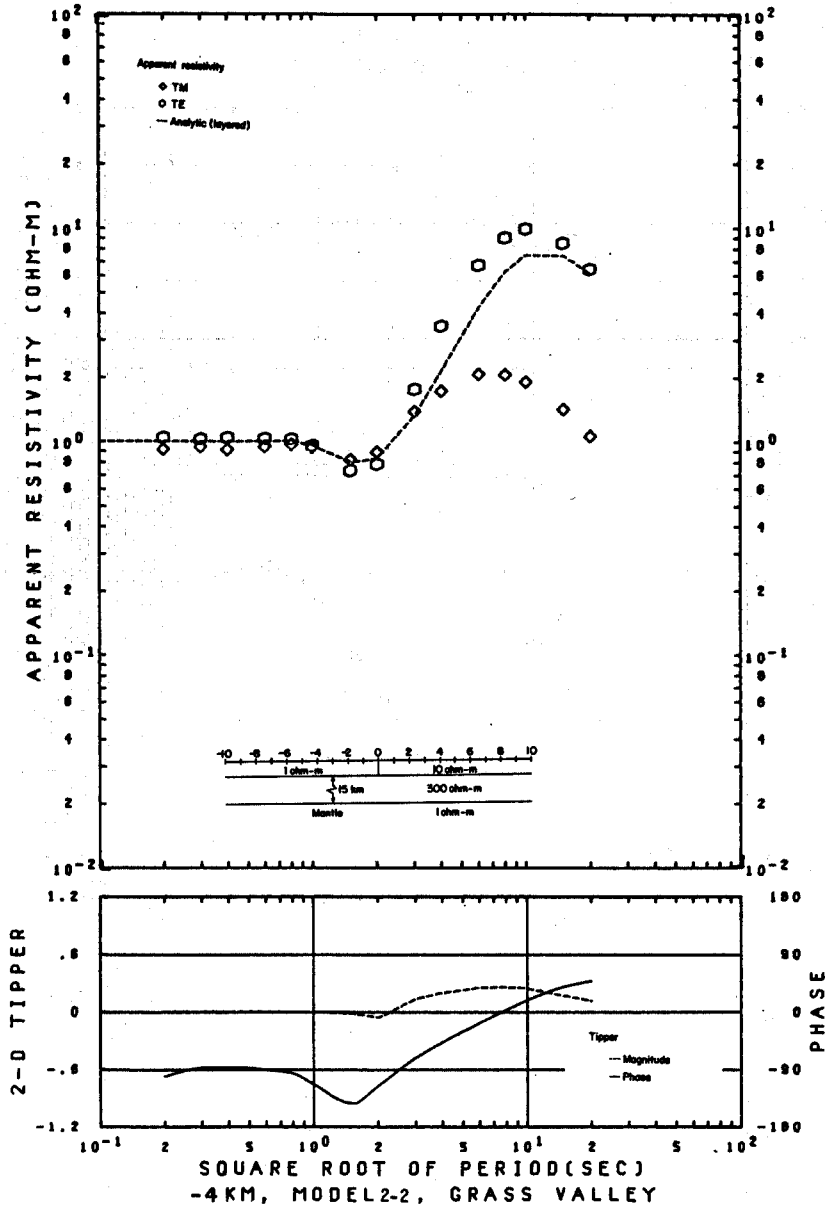
Apparent resistivity
TM
TE
Analytic (layered)
APPARENT RESISTIVITY (OHM-M)
1 ohm-m
10 ohm-m
15 km
300 ohm-m
Mantle
1 ohm-m
2-D TIPPER
PHASE
Tipper
Magnitude
Phase
SQUARE ROOT OF PERIOD(SEC)
-4 KM, MODEL 2-2, GRASS VALLEY

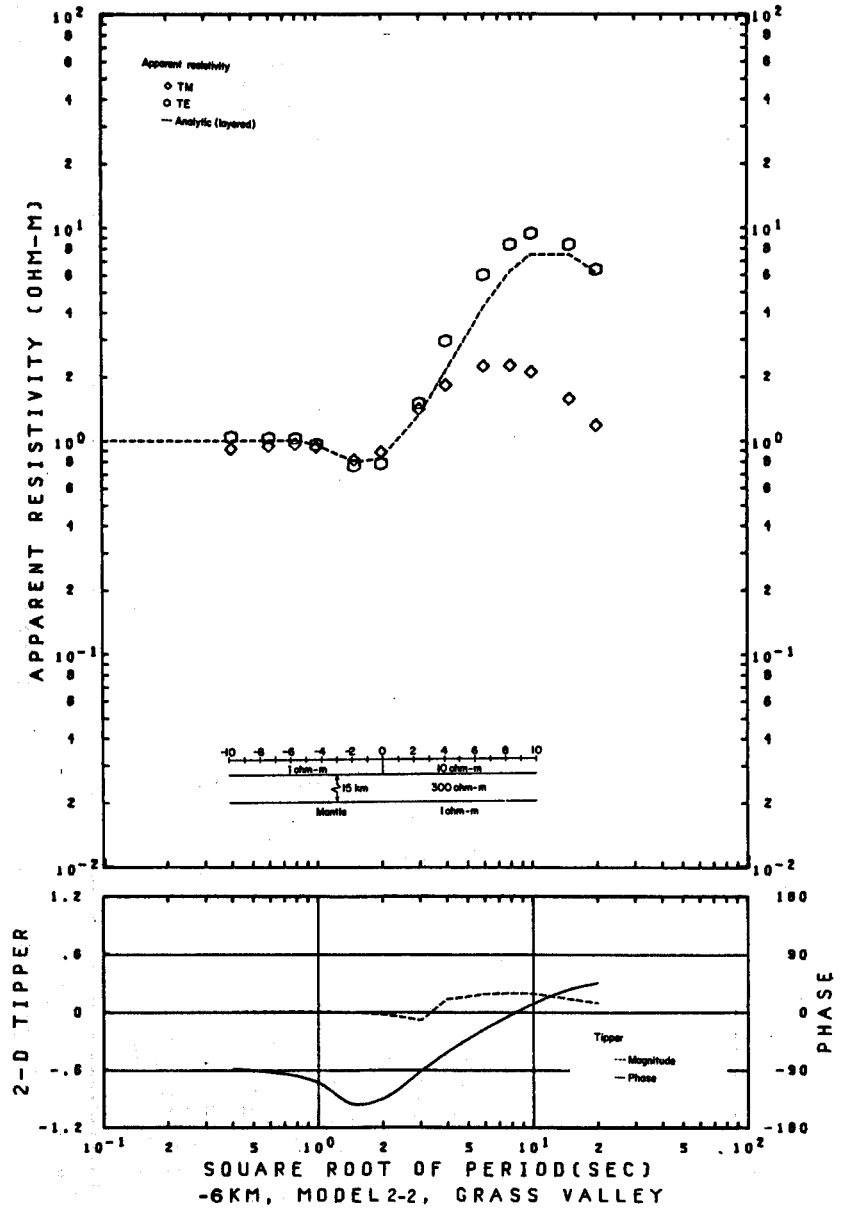
Apparent resistivity
TM
TE
Analytic (layered)
APPARENT RESISTIVITY (OHM-M)
1 ohm-m
10 ohm-m
15 km
300 ohm-m
Mantle
1 ohm-m
2-D TIPPER
PHASE
Tipper
Magnitude
Phase
SQUARE ROOT OF PERIOD(SEC)
-6KM, MODEL 2-2, GRASS VALLEY

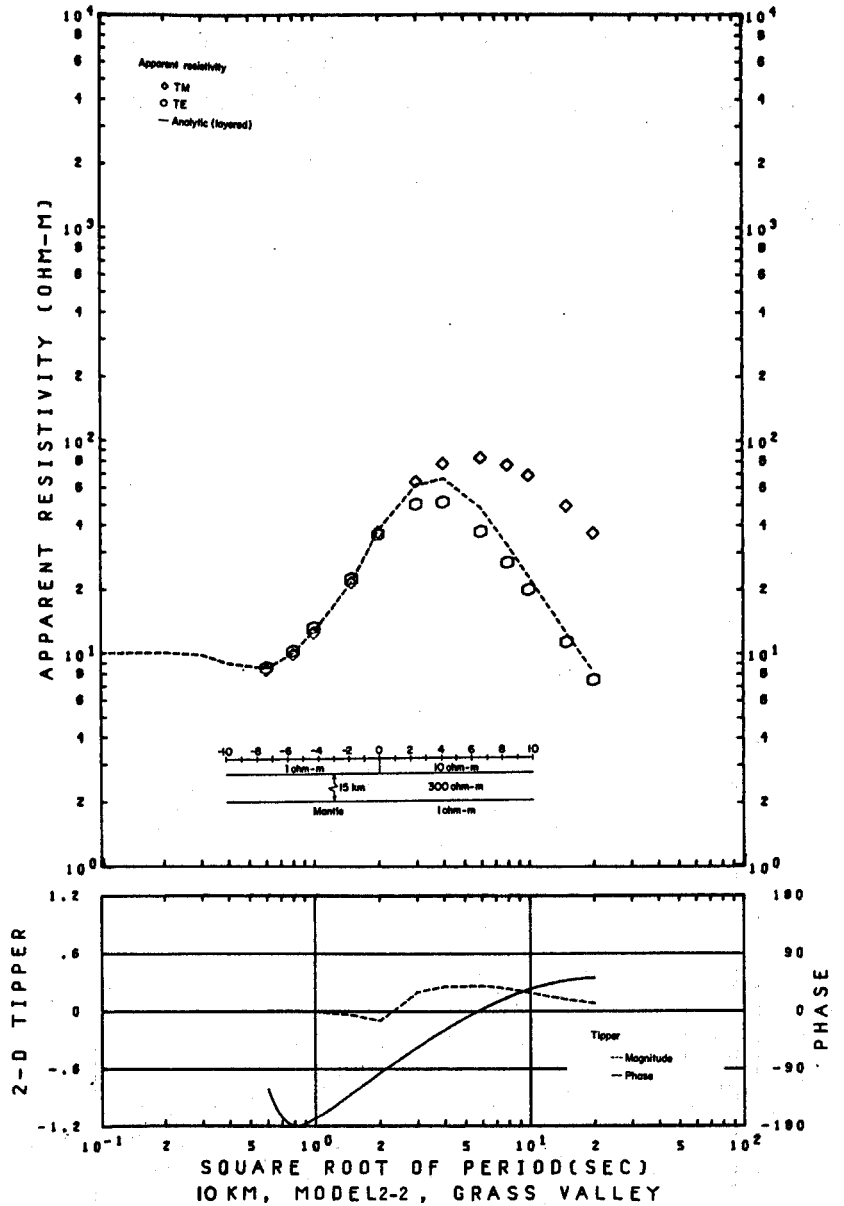
Apparent resistivity
TM
TE
Analytic (layered)
APPARENT RESISTIVITY (OHM-M)
1 ohm-m
10 ohm-m
15 km
300 ohm-m
Mantle
1 ohm-m
2-D TIPPER
PHASE
Tipper
Magnitude
Phase
SQUARE ROOT OF PERIOD(SEC)
10 KM, MODEL 2-2, GRASS VALLEY

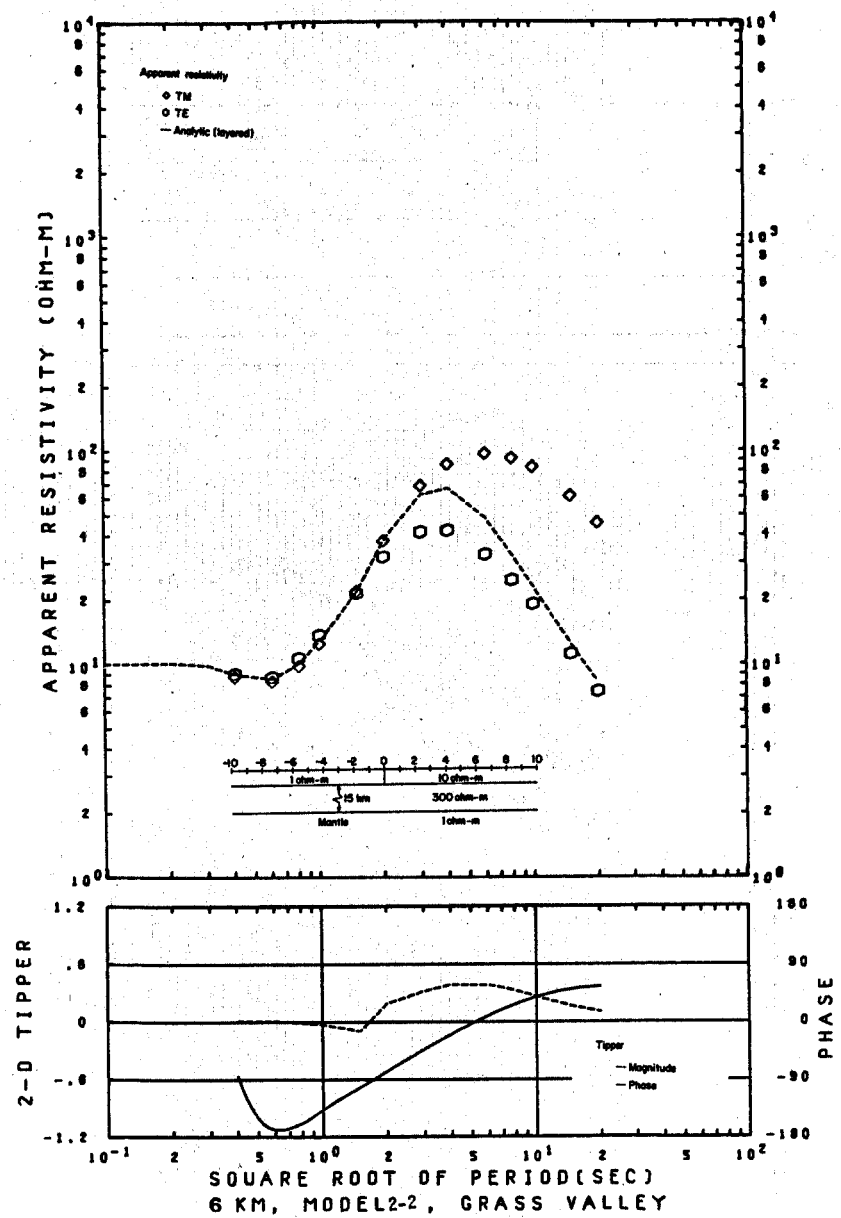

6 KM, MODEL2-2, GRASS VALLEY

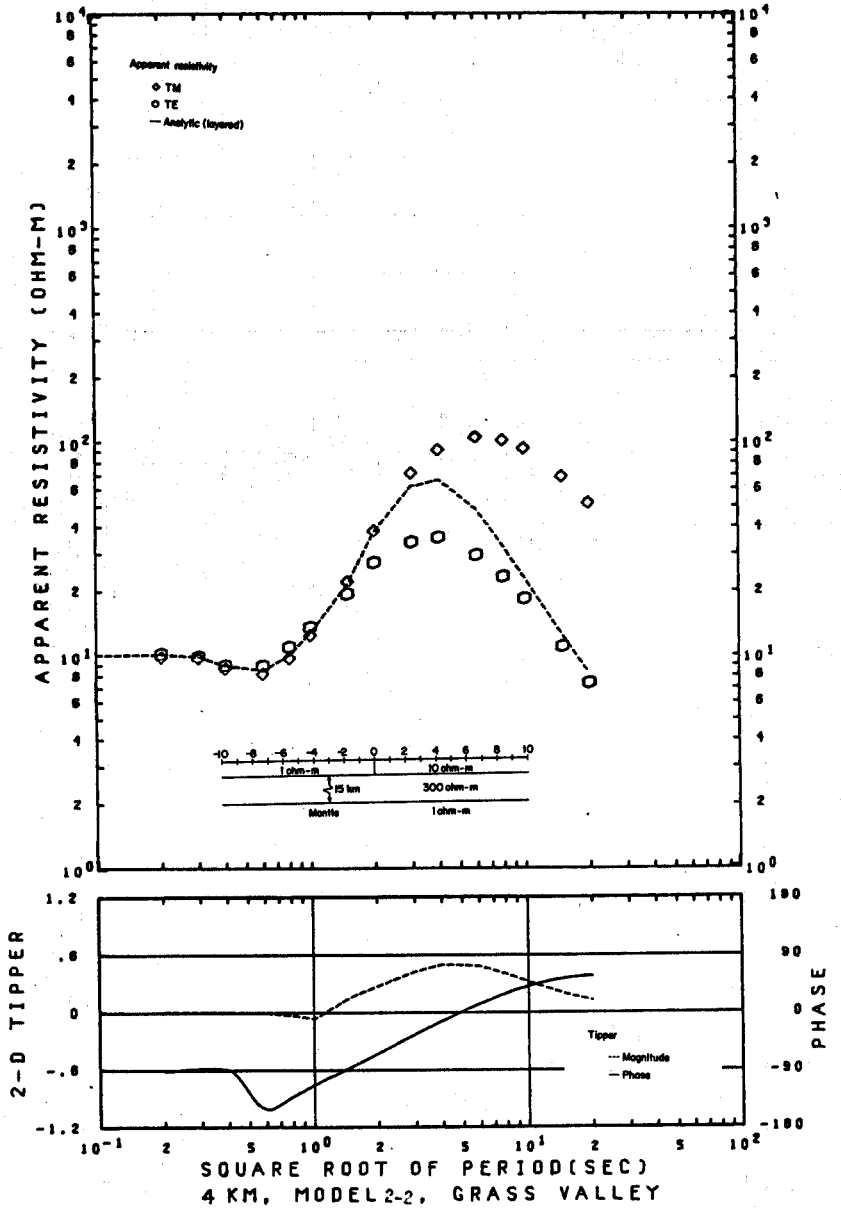

4 KM, MODEL2-2, GRASS VALLEY

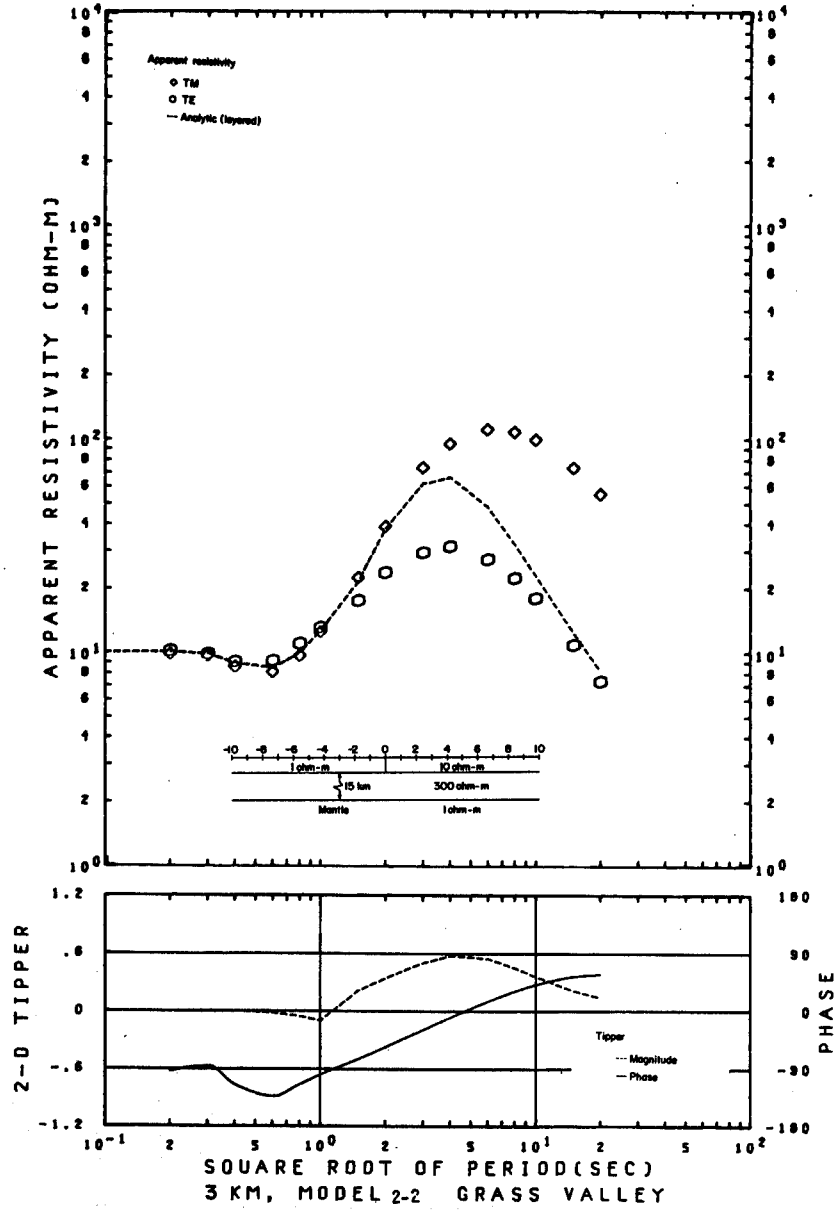
Apparent resistivity
TM
TE
Analytic (layered)
APPARENT RESISTIVITY (OHM-M)
1 ohm-m
10 ohm-m
15 km
300 ohm-m
Mantle
1 ohm-m
2-D TIPPER
PHASE
Tipper
Magnitude
Phase
SQUARE ROOT OF PERIOD(SEC)
3 KM, MODEL 2-2 GRASS VALLEY

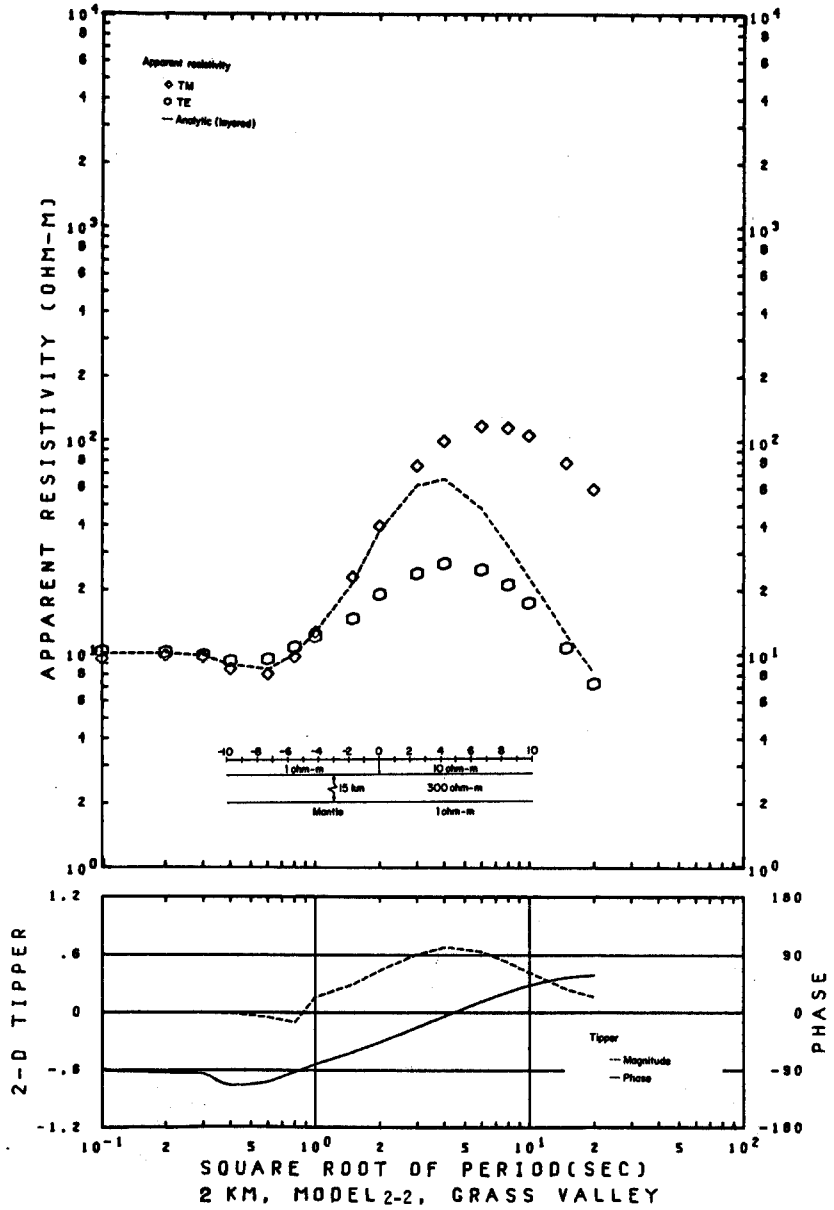
Apparent resistivity
TM
TE
Analytic (layered)
APPARENT RESISTIVITY (OHM-M)
1 ohm-m
10 ohm-m
15 km
300 ohm-m
Mantle
1 ohm-m
2-D TIPPER
PHASE
Tipper
Magnitude
Phase
SQUARE ROOT OF PERIOD(SEC)
2 KM, MODEL 2-2, GRASS VALLEY

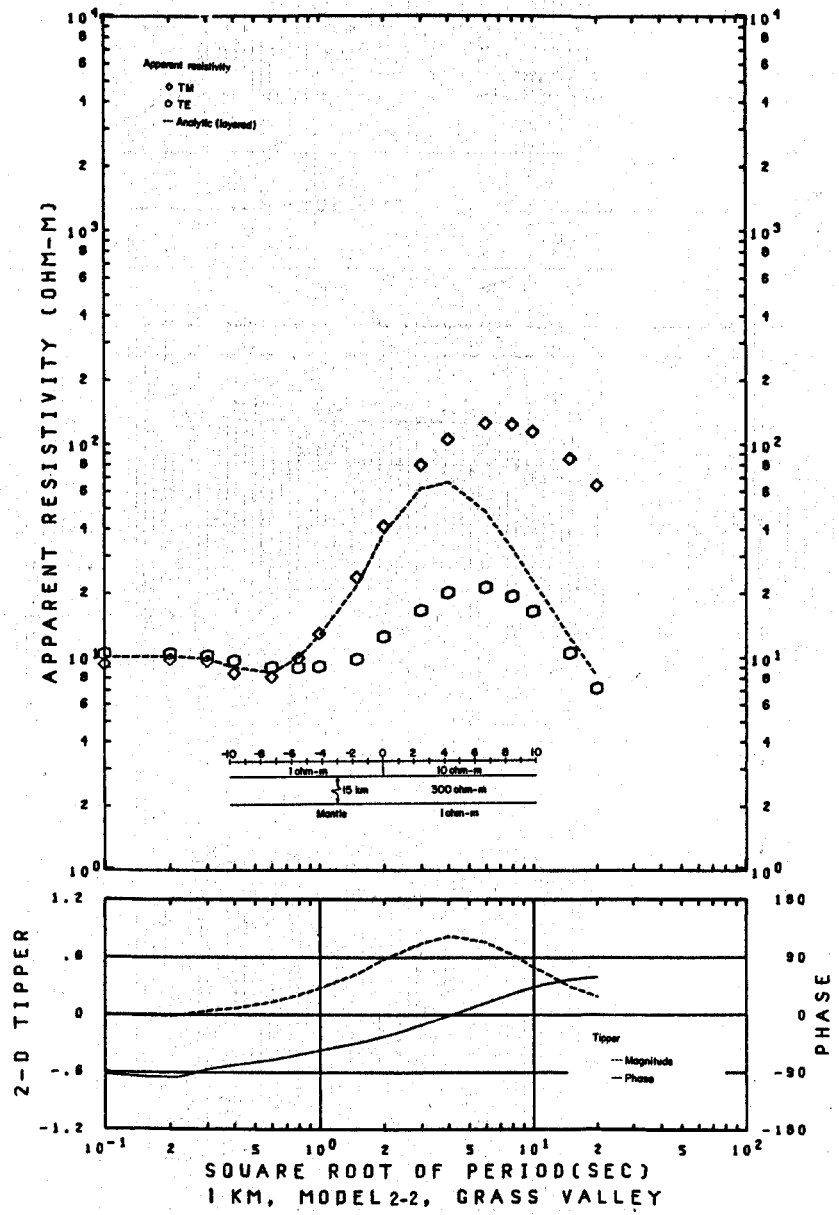
Apparent resistivity
TM
TE
Analytic (layered)
APPARENT RESISTIVITY (OHM-M)
1 ohm-m
10 ohm-m
15 km
300 ohm-m
Mantle
1 ohm-m
2-D TIPPER
PHASE
Tipper
Magnitude
Phase
SQUARE ROOT OF PERIOD(SEC)
1 KM, MODEL 2-2, GRASS VALLEY

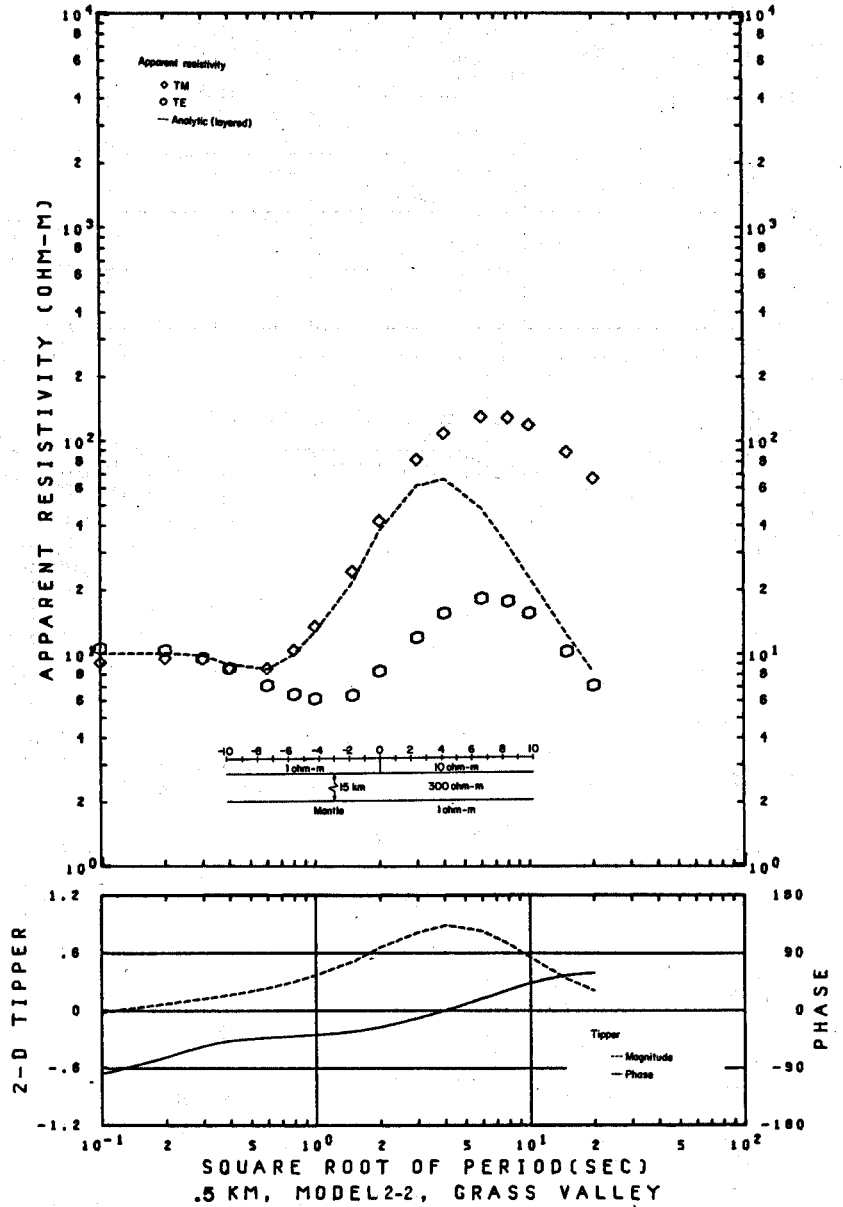
Apparent resistivity
TM
TE
Analytic (layered)
APPARENT RESISTIVITY (OHM-M)
1 ohm-m
10 ohm-m
15 km
300 ohm-m
Mantle
1 ohm-m
2-D TIPPER
PHASE
Tipper
Magnitude
Phase
SQUARE ROOT OF PERIOD(SEC)
.5 KM, MODEL 2-2, GRASS VALLEY

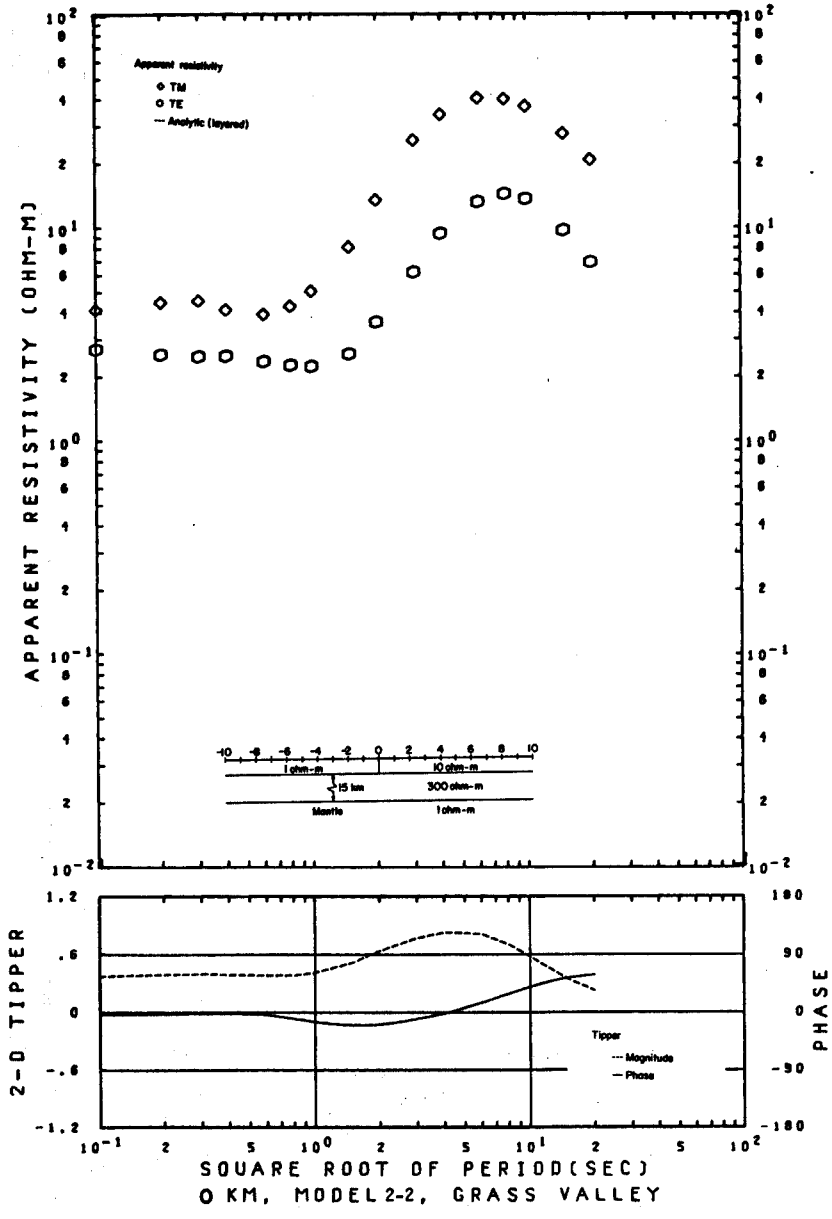
Apparent resistivity
TM
TE
Analytic (layered)
APPARENT RESISTIVITY (OHM-M)
1 ohm-m
10 ohm-m
15 km
300 ohm-m
Mantle
1 ohm-m
2-D TIPPER
PHASE
Tipper
Magnitude
Phase
SQUARE ROOT OF PERIOD(SEC)
0 KM, MODEL 2-2, GRASS VALLEY

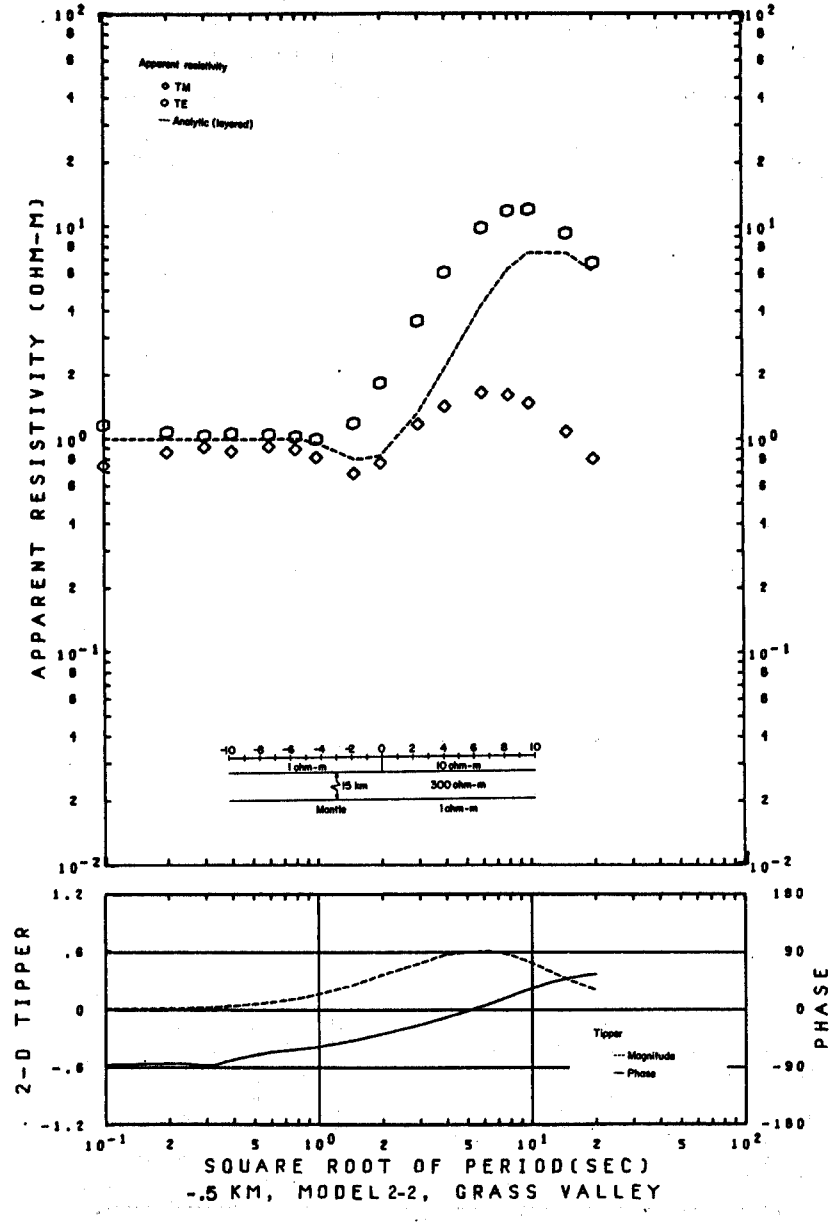
Apparent resistivity
TM
TE
Analytic (layered)
APPARENT RESISTIVITY (OHM-M)
1 ohm-m
10 ohm-m
15 km
300 ohm-m
Mantle
1 ohm-m
2-D TIPPER
PHASE
Tipper
Magnitude
Phase
SQUARE ROOT OF PERIOD(SEC)
-.5 KM, MODEL 2-2, GRASS VALLEY

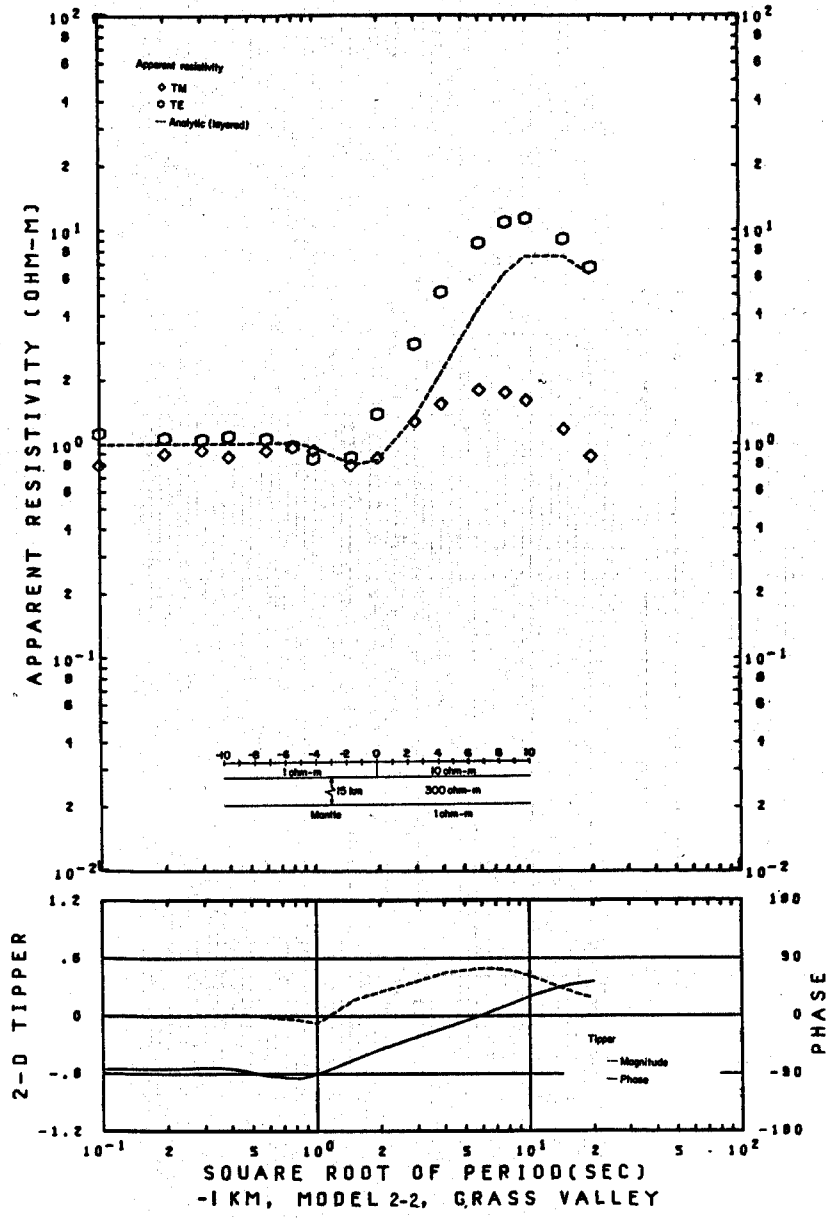
Apparent resistivity
TM
TE
Analytic (layered)
APPARENT RESISTIVITY (OHM-M)
1 ohm-m
10 ohm-m
15 km
300 ohm-m
Mantle
1 ohm-m
2-D TIPPER
PHASE
Tipper
Magnitude
Phase
SQUARE ROOT OF PERIOD(SEC)
-1 KM, MODEL 2-2, GRASS VALLEY

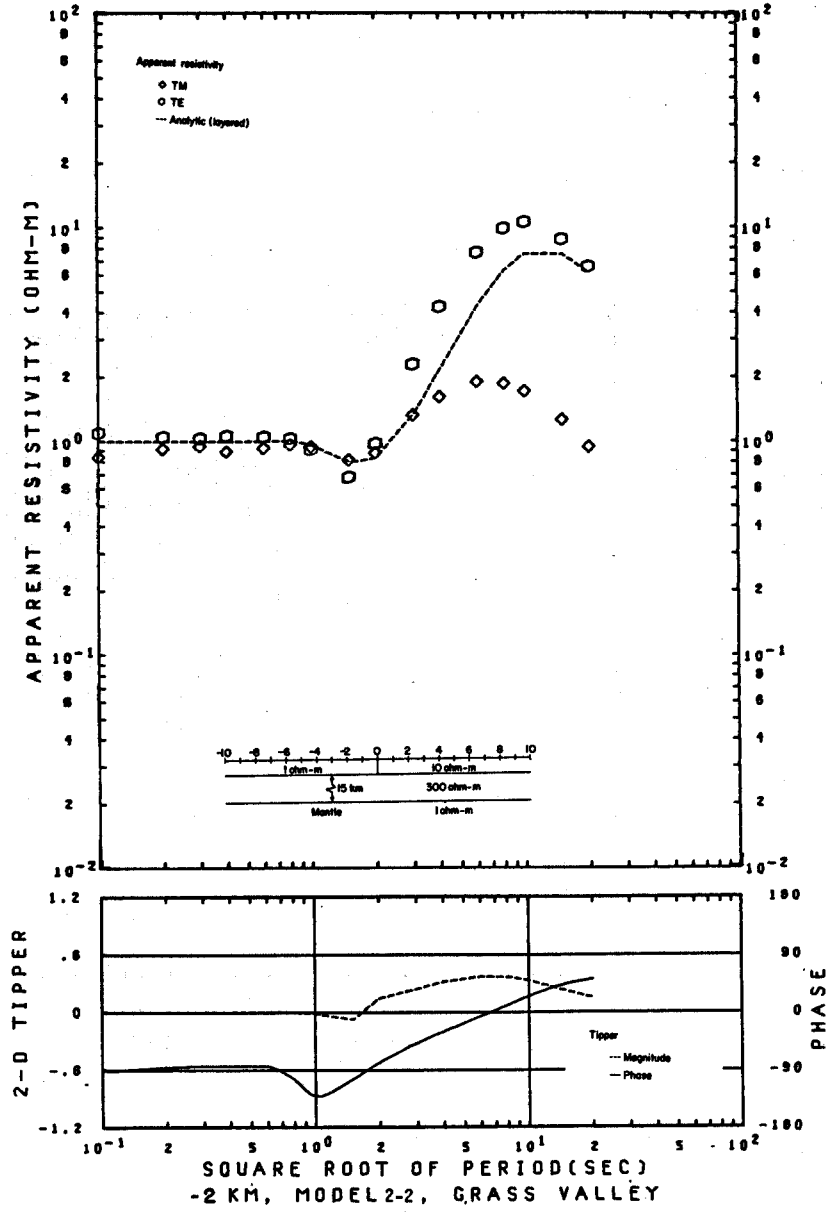
Apparent resistivity
TM
TE
Analytic (layered)
APPARENT RESISTIVITY (OHM-M)
1 ohm-m
10 ohm-m
15 km
300 ohm-m
Mantle
1 ohm-m
2-D TIPPER
PHASE
Tipper
Magnitude
Phase
SQUARE ROOT OF PERIOD(SEC)
-2 KM, MODEL 2-2, GRASS VALLEY

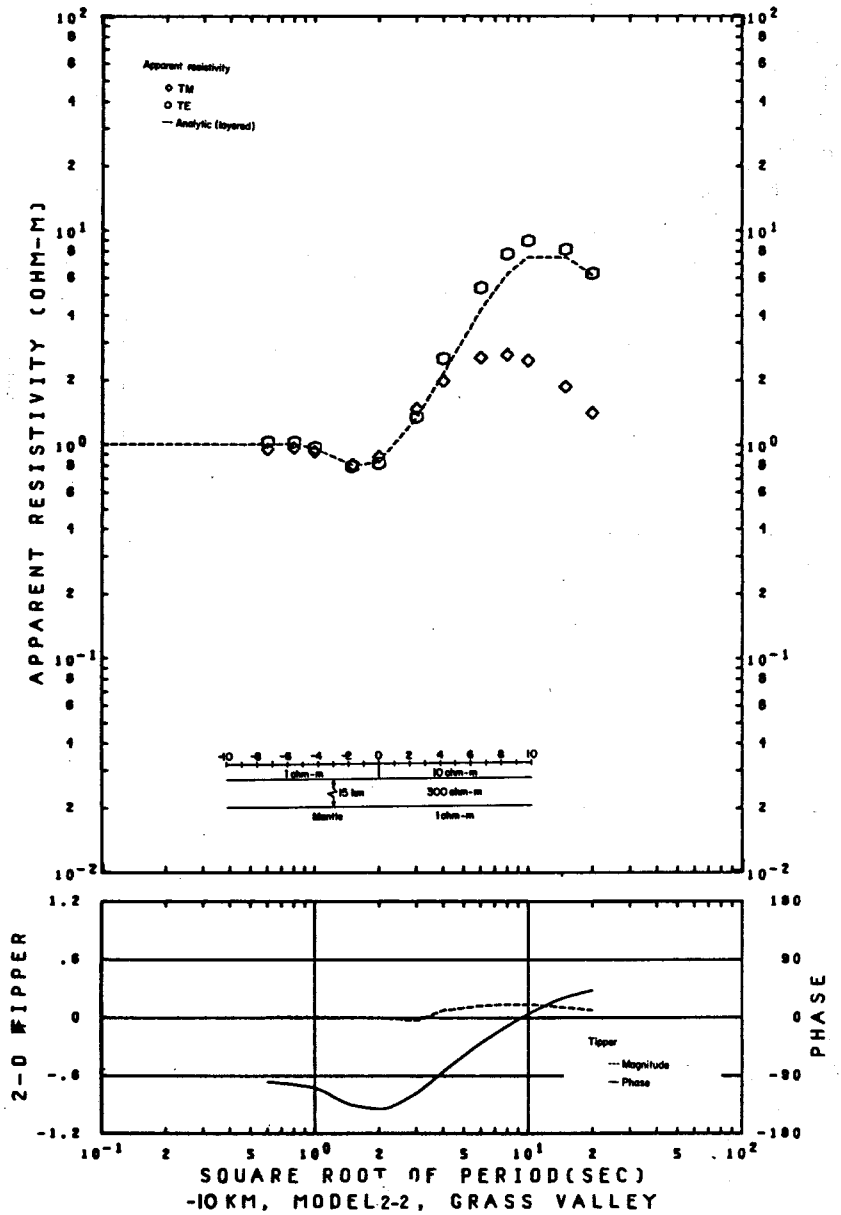
Apparent resistivity
TM
TE
Analytic (layered)
APPARENT RESISTIVITY (OHM-M)
1 ohm-m
10 ohm-m
15 km
300 ohm-m
Mantle
1 ohm-m
2-D TIPPER
PHASE
Tipper
Magnitude
Phase
SQUARE ROOT OF PERIOD(SEC)
-10KM, MODEL2-2, GRASS VALLEY

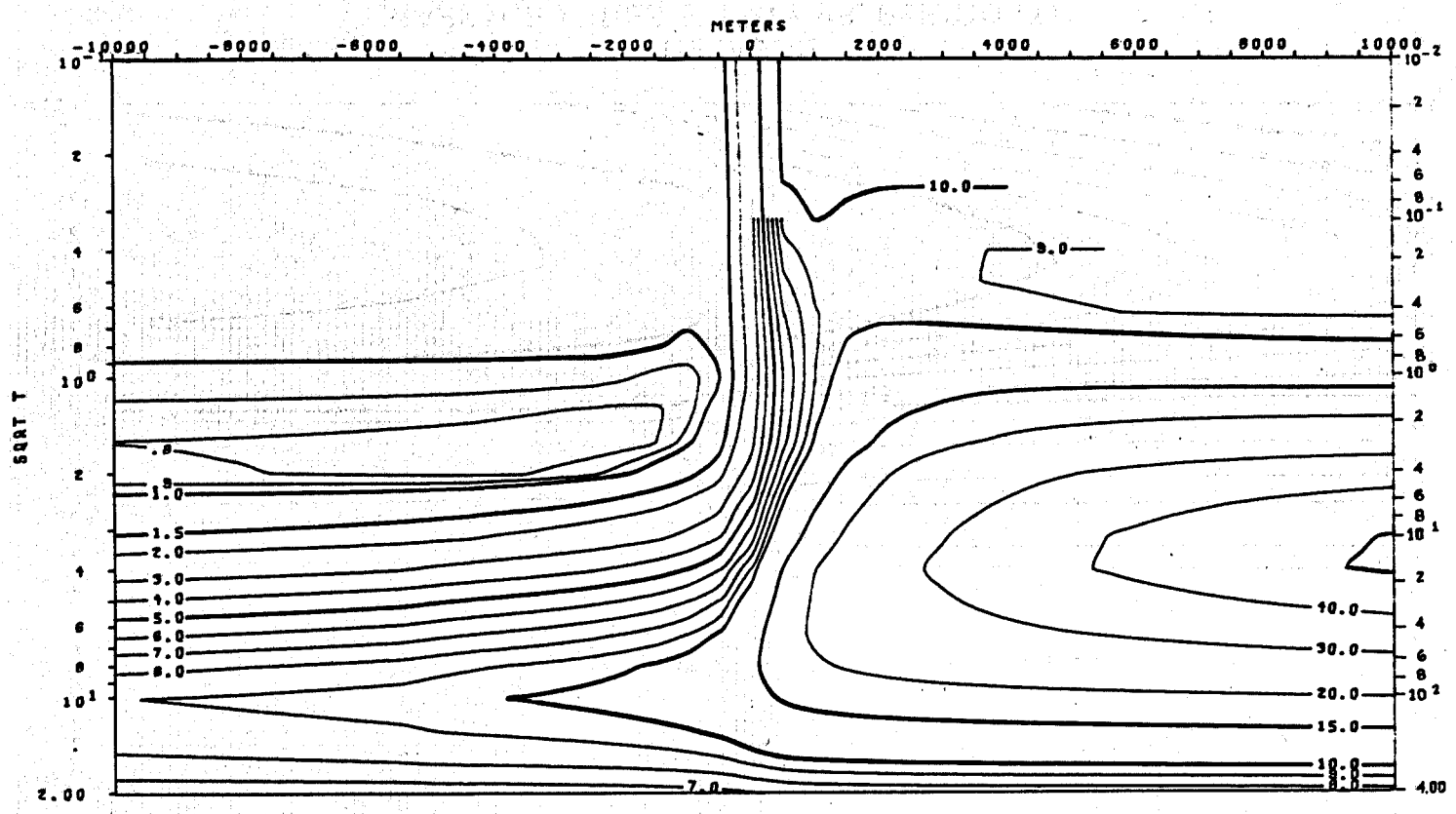

TE MODE
APPARENT RESISTIVITY VS. PERIOD (T)
MODEL 2-2

XBL 786-1926

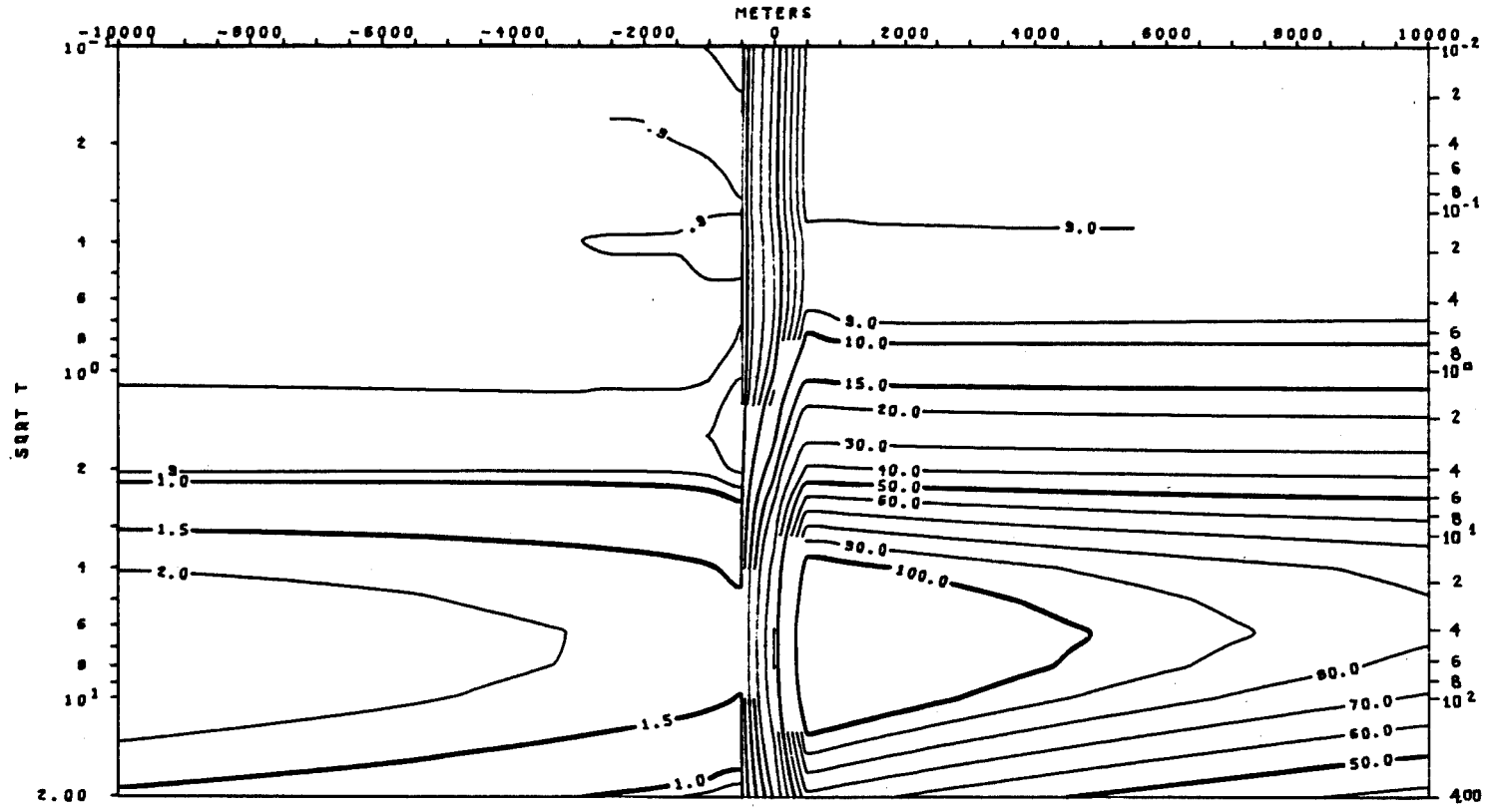

T

TM MODE
APPARENT RESISTIVITY VS. PERIOD (T)
MODEL 2-2

XBL 786-1913

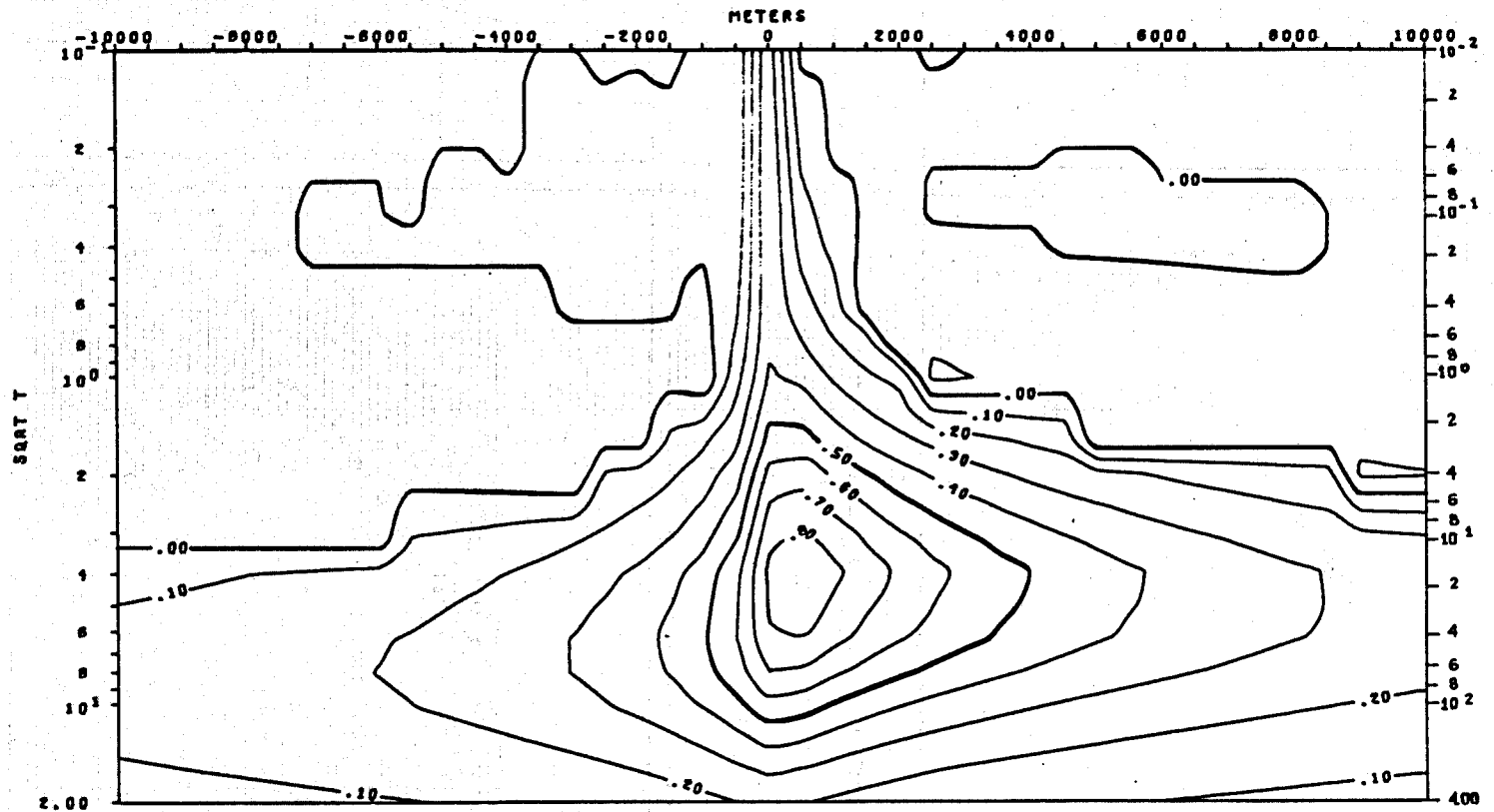

TIPPER VS. PERIOD (T)
MODEL 2-2

XBL 786-1912

T

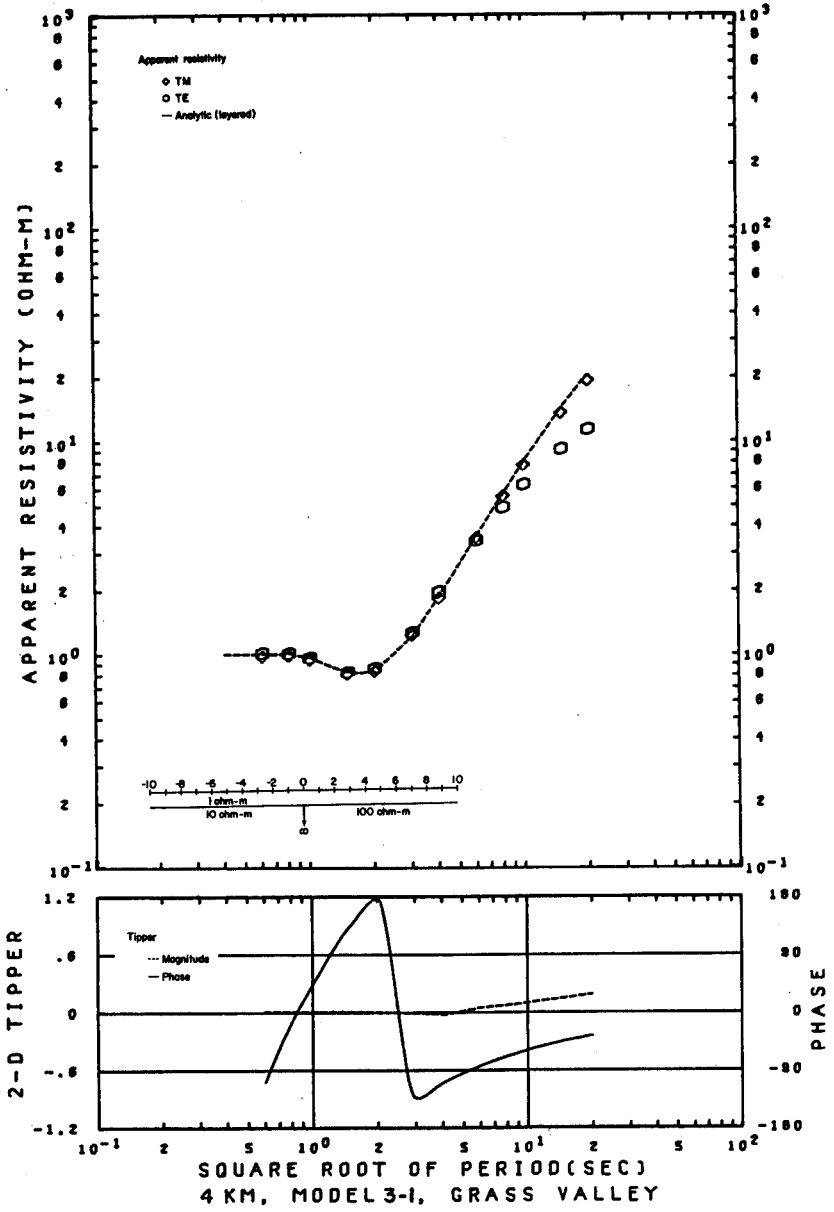
Apparent resistivity
TM
TE
Analytic (layered)
APPARENT RESISTIVITY (OHM-M)
1 ohm-m
10 ohm-m
100 ohm-m
Tipper
Magnitude
Phase
2-D TIPPER
PHASE
SQUARE ROOT OF PERIOD(SEC)
4 KM, MODEL 3-1, GRASS VALLEY

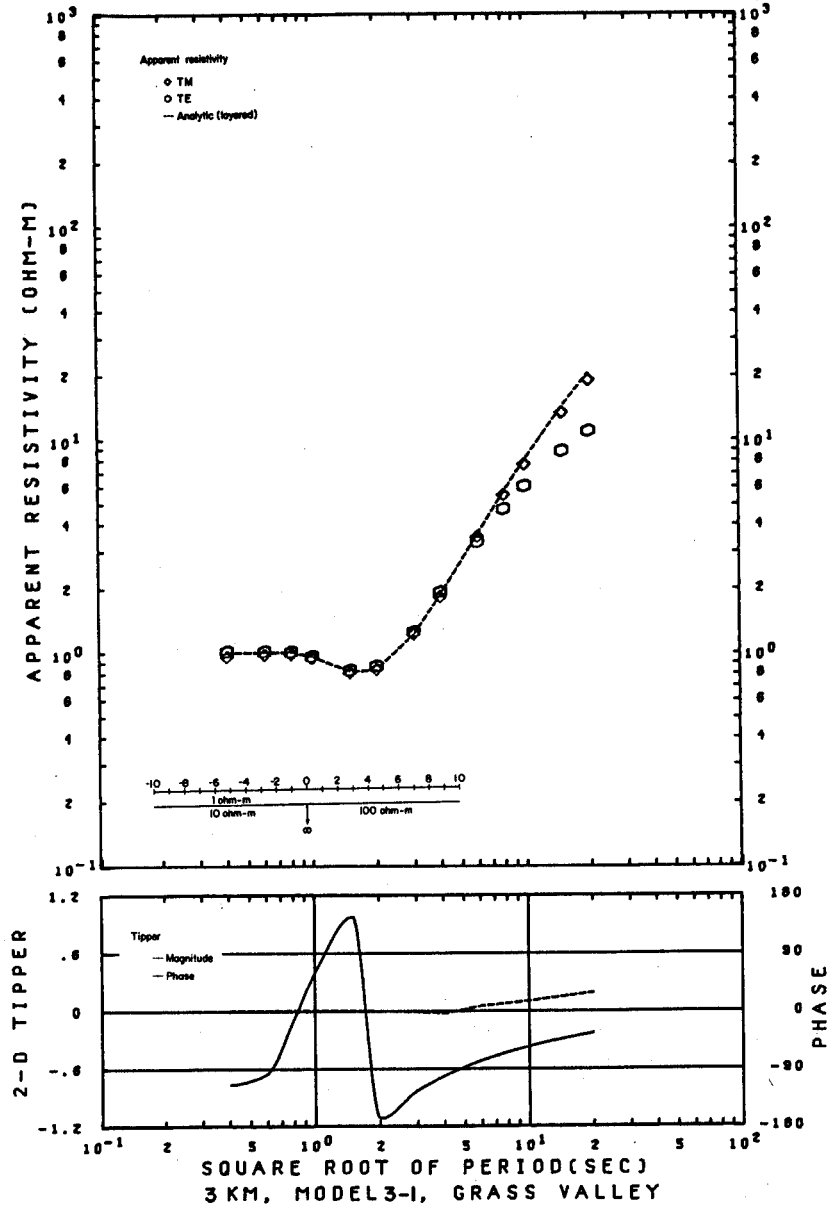
Apparent resistivity
TM
TE
Analytic (layered)
APPARENT RESISTIVITY (OHM-M)
1 ohm-m
10 ohm-m
100 ohm-m
Tipper
Magnitude
Phase
2-D TIPPER
PHASE
SQUARE ROOT OF PERIOD(SEC)
3 KM, MODEL 3-1, GRASS VALLEY

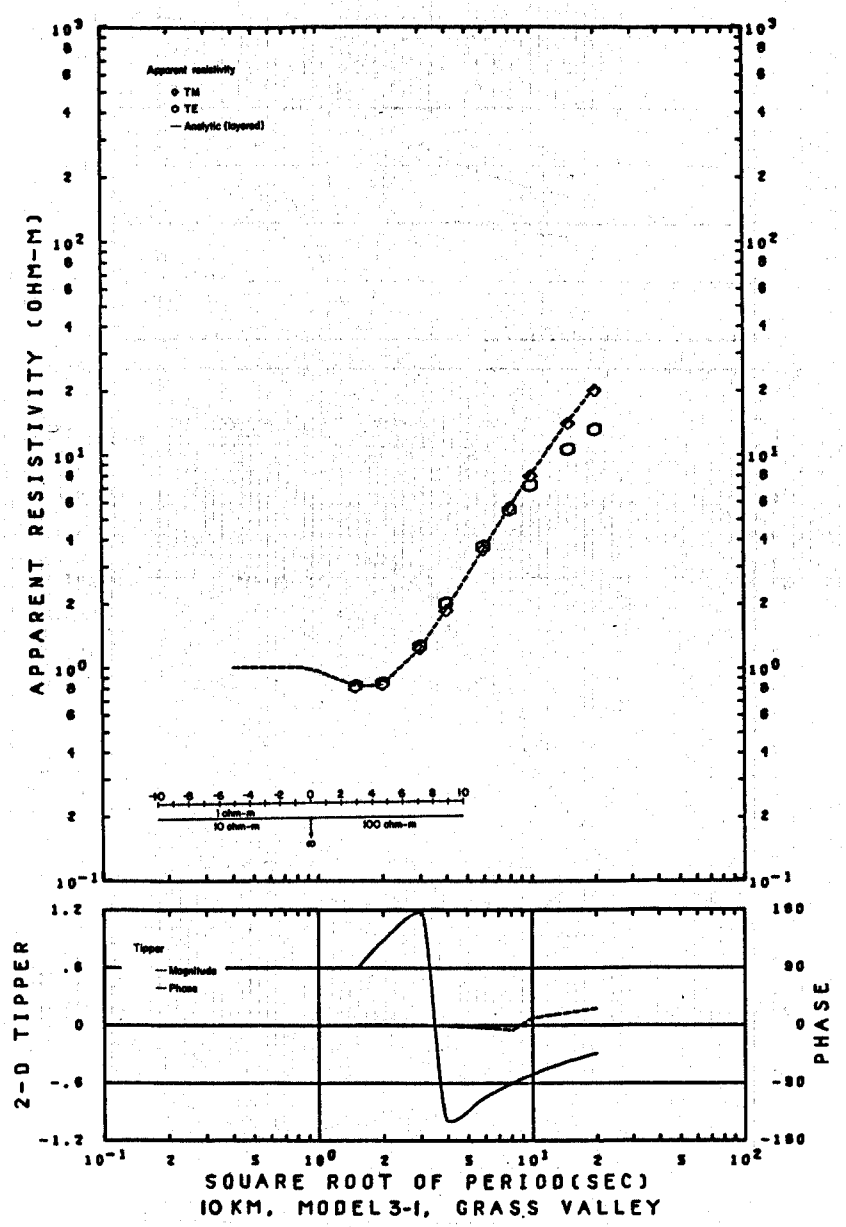
Apparent resistivity
TM
TE
Analytic (layered)
APPARENT RESISTIVITY (OHM-M)
1 ohm-m
10 ohm-m
100 ohm-m
Tipper
Magnitude
Phase
2-D TIPPER
PHASE
SQUARE ROOT OF PERIOD(SEC)
10KM, MODEL3-1, GRASS VALLEY

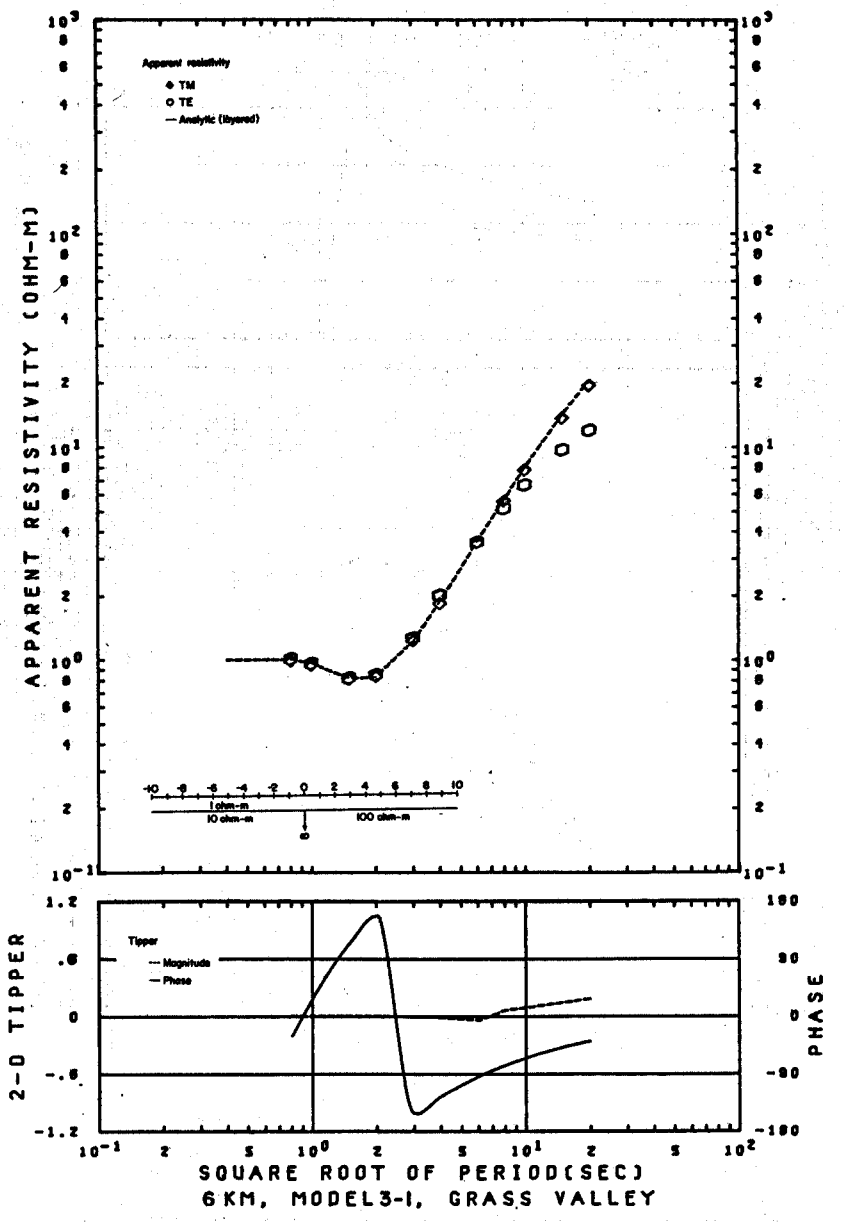
Apparent resistivity
TM
TE
Analytic (layered)
APPARENT RESISTIVITY (OHM-M)
1 ohm-m
10 ohm-m
100 ohm-m
Tipper
Magnitude
Phase
2-D TIPPER
PHASE
SQUARE ROOT OF PERIOD(SEC)
6KM, MODEL3-1, GRASS VALLEY

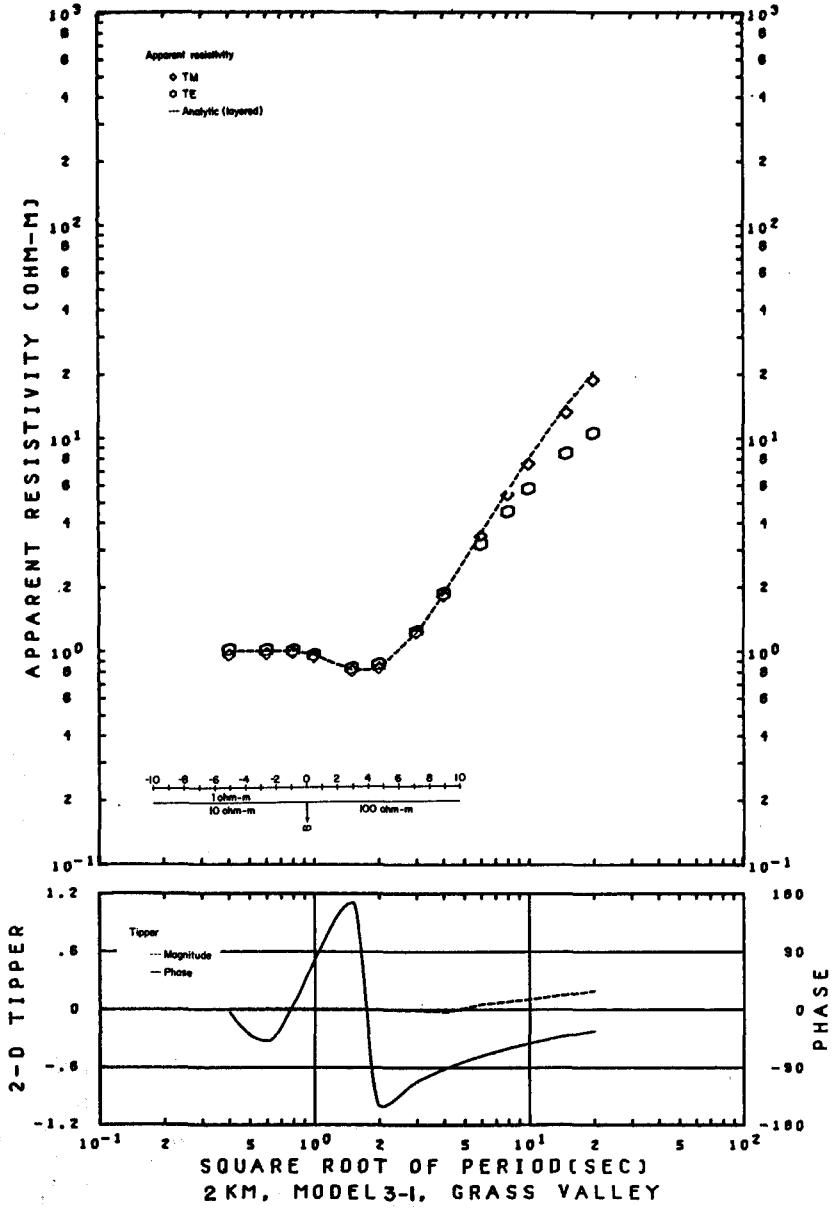
Apparent resistivity
TM
TE
Analytic (layered)
APPARENT RESISTIVITY (OHM-M)
1 ohm-m
10 ohm-m
100 ohm-m
Tipper
Magnitude
Phase
2-D TIPPER
PHASE
SQUARE ROOT OF PERIOD(SEC)
2 KM, MODEL 3-I, GRASS VALLEY

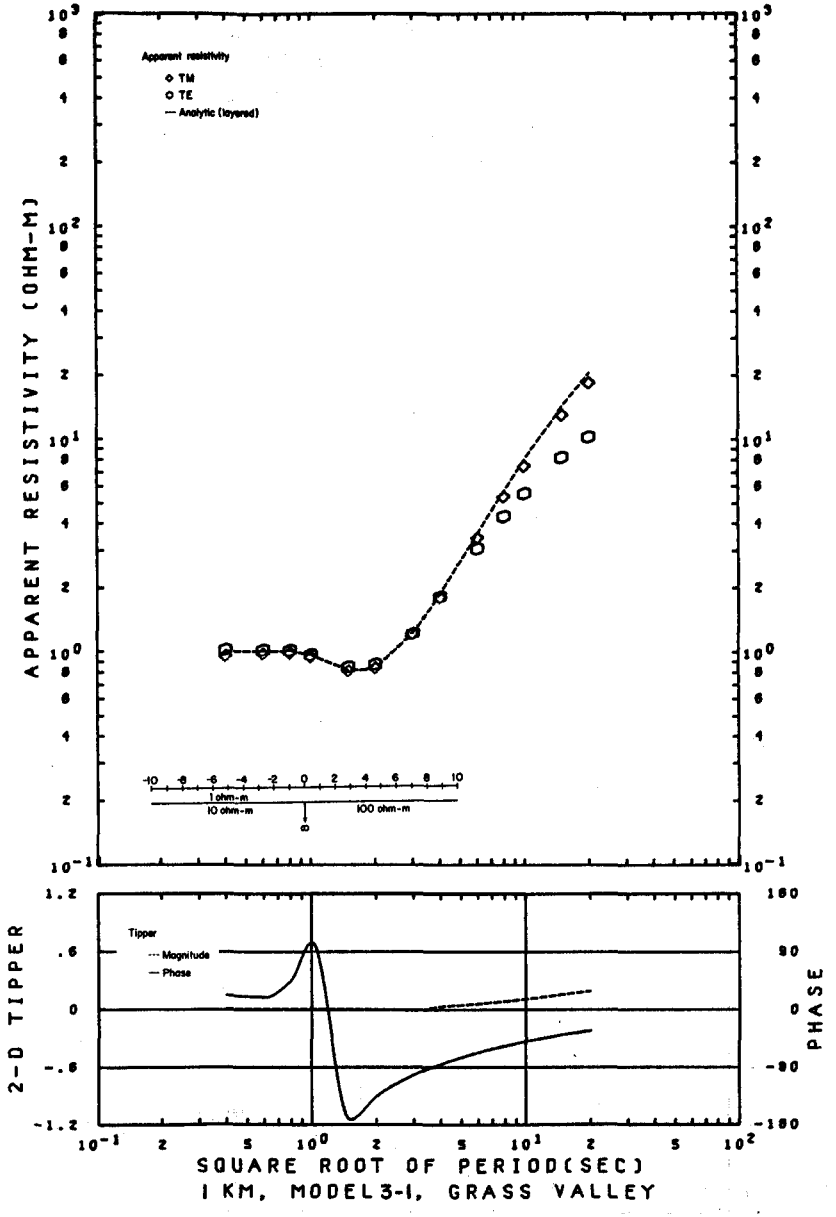
Apparent resistivity
TM
TE
Analytic (layered)
APPARENT RESISTIVITY (OHM-M)
1 ohm-m
10 ohm-m
100 ohm-m
Tipper
Magnitude
Phase
2-D TIPPER
PHASE
SQUARE ROOT OF PERIOD(SEC)
1 KM, MODEL 3-I, GRASS VALLEY

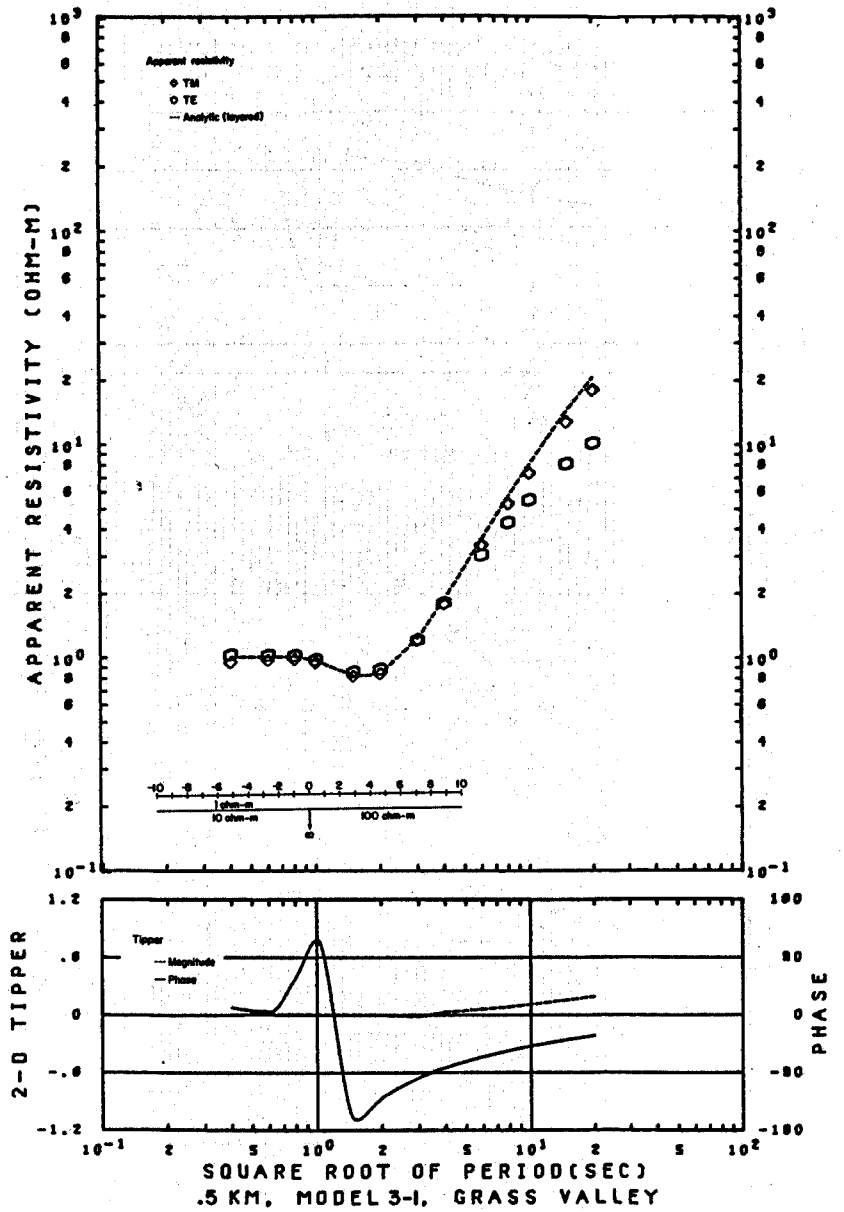

.5 KM, MODEL 3-I, GRASS VALLEY

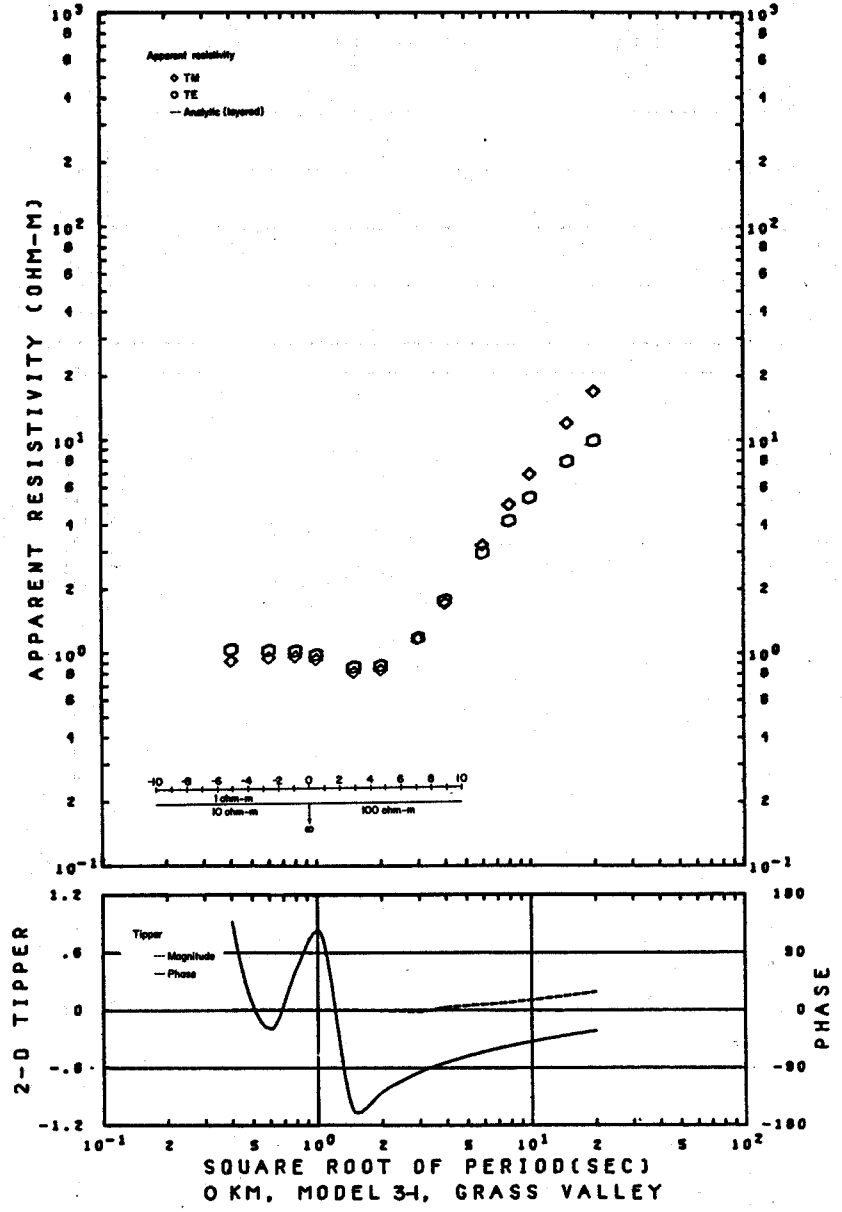

0 KM, MODEL 3-I, GRASS VALLEY

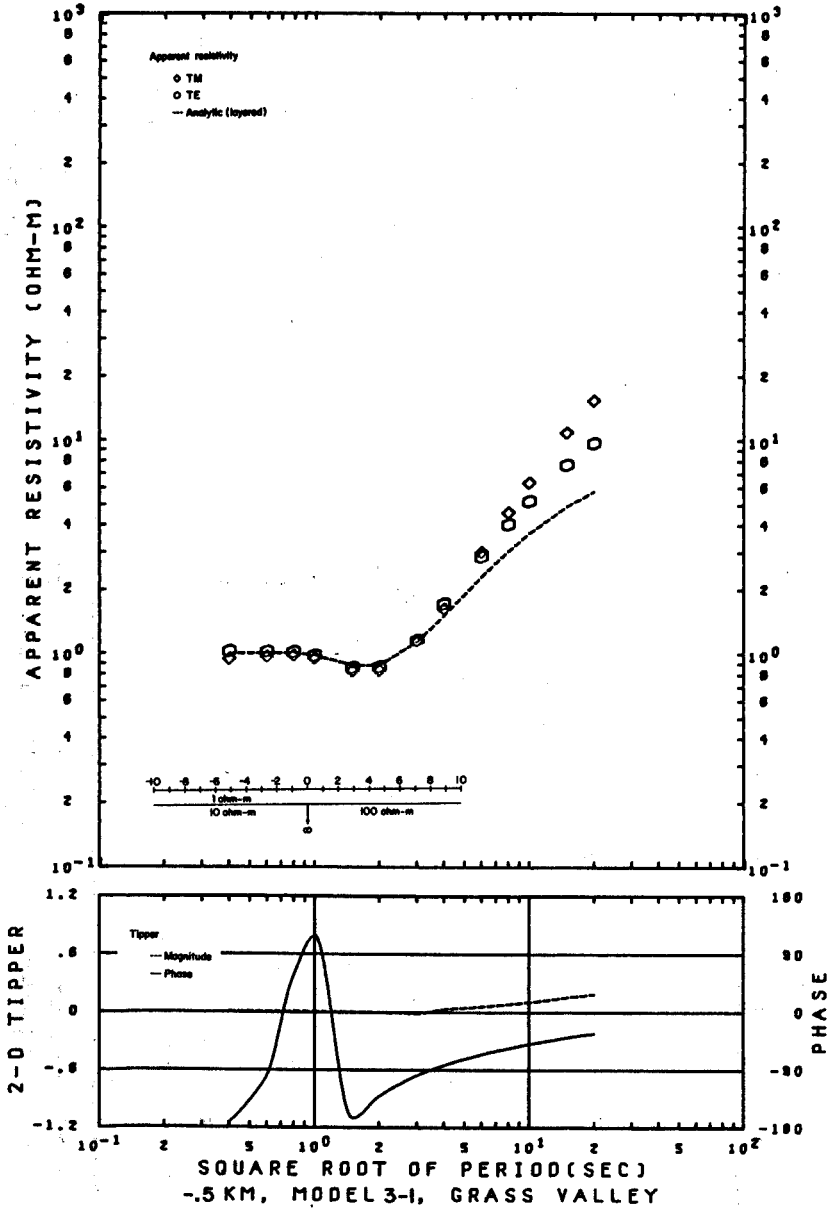
Apparent resistivity
TM
TE
Analytic (layered)
APPARENT RESISTIVITY (OHM-M)
1 ohm-m
10 ohm-m
100 ohm-m
Tipper
Magnitude
Phase
2-D TIPPER
PHASE
SQUARE ROOT OF PERIOD(SEC)
-.5 KM, MODEL 3-1, GRASS VALLEY

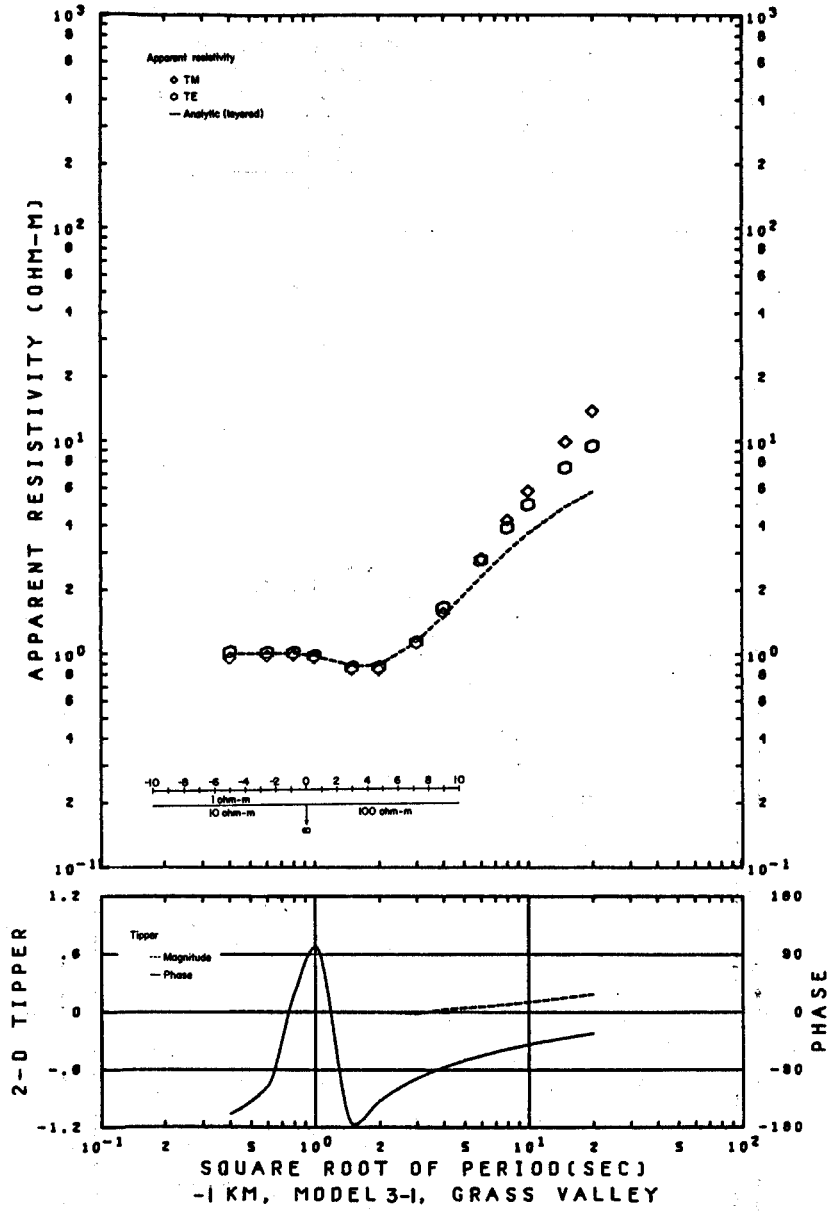
Apparent resistivity
TM
TE
Analytic (layered)
APPARENT RESISTIVITY (OHM-M)
1 ohm-m
10 ohm-m
100 ohm-m
Tipper
Magnitude
Phase
2-D TIPPER
PHASE
SQUARE ROOT OF PERIOD(SEC)
-1 KM, MODEL 3-1, GRASS VALLEY

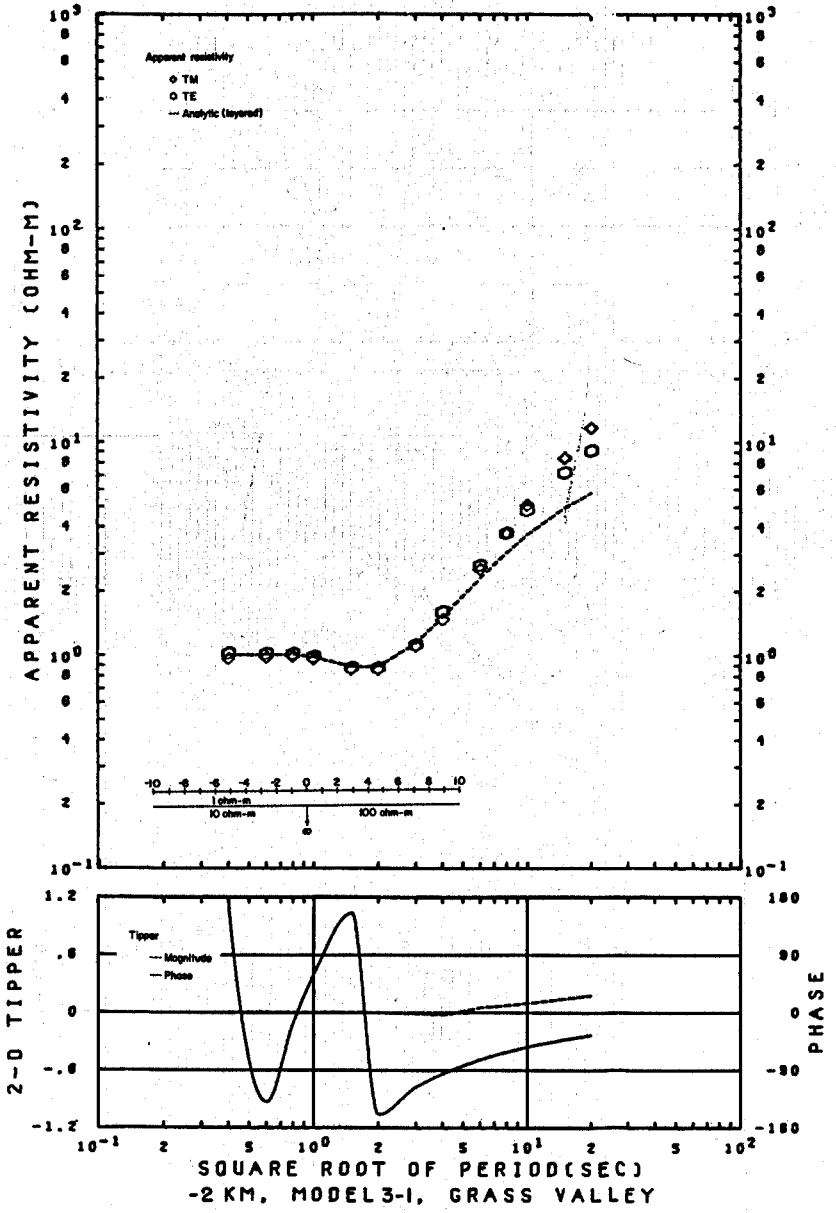
Apparent resistivity
TM
TE
Analytic (layered)
APPARENT RESISTIVITY (OHM-M)
1 ohm-m
10 ohm-m
100 ohm-m
Tipper
Magnitude
Phase
2-D TIPPER
PHASE
SQUARE ROOT OF PERIOD(SEC)
-2 KM, MODEL 3-1, GRASS VALLEY

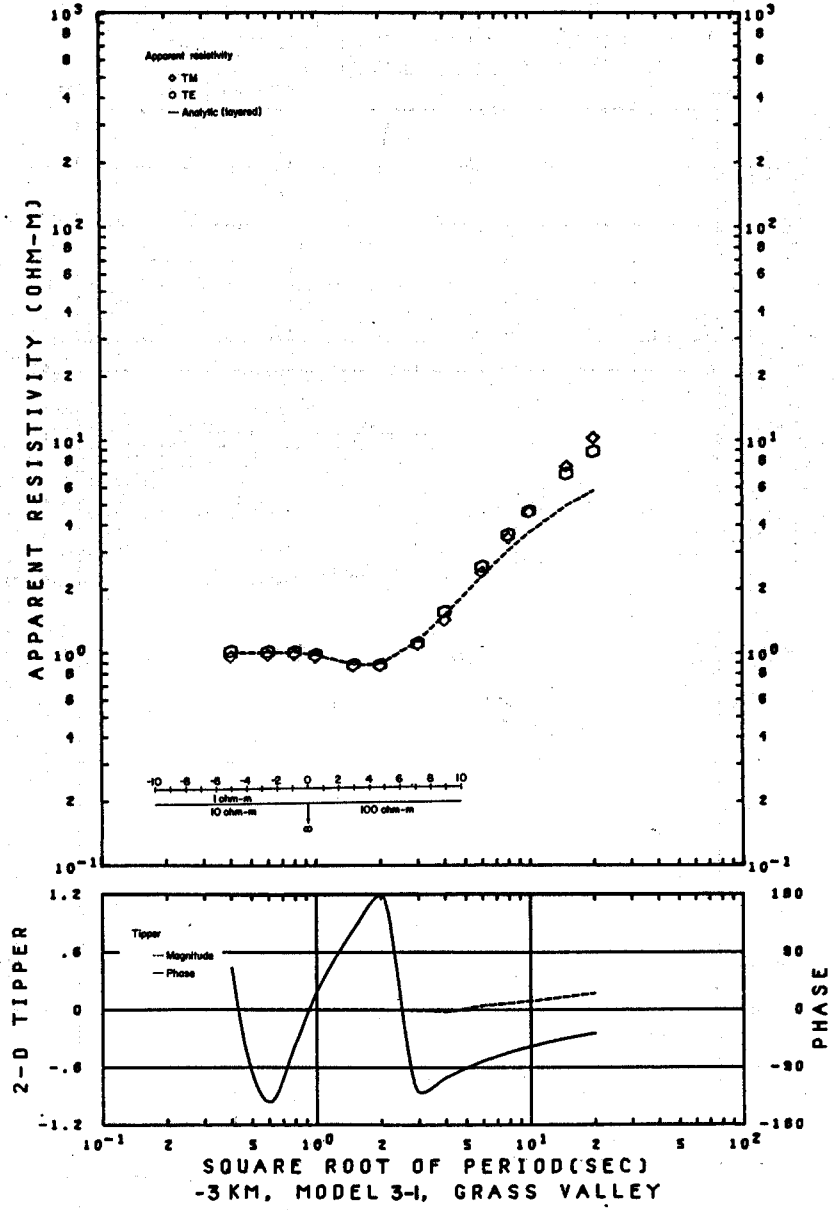
Apparent resistivity
TM
TE
Analytic (layered)
APPARENT RESISTIVITY (OHM-M)
1 ohm-m
10 ohm-m
100 ohm-m
Tipper
Magnitude
Phase
2-D TIPPER
PHASE
SQUARE ROOT OF PERIOD(SEC)
-3 KM, MODEL 3-1, GRASS VALLEY

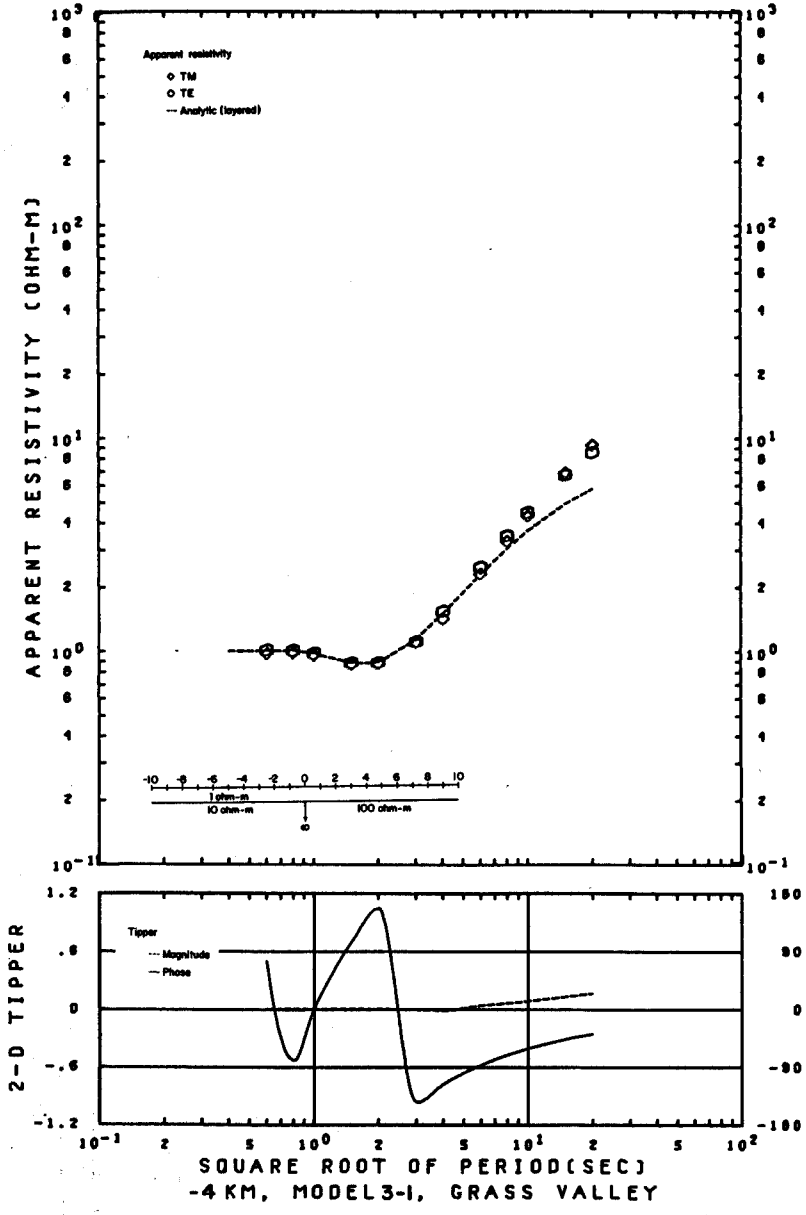
Apparent resistivity
TM
TE
Analytic (layered)
APPARENT RESISTIVITY (OHM-M)
1 ohm-m
10 ohm-m
100 ohm-m
Tipper
Magnitude
Phase
2-D TIPPER
PHASE
SQUARE ROOT OF PERIOD(SEC)
-4 KM, MODEL 3-I, GRASS VALLEY

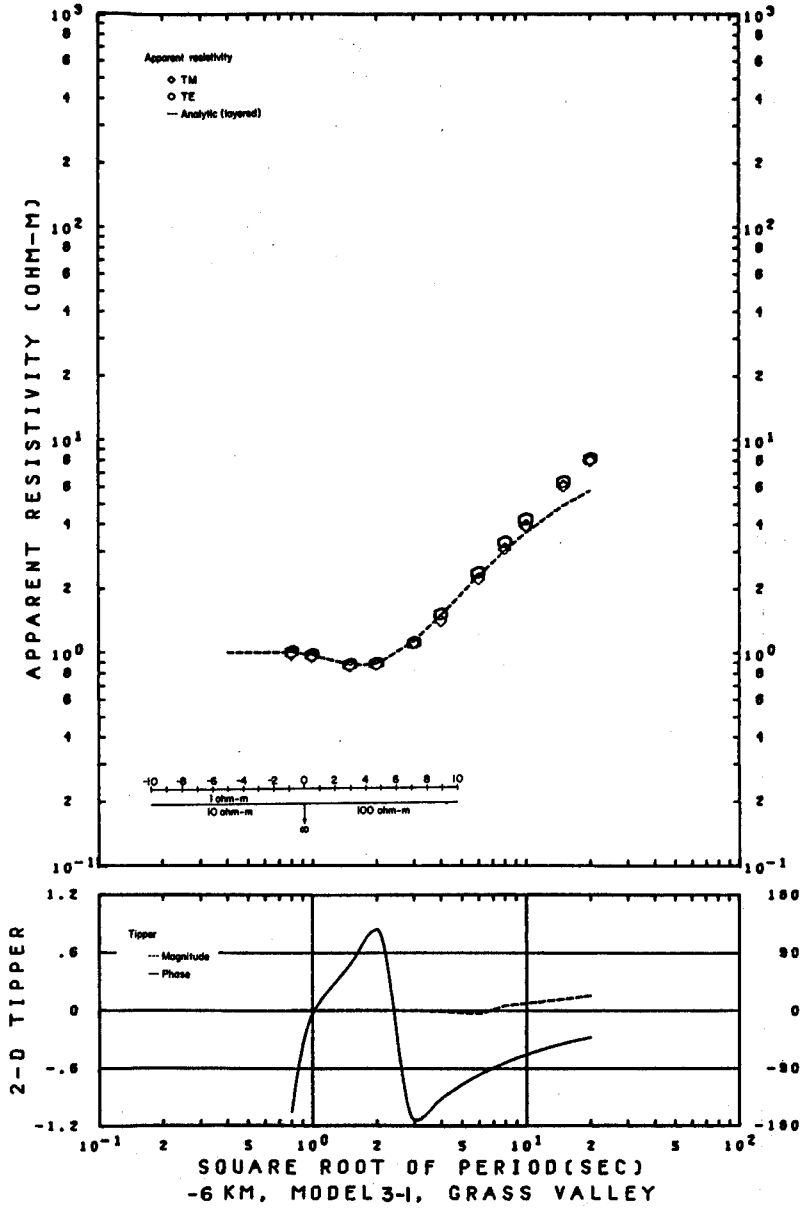
Apparent resistivity
TM
TE
Analytic (layered)
APPARENT RESISTIVITY (OHM-M)
1 ohm-m
10 ohm-m
100 ohm-m
Tipper
Magnitude
Phase
2-D TIPPER
PHASE
SQUARE ROOT OF PERIOD(SEC)
-6 KM, MODEL 3-I, GRASS VALLEY

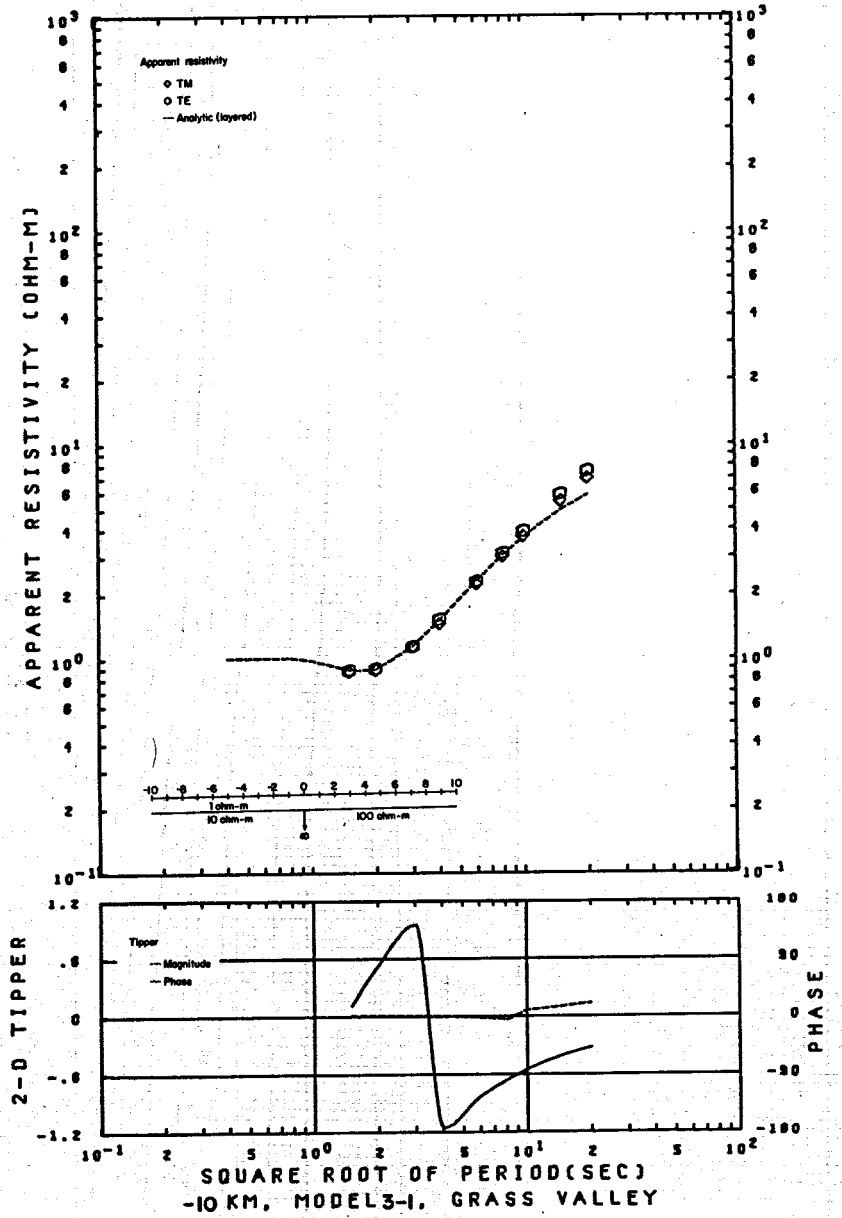
Apparent resistivity
TM
TE
Analytic (layered)
APPARENT RESISTIVITY (OHM-M)
1 ohm-m
10 ohm-m
100 ohm-m
Tipper
Magnitude
Phase
2-D TIPPER
PHASE
SQUARE ROOT OF PERIOD(SEC)
-10 KM, MODEL3-1, GRASS VALLEY

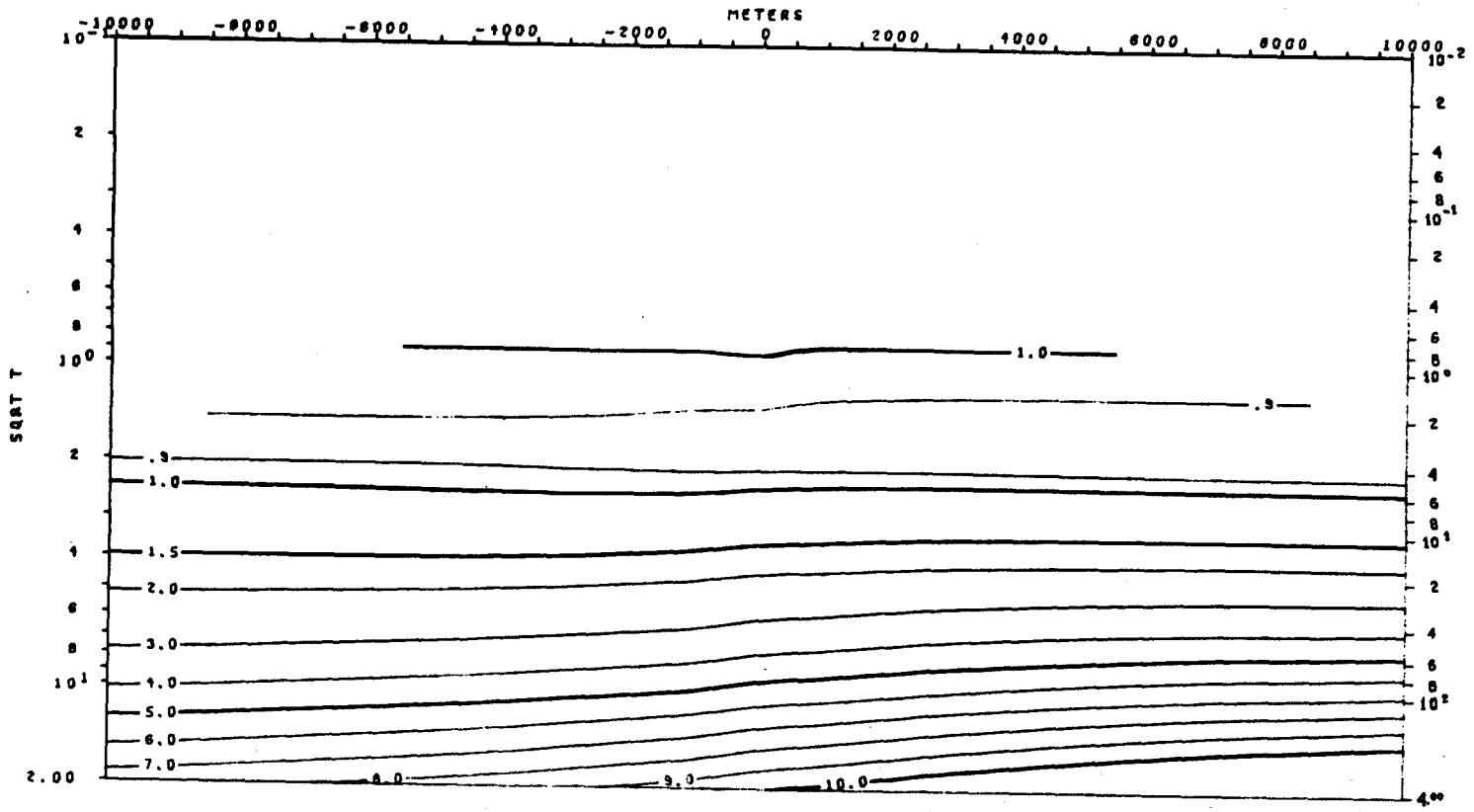

TE MODE
APPARENT RESISTIVITY VS. PERIOD (T)
MODEL 3-1

XBL 786-1936

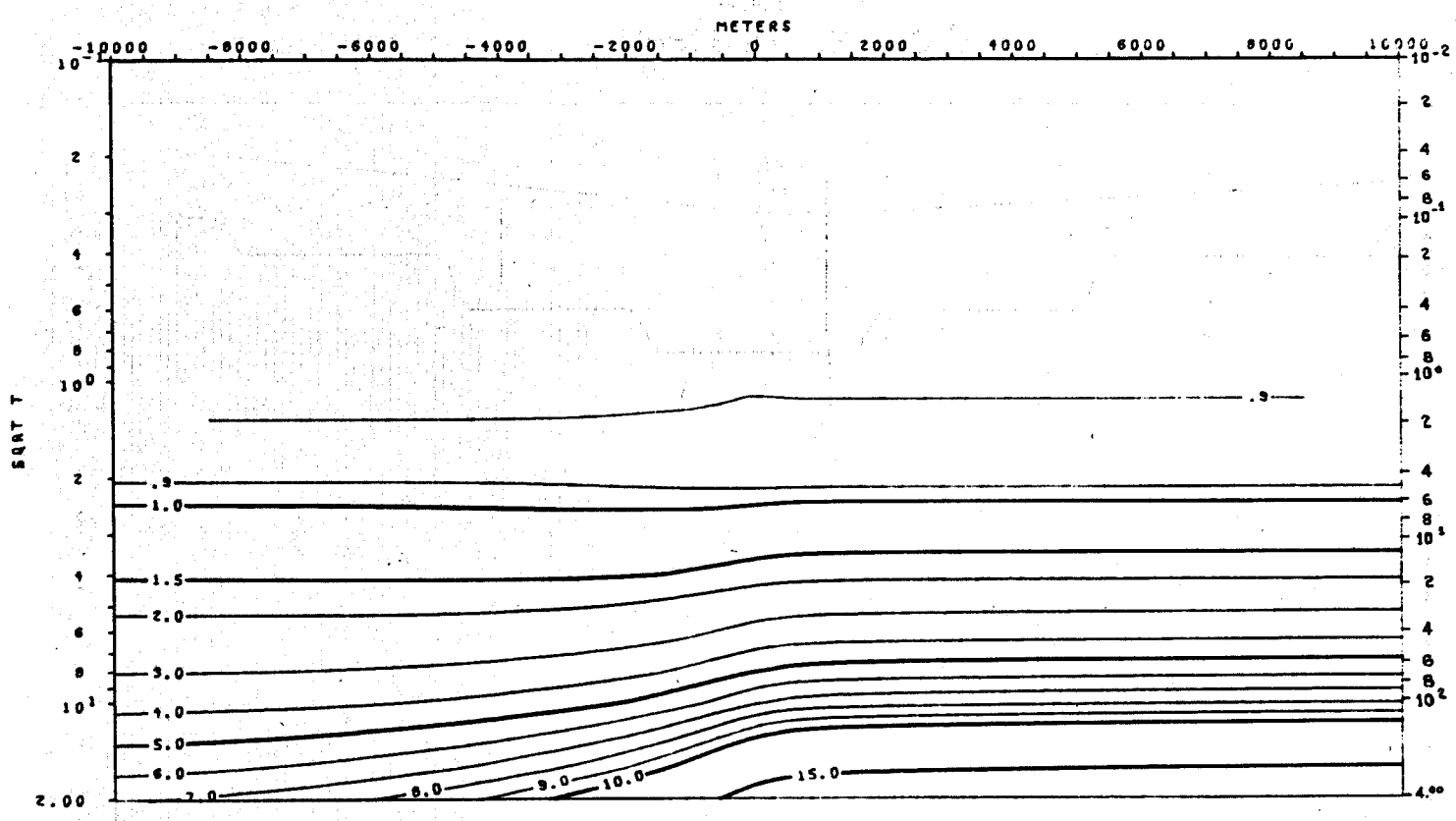

TM MODE
APPARENT RESISTIVITY VS. PERIOD (T)
MODEL 3-1

XBL 786-1919

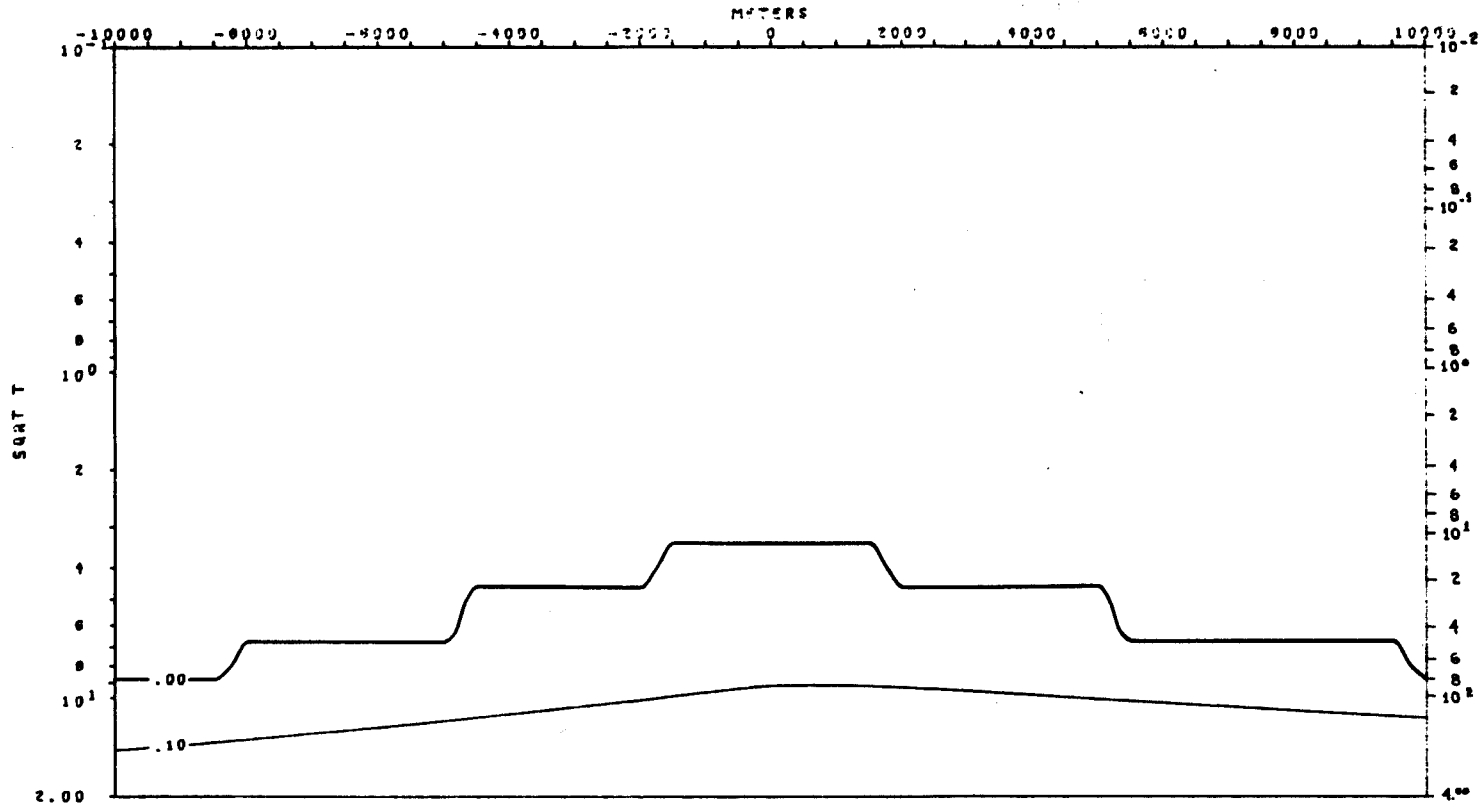

TIPPER VS. PERIOD (T)
MODEL 3-1

XBL 786-1918

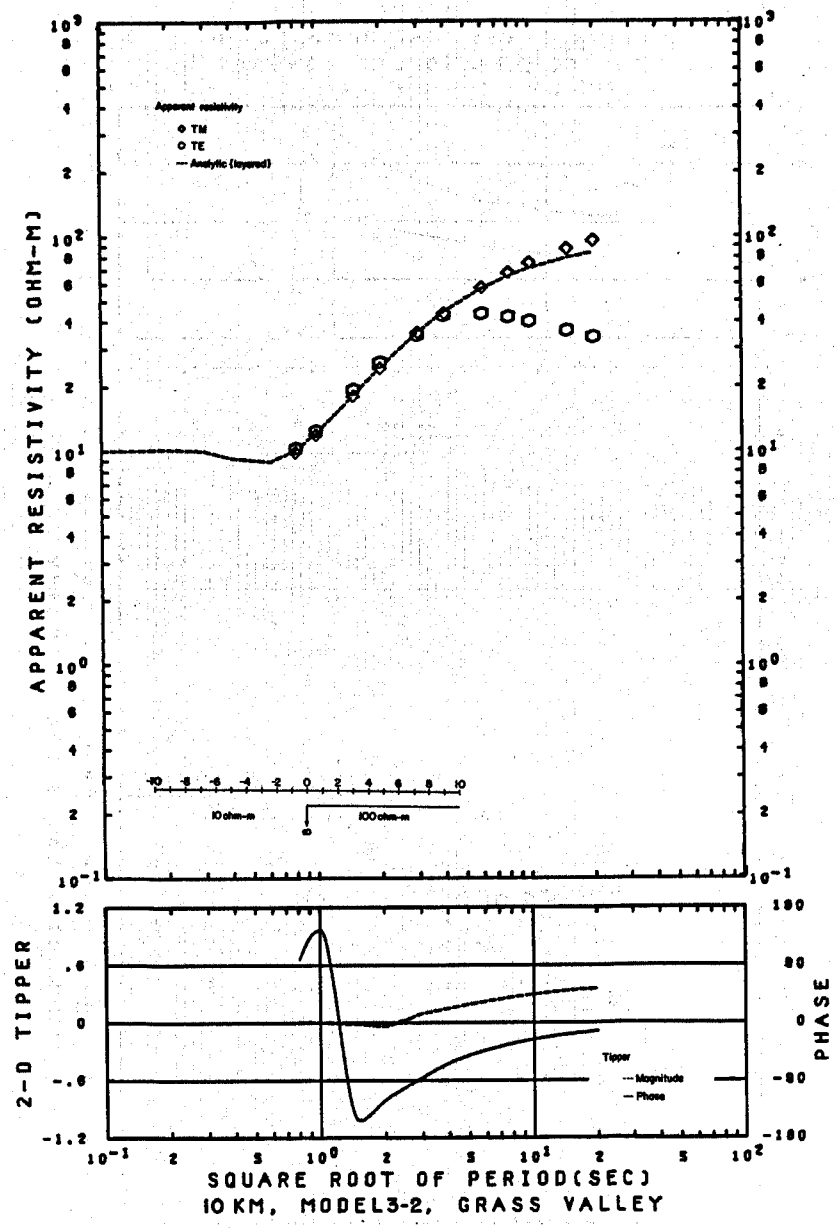
Apparent resistivity
TM
TE
Analytic (layered)
APPARENT RESISTIVITY (OHM-M)
10 ohm-m
100 ohm-m
2-D TIPPER
PHASE
Tipper
Magnitude
Phase
SQUARE ROOT OF PERIOD(SEC)
10 KM, MODEL3-2, GRASS VALLEY

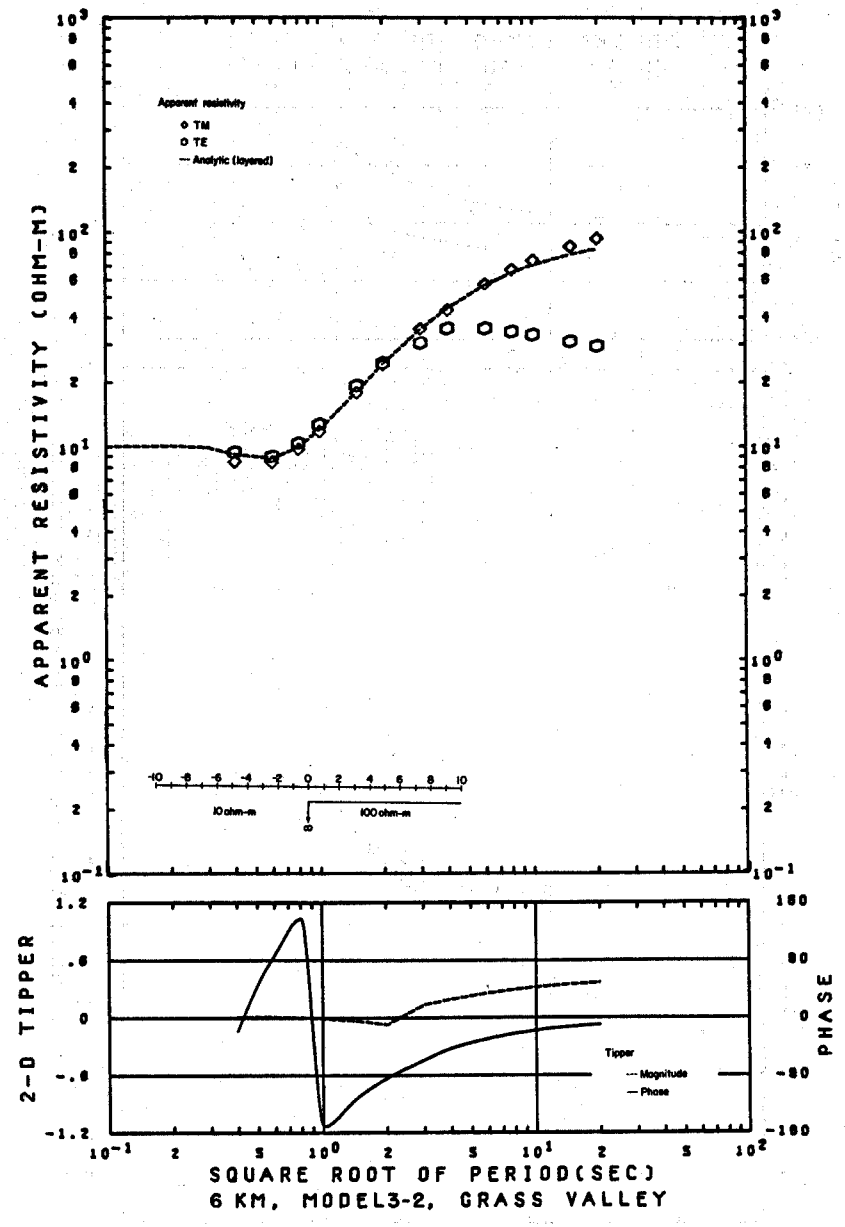
Apparent resistivity
TM
TE
Analytic (layered)
APPARENT RESISTIVITY (OHM-M)
10 ohm-m
100 ohm-m
2-D TIPPER
PHASE
Tipper
Magnitude
Phase
SQUARE ROOT OF PERIOD(SEC)
6 KM, MODEL3-2, GRASS VALLEY

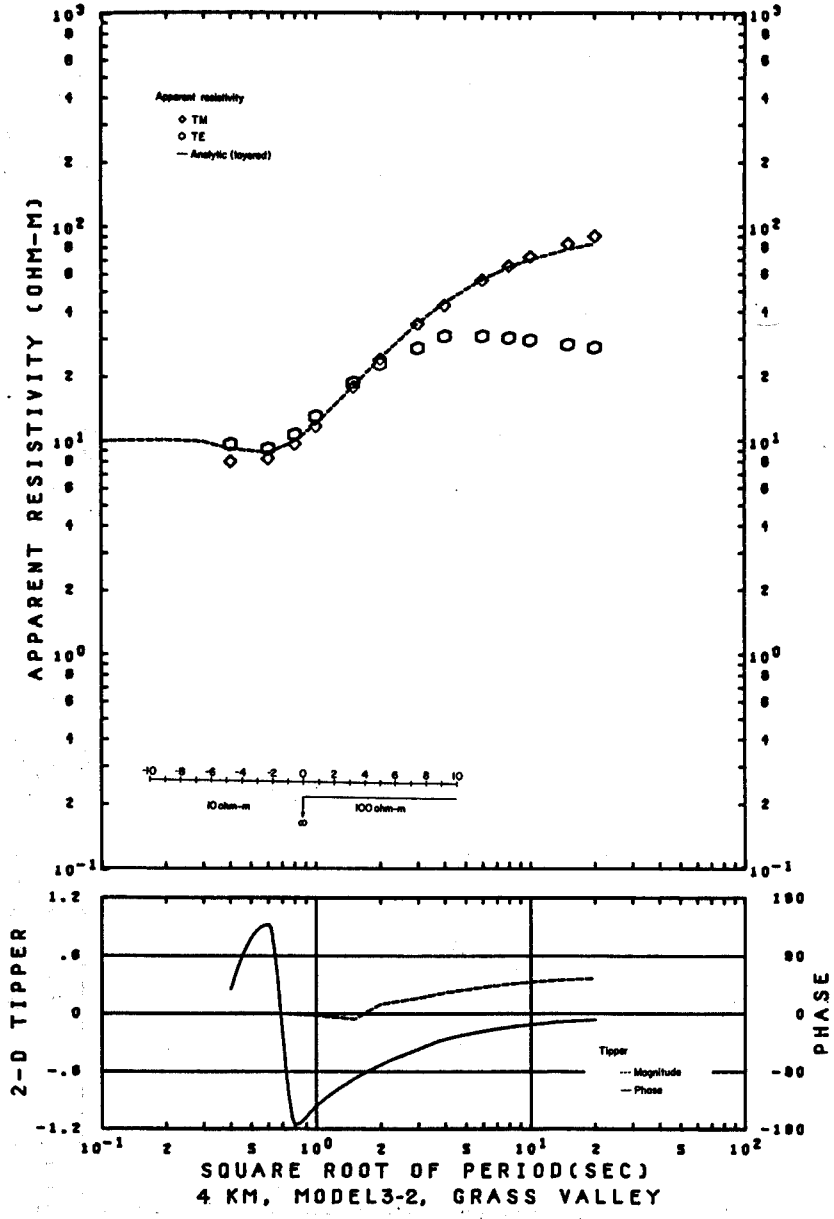
Apparent resistivity
TM
TE
Analytic (layered)
APPARENT RESISTIVITY (OHM-M)
10 ohm-m
100 ohm-m
2-D TIPPER
PHASE
Tipper
Magnitude
Phase
SQUARE ROOT OF PERIOD(SEC)
4 KM, MODEL3-2, GRASS VALLEY

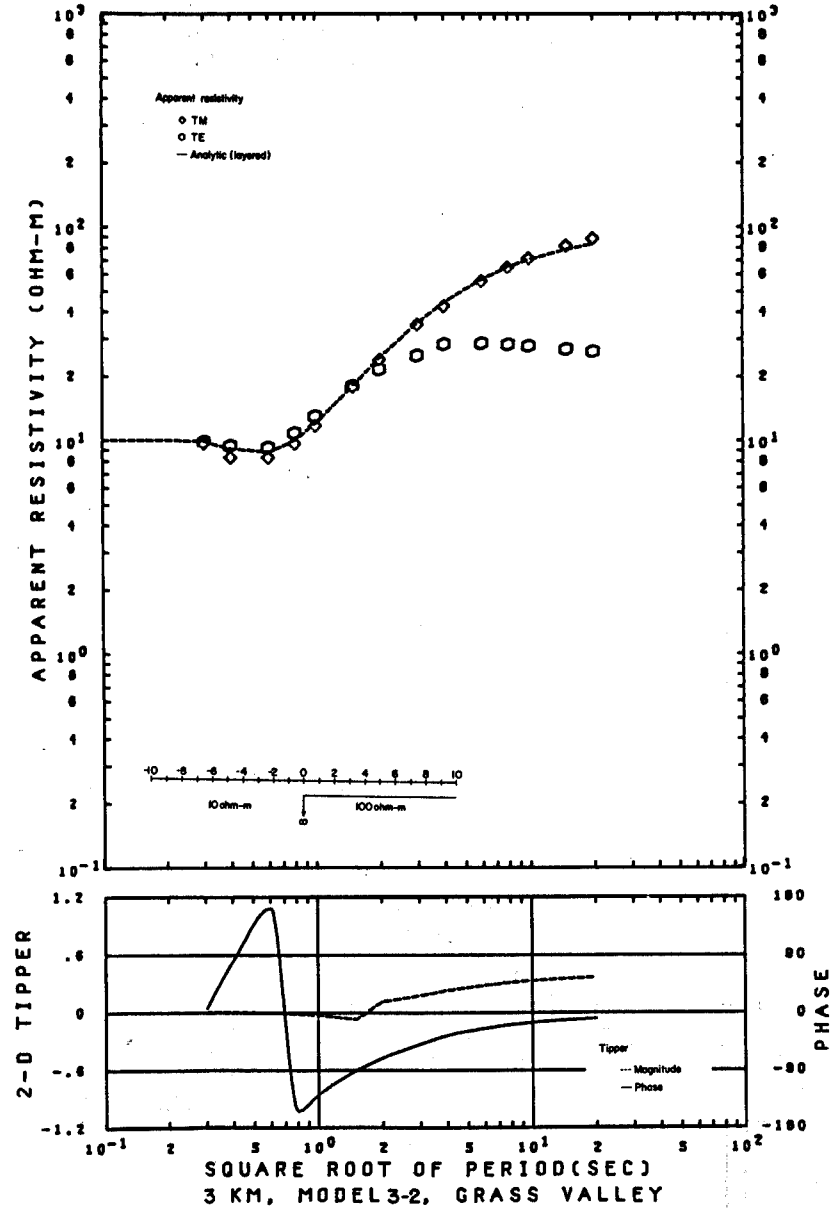
Apparent resistivity
TM
TE
Analytic (layered)
APPARENT RESISTIVITY (OHM-M)
10 ohm-m
100 ohm-m
2-D TIPPER
PHASE
Tipper
Magnitude
Phase
SQUARE ROOT OF PERIOD(SEC)
3 KM, MODEL3-2, GRASS VALLEY

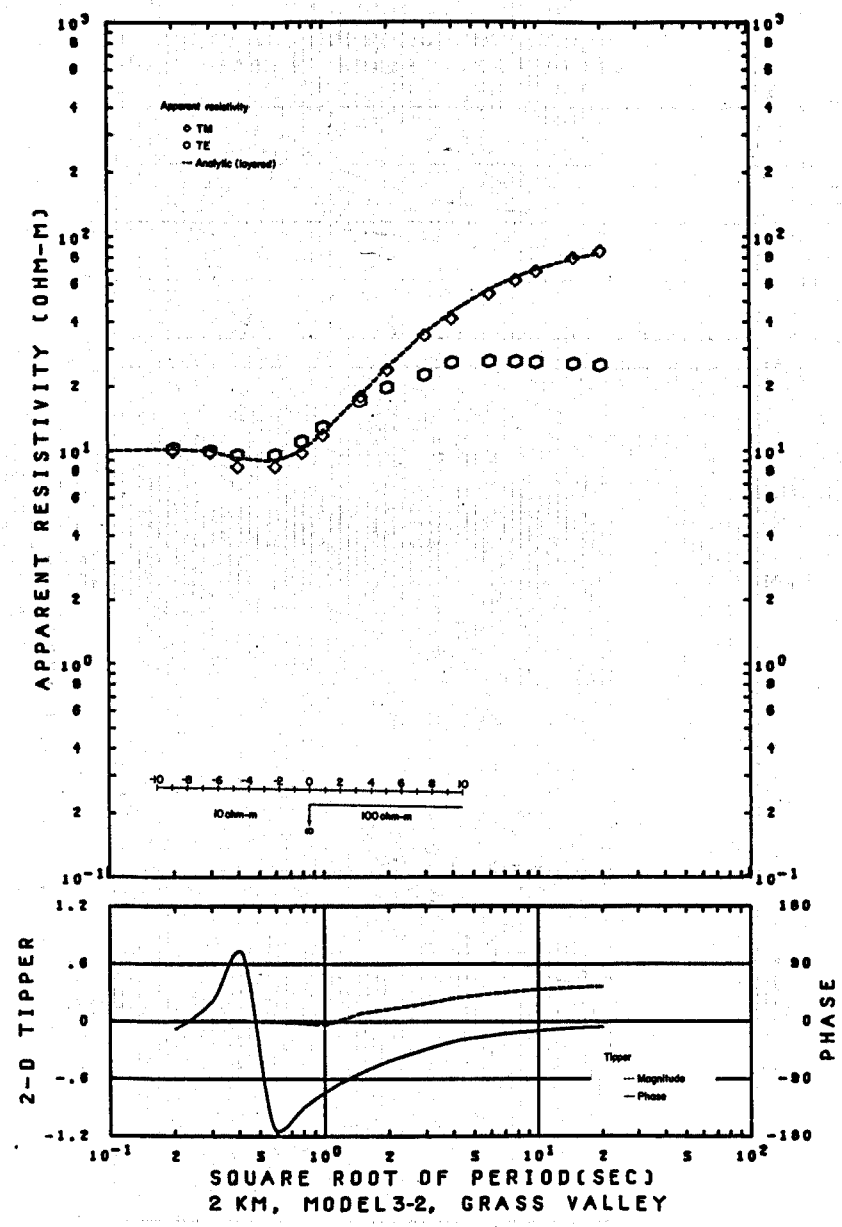
Apparent resistivity
TM
TE
Analytic (layered)
APPARENT RESISTIVITY (OHM-M)
10 ohm-m
100 ohm-m
2-D TIPPER
PHASE
Tipper
Magnitude
Phase
SQUARE ROOT OF PERIOD(SEC)
2 KM, MODEL3-2, GRASS VALLEY

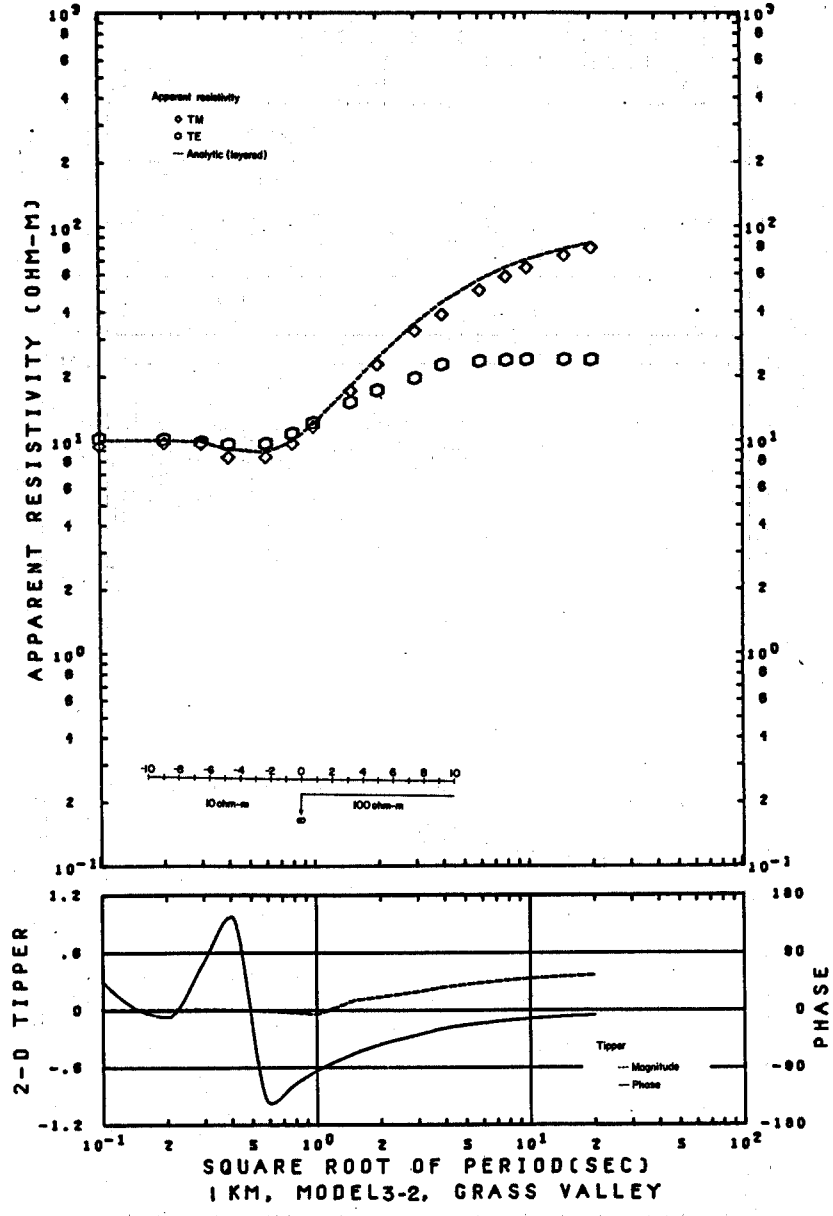
Apparent resistivity
TM
TE
Analytic (layered)
APPARENT RESISTIVITY (OHM-M)
10 ohm-m
100 ohm-m
2-D TIPPER
PHASE
Tipper
Magnitude
Phase
SQUARE ROOT OF PERIOD(SEC)
1 KM, MODEL3-2, GRASS VALLEY

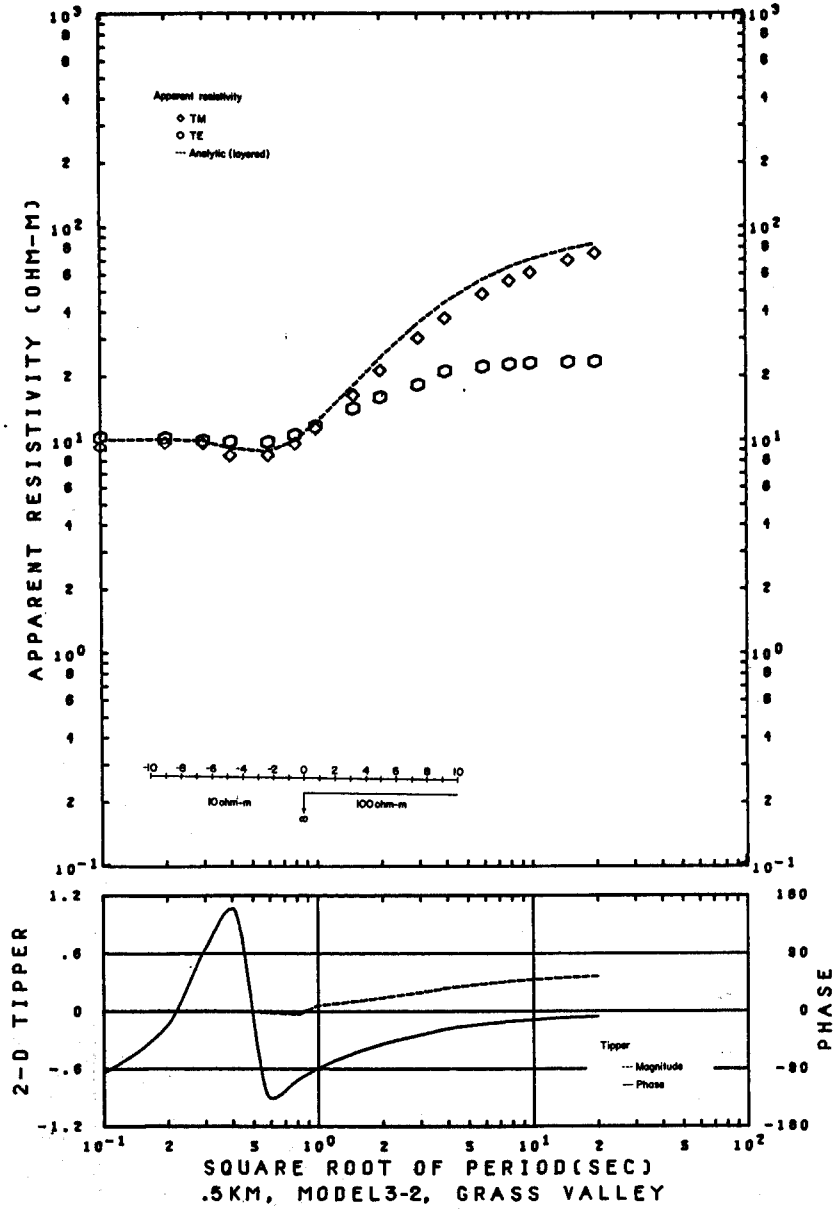
Apparent resistivity
TM
TE
Analytic (layered)
APPARENT RESISTIVITY (OHM-M)
10 ohm-m
100 ohm-m
2-D TIPPER
PHASE
Tipper
Magnitude
Phase
SQUARE ROOT OF PERIOD(SEC)
.5KM, MODEL3-2, GRASS VALLEY

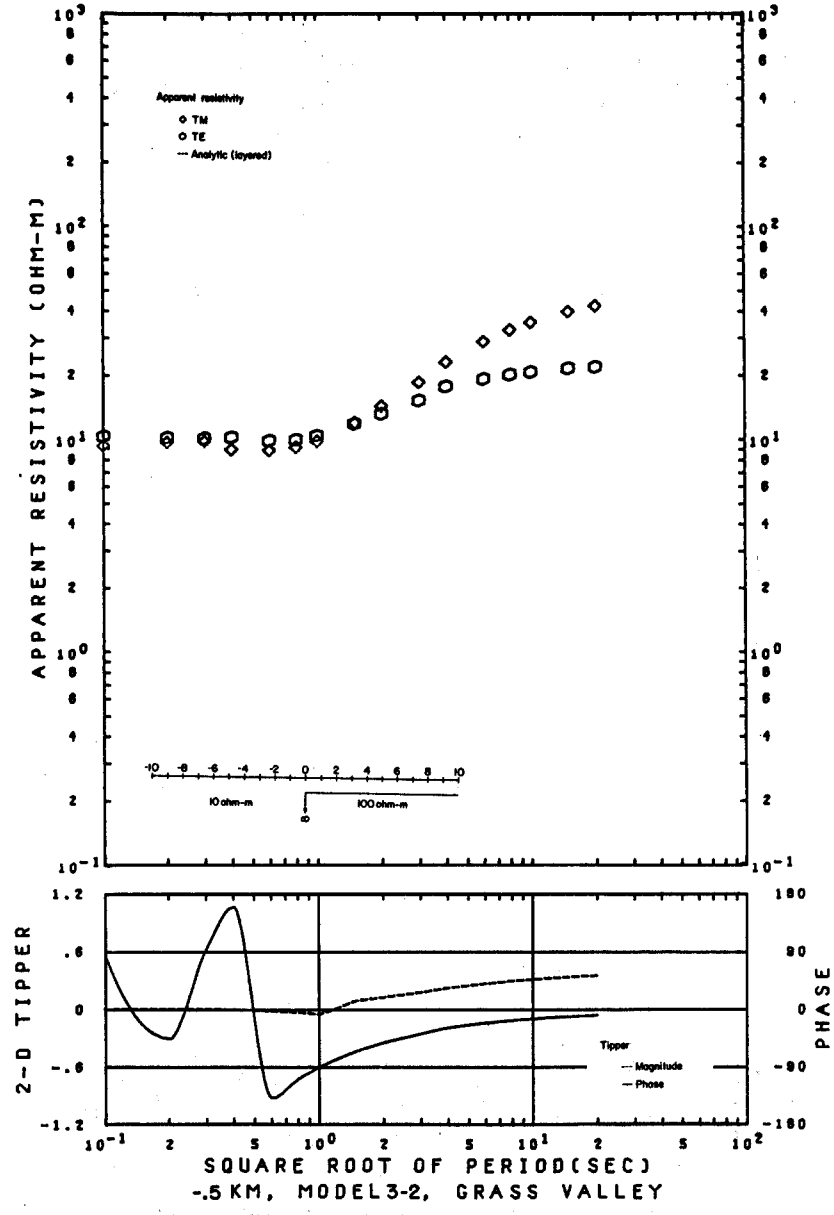
Apparent resistivity
TM
TE
Analytic (layered)
APPARENT RESISTIVITY (OHM-M)
10 ohm-m
100 ohm-m
2-D TIPPER
PHASE
Tipper
Magnitude
Phase
SQUARE ROOT OF PERIOD(SEC)
-.5 KM, MODEL3-2, GRASS VALLEY

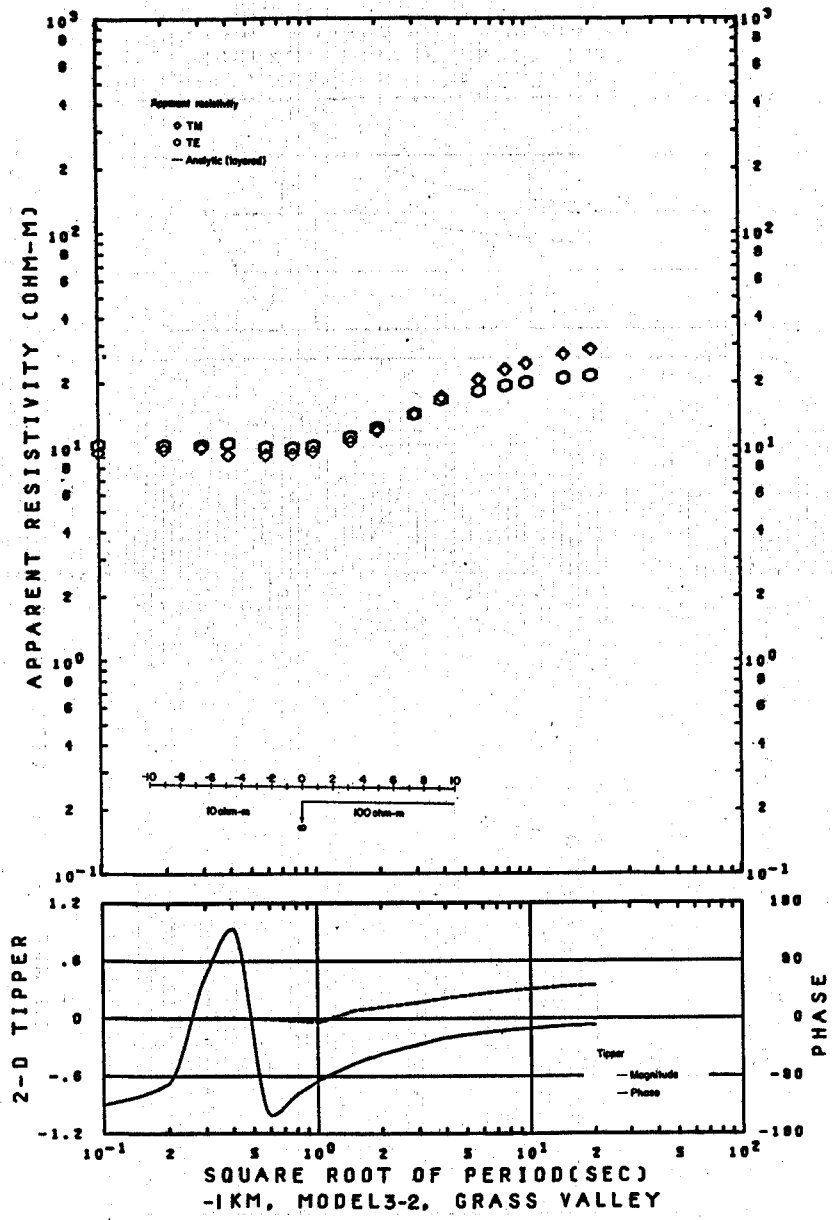
Apparent resistivity
TM
TE
Analytic (layered)
APPARENT RESISTIVITY (OHM-M)
10 ohm-m
100 ohm-m
2-D TIPPER
PHASE
Tipper
Magnitude
Phase
SQUARE ROOT OF PERIOD(SEC)
-1KM, MODEL3-2, GRASS VALLEY

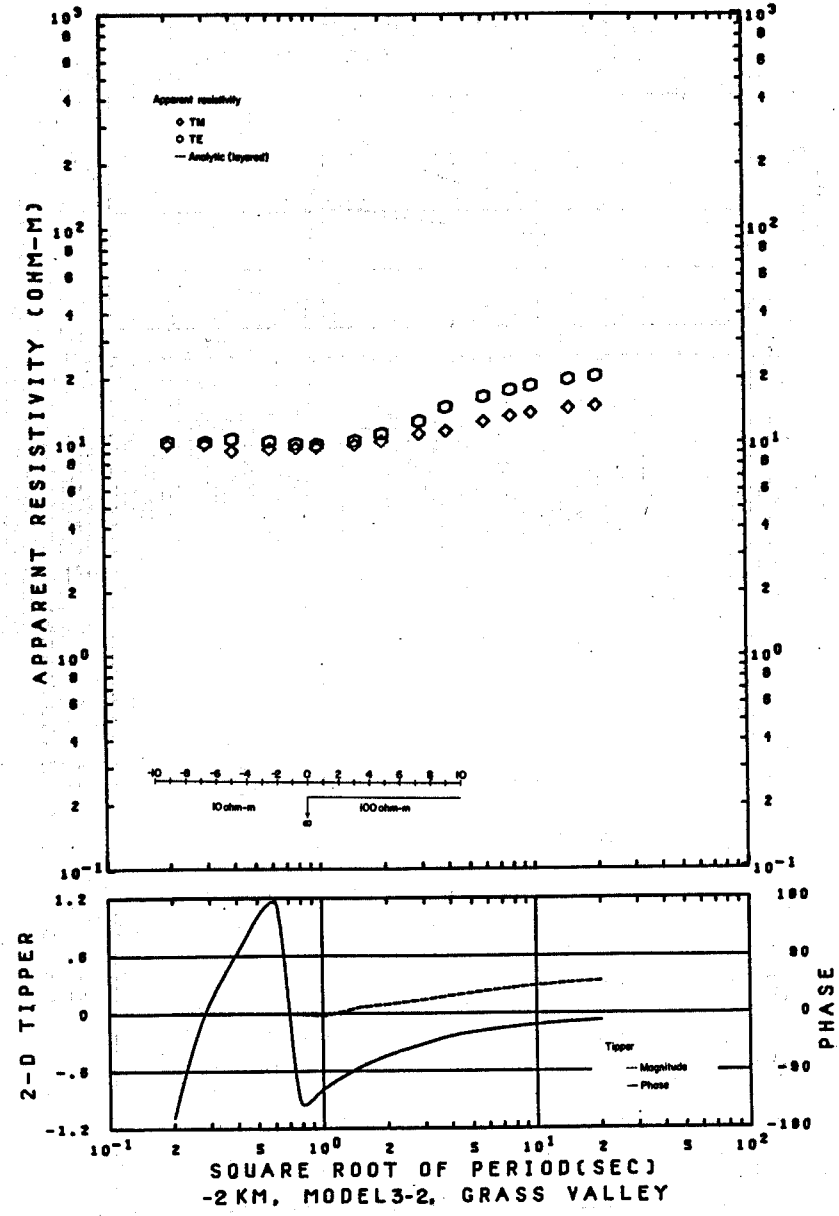
Apparent resistivity
TM
TE
Analytic (layered)
APPARENT RESISTIVITY (OHM-M)
10 ohm-m
100 ohm-m
2-D TIPPER
PHASE
Tipper
Magnitude
Phase
SQUARE ROOT OF PERIOD(SEC)
-2 KM, MODEL3-2, GRASS VALLEY

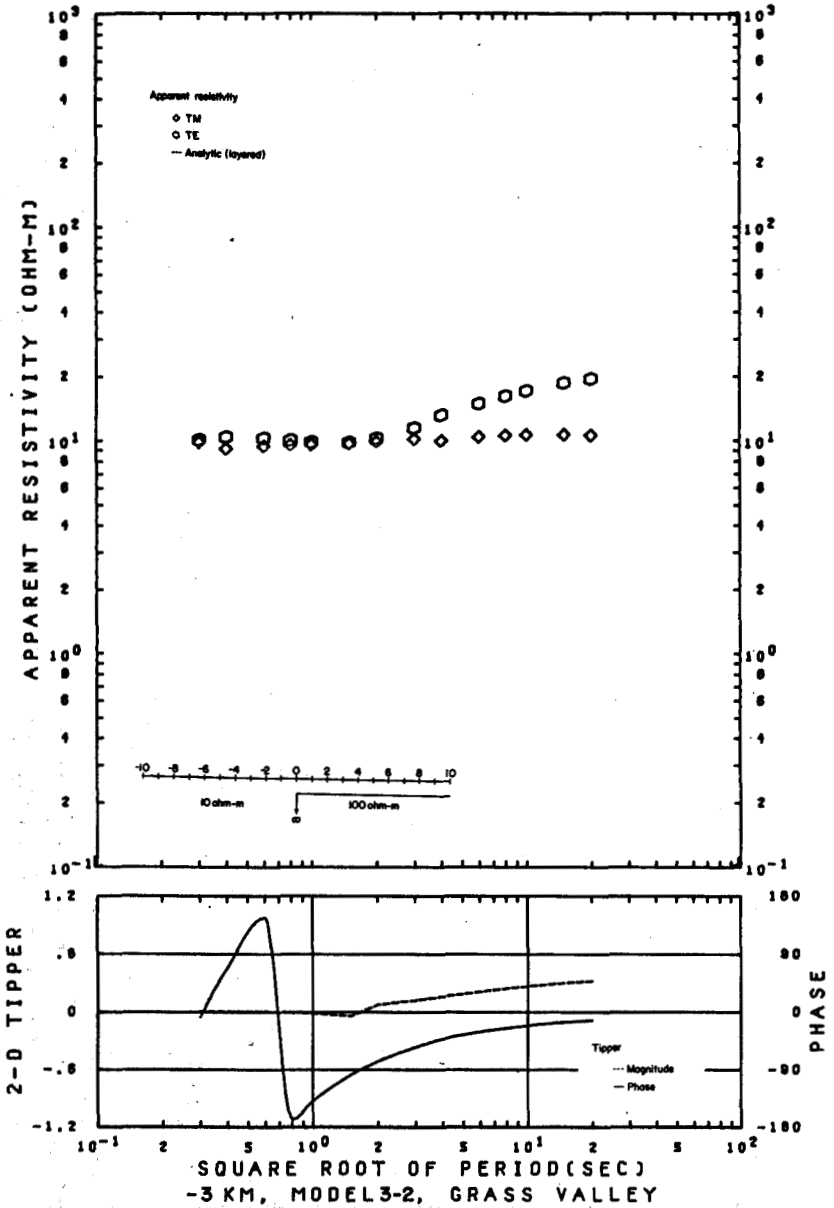

-3 KM, MODEL3-2, GRASS VALLEY

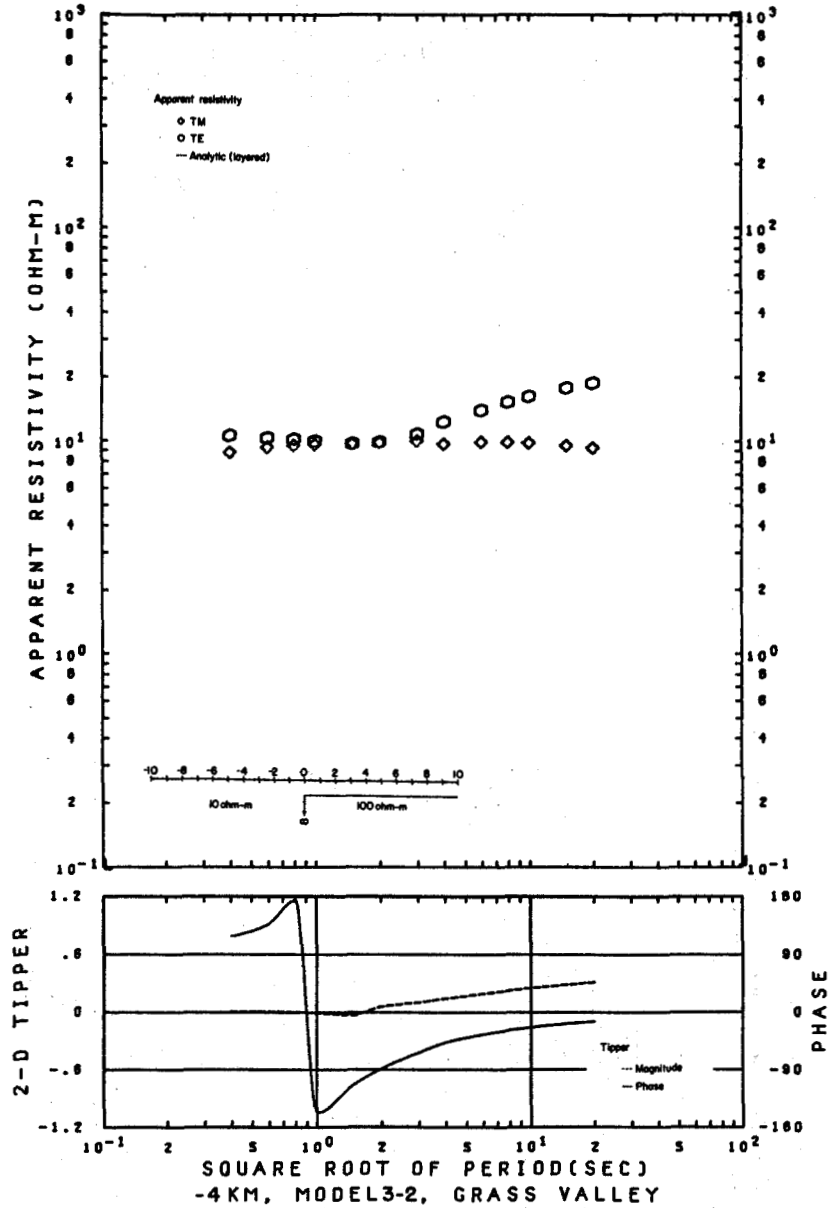

-4 KM, MODEL3-2, GRASS VALLEY

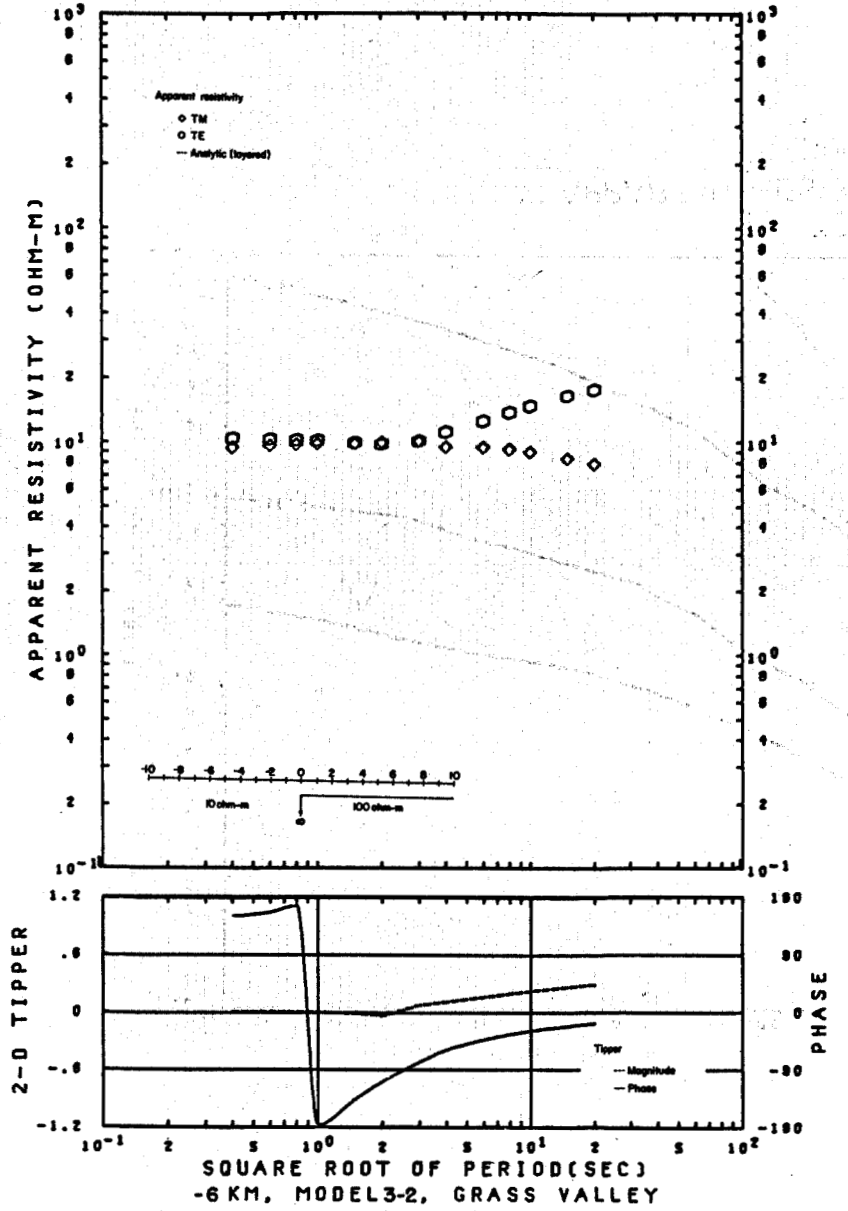

-6 KM, MODEL3-2, GRASS VALLEY

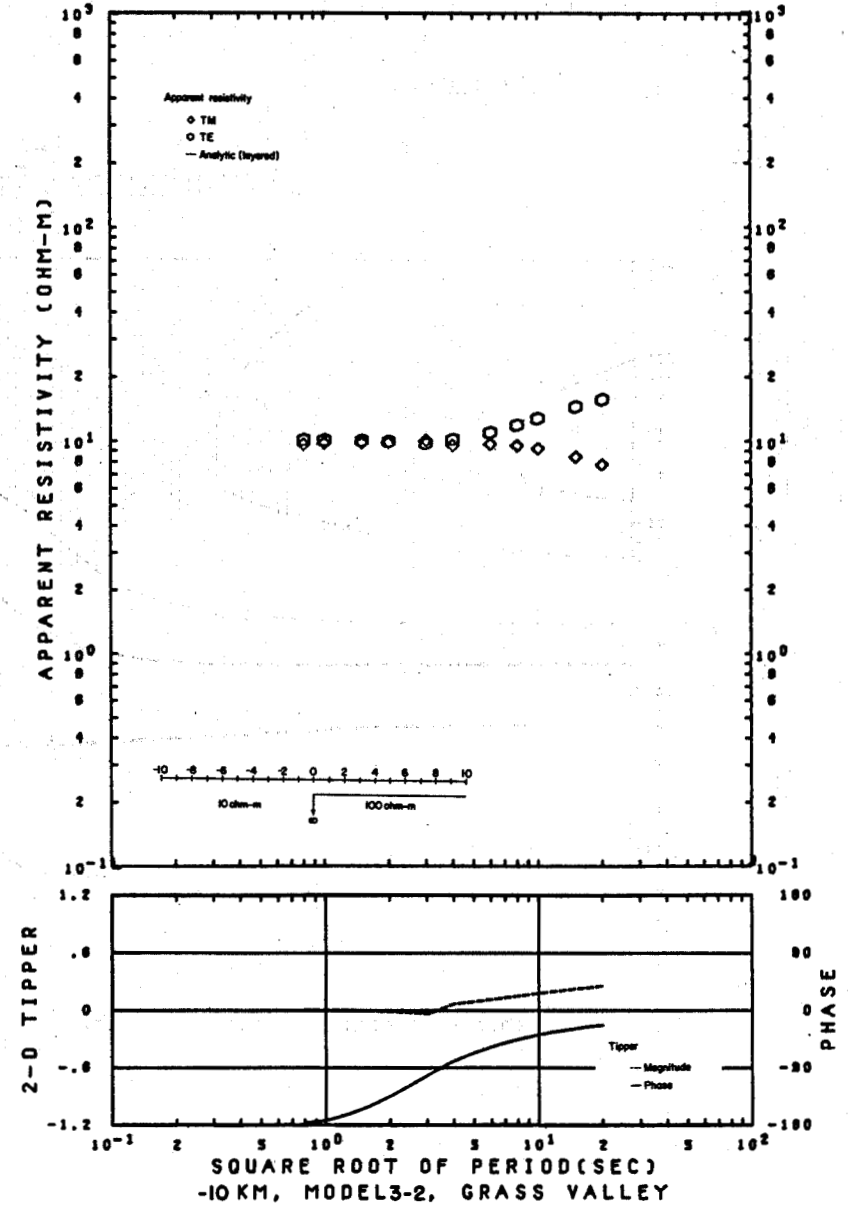

-10 KM, MODEL3-2, GRASS VALLEY

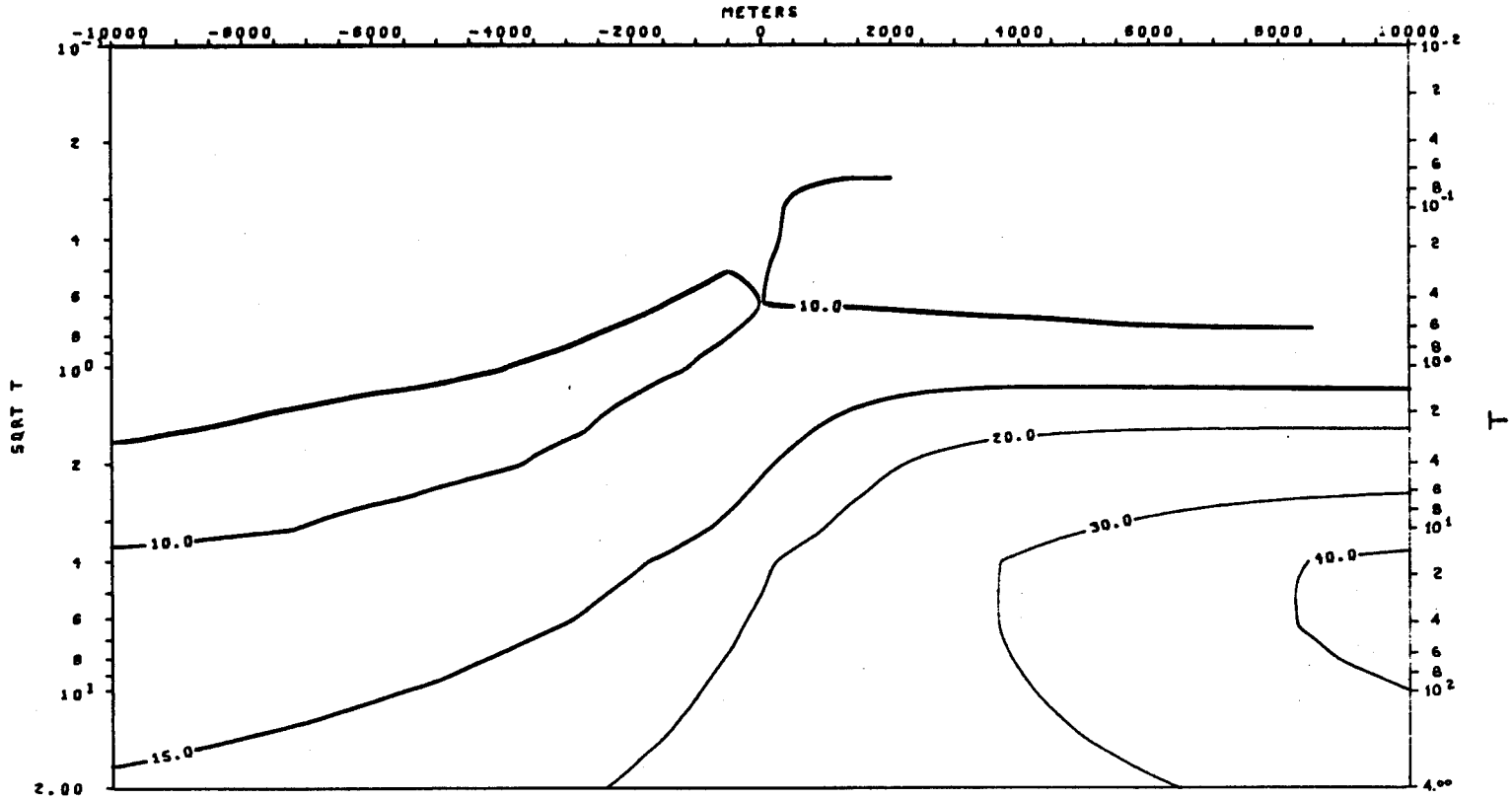

TE MODE
APPARENT RESISTIVITY VS. PERIOD (T)
MODEL 3-2

XBL 786-1907

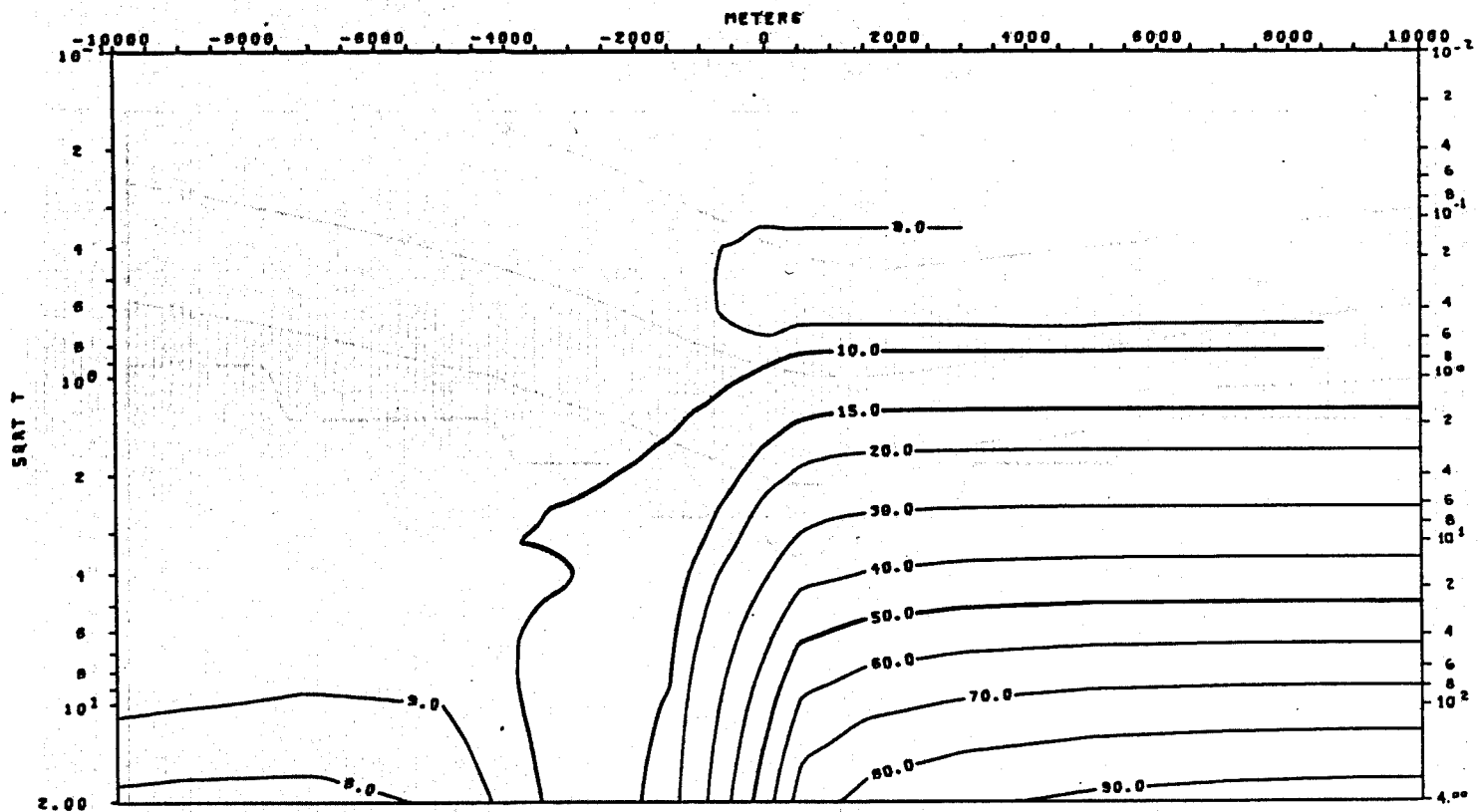

TM MODE
APPARENT RESISTIVITY VS. PERIOD (T)
MODEL 3-2

XBL 786-1909

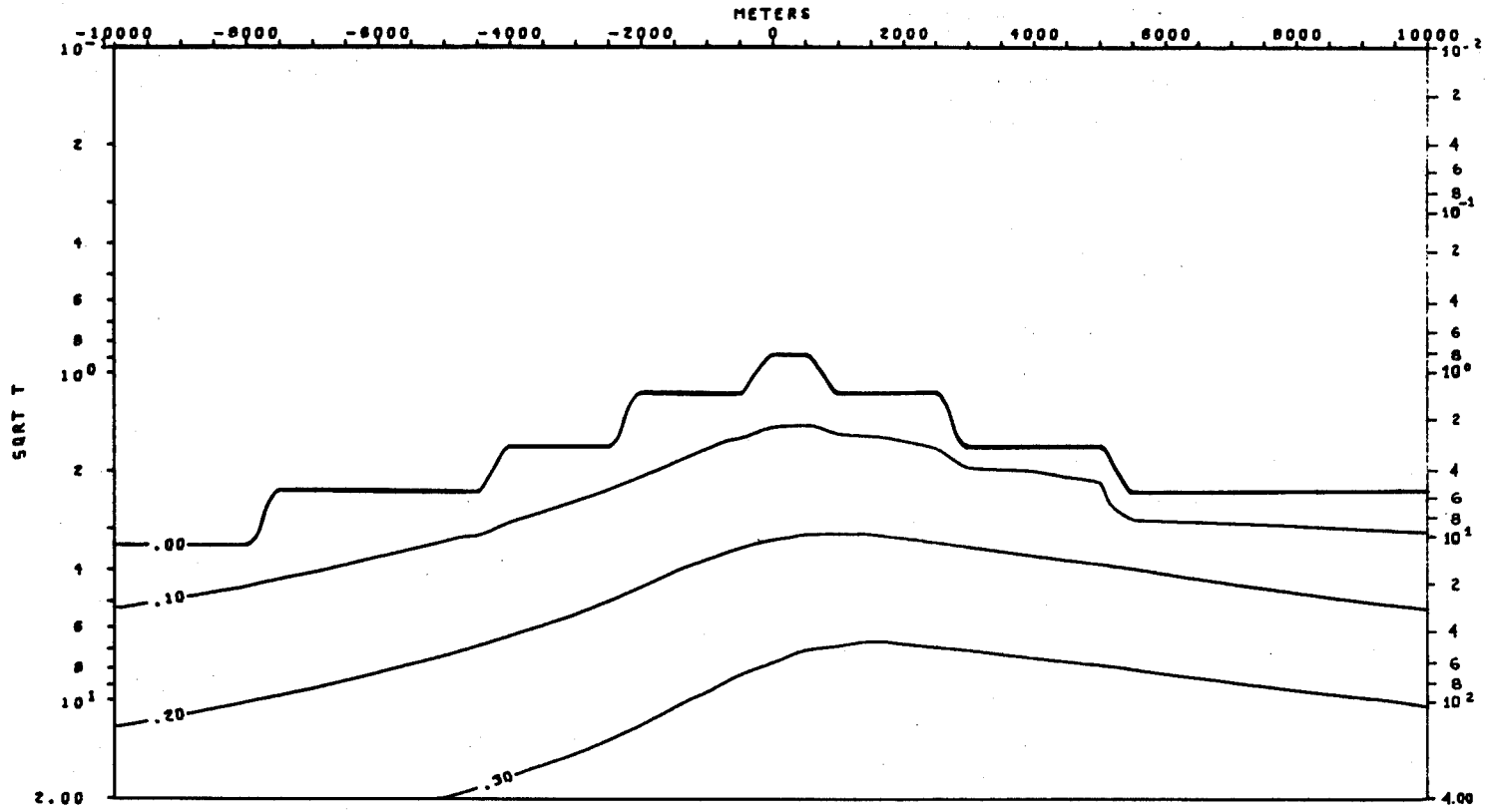

TIPPER VS. PERIOD (T)
MODEL 3-2

XBL 786-1944

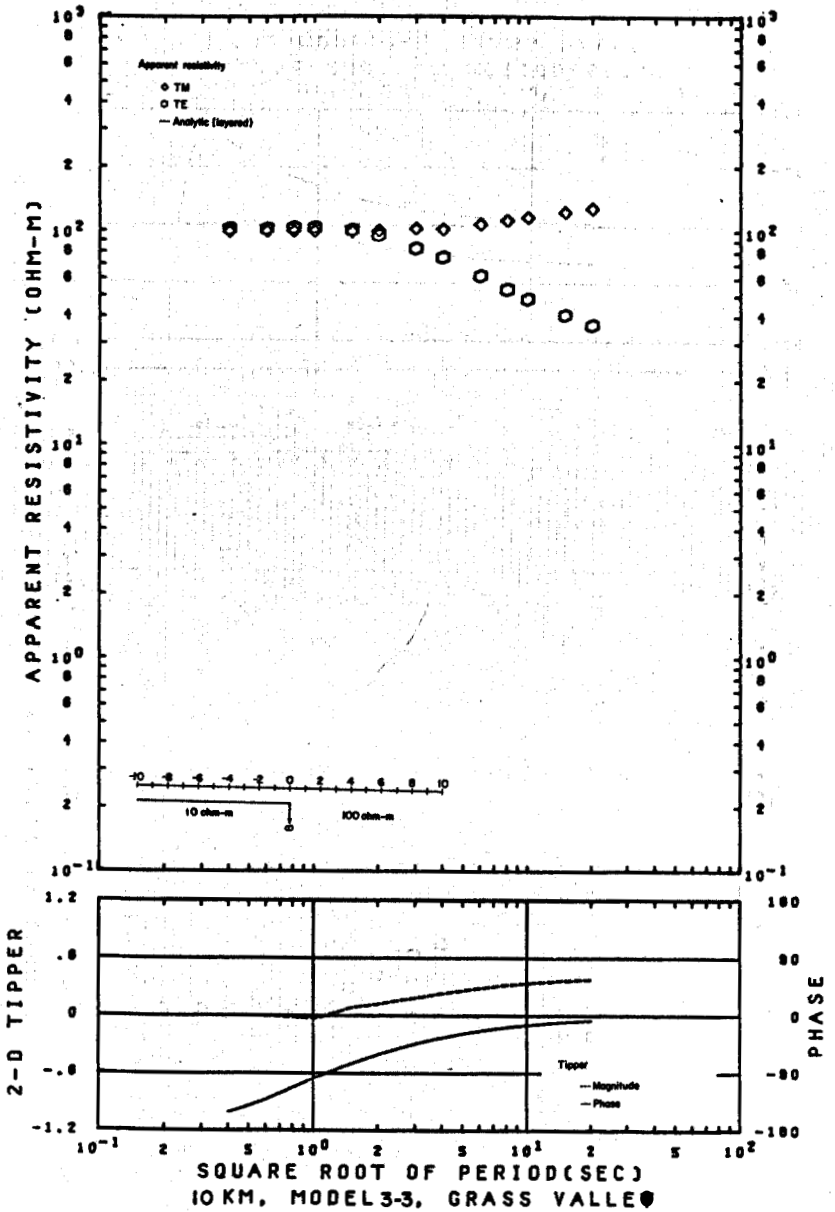

10 KM, MODEL 3-3, GRASS VALLEY

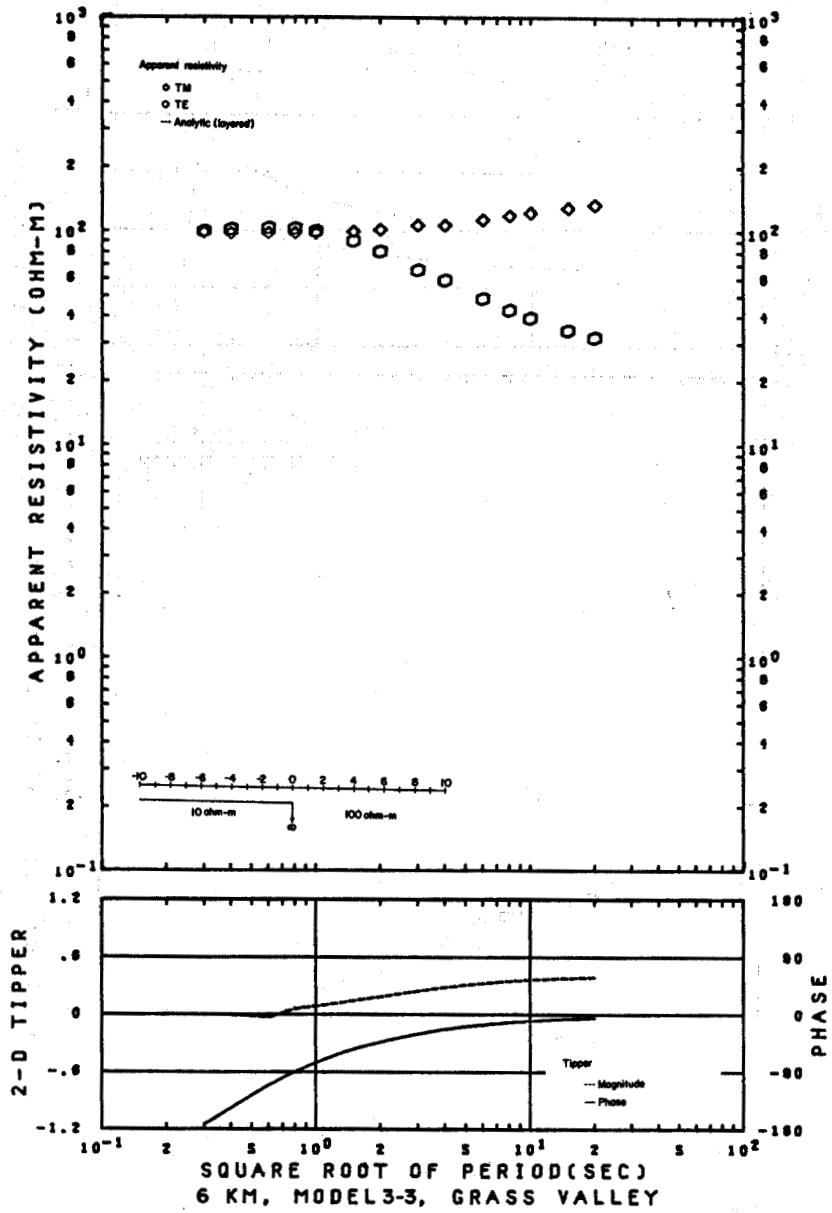

6 KM, MODEL 3-3, GRASS VALLEY

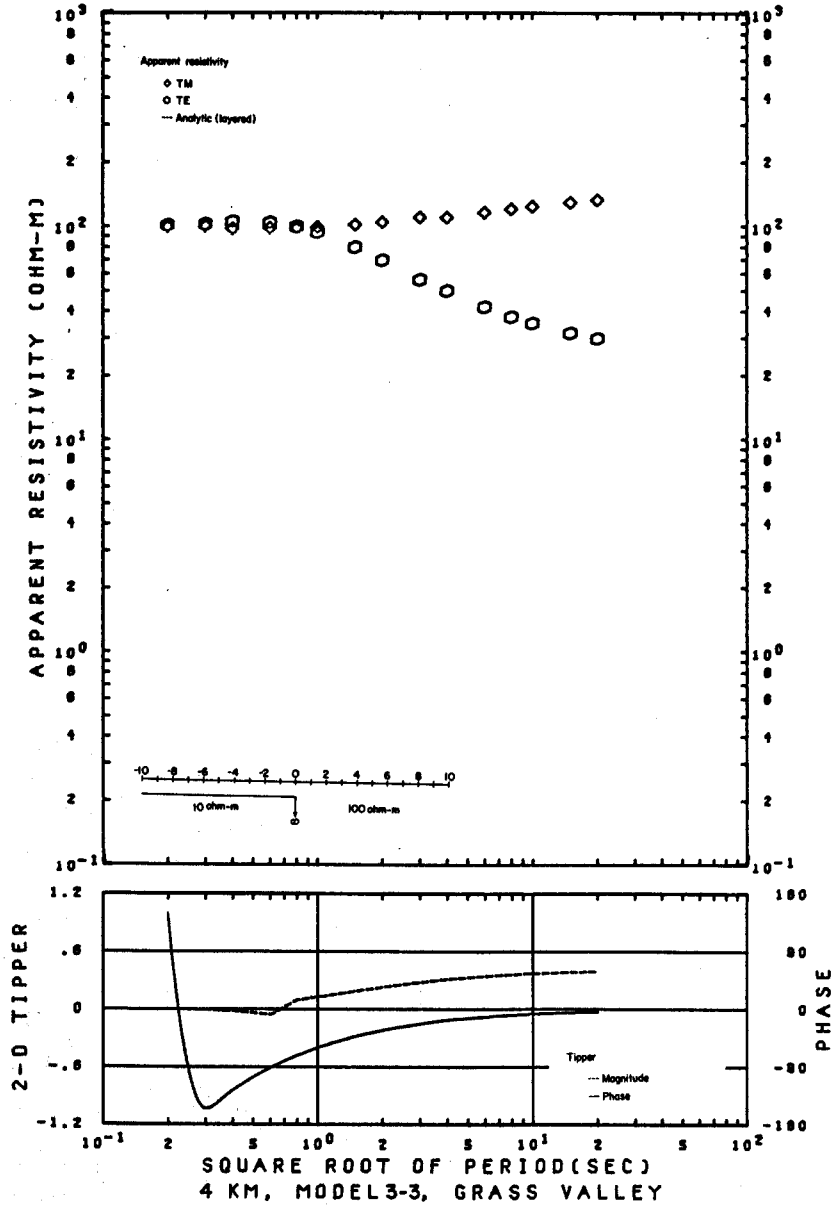

4 KM, MODEL3-3, GRASS VALLEY

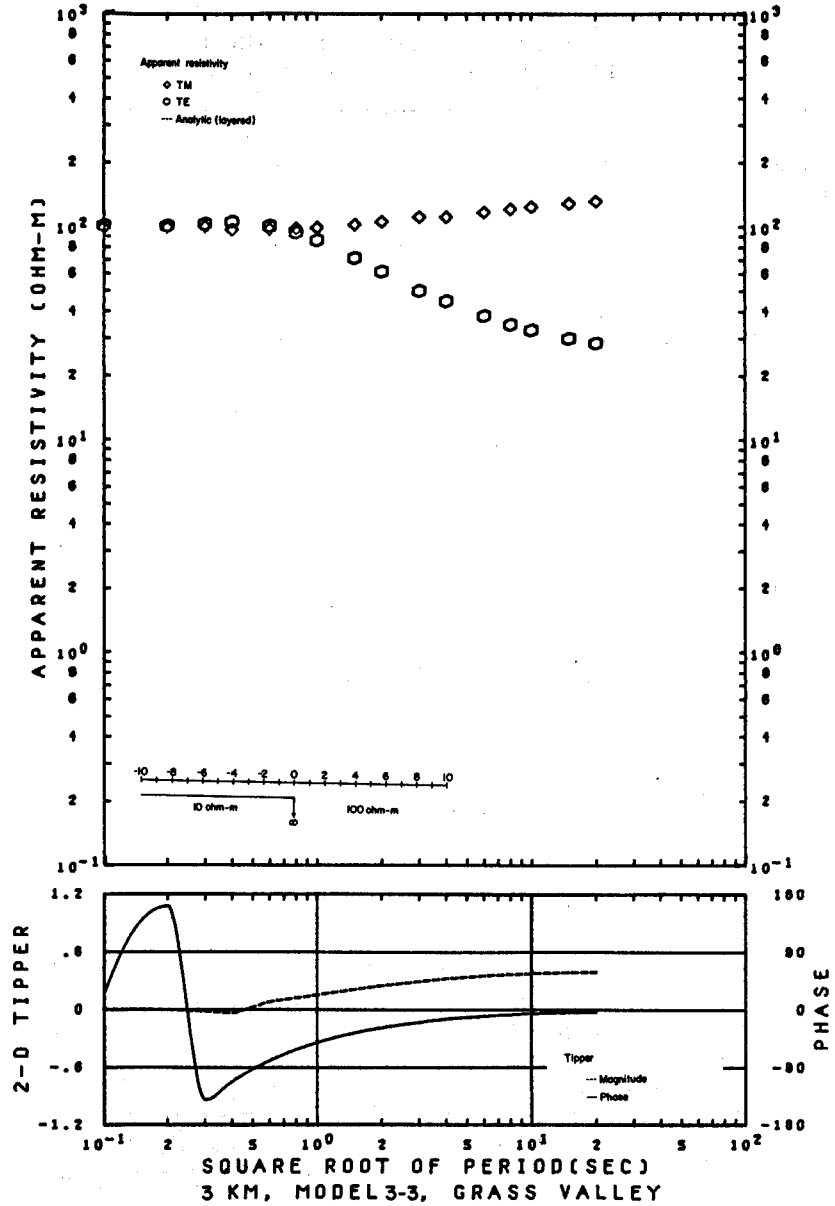

3 KM, MODEL3-3, GRASS VALLEY

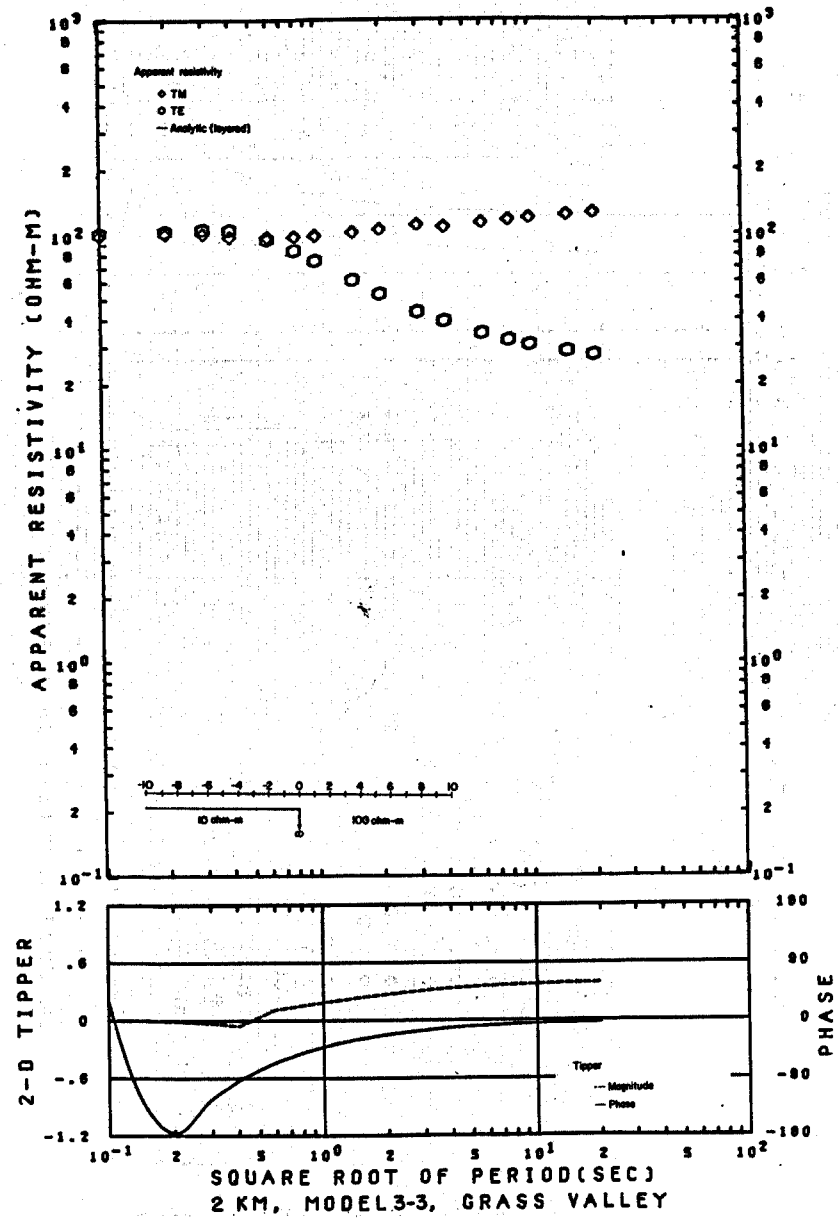
Apparent resistivity
TM
TE
Analytic (layered)
APPARENT RESISTIVITY (OHM-M)
10 ohm-m
100 ohm-m
2-D TIPPER
PHASE
Tipper
Magnitude
Phase
SQUARE ROOT OF PERIOD(SEC)
2 KM, MODEL3-3, GRASS VALLEY

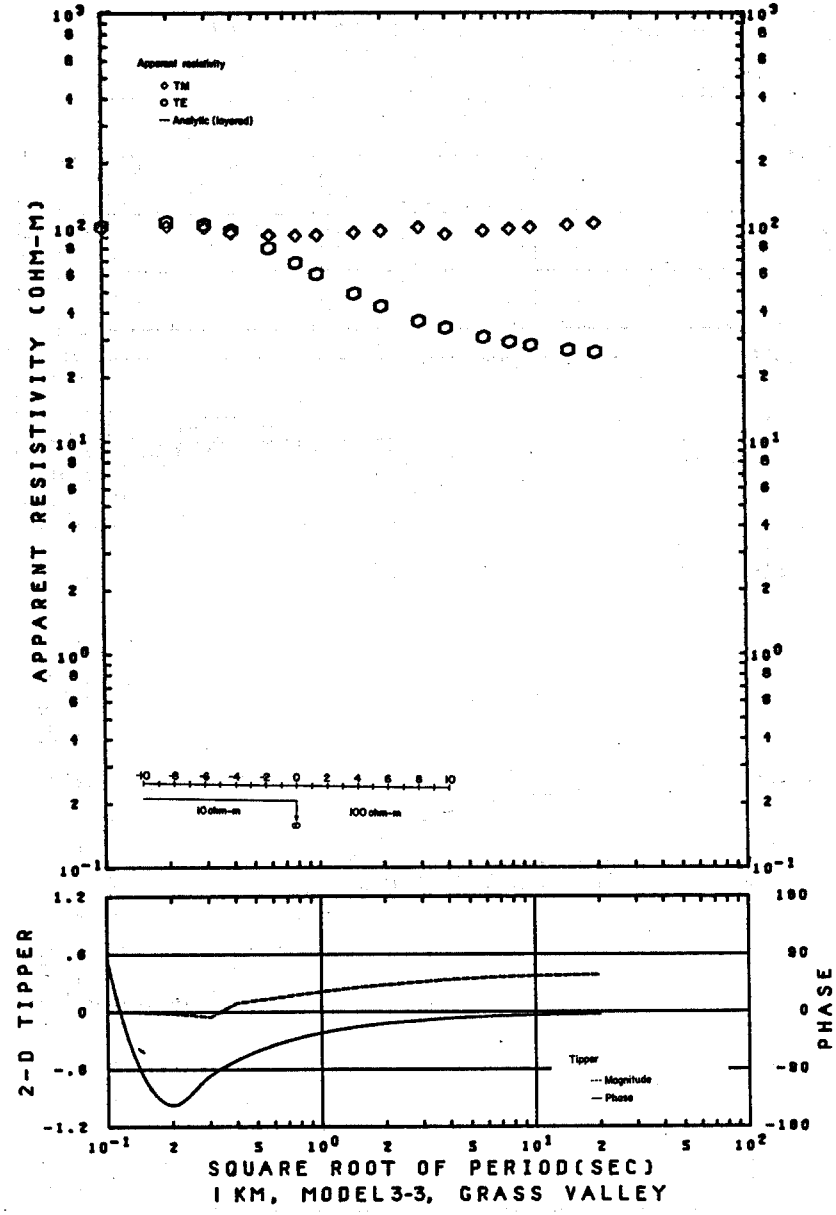
Apparent resistivity
TM
TE
Analytic (layered)
APPARENT RESISTIVITY (OHM-M)
10 ohm-m
100 ohm-m
2-D TIPPER
PHASE
Tipper
Magnitude
Phase
SQUARE ROOT OF PERIOD(SEC)
1 KM, MODEL3-3, GRASS VALLEY

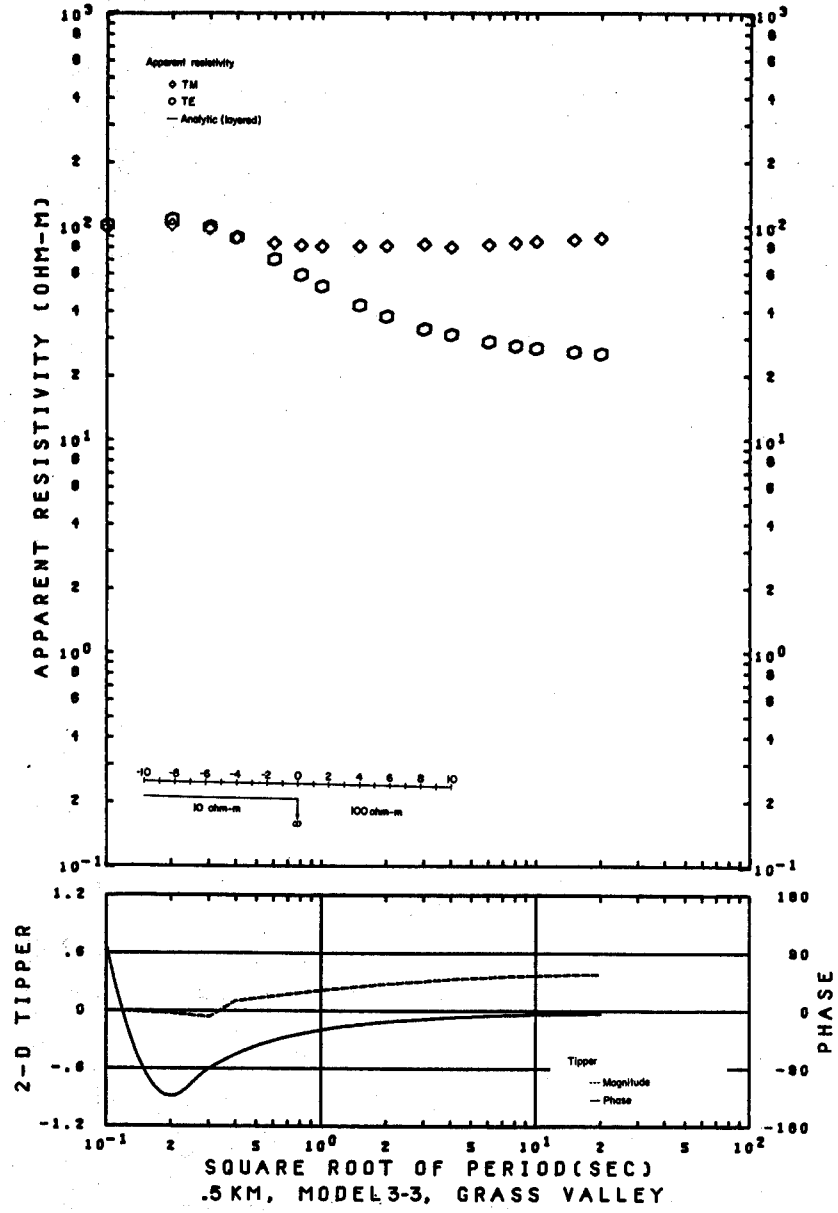
Apparent resistivity
TM
TE
Analytic (layered)
APPARENT RESISTIVITY (OHM-M)
10 ohm-m
100 ohm-m
2-D TIPPER
PHASE
Tipper
Magnitude
Phase
SQUARE ROOT OF PERIOD(SEC)
.5 KM, MODEL 3-3, GRASS VALLEY

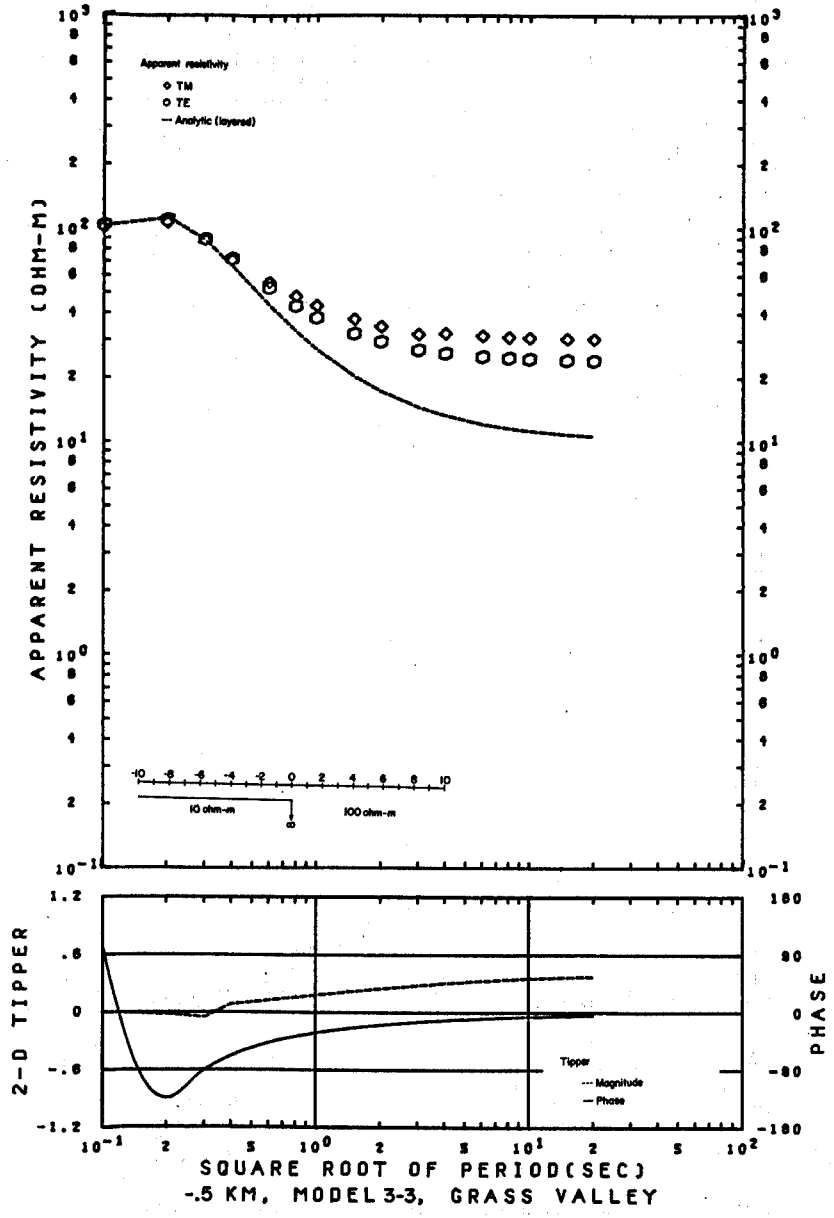
Apparent resistivity
TM
TE
Analytic (layered)
APPARENT RESISTIVITY (OHM-M)
10 ohm-m
100 ohm-m
2-D TIPPER
PHASE
Tipper
Magnitude
Phase
SQUARE ROOT OF PERIOD(SEC)
-.5 KM, MODEL 3-3, GRASS VALLEY

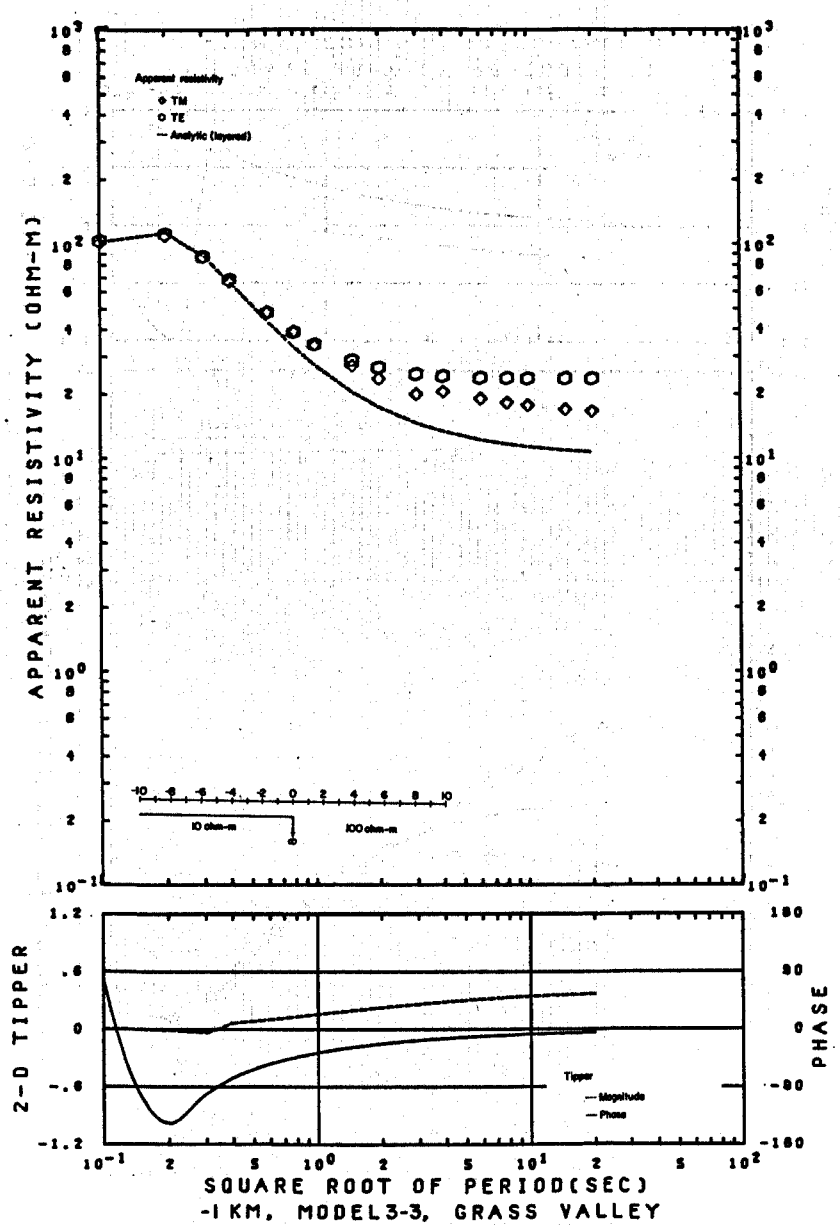
Apparent resistivity
TM
TE
Analytic (layered)
APPARENT RESISTIVITY (OHM-M)
10 ohm-m
100 ohm-m
2-D TIPPER
PHASE
Tipper
Magnitude
Phase
SQUARE ROOT OF PERIOD(SEC)
-1 KM, MODEL3-3, GRASS VALLEY

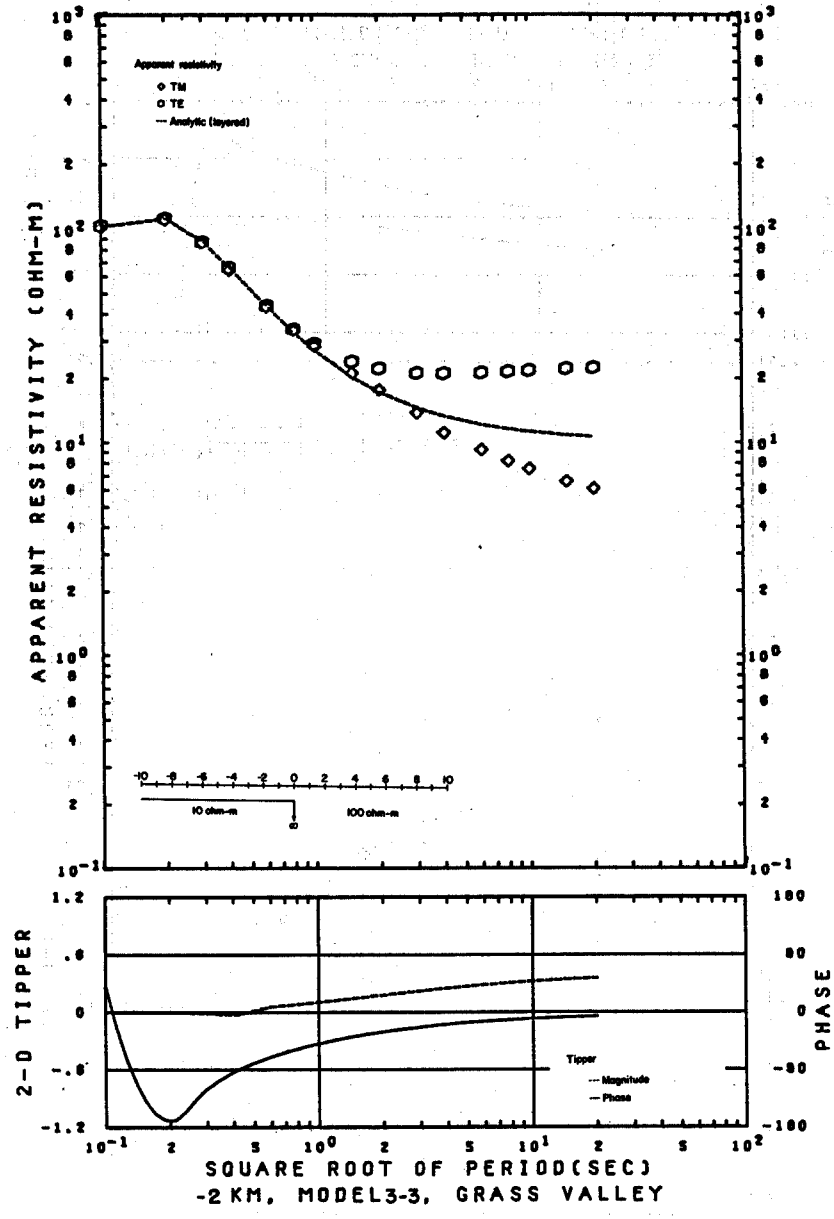
Apparent resistivity
TM
TE
Analytic (layered)
APPARENT RESISTIVITY (OHM-M)
10 ohm-m
100 ohm-m
2-D TIPPER
PHASE
Tipper
Magnitude
Phase
SQUARE ROOT OF PERIOD(SEC)
-2 KM, MODEL3-3, GRASS VALLEY

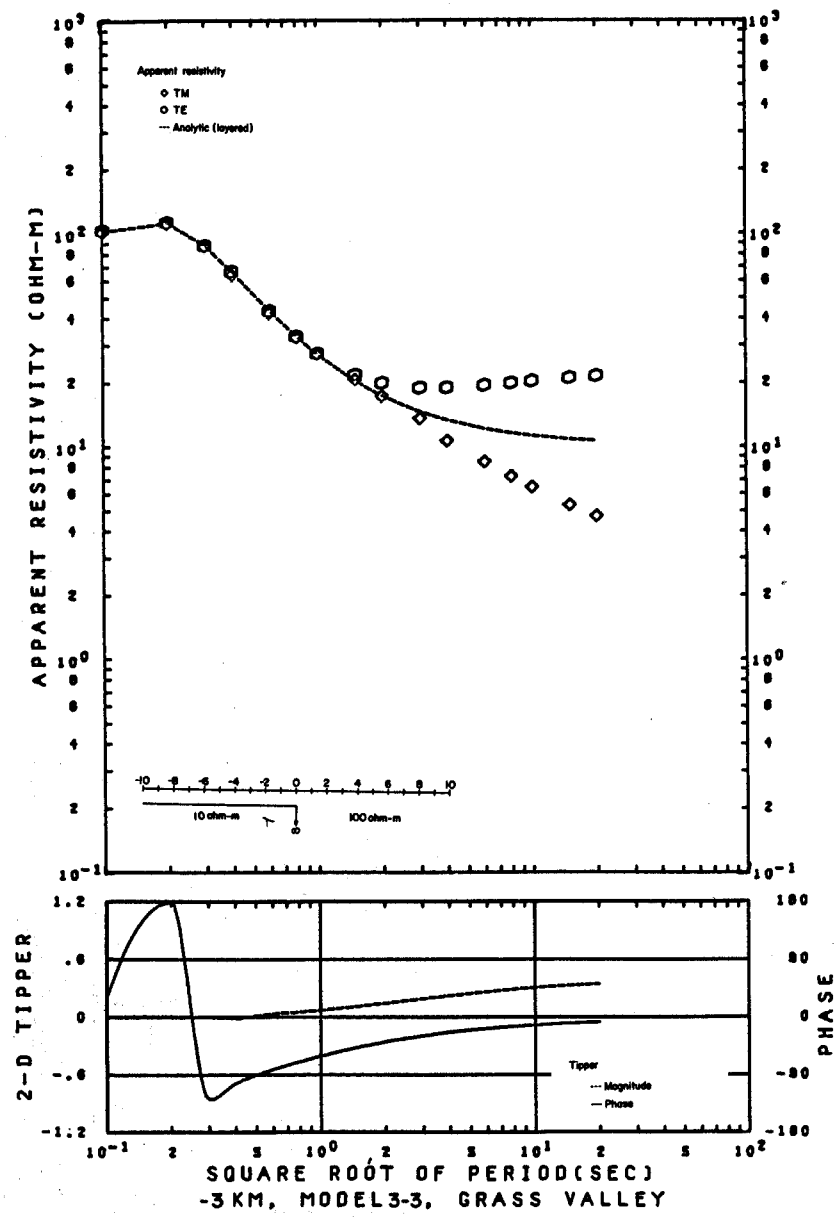
Apparent resistivity
TM
TE
Analytic (layered)
APPARENT RESISTIVITY (OHM-M)
10 ohm-m
100 ohm-m
2-D TIPPER
PHASE
Tipper
Magnitude
Phase
SQUARE ROOT OF PERIOD(SEC)
-3 KM, MODEL3-3, GRASS VALLEY

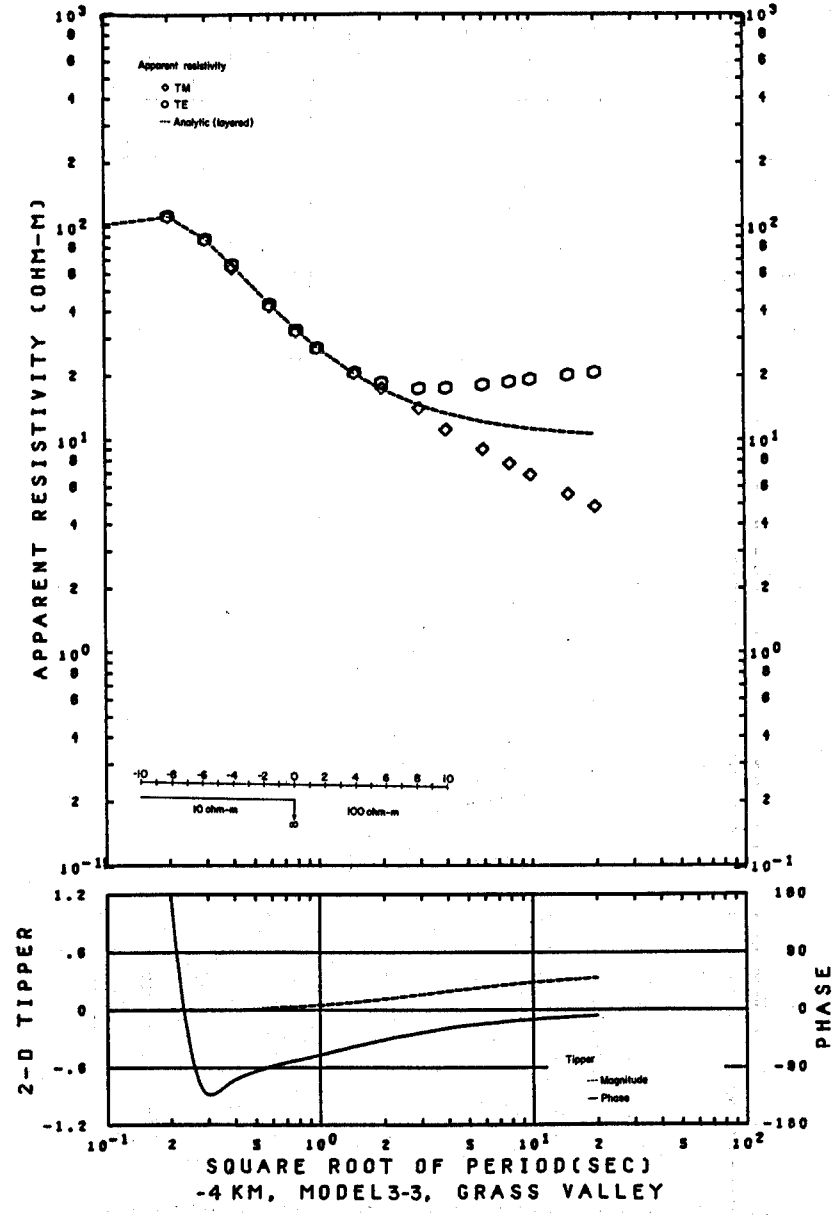
Apparent resistivity
TM
TE
Analytic (layered)
APPARENT RESISTIVITY (OHM-M)
10 ohm-m
100 ohm-m
2-D TIPPER
PHASE
Tipper
Magnitude
Phase
SQUARE ROOT OF PERIOD(SEC)
-4 KM, MODEL3-3, GRASS VALLEY

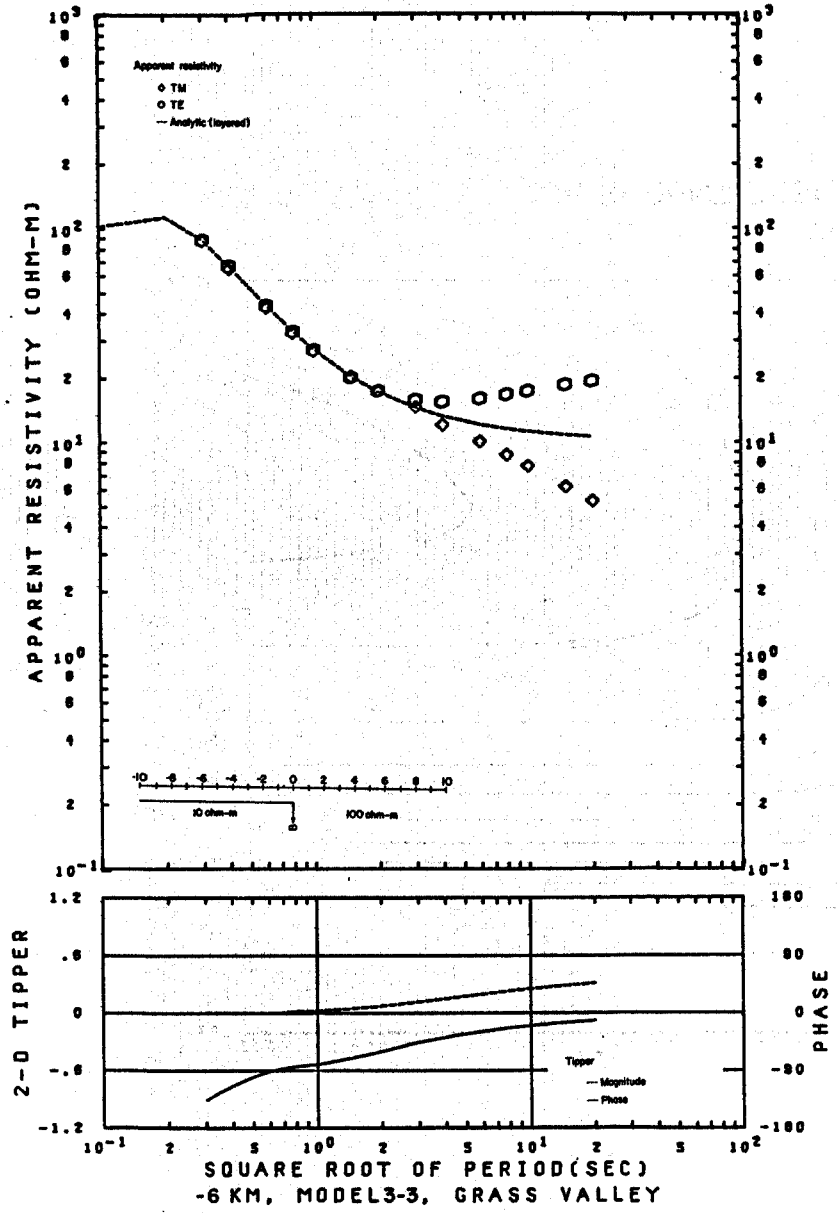
Apparent resistivity
TM
TE
Analytic (layered)
APPARENT RESISTIVITY (OHM-M)
10 ohm-m
100 ohm-m
2-D TIPPER
PHASE
Tipper
Magnitude
Phase
SQUARE ROOT OF PERIOD(SEC)
-6 KM, MODEL3-3, GRASS VALLEY

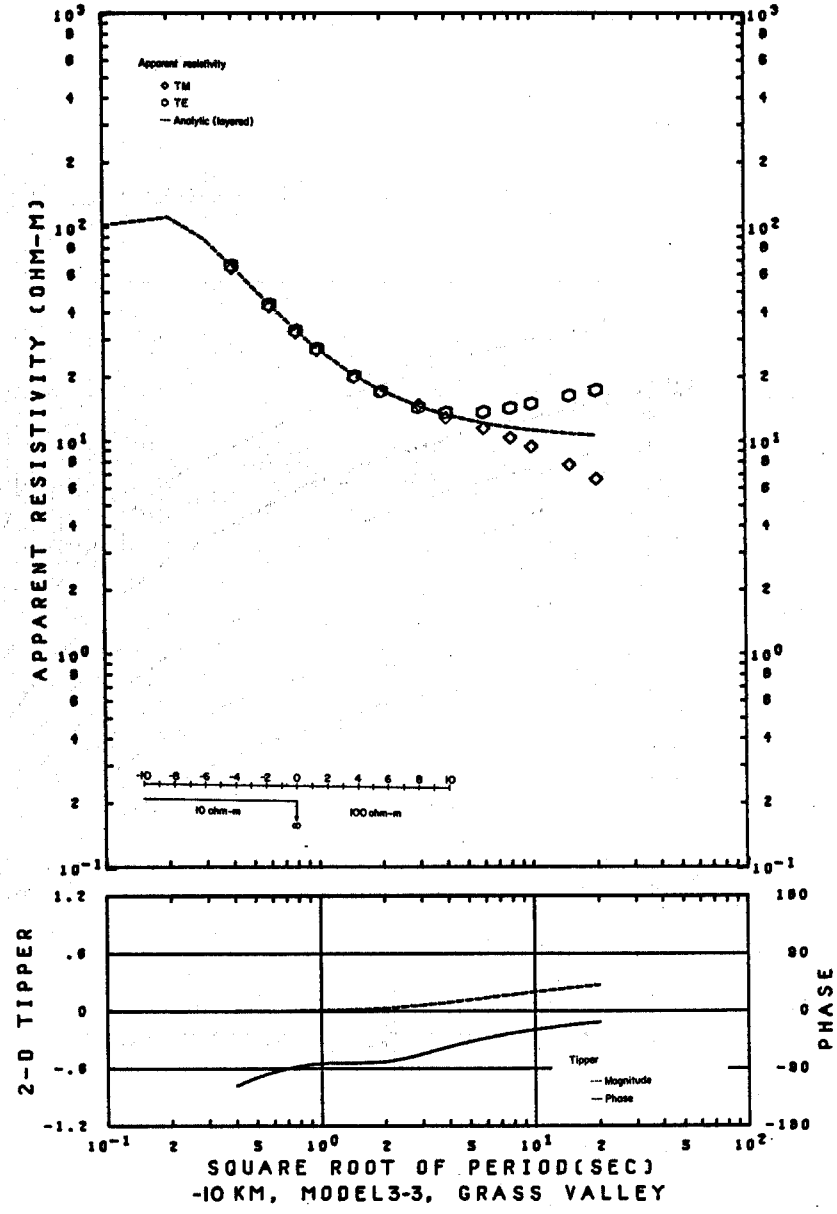
Apparent resistivity
TM
TE
Analytic (layered)
APPARENT RESISTIVITY (OHM-M)
10 ohm-m
100 ohm-m
2-D TIPPER
PHASE
Tipper
Magnitude
Phase
SQUARE ROOT OF PERIOD(SEC)
-10 KM, MODEL3-3, GRASS VALLEY

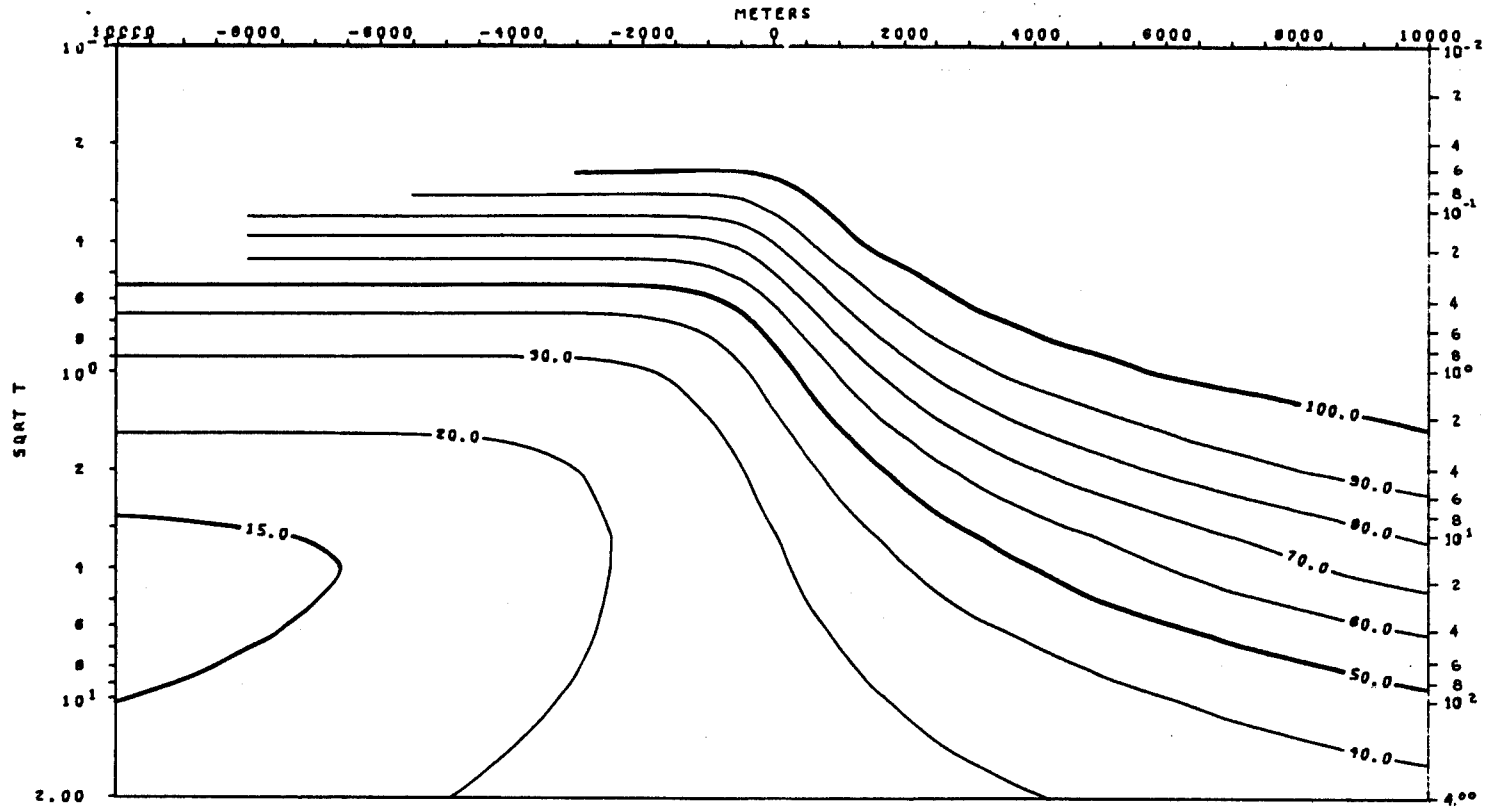

TE MODE
APPARENT RESISTIVITY VS. PERIOD (T)
MODEL 3-3

XBL 786-1908

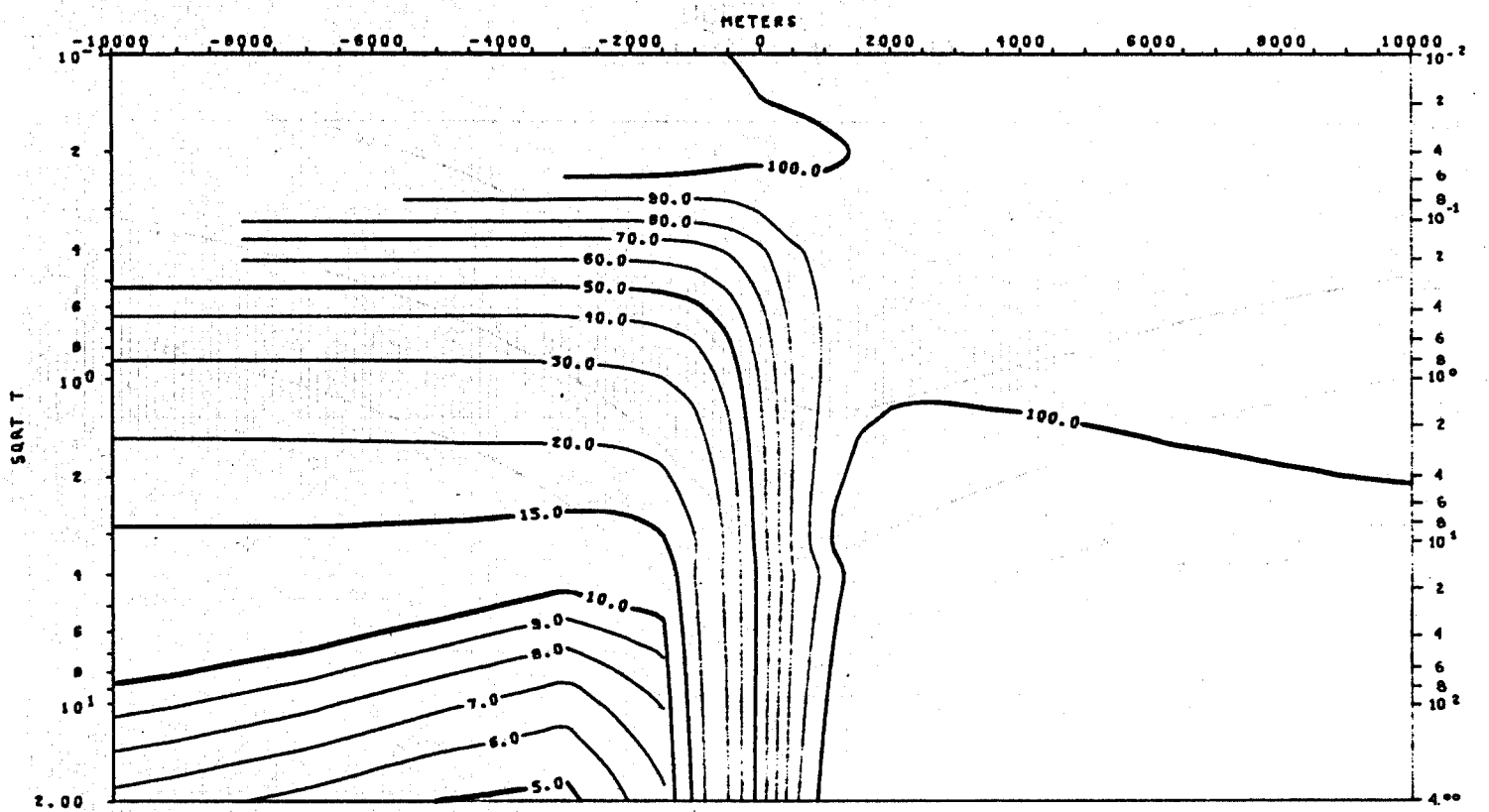

TM MODE
APPARENT RESISTIVITY VS. PERIOD (T)
MODEL 3-3

XBL 786-1928

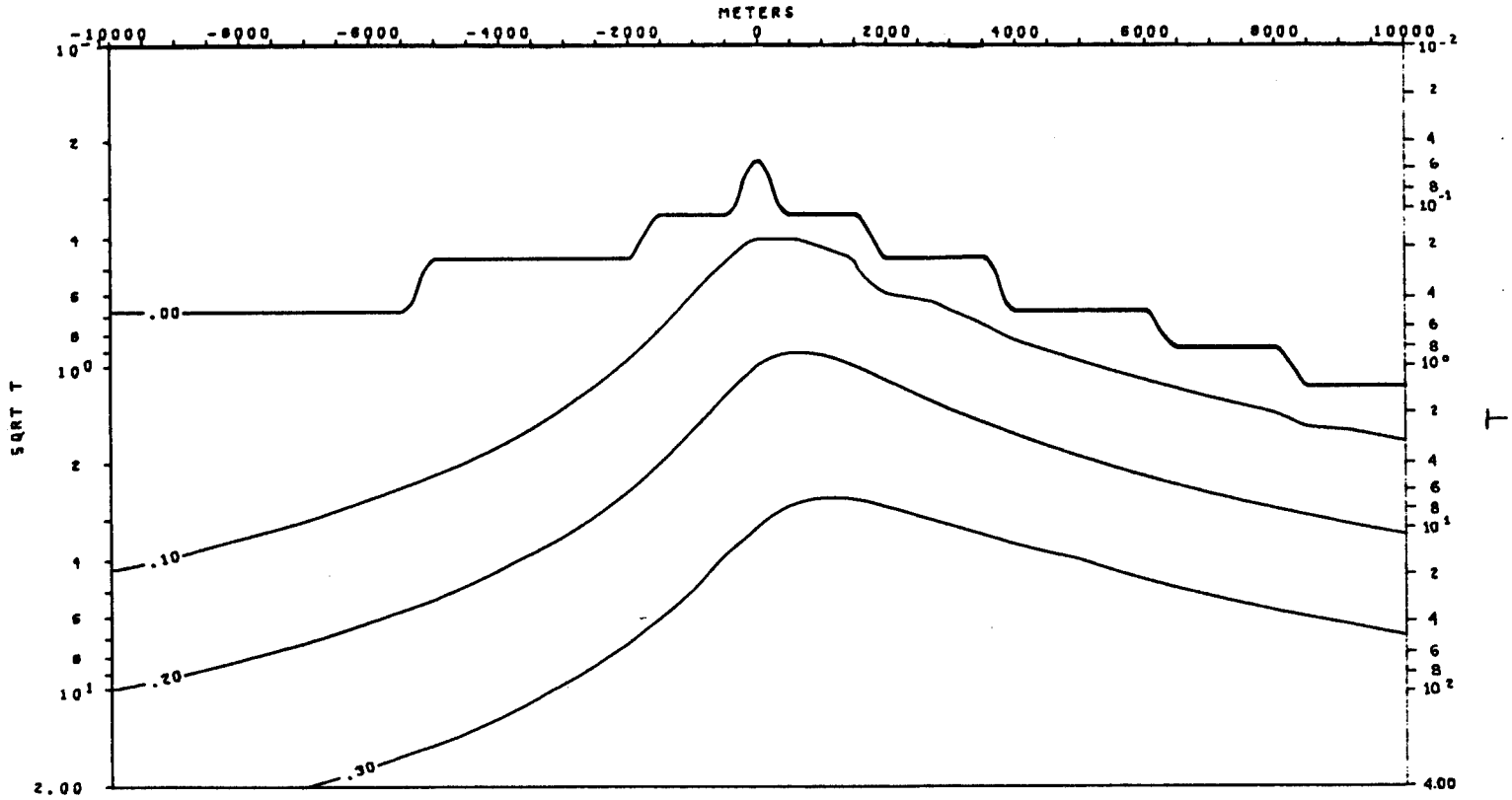

TIPPER VS. PERIOD (T)
MODEL 3-3

XBL 786-1923

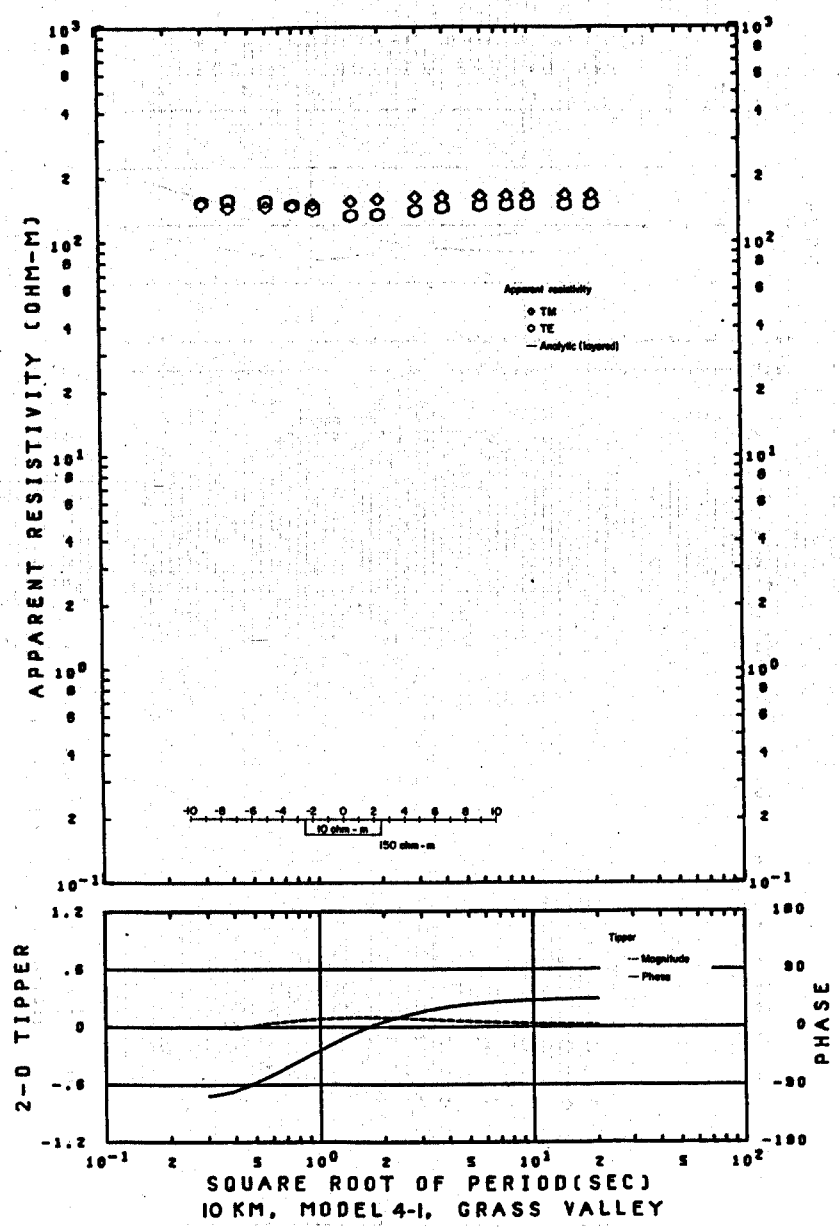
APPARENT RESISTIVITY (OHM-M)
Apparent resistivity
TM
TE
Analytic (layered)
10 ohm - m
150 ohm - m
2-D TIPPER
PHASE
Tipper
Magnitude
Phase
SQUARE ROOT OF PERIOD(SEC)
10 KM, MODEL 4-1, GRASS VALLEY

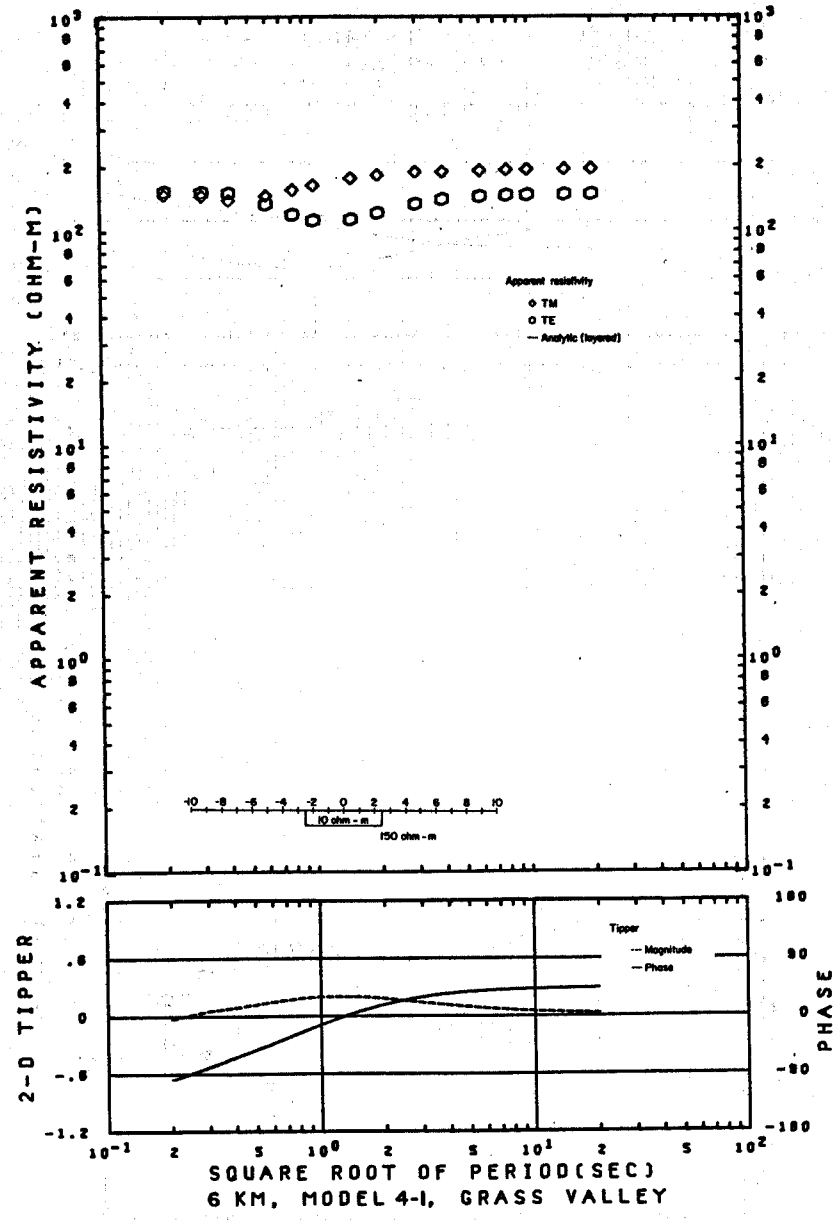
APPARENT RESISTIVITY (OHM-M)
Apparent resistivity
TM
TE
Analytic (layered)
10 ohm - m
150 ohm - m
2-D TIPPER
PHASE
Tipper
Magnitude
Phase
SQUARE ROOT OF PERIOD(SEC)
6 KM, MODEL 4-1, GRASS VALLEY

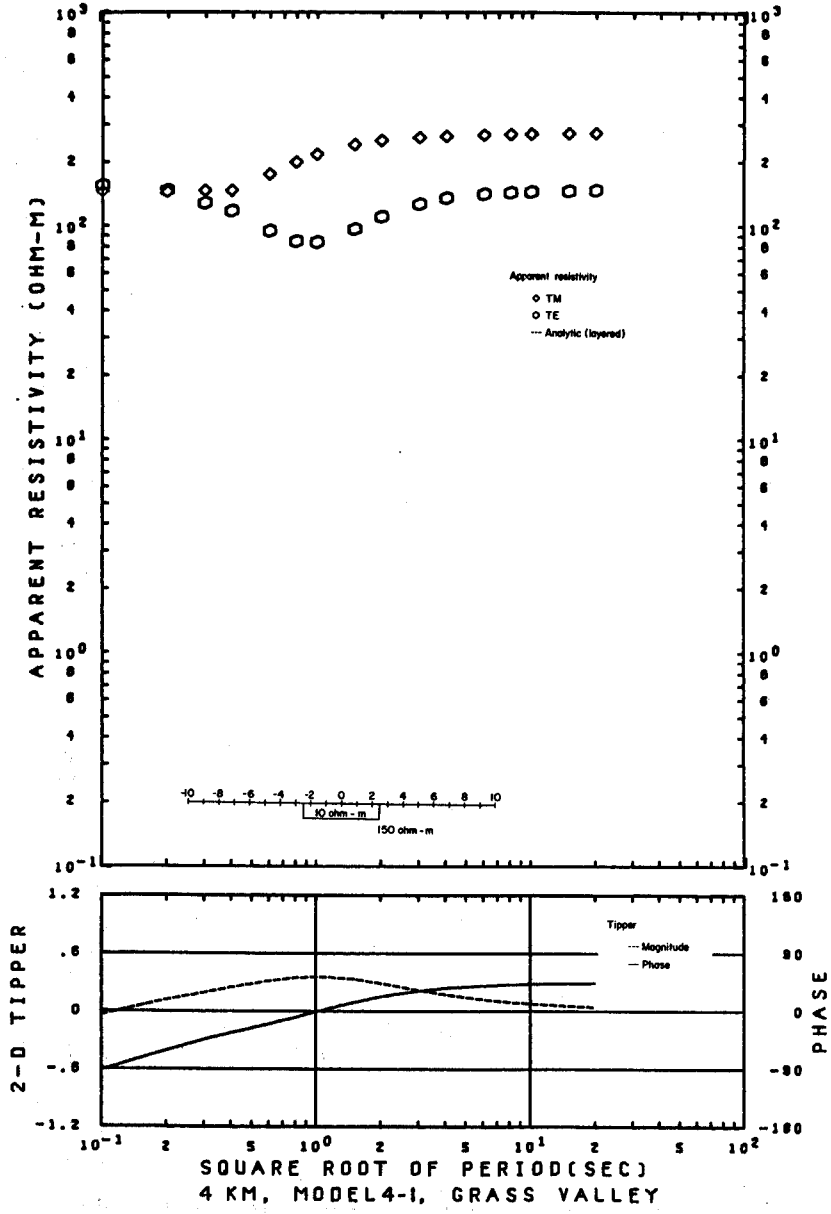
APPARENT RESISTIVITY (OHM-M)
Apparent resistivity
TM
TE
Analytic (layered)
10 ohm - m
150 ohm - m
2-D TIPPER
Tipper
Magnitude
Phase
PHASE
SQUARE ROOT OF PERIOD(SEC)
4 KM, MODEL4-1, GRASS VALLEY

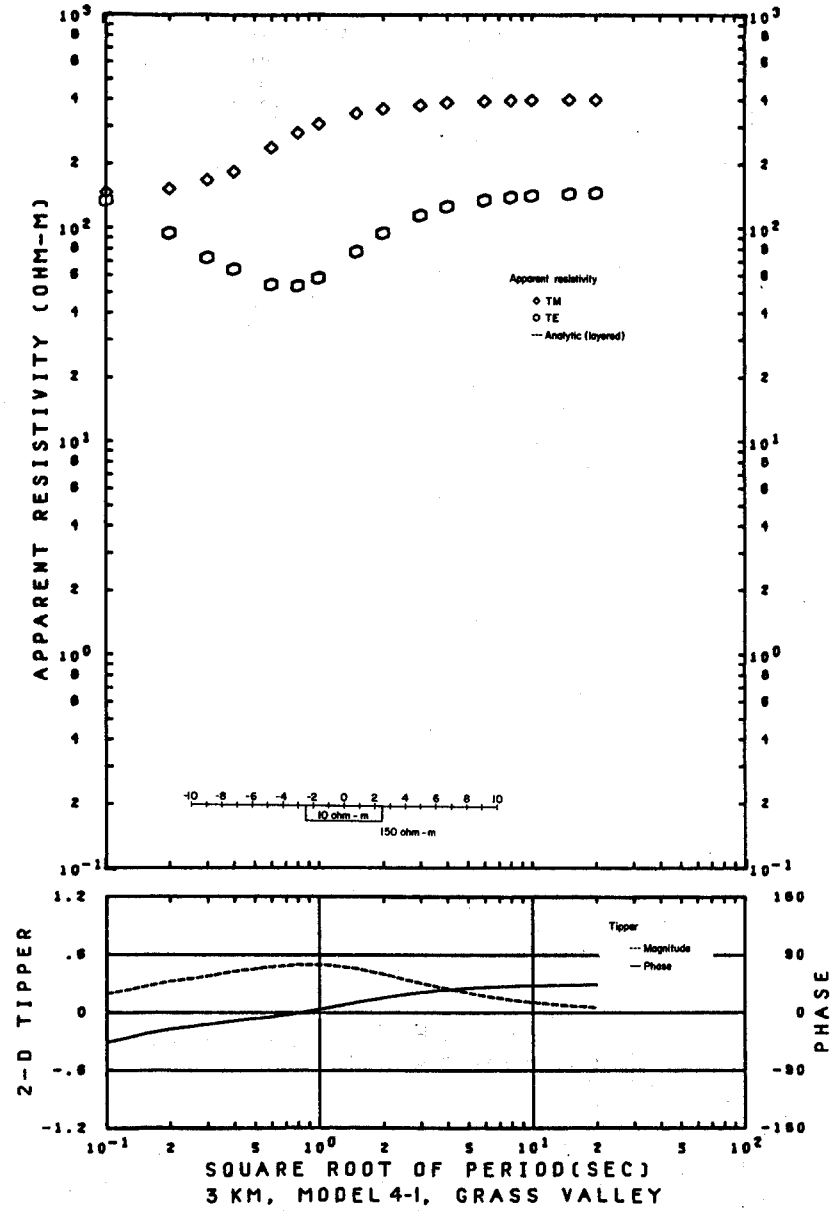
APPARENT RESISTIVITY (OHM-M)
Apparent resistivity
TM
TE
Analytic (layered)
10 ohm - m
150 ohm - m
2-D TIPPER
Tipper
Magnitude
Phase
PHASE
SQUARE ROOT OF PERIOD(SEC)
3 KM, MODEL 4-1, GRASS VALLEY

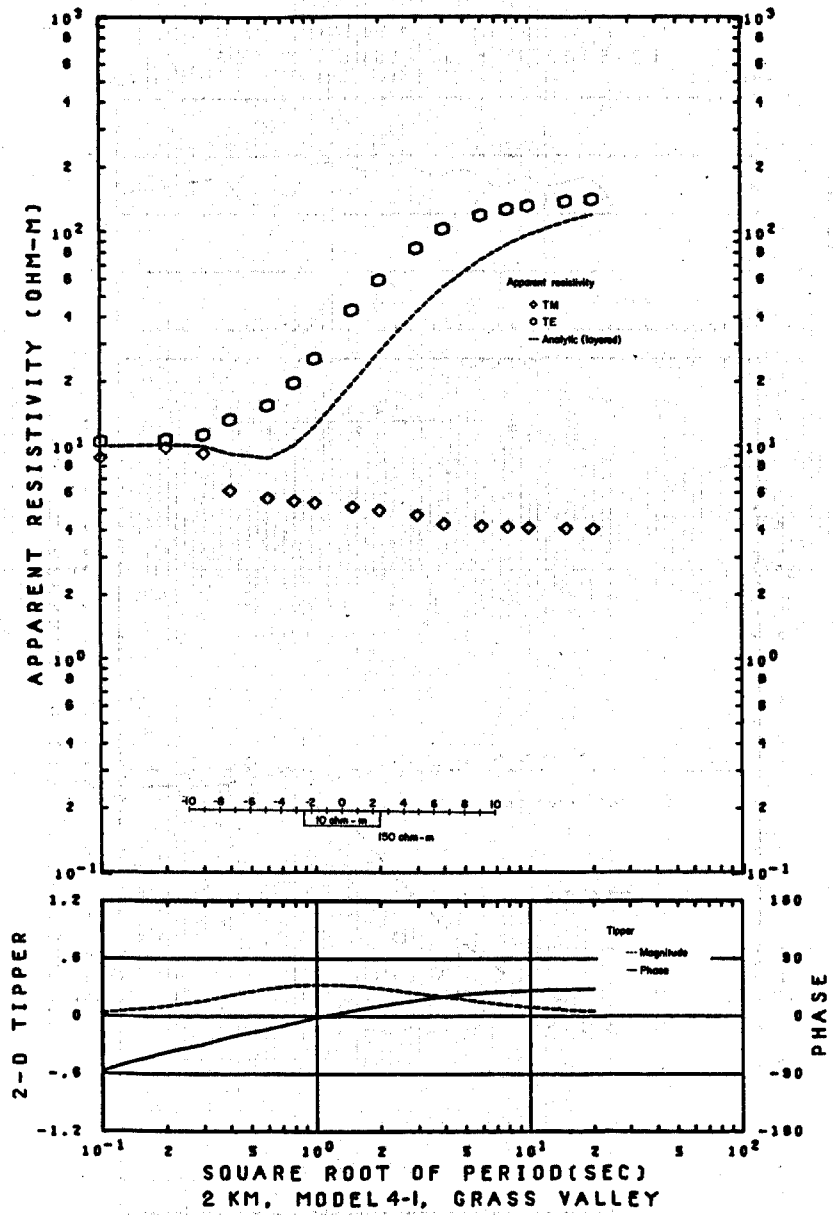
APPARENT RESISTIVITY (OHM-M)
Apparent resistivity
TM
TE
Analytic (layered)
10 ohm-m
150 ohm-m
2-D TIPPER
PHASE
Tipper
Magnitude
Phase
SQUARE ROOT OF PERIOD(SEC)
2 KM, MODEL 4-1, GRASS VALLEY

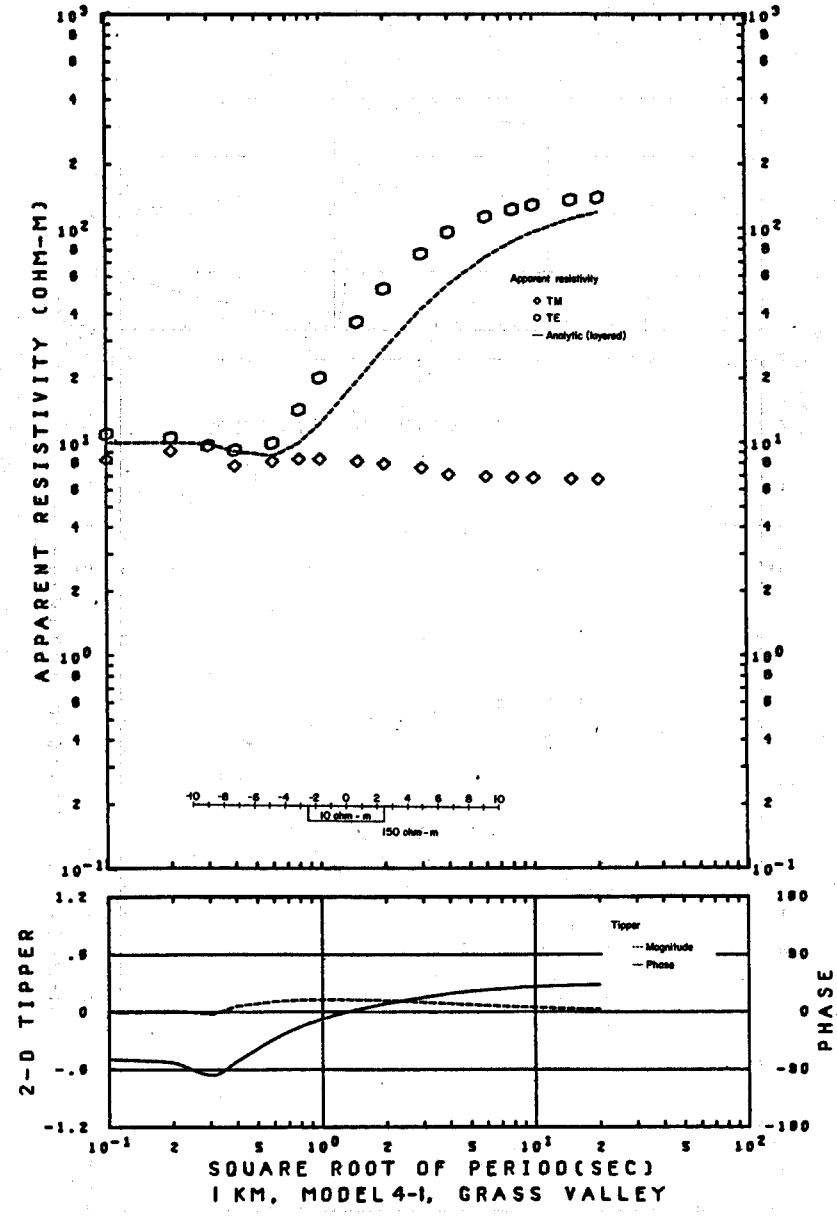
APPARENT RESISTIVITY (OHM-M)
Apparent resistivity
TM
TE
Analytic (layered)
10 ohm-m
150 ohm-m
2-D TIPPER
PHASE
Tipper
Magnitude
Phase
SQUARE ROOT OF PERIOD(SEC)
1 KM, MODEL 4-1, GRASS VALLEY

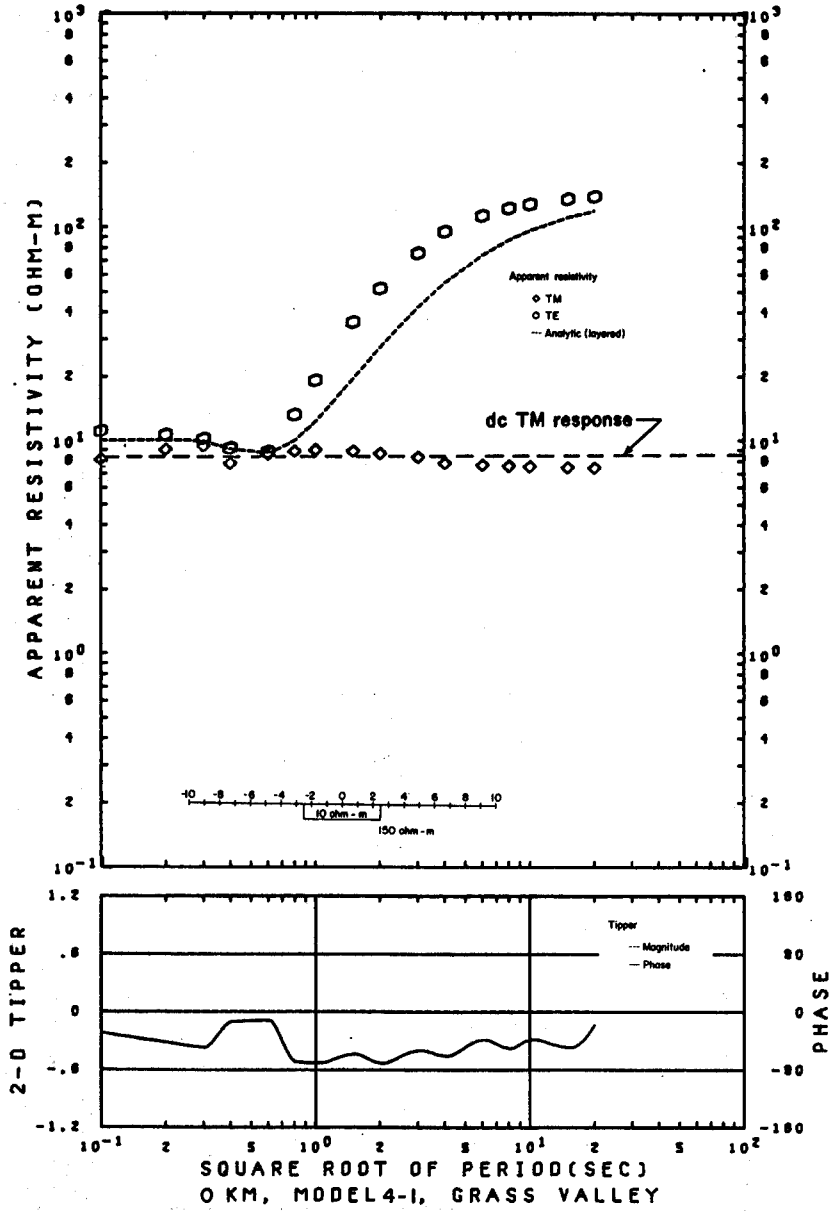
APPARENT RESISTIVITY (OHM-M)
Apparent resistivity
TM
TE
Analytic (layered)
dc TM response
10 ohm - m
150 ohm - m
2-D TIPPER
Tipper
Magnitude
Phase
PHASE
SQUARE ROOT OF PERIOD(SEC)
0 KM, MODEL 4-I, GRASS VALLEY

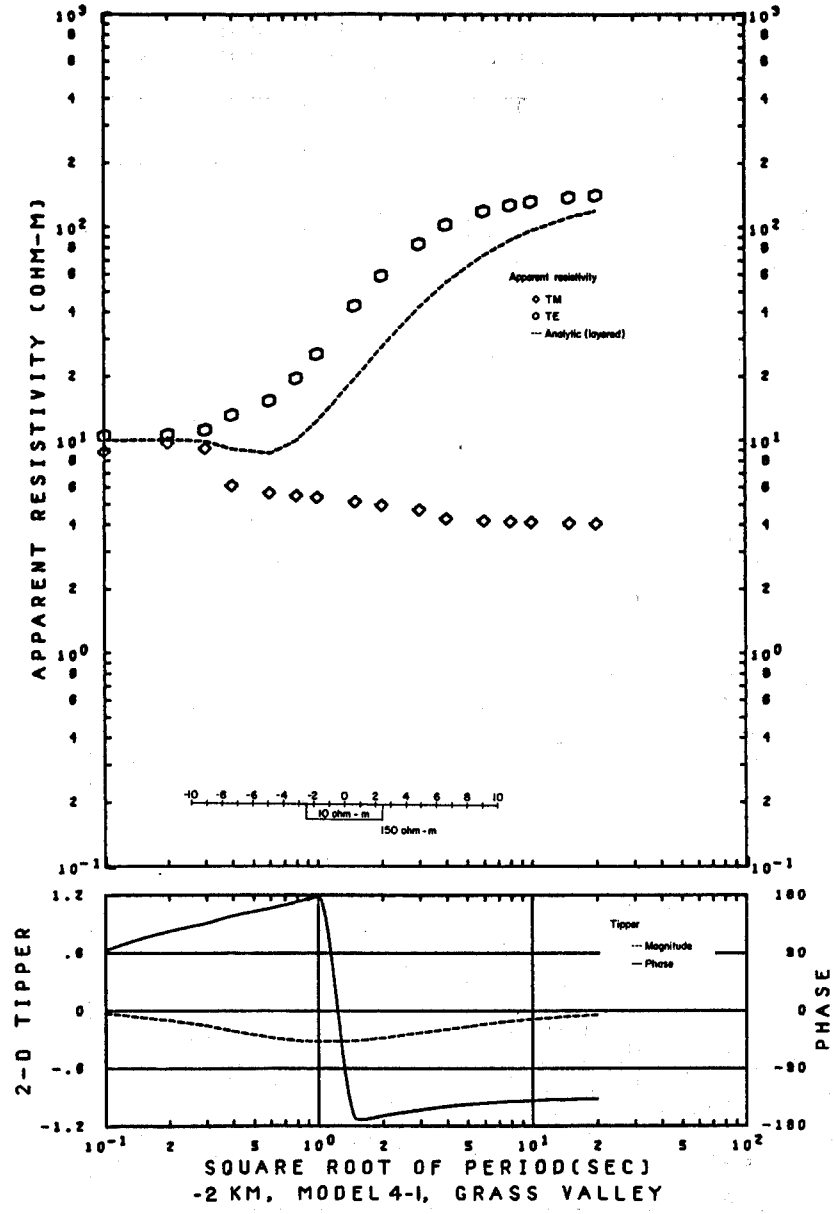
APPARENT RESISTIVITY (OHM-M)
Apparent resistivity
TM
TE
Analytic (layered)
10 ohm - m
150 ohm - m
2-D TIPPER
Tipper
Magnitude
Phase
PHASE
SQUARE ROOT OF PERIOD(SEC)
-2 KM, MODEL 4-I, GRASS VALLEY

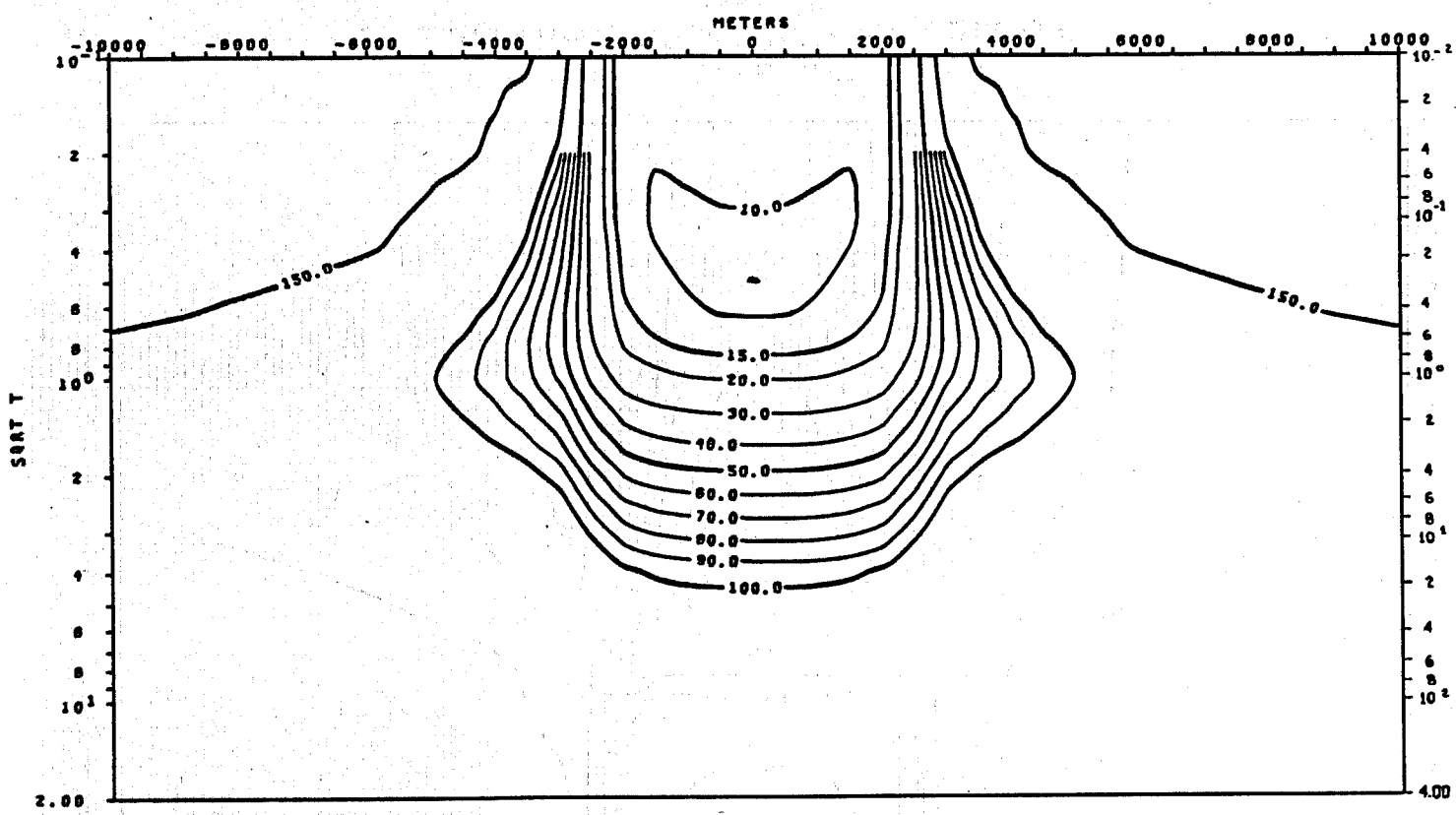

TE MODE
APPARENT RESISTIVITY VS. PERIOD (T)
MODEL 4-1

XBL 786-1901

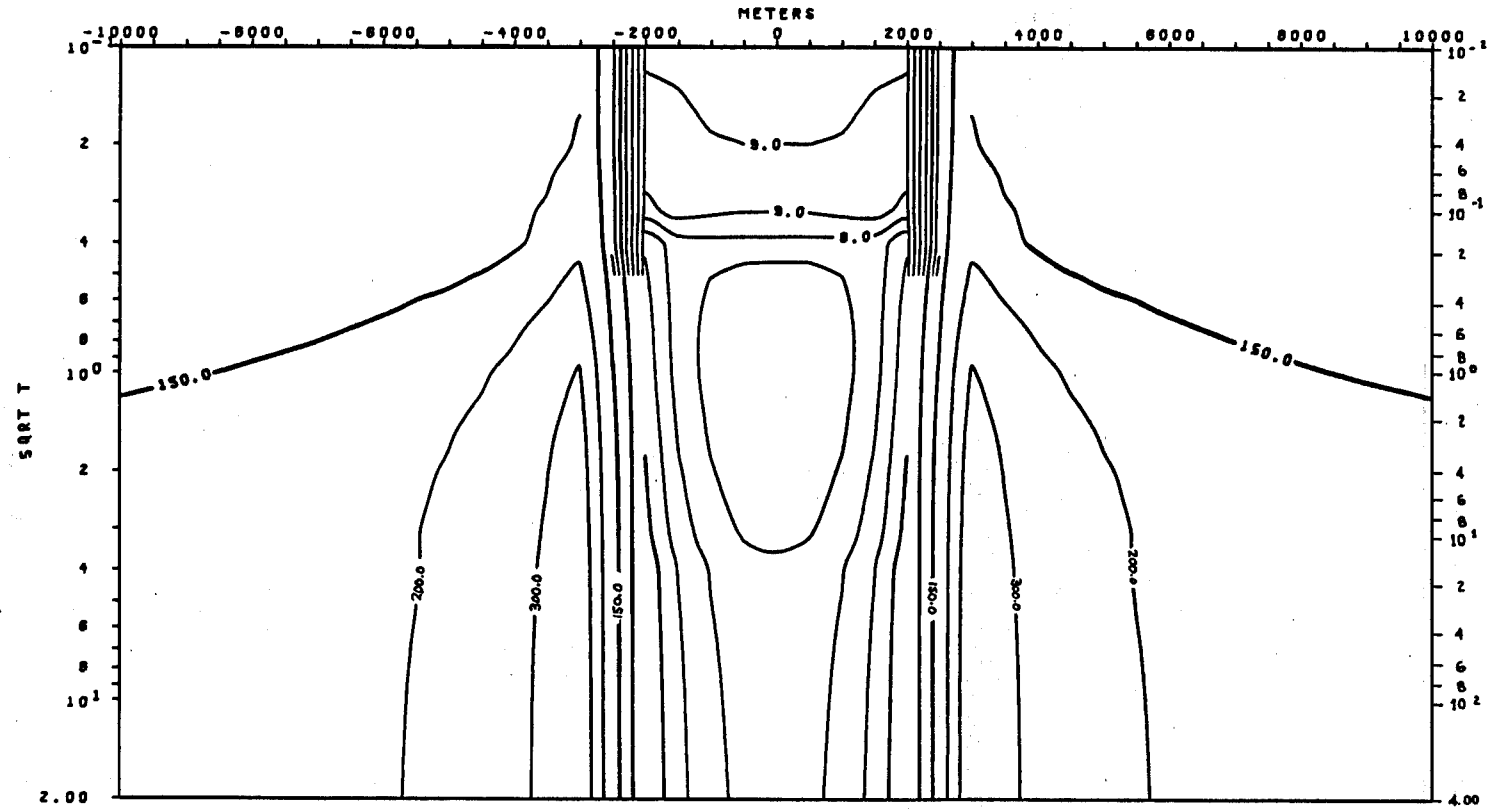

TM MODE
APPARENT RESISTIVITY VS. PERIOD (T)
MODEL 4-1

XBL 786-1946

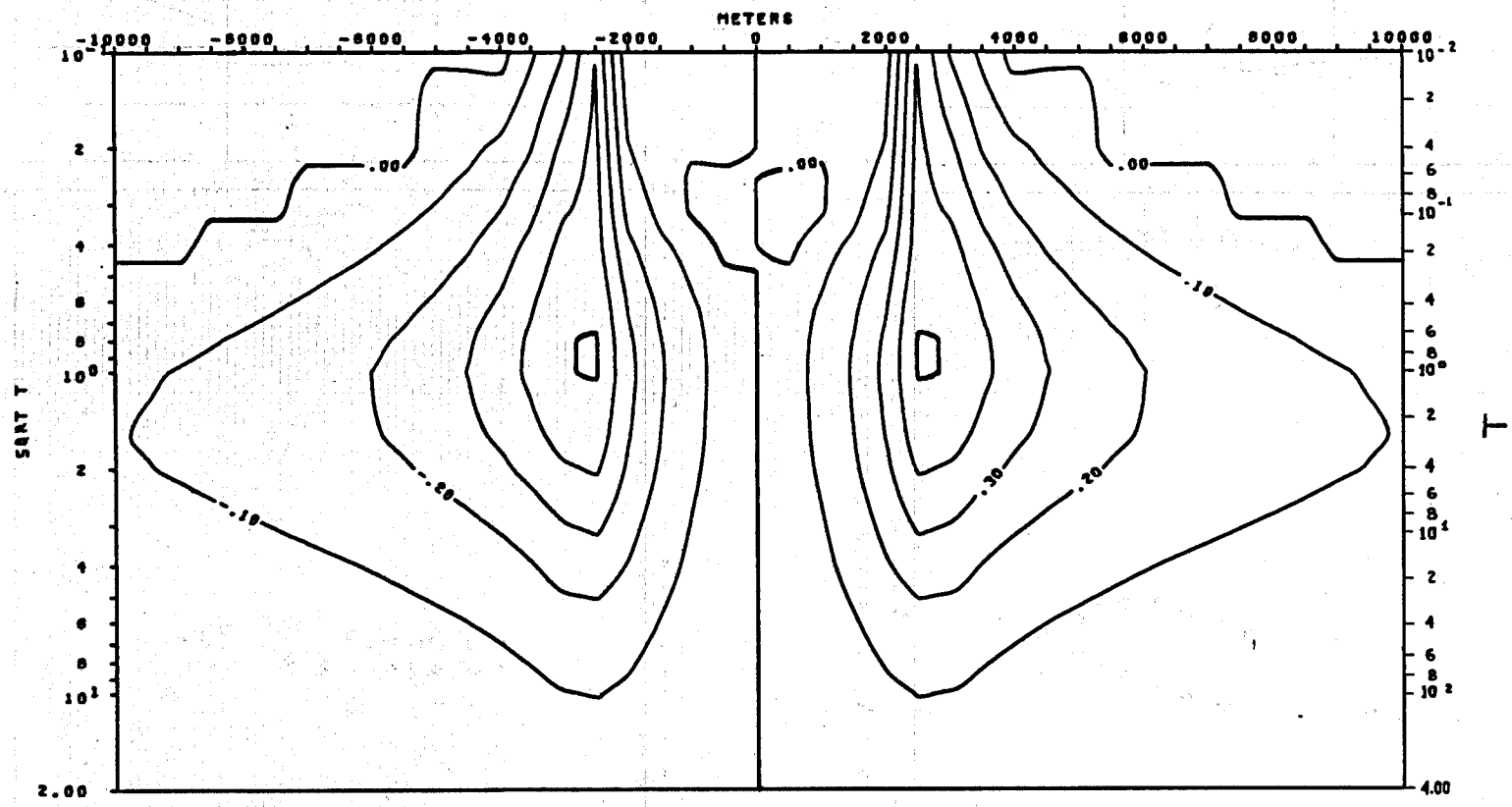

T

TIPPER VS. PERIOD (T)
MODEL 4-1

XBL 786-1933

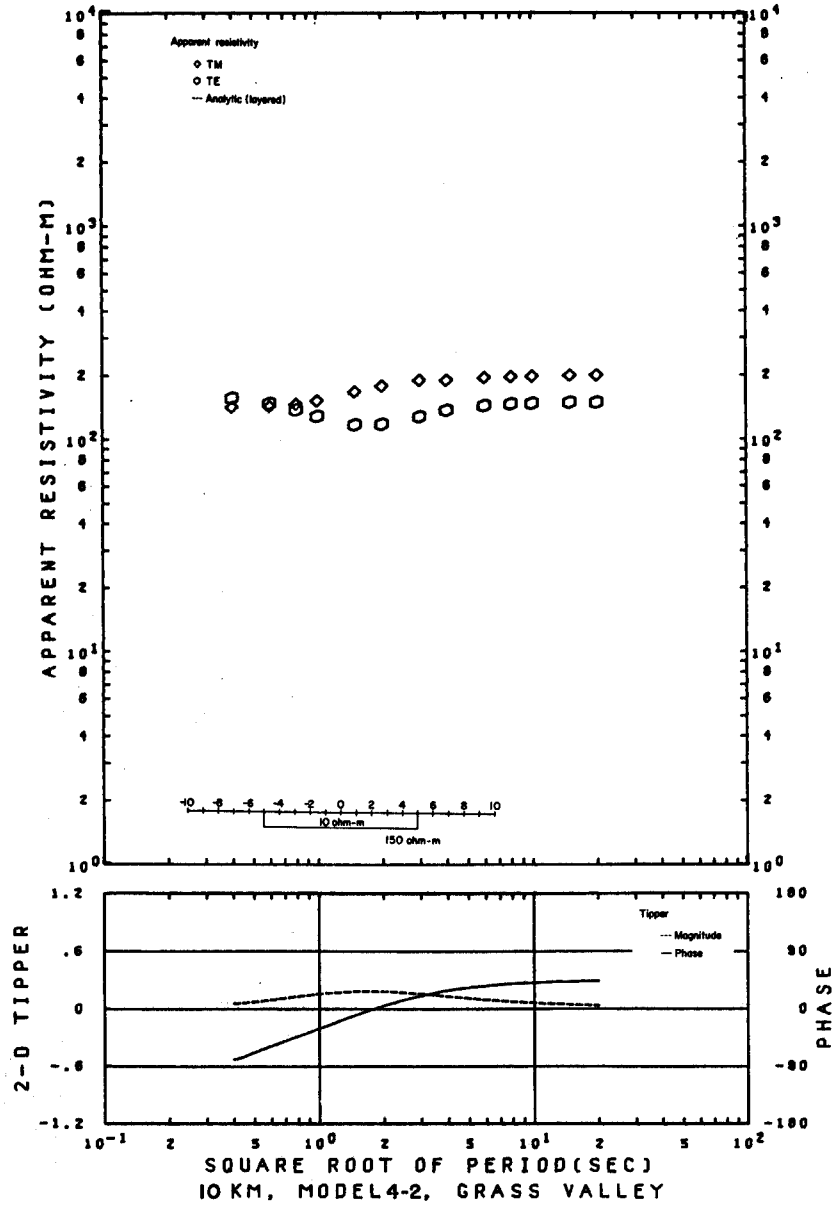
Apparent resistivity
TM
TE
Analytic (layered)
APPARENT RESISTIVITY (OHM-M)
10 ohm-m
150 ohm-m
Tipper
Magnitude
Phase
2-D TIPPER
PHASE
SQUARE ROOT OF PERIOD(SEC)
10KM, MODEL4-2, GRASS VALLEY

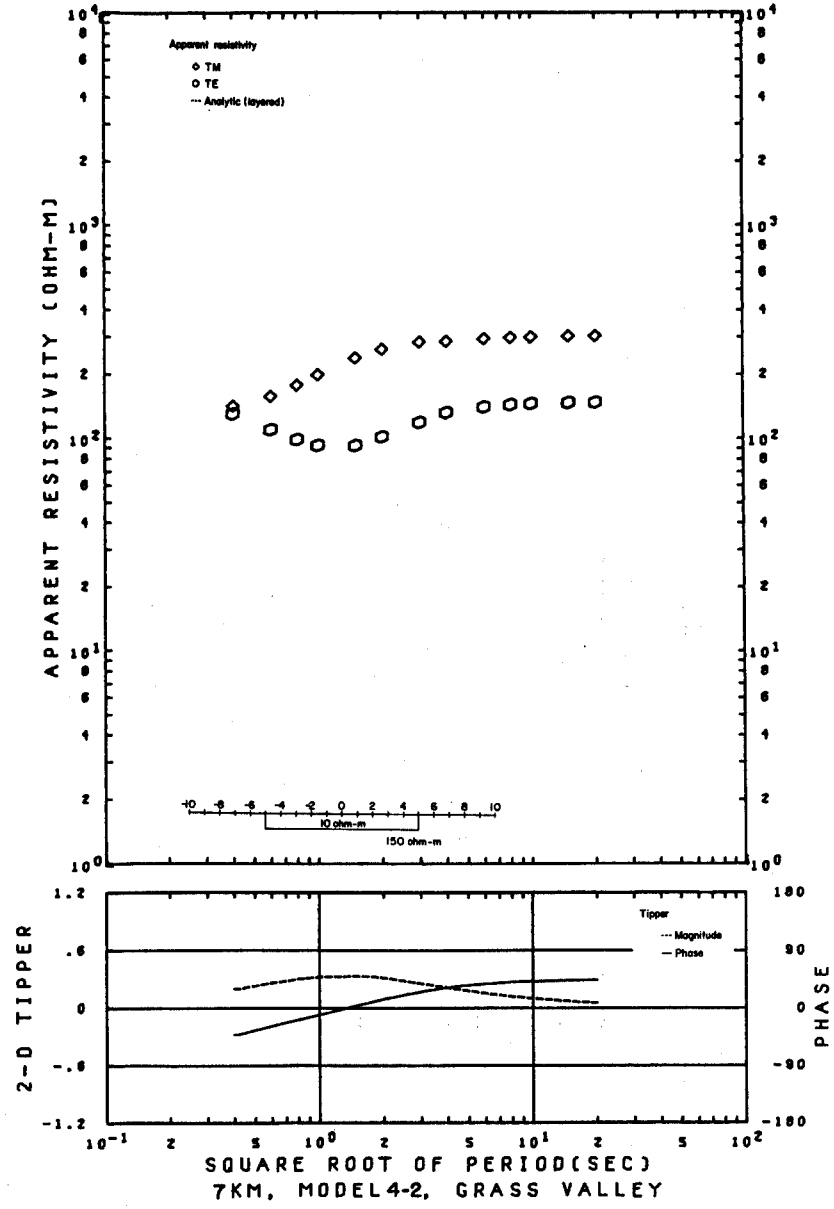
Apparent resistivity
TM
TE
Analytic (layered)
APPARENT RESISTIVITY (OHM-M)
10 ohm-m
150 ohm-m
Tipper
Magnitude
Phase
2-D TIPPER
PHASE
SQUARE ROOT OF PERIOD(SEC)
7KM, MODEL4-2, GRASS VALLEY

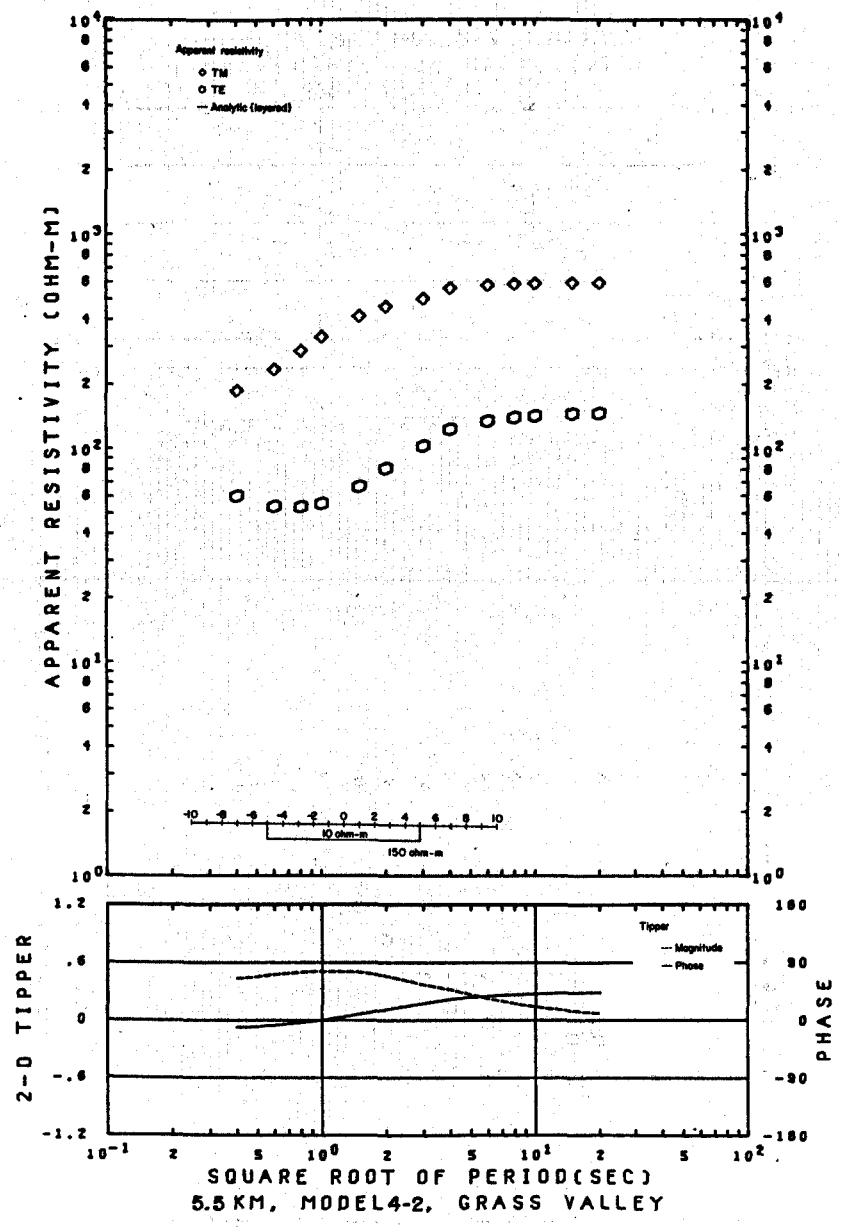

5.5 KM, MODEL4-2, GRASS VALLEY

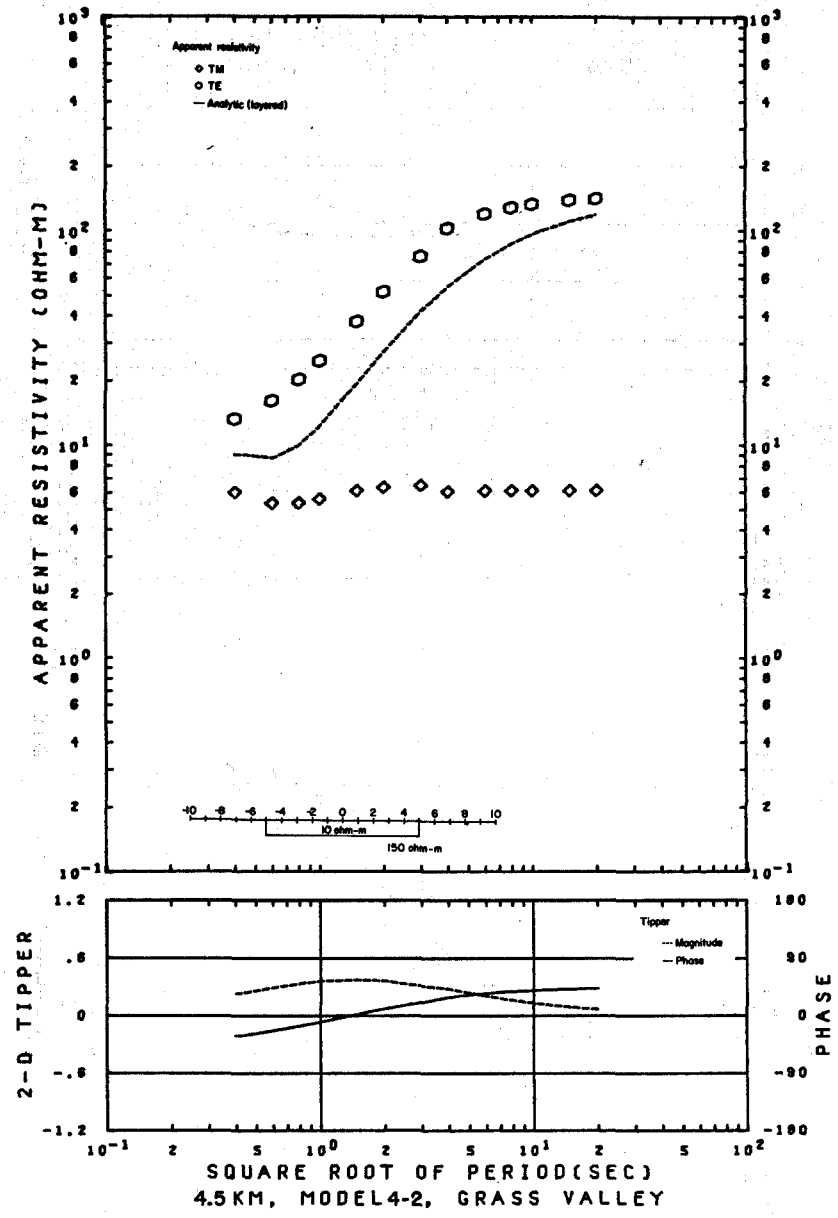

4.5 KM, MODEL4-2, GRASS VALLEY

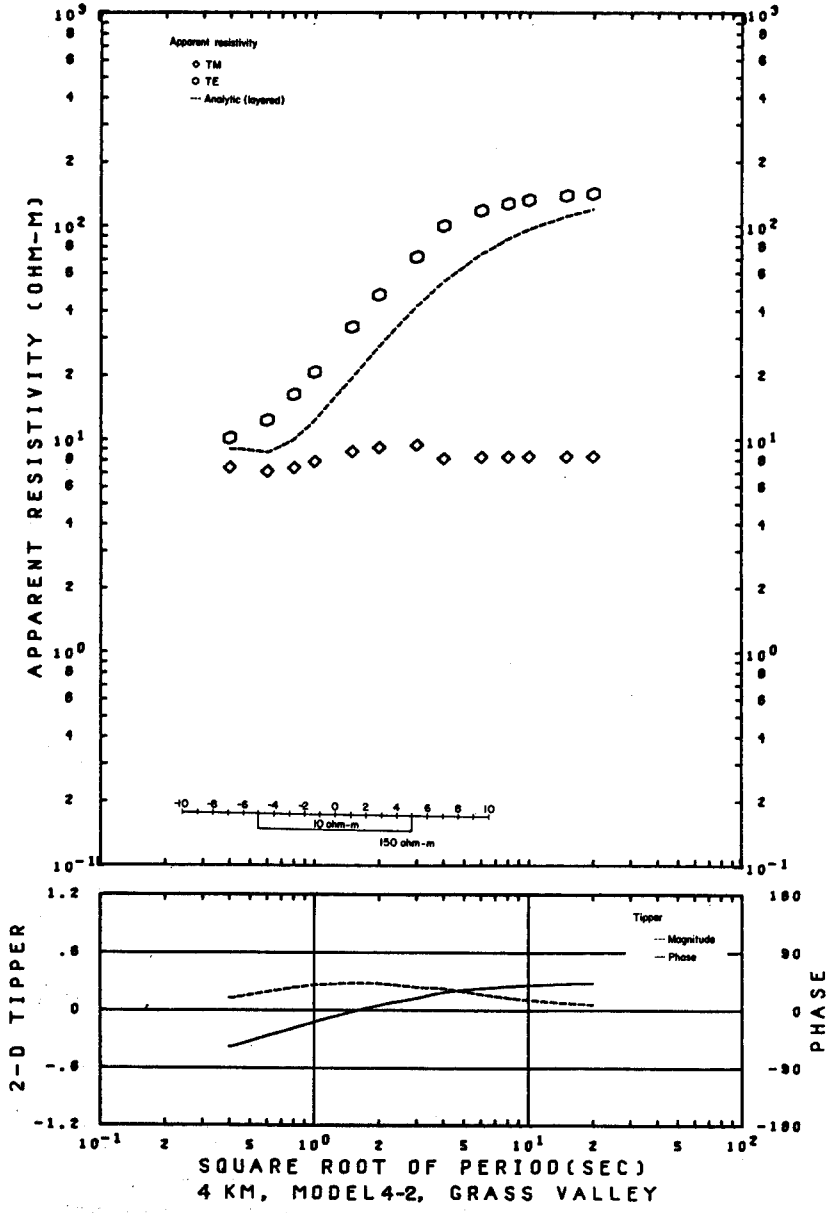
Apparent resistivity
TM
TE
Analytic (layered)
APPARENT RESISTIVITY (OHM-M)
10 ohm-m
150 ohm-m
Tipper
Magnitude
Phase
2-D TIPPER
PHASE
SQUARE ROOT OF PERIOD(SEC)
4 KM, MODEL 4-2, GRASS VALLEY

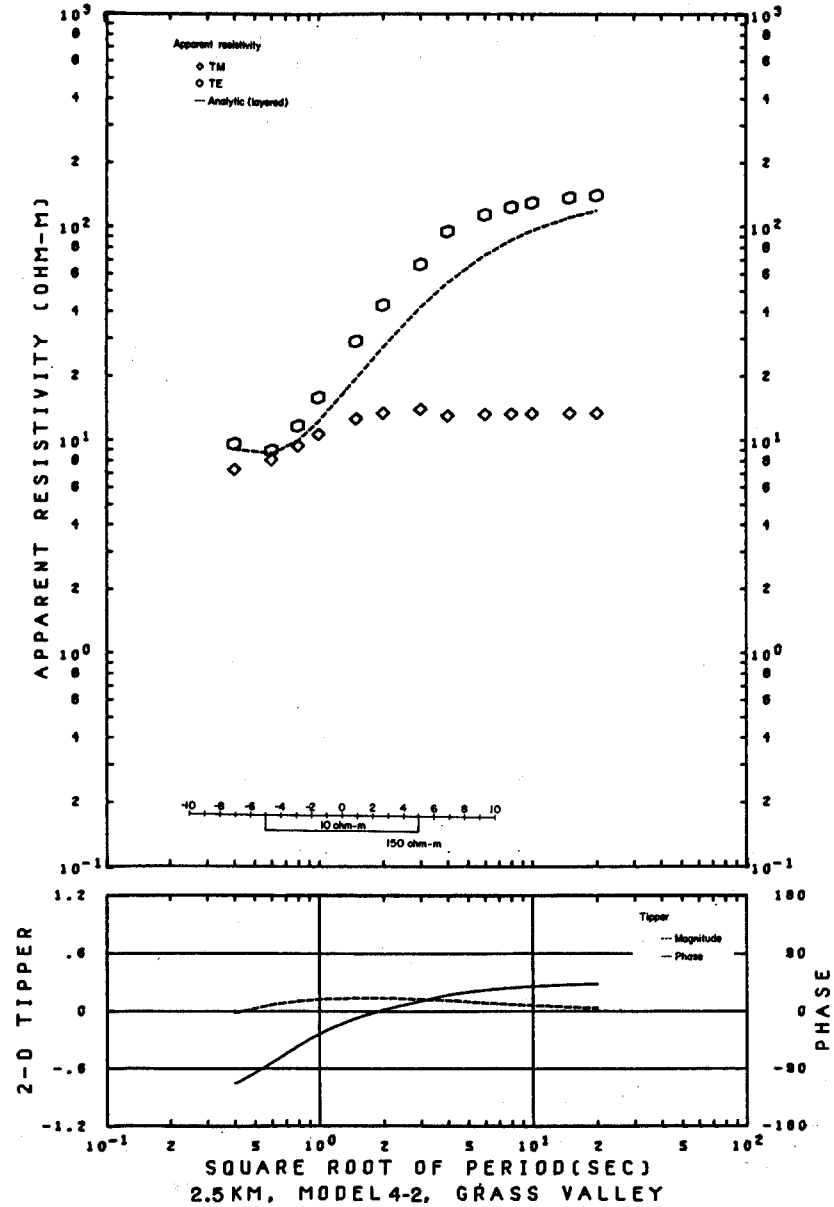
Apparent resistivity
TM
TE
Analytic (layered)
APPARENT RESISTIVITY (OHM-M)
10 ohm-m
150 ohm-m
Tipper
Magnitude
Phase
2-D TIPPER
PHASE
SQUARE ROOT OF PERIOD(SEC)
2.5 KM, MODEL 4-2, GRASS VALLEY

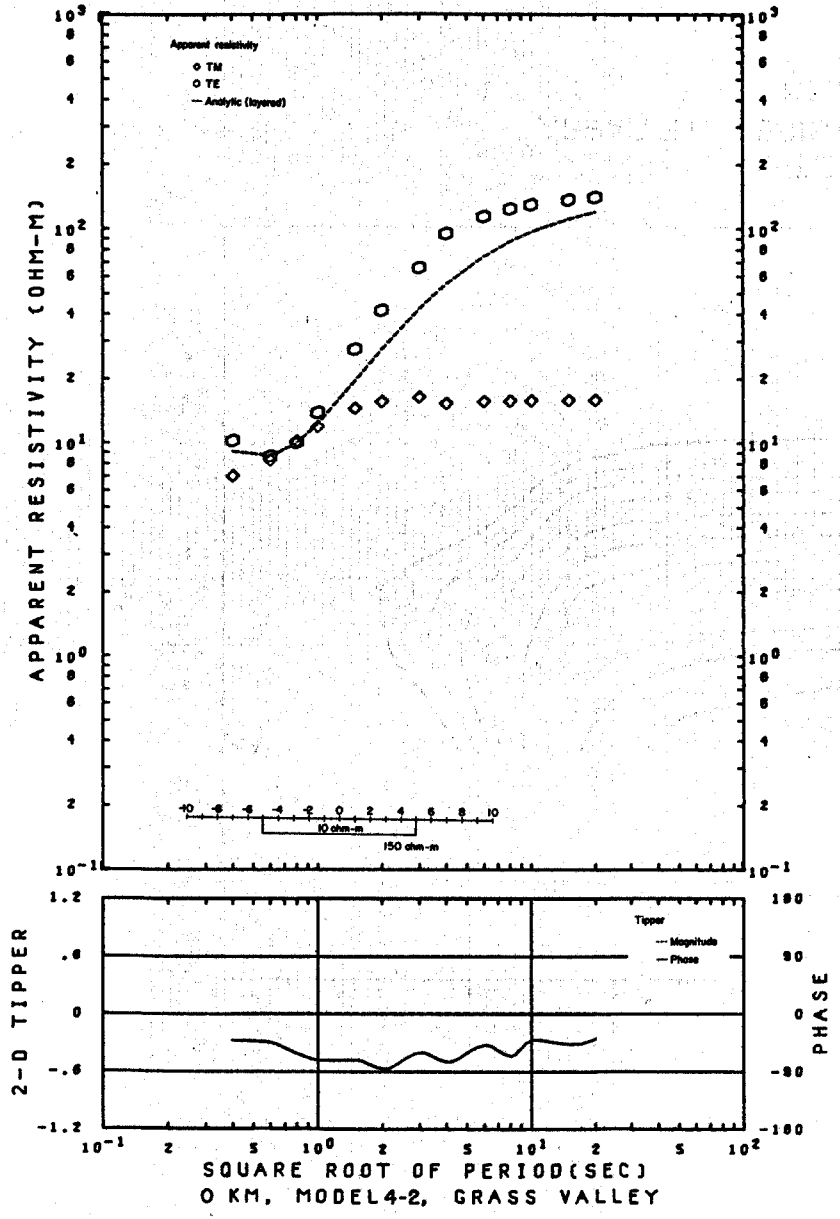
Apparent resistivity
TM
TE
Analytic (layered)
APPARENT RESISTIVITY (OHM-M)
10 ohm-m
150 ohm-m
Tipper
Magnitude
Phase
2-D TIPPER
PHASE
SQUARE ROOT OF PERIOD(SEC)
0 KM, MODEL4-2, GRASS VALLEY

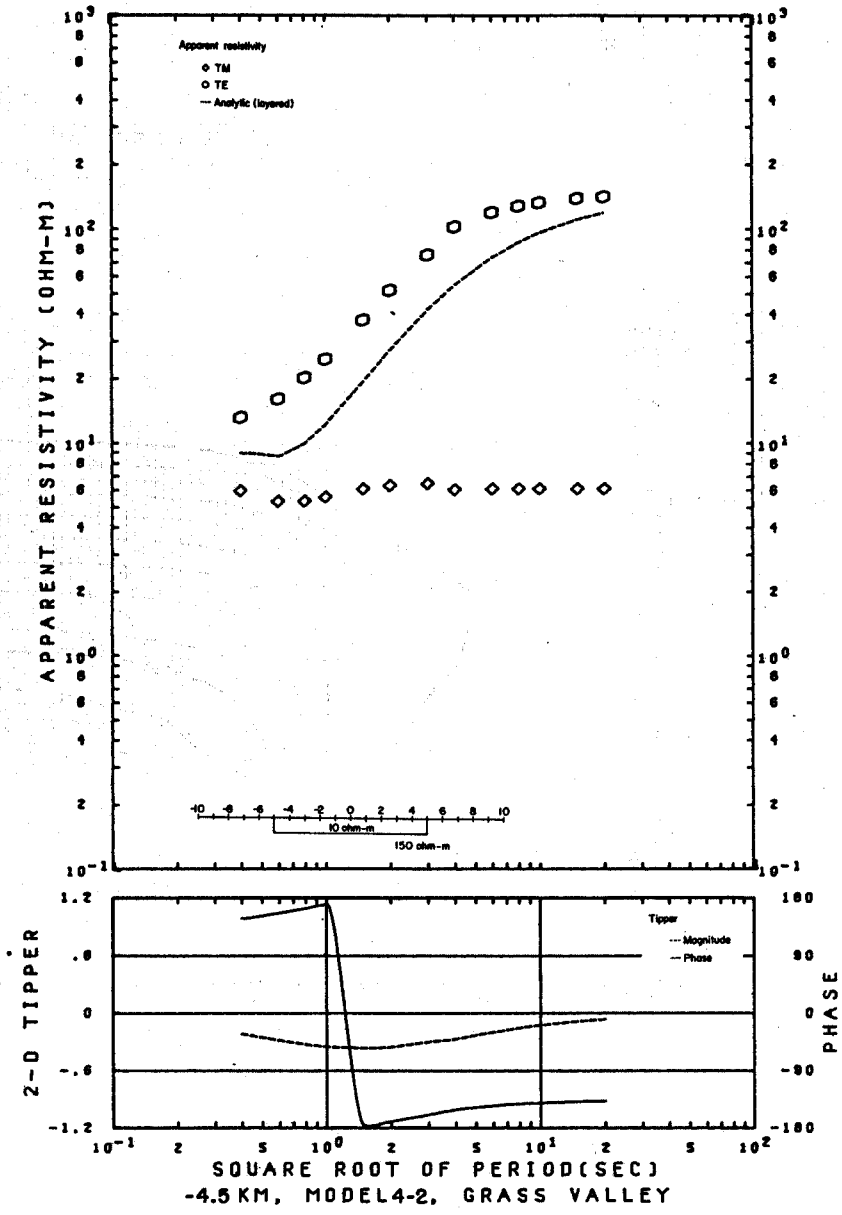
Apparent resistivity
TM
TE
Analytic (layered)
APPARENT RESISTIVITY (OHM-M)
10 ohm-m
150 ohm-m
Tipper
Magnitude
Phase
2-D TIPPER
PHASE
SQUARE ROOT OF PERIOD(SEC)
-4.5 KM, MODEL4-2, GRASS VALLEY

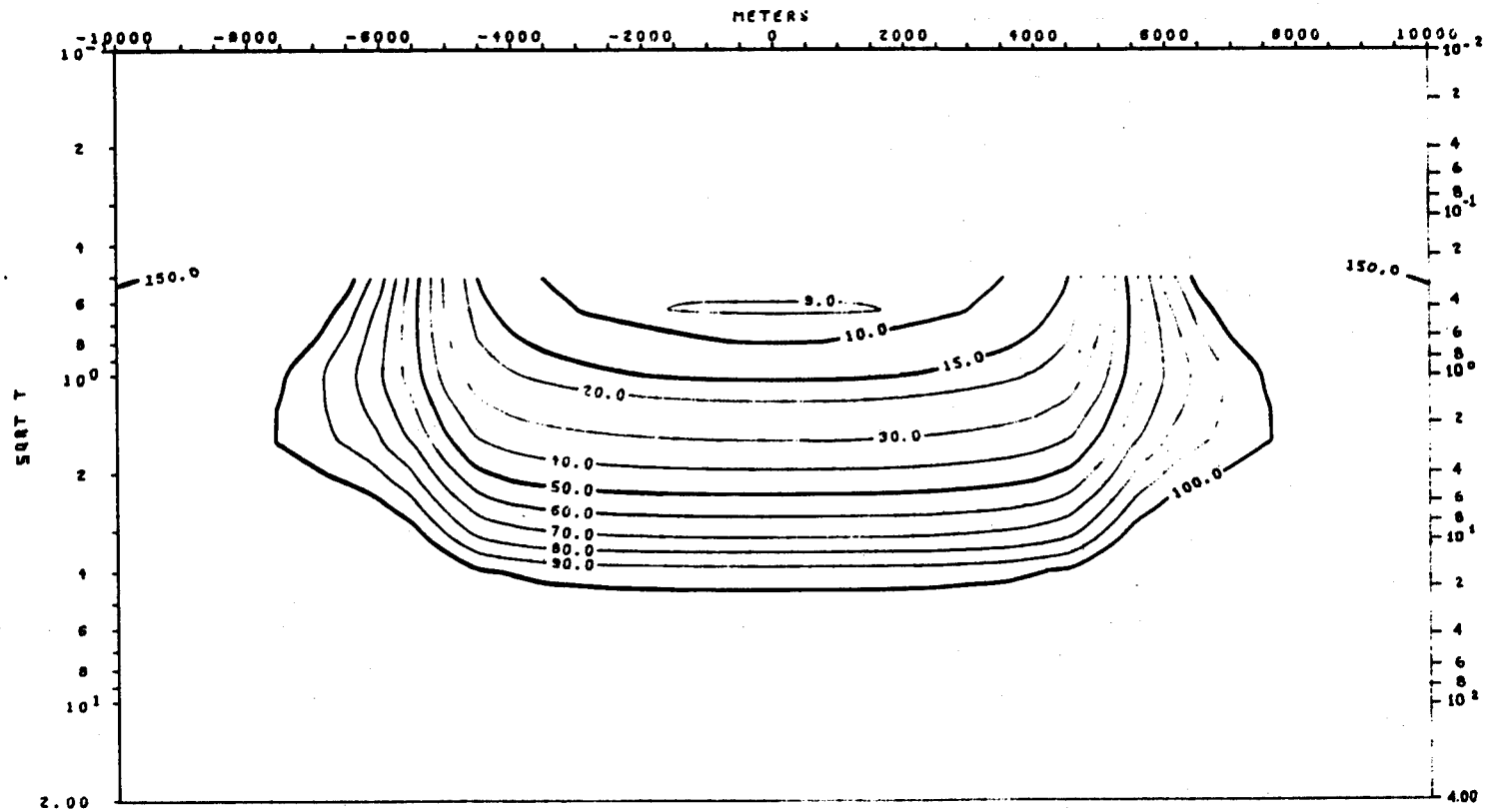

TE MODE
APPARENT RESISTIVITY VS. PERIOD (T)
MODEL 4-2

XBL 786-1935

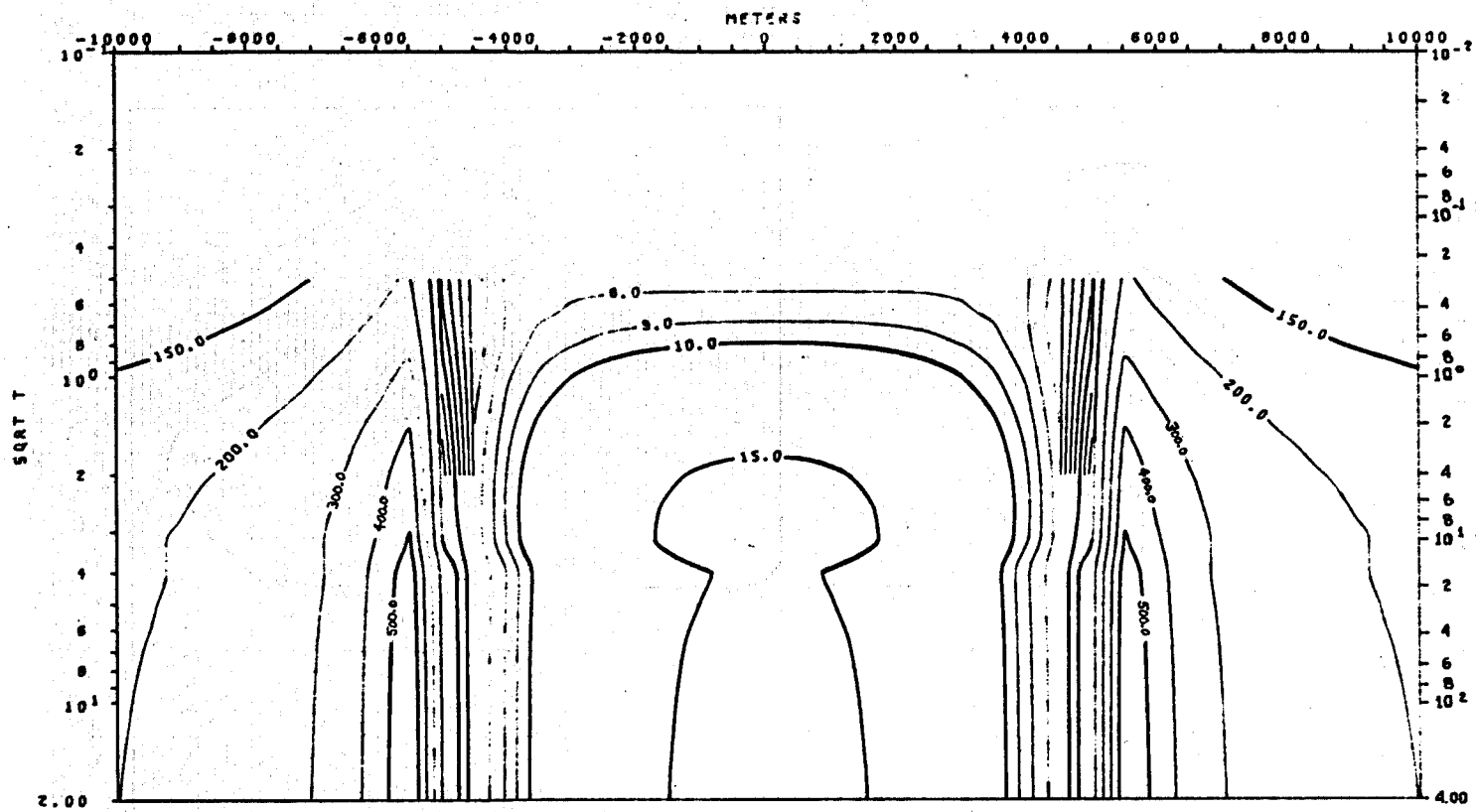

TM MODE
APPARENT RESISTIVITY VS. PERIOD (T)
MODEL 4-2

XBL 786-1934

T

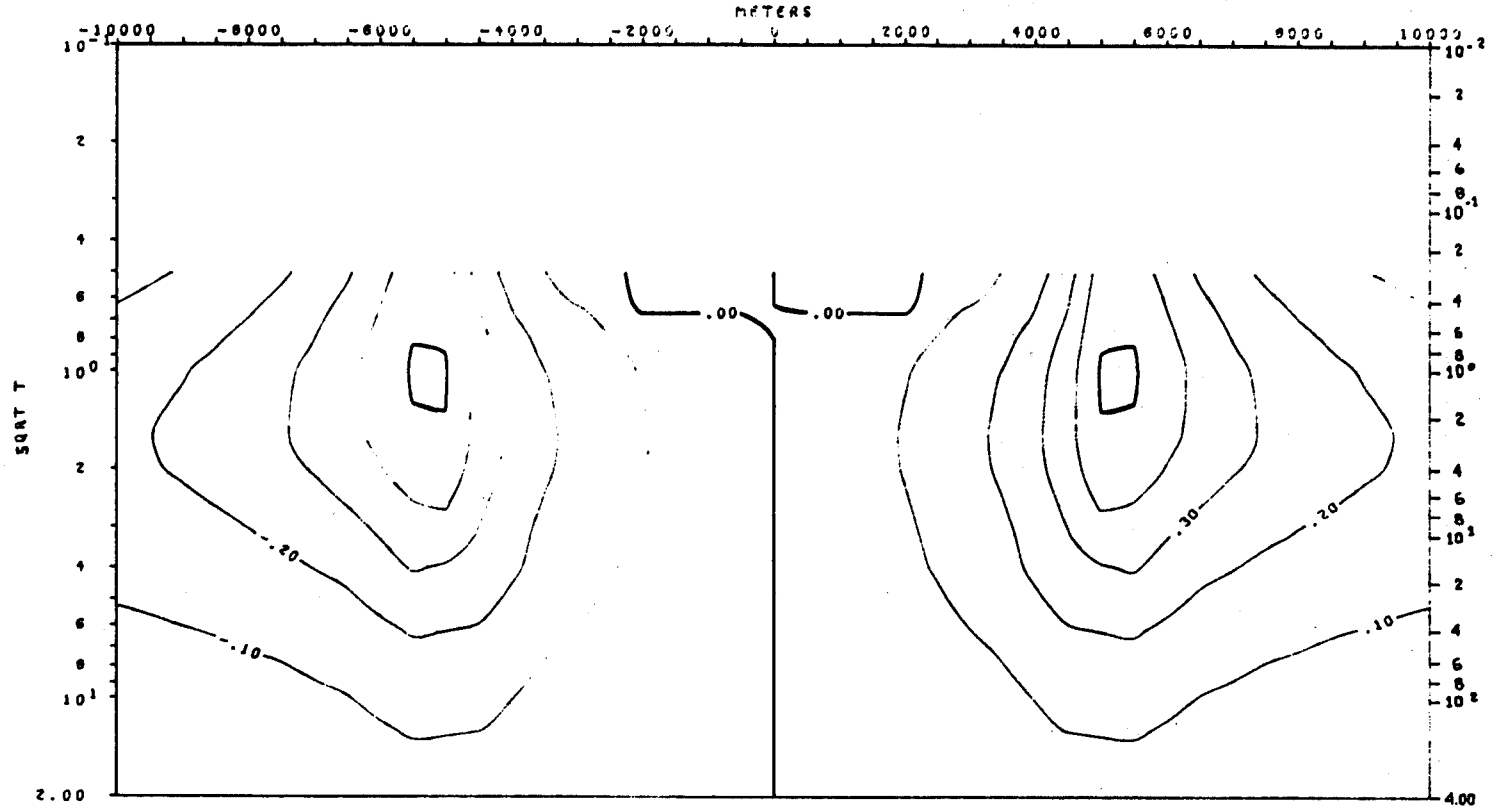

TIPPER VS. PERIOD (T)
MODEL 4-2

XBL 786-1937

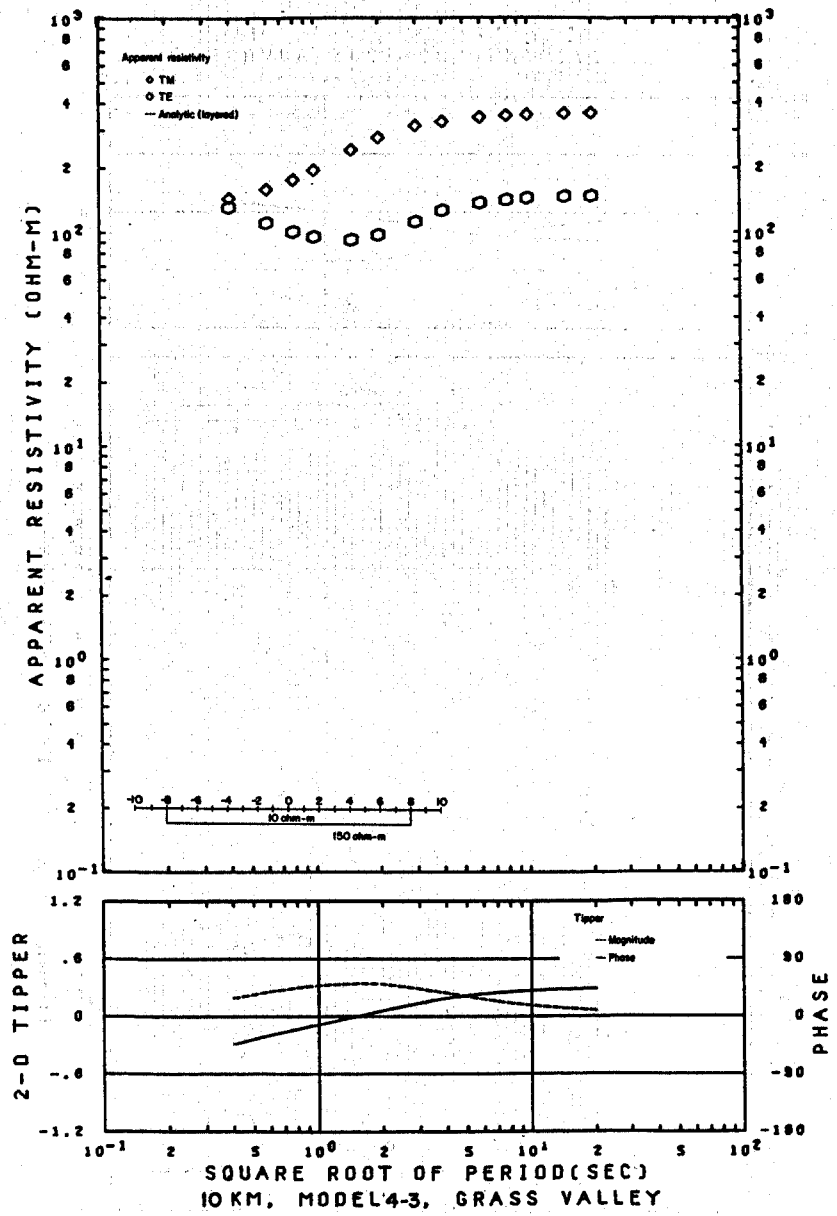
Apparent resistivity
TM
TE
Analytic (layered)
APPARENT RESISTIVITY (OHM-M)
10 ohm-m
150 ohm-m
Tipper
Magnitude
Phase
2-D TIPPER
PHASE
SQUARE ROOT OF PERIOD(SEC)
10 KM, MODEL 4-3, GRASS VALLEY

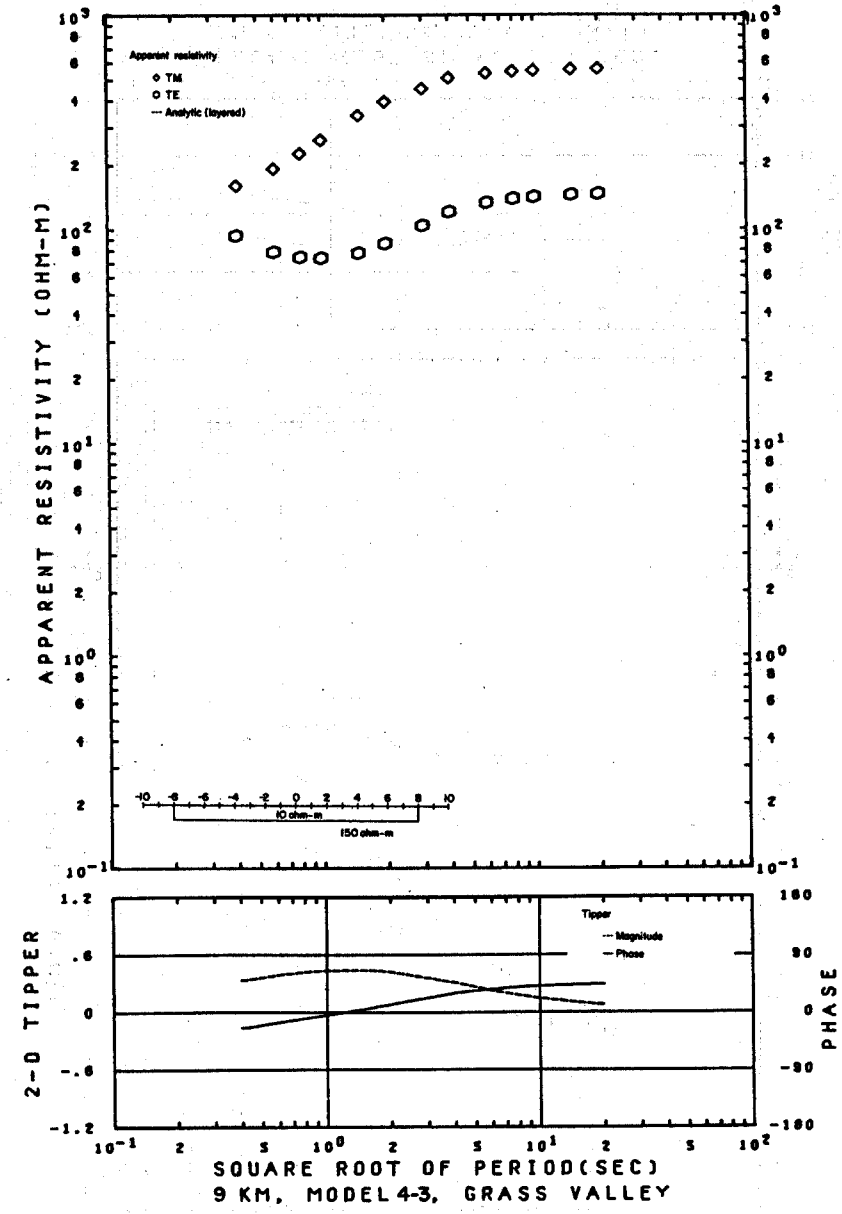
Apparent resistivity
TM
TE
Analytic (layered)
APPARENT RESISTIVITY (OHM-M)
10 ohm-m
150 ohm-m
Tipper
Magnitude
Phase
2-D TIPPER
PHASE
SQUARE ROOT OF PERIOD(SEC)
9 KM, MODEL 4-3, GRASS VALLEY

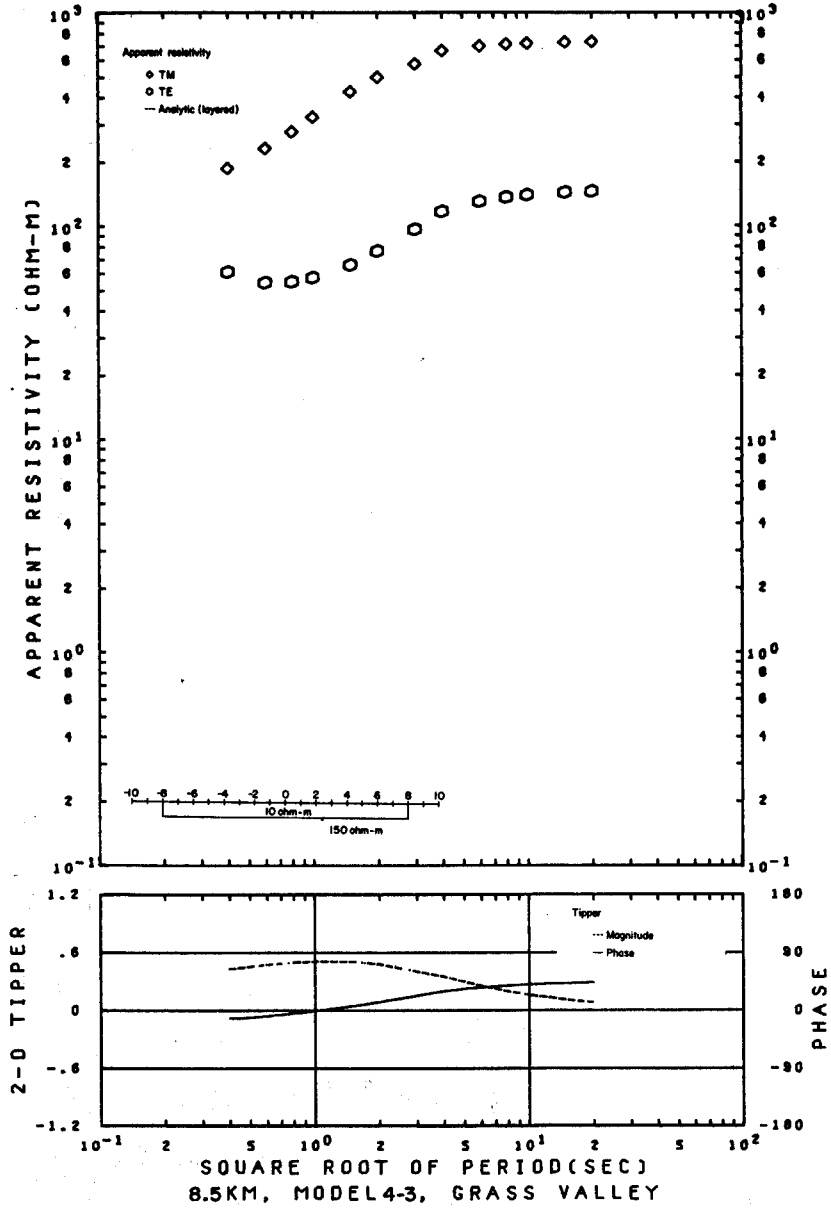
Apparent resistivity
TM
TE
Analytic (layered)
APPARENT RESISTIVITY (OHM-M)
10 ohm-m
150 ohm-m
Tipper
Magnitude
Phase
2-D TIPPER
PHASE
SQUARE ROOT OF PERIOD(SEC)
8.5KM, MODEL4-3, GRASS VALLEY

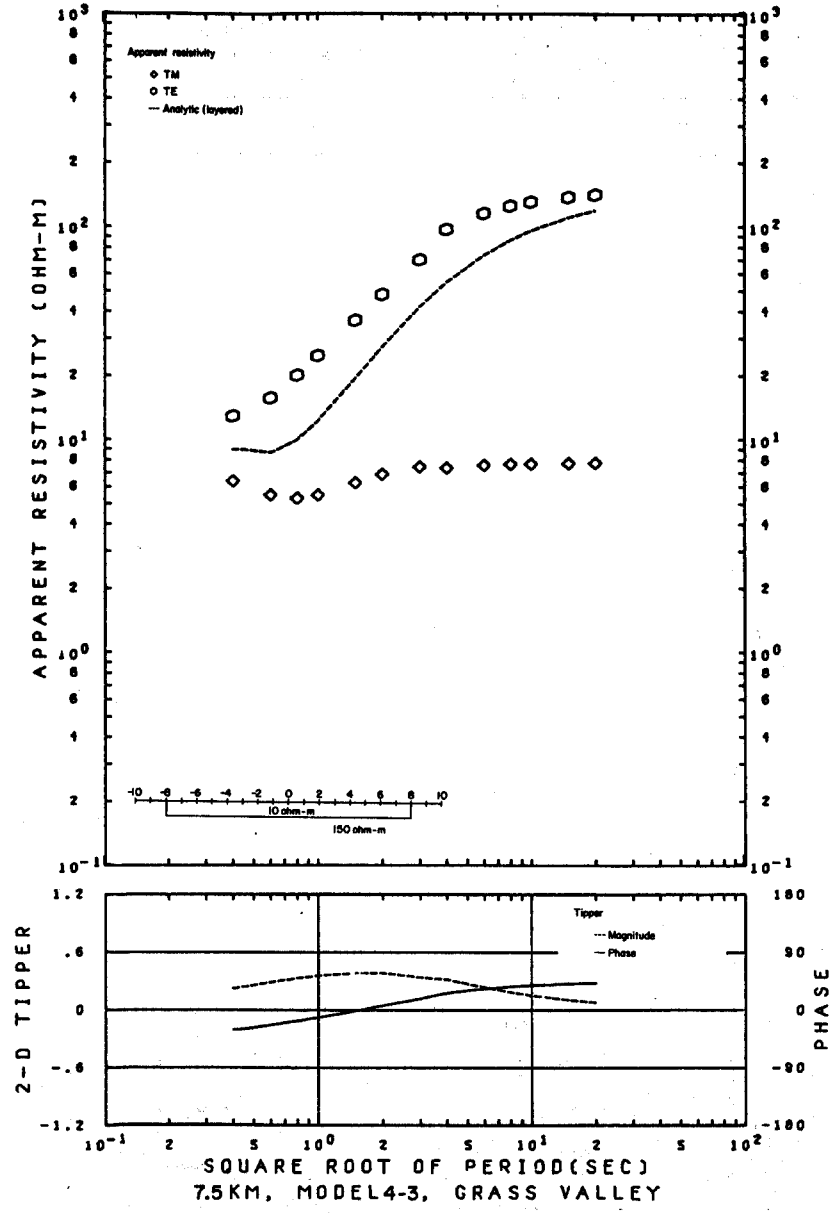
Apparent resistivity
TM
TE
Analytic (layered)
APPARENT RESISTIVITY (OHM-M)
10 ohm-m
150 ohm-m
Tipper
Magnitude
Phase
2-D TIPPER
PHASE
SQUARE ROOT OF PERIOD(SEC)
7.5KM, MODEL4-3, GRASS VALLEY

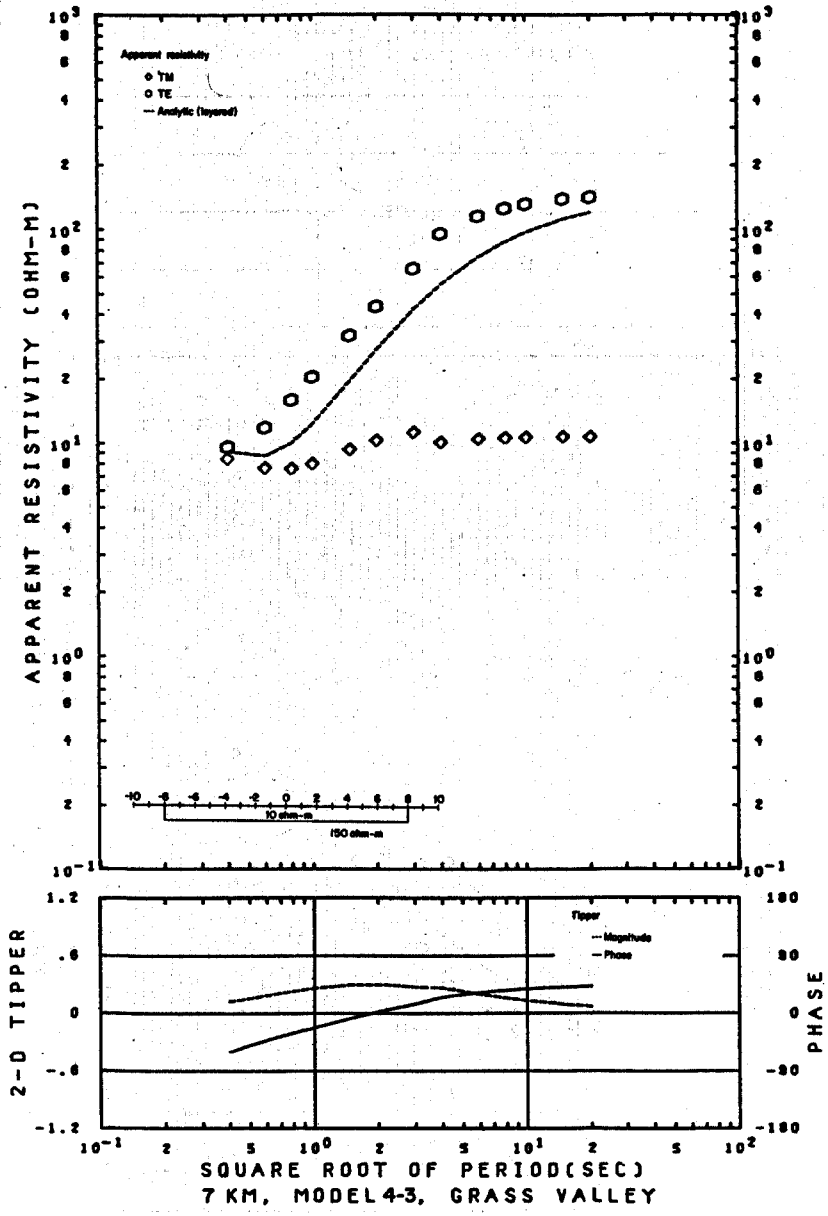
Apparent resistivity
TM
TE
Analytic (layered)
APPARENT RESISTIVITY (OHM-M)
10 ohm-m
150 ohm-m
Tipper
Magnitude
Phase
2-D TIPPER
PHASE
SQUARE ROOT OF PERIOD(SEC)
7 KM, MODEL4-3, GRASS VALLEY

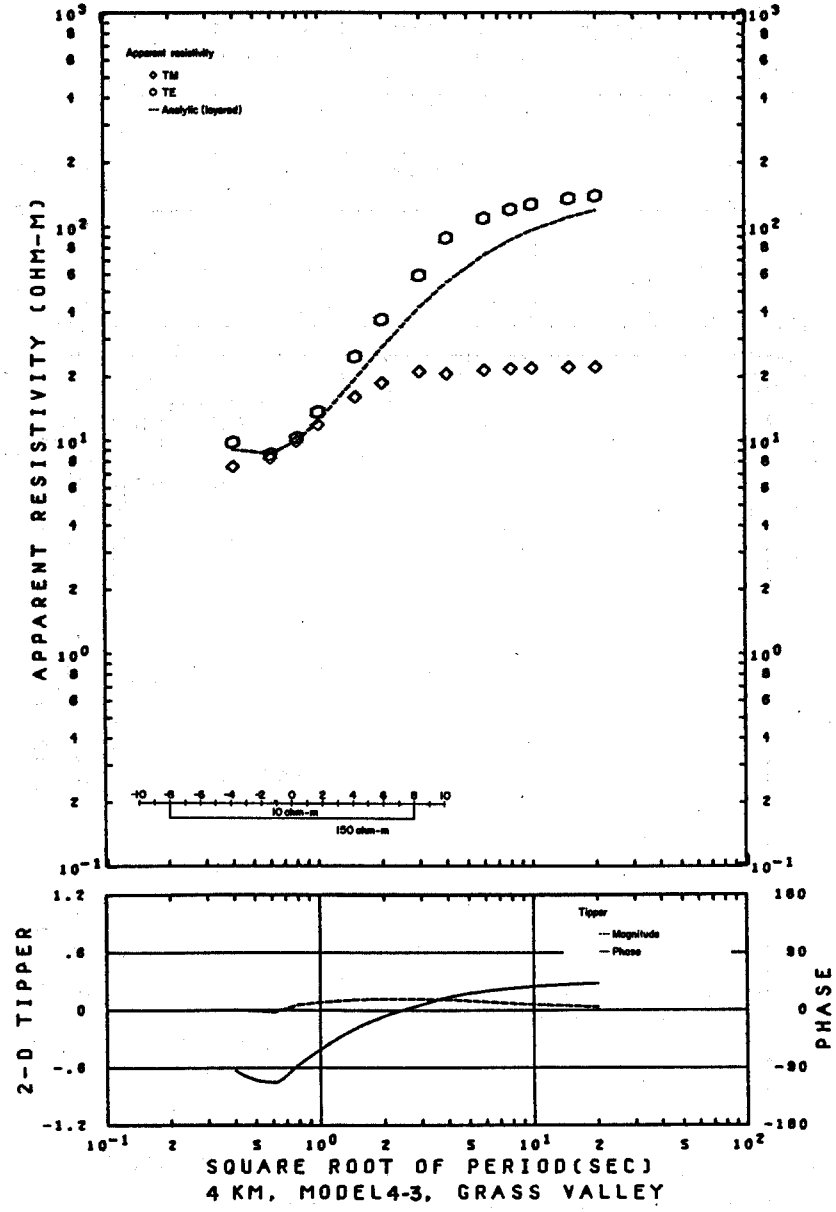
Apparent resistivity
TM
TE
Analytic (layered)
APPARENT RESISTIVITY (OHM-M)
10 ohm-m
150 ohm-m
Tipper
Magnitude
Phase
2-D TIPPER
PHASE
SQUARE ROOT OF PERIOD(SEC)
4 KM, MODEL4-3, GRASS VALLEY

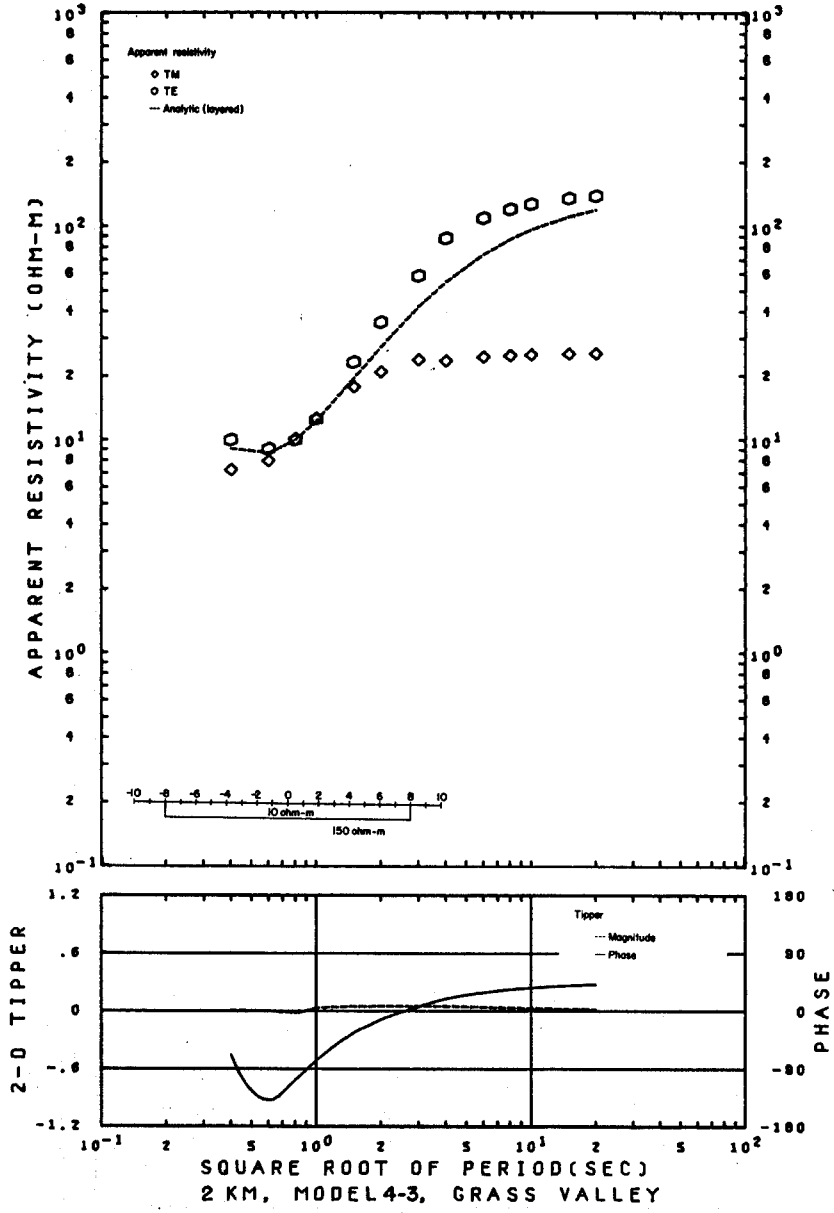
Apparent resistivity
TM
TE
Analytic (layered)
APPARENT RESISTIVITY (OHM-M)
10 ohm-m
150 ohm-m
Tipper
Magnitude
Phase
2-D TIPPER
PHASE
SQUARE ROOT OF PERIOD(SEC)
2 KM, MODEL4-3, GRASS VALLEY

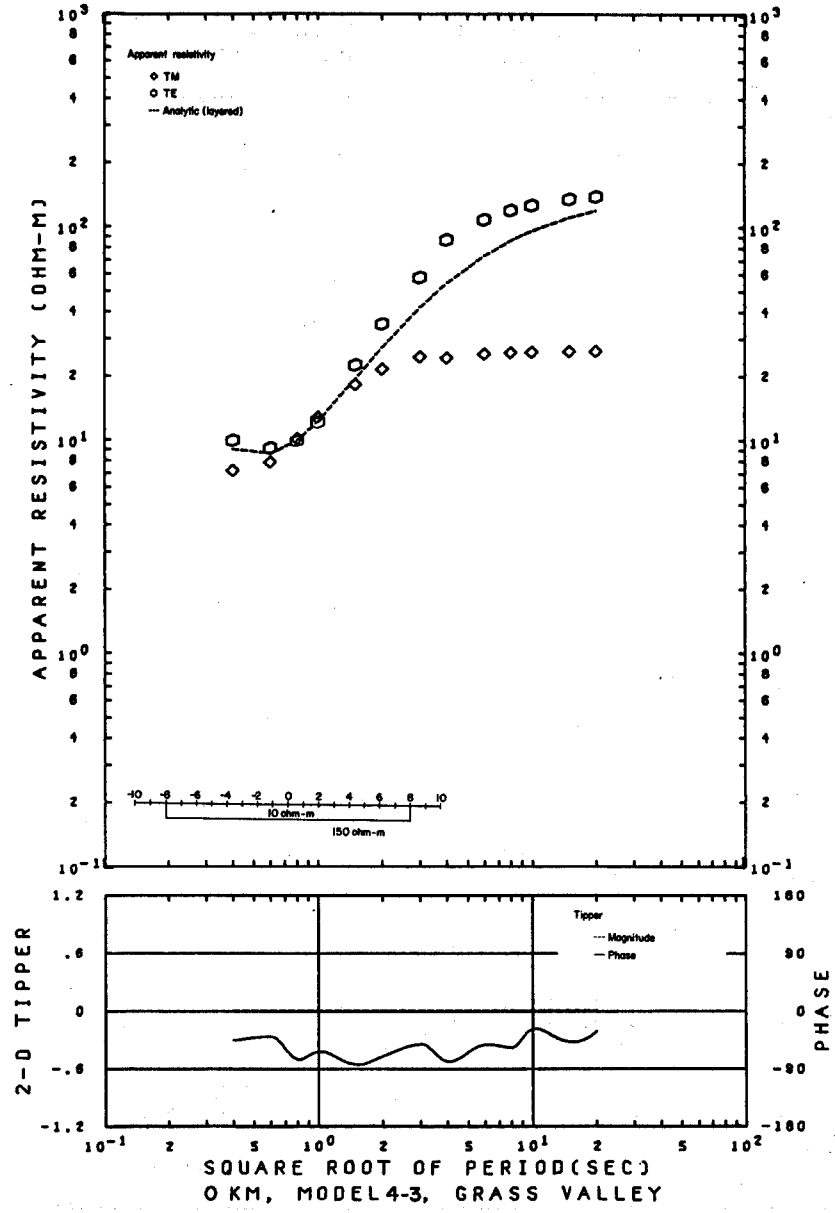
Apparent resistivity
TM
TE
Analytic (layered)
APPARENT RESISTIVITY (OHM-M)
10 ohm-m
150 ohm-m
Tipper
Magnitude
Phase
2-D TIPPER
PHASE
SQUARE ROOT OF PERIOD(SEC)
0 KM, MODEL4-3, GRASS VALLEY

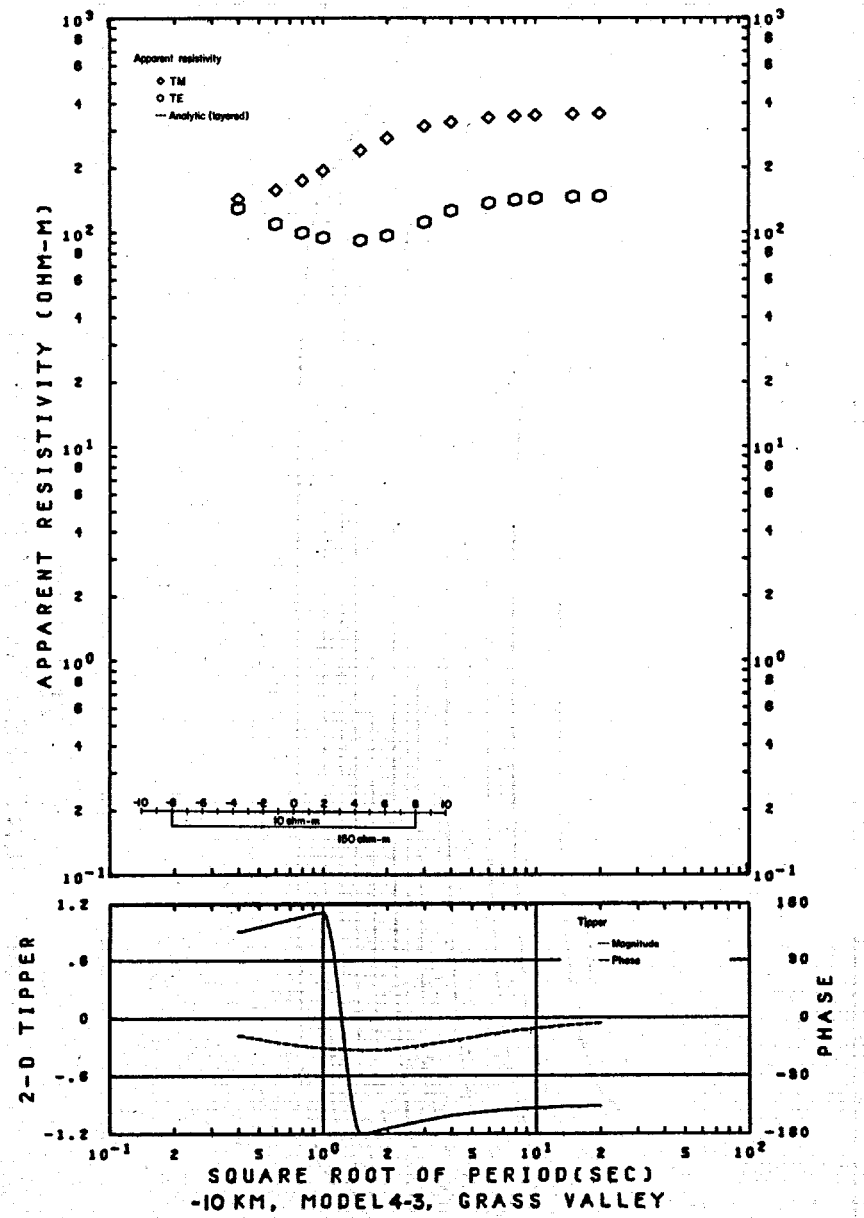
Apparent resistivity
TM
TE
Analytic (layered)
APPARENT RESISTIVITY (OHM-M)
10 ohm-m
150 ohm-m
Tipper
Magnitude
Phase
2-D TIPPER
PHASE
SQUARE ROOT OF PERIOD(SEC)
-10 KM, MODEL 4-3, GRASS VALLEY

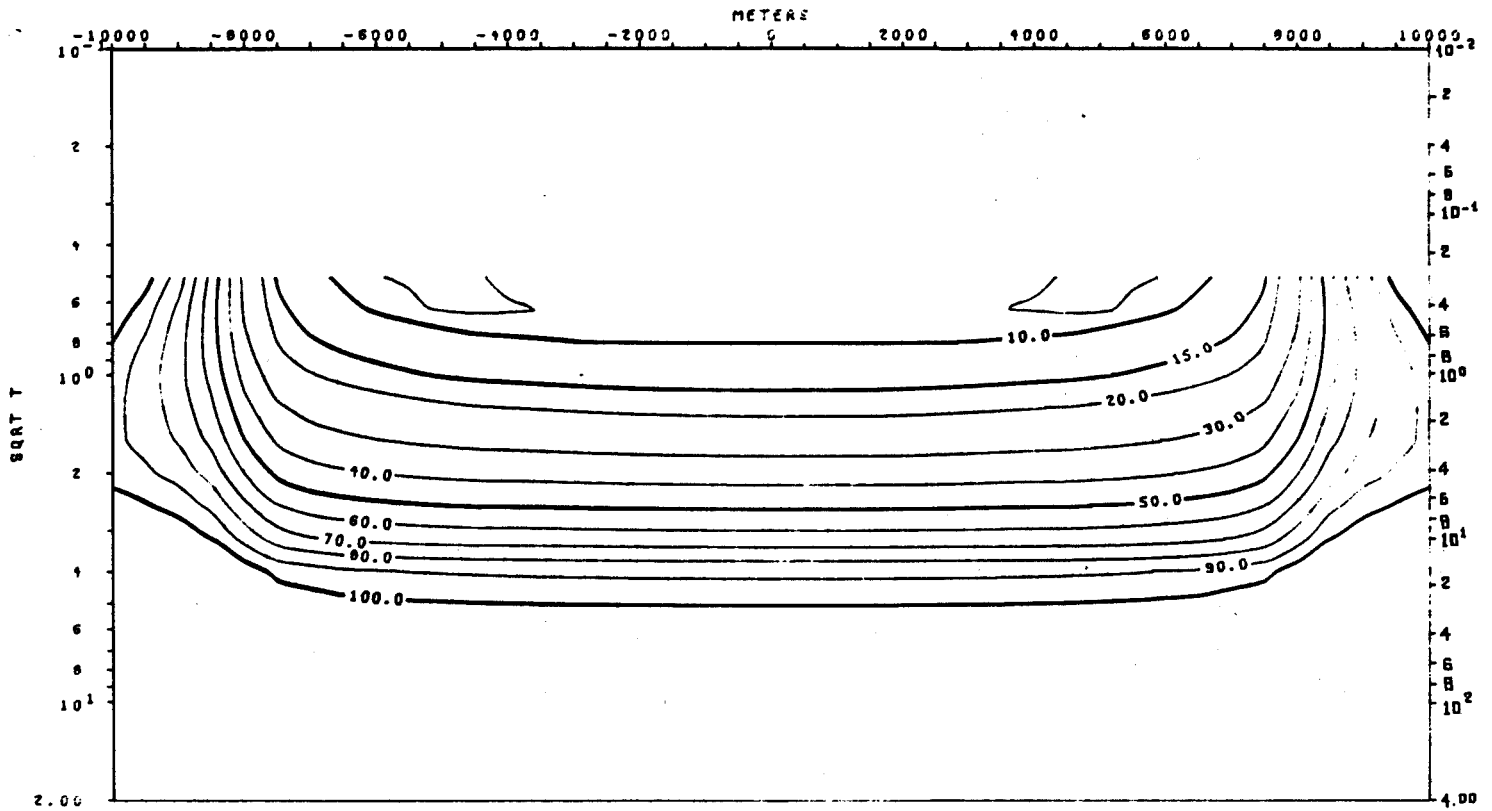

TE MODE
APPARENT RESISTIVITY VS. PERIOD (T)
MODEL 4-3

XBL 786-1911

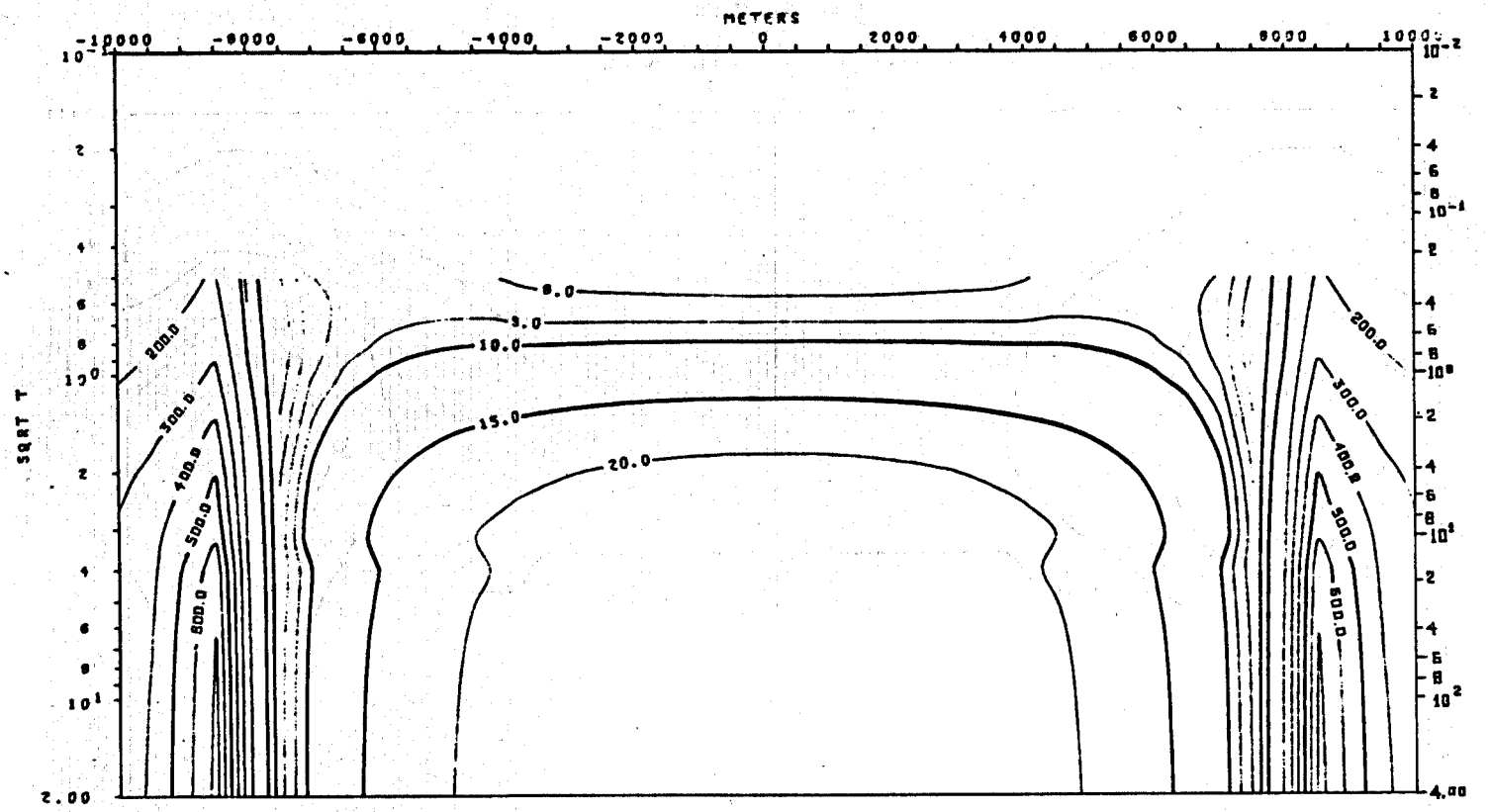

TM MODE
APPARENT RESISTIVITY VS. PERIOD (T)
MODEL 4-3

XBL 786-1910

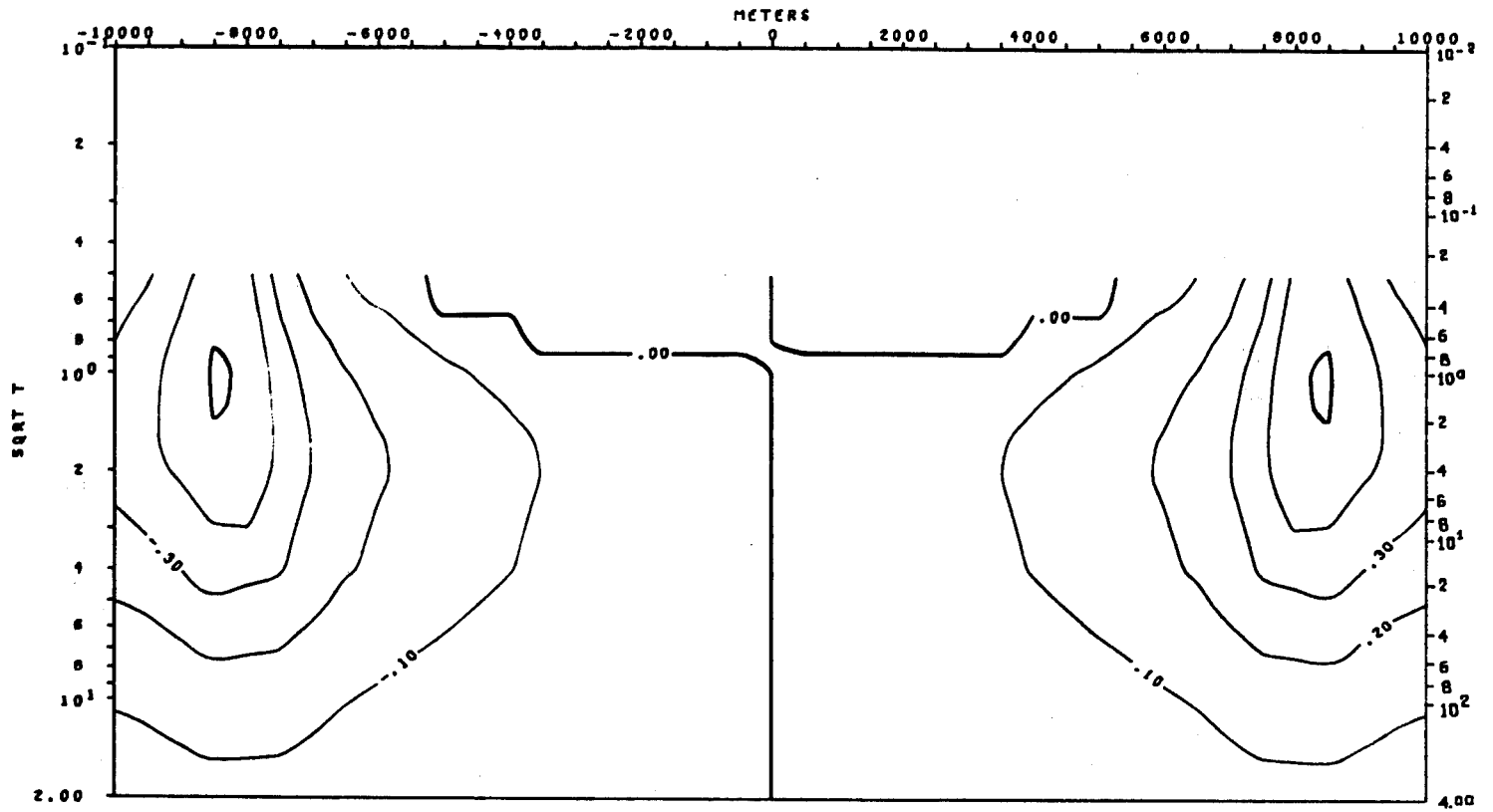

TIPPER VS. PERIOD (T)
MODEL 4-3

XBL 786-1917

T

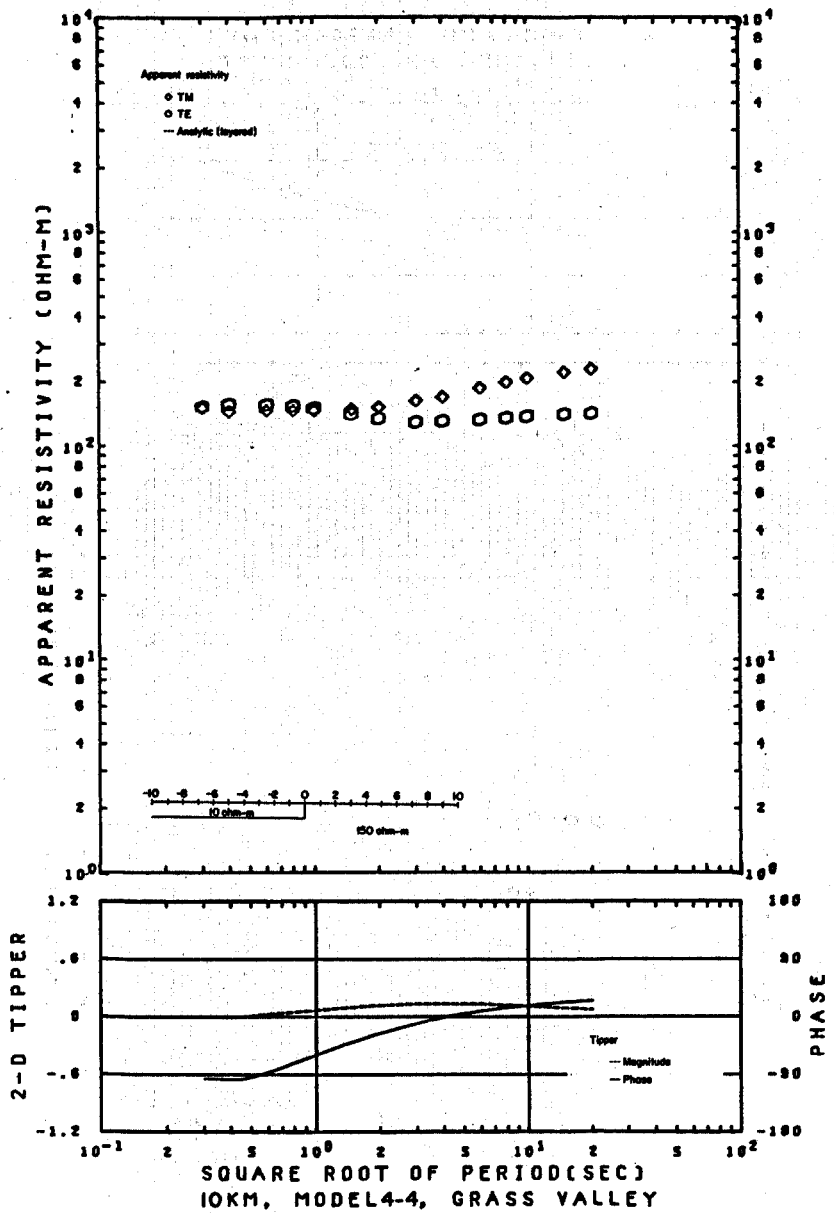

10KM, MODEL4-4, GRASS VALLEY

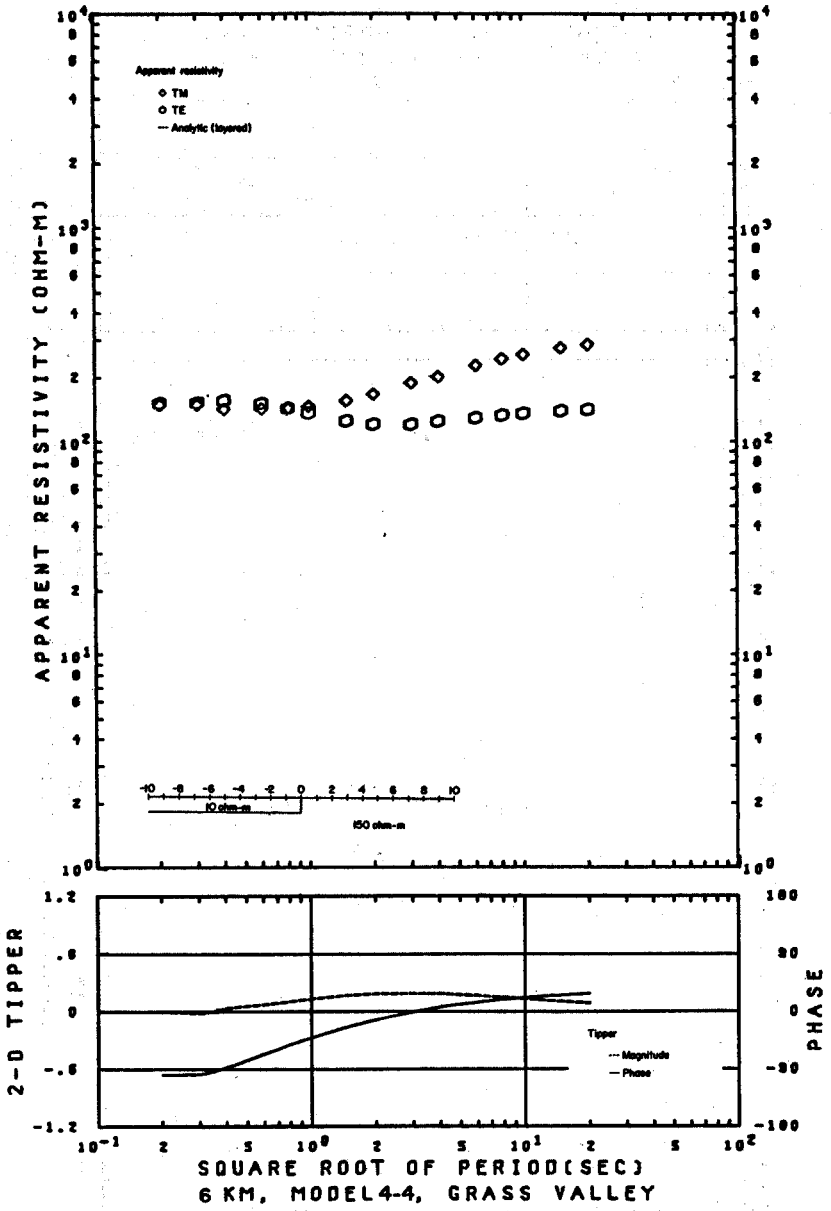

6 KM, MODEL4-4, GRASS VALLEY

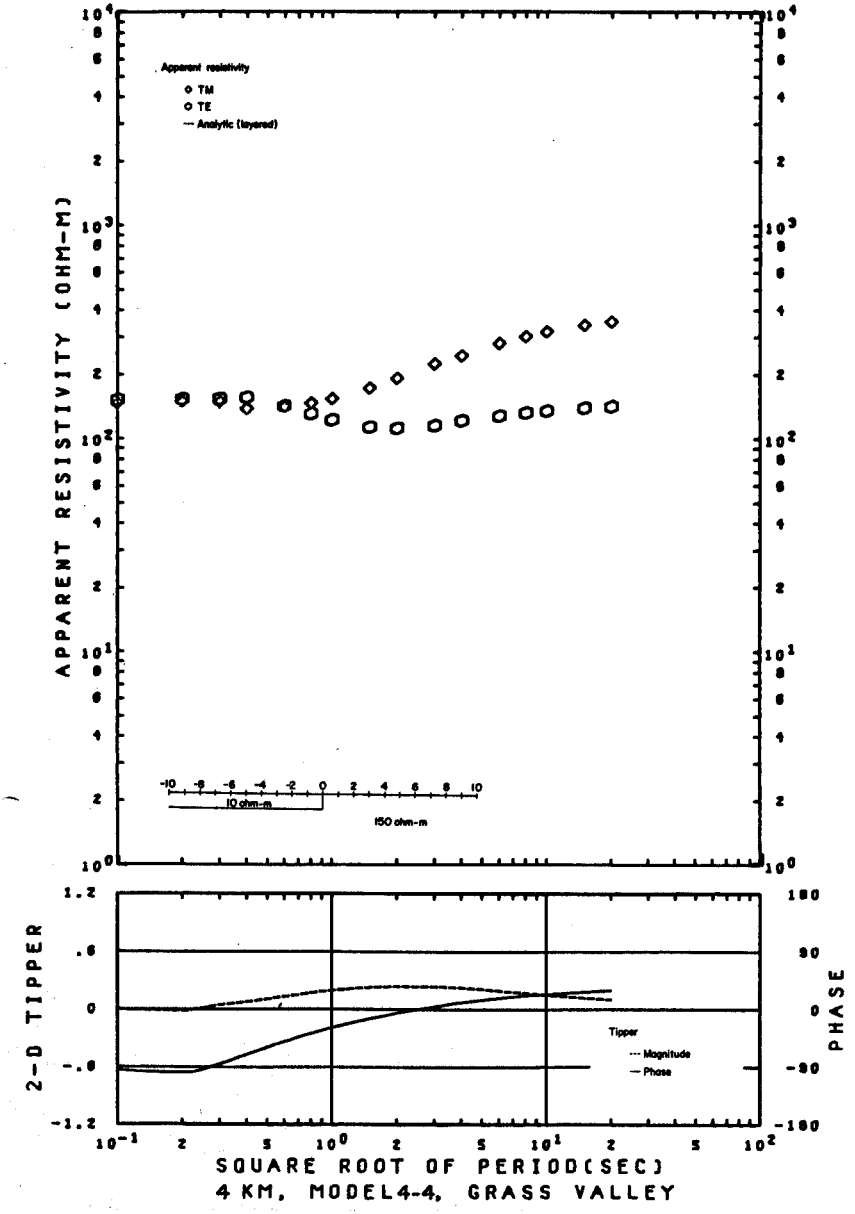
Apparent resistivity
TM
TE
Analytic (layered)
APPARENT RESISTIVITY (OHM-M)
10 ohm-m
150 ohm-m
2-D TIPPER
PHASE
Tipper
Magnitude
Phase
SQUARE ROOT OF PERIOD(SEC)
4 KM, MODEL4-4, GRASS VALLEY

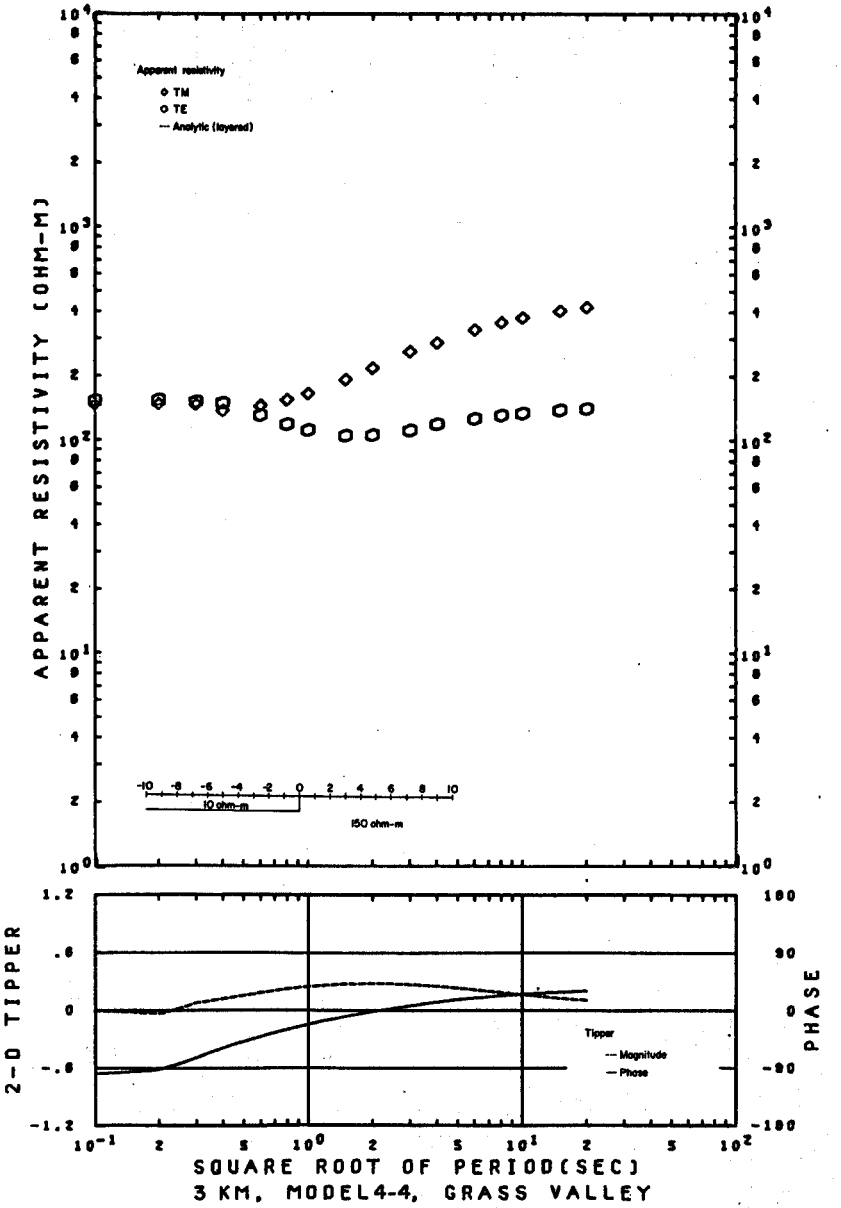
Apparent resistivity
TM
TE
Analytic (layered)
APPARENT RESISTIVITY (OHM-M)
10 ohm-m
150 ohm-m
2-D TIPPER
PHASE
Tipper
Magnitude
Phase
SQUARE ROOT OF PERIOD(SEC)
3 KM, MODEL4-4, GRASS VALLEY

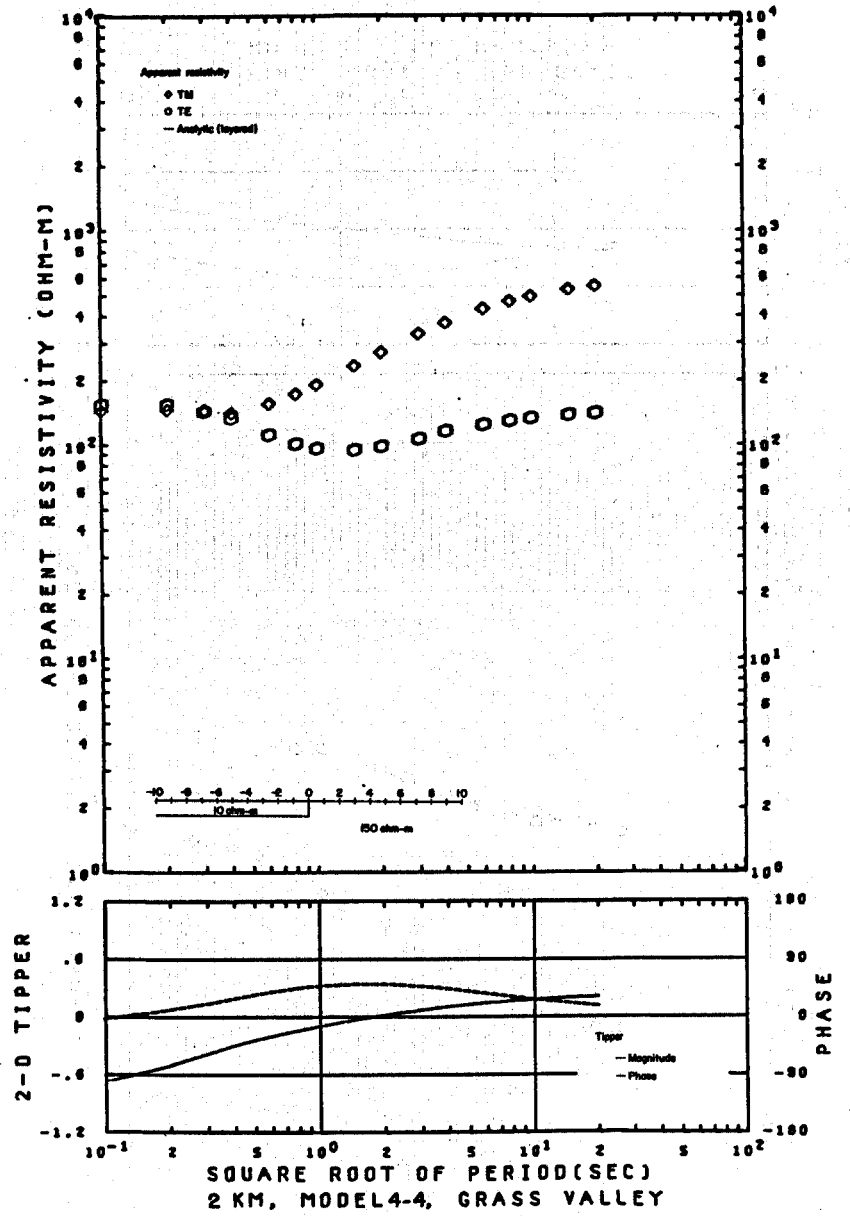

2 KM, MODEL4-4, GRASS VALLEY

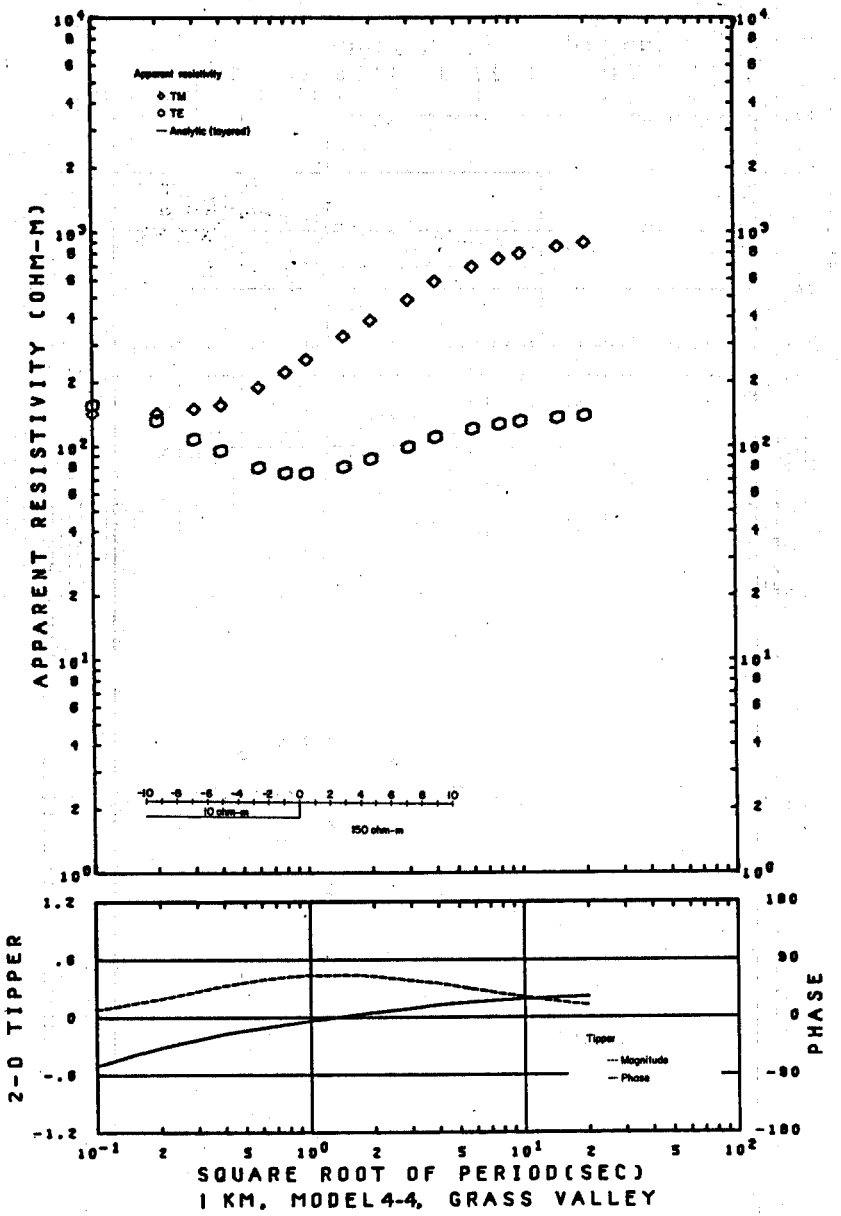

1 KM, MODEL4-4, GRASS VALLEY

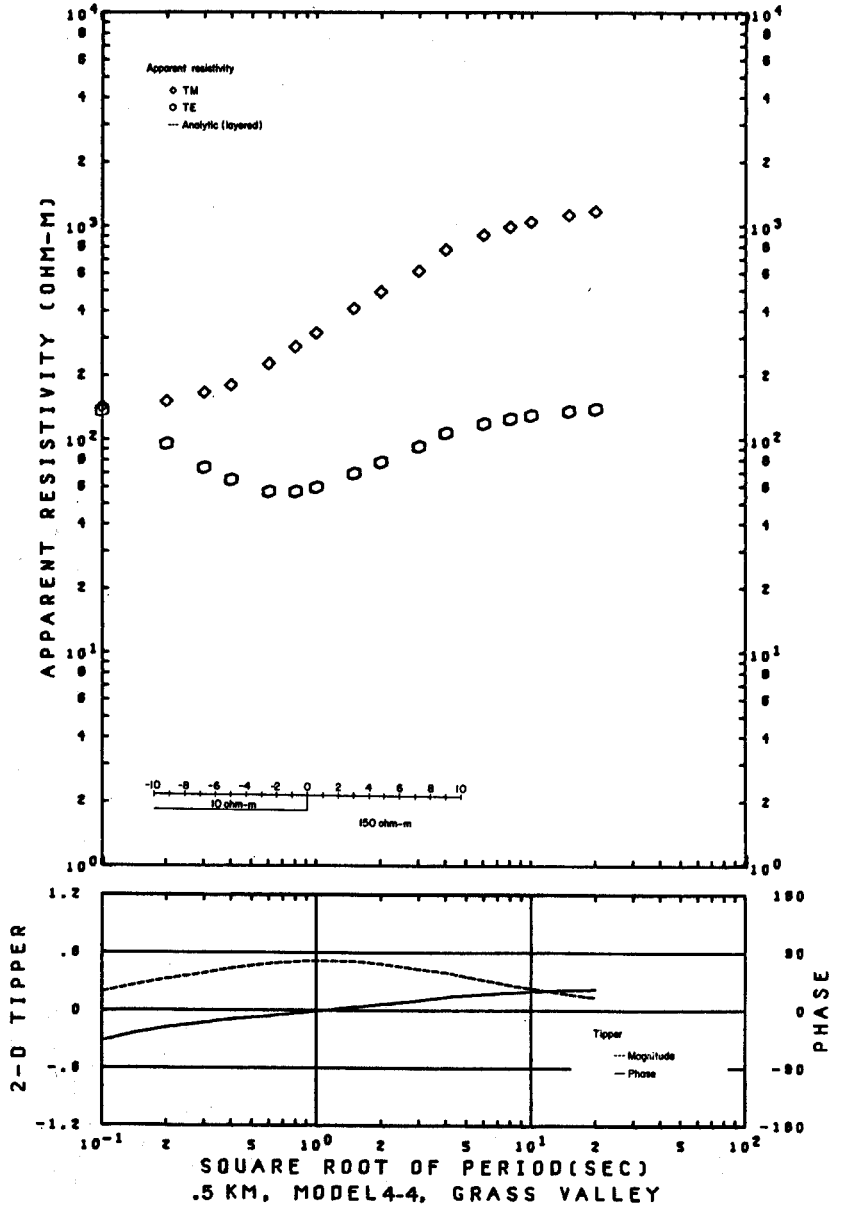
Apparent resistivity
TM
TE
Analytic (layered)
APPARENT RESISTIVITY (OHM-M)
10 ohm-m
150 ohm-m
2-D TIPPER
PHASE
Tipper
Magnitude
Phase
SQUARE ROOT OF PERIOD(SEC)
.5 KM, MODEL4-4, GRASS VALLEY

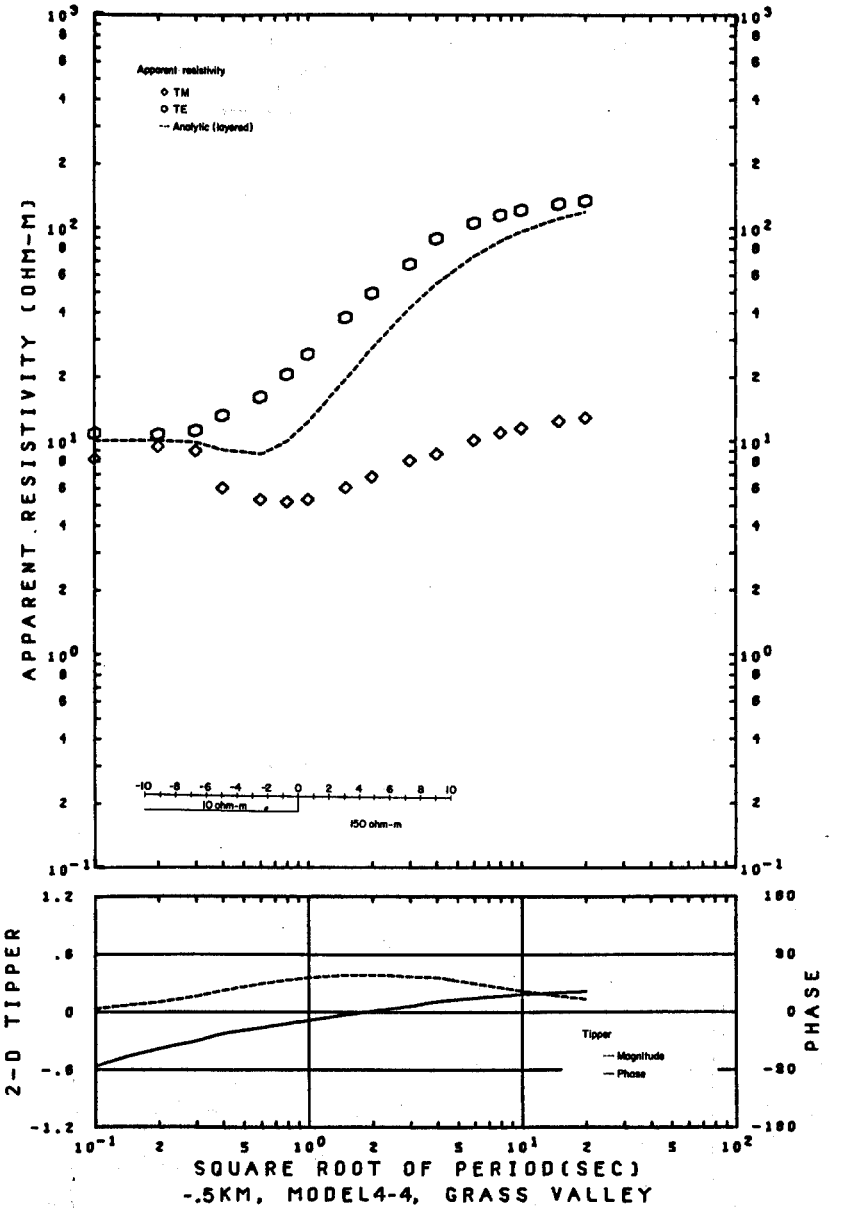
Apparent resistivity
TM
TE
Analytic (layered)
APPARENT RESISTIVITY (OHM-M)
10 ohm-m
150 ohm-m
2-D TIPPER
PHASE
Tipper
Magnitude
Phase
SQUARE ROOT OF PERIOD(SEC)
-.5KM, MODEL4-4, GRASS VALLEY

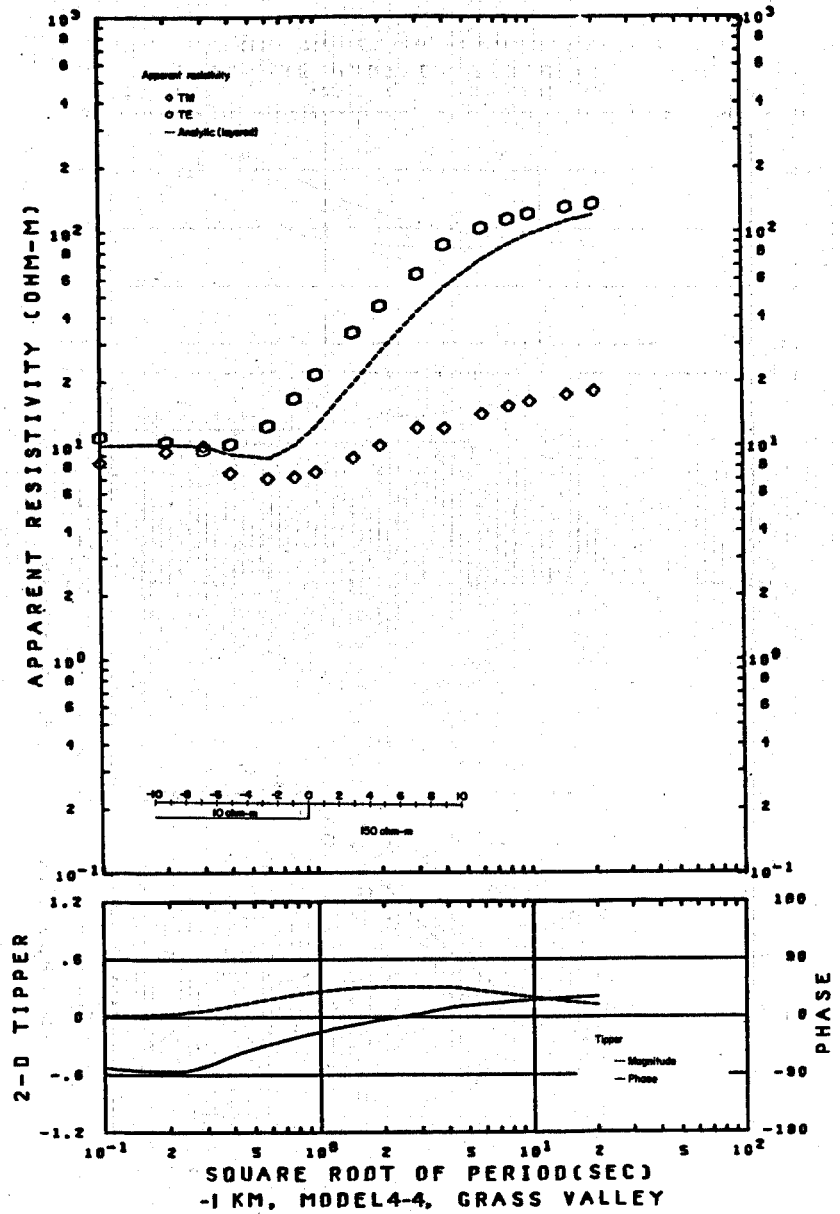

-1 KM, MODEL4-4, GRASS VALLEY

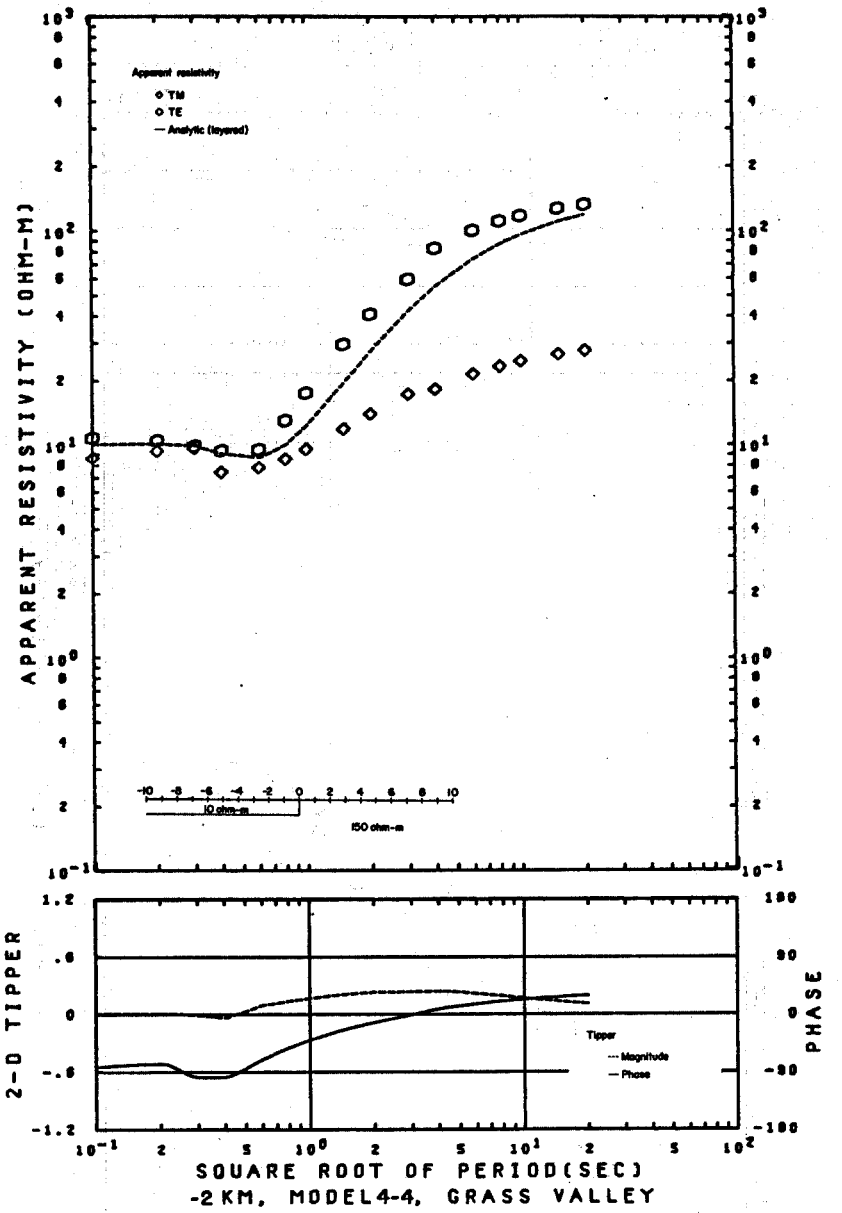

-2 KM, MODEL4-4, GRASS VALLEY

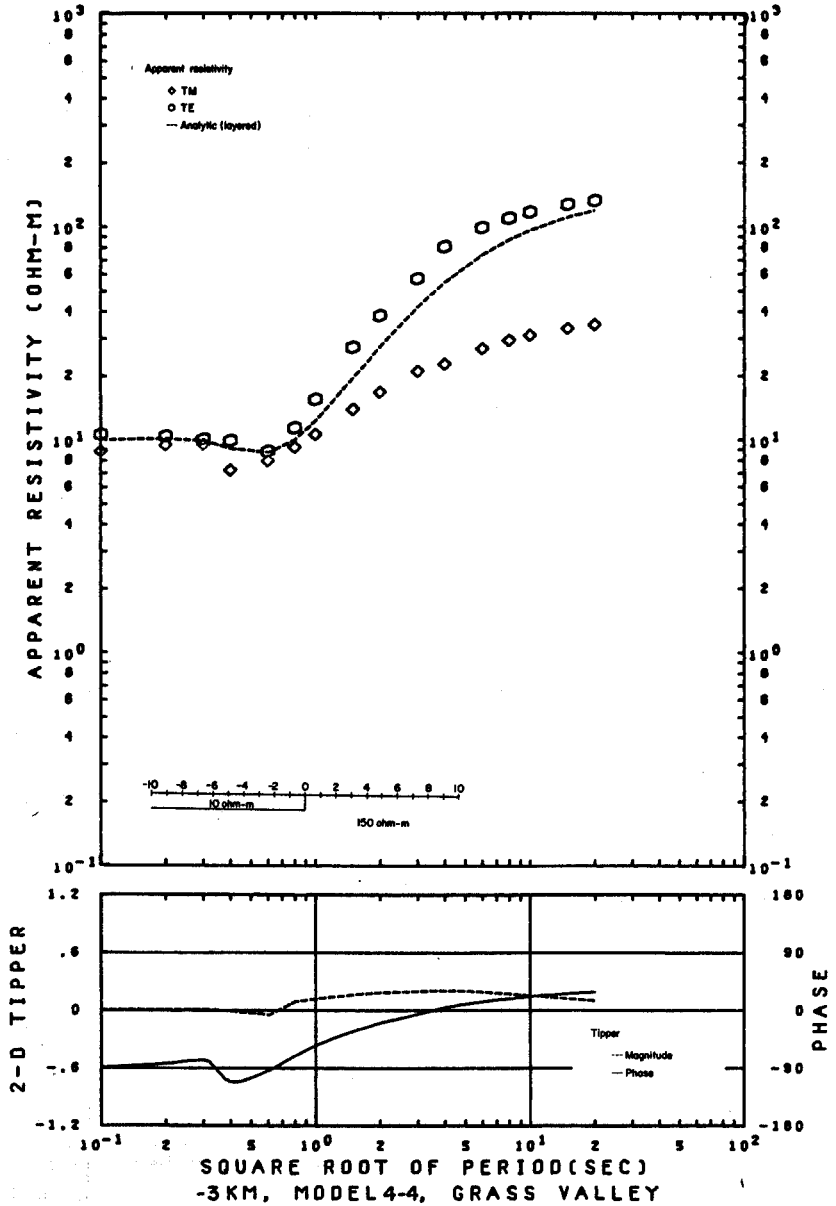
Apparent resistivity
TM
TE
Analytic (layered)
APPARENT RESISTIVITY (OHM-M)
10 ohm-m
150 ohm-m
2-D TIPPER
PHASE
Tipper
Magnitude
Phase
SQUARE ROOT OF PERIOD(SEC)
-3KM, MODEL4-4, GRASS VALLEY

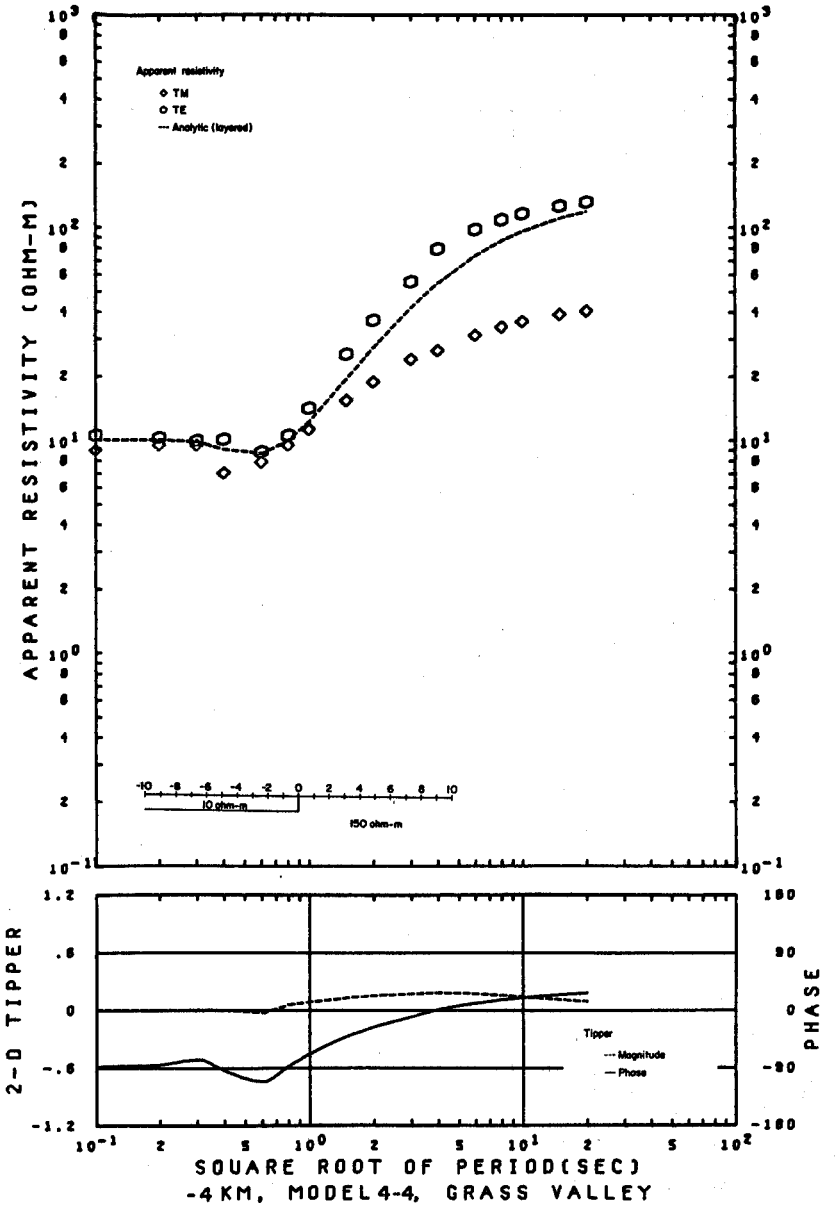
Apparent resistivity
TM
TE
Analytic (layered)
APPARENT RESISTIVITY (OHM-M)
10 ohm-m
150 ohm-m
2-D TIPPER
PHASE
Tipper
Magnitude
Phase
SQUARE ROOT OF PERIOD(SEC)
-4KM, MODEL4-4, GRASS VALLEY

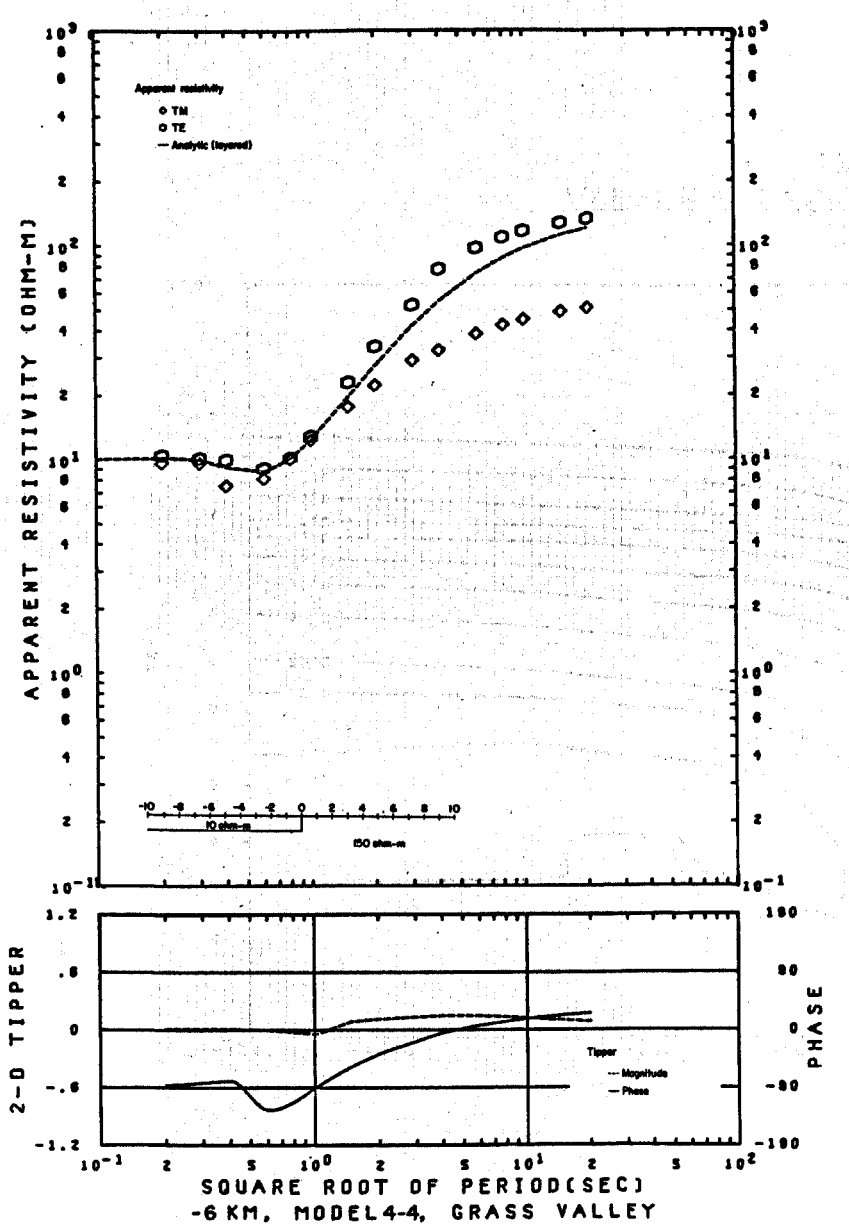

-6 KM, MODEL4-4, GRASS VALLEY

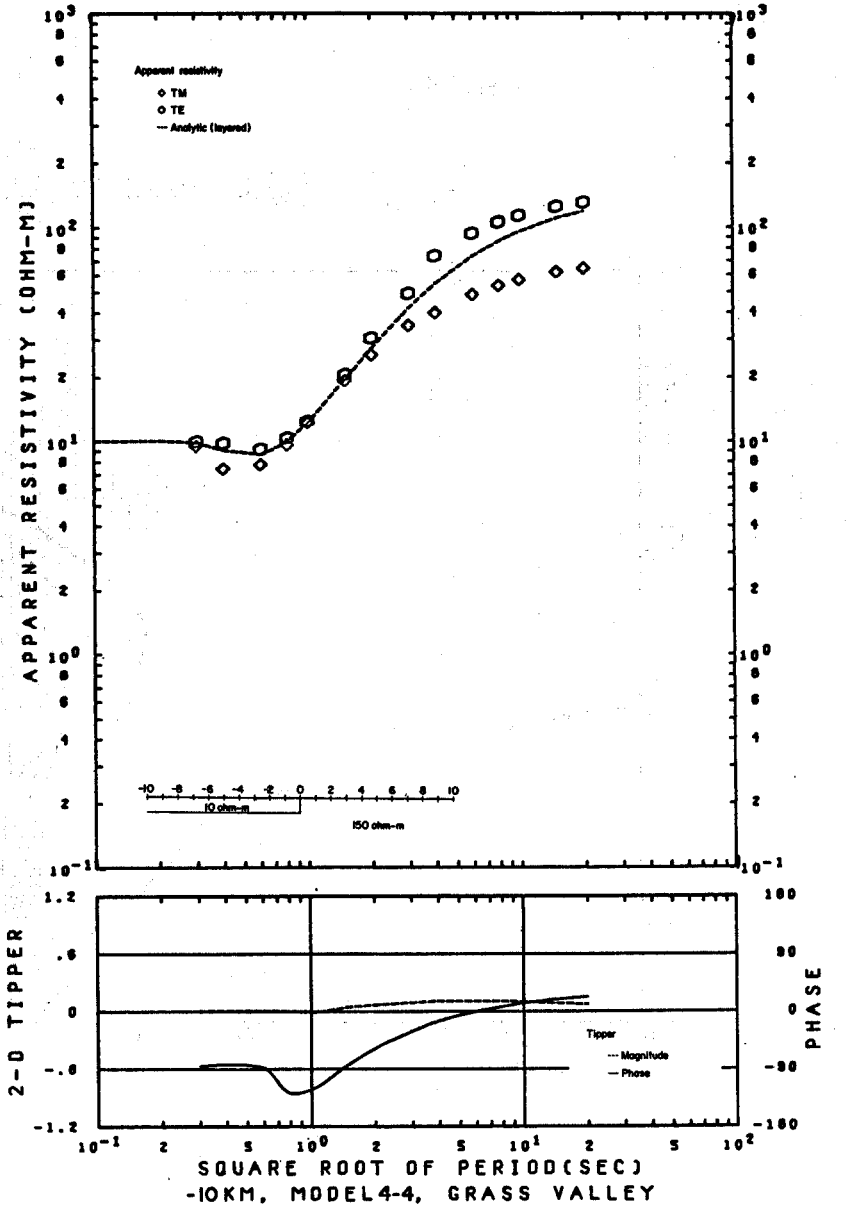

-10KM, MODEL4-4, GRASS VALLEY

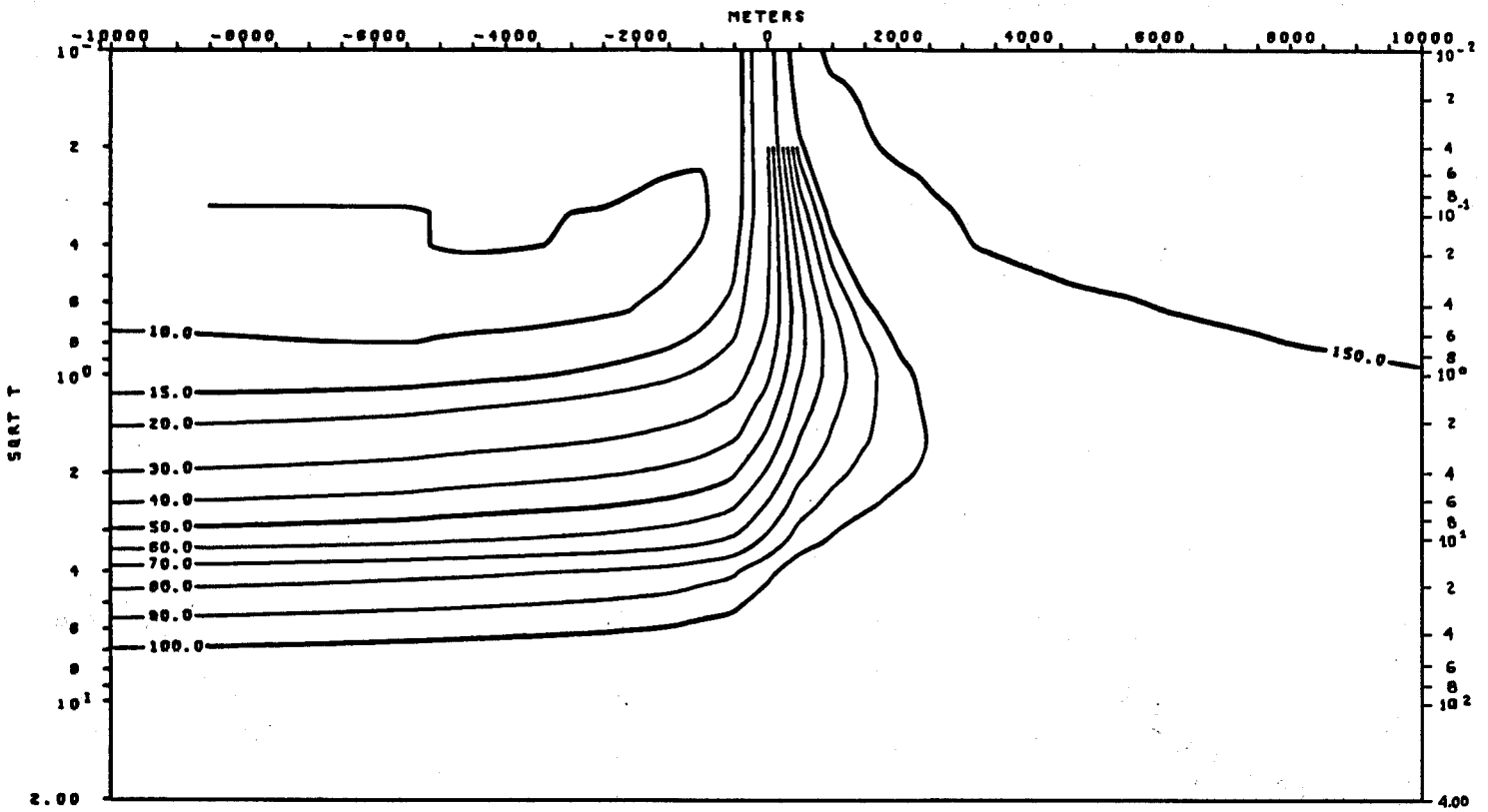

TE MODE
APPARENT RESISTIVITY VS. PERIOD (T)
MODEL 4-4

XBL 786-1905

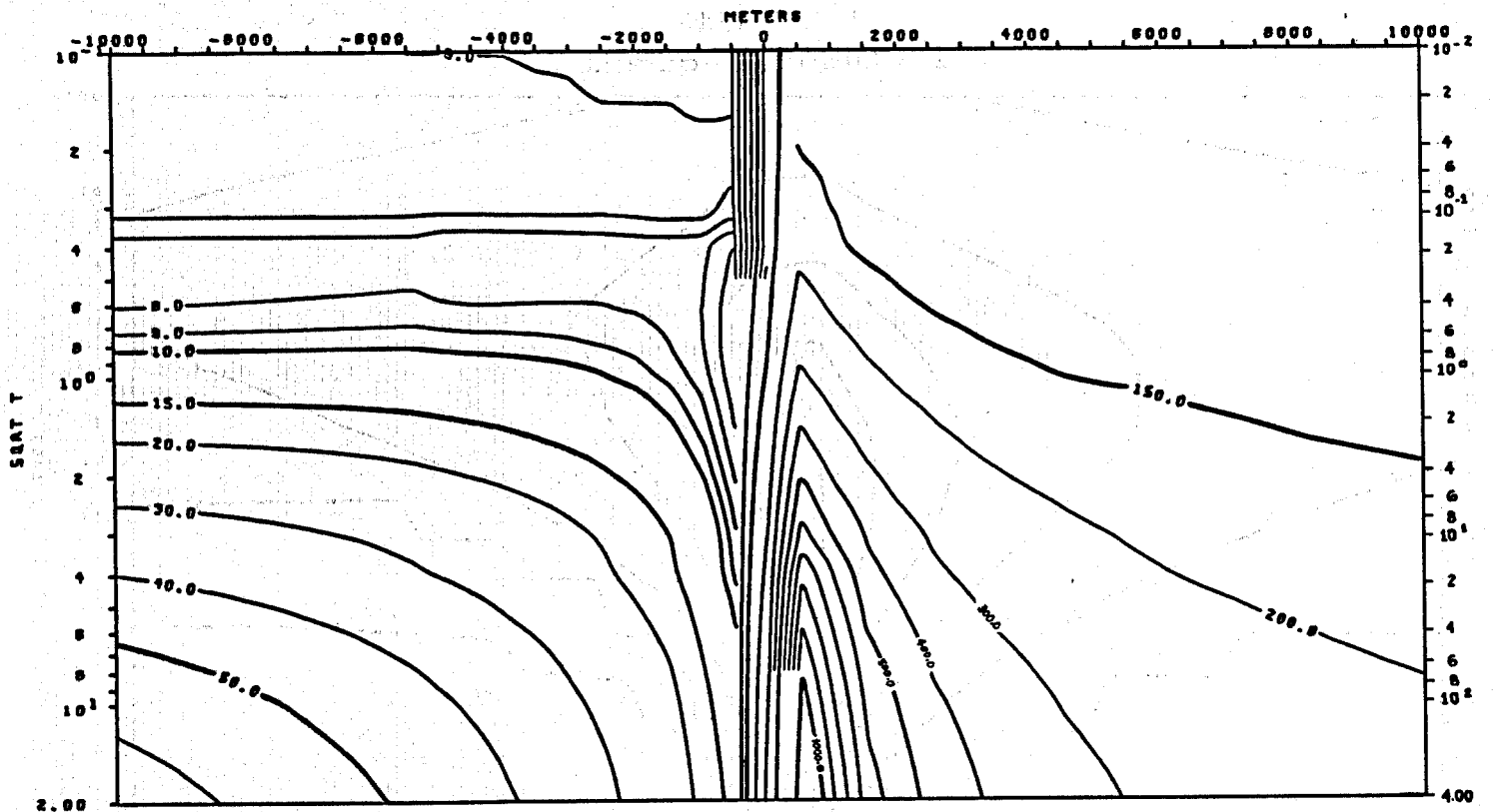

TM MODE
APPARENT RESISTIVITY VS. PERIOD (T)
MODEL 4-4

XBL 786-1931

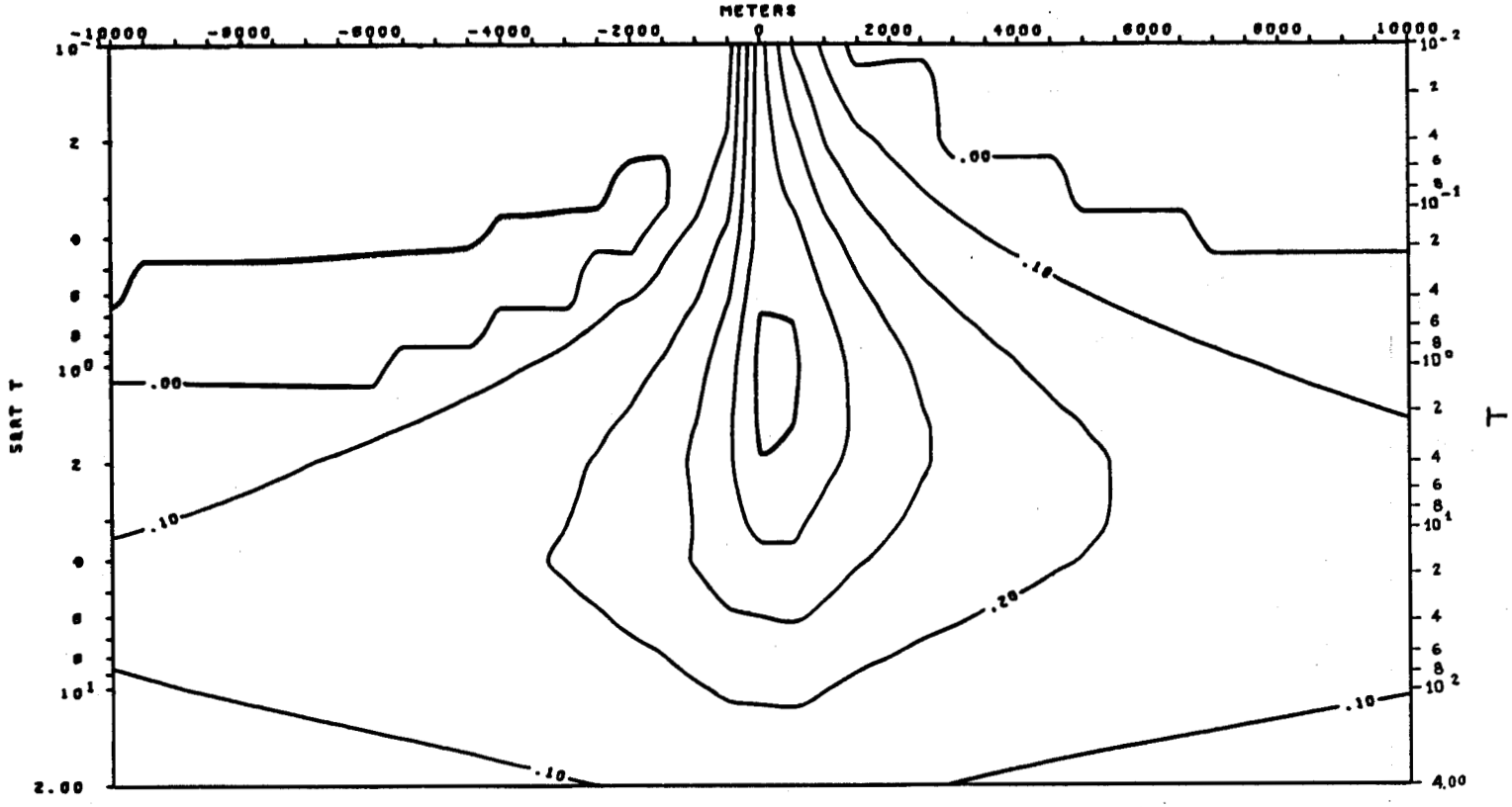

TIPPER VS. PERIOD (T)
MODEL 4-4

XBL 786-1945

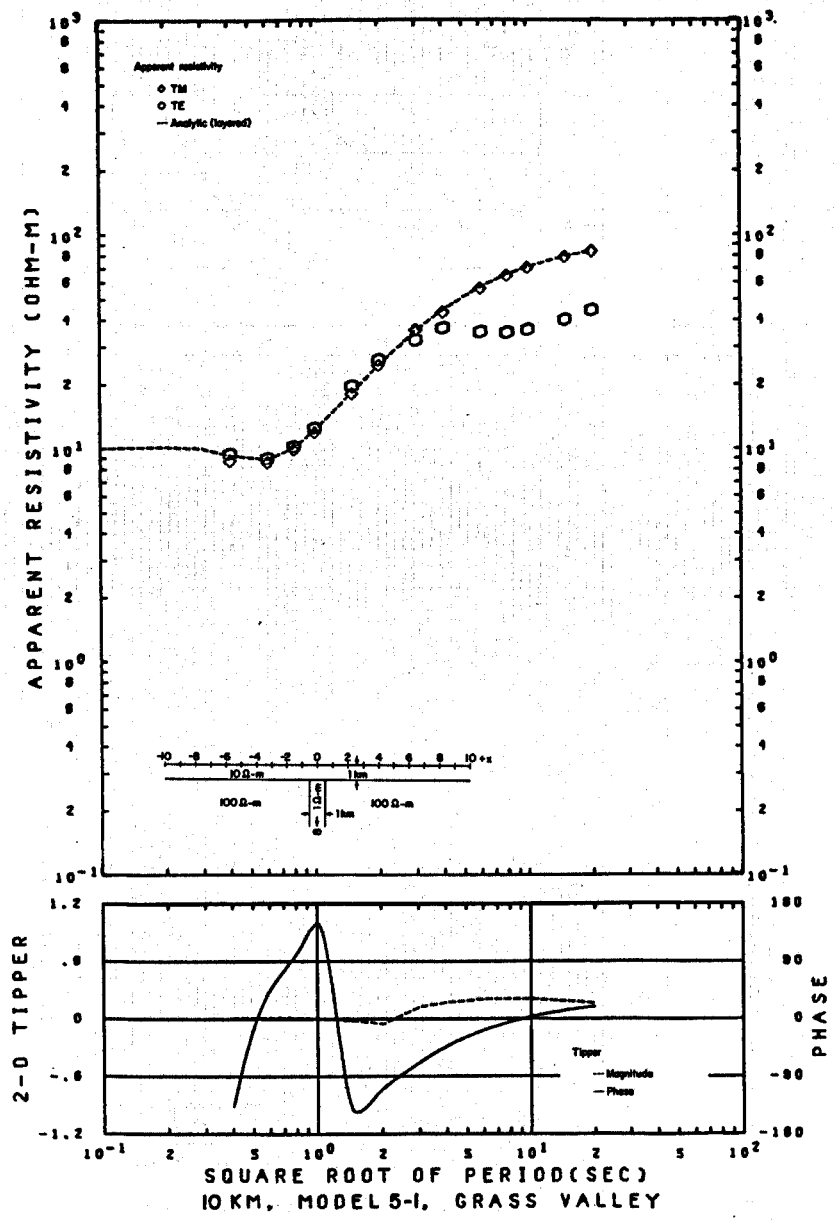

10 KM, MODEL 5-1, GRASS VALLEY

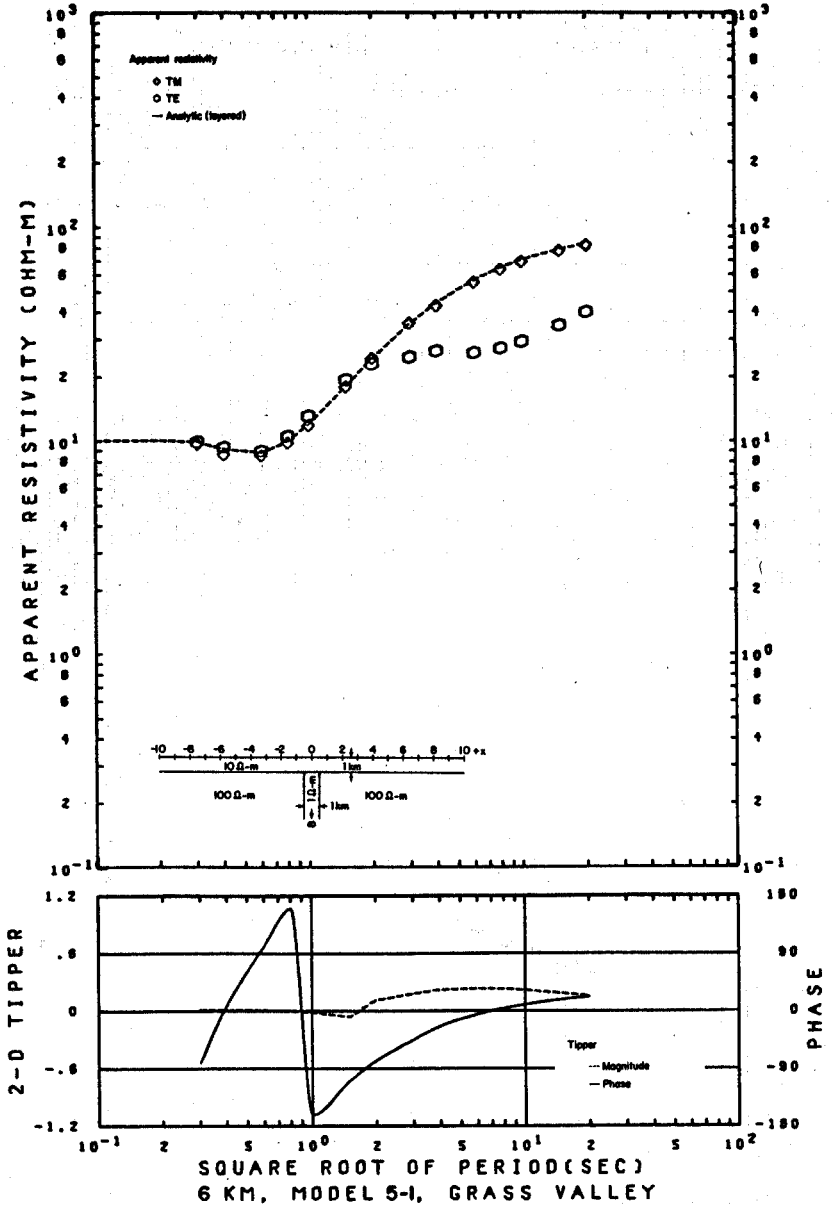

6 KM, MODEL 5-1, GRASS VALLEY

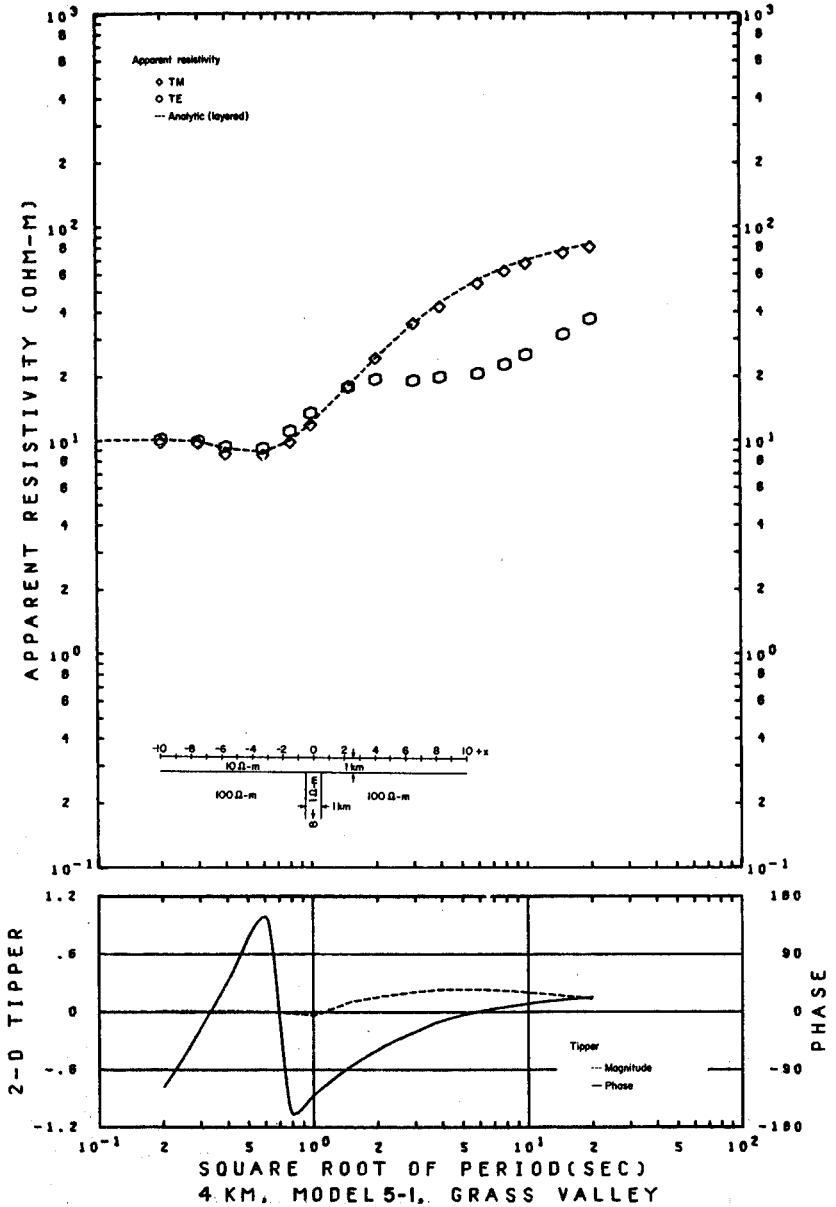
Apparent resistivity
TM
TE
Analytic (layered)
APPARENT RESISTIVITY (OHM-M)
10 Ω-m
1 km
100 Ω-m
100 Ω-m
10 Ω-m
1 km
2-D TIPPER
PHASE
Tipper
Magnitude
Phase
SQUARE ROOT OF PERIOD(SEC)
4 KM, MODEL 5-I, GRASS VALLEY

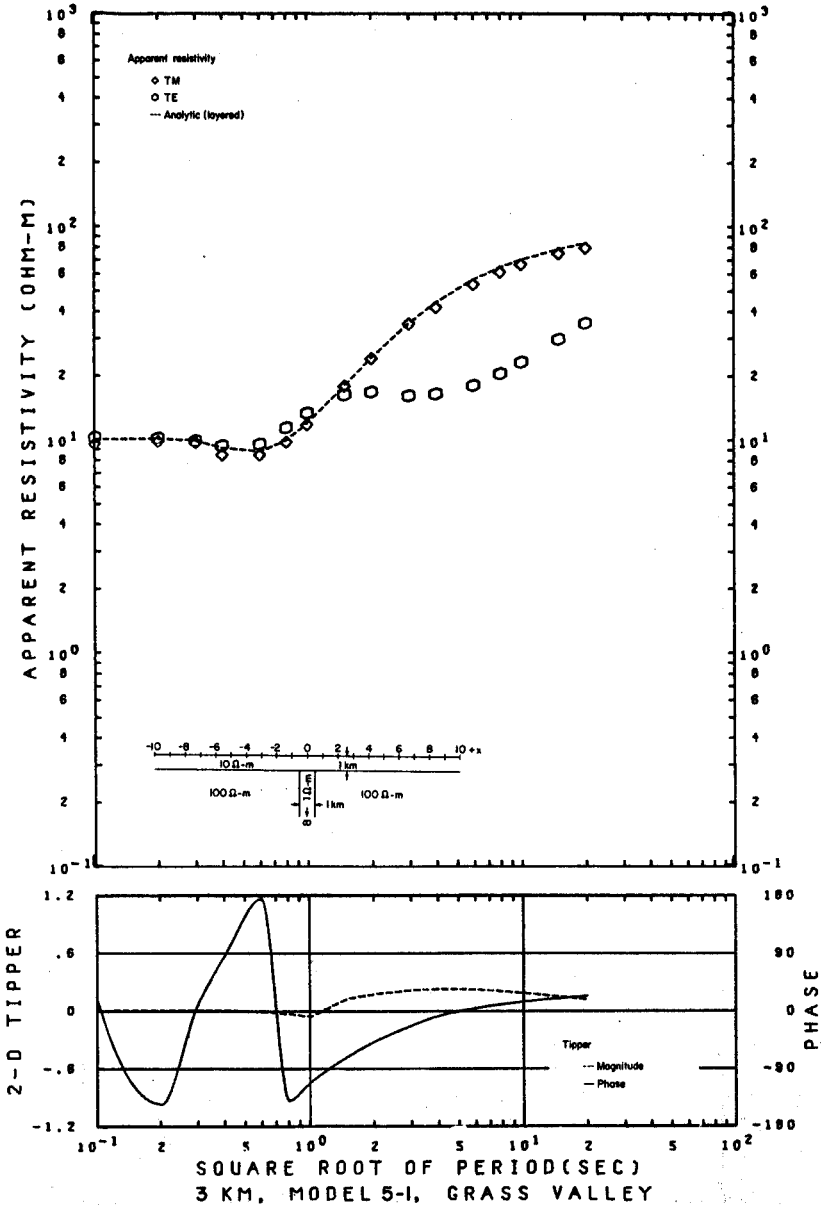
Apparent resistivity
TM
TE
Analytic (layered)
APPARENT RESISTIVITY (OHM-M)
10 Ω-m
1 km
100 Ω-m
100 Ω-m
10 Ω-m
1 km
2-D TIPPER
PHASE
Tipper
Magnitude
Phase
SQUARE ROOT OF PERIOD(SEC)
3 KM, MODEL 5-I, GRASS VALLEY

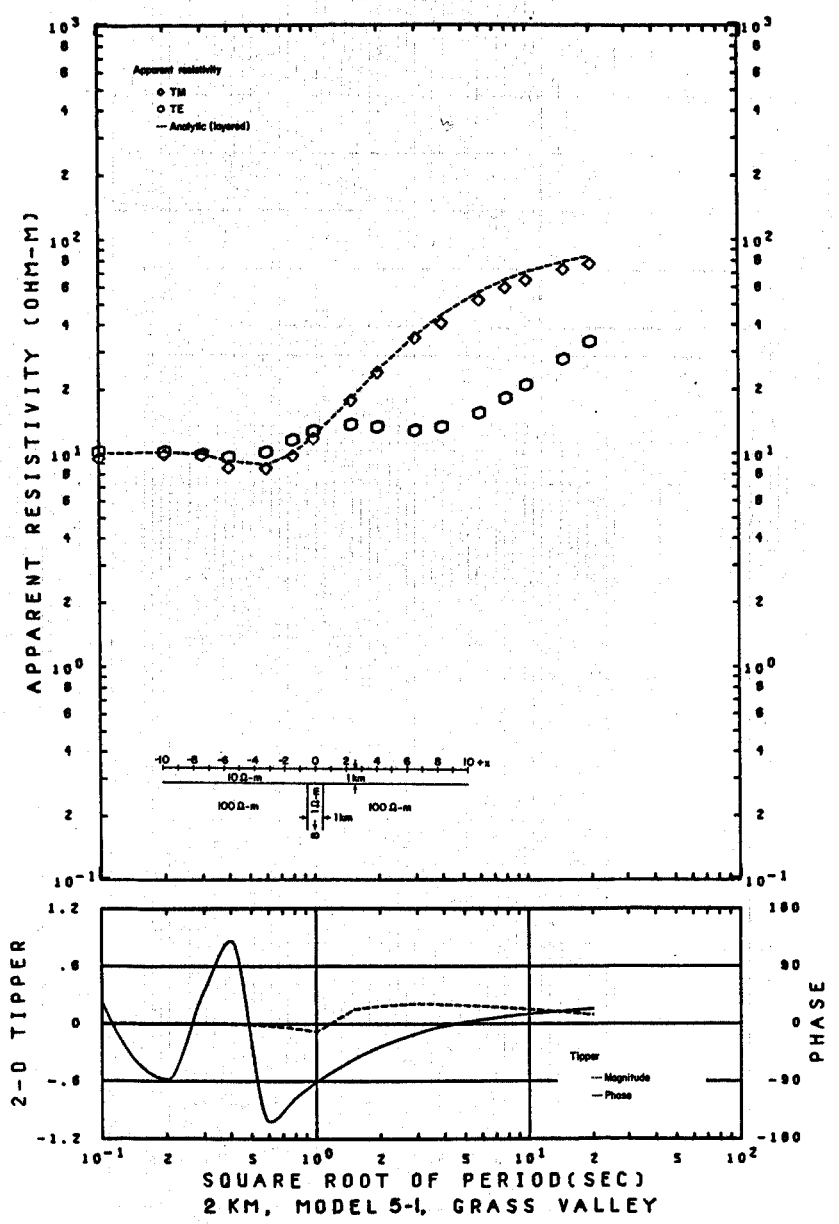
Apparent resistivity
TM
TE
Analytic (layered)
APPARENT RESISTIVITY (OHM-M)
10 Ω-m
1 km
100 Ω-m
100 Ω-m
10 Ω-m
1 km
2-D TIPPER
PHASE
Tipper
Magnitude
Phase
SQUARE ROOT OF PERIOD(SEC)
2 KM, MODEL 5-I, GRASS VALLEY

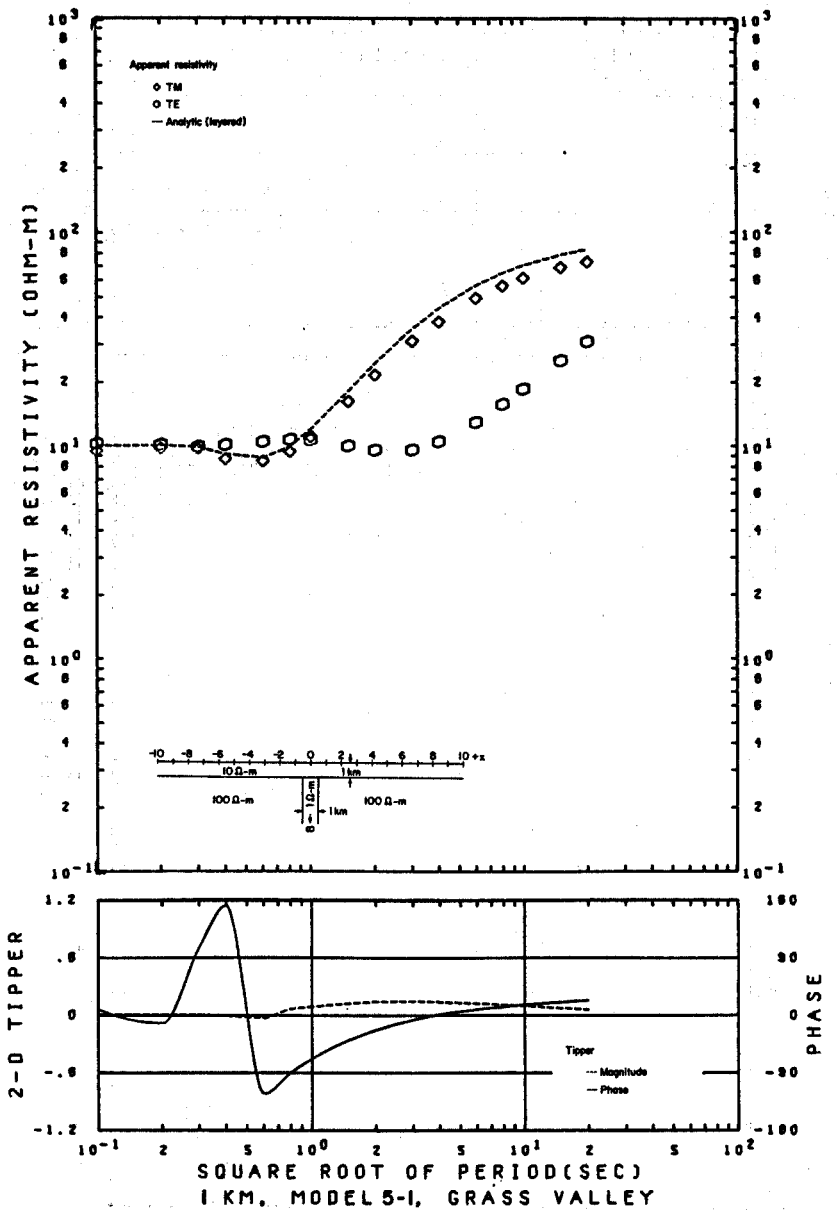
Apparent resistivity
TM
TE
Analytic (layered)
APPARENT RESISTIVITY (OHM-M)
10 Ω-m
1 km
100 Ω-m
100 Ω-m
10 Ω-m
1 km
2-D TIPPER
PHASE
Tipper
Magnitude
Phase
SQUARE ROOT OF PERIOD(SEC)
1 KM, MODEL 5-I, GRASS VALLEY

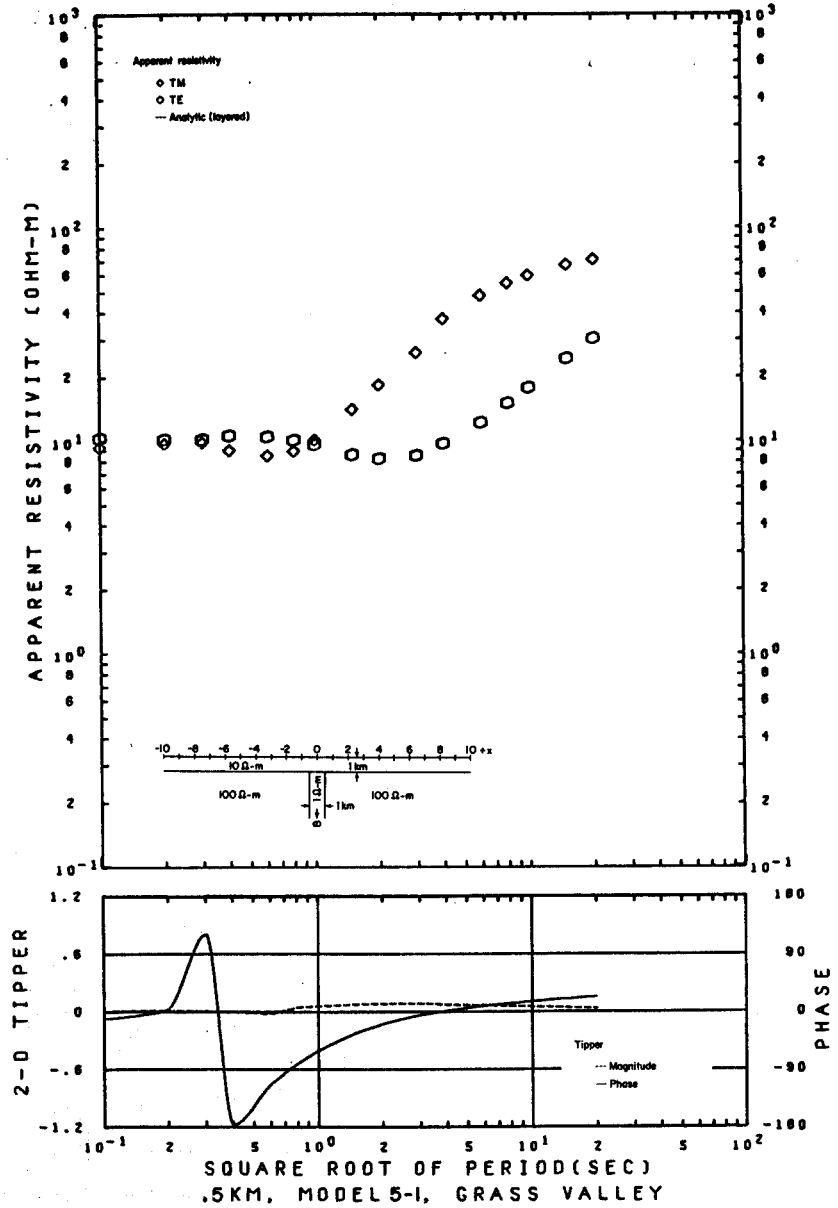
Apparent resistivity
TM
TE
Analytic (layered)
APPARENT RESISTIVITY (OHM-M)
10 Ω-m
1km
100 Ω-m
100 Ω-m
1 Ω-m
1km
2-D TIPPER
PHASE
Tipper
Magnitude
Phase
SQUARE ROOT OF PERIOD(SEC)
.5KM, MODEL 5-1, GRASS VALLEY

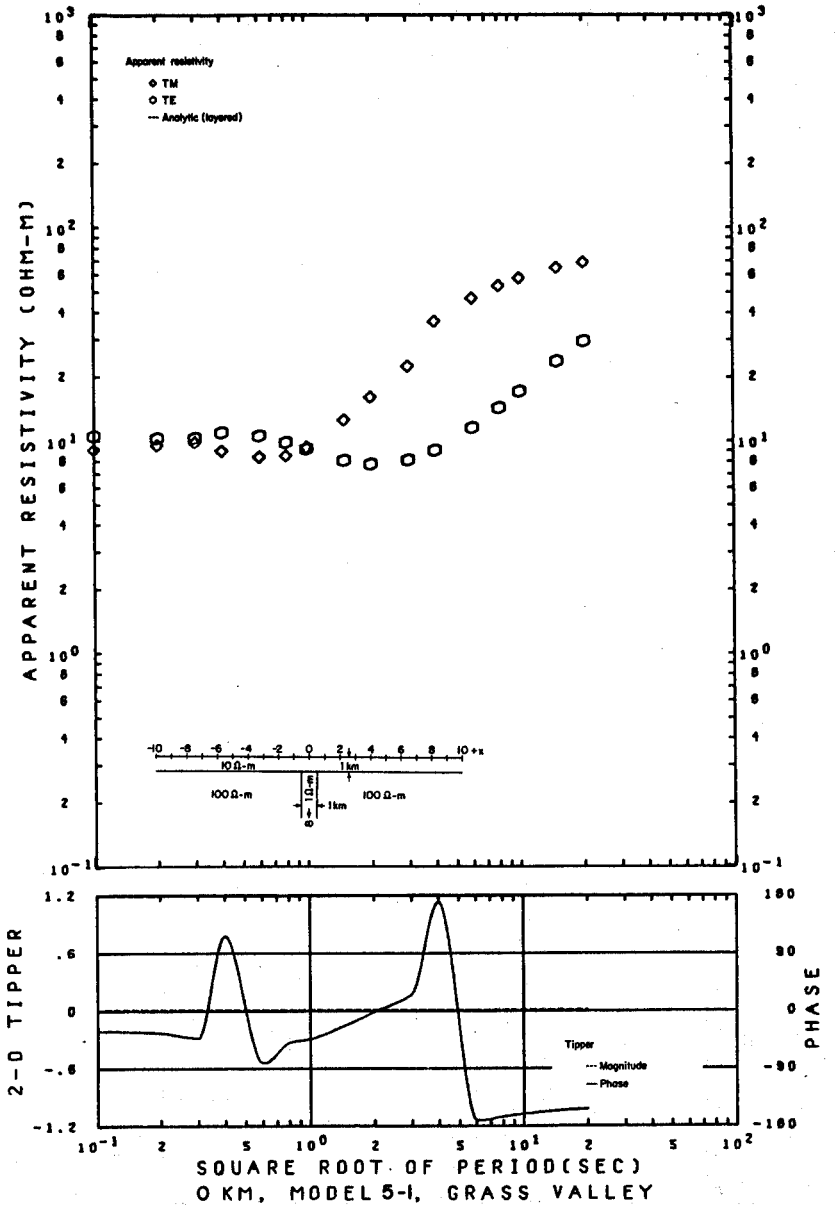
Apparent resistivity
TM
TE
Analytic (layered)
APPARENT RESISTIVITY (OHM-M)
10 Ω-m
1km
100 Ω-m
100 Ω-m
1 Ω-m
1km
2-D TIPPER
PHASE
Tipper
Magnitude
Phase
SQUARE ROOT OF PERIOD(SEC)
0 KM, MODEL 5-1, GRASS VALLEY

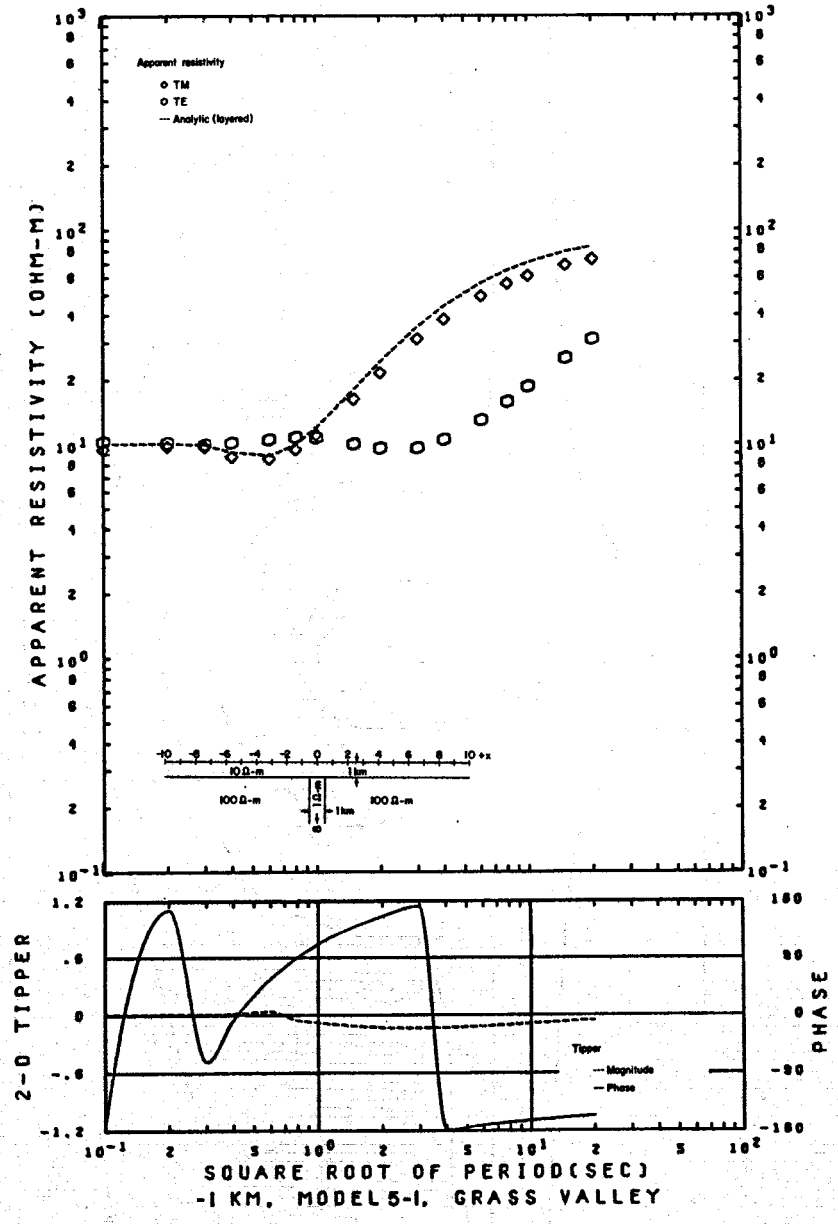
Apparent resistivity
TM
TE
Analytic (layered)
APPARENT RESISTIVITY (OHM-M)
100 Ω-m
1 km
100 Ω-m
10 Ω-m
1 km
2-D TIPPER
PHASE
Tipper
Magnitude
Phase
SQUARE ROOT OF PERIOD(SEC)
-1 KM, MODEL 5-1, GRASS VALLEY

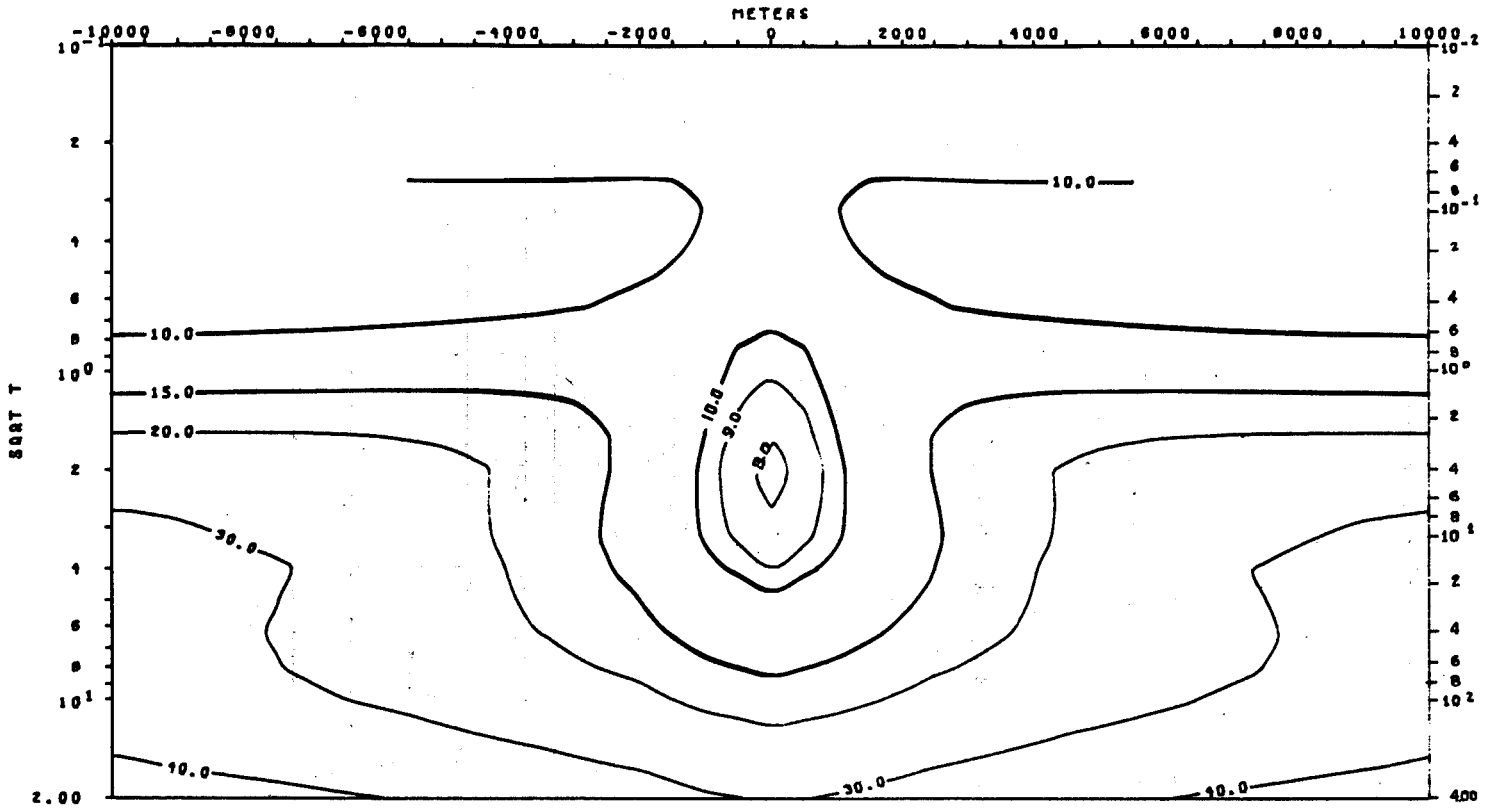

TE MODE
APPARENT RESISTIVITY VS. PERIOD (T)
MODEL 5-1

XBL 786-1927

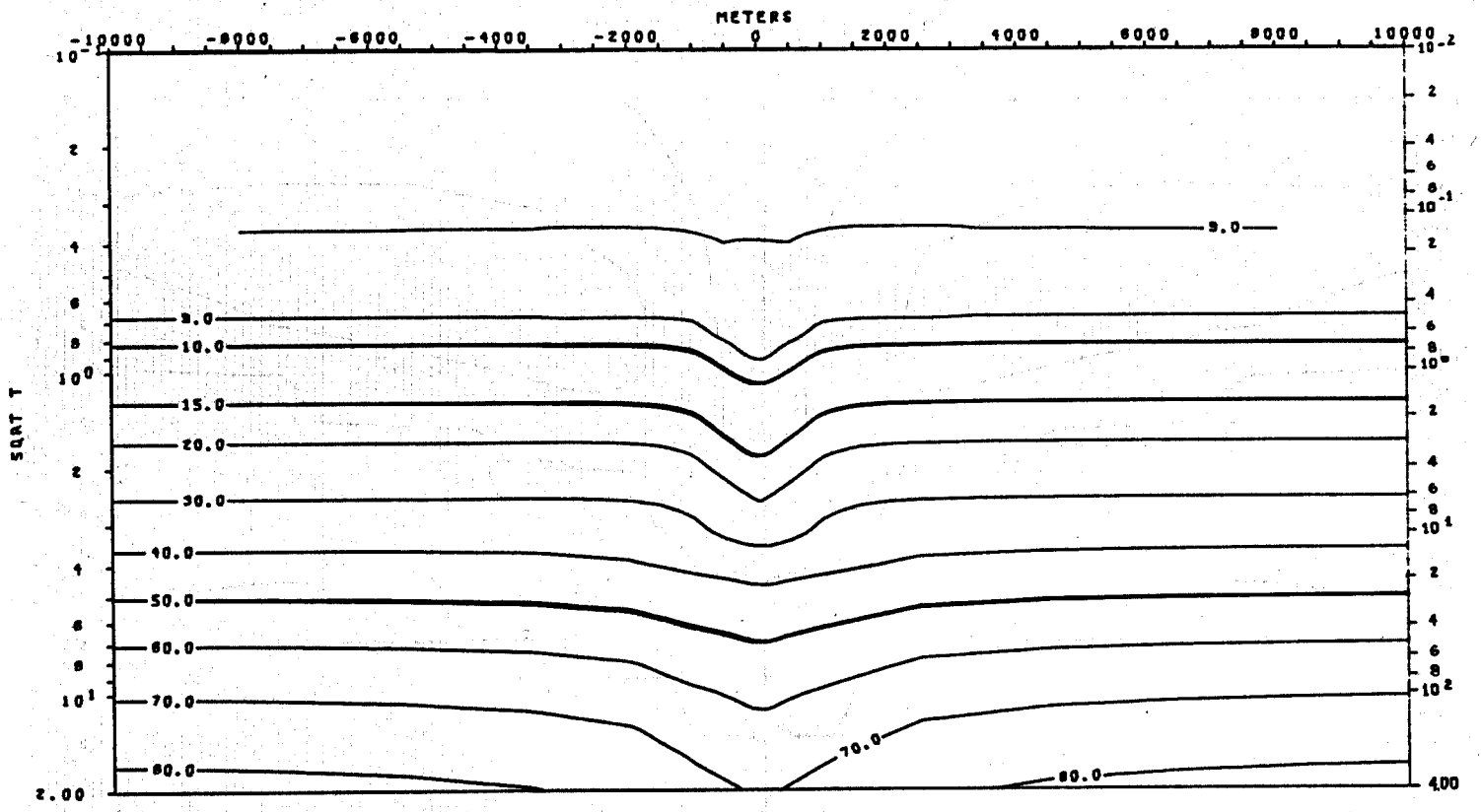

TM MODE
APPARENT RESISTIVITY VS. PERIOD (T)
MODEL 5-1

XBL 786-1914

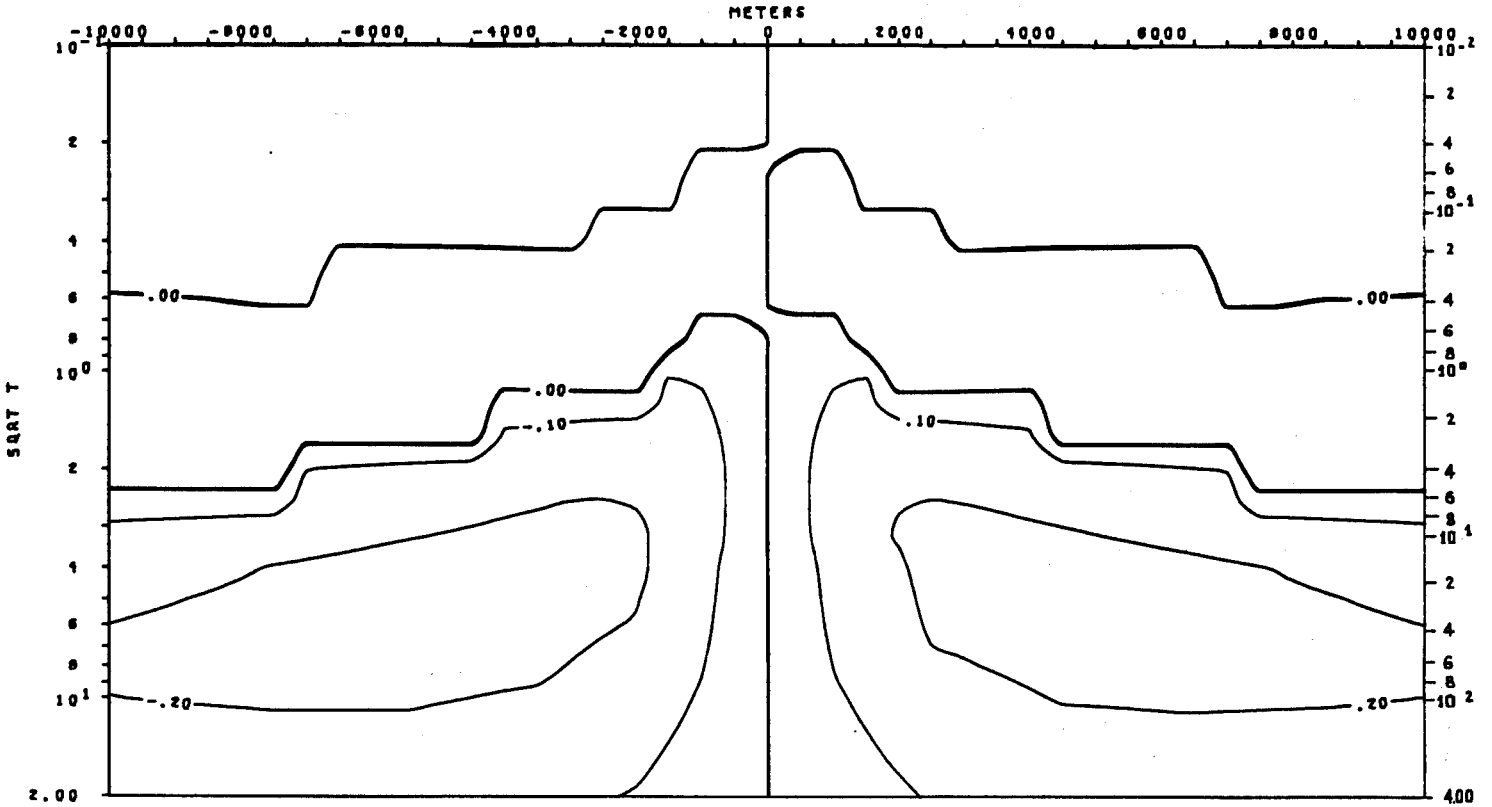

TIPPER VS. PERIOD (T)
MODEL 5-1

XBL 786-1899

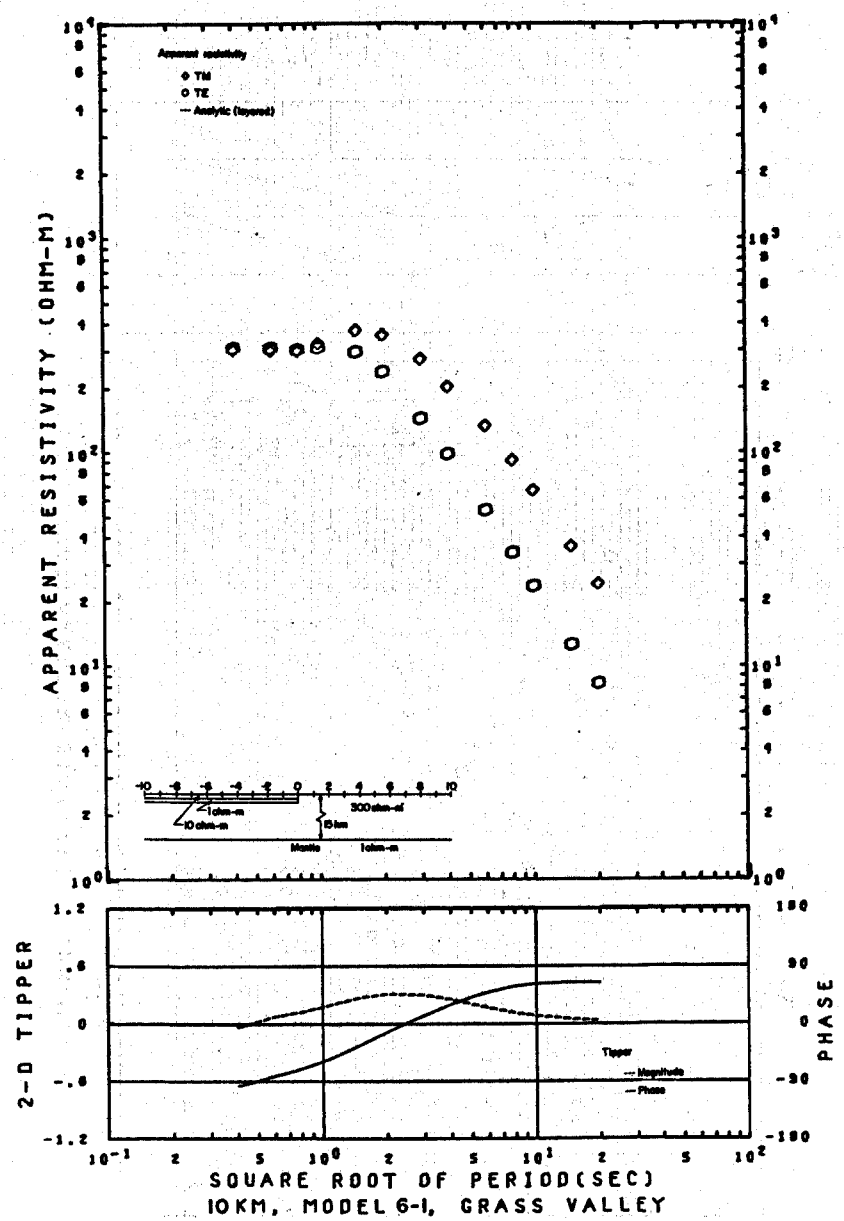
Apparent resistivity
TM
TE
Analytic (layered)
APPARENT RESISTIVITY (OHM-M)
1 ohm-m
10 ohm-m
300 ohm-m
15 km
Mantle
1 ohm-m
2-D TIPPER
PHASE
Tipper
Magnitude
Phase
SQUARE ROOT OF PERIOD(SEC)
10KM, MODEL 6-1, GRASS VALLEY

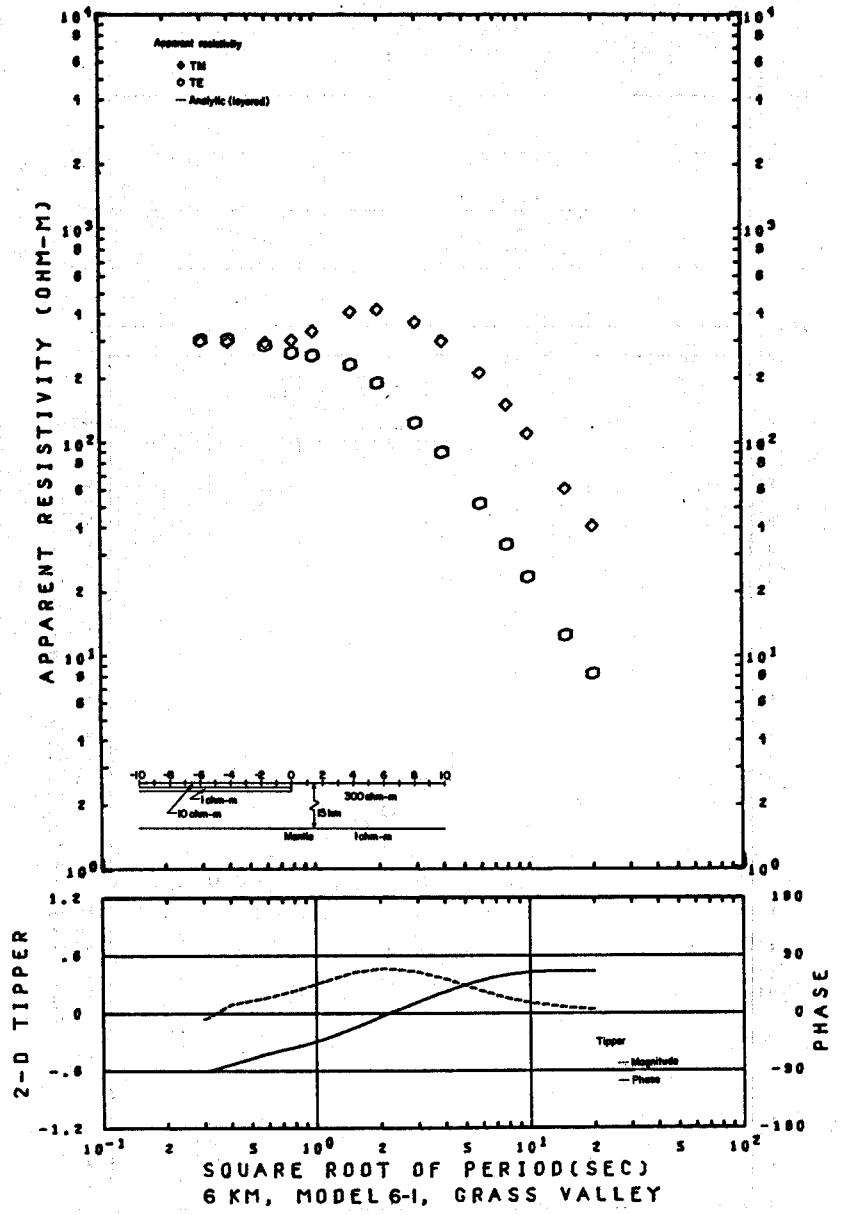
Apparent resistivity
TM
TE
Analytic (layered)
APPARENT RESISTIVITY (OHM-M)
1 ohm-m
10 ohm-m
300 ohm-m
15 km
Mantle
1 ohm-m
2-D TIPPER
PHASE
Tipper
Magnitude
Phase
SQUARE ROOT OF PERIOD(SEC)
6 KM, MODEL 6-1, GRASS VALLEY

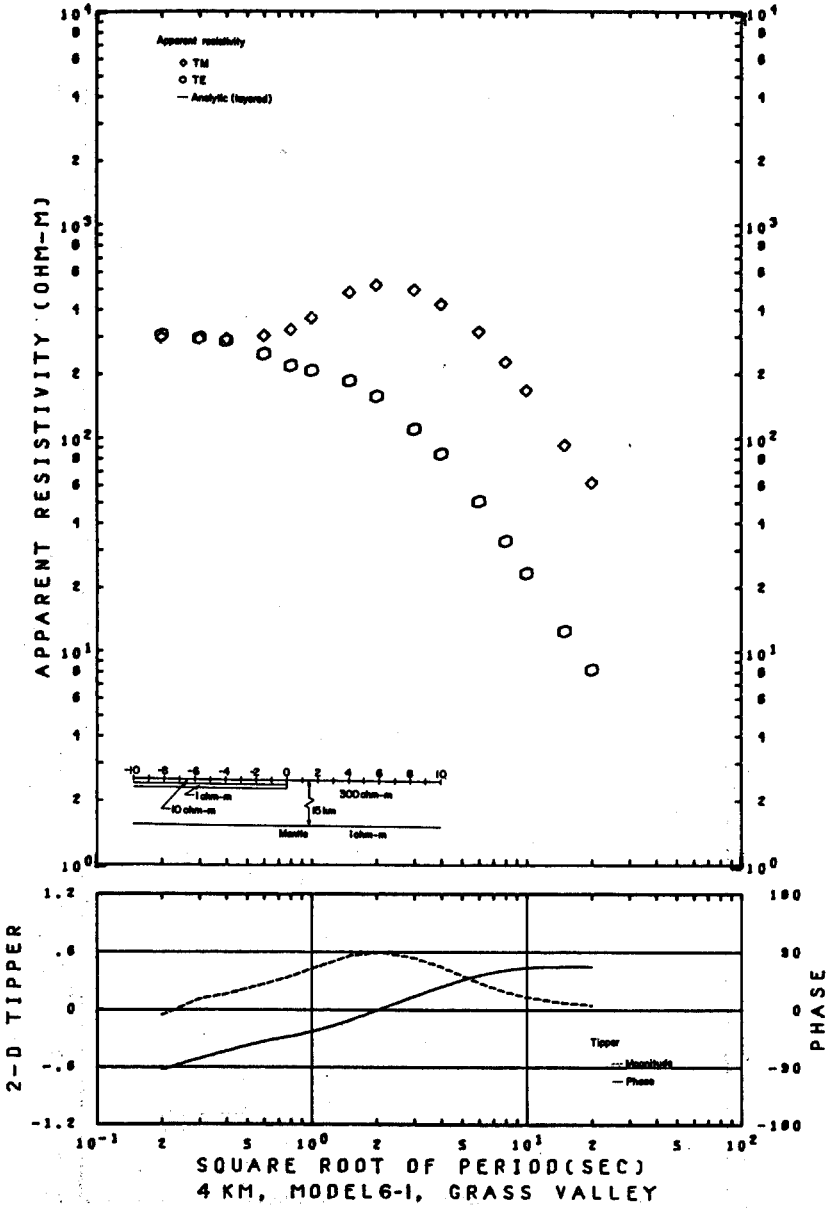
Apparent resistivity
TM
TE
Analytic (layered)
APPARENT RESISTIVITY (OHM-M)
2-D TIPPER
PHASE
Tipper
Magnitude
Phase
SQUARE ROOT OF PERIOD(SEC)
4 KM, MODEL6-I, GRASS VALLEY

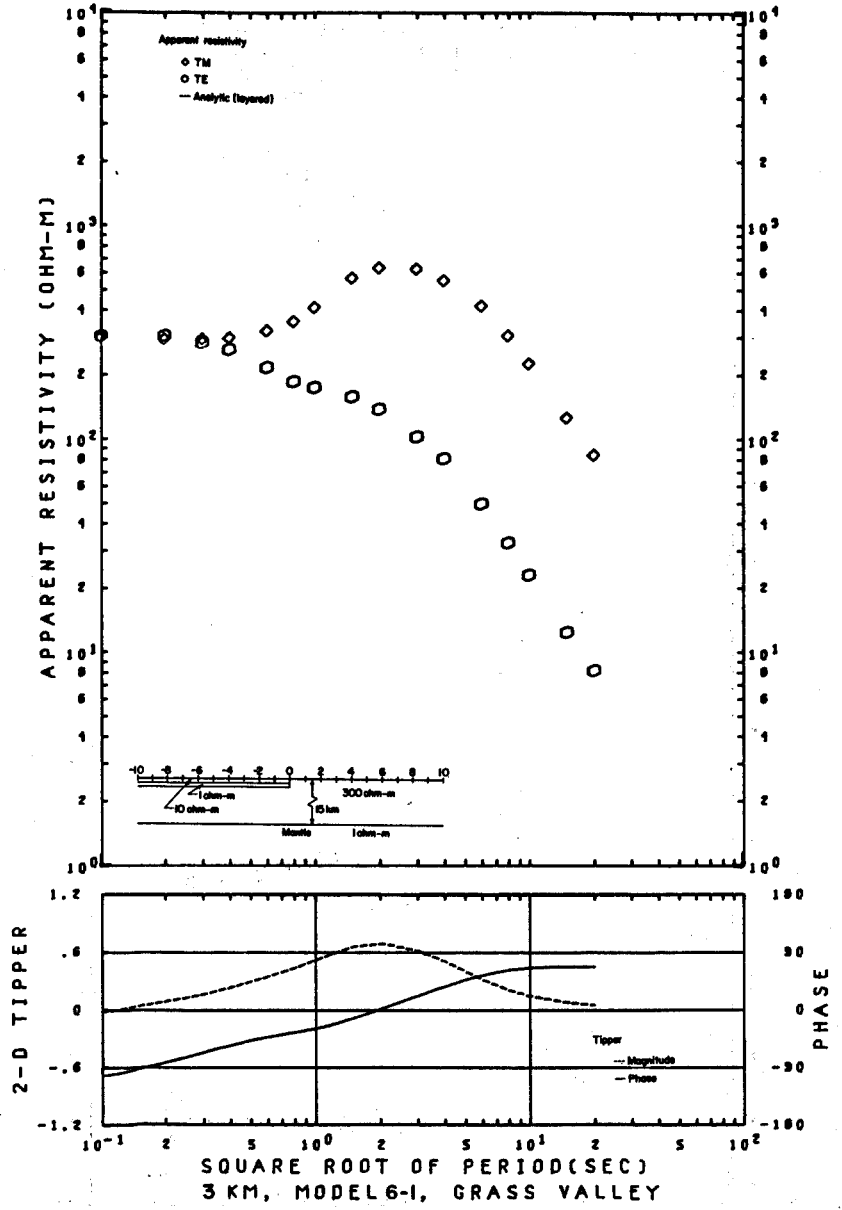
Apparent resistivity
TM
TE
Analytic (layered)
APPARENT RESISTIVITY (OHM-M)
2-D TIPPER
PHASE
Tipper
Magnitude
Phase
SQUARE ROOT OF PERIOD(SEC)
3 KM, MODEL6-I, GRASS VALLEY

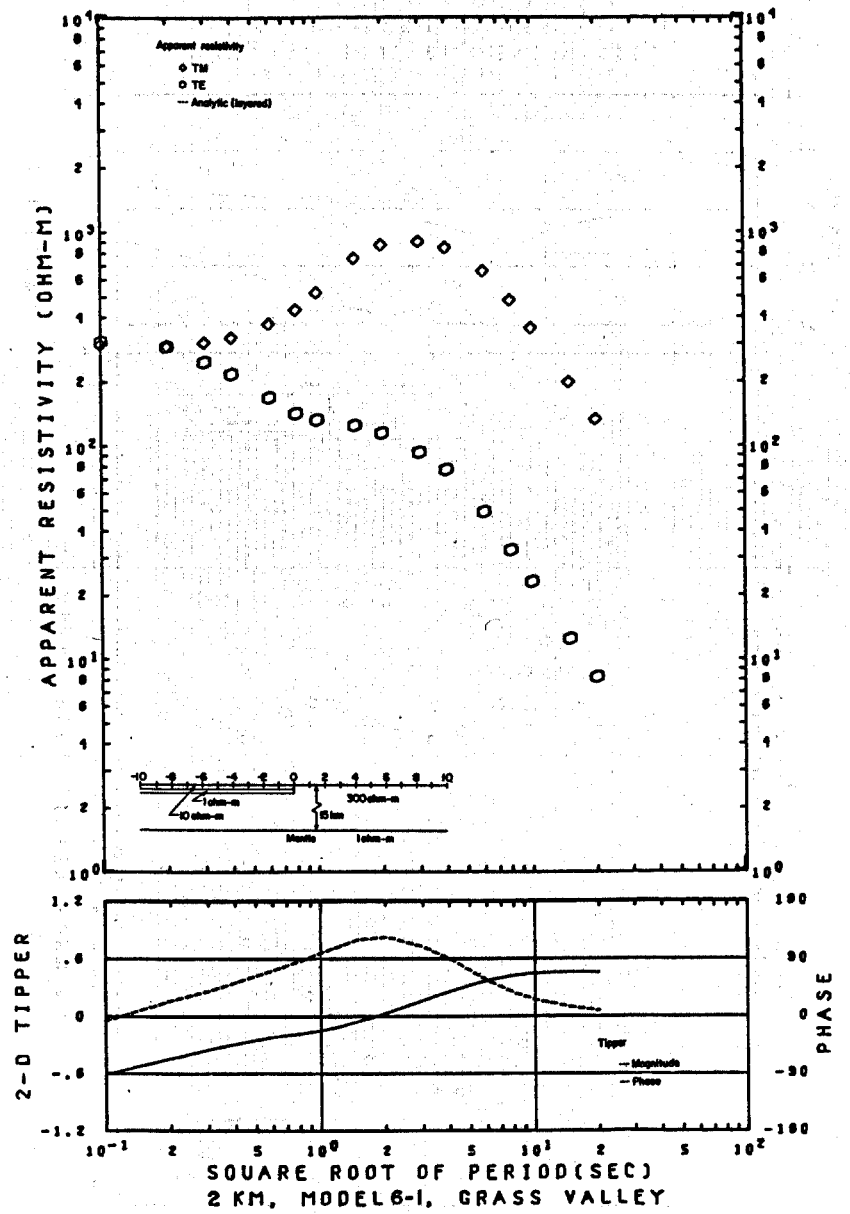
Apparent resistivity
TM
TE
Analytic (layered)
APPARENT RESISTIVITY (OHM-M)
1 ohm-m
10 ohm-m
300 ohm-m
15 km
Mantle
1 ohm-m
2-D TIPPER
PHASE
Tipper
Magnitude
Phase
SQUARE ROOT OF PERIOD(SEC)
2 KM, MODEL 6-1, GRASS VALLEY

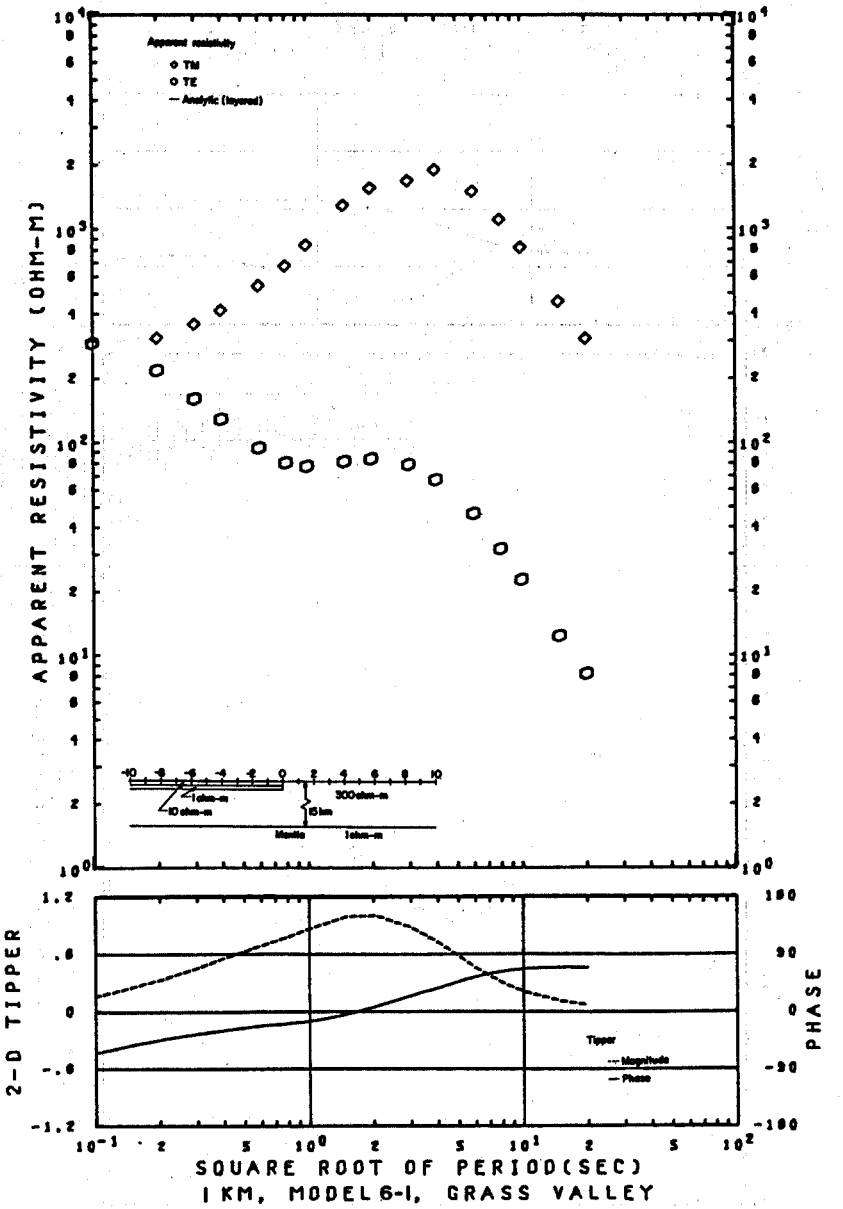
Apparent resistivity
TM
TE
Analytic (layered)
APPARENT RESISTIVITY (OHM-M)
1 ohm-m
10 ohm-m
300 ohm-m
15 km
Mantle
1 ohm-m
2-D TIPPER
PHASE
Tipper
Magnitude
Phase
SQUARE ROOT OF PERIOD(SEC)
1 KM, MODEL 6-1, GRASS VALLEY

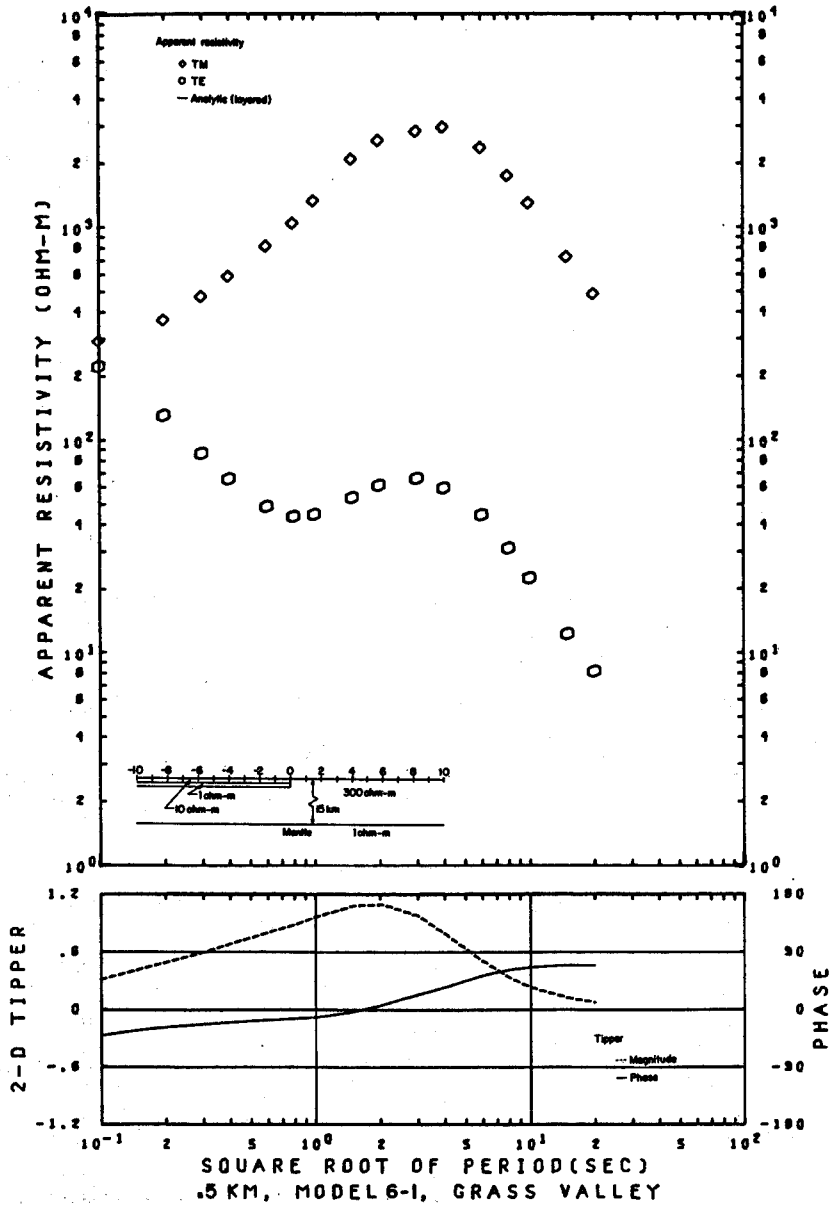
Apparent resistivity
TM
TE
Analytic (layered)
APPARENT RESISTIVITY (OHM-M)
1 ohm-m
10 ohm-m
300 ohm-m
15 km
Mantle
1 ohm-m
2-D TIPPER
PHASE
Tipper
Magnitude
Phase
SQUARE ROOT OF PERIOD(SEC)
.5 KM, MODEL 6-1, GRASS VALLEY

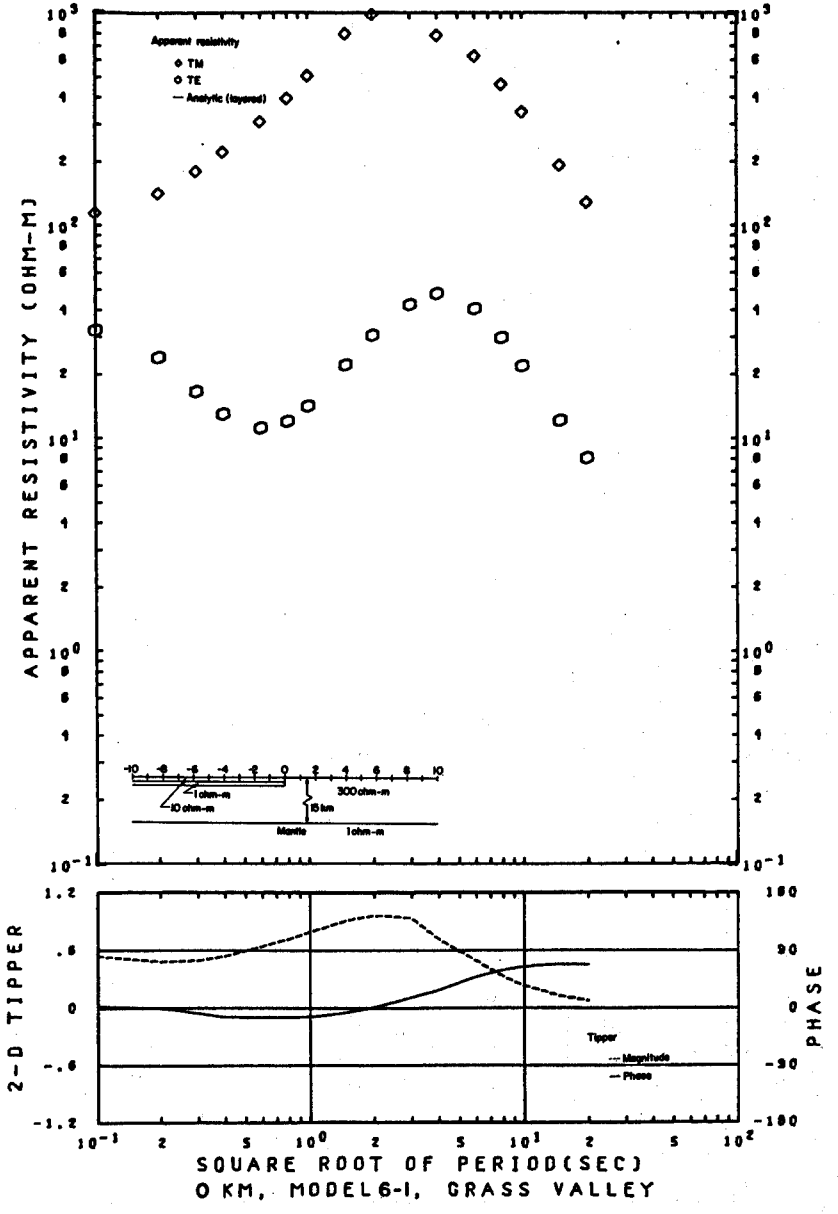
Apparent resistivity
TM
TE
Analytic (layered)
APPARENT RESISTIVITY (OHM-M)
1 ohm-m
10 ohm-m
300 ohm-m
15 km
Mantle
1 ohm-m
2-D TIPPER
PHASE
Tipper
Magnitude
Phase
SQUARE ROOT OF PERIOD(SEC)
0 KM, MODEL 6-1, GRASS VALLEY

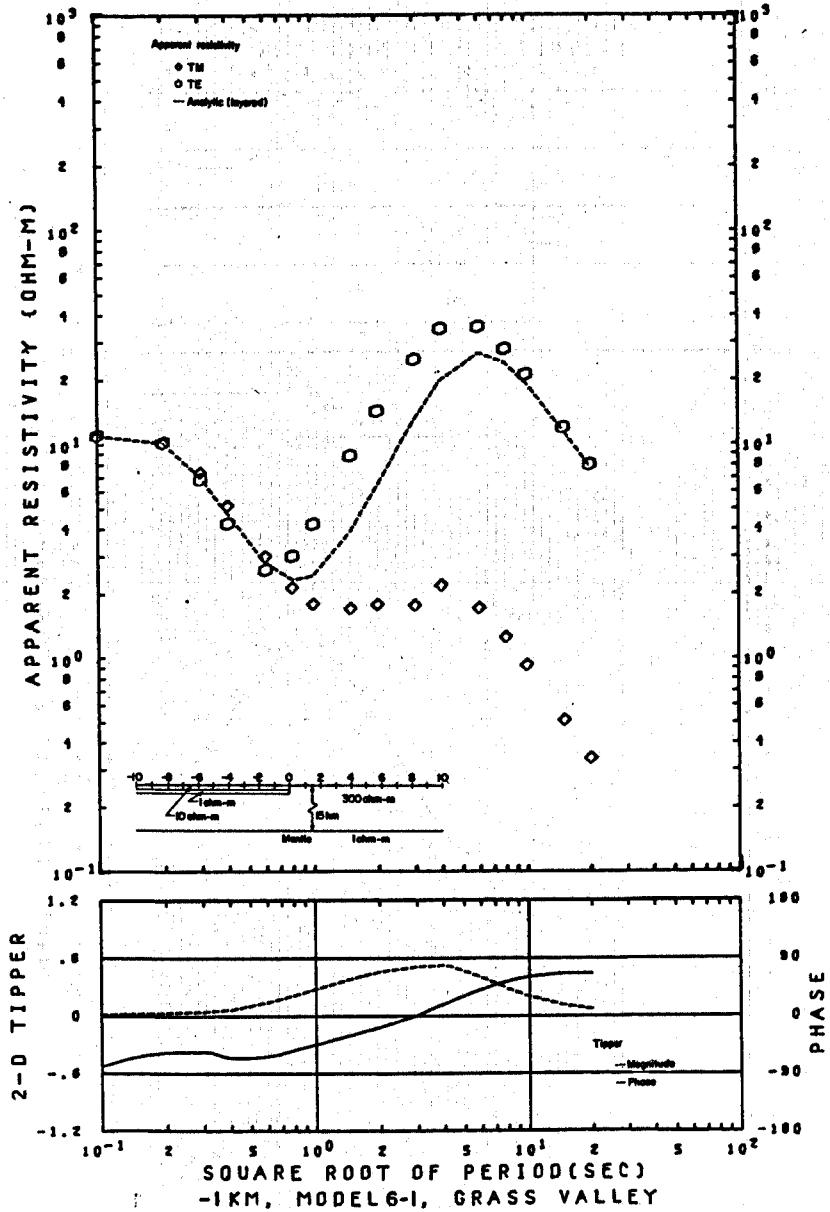
Apparent resistivity
TM
TE
Analytic (layered)
APPARENT RESISTIVITY (OHM-M)
2-D TIPPER
PHASE
Tipper
Magnitude
Phase
SQUARE ROOT OF PERIOD(SEC)
-1KM, MODEL6-I, GRASS VALLEY

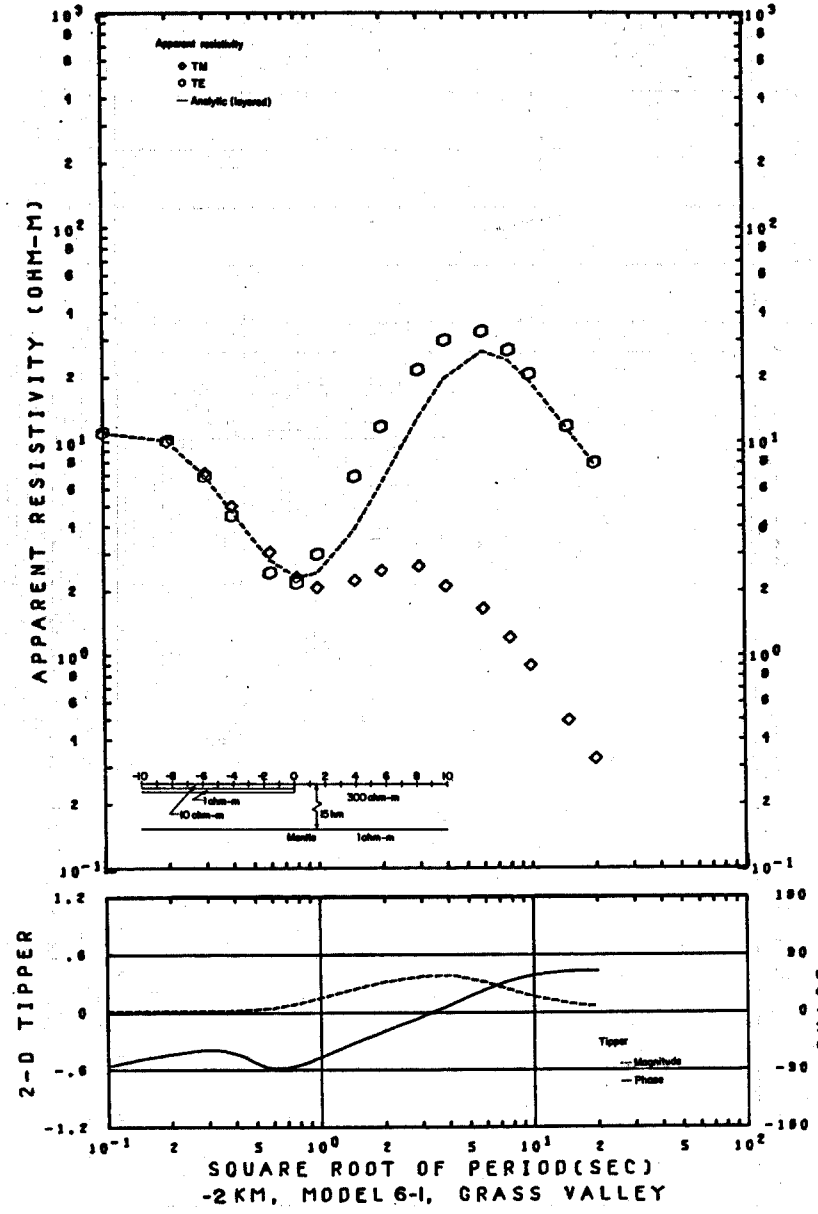
Apparent resistivity
TM
TE
Analytic (layered)
APPARENT RESISTIVITY (OHM-M)
2-D TIPPER
PHASE
Tipper
Magnitude
Phase
SQUARE ROOT OF PERIOD(SEC)
-2KM, MODEL 6-I, GRASS VALLEY

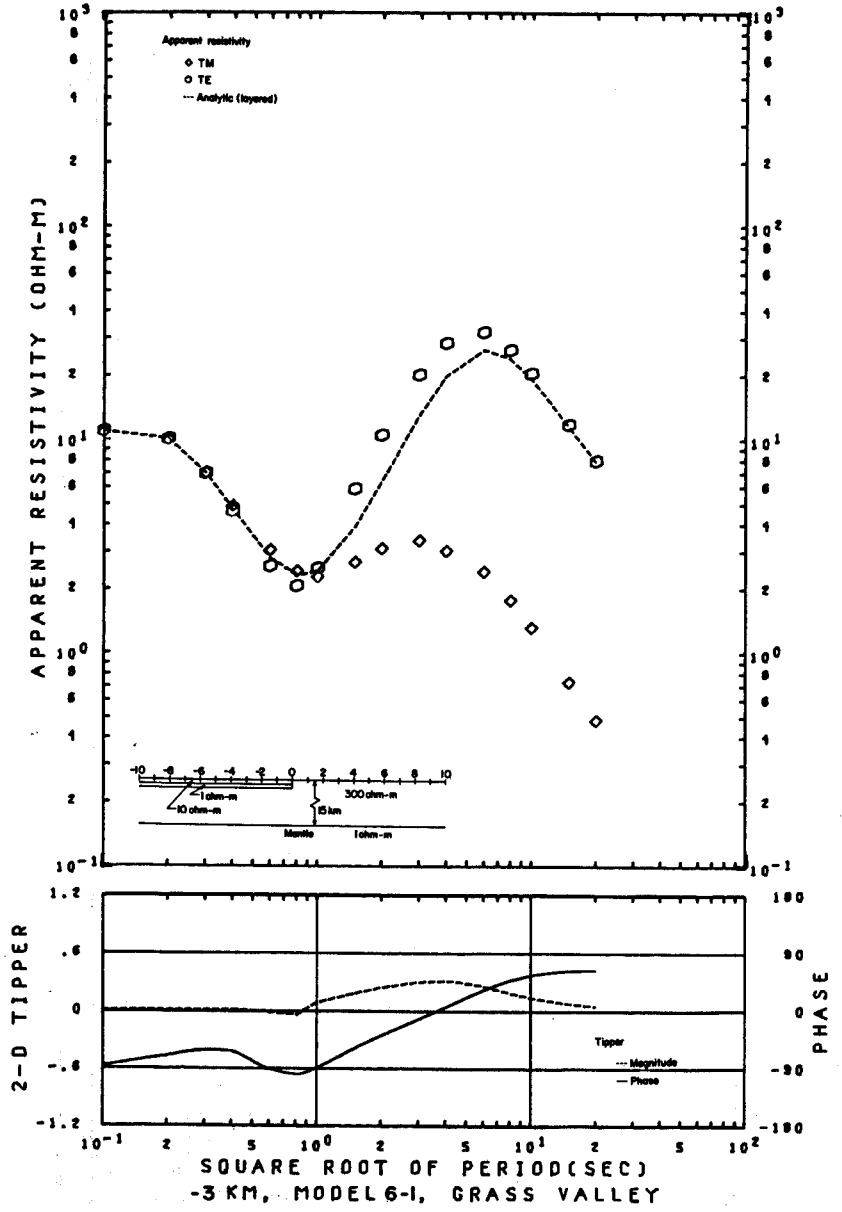
Apparent resistivity
TM
TE
Analytic (layered)
APPARENT RESISTIVITY (OHM-M)
1 ohm-m
10 ohm-m
300 ohm-m
15 km
Mantle
1 ohm-m
2-D TIPPER
PHASE
Tipper
Magnitude
Phase
SQUARE ROOT OF PERIOD(SEC)
-3 KM, MODEL 6-I, GRASS VALLEY

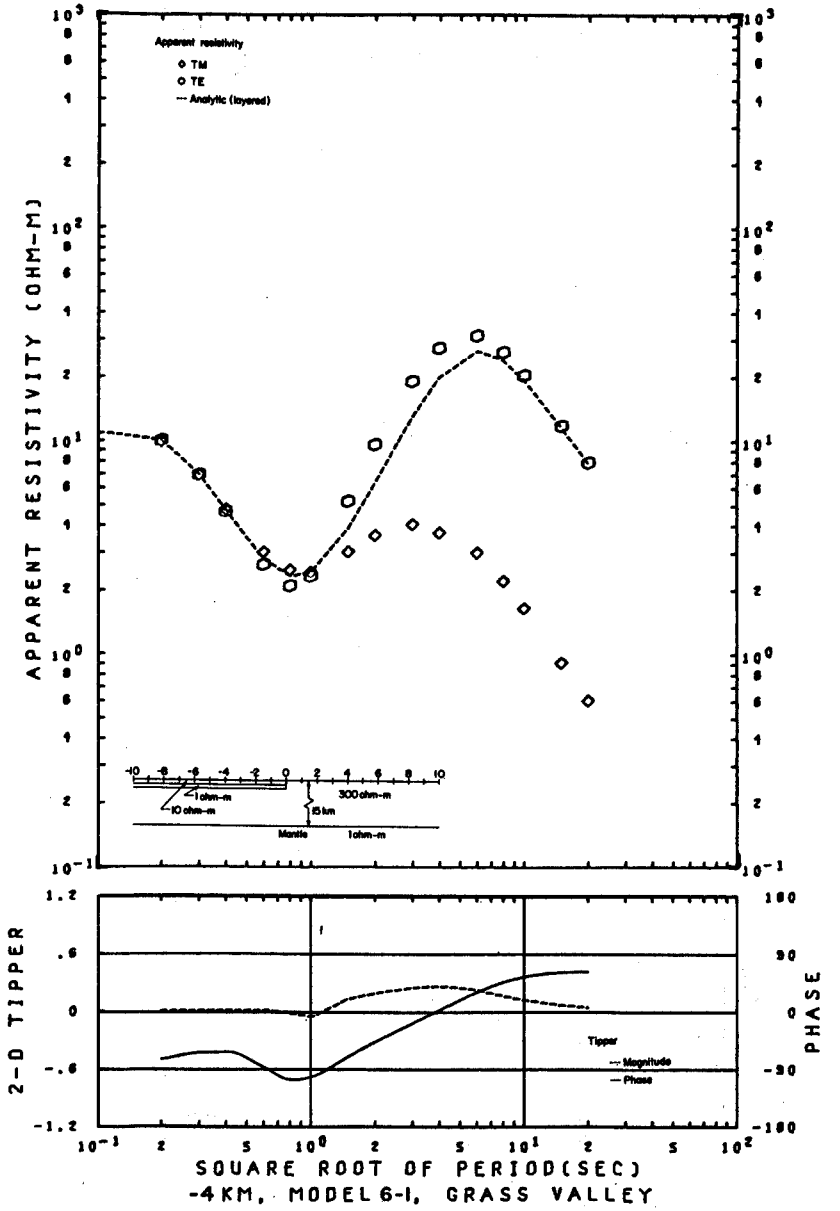
Apparent resistivity
TM
TE
Analytic (layered)
APPARENT RESISTIVITY (OHM-M)
1 ohm-m
10 ohm-m
300 ohm-m
15 km
Mantle
1 ohm-m
2-D TIPPER
PHASE
Tipper
Magnitude
Phase
SQUARE ROOT OF PERIOD(SEC)
-4 KM, MODEL 6-I, GRASS VALLEY

Apparent resistivity
TM
TE
Analytic (layered)
APPARENT RESISTIVITY (OHM-M)
2-D TIPPER
PHASE
Tipper
Magnitude
Phase
SQUARE ROOT OF PERIOD(SEC)
-6 KM, MODEL 6-1, GRASS VALLEY

Apparent resistivity
TM
TE
Analytic (layered)
APPARENT RESISTIVITY (OHM-M)
2-D TIPPER
PHASE
Tipper
Magnitude
Phase
SQUARE ROOT OF PERIOD(SEC)
-10 KM, MODEL 6-1, GRASS VALLEY

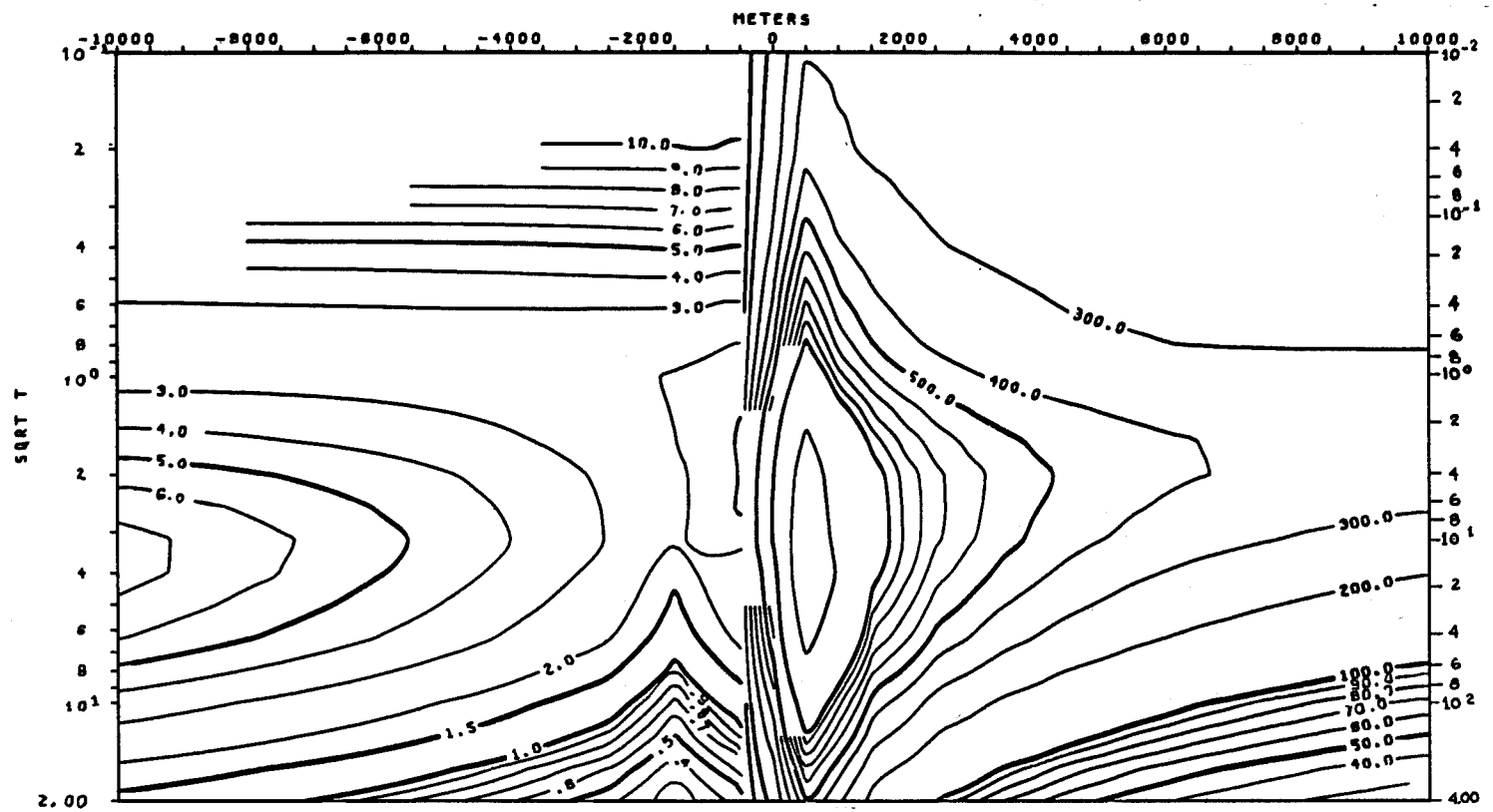

TM MODE
APPARENT RESISTIVITY VS. PERIOD (T)
MODEL 6-1

XBL 786-1942

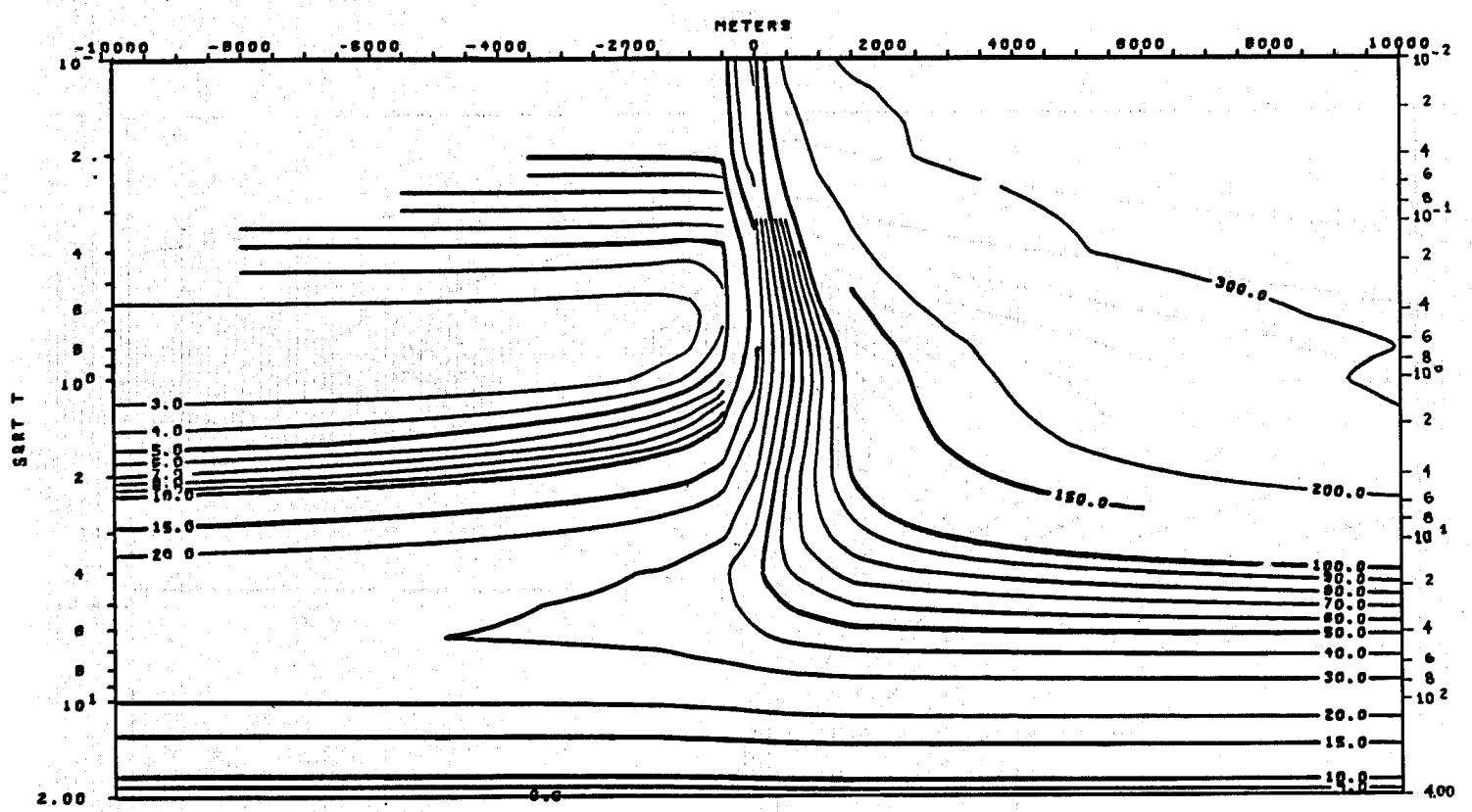

TE MODE
APPARENT RESISTIVITY VS. PERIOD (T)
MODEL 6-1

XBL 786-1938

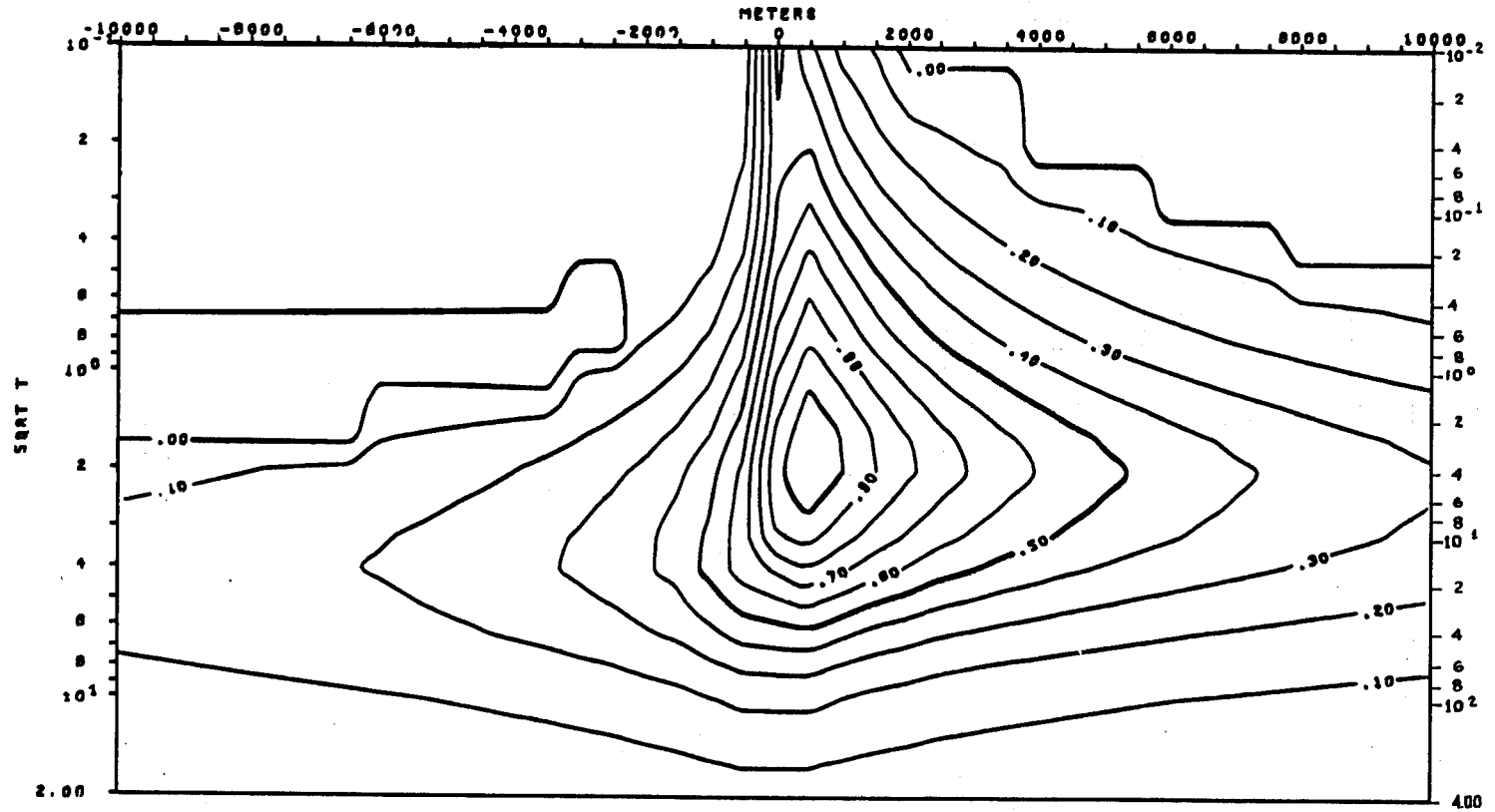

TIPPER VS. PERIOD (T)
MODEL 6-1

XBL 786-1920

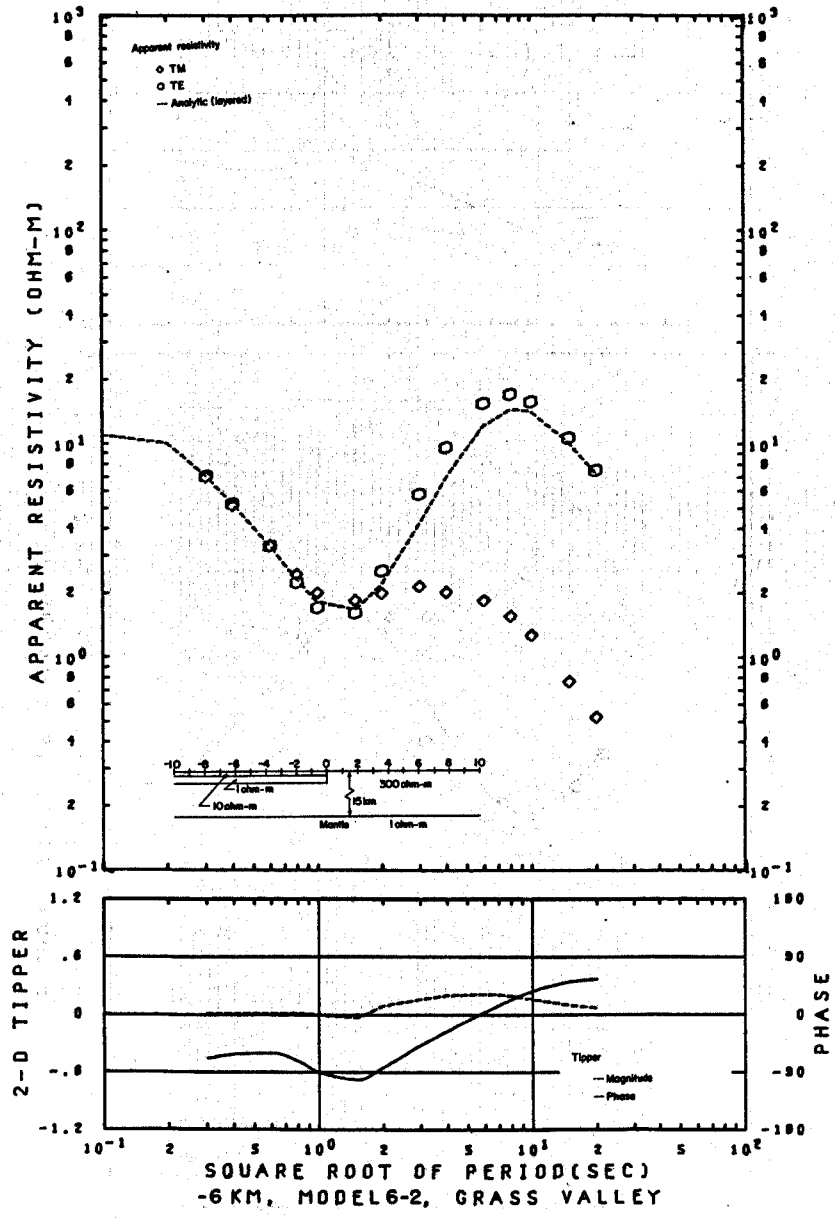

-6KM, MODEL6-2, GRASS VALLEY

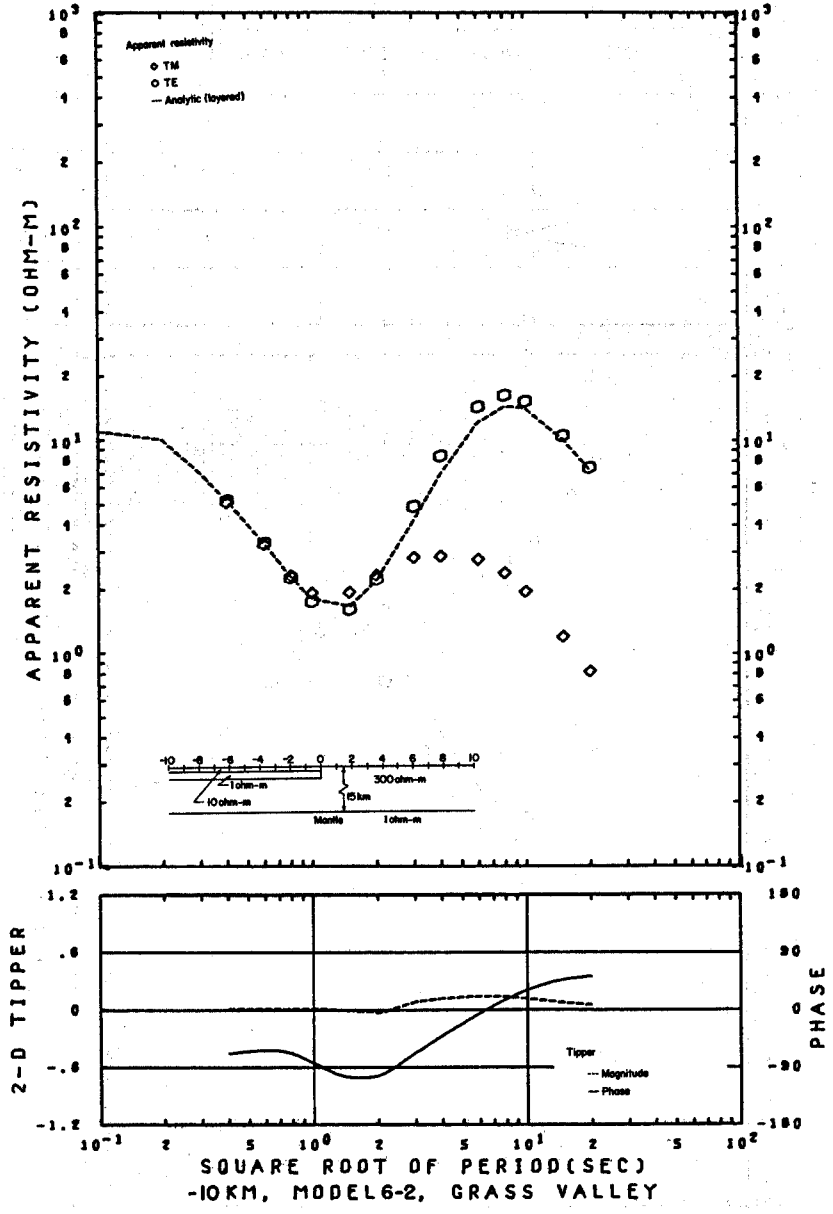

-10KM, MODEL6-2, GRASS VALLEY

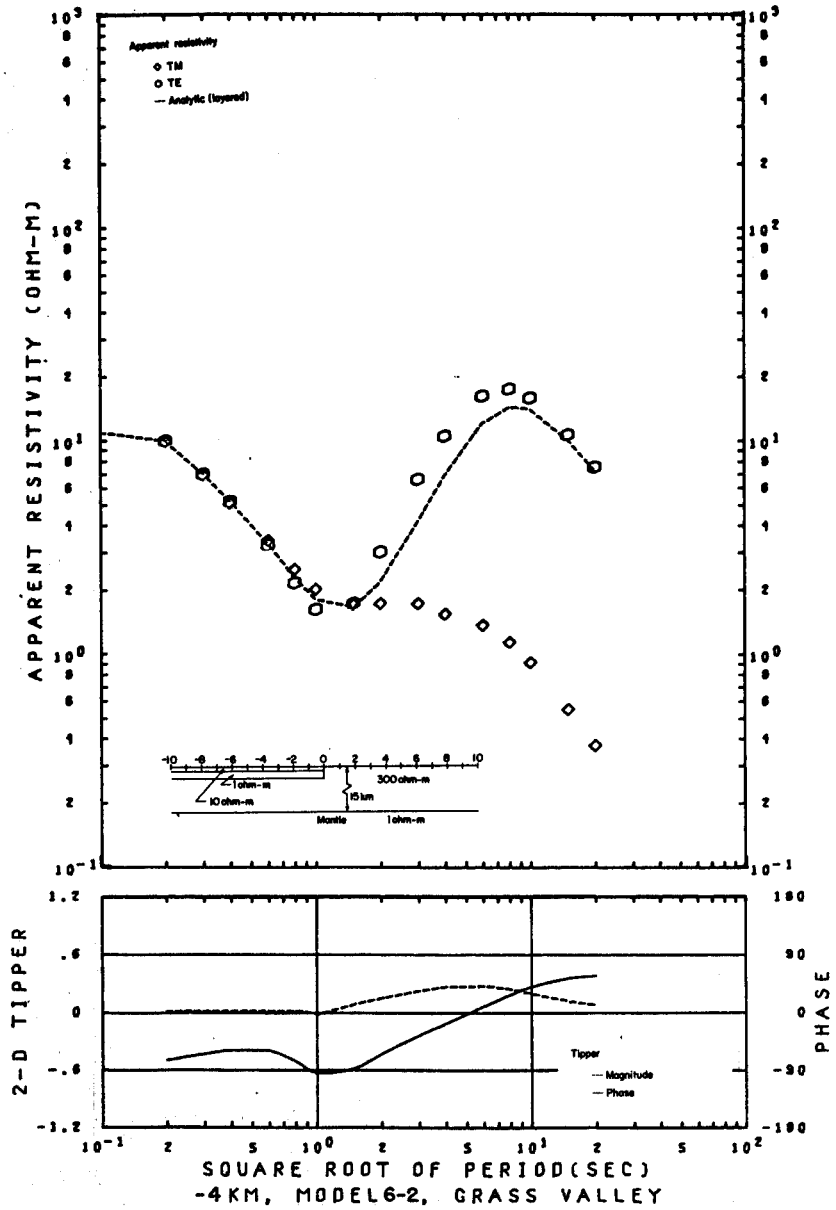
Apparent resistivity
TM
TE
Analytic (layered)
APPARENT RESISTIVITY (OHM-M)
1 ohm-m
10 ohm-m
300 ohm-m
15 km
Mantle
1 ohm-m
2-D TIPPER
PHASE
Tipper
Magnitude
Phase
SQUARE ROOT OF PERIOD(SEC)
-4 KM, MODEL 6-2, GRASS VALLEY

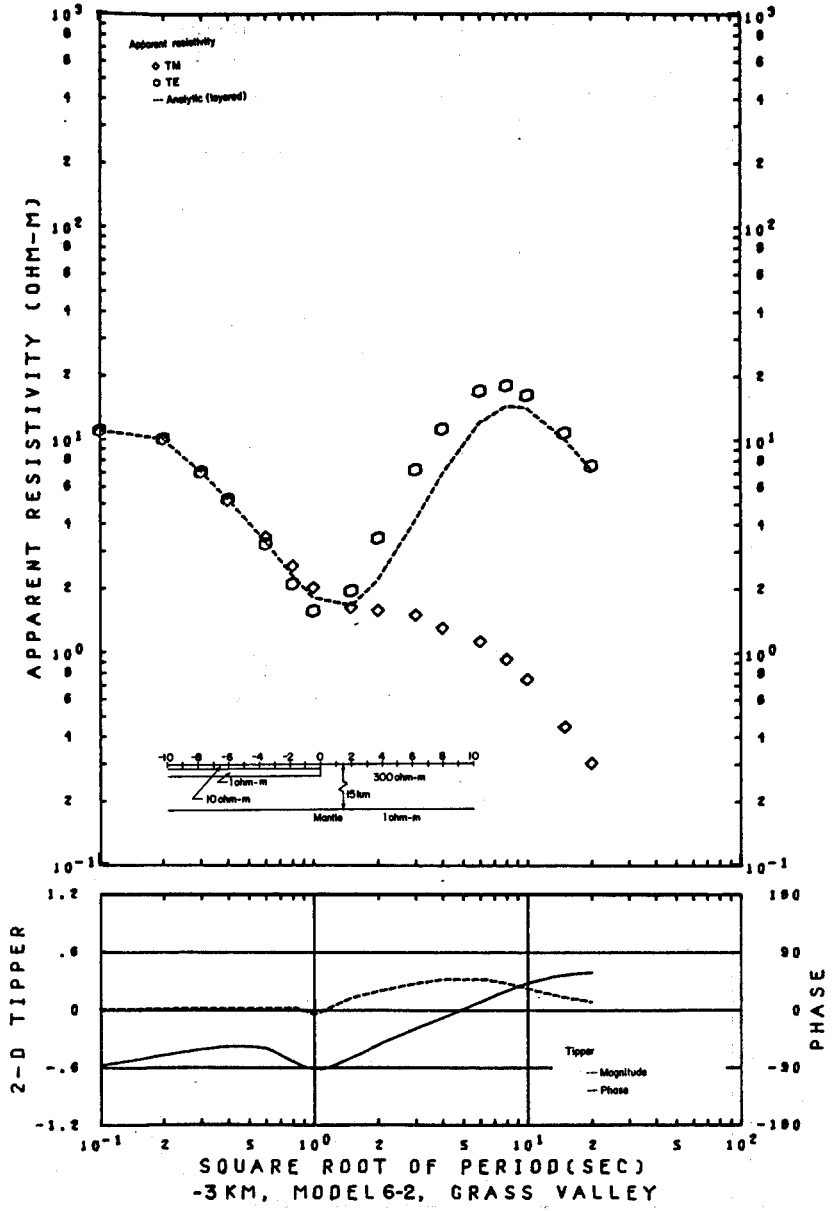
Apparent resistivity
TM
TE
Analytic (layered)
APPARENT RESISTIVITY (OHM-M)
1 ohm-m
10 ohm-m
300 ohm-m
15 km
Mantle
1 ohm-m
2-D TIPPER
PHASE
Tipper
Magnitude
Phase
SQUARE ROOT OF PERIOD(SEC)
-3 KM, MODEL 6-2, GRASS VALLEY

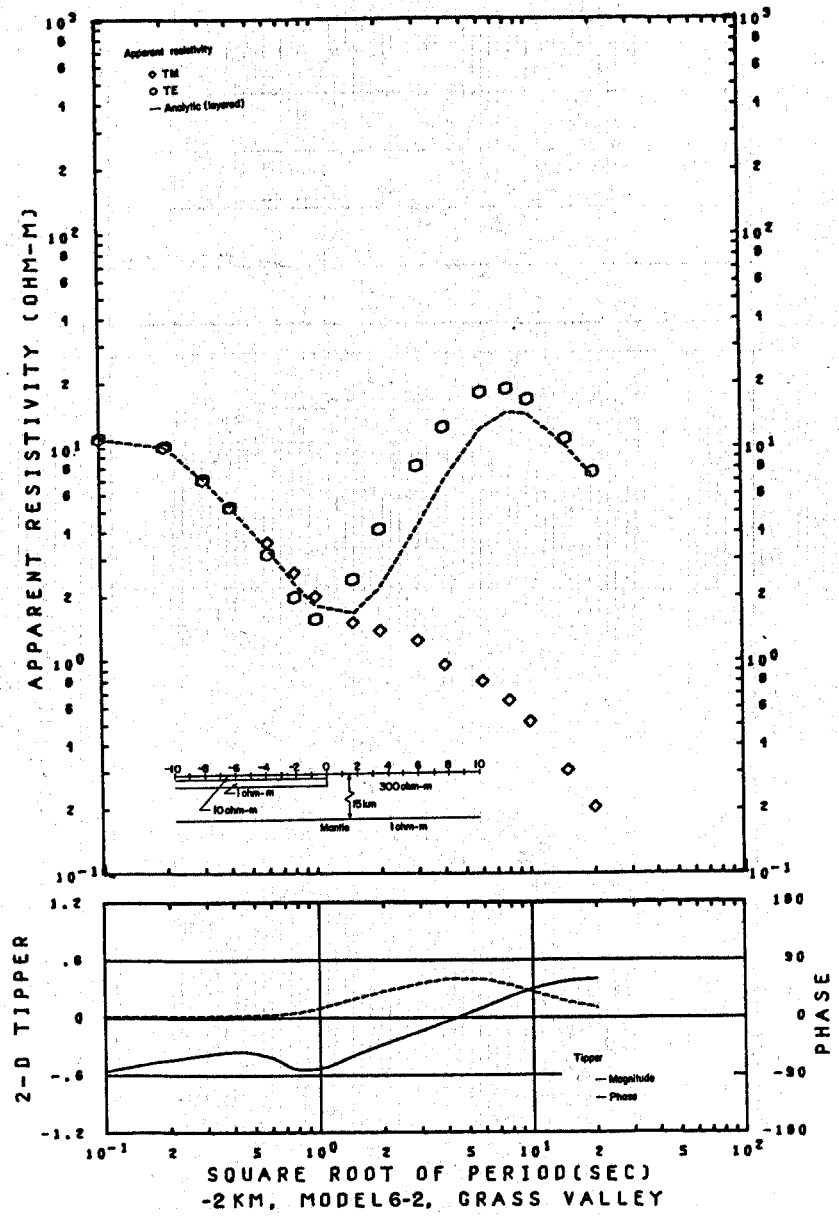
Apparent resistivity
TM
TE
Analytic (layered)
APPARENT RESISTIVITY (OHM-M)
1 ohm-m
10 ohm-m
300 ohm-m
15 km
Mantle
1 ohm-m
2-D TIPPER
PHASE
Tipper
Magnitude
Phase
SQUARE ROOT OF PERIOD(SEC)
-2 KM, MODEL6-2, GRASS VALLEY

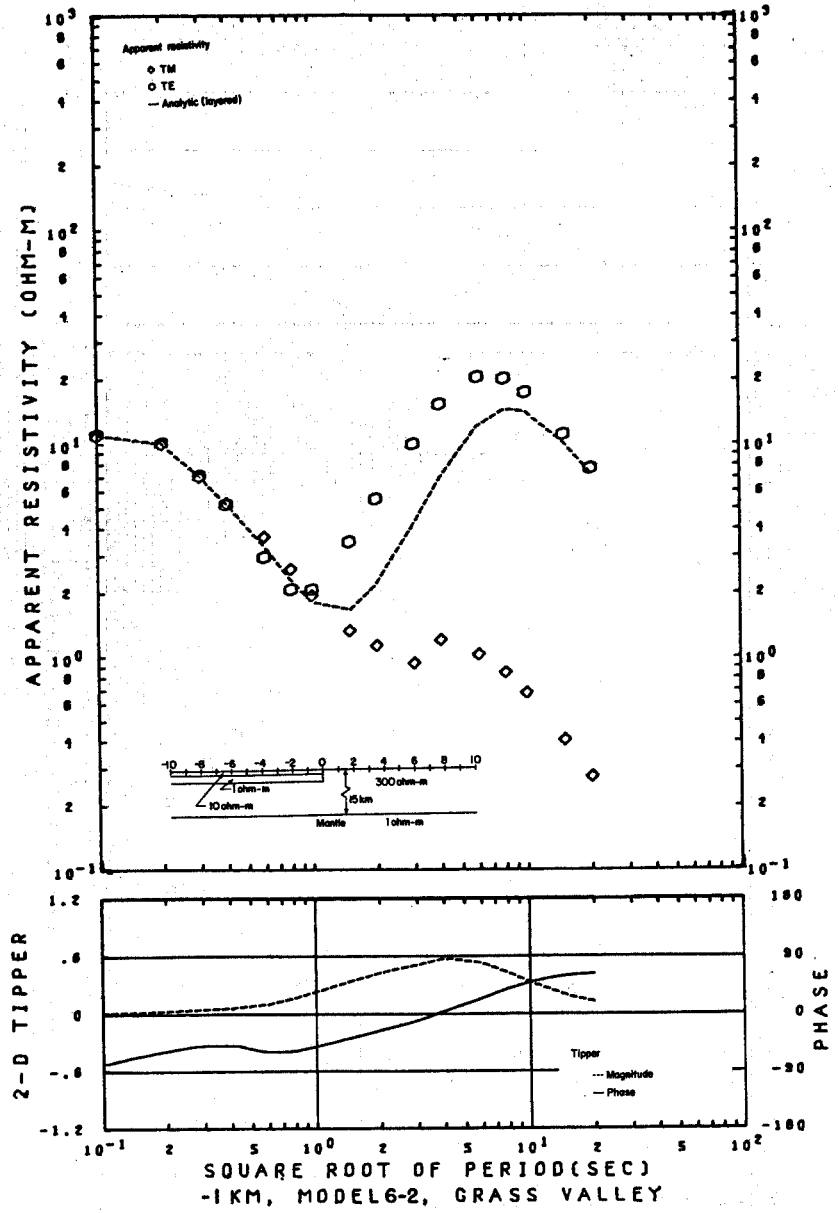
Apparent resistivity
TM
TE
Analytic (layered)
APPARENT RESISTIVITY (OHM-M)
1 ohm-m
10 ohm-m
300 ohm-m
15 km
Mantle
1 ohm-m
2-D TIPPER
PHASE
Tipper
Magnitude
Phase
SQUARE ROOT OF PERIOD(SEC)
-1 KM, MODEL6-2, GRASS VALLEY

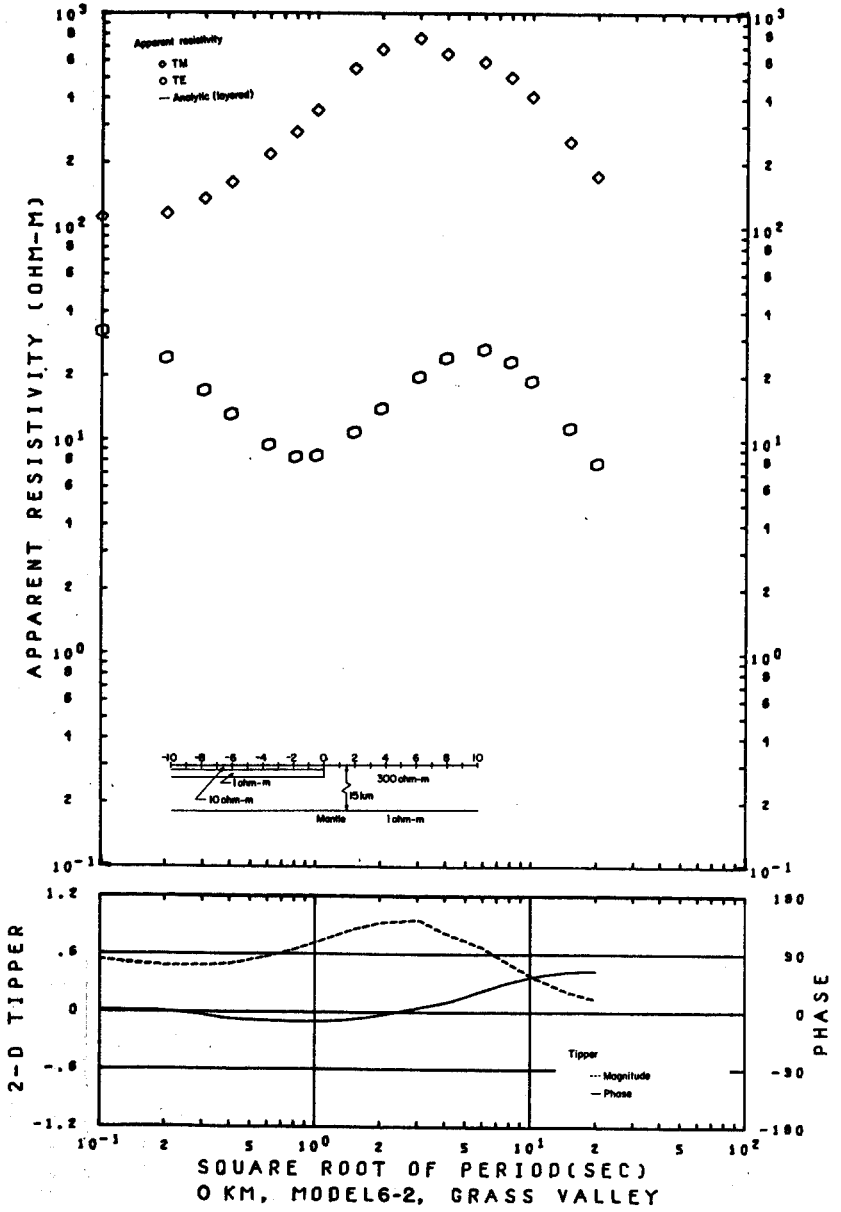
Apparent resistivity
TM
TE
Analytic (layered)
APPARENT RESISTIVITY (OHM-M)
1 ohm-m
10 ohm-m
300 ohm-m
15 km
Mantle
1 ohm-m
2-D TIPPER
PHASE
Tipper
Magnitude
Phase
SQUARE ROOT OF PERIOD(SEC)
0 KM, MODEL6-2, GRASS VALLEY

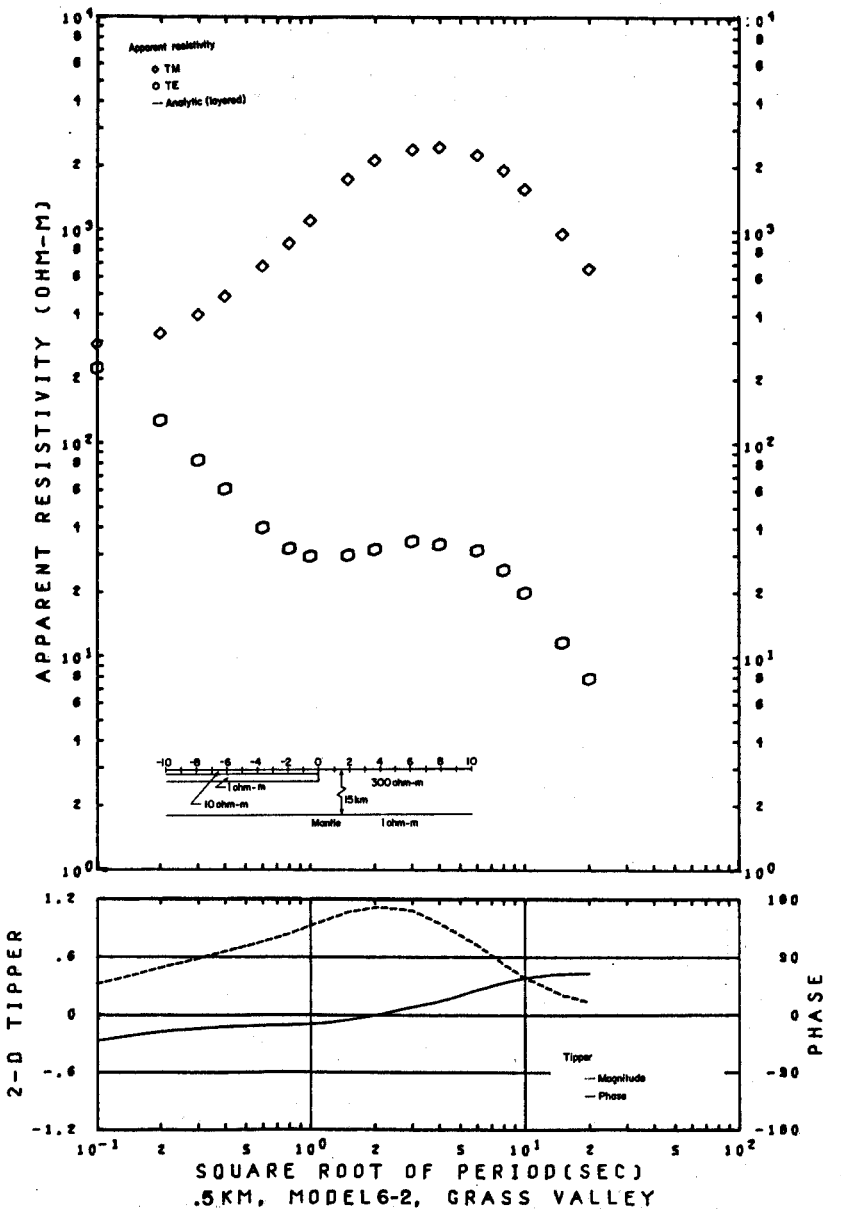
Apparent resistivity
TM
TE
Analytic (layered)
APPARENT RESISTIVITY (OHM-M)
1 ohm-m
10 ohm-m
300 ohm-m
15 km
Mantle
1 ohm-m
2-D TIPPER
PHASE
Tipper
Magnitude
Phase
SQUARE ROOT OF PERIOD(SEC)
.5 KM, MODEL6-2, GRASS VALLEY

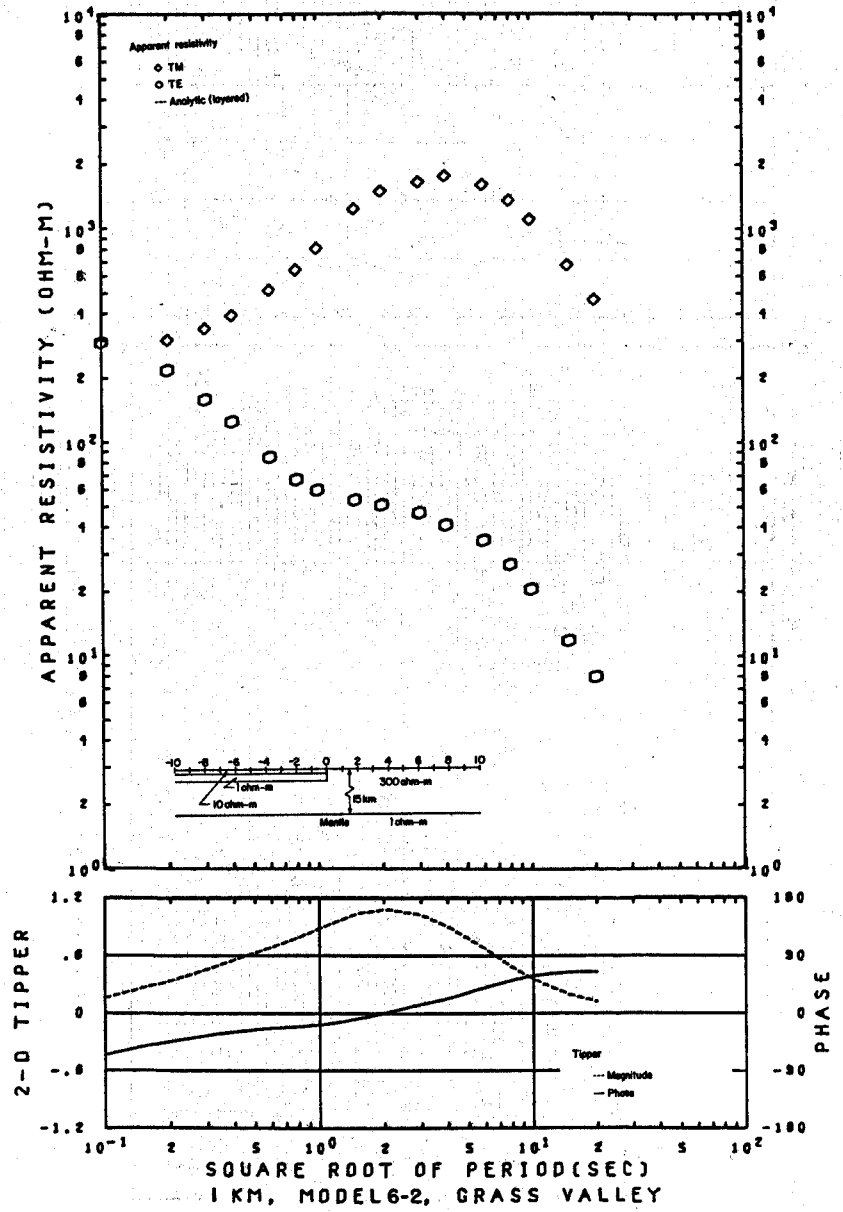
Apparent resistivity
TM
TE
Analytic (layered)
APPARENT RESISTIVITY (OHM-M)
1 ohm-m
10 ohm-m
300 ohm-m
15 km
Mantle
1 ohm-m
2-D TIPPER
PHASE
Tipper
Magnitude
Phase
SQUARE ROOT OF PERIOD(SEC)
1 KM, MODEL6-2, GRASS VALLEY

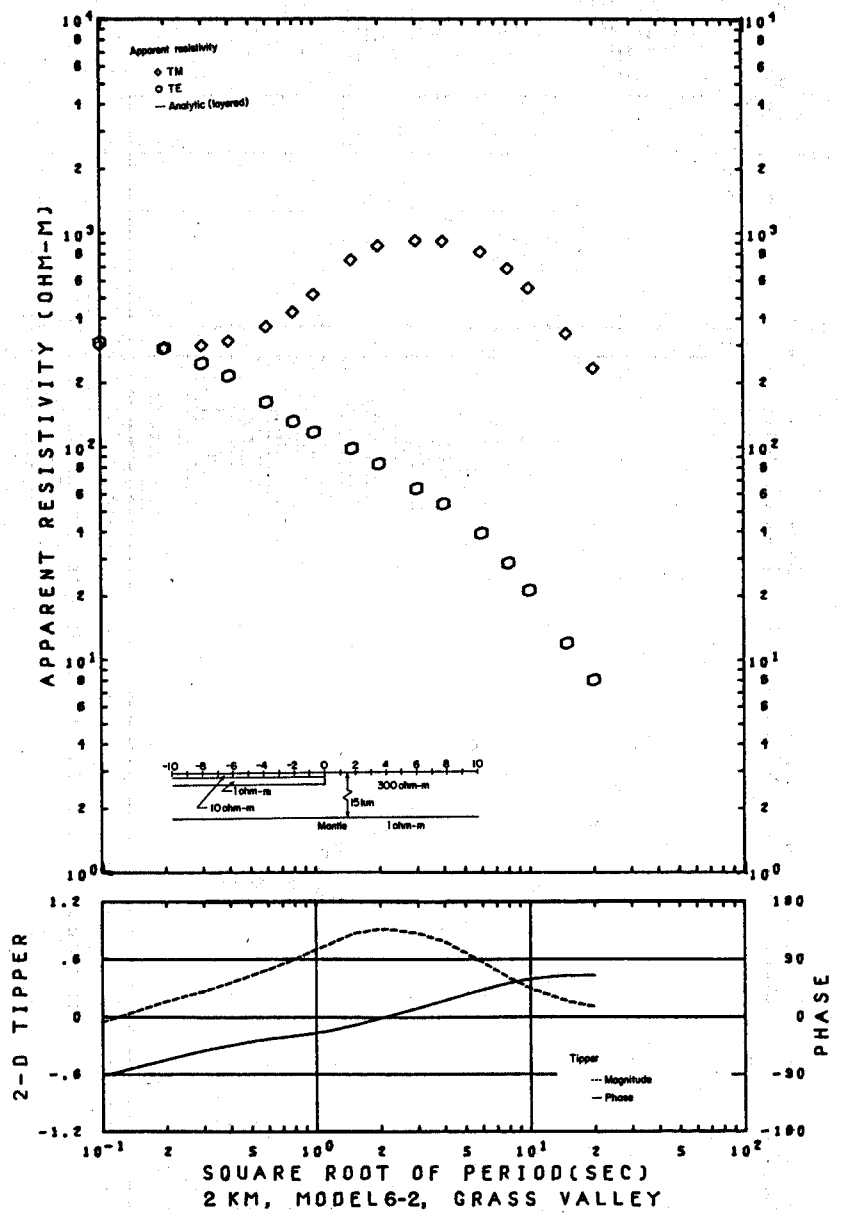
Apparent resistivity
TM
TE
Analytic (layered)
APPARENT RESISTIVITY (OHM-M)
1 ohm-m
10 ohm-m
300 ohm-m
15 km
Mantle
1 ohm-m
2-D TIPPER
PHASE
Tipper
Magnitude
Phase
SQUARE ROOT OF PERIOD(SEC)
2 KM, MODEL6-2, GRASS VALLEY

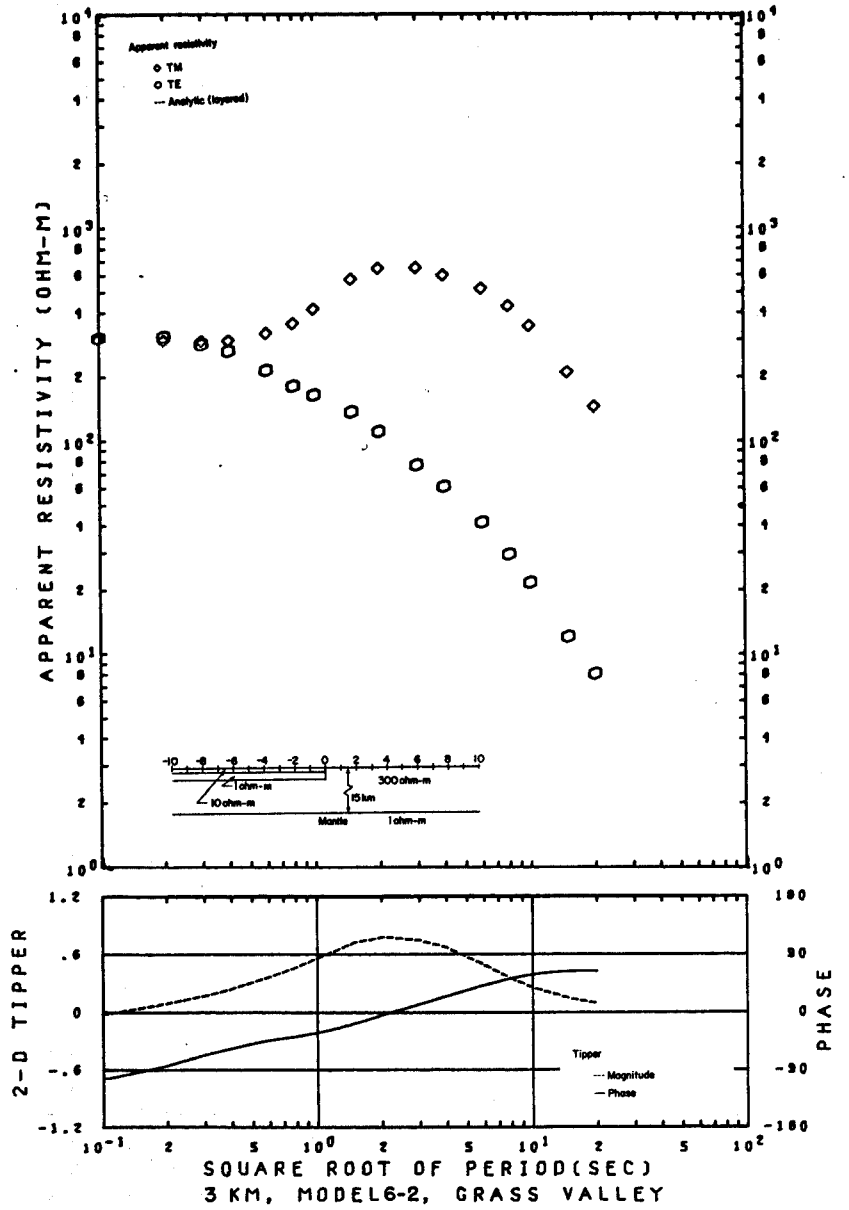
Apparent resistivity
TM
TE
Analytic (layered)
APPARENT RESISTIVITY (OHM-M)
1 ohm-m
10 ohm-m
300 ohm-m
15 km
Mantle
1 ohm-m
2-D TIPPER
PHASE
Tipper
Magnitude
Phase
SQUARE ROOT OF PERIOD(SEC)
3 KM, MODEL6-2, GRASS VALLEY

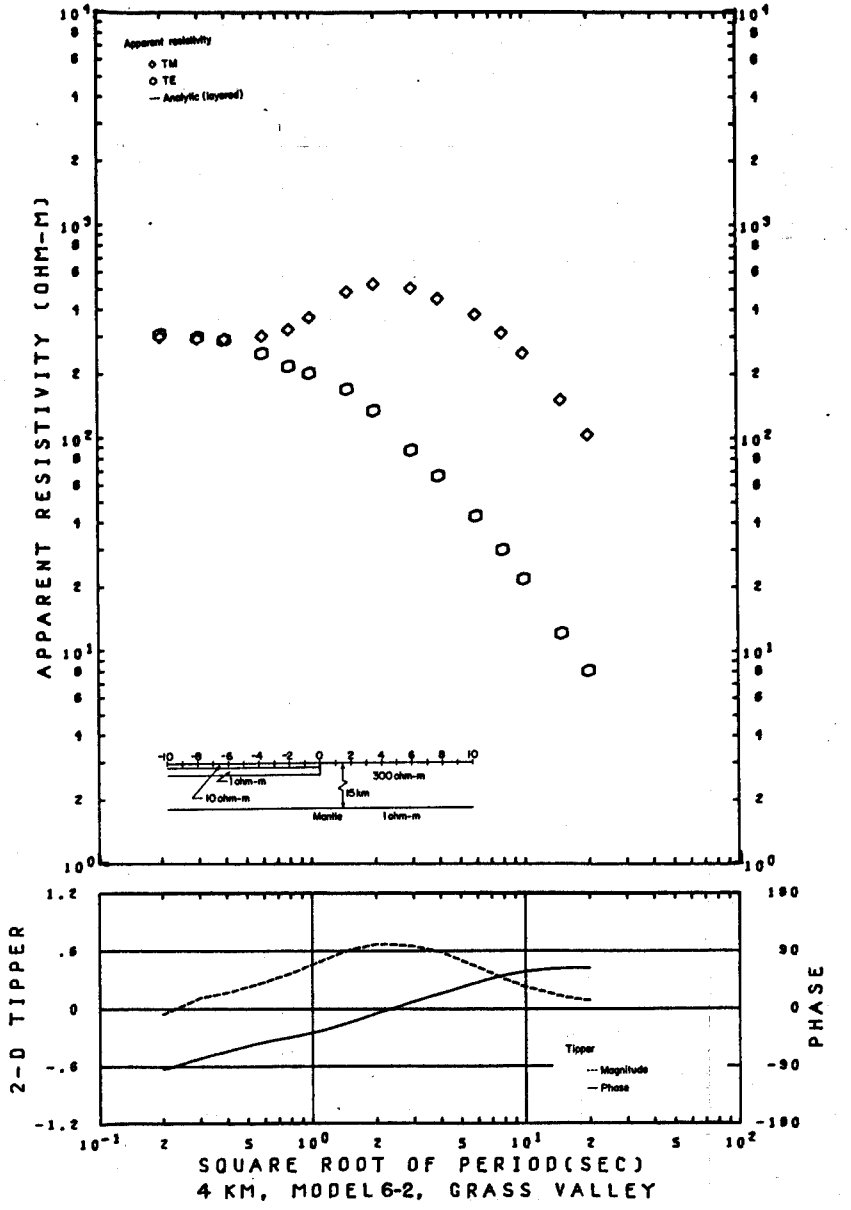
Apparent resistivity
TM
TE
Analytic (layered)
APPARENT RESISTIVITY (OHM-M)
1 ohm-m
10 ohm-m
300 ohm-m
15 km
Mantle
1 ohm-m
2-D TIPPER
PHASE
Tipper
Magnitude
Phase
SQUARE ROOT OF PERIOD(SEC)
4 KM, MODEL6-2, GRASS VALLEY

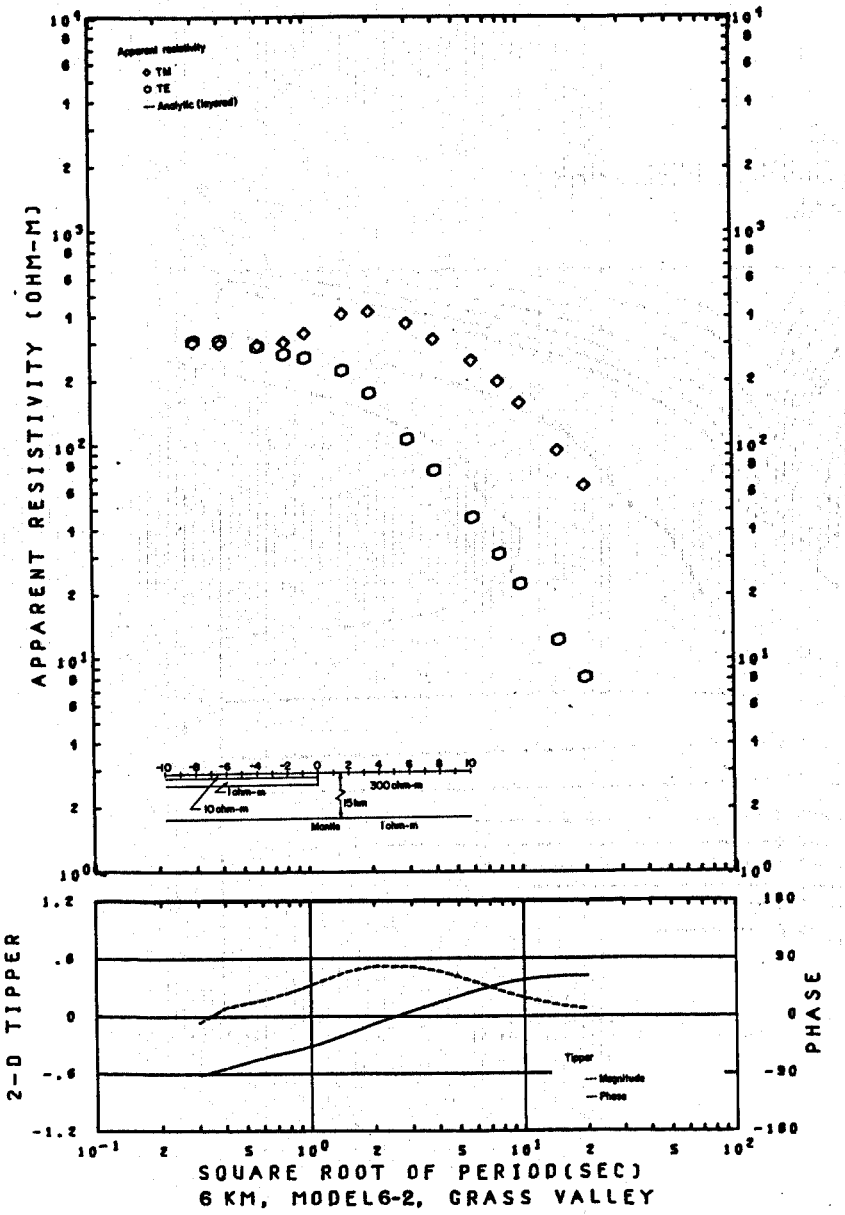
Apparent resistivity
TM
TE
Analytic (layered)
APPARENT RESISTIVITY (OHM-M)
300 ohm-m
1 ohm-m
10 ohm-m
15 km
Mantle
1 ohm-m
2-D TIPPER
PHASE
Tipper
Magnitude
Phase
SQUARE ROOT OF PERIOD(SEC)
6 KM, MODEL6-2, GRASS VALLEY

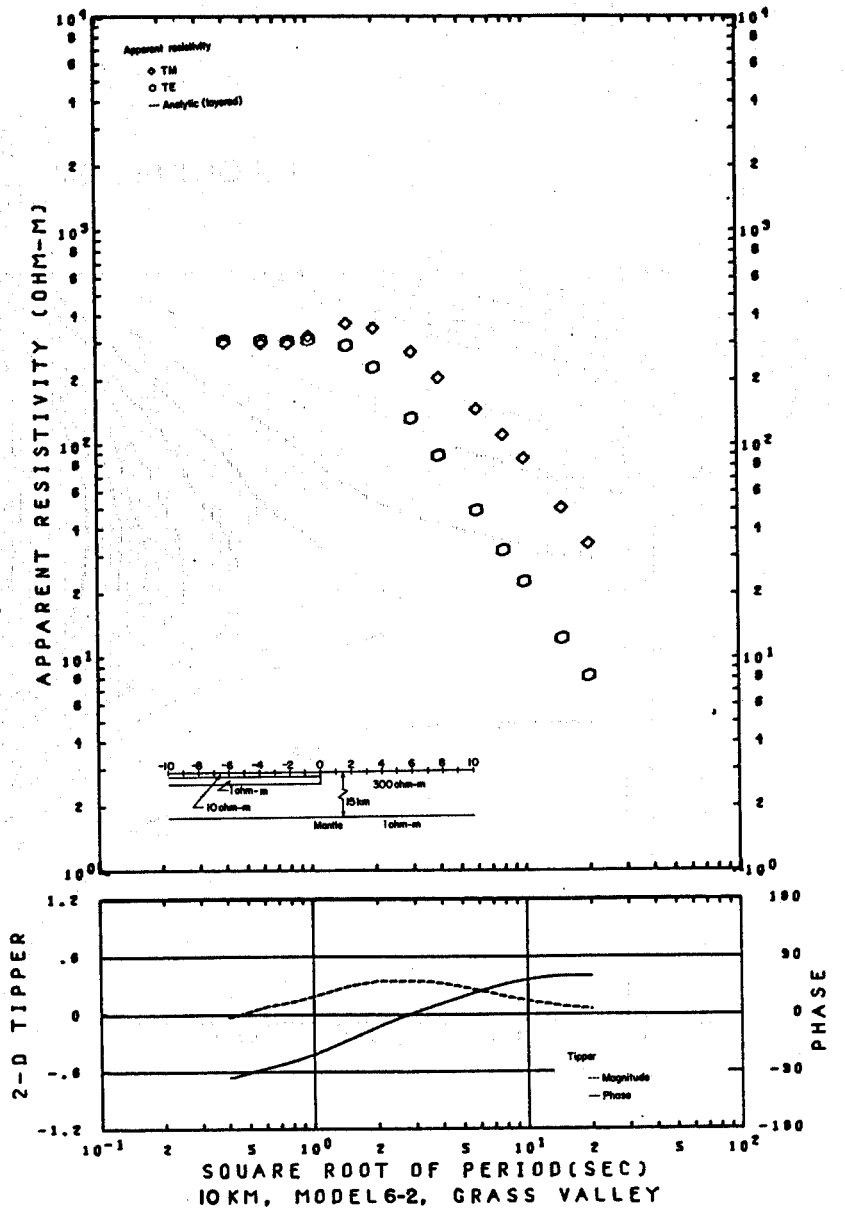
Apparent resistivity
TM
TE
Analytic (layered)
APPARENT RESISTIVITY (OHM-M)
300 ohm-m
1 ohm-m
10 ohm-m
15 km
Mantle
1 ohm-m
2-D TIPPER
PHASE
Tipper
Magnitude
Phase
SQUARE ROOT OF PERIOD(SEC)
10 KM, MODEL6-2, GRASS VALLEY

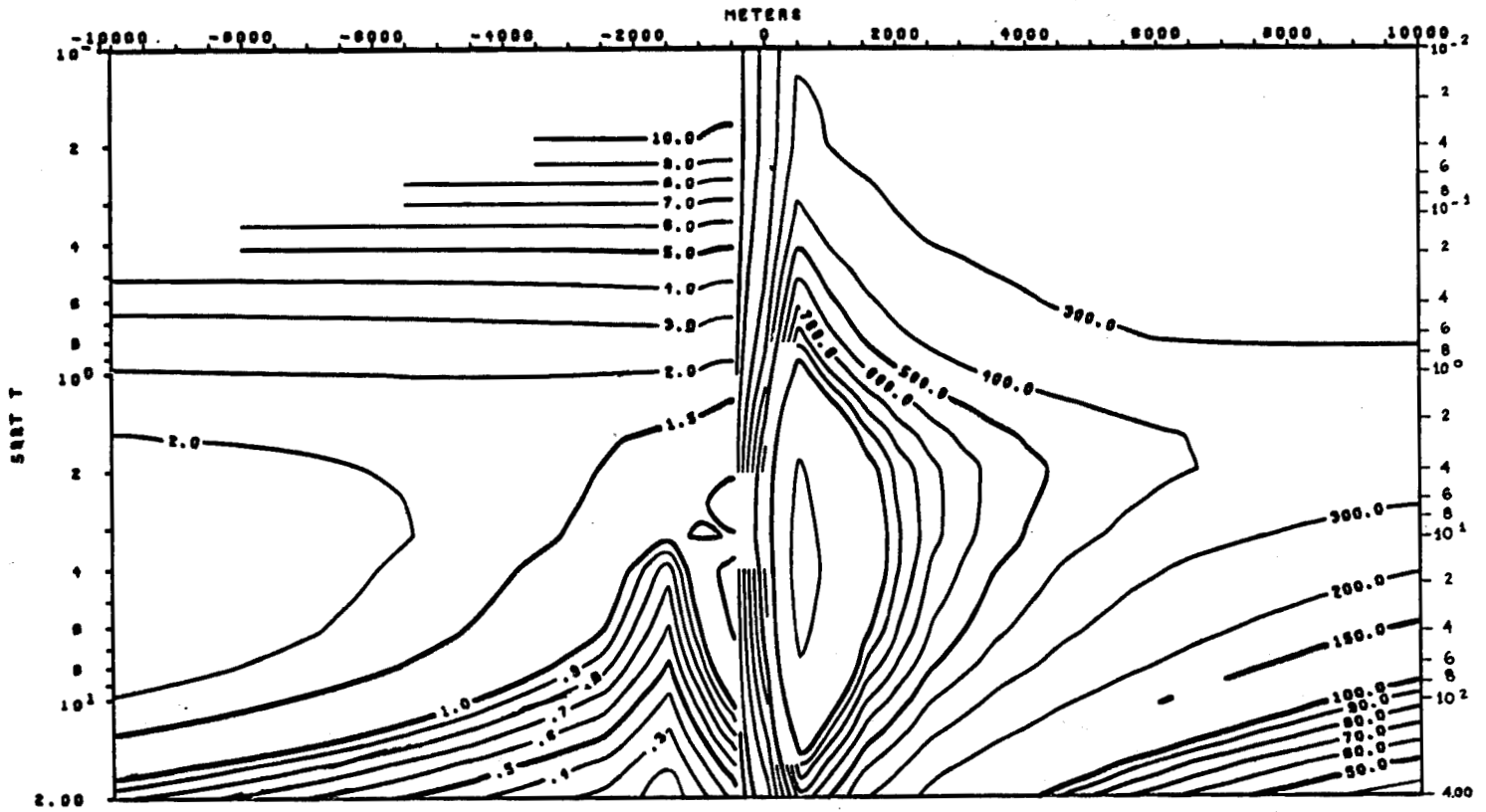

TM MODE
APPARENT RESISTIVITY VS. PERIOD (T)
MODEL 6-2

XBL 786-1922

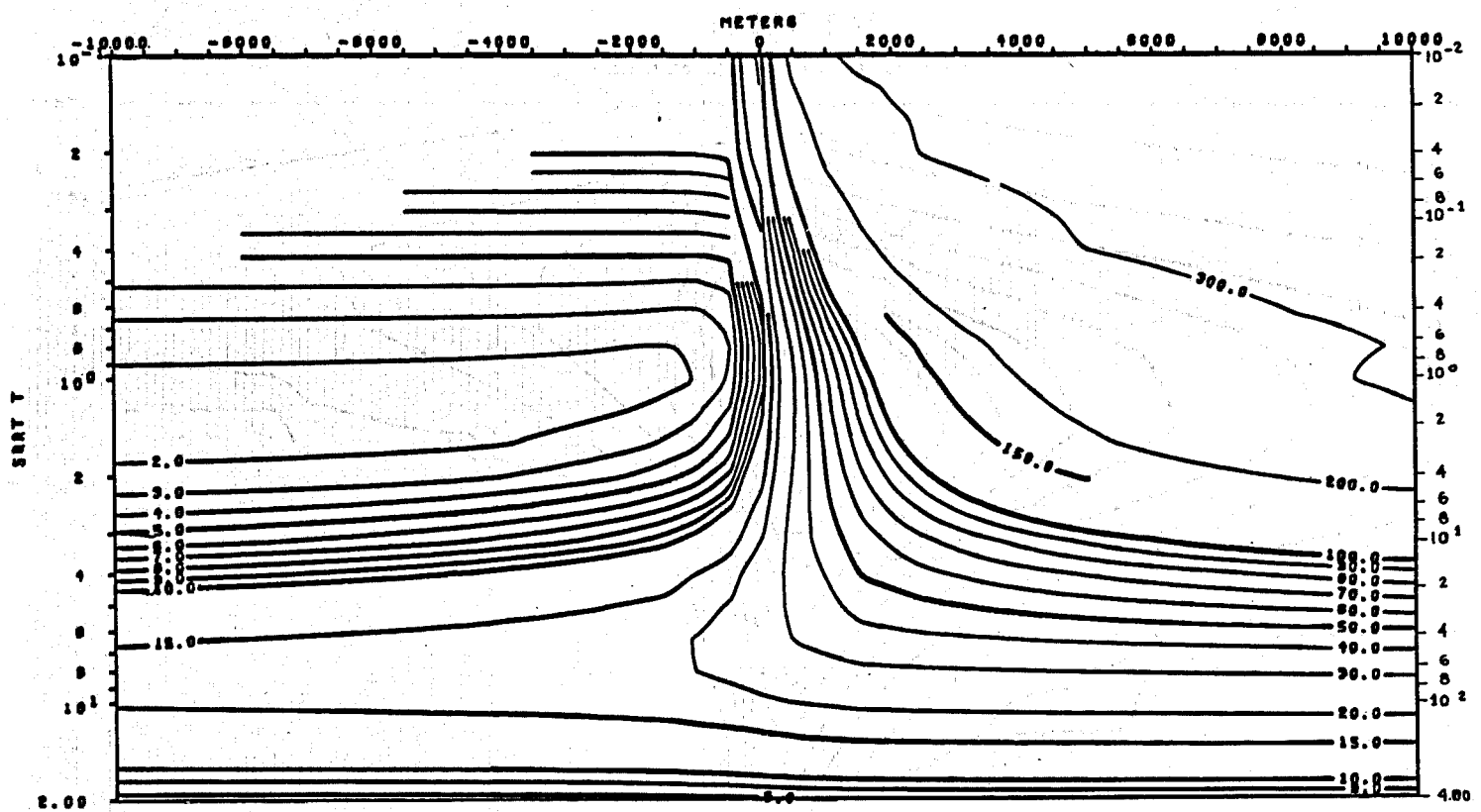

TE MODE
APPARENT RESISTIVITY VS. PERIOD (T)
MODEL 6-2

XBL 786-1921

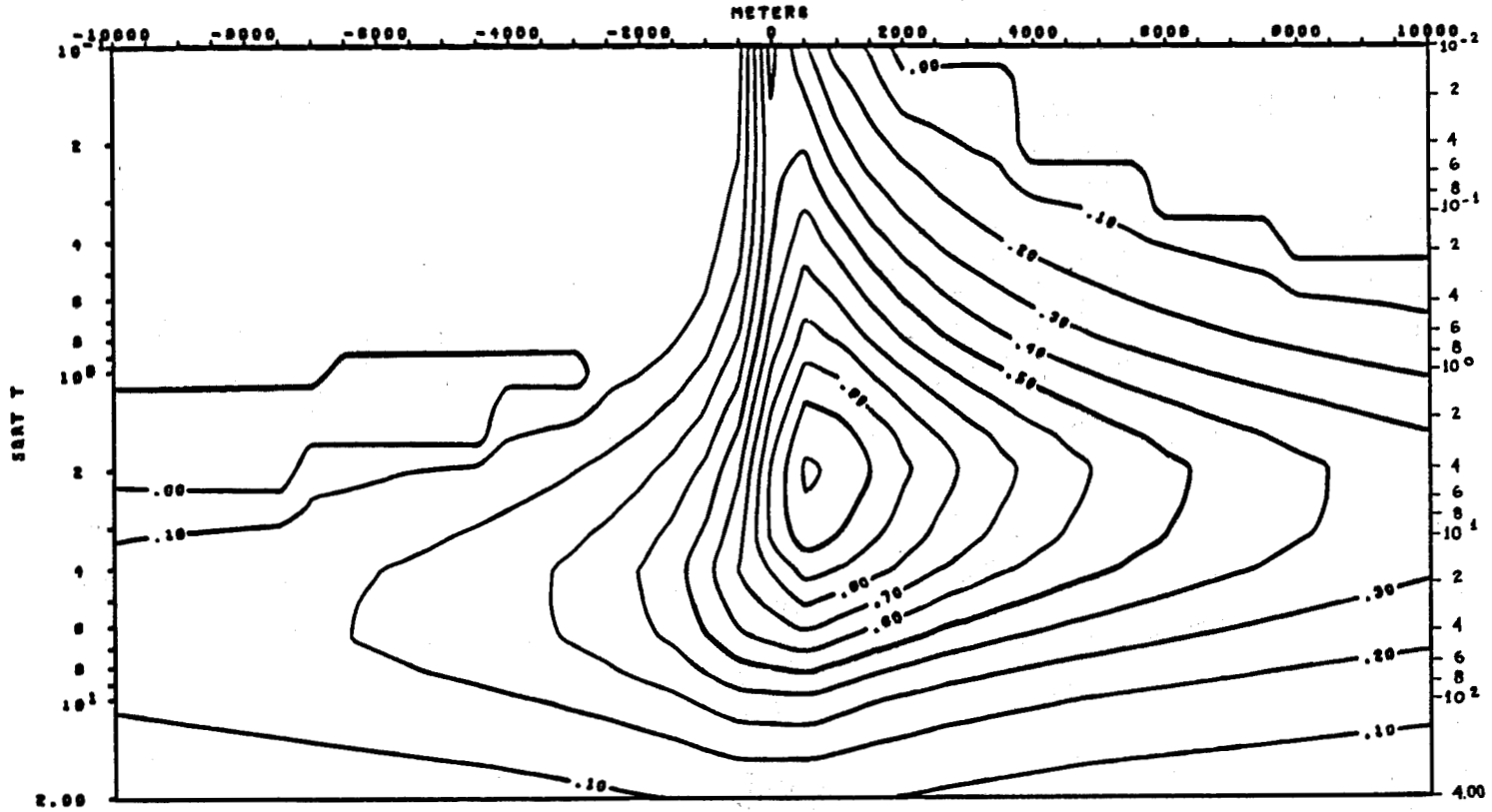

TIPPER VS. PERIOD (T)
MODEL 6-2

XBL 786-1939

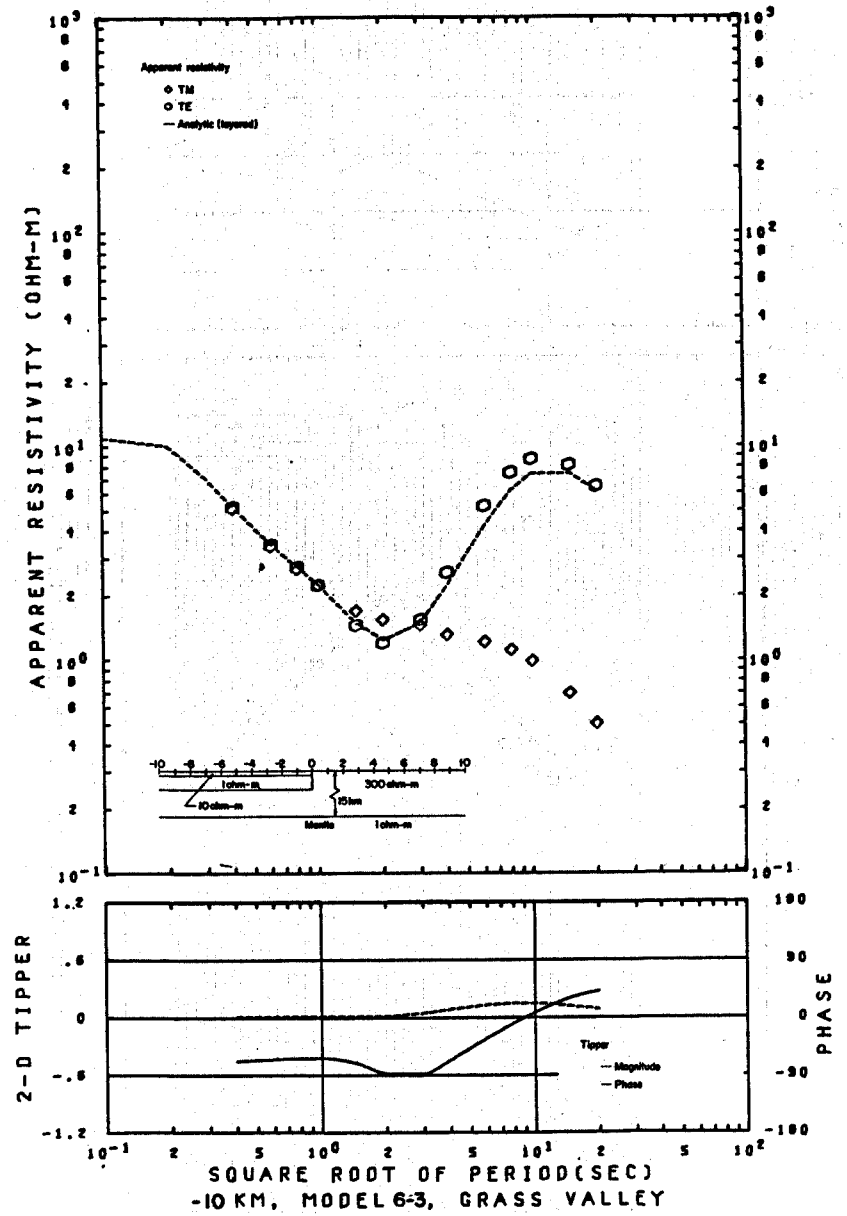
Apparent resistivity
TM
TE
Analytic (layered)
APPARENT RESISTIVITY (OHM-M)
1ohm-m
300 ohm-m
10ohm-m
15km
Mantle
1ohm-m
2-D TIPPER
PHASE
Tipper
Magnitude
Phase
SQUARE ROOT OF PERIOD(SEC)
-10 KM, MODEL 6-3, GRASS VALLEY

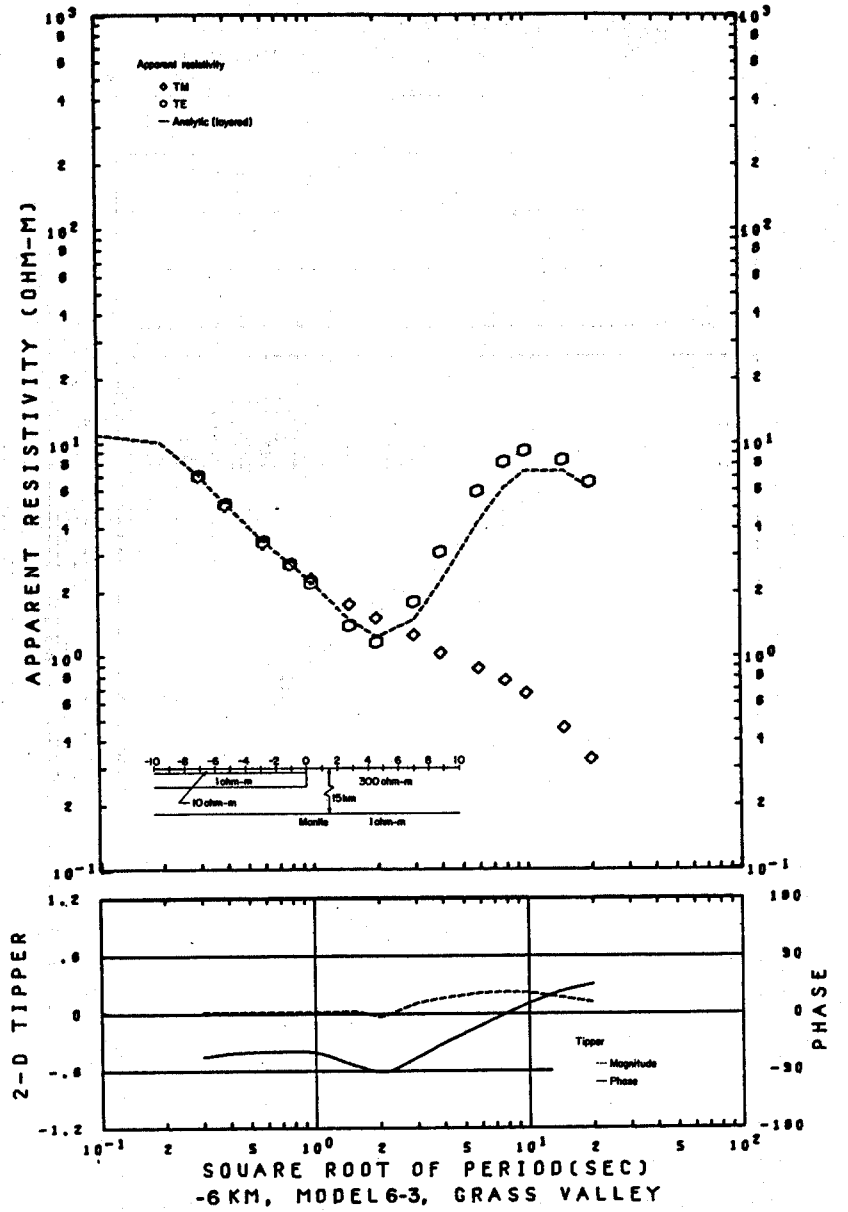
Apparent resistivity
TM
TE
Analytic (layered)
APPARENT RESISTIVITY (OHM-M)
1ohm-m
300 ohm-m
10ohm-m
15km
Mantle
1ohm-m
2-D TIPPER
PHASE
Tipper
Magnitude
Phase
SQUARE ROOT OF PERIOD(SEC)
-6 KM, MODEL 6-3, GRASS VALLEY

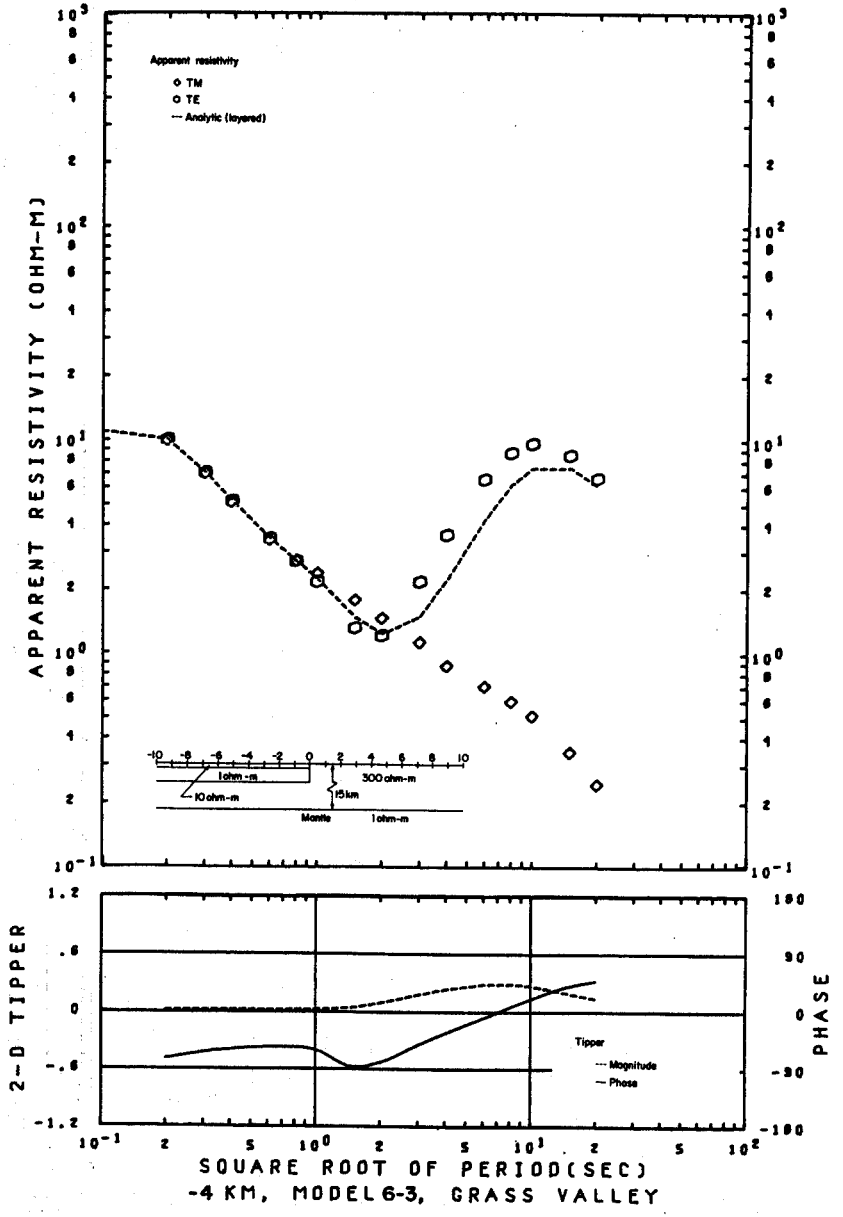
Apparent resistivity
TM
TE
Analytic (layered)
APPARENT RESISTIVITY (OHM-M)
1 ohm-m
10 ohm-m
15 km
300 ohm-m
Mantle
1 ohm-m
2-D TIPPER
PHASE
Tipper
Magnitude
Phase
SQUARE ROOT OF PERIOD(SEC)
-4 KM, MODEL 6-3, GRASS VALLEY

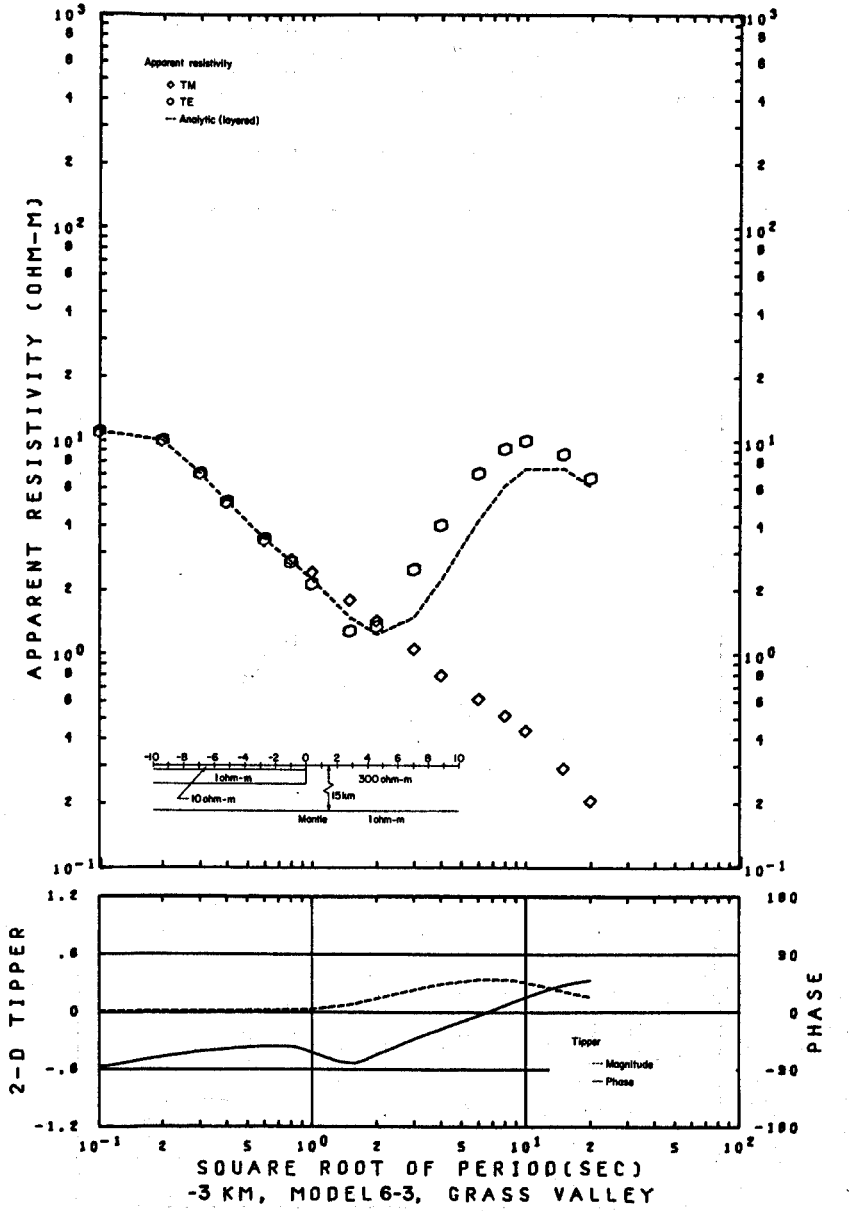
Apparent resistivity
TM
TE
Analytic (layered)
APPARENT RESISTIVITY (OHM-M)
1 ohm-m
10 ohm-m
15 km
300 ohm-m
Mantle
1 ohm-m
2-D TIPPER
PHASE
Tipper
Magnitude
Phase
SQUARE ROOT OF PERIOD(SEC)
-3 KM, MODEL 6-3, GRASS VALLEY

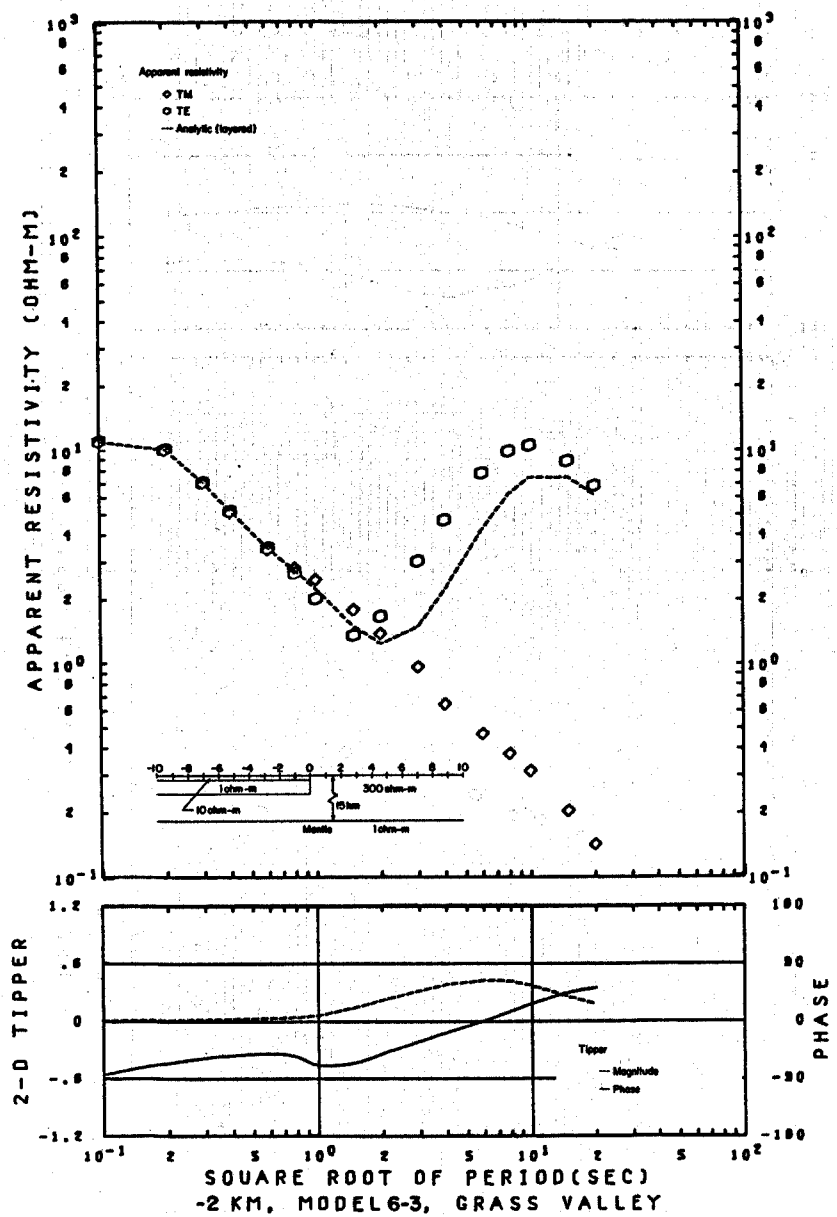
Apparent resistivity
TM
TE
Analytic (layered)
APPARENT RESISTIVITY (OHM-M)
1 ohm-m
300 ohm-m
10 ohm-m
15 km
Mantle
1 ohm-m
2-D TIPPER
PHASE
Tipper
Magnitude
Phase
SQUARE ROOT OF PERIOD(SEC)
-2 KM, MODEL6-3, GRASS VALLEY

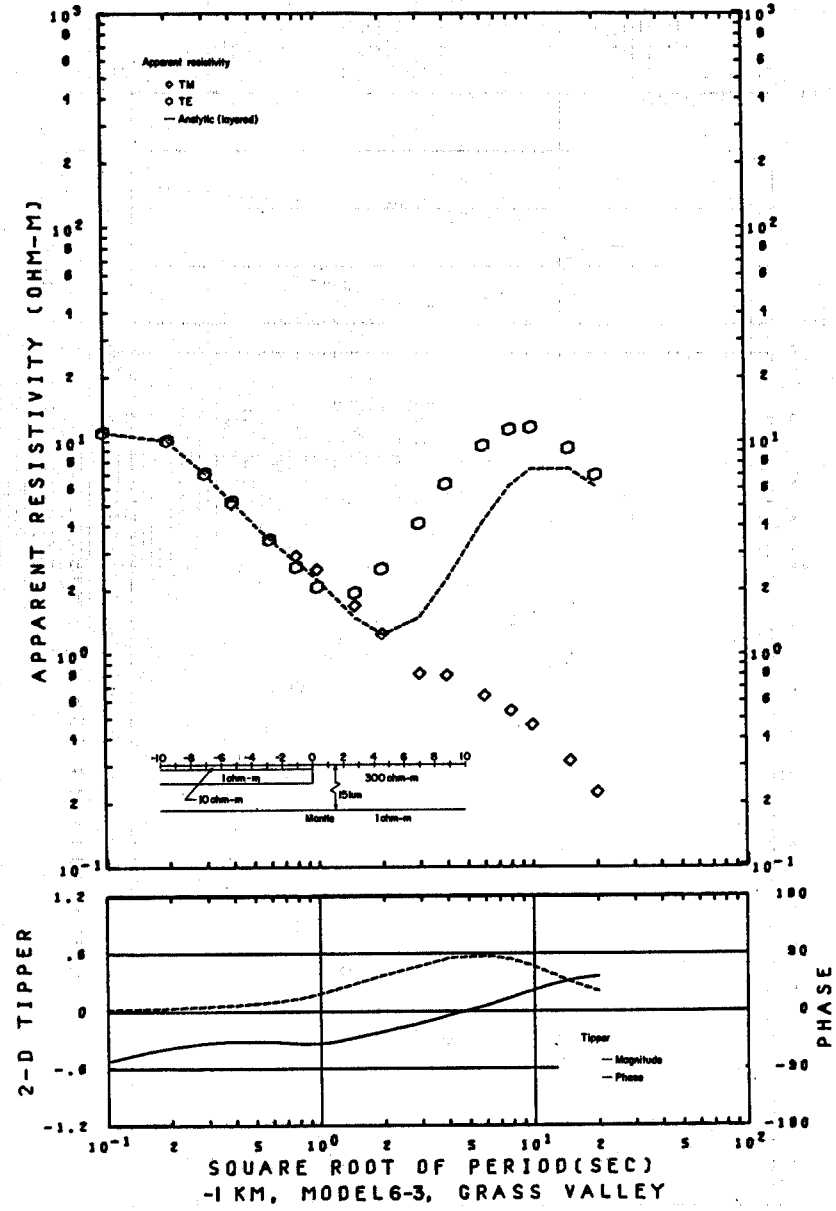
Apparent resistivity
TM
TE
Analytic (layered)
APPARENT RESISTIVITY (OHM-M)
1 ohm-m
300 ohm-m
10 ohm-m
15 km
Mantle
1 ohm-m
2-D TIPPER
PHASE
Tipper
Magnitude
Phase
SQUARE ROOT OF PERIOD(SEC)
-1 KM, MODEL6-3, GRASS VALLEY

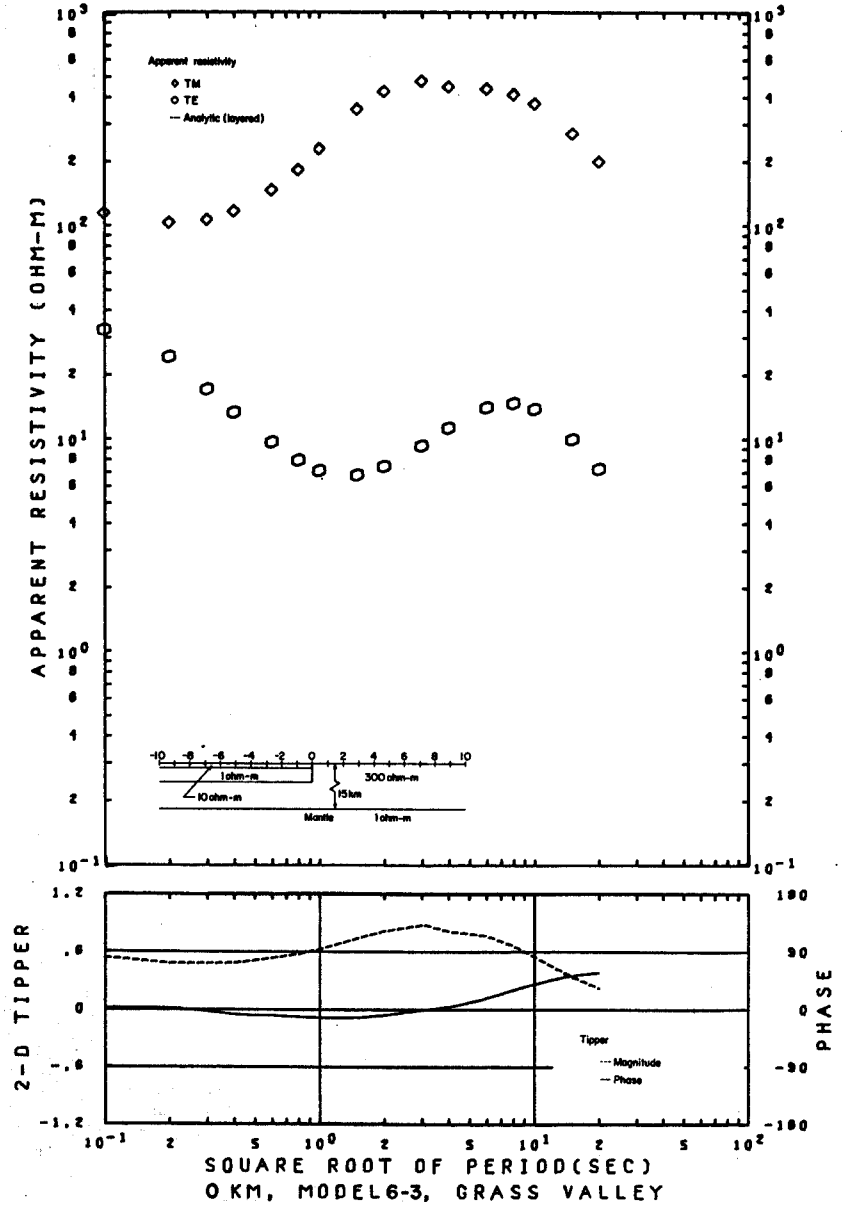
Apparent resistivity
TM
TE
Analytic (layered)
APPARENT RESISTIVITY (OHM-M)
1 ohm-m
300 ohm-m
10 ohm-m
15 km
Mantle
1 ohm-m
2-D TIPPER
PHASE
Tipper
Magnitude
Phase
SQUARE ROOT OF PERIOD(SEC)
0 KM, MODEL6-3, GRASS VALLEY

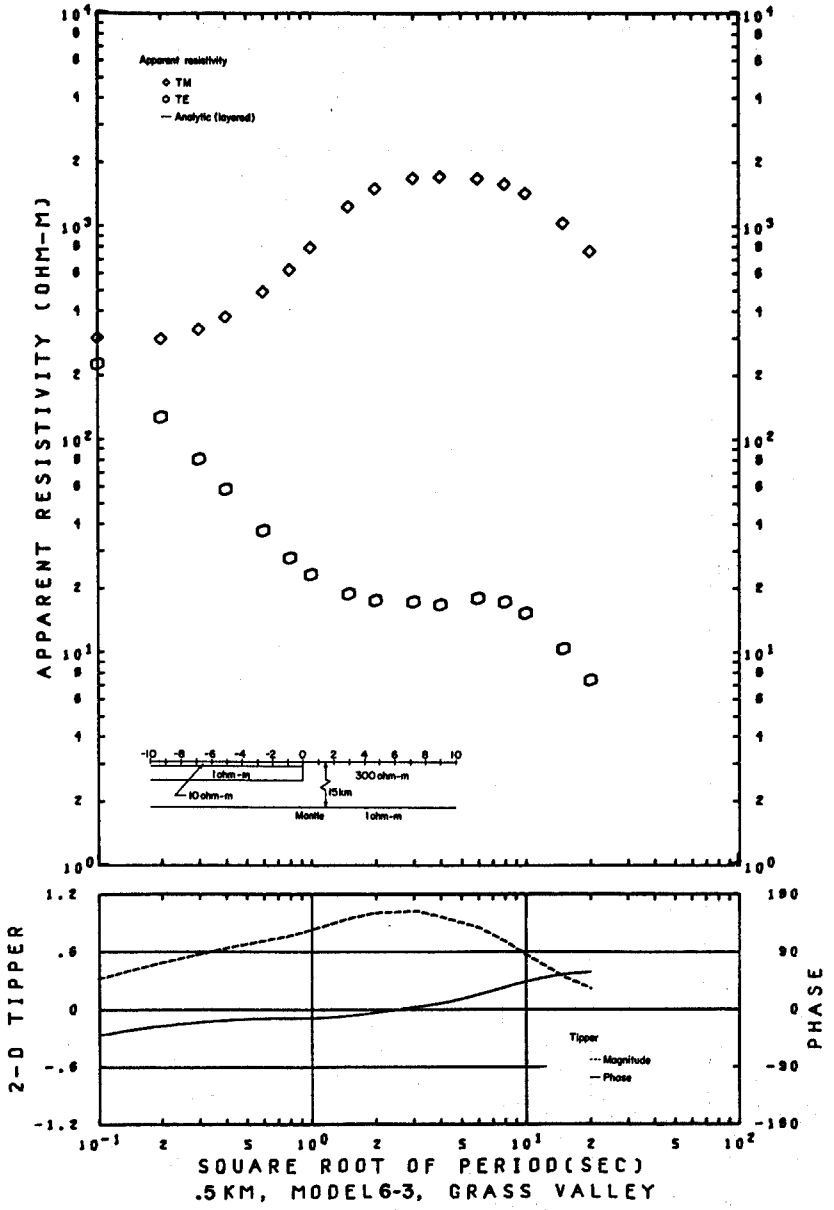
Apparent resistivity
TM
TE
Analytic (layered)
APPARENT RESISTIVITY (OHM-M)
1 ohm-m
300 ohm-m
10 ohm-m
15 km
Mantle
1 ohm-m
2-D TIPPER
PHASE
Tipper
Magnitude
Phase
SQUARE ROOT OF PERIOD(SEC)
.5 KM, MODEL6-3, GRASS VALLEY

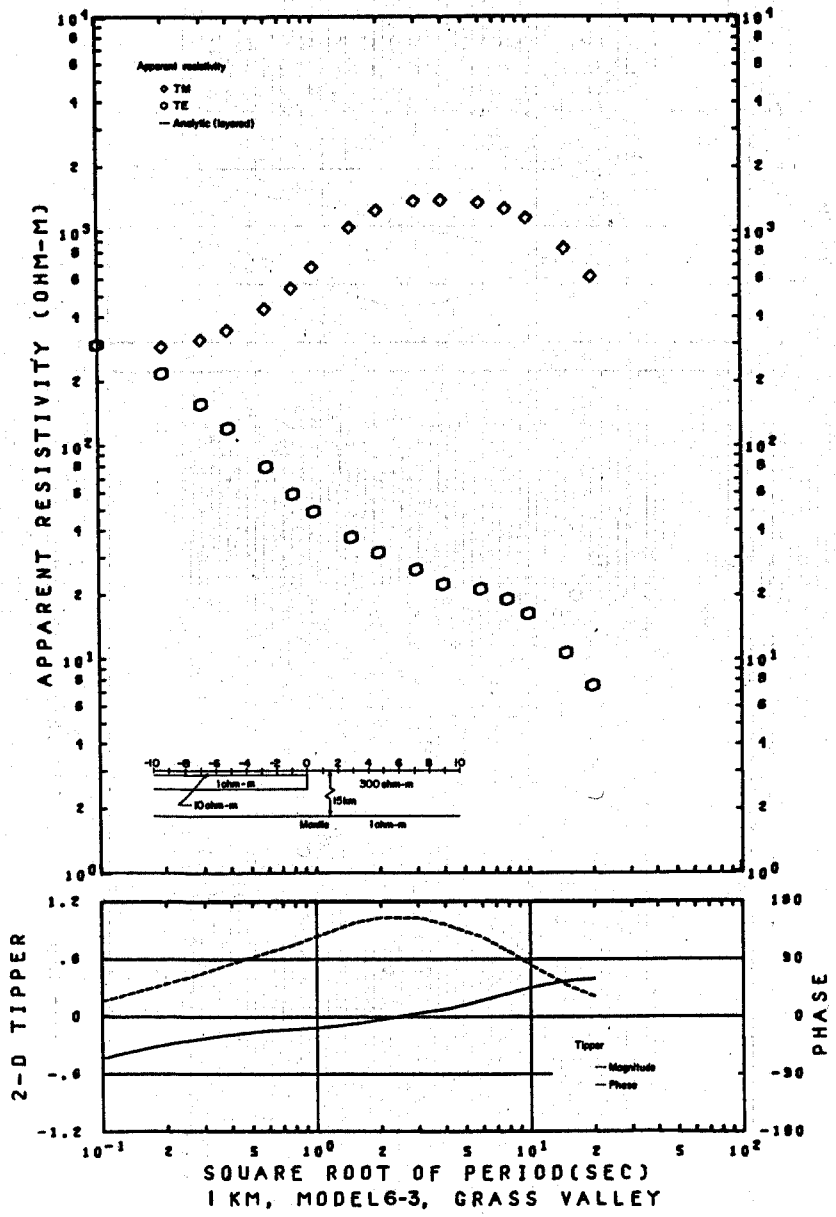
Apparent resistivity
TM
TE
Analytic (layered)
APPARENT RESISTIVITY (OHM-M)
1ohm-m
300 ohm-m
10ohm-m
15km
Mantle
1ohm-m
2-D TIPPER
PHASE
Tipper
Magnitude
Phase
SQUARE ROOT OF PERIOD(SEC)
1 KM, MODEL6-3, GRASS VALLEY

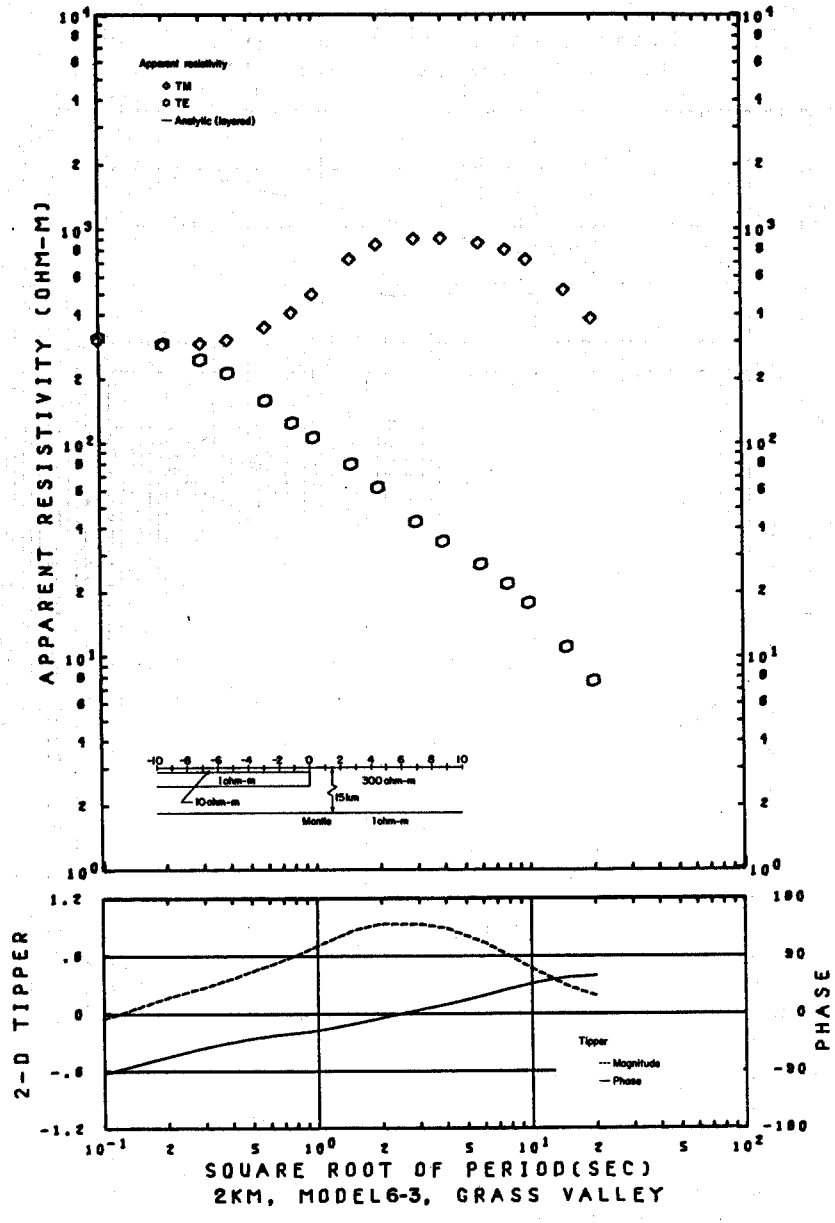
Apparent resistivity
TM
TE
Analytic (layered)
APPARENT RESISTIVITY (OHM-M)
1ohm-m
300 ohm-m
10ohm-m
15km
Mantle
1ohm-m
2-D TIPPER
PHASE
Tipper
Magnitude
Phase
SQUARE ROOT OF PERIOD(SEC)
2KM, MODEL6-3, GRASS VALLEY

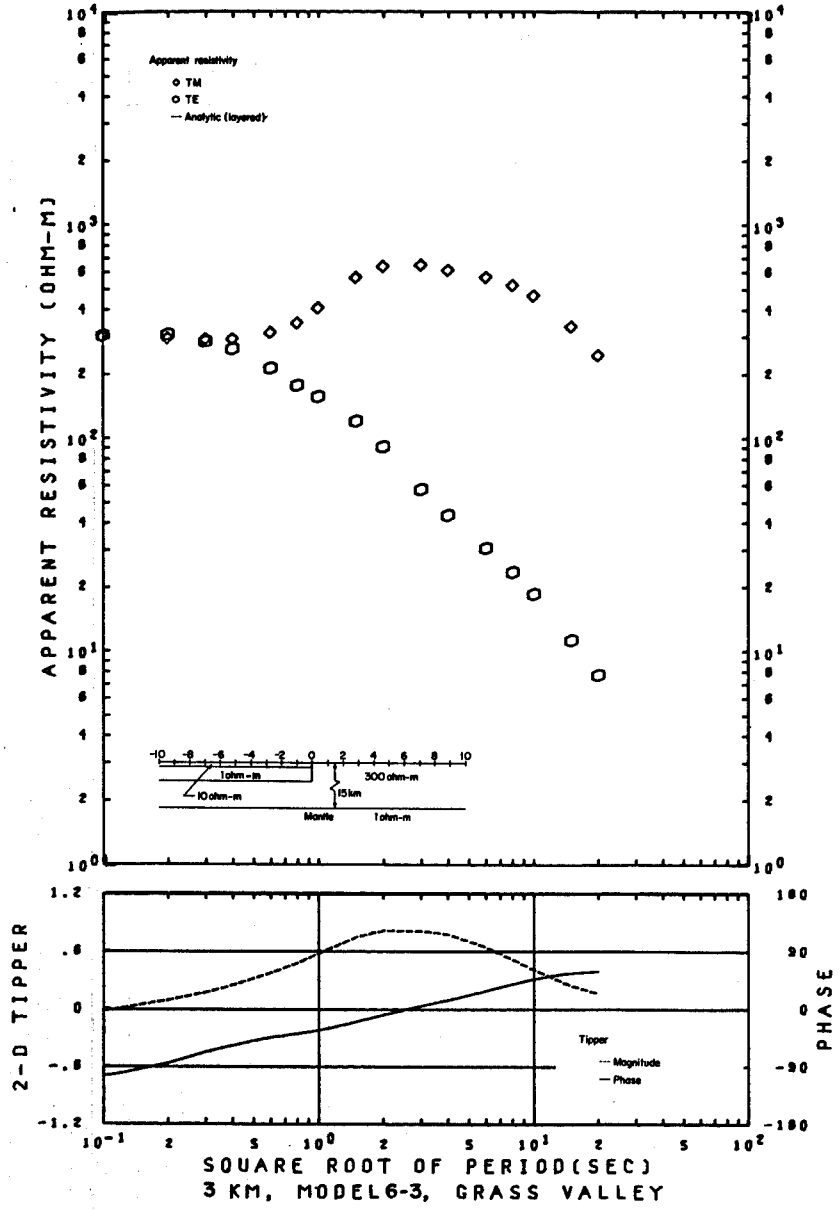
Apparent resistivity
TM
TE
Analytic (layered)
APPARENT RESISTIVITY (OHM-M)
1 ohm-m
300 ohm-m
10 ohm-m
15 km
Mantle
1 ohm-m
2-D TIPPER
Tipper
Magnitude
Phase
PHASE
SQUARE ROOT OF PERIOD(SEC)
3 KM, MODEL6-3, GRASS VALLEY

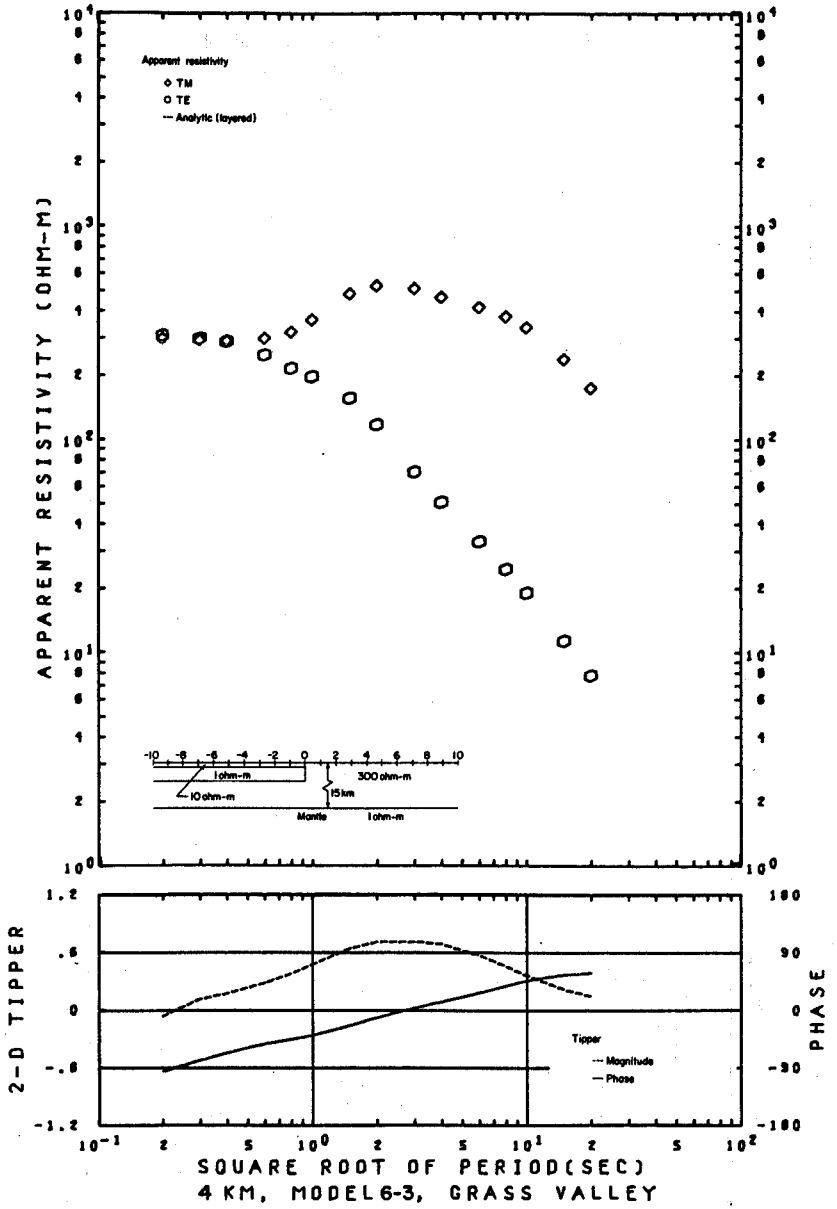
Apparent resistivity
TM
TE
Analytic (layered)
APPARENT RESISTIVITY (OHM-M)
1 ohm-m
300 ohm-m
10 ohm-m
15 km
Mantle
1 ohm-m
2-D TIPPER
Tipper
Magnitude
Phase
PHASE
SQUARE ROOT OF PERIOD(SEC)
4 KM, MODEL6-3, GRASS VALLEY

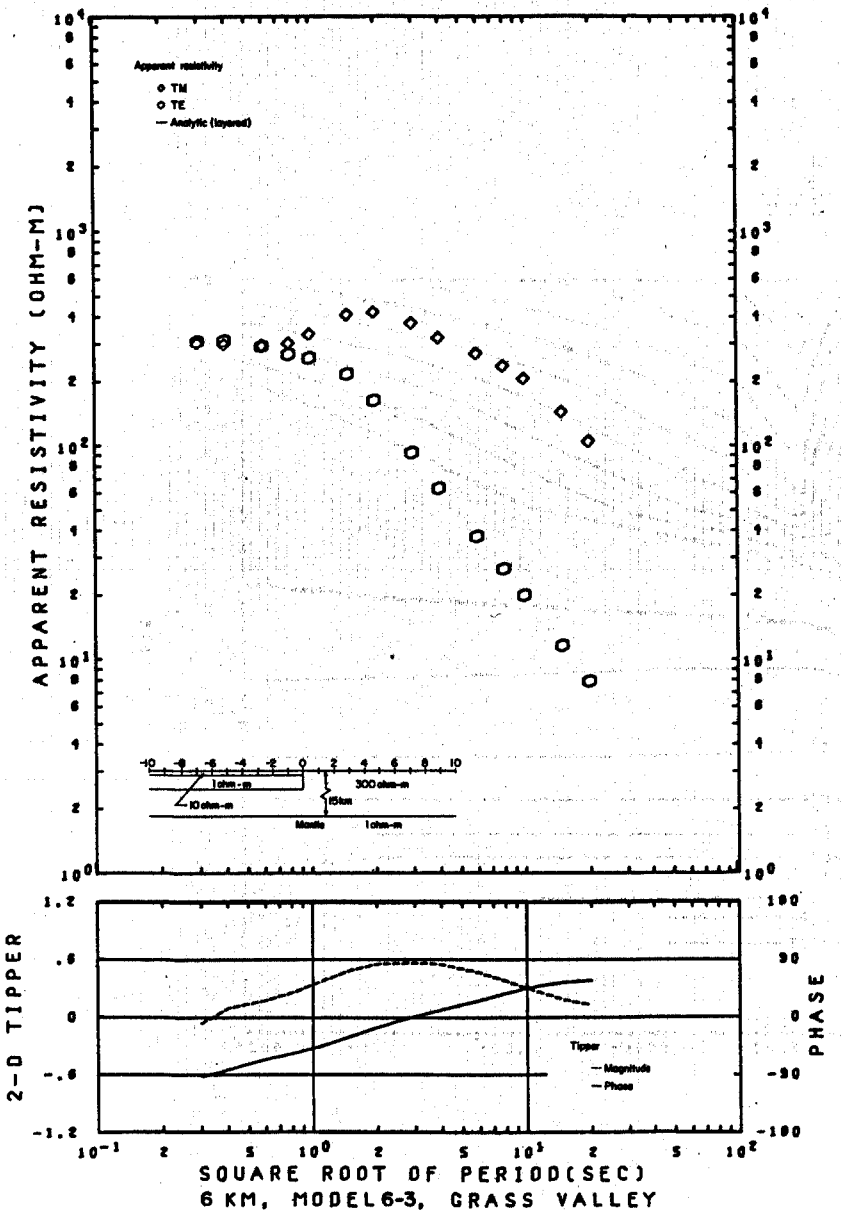
Apparent resistivity
TM
TE
Analytic (layered)
APPARENT RESISTIVITY (OHM-M)
1 ohm-m
300 ohm-m
10 ohm-m
15km
Mantle
1 ohm-m
2-D TIPPER
Tipper
Magnitude
Phase
PHASE
SQUARE ROOT OF PERIOD(SEC)
6 KM, MODEL6-3, GRASS VALLEY

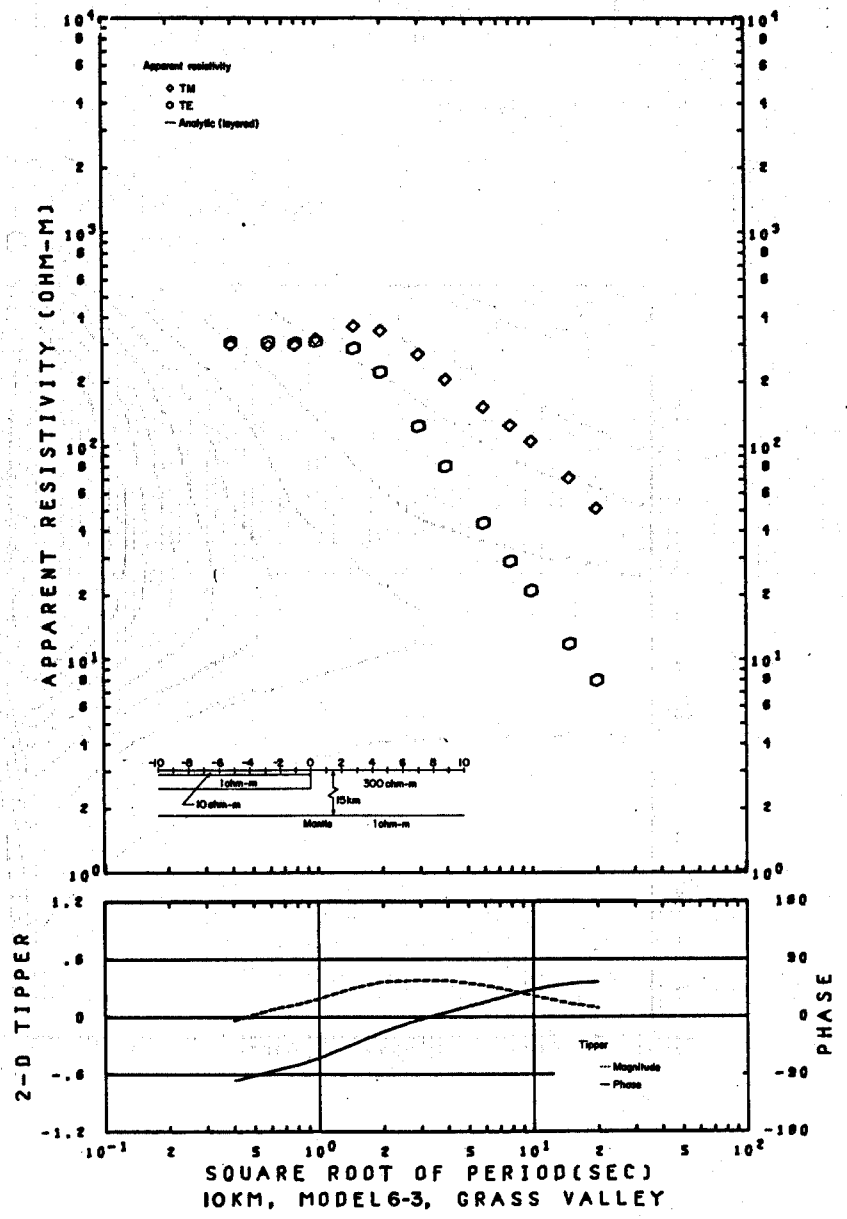
Apparent resistivity
TM
TE
Analytic (layered)
APPARENT RESISTIVITY (OHM-M)
1 ohm-m
300 ohm-m
10 ohm-m
15km
Mantle
1 ohm-m
2-D TIPPER
Tipper
Magnitude
Phase
PHASE
SQUARE ROOT OF PERIOD(SEC)
10KM, MODEL6-3, GRASS VALLEY

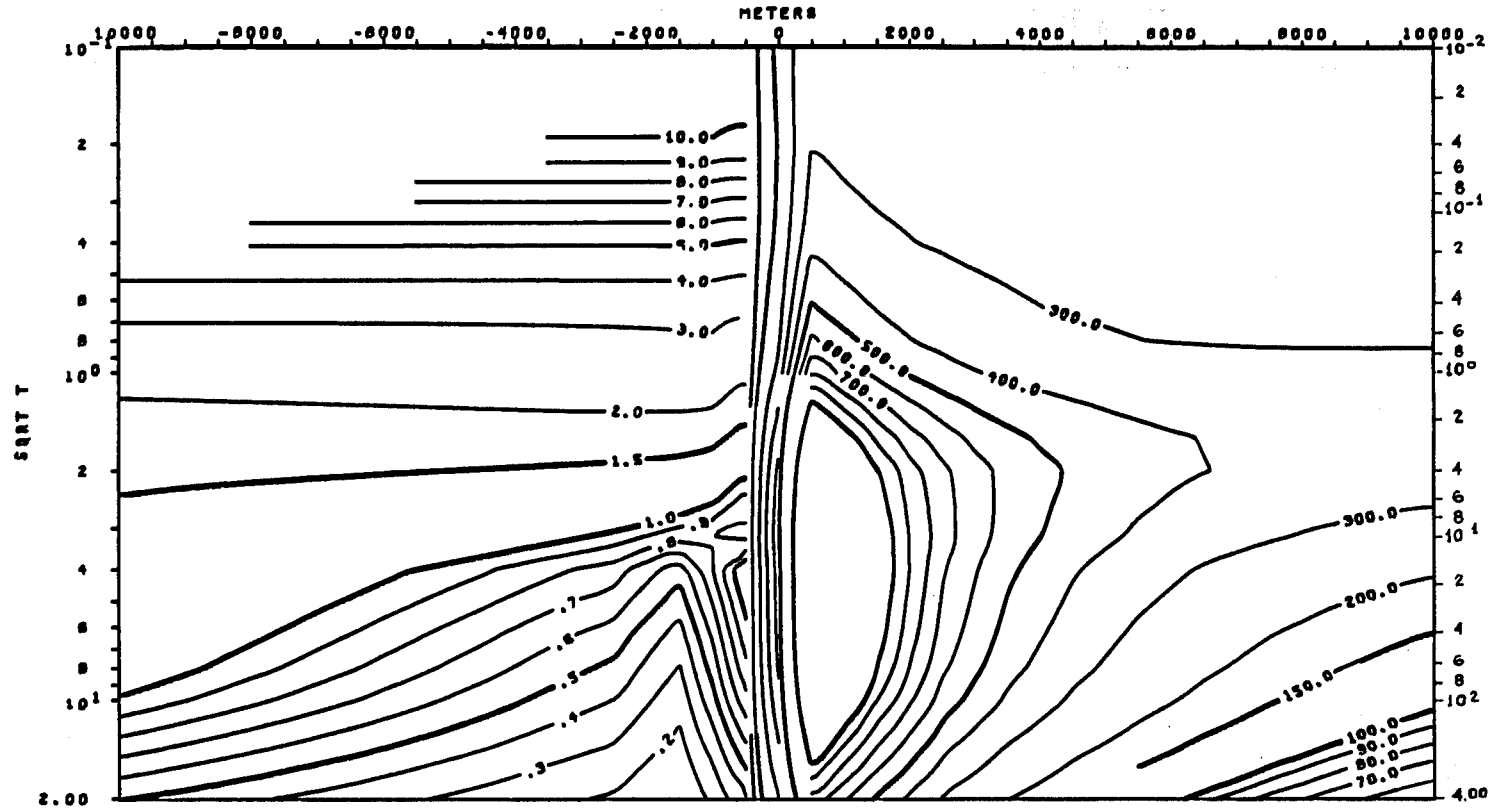

TM MODE
APPARENT RESISTIVITY VS. PERIOD (T)
MODEL 6-3

XBL 786-1924

T

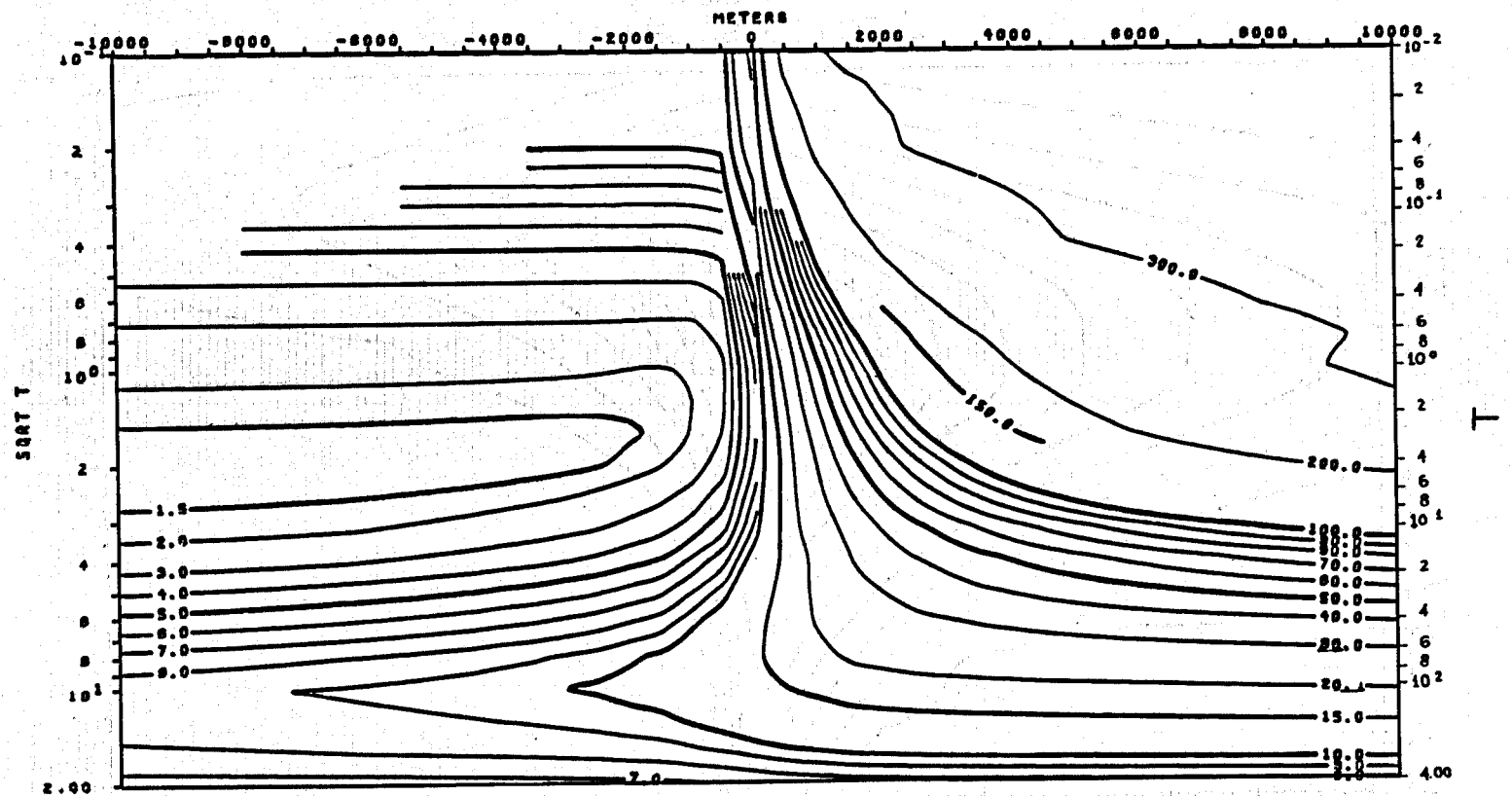

TE MODE
APPARENT RESISTIVITY VS. PERIOD (T)
MODEL 6-3

XBL 786-1940

U.S.GPO:1979-689-058(P)59

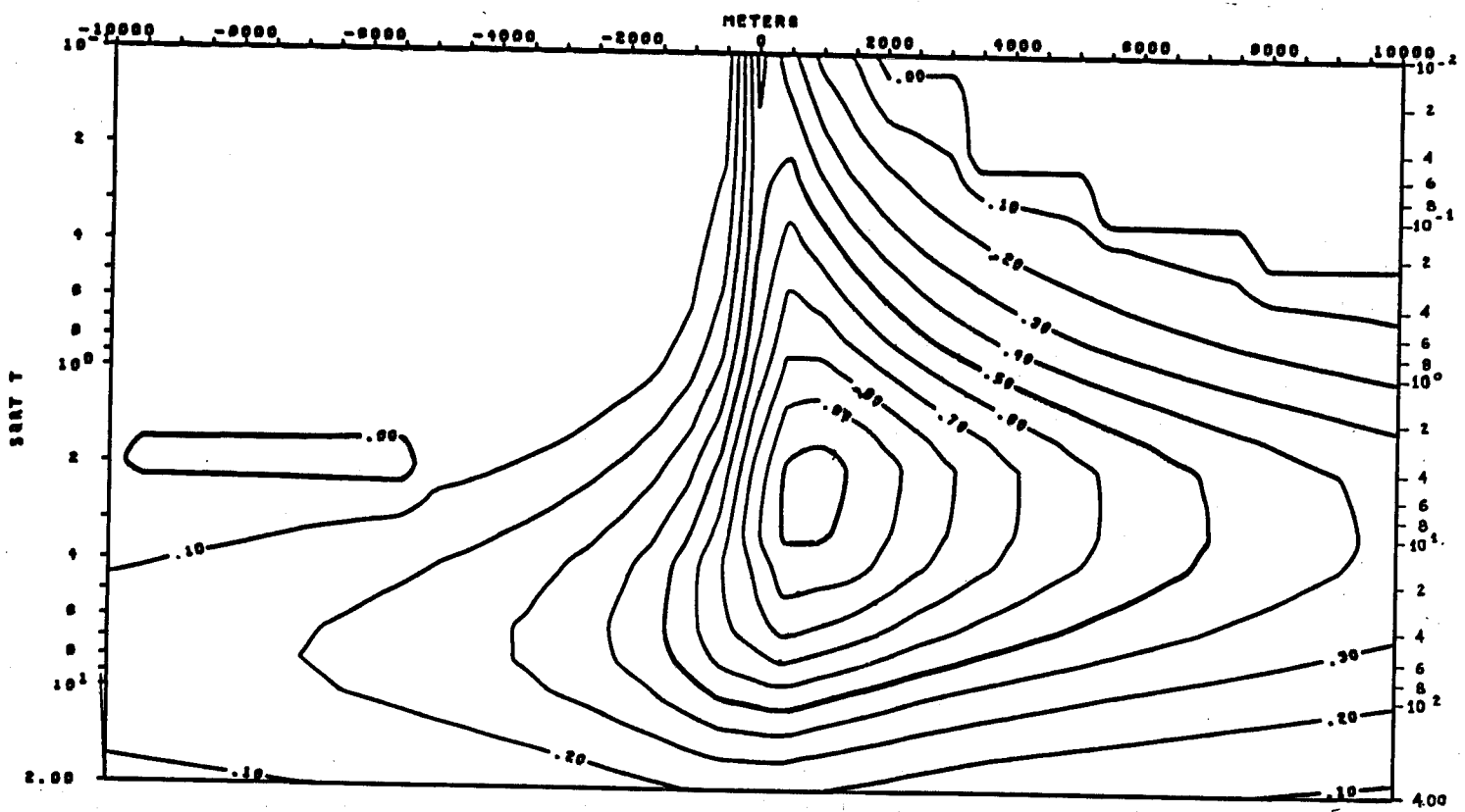

TIPPER VS. PERIOD (T)
MODEL 6-3

XBL 786-1941